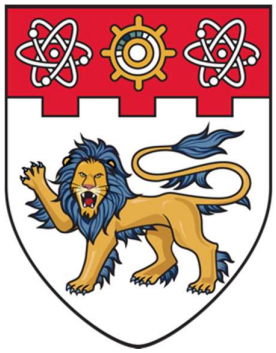

NANYANG TECHNOLOGICAL UNIVERSITY
SINGAPORE

SYNTHESIS OF *MYCOBACTERIUM TUBERCULOSIS* ATP SYNTHASE INHIBITORS

SEANKONGSUK PATTARAKIAT

SCHOOL OF PHYSICAL AND MATHEMATICAL SCIENCES

2022

SYNTHESIS OF *MYCOBACTERIUM TUBERCULOSIS* ATP SYNTHASE INHIBITORS

SEANKONGSUK PATTARAKIAT

SCHOOL OF PHYSICAL AND MATHEMATICAL SCIENCES

A thesis submitted to the Nanyang Technological University in partial fulfilment of the requirement for the degree of Doctor of Philosophy

2022

Statement of Originality

I hereby certify that the work embodied in this thesis is the result of original research done by me except where otherwise stated in this thesis. The thesis work has not been submitted for a degree or professional qualification to any other university or institution. I declare that this thesis is written by myself and is free of plagiarism and of sufficient grammatical clarity to be examined. I confirm that the investigations were conducted in accord with the ethics policies and integrity standards of Nanyang Technological University and that the research data are presented honestly and without prejudice.

20th June 2022

Date

Seankongsuk Pattarakiat

Supervisor Declaration Statement

I have reviewed the content and presentation style of this thesis and declare it of sufficient grammatical clarity to be examined. To the best of my knowledge, the thesis is free of plagiarism, and the research and writing are those of the candidate's except as acknowledged in the Author Attribution Statement. I confirm that the investigations were conducted in accord with the ethics policies and integrity standards of Nanyang Technological University and that the research data are presented honestly and without prejudice.

20th June 2022
Date

Rod Bates
Assoc. Prof. Roderick W. Bates

Authorship Attribution Statement

This thesis contains material from 1 paper published in the following peer-reviewed journal in which I am listed as an author.

Chapter 2 is published as Hotra, A.; Ragunathan P.; Ng P. S.; **Seankongsuk, P.**; Harikishore, A.; Sarathy, J. P.; Saw W. G.; Lakshmanan, U.; Sae-Lao P.; Kalia N. P.; Shin, J.; Kalyanasundaram, R.; Anbarasu, S.; Parthasarathy, K.; Pradeep, C. N.; Makhija, H.; Dröge, P.; Poulsen, A.; Tan, J. H. L.; Pethe, K.; Dick, T.; Bates, R. W.; Grüber, G. Discovery of a Novel Mycobacterial F-ATP Synthase Inhibitor and its Potency in Combination with Diarylquinolines. *Angew. Chem. Int. Ed.*, **2020**, *59*, 2 – 12. DOI: 10.1002/anie.202002546.

The contributions of the co-authors are as follows:

- Grüber, G. and Bates, R. W. provided the initial project direction and gave guidance throughout the entire project.
- Hotra, A. performed computational homology and compound screening modeling to discover GaMF1 as a mycobacterial F-ATP synthase inhibitor, as well as enzymatic and antimycobacterial growth assays, initiated the structural activity relationship (SAR) of GaMF1 by synthesis and investigation of compounds **S8a – g**, **S9**, **S10a – b**, and **S11a – e**, and studied with Kalia N. P. the synergistic effect between Bedaquiline and GaMF1 on cell growth of *M. smegmatis*.
- Ragunathan P., Sarathy, J. P., and Lakshmanan, U. conducted the enzymatic and antimycobacterial growth assays for GaMF1 and its analogs.
- Ragunathan P. investigated the GaMF1 target specificity.

- Shin, J. performed and analyzed the HSQC-NMR titration data.
- Harikishore, A. computed the molecular modeling of GaMF1 binding the targeted subunit based on the HSQC-NMR titration results.
- Sae-Lao P. investigated the approach and synthesized the TBAJ-analogs (±)-**5307**, (±)-**5316**, and (±)-**5366** to test enhanced potency with GaMF1.
- Pradeep, C.N., Makhija, H. and Dröge, P. studied the toxicology of combinations between Bedaquiline/**(±)-5307** and GaMF1 with human stem cell technologies.
- Bates, R. W., Ng P. S., **Seankongsuk, P.**, Harikishore, A., Tan, J. H. L., and Poulsen, A. designed the GaMF1 analogs and interpreted the SAR data.
- Ng P. S., Tan, J. H. L., and Poulsen, A. designed the approach and synthesized GaMF1 analogs **3** – **8**, **S5**, and **S8h – j** for SAR studies.
- **Seankongsuk, P.** designed and studied the synthetic route to make their compounds and synthesized **S14 a – k**, **S15a – g**, and **S26 – S35** for GaMF1 SAR investigation.
- Kalyanasundaram, R., Anbarasu, S., and Parthasarathy, K. demonstrated the killing potency of GaMF1 against three drug-resistant clinical *Mtb* isolates
- Dick, T. and Pethe, K. contributed to the microbiology aspects of the studies.

P. Seankongsuk.

20th June 2022
Date

Seankongsuk Pattarakiat

Abstract

Tuberculosis (TB) is a lethal disease considered a direct threat to human wellbeing in all regions worldwide *Mycobacterium tuberculosis* (*Mtb*) is a species of bacteria that causes almost all cases of TB in humans. Currently, multidrug therapy is a *key* strategy for treating TB. However, TB can mutate to resist the common TB drugs; therefore, more potent drugs, which commonly come with greater side effects, are required to cure MDR-TB. One of the potent second-line drugs with a high success rate is Bedaquiline (BDQ). However, it carries a risk of arrhythmias, which is potentially lethal. Nonetheless, the BDQ binding site of *Mtb* F_1F_0 ATP synthase remains a promising drug target. In this work, the development of novel *Mtb* ATP synthase inhibitors was studied.

Recently, GaMF1 was reported to exhibit good inhibition in ATP synthesis of *Mtb* by binding at a unique and crucial peptide loop in the γ-subunit of *Mycobacterium* F_oF_1-ATP synthase. Nevertheless, the water solubility and in *vivo* stability of GaMF1 are potentially problematic. In this work, 28 GaMF1 analogs are synthesized to overcome those issues and improve both ATP synthesis and mycobacterial growth inhibition. Inverted Membrane Vesicle (IMV) and *M. smeg.* growth inhibition assays were done to evaluate the synthetic analogs' properties. The pyrimidine (ring C) substituents are crucial moieties for inhibition, and the modification of this ring results in a significant decrease in potency. However, the modification of the middle *p*-phenylenediamine (ring B) is quite well-tolerated, and aromatic or cyclic alkanes are favored for efficiency.

Recently, EGCG was discovered to have promising enzymatic activity at the nanomolar level to inhibit *Mycobacterium* ATP synthesis by interfering with *Mycobacterium* F_oF_1-ATP synthase at the ε subunit. However, EGCG does not show mycobacterial growth activity. In this work, 16 EGCG analogs are synthesized to understand the structure-activity relationship in which both catechin and gallate ester moieties are required for mycobacterial ATP synthesis inhibition. However, catechin gallate and gallocatechin gallate derivatives revealed different patterns in structural activity relationships. Additionally, catechol ester can improve the effectiveness of inhibiting ATP synthesis in catechin analogs. The bacterial growth assay showed that EGCG analogs still lack the mycobacterial growth inhibition property. The lipophilic ester-protected catechin gallate could not solve the bacterial growth inhibition problem.

Acknowledgments

Firstly, I would like to sincerely thank and express my deepest gratitude to my advisor, Assoc. Prof. Roderick Wayland Bates and co-advisor, Prof. Gerhard Grüber, for their guidance not only in my research but also in integrating knowledge in organic synthesis, biochemistry, as well as medicinal chemistry, and for being influential on my logical and critical thinking skills. Their advice and encouragement helped me understand and overcome challenges with my research and thesis writing. I am also grateful to my thesis advisor committee, Prof. Xing Bengang, and Assoc. Prof. Judeh Zaher for their valuable comments and suggestions.

Moreover, I would like to thank the Targeting Oxidative Phosphorylation Network (TOP Net), which is composed of Chemistry and Biological Chemistry – School of Physical and Mathematical Science – Nanyang Technological University (NTU), School of Biological Science – NTU, National University of Singapore, and Experimental Drug Development Centre – The Agency for Science, Technology, and Research (A*star), Singapore, for their excellent collaboration, especially Priya Ragunathan and Umayal Lakshmanan for the ATP synthesis inhibition assay, Jickky Palmae Sarathy for the antimycobacterial activity assay, and Amaravadhi Harikishore for molecular modeling. The research of this thesis was supported by the National Research Foundation (NRF) Singapore, NRF Competitive Research Programme (CRP), Grant Award Number NRF–CRP18–2017–01.

In addition, I would like to express my gratitude to Patcharaporn Sae-Lao for her advice and encouragement to strengthen and broaden my chemistry and medicinal chemistry knowledge as a senior in our research group. I would like to thank Bates' and Grüber's research group members for their stimulating discussion, friendship, and advice. Last but never least, I am deeply indebted to my family and friends for their moral support throughout the research.

Contents

Abbreviations

Ac	Acetyl
ADP	adenosine diphosphate
ATP	Adenosine triphosphate
ATPase	adenosine triphosphatase
ATR	attenuated total reflection
BCA	bicinchoninic acid
B-cells	Bone marrow cells
BDQ	Bedaquiline
Bn	Benzyl
Boc	*tert*-Butyloxycarbonyl
c-hex	Cyclohexyl
COD	1,5-cyclooctadiene
COVID-19	Coronavirus disease 2019
DCE	1,2-dichloroethene
DCM	Dichloromethane
dec.	Decompose
DIBAL	diisobutylaluminium hydride
DIPEA	*N*,*N*-Diisopropylethylamine
diphos	1,2-Bis(diphenylphosphino)ethane
DMAP	4-dimethylaminopyridine
DMF	Dimethylformamide
DMPU	*N*,*N*′-Dimethylpropyleneurea
DMSO	dimethyl sulfoxide

DNA	Deoxyribonucleic acid
DNAse	Deoxyribonuclease
E. coli	*Escherichia coli*
EAS	electrophilic aromatic substitution
ECG	epicatechin gallate
EDCI	1-ethyl-3-(3-dimethylaminopropyl)carbodiimide
EDTA	ethylenediaminetetraacetic acid
EGCG	epigallocatechin gallate
EMA	European Medicines Agency
EMB	Ethambutol
Et	Ethyl
ETC	electron transport chain
FDA	Food and Drugs Administration
FM	lipid-rich Foamy Cells
GCG	gallocatechin gallate
H. sap.	*Homo sapiens*
HIV	Human Immunodeficiency Virus
HRMS	high-resolution mass spectrometry
HSQC	heteronuclear single quantum coherence
Hz	Hertz
IC_{50}	half-maximal inhibitory concentration
IMV	inversed membrane vesicle
INH	Isoniazid
InhA	enoyl-acyl carrier protein reductase
i-Pr	*iso*-propyl

IR	Infrared spectroscopy
KatG	bacterial catalase-peroxidase enzyme
LRMS	low-resolution mass spectrometry
LTBI	Latent Tuberculosis infection
M. aficanum	*Mycobacterium aficanum*
M. bovis	*Mycobacterium bovis*
M. microti	*Mycobacterium microti*
M. smeg.	*Mycobacterium smegmatis*
MDR-TB	Multidrug-resistant TB
Me	Methyl
MGCs	multinucleated Langhans giant cells
MIC_{50}	minimum inhibitory concentration inhibiting 50% of the bacterial growth
MK	Menaquinone
MKH_2	Menaquinol
MOPS	3-(*N*-morpholino)propanesulfonic acid
mp	melting point
Mtb	*Mycobacterium tuberculosis*
NAD	nicotinamide adenine dinucleotide
NADPH	Reduced nicotinamide adenine dinucleotide phosphate
NAS	nucleophilic aromatic substitution
NDH	NADH dehydrogenase
n-hex	normal hexyl
NMO	*N*-methylmorpholine *N*-oxide
NMR	nuclear magnetic resonance
n-Pr	normal propyl

OD	optical density
PanD	aspartate decarboxylase enzyme
POA	Pyrazinoic acid
PPTS	pyridinium *p*-toluenesulfonate
Py	Pyridine
PZA	Pyrazinamide
RCM	ring-closing metathesis
RIF	Rifampicin
RNA	Ribonucleic acid
rpm	round per minutes
RT	room temperature
SAR	structural activity relationship
SARS-CoV 2	severe acute respiratory syndrome Coronavirus 2
SDH	succinate dehydrogenase
SEM	standard error of the mean
TB	Tuberculosis
TBAF	tetra-*n*-butylammonium fluoride
TBS	*tert*-butyldimethylsilyl
*t*Bu	*tert*-butyl
T-cells	Thymus cells
TES	Triethylsilane
Tf	Triflate
TFA	trifluoroacetic acid
THF	Tetrahydrofuran
TLC	thin layer chromatography

TNF	Tumor Necrosis Factor alpha
UV	Ultraviolet
WHO	World Health Organization

Chapter 1

Introduction

CHAPTER 1: Introduction

1.1 Background and Epidemiology of Tuberculosis

Tuberculosis (TB) is one of the top 10 deadly diseases caused by *Mycobacterium tuberculosis* (*Mtb*).[1] In 2019, approximately 10 million active TB cases and around 1.2 million deaths were reported, equating to 1 death every 26 seconds.[1] In particular, most TB cases occurred in Southeast Asia and Africa, contributing to two-thirds of the worldwide TB cases. The eight most affected countries in these regions were India (26%), Indonesia (8.5%), China (8.4%), the Philippines (6.0%), Pakistan (5.7%), Nigeria (4.4%), Bangladesh (3.6%) and South Africa (3.6%). Another one-third was in the Western Pacific (18%), Eastern Mediterranean (8.2%), the Americas (2.9%), and Europe (2.5%).[1] Therefore, TB directly threatens human well-being in all regions of the world.

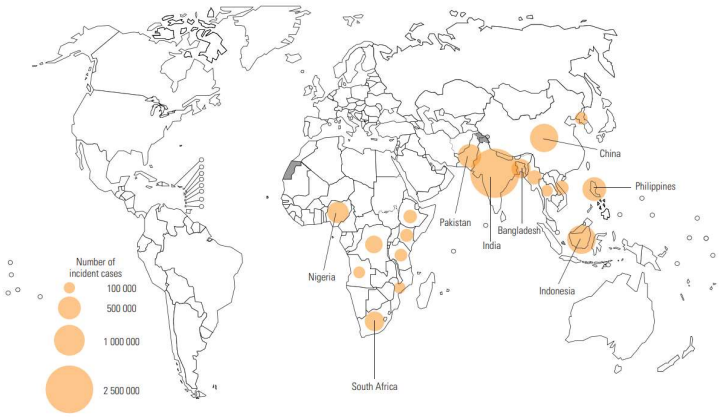

Figure 1.1 Estimated TB incidence with at least 10,000 cases in 2019.[1] Reprinted with permission from Global Tuberculosis Report 2020, Progress towards global TB targets – an overview, page 8, Copyright (2021).

Nowadays, TB is known to be a widespread disease since bacteria can be easily transmitted from one person to another through airborne transmission. When a patient excretes droplets containing *Mtb* by coughing or sneezing, each droplet will evaporate to a size of around 1 μm suspended in the air and can be inhaled into the lungs by people nearby.[2] In general, TB that targets the lungs, or pulmonary TB, commonly results in chest pains and prolonged coughs (sometimes including blood) in patients.[1] Moreover, in immunosuppressed people, *Mtb* can spread from the lungs to other organs, called extrapulmonary TB. This causes a variety of symptoms, depending on the infected organ.[3]

1.2 Pathophysiology of TB

There are four bacteria species that can cause TB: *Mycobacterium tuberculosis* (*Mtb*), *Mycobacterium bovis* (*M. bovis*), *Mycobacterium aficanum* (*M. aficanum*), and *Mycobacterium microti* (*M. microti*). However, only *Mtb* has been reported to be a causative agent for almost all causes of human TB.[4]

Mtb is an aerobic, non-spore producing, slow-growing, non-motile bacterium in the *Mycobacteriaceae* family. In general, the *Mtb* bacillus shape and size vary from short oval about 0.5 to 1 μm in length to the rod shape with a length of 2-4 μm, and long filamentous forms over 6-7 μm in length. Nevertheless, the width does not significantly differ at 0.2 – 0.5 μm.[5] The envelope of *Mycobacteria* has a unique structure, providing special properties to the organism. The outer layer of the bacterial cell wall is composed of a combination of lipid and lipoglycan, which covers a layer of mycolic acid, a long-chain fatty acid.[6] This lipophilic layer accounts for 50% of the dry cell wall weight and is not classified as a real membrane.[7] The next two inner layers, arabinogalactan, and peptidoglycan, provide rigidity and optimal osmotic stability to the bacteria. These two layers cover the phospholipid bilayer cell membrane (Figure 1.2).[6] The *Mycobacteria* envelope structure is waxy and highly lipophilic, which is more

complex than the cell walls of most bacteria, and other organisms, resulting in unique properties that enable *Mtb* to survive the immune system of the host and prevent drug penetration through its cell membrane.

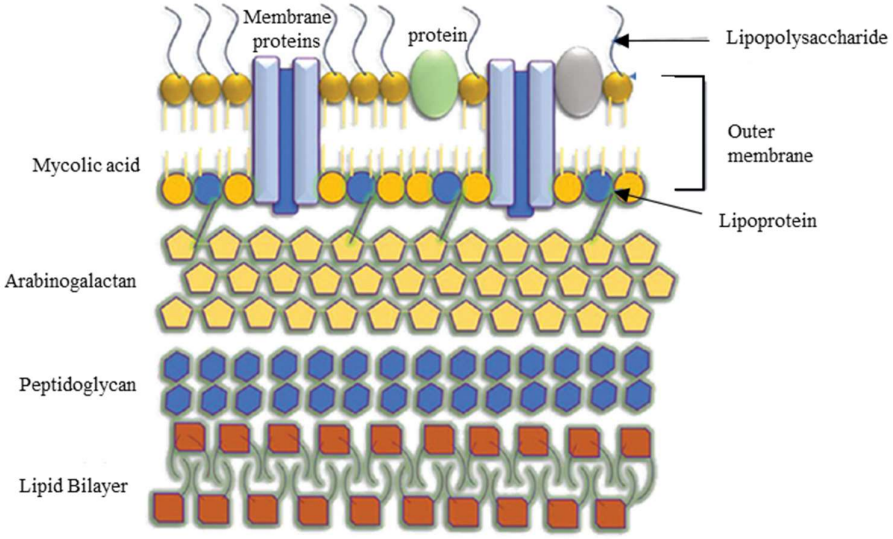

Figure 1.2 Lipid-rich *Mycobacteria* envelop structure.[7] Reprinted with permission from Ghazaei, C. *J Res Med Sci* **2018,** *23*, 63-63. Copyright © 2018 Journal of Research in Medical Sciences

Mtb infection in humans is initiated when the bacilli enter the lower respiratory tract. Alveolar macrophages then take up the bacilli as a common immune response (Scheme 1.1a). However, the bacilli can prevent lysosomal degradation by inhibiting phagosome-lysosome fusion. This defense mechanism involves sulfatide (anionic glycolipid) in the unique bacterial cell wall, which has an anti-fusion effect.[8] Moreover, phagosomal acidification by vesicular proton-adenosine triphosphatase (ATPase) is interrupted to make the environment in the phagosome less acidic.[9] In addition, reactive oxygen species from the environment are encountered by overexpressing a protein that increases the amount of cyclopropanated mycolic acid double bonds on the cell wall.[10] Therefore, the bacteria are to survive, grow, and undergo cell division inside the infected macrophage.

The infected macrophage produces and releases various chemokines and cytokines, mainly Tumor Necrosis Factor alpha (TNF) and interleukin 12 (IL-12), to recruit other immune cells such as more macrophages, dendritic cells, and lymphocytes (Thymus cells (T-cells), and bone marrow cells (B-cells)) to the infected area (Scheme 1.1b).[11] The bacilli grow and multiply in the macrophage until the host cell bursts. These multiplied bacilli infect more macrophages in the infected site.

Lymphocytes form a spherical structure with the infected macrophages in the middle to initiate granuloma formation. In this state, the macrophages can fuse to give multinucleated Langhans giant cells (MGCs) or differentiate into lipid-rich Foamy Cells (FM). B-cells are accumulated into a follicular structure beside the granuloma (Scheme 1.1c).[11] After that, necrosis occurs at the center of the granuloma to form a necrotic area (Caseum) (Scheme 1.1d).[11] However, the key factors that cause necrosis are still not fully understood. Finally, the granuloma collapses and releases *Mtb* to other parts of the lung (Scheme 1.1e).[11] Extrapulmonary TB occurs when the bacilli invade the arteries or other blood vessels.[3] Moreover, extracellular *Mtb* escaping from the granuloma can spread *via* airborne transmission to other individuals by coughing or sneezing.

Long-term infection of *Mtb* results in permanent lung impairment, even after *Mtb* infection is cured.[12-14] Currently, the factors and specific conditions that lead to post-TB lung injury remain unclear. However, it has been hypothesized that host immune responses to the pathogen may play a dominant role by triggering excessive inflammation and large expression of lung-matrix degrading proteases.[15]

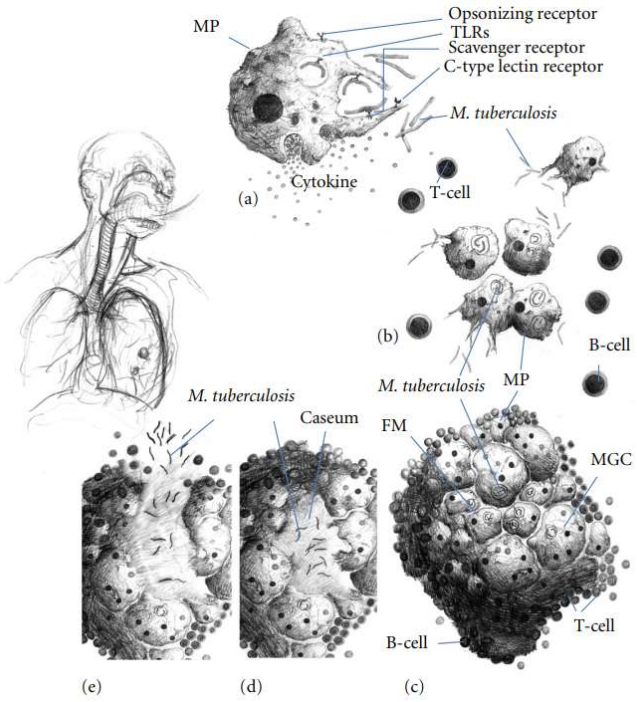

Scheme 1.1 Maturation of lung *Mtb*; macrophage phagocytosis (a), induction of immune cells (b), formation of the granuloma (c), Necrosis of the macrophage at the center of the granuloma (d), and breakdown of the granuloma (e).[11] Reprinted with permission from Silva Miranda, M. *et al. Clinical and Developmental Immunology* **2012,** *2012*, 139127.

1.2.1 Latent TB infection

Latent TB is a non-contagious and asymptomatic infection. However, there is a roughly 5-10% probability that latent TB develops into active TB (contagious and symptomatic TB) during the lifetime of the human host.[16] In 2019, an estimated 1.9 billion people (approximately 24.8% of the world population) are infected with latent TB.[17]

The mechanism of the latent infection can be described as follows. During granuloma formation (Scheme 1.1), the granuloma becomes a good shelter to prevent the elimination of *Mtb* by active immune cells. This shelter allows *Mtb* to survive in the host for decades.[18]

Although the exact factors that trigger the necrosis step remain unclear; this step is a crucial mechanism for reactivating the latent state of symptomatic TB.

Nowadays, latent TB infection is treated only in specific groups, for instance, immunosuppressed patients (mostly HIV-infected patients and immunosuppressant drug users) or high-risk people (prisoners, homeless, drug addicts, and healthcare workers in contact with TB). The latent TB treatment also depends on the resource availability of each country. For example, countries with high TB incidents or limited resources must prioritize treatment of active TB over latent TB.[19]

1.2.2 Human Immunodeficiency Virus (HIV) coinfection

HIV coinfection increases the mortality rate massively due to the patient's weakened immune system. In 2019, approximately 208,000 additional deaths resulting from 820,000 HIV-TB coinfected patients were reported by WHO.[1] Moreover, HIV is known to dramatically increase the risk of reactivating latent TB to active TB.[20]

1.3 Predicted impacts of the Coronavirus disease 2019 (COVID-19) pandemic on the TB situation

In late 2019, Coronavirus disease 2019 (COVID-19), caused by severe acute respiratory syndrome Coronavirus 2 (SARS-CoV 2), spread worldwide, creating a global pandemic. Symptoms differ from patient to patient but generally include headaches, loss of taste and smell, runny nose, cough, muscle pain, sore throat, diarrhea, fever, and breathing difficulty.[21] In some cases, the severity of the symptoms progresses to death through respiratory failure, shock, and organ dysfunction.[22]

TB-COVID-19 coinfection typically causes fever, dry cough, and shortness of breath. The mortality rate was reported to be more than 10%, which is much higher than the COVID-19 infection alone (1.1% death rate in unvaccinated patients)[23], and a higher rate in elderly

patients[24]. An *in vitro* investigation[25] revealed that the immune response to *Mtb* antigen in COVID-19 patients infected with either symptomatic or latent TB was substantially related to TB status. However, the patients had a lower immune response to SARS-CoV 2.[25]

During the COVID-19 pandemic, reported TB cases significantly decreased, especially in India (Graph 1.1).[1] One of the reasons for this was a strict social distancing policy. However, essential TB services (diagnosis and treatment) were also limited since medical facilities and services were prioritized for COVID-19.[1] Thus, the number of TB cases detected during this period did not reflect the actual number of TB infections. The actual number of TB incidents and deaths is likely much higher than reported.

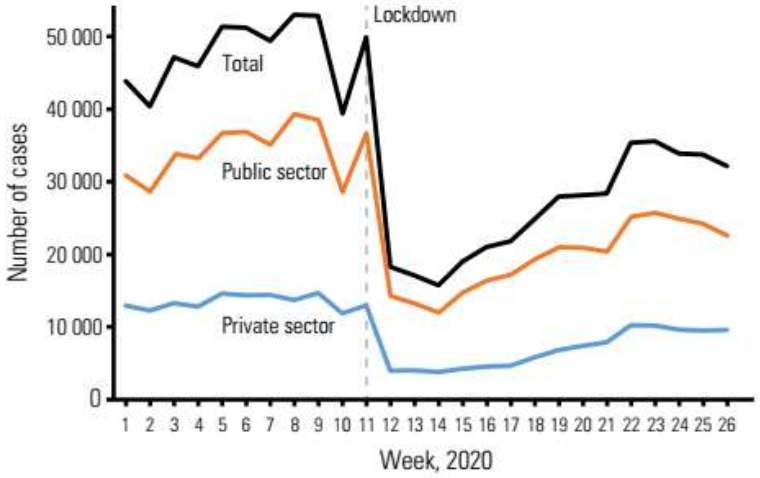

Graph 1.1 Trend of TB detection in India in 2020 under COVID-19 pandemic.[1] Reprinted from Global Tuberculosis Report 2020, The COVID-19 pandemic and TB – impact and implications, page 15, Copyright (2021).

The WHO estimated that the disruption in healthcare services and facilities for TB could lead to 1.4 million more TB deaths during the 2020 – 2025 period.[1, 26, 27] Therefore, TB cannot be ignored during the COVID-19 pandemic. The development of effective TB drugs and treatments remains crucial.

1.4 Current TB Treatments

To date, many drugs have received United States Food and Drugs Administration (FDA) approval to treat TB. The main treatment option for TB is multi-drug therapy, using a combination of several TB drugs for 6 – 9 months.[28] The types of drugs and doses in the drug combination depend on the patients' medical condition and the infecting TB strain. In general, first-line drugs are used as the first response. However, some patients are infected with first-line drug-resistant TB.[1] In such cases, more potent drugs with more severe side effects must be considered to achieve the treatment.

1.4.1 First-line TB drugs

Isoniazid (INH), rifampicin (RIF), ethambutol (EMB), and pyrazinamide (PZA) are four TB drugs that are fairly effective against TB and exhibit low-risk side effects.[28] Therefore, these drugs have been used in combination as the first response to TB, so-called first-line drugs. The structures of these drugs are shown in Figure 1.3. The treatment regimens begin with an intensive phase in which a patient is treated with all four first-line drugs for two months. The following is a continuous phase in which only INH and RIF are required for 4 to 7 months.[29]

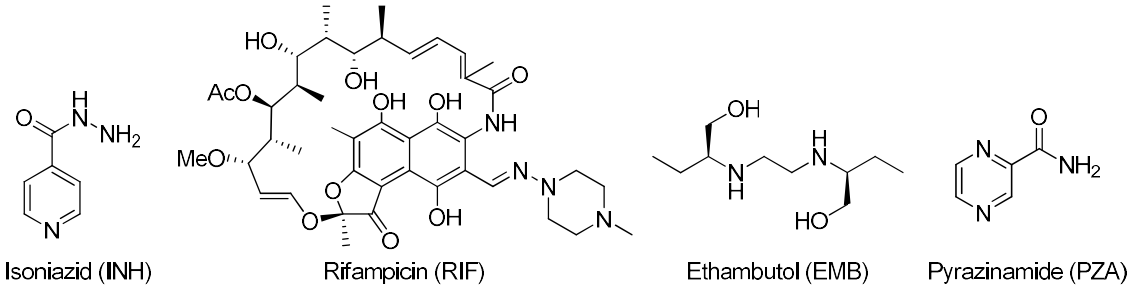

Figure 1.3 Structures of Isoniazid, Rifampicin, Ethambutol, and Pyrazinamide.

1.4.1.1 Isoniazid (INH)

Isoniazid (INH) is one of the major TB drugs which is commonly used for the entire treatment. The mechanism of action involves interfering with the synthesis of the *Mtb* cell wall component, mycolic acid. INH is a prodrug and has the following mechanism of action. First, INH is activated by the bacterial catalase-peroxidase enzyme (KatG). The activated species then reacts with nicotinamide adenine dinucleotide (NAD) (Scheme 1.2). The isonicotinic acyl-NADH inhibits mycolic acid synthesis by blocking enoyl-acyl carrier protein reductase (InhA).[30] However, this drug may cause side effects, including nausea, vomiting, and peripheral neuropathy.[31]

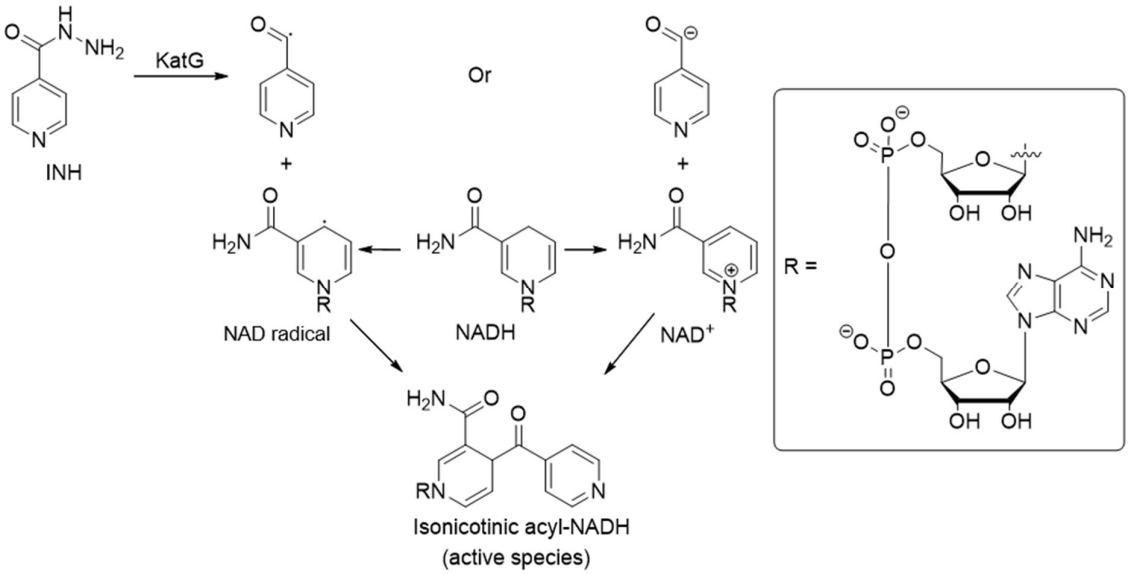

Scheme 1.2 Mechanism by INH, which generates Isonicotinic acyl-NADH

1.4.1.2 Rifampicin (RIF)

Rifampicin (RIF) is one of the major TB drugs required for both intensive and continuous phases.[29] The mechanism of action involves the interruption of RNA polymerase by inhibiting the synthesis of the second or third phosphodiester bond between RNA nucleotides.[32] This process disrupts protein synthesis in *Mtb* cells and terminates the binary fission process in the bacteria. Common side effects of RIF include nausea, vomiting, diarrhea, and loss of appetite.[31]

1.4.1.3 Ethambutol (EMB)

Ethambutol (EMB) is commonly used as a bacteriostatic agent in the treatment's first two months (intensive phase).[29] The proposed mechanism of action involves inhibition of the synthesis of a cell wall component, arabinogalactan, by blocking arabinosyl transferase.[32] There are some side effects, including vision problems, joint pain, nausea, headaches, and exhaustion.[31]

1.4.1.4 Pyrazinamide (PZA)

Pyrazinamide (PZA) is required during the intensive phase (the first eight weeks) of the treatment.[29] PZA is classified as a prodrug. Its mechanism involves the degradation of PanD, the critical enzyme for coenzyme A biosynthesis. The process begins with PZA hydrolysis to generate the active species, Pyrazinoic acid (POA). Then, POA binds with the aspartate decarboxylase enzyme (PanD). Finally, the PanD-POA complex triggers the ClpP-ClpC1 bacterial protease to digest PanD itself (Scheme 1.3).[33] Side effects include neuropathy, anorexia, nausea, vomiting, and skin hypersensitivity.[31]

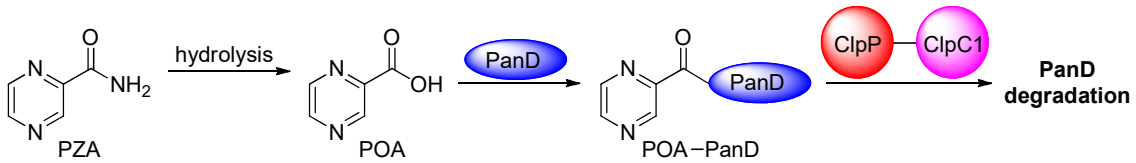

Scheme 1.3 Mechanism of action for PZA

1.4.2 Problems with the current TB treatments

Recent findings highlight three main problems in current TB treatment strategies. First, HIV-positive patients are reported to have a higher chance of being coinfected by *Mtb*. Treatment needs to be adjusted as HIV drugs are incompatible with TB drugs, resulting in less effective treatment than the standard TB treatment.[34] Second, the long-term nature of the TB treatment (at least 6–9 months) reduces patients' compliance with the doctor's prescription. Commonly, patients may feel better within a few weeks after starting the therapy and tend to avoid their remaining treatments.[35] Third, incomplete treatment can also allow *Mtb* to mutate to become drug-resistant *Mtb*. This mutation can accelerate its spread.[35]

1.4.3 Second-line TB drugs

In some cases, TB may mutate to resist more than one anti-TB drug. TB may be resistant to at least one of the main first-line drugs (INH and RIF) and is called Multidrug-resistant TB (MDR-TB).[1] In such situations, the first-line drugs are not an effective strategy. More potent drugs with higher-risk side effects, called second-line TB drugs, are required to overcome MDR-TB. Nowadays, there are many approved second-line TB drugs to treat MDR-TB, for instance, Fluoroquinolones (Levofloxacin and Moxifloxacin), Linezolid, Pretomanid, Delamanid, and Bedaquiline.

1.4.3.1 Fluoroquinolones

Fluoroquinolones are a family of antibacterial agents that are effective against Gram-positive and Gram-negative bacteria, as well as Mycobacteria.[36] These compounds are generally used for the treatment of bacterial infections in the respiratory, urinary, and gastrointestinal tracts, as well as sexually transmitted infections and osteomyelitis.[37] Fluoroquinolones are some of the most valuable second-line TB drugs since they show interesting *in vivo* and *in vitro* activities against *Mtb.*[38, 39]

The mechanism of action of compounds in this class involves inhibition of the bacterial DNA gyrase and topoisomerase IV.[40] Since DNA gyrase is involved in supercoiling DNA, and the topoisomerase IV is responsible for DNA strand separation during DNA replication, inhibition of both enzymes leads to incomplete bacterial cell division, which eventually kills the bacteria. Herein, two of the most potent Fluoroquinolones on the WHO model list of essential medicines, Levofloxacin and Moxifloxacin,[41] are discussed. The structures of both drugs are shown in Figure 1.4.

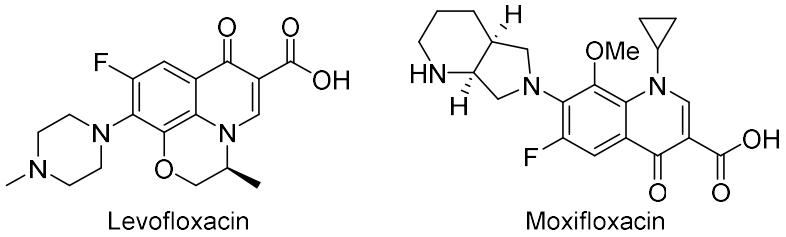

Figure 1.4 Structures of Levofloxacin and Moxifloxacin

1.4.3.1.1 Levofloxacin

Levofloxacin is currently in a phase IV clinical trial to treat pulmonary and meningitis TB[42] and a phase II clinical trial for MDR-TB. This compound is recommended for use in a drug regimen for treating isoniazid-resistant TB.[1] Common side effects include nausea, diarrhea, and insomnia. In some patients, rare severe side effects, such as tendon rupture, tendon inflammation, seizures, psychosis, and permanent peripheral nerve damage, have been reported.[43]

1.4.3.1.2 Moxifloxacin

Moxifloxacin is currently undergoing phase III clinical development for treating TB,[42] and is one of the preferred component drugs for an intensive phase treatment of MDR-TB for the first four months.[44] This compound is also under a component in a longer drug regime for the treatment of MDR-TB and rifampicin-resistant TB.[1]

However, common side effects of Moxifloxacin include diarrhea, dizziness, and headaches. There are rarely observed severe side effects, such as tendon ruptures, nerve damage, and myasthenia gravis.[45]

1.4.3.2 Linezolid

Linezolid (Figure 1.5) is one of the priority compounds in the class of second-line TB drugs to treat rifampicin-resistant TB and MDR-TB. This compound is also on the WHO model list of essential medicines.[41] Its mechanism involves the binding to the bacterial 23S ribosomal RNA component of the 50S subunit, leading to the inhibition of the initiation step of the protein synthesis process, thus, disrupting protein synthesis.[46]

Linezolid is safer than other antibiotic agents as long as it is used over a short period. Common side effects of short-term use include headaches, diarrhea, and nausea.[47] However, side effects are reported to be more severe with long-term use of over two weeks. More severe symptoms are observed, such as serotonin syndrome, bone marrow suppression, high blood lactate levels,[48] and nerve damage.[49]

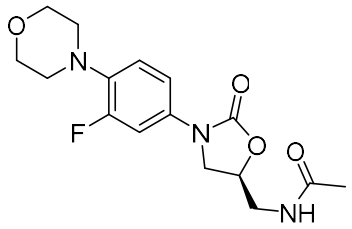

Figure 1.5 Structure of Linezolid

1.4.3.3 Pretomanid

Pretomanid (Figure 1.6) is a drug currently undergoing a phase III clinical trial to treat MDR-TB. It is approved only when used with Linezolid and Bedaquiline (details as shown in 1.4.3.5) by the FDA.[1] Its mechanism of action remains unclear.[50] However, it is believed to involve mycolic acid synthesis inhibition.[51] Common side effects include nerve damage, vomiting, headaches, hypoglycemia, diarrhea, and liver inflammation.[52]

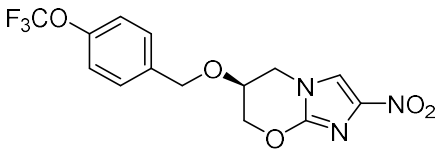

Figure 1.6 Structure of Pretomanid

1.4.3.4 Delamanid

Delamanid (Figure 1.7) is currently undergoing phase III clinical development.[1] This drug is included in a longer drug regime to treat rifampicin-resistant TB and MDR-TB.[1] It is approved for MDR-TB treatment by the European Medicines Agency (EMA) in 2014.[53] Even though this molecule is effective in curing TB, there are some side effects. Common side effects include headaches, dizziness, and nausea. One serious side effect is QT prolongation, which may lead to cardiac arrest.[54]

Delamanid is a prodrug whose entire mechanism of action is not fully understood. The generation of the active species is believed to involve the mycobacterial F420 system, including the nitroreductase Rv3547.[55] The active species then inhibits the mycolic acid synthesis, resulting in the disruption of bacterial cell wall synthesis.[56]

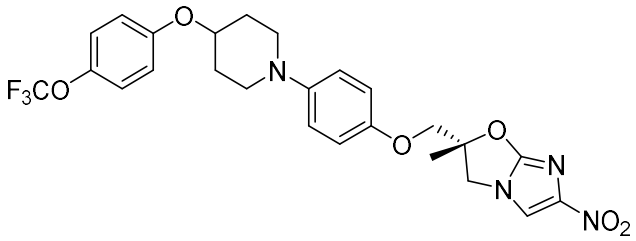

Figure 1.7 Structures of Delamanid

1.4.3.5 Bedaquiline

Bedaquiline (BDQ, Figure 1.8a), approved by the FDA in 2012,[57] is also undergoing the second stage of phase III clinical development to treat MDR-TB.[1] BDQ was reported to bind with the F-ATP synthase of *Mycobacterium* species. This limits the amount of intracellular ATP, eventually killing the bacteria.[58, 59] There are currently two widely accepted mechanisms of action: interrupting the rotation of the *c*-ring by binding with one of the *c*-ring subunits (Figure 1.8b),[58] or binding with the ε subunit, resulting in miscommunication between the *c*-ring and other subunits.[59] (The details of F-ATP synthase are discussed in Section 1.6.)

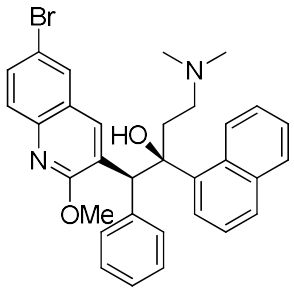

a

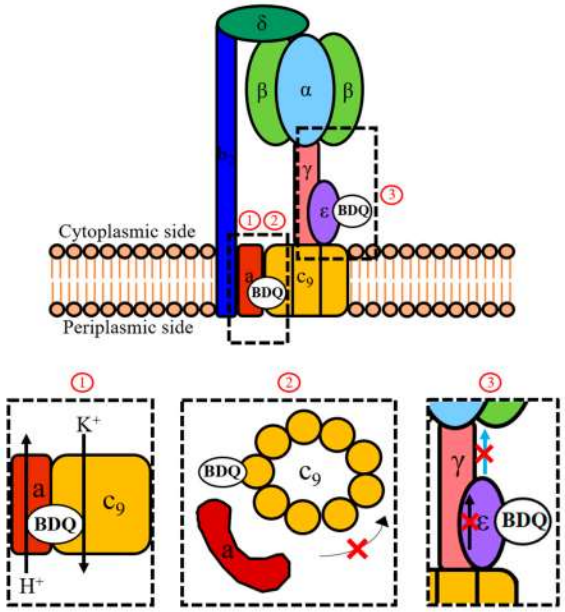

b

Figure 1.8 Structure of BDQ (a) and two mechanisms of action of BDQ to inhibit the F-ATP synthase of *Mycobacterium* species[58] (b) Reprinted with permission from Sarathy, J. P. *et al. Antibiotics (Basel)* **2019,** *8* (4), 261. Copyright © 2019 by Sarathy, J. P. *et al.*

BDQ exhibits excellent efficiency against both general *Mtb* and MDR-TB strains,[60] but it causes side effects such as coughing, fever, and headaches. Other serious side effects include arrhythmia, which may cause BDQ treatment to be lethal. The clinical treatment of BDQ to MDR-TB showed a favorable success rate of 65.8%.[61] However, an 11.7% mortality rate by the BDQ's side effects was also observed.[61]

The side effects of BDQ are a result of its ionophore property. BDQ can insert into the cell membrane and transfer H^+ and K^+ ions between the inner membrane space and the cell matrix, leading to equilibration of the transmembrane pH and K^+ gradient. This process interferes with the cardiac K^+ channel, resulting in arrhythmia.[62] Moreover, it can also unspecifically inhibit cellular ATP synthesis without affecting the respiratory chain and ATP synthase by disconnecting the electron transport from phosphorylation reactions, called the uncoupler effect,[63] leading to human cell death.

1.4.4 Drug regimen strategy to overcome multi-drug resistant TB (MDR-TB)

Currently, the main strategy for treating MDR-TB is to use a second-line drug. However, most of these drugs can induce severe side effects that may lead to patients' deaths. One strategy to improve the efficacy of the medicines while decreasing their side effects is to use a combination of drugs that are synergistic with each other.

Recently, the drug combination named SimpliciTB, which contains BDQ as the main compound along with Pretomanid, Moxifloxacin, and Pyrazinamide was developed to treat drug-sensitive TB and MDR-TB.[1] This drug cocktail is currently in phase III clinical trial, and the results to date show that the treatment exhibits a very high success rate of about 90% for both drug-sensitive TB and drug-resistant TB within six months.[64] Through the synergistic effects of the combined drugs, the amount of BDQ can be decreased to make use of its therapeutic effect while avoiding its severe side effects. Analysis of the results shows that

patients' deaths were not related to the drug effects, but there were some instances of liver toxicity arising from the drug cocktail.[65]

Although using BDQ in the drug combination increased the success rate and decreased the side effects, some severe side effects were still reported. Therefore, developing new TB drugs with milder side effects is of great importance in curing MDR-TB. From the high success rate of BDQ, the inhibition of ATP synthase on the electron transport chain appears to be a promising target for the next generation of TB drugs.

1.5 Mycobacterial ATP synthesis by Electron Transport Chain and ATP synthase

The mycobacterial electron transport chain (ETC) is a series of enzymes embedded in the cell membrane involving NADH dehydrogenase (NDH), succinate dehydrogenase (SDH), NADH dehydrogenase (NDH), and succinate dehydrogenase (SDH) that create an electrochemical gradient to produce the majority of the cell's ATP energy source by ATP synthase.[66] In mycobacteria, the process begins with the conversion of menaquinone (MK) to menaquinol (MKH_2) by NADH dehydrogenase (NDH) and succinate dehydrogenase (SDH). The subsequent MKH_2 is passed through two electron-accepting complexes – Cytochrome bc complex and Cytochrome bd oxidase – leading to the reduction of O_2 to water. This redox process allows NDH and electron-accepting complexes to pump H^+ from the intercellular space to the extracellular matrix against the H^+ gradient. Finally, energy in the form of the electrochemical H^+ gradient is converted to ATP by ATP synthase (Figure 1.9).[66]

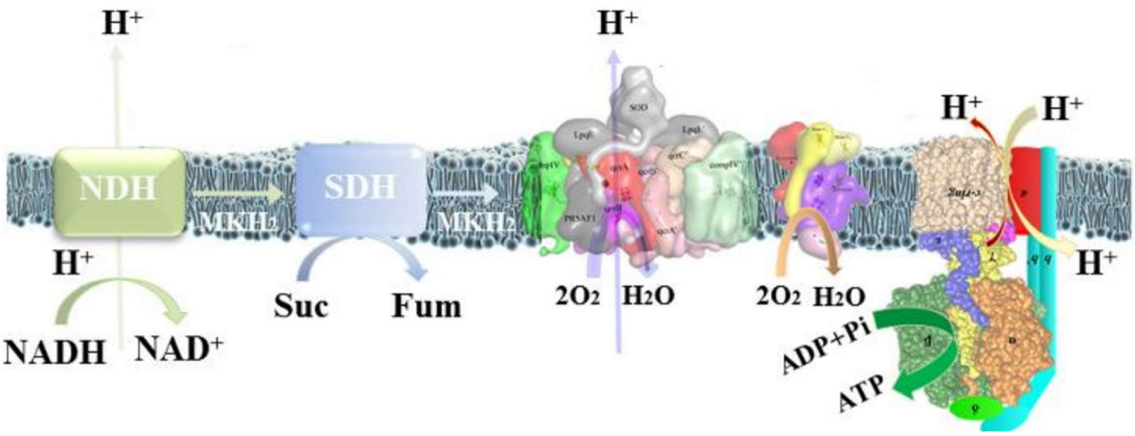

Figure 1.9 Mycobacterial electron transport chain and ATP synthase[67] Reprinted with permission from Hotra, A. *et al.* Angew. Chem. Int. Ed. **2020,** *59*, 2-12. Copyright 2021 Angewandte Chemie International Edition.

Recently, there has been great interest in targeting the electron transport chain and ATP synthase for *Mtb* drug development. For instance, NDH is the drug target for clofazimine,[68] a *Mtb* drug currently undergoing a phase III clinical trial.[69] Another example is Telacebec (Q203), a drug in phase II clinical development that interferes with the Cytochrome *bcc* complex.[70] In addition, one of the most potent MDR-TB drugs, BDQ, also disrupts the mycobacterial ATP synthasis by inhibiting ATP synthase activity.[58, 59] Based on the effectiveness of BDQ in treating MDR-TB, the F-ATP synthase has proven to be a promising *Mtb* drug target. Hence, developing ATP synthase inhibitors is of great importance in creating the next generation of *Mtb* drugs.

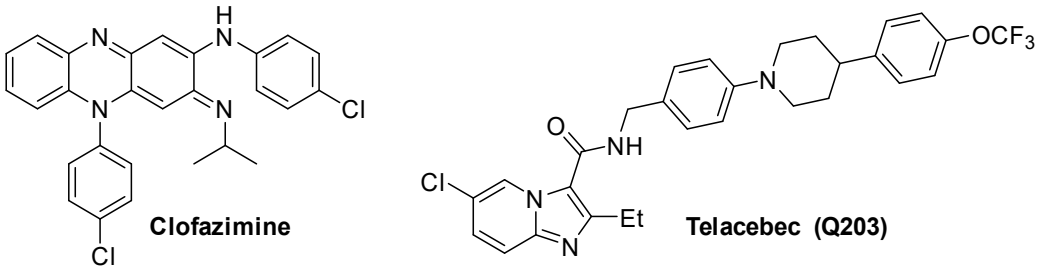

Figure 1.10 Structures of Clofazimine and Telacebed (Q203)

1.6 F_1F_0 ATP synthase

F_1F_0 ATP synthase is a protein on the *Mtb* cell membrane that acts as an enzyme for ATP synthesis and hydrolysis in the electron transport chain. The structure of the enzyme can be divided into two parts designated F_0 and F_1, as illustrated in Figure 1.11. The F_0 part is located in the cell membrane and consists of the *a*, *b*, *b'*, and *c*-ring subunits ($a : b_2 : c_9$). The F_1 part is placed in the intracellular space, and it comprises the α, β, γ, δ, and ε subunits ($\alpha_3 : \beta_3 : \gamma : \delta : \varepsilon$). The core structure of this enzyme is a stalk formed by the γ and ε subunits that link the $\alpha_3\beta_3$ hexamer complex and the *c*-ring subunit. The δ subunit is located at the top of the hexamer complex and interacts with the *b* subunits, which are also connected to the *a* subunit (Figure 1.11). The *c*-ring contacts the *a* subunit to allow the two-half channel system to maintain the coupling of ATP synthase to the transmembrane proton motive force. Protons can enter the inlet channel from the *a* subunit, pass through the *c*-ring, and escape through the *a* subunit outlet channel. This process initiates the *c*-ring rotation from the transmembrane proton gradient,[71] causing conformational changes through the γ, and ε subunits, which connect to the $\alpha_3\beta_3$ hexamer complex to trigger ATP synthesis and hydrolysis at the hexamer complex.[72]

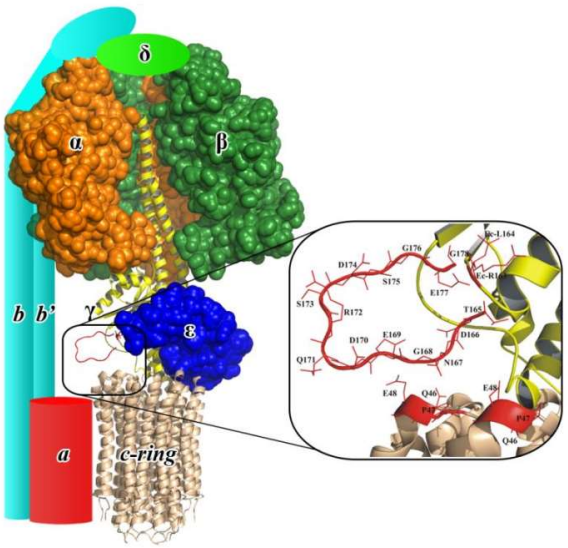

Figure 1.11 Overall structure of *Mtb* F-ATP synthase.[73] Subunits α (orange) and β (green) form the hexamer complex. In this figure, one α and β subunits were removed to reveal the subunit γ (yellow). The regulatory ε subunit is shown in blue. The unique mycobacterial γ-loop is shown in the expansion (red loop) in the vicinity of the *c*-ring loop residues Q46 to E48 of *M. phlei*. The subunits *a*, *b*, *b'*, and δ are shown as cartoon figures and colored in red, light blue, and light green, respectively. Reprinted with permission from Hotra, A. *et al.* FEBS J. **2016,** *283* (10), 1947-1961. Copyright 2021 FEBS J.

The *Mtb* F-ATP synthase has unique features that distinguish it from human and other bacterial enzymes. First, the C-terminal domain of the ε subunit (α-helix) of *Mtb* has a shorter amino acid sequence than in other bacteria. (The ε subunit consists of an β-barrel at the N-terminal domain and two α-helices at the C-terminal. The C-terminal helical domain interacts with the β subunit of the hexamer complex.)[59] The C-terminal domain of the α subunit is also longer than in other species. The *Mtb* δ subunit is fused to the b subunit, while the shorter b' subunit is missing the C-terminal part usually present in other species.[74] Lastly, the *Mycobacterium* γ subunit contains a 13 amino acid loop.[73] These unique features suggest that

it is possible to develop a drug that specifically targets *Mtb* F-ATP synthase without affecting ATP synthase in humans and other bacteria.

1.7 Drug discovery and development

The discovery of novel drugs is a complicated process. After the target is validated, compounds that bind to the target have to be then identified and screened by suitable biological assays to get hit or lead compounds. The structural activity relationship (SAR) of the selected potent compounds has to be investigated so that the potency, target specificity, stability, and drug-likeness can be optimized. Subsequently, the developed compounds from SAR are animal tested, after which the successful compounds are chosen for clinical trials.[75]

High-throughput screening (HTS) is a useful method to identify hit or lead compounds by screening a large number of chemical substrates against a biological target (commonly more than 10,000 to 1,000,000 studied substrates). Even though HTS is an effective approach to find hits or leads to be the starting point for further drug development, it is a costly technique as a massive number of compounds must be tested.[76]

In silico screening is a computational approach for screening possible drug candidates, which is widely used in drug discovery.[77] As long as detailed structural knowledge of the targeted enzyme is adequate, this approach can be applied to lessen the burden of experimental work by providing guidance to drug development, resulting in more efficient discovery and lower costs.[77]

Recently, *Mtb* F-ATP synthase at γ and ε subunits, for which the protein structures and amino acid sequences are different from human and other bacterial enzymes (discussed in 1.6), were investigated using *in silico* screening to discover GaMF1 (targeting mycobacterial γ subunit)[78] and EGCG (targeting mycobacterial ε subunit)[79]. Both GaMF1 and EGCG show promising mycobacterial ATP synthesis inhibition properties with minimum inhibitory

concentrations at the micromolar and nanomolar levels, respectively (Figure 1.12). However, although GaMF1 has an interesting bacterial growth inhibition property against *M. smeg.* and *Mtb* in micromolar, its water solubility is limited, restricting future research on this species.[78] EGCG is unable to inhibit mycobacterial growth.[79]

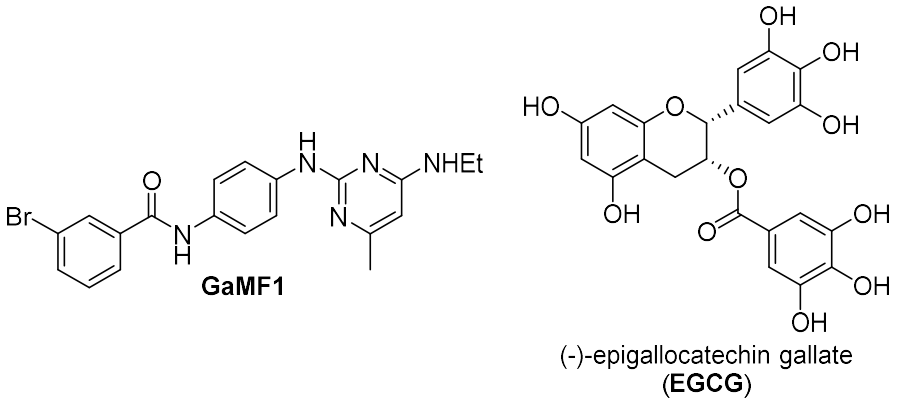

Figure 1.12 Structure of **GaMF1** and epigallocatechin gallate (**EGCG**)

Hence, in this work, SAR investigations of GaMF1 and EGCG were performed to understand the relationship between the chemical structures and ATP synthesis inhibition activities; consequently, more potent compounds can be discovered. It is hoped that, from the SAR results, the GaMF1 water solubility problem could be solved, and the lack of mycobacterial growth inhibition of EGCG could be resolved.

1.8 References

1. Geneva: *World Health Organization, Global tuberculosis report 2020*; 2020.

2. Council of the Infectious Disease Society of America, September 1999. *Am. J. Respir. Crit. Care. Med.* **2000,** *161* (4 Pt 1), 1376-95.

3. Ramírez-Lapausa, M.; Menéndez-Saldaña, A.; Noguerado-Asensio, A. *Rev. Esp. Sanid. Penit.* **2015,** *17* (1), 3-11.

4. Talbot, E. A.; Raffa, B. J.; Tang, Y.-W.; Sussman, M.; Liu, D.; Poxton, I.; Schwartzman, J. Eds. Academic Press: Boston, 2015; pp 1637-1653.

5. Ufimtseva, E.; Eremeeva, N.; Vakhrusheva, D.; Skornyakov, S. *Eur. Respir. J.* **2019,** *54* (suppl 63), PA4605.

6. Vincent, A. T.; Nyongesa, S.; Morneau, I.; Reed, M. B.; Tocheva, E. I.; Veyrier, F. J. *Front. Microbiol.* **2018,** *9* (2341).

7. Ghazaei, C. *J. Res. Med. Sci.* **2018,** *23*, 63-63.

8. Armstrong , J. A.; Hart , P. D. A. *J. Exp. Med.* **1971,** *134* (3), 713-740.

9. Sturgill-Koszycki, S.; Schlesinger, P.; Chakraborty, P.; Haddix, P.; Collins, H.; Fok, A.; Allen, R.; Gluck, S.; Heuser, J.; Russell, D. *Science* **1994,** *263* (5147), 678-681.

10. Rajni, L. S. M. *FEBS J.* **2010,** *277*, 2416–2427

11. Silva Miranda, M.; Breiman, A.; Allain, S.; Deknuydt, F.; Altare, F. *Clin. Exp. Immunol.* **2012,** *2012*, 139127.

12. Plit, M.; Anderson, R.; Van Rensburg, C.; Page-Shipp, L.; Blott, J.; Fresen, J.; Feldman, C. *Eur. Respir. J.* **1998,** *12* (2), 351-356.

13. Maguire, G. P.; Anstey, N. M.; Ardian, M.; Waramori, G.; Tjitra, E.; Kenangalem, E.; Handojo, T.; Kelly, P. M. *Int. J. Tuberc. Lung. Dis.* **2009,** *13* (12), 1500-6.

14. Ralph, A. P.; Kenangalem, E.; Waramori, G.; Pontororing, G. J.; Sandjaja; Tjitra, E.; Maguire, G. P.; Kelly, P. M.; Anstey, N. M. *PLoS One.* **2013,** *8* (11), e80302.

15. Ravimohan, S.; Kornfeld, H.; Weissman, D.; Bisson, G. P. *Eur. Respir. Rev.* **2018,** *27* (147), 170077.

16. Comstock, G. W.; Livesay, V. T.; Woolpert, S. F. *Am. J. Epidemiol.* **1974,** *99* (2), 131-138.

17. Cohen, A.; Mathiasen, V. D.; Schön, T.; Wejse, C. *Eur. Respir. J.* **2019,** *54* (3), 1900655.

18. Ulrichs, T.; Kosmiadi, G. A.; Jörg, S.; Pradl, L.; Titukhina, M.; Mishenko, V.; Gushina, N.; Kaufmann, S. H. E. *J. Infect. Dis.* **2005,** *192* (1), 89-97.

19. Geneva:, *World Health Organization, Guidelines on the Management of Latent Tuberculosis Infection*. 2015.

20. Selwyn, P. A.; Hartel, D.; Lewis, V. A.; Schoenbaum, E. E.; Vermund, S. H.; Klein, R. S.; Walker, A. T.; Friedland, G. H. *N. Engl. J. Med.* **1989,** *320* (9), 545-550.

21. U.S. Centers for Disease Control and Prevention (CDC), Symptoms of COVID-19. 2021.

22. U.S. Centers for Disease Control and Prevention (CDC), Interim Clinical Guidance for Management of Patients with Confirmed Coronavirus Disease (COVID-19). 2021.

23. Stanley, X.; Runxin, H.; Lina, S. S.; Sungching, C. G.; Denison, S. R.; Kerresa, M.; David, K. S.; Gabriela, V.-B.; Jason, M. G.; Nicola, P. K.; David, M.; Elizabeth, G. L.; Eric, S. W.; Hung-Fu, T.; Lei, Q. *COVID-19 Vaccination and Non–COVID-19 Mortality Risk —Seven Integrated Health Care Organizations, United States, December 14, 2020–July 31, 2021*; 2021; pp 1521-1524.

24. Mishra, A.; George, A. A.; Sahu, K. K.; Lal, A.; Abraham, G. *Acta. Biomed.* **2020,** *92* (1), e2021025.

25. Petrone, L.; Petruccioli, E.; Vanini, V.; Cuzzi, G.; Gualano, G.; Vittozzi, P.; Nicastri, E.; Maffongelli, G.; Grifoni, A.; Sette, A.; Ippolito, G.; Migliori, G. B.; Palmieri, F.; Goletti, D. *Int. J. Infect. Dis.* **2020**.

26. Glaziou, P. *medRxiv* **2020**, 2020.04.28.20079582.

27. *Stop TB Partnership, The potential impact of the COVID-19 response on tuberculosis in high-burden countries: a modelling analysis*; 2020.

28. Curry, F. J., *Drug-resistant tuberculosis: a survival guide for clinicians*. 2nd ed.; National Tuberculosis Center, California Department of Health Service. San Francisco, CA, 2011.

29. Nahid, P.; Dorman, S. E.; Alipanah, N.; Barry, P. M.; Brozek, J. L.; Cattamanchi, A.; Chaisson, L. H.; Chaisson, R. E.; Daley, C. L.; Grzemska, M.; Higashi, J. M.; Ho, C. S.; Hopewell, P. C.; Keshavjee, S. A.; Lienhardt, C.; Menzies, R.; Merrifield, C.; Narita, M.; O'Brien, R.; Peloquin, C. A.; Raftery, A.; Saukkonen, J.; Schaaf, H. S.; Sotgiu, G.; Starke, J. R.; Migliori, G. B.; Vernon, A. *Clin. Infect. Dis.* **2016,** *63* (7), e147-e195.

30. Rozwarski, D. A.; Grant, G. A.; Barton, D. H.; Jacobs, W. R., Jr.; Sacchettini, J. C. *Science* **1998,** *279* (5347), 98-102.

31. Derek G.; Waller, A. S., *Medical Pharmacology and Therapeutics*. 5th ed.; Elsevier Health Sciences: London, United Kingdom, 2017.

32. Farrell, D. J.; Putnam, S. D.; Biedenbach, D. J.; Moro, L.; Bozzella, R.; Celasco, G.; Jones, R. N. *Antimicrob. Agents Chemother.* **2011,** *55* (3), 992-996.

33. Gopal, P.; Sarathy, J. P.; Yee, M.; Ragunathan, P.; Shin, J.; Bhushan, S.; Zhu, J.; Akopian, T.; Kandror, O.; Lim, T. K.; Gengenbacher, M.; Lin, Q.; Rubin, E. J.; Grüber, G.; Dick, T. *Nat. Commun.* **2020,** *11* (1), 1661.

34. Blumberg, H. M.; Leonard, M. K.; Jasmer, R. M. *JAMA.* **2005,** *293* (22), 2776-2784.

35. U.S. Centers for Disease Control and Prevention (CDC), *Questions and Answers About Tuberculosis*. USA., 2014.

36. Ball, P. *J. Antimicrob. Chemother.* **2000,** *46* (suppl_3), 17-24.

37. Feng, L.-S.; Liu, M.-L.; Wang, B.; Chai, Y.; Hao, X.-Q.; Meng, S.; Guo, H.-Y. *Eur. J. Med. Chem.* **2010,** *45* (8), 3407-3412.

38. Wang, J. Y.; Hsueh, P. R.; Jan, I. S.; Lee, L. N.; Liaw, Y. S.; Yang, P. C.; Luh, K. T. *Thorax* **2006,** *61* (10), 903-8.

39. Bartlett, J. G.; Dowell, S. F.; Mandell, L. A.; File, T. M., Jr.; Musher, D. M.; Fine, M. J. *Clin. Infect. Dis.* **2000,** *31* (2), 347-382.

40. Drlica, K.; Zhao, X. *Microbiol. Mol. Biol. Rev.* **1997,** *61* (3), 377-392.

41. Geneva: *World Health Organization, model list of essential medicines: 21st list 2019*; World Health Organization: Geneva, 2019, 2019.

42. Pranger, A. D.; van der Werf, T. S.; Kosterink, J. G. W.; Alffenaar, J. W. C. *Drugs* **2019,** *79* (2), 161-171.

43. Kahn, J. B. *Chemotherapy* **2001,** *47* (Suppl. 3), 32-37.

44. Falzon, D.; Schünemann, H. J.; Harausz, E.; González-Angulo, L.; Lienhardt, C.; Jaramillo, E.; Weyer, K. *Eur. Respir. J.* **2017,** *49* (3), 2003300.

45. Iannini, P. B.; Kubin, R.; Reiter, C.; Tillotson, G. *Clin. Infect. Dis.* **2001,** *32* (7), 1112-4.

46. Swaney, S. M.; Aoki, H.; Ganoza, M. C.; Shinabarger, D. L. *Antimicrob. Agents Chemother.* **1998,** *42* (12), 3251-3255.

47. Gerson, S. L.; Kaplan, S. L.; Bruss, J. B.; Le, V.; Arellano, F. M.; Hafkin, B.; Kuter, D. J. *Antimicrob. Agents Chemother.* **2002,** *46* (8), 2723-2726.

48. Morales-Molina, J. A.; Antonio, J. M.-d.; Marín-Casino, M.; Grau, S. *J. Antimicrob. Chemother.* **2005,** *56* (6), 1176-1178.

49. Lee, E.; Burger, S.; Shah, J.; Melton, C.; Mullen, M.; Warren, F.; Press, R. *Clin. Infect. Dis.* **2003,** *37* (10), 1389-91.

50. Baptista, R.; Fazakerley, D. M.; Beckmann, M.; Baillie, L.; Mur, L. A. J. *Sci. Rep.* **2018,** *8* (1), 5084.

51. Manjunatha, U.; Boshoff, H. I.; Barry, C. E. *Commun. Integr. Biol.* **2009,** *2* (3), 215-218.

52. Diacon, A. H.; Dawson, R.; von Groote-Bidlingmaier, F.; Symons, G.; Venter, A.; Donald, P. R.; van Niekerk, C.; Everitt, D.; Winter, H.; Becker, P.; Mendel, C. M.; Spigelman, M. K. *Lancet* **2012,** *380* (9846), 986-993.

53. Ryan, N. J.; Lo, J. H. *Drugs* **2014,** *74* (9), 1041-5.

54. Geneva:, *World Health Organization, The selection and use of essential medicines. Twentieth report of the WHO Expert Committee 2015 (including 19th WHO Model List of Essential Medicines and 5th WHO Model List of Essential Medicines for Children)*. World Health Organization: Geneva, 2015.

55. Stover, C. K.; Warrener, P.; VanDevanter, D. R.; Sherman, D. R.; Arain, T. M.; Langhorne, M. H.; Anderson, S. W.; Towell, J. A.; Yuan, Y.; McMurray, D. N.; Kreiswirth, B. N.; Barry, C. E.; Baker, W. R. *Nature* **2000,** *405* (6789), 962-6.

56. Blair, H. A.; Scott, L. J. *Drugs* **2015,** *75* (1), 91-100.

57. Mahajan, R. *Int. J. Appl. Basic. Med. Res.* **2013,** *3* (1), 1-2.

58. Sarathy, J. P.; Gruber, G.; Dick, T. *Antibiotics (Basel)* **2019,** *8* (4), 261.

59. Joon, S.; Ragunathan, P.; Sundararaman, L.; Nartey, W.; Kundu, S.; Manimekalai, M. S. S.; Bogdanović, N.; Dick, T.; Grüber, G. *FEBS J.* **2018,** *285* (6), 1111-1128.

60. Field, S. K. *Ther. Adv. Chronic. Dis.* **2015,** *6* (4), 170-184.

61. Mbuagbaw, L.; Guglielmetti, L.; Hewison, C.; Bakare, N.; Bastard, M.; Caumes, E.; Fréchet-Jachym, M.; Robert, J.; Veziris, N.; Khachatryan, N.; Kotrikadze, T.;

Hayrapetyan, A.; Avaliani, Z.; Schünemann, H. J.; Lienhardt, C. *Emerg. Infect. Dis.* **2019,** *25* (5), 936-943.

62. Giraud-Gatineau, A.; Coya, J. M.; Maure, A.; Biton, A.; Thomson, M.; Bernard, E. M.; Marrec, J.; Gutierrez, M. G.; Larrouy-Maumus, G.; Brosch, R.; Gicquel, B.; Tailleux, L. *Elife* **2020,** *9*, e55692.

63. Hards, K.; McMillan, D. G. G.; Schurig-Briccio, L. A.; Gennis, R. B.; Lill, H.; Bald, D.; Cook, G. M. *PNAS.* **2018,** *115* (28), 7326-7331.

64. Kendall, E. A.; Malhotra, S.; Cook-Scalise, S.; Denkinger, C. M.; Dowdy, D. W. *BMC Infect. Dis.* **2019,** *19* (1), 794.

65. Haraka, F.; Tweed, C.; Dawson, R.; Conradie, A.; Crook, A.; Mendel, C.; Conradie, F.; Diacon, A.; Ntinginya, N.; Everitt, D.; Haraka, F.; Li, M.; van Niekerk, C.; Okwera, A.; Rassool, M.; Reither, K.; Sebe, M.; Staples, S.; Variava, E.; Spigelman, M., Bedaquiline, moxifloxacin, pretomanid, and pyrazinamide during the first 8 weeks of treatment of patients with drug-susceptible or drug-resistant pulmonary tuberculosis: a multicentre, open-label, partially randomised, phase 2b trial. **2019**, 1048-58.

66. Black, P.; Warren, R.; Louw, G.; Helden, P.; Victor, T.; Kana, B. *Antimicrob. Agents Chemother.* **2014,** *58*.

67. Hotra, A.; Priya, R.; Ng, P.; Seankongsuk, P.; Harikishore, A.; Sarathy, J.; Geok, S.; Lakshmanan, U.; Sae-Lao, P.; Kalia, N.; Shin, J.; Kalyanasundaram, R.; Anbarasu, S.; Parthasarathy, K.; Pradeep, C.; Makhija, H.; Dröge, P.; Poulsen, A.; Tan, J.; Grüber, G. *Angew. Chem. Int. Ed.* **2020,** *59*, 2-12.

68. Yano, T.; Kassovska-Bratinova, S.; Teh, J. S.; Winkler, J.; Sullivan, K.; Isaacs, A.; Schechter, N. M.; Rubin, H. *J. Biol. Chem.* **2011,** *286* (12), 10276-10287.

69. Vjecha, M. J.; Tiberi, S.; Zumla, A. *Nat. Rev. Drug Discov.* **2018,** *17* (9), 607-608.

70. Pethe, K.; Bifani, P.; Jang, J.; Kang, S.; Park, S.; Ahn, S.; Jiricek, J.; Jung, J.; Jeon, H. K.; Cechetto, J.; Christophe, T.; Lee, H.; Kempf, M.; Jackson, M.; Lenaerts, A. J.; Pham, H.; Jones, V.; Seo, M. J.; Kim, Y. M.; Seo, M.; Seo, J. J.; Park, D.; Ko, Y.; Choi, I.; Kim, R.; Kim, S. Y.; Lim, S.; Yim, S.-A.; Nam, J.; Kang, H.; Kwon, H.; Oh, C.-T.; Cho, Y.; Jang, Y.; Kim, J.; Chua, A.; Tan, B. H.; Nanjundappa, M. B.; Rao, S. P. S.; Barnes, W. S.; Wintjens, R.; Walker, J. R.; Alonso, S.; Lee, S.; Kim, J.; Oh, S.; Oh, T.; Nehrbass, U.; Han, S.-J.; No, Z.; Lee, J.; Brodin, P.; Cho, S.-N.; Nam, K.; Kim, J. *Nat. Med.* **2013,** *19* (9), 1157-1160.

71. Montgomery, M. G.; Petri, J.; Spikes, T. E.; Walker, J. E. *PNAS.* **2021,** *118* (47), e2111899118.

72. von Ballmoos, C.; Wiedenmann, A.; Dimroth, P. *Annu. Rev. Biochem.* **2009,** *78*, 649-72.

73. Hotra, A.; Suter, M.; Biuković, G.; Ragunathan, P.; Kundu, S.; Dick, T.; Grüber, G. *FEBS J.* **2016,** *283* (10), 1947-1961.

74. Lu, P.; Lill, H.; Bald, D. *Biochim. Biophys. Acta.* **2014,** *1837* (7), 1208-18.

75. Carnero, A. *Clin. Transl. Oncol.* **2006,** 8, 482-90.

76. Gangadharan, N. T.; Venkatachalam, A. B.; Sugathan, S. Bioresources and Bioprocess in Biotechnology: Volume 1: Status and Strategies for Exploration.; Springer Singapore: Singapore, 2017.

77. Ekins, S.; Mestres, J.; Testa, B. *Br. J. Pharmacol*. **2007,** *152* (1), 9-20.

78. Hotra, A. Design of Novel F-ATP Synthase Inhibitors of Mycobacterium Tuberculosis Nanyang Technological University, Singapore, Unpublished doctoral dissertation, 2018.

79. Saw, W.-G.; Wu, M.-L.; Ragunathan, P.; Biuković, G.; Lau, A.-M.; Shin, J.; Harikishore, A.; Cheung, C.-Y.; Hards, K.; Sarathy, J. P.; Bates, R. W.; Cook, G. M.; Dick, T.; Grüber, G. *Sci. Rep.* **2019,** *9* (1), 16759.

Chapter 2

Synthesis and investigation of *Mycobacterium tuberculosis* F-ATP synthase inhibitors with GaMF1

CHAPTER 2: Synthesis and investigation of *Mycobacterium tuberculosis* F-ATP synthase inhibitors with GaMF1

2.1 Introduction

The mycobacterial F-ATP synthase γ subunit is an essential component of the engine for ATP synthesis and ATP hydrolysis activities. The protein structure and amino acid sequence of the γ subunit of *Mtb* are significantly different from other organisms.[1] Thus, the γ subunit may be a potential target with high selectivity to cure *Mtb* for the next drug generation.

2.1.1 Mycobacterial F-ATP synthase subunit γ: An interesting binding site for the next drug generation

The role of the mycobacterial γ subunit is to communicate between the rotation of the *c*-ring and the $\alpha_3\beta_3$ hexamer catalytic site, which is essential for both ATP synthesis and hydrolysis. This subunit is composed of two different protein structures. The first element is an extended coiled-coil that links to the $\alpha_3\beta_3$ cavity and is produced by the *N*- and *C*-terminal helices.[2] Another component is a globular structure of mixed an α-helical/β-sheet domain located near the *c*-ring[3, 4] (Figure 2.1).

According to amino acid sequence analysis of the γ subunit, the mycobacterial coiled-coil component has a high degree of sequence similarity to other organisms (*Escherichia coli* (*E. coli*) and *Homo sapiens* (*H. sap.*)). In contrast, the mycobacterial globular amino acid sequence is largely unmatched by *E. coli.* and *H. sap.* with 63% and 75% differences, respectively.[1] One of the main differences in this globular region is a unique 13-amino acid loop (γ-loop), which is found only in *Mycobacterium* species.[1] This region, therefore, represents a valuable drug target as a molecule that binds to this region would unlikely affect ATP synthase in other organisms, including humans and our microbiome.

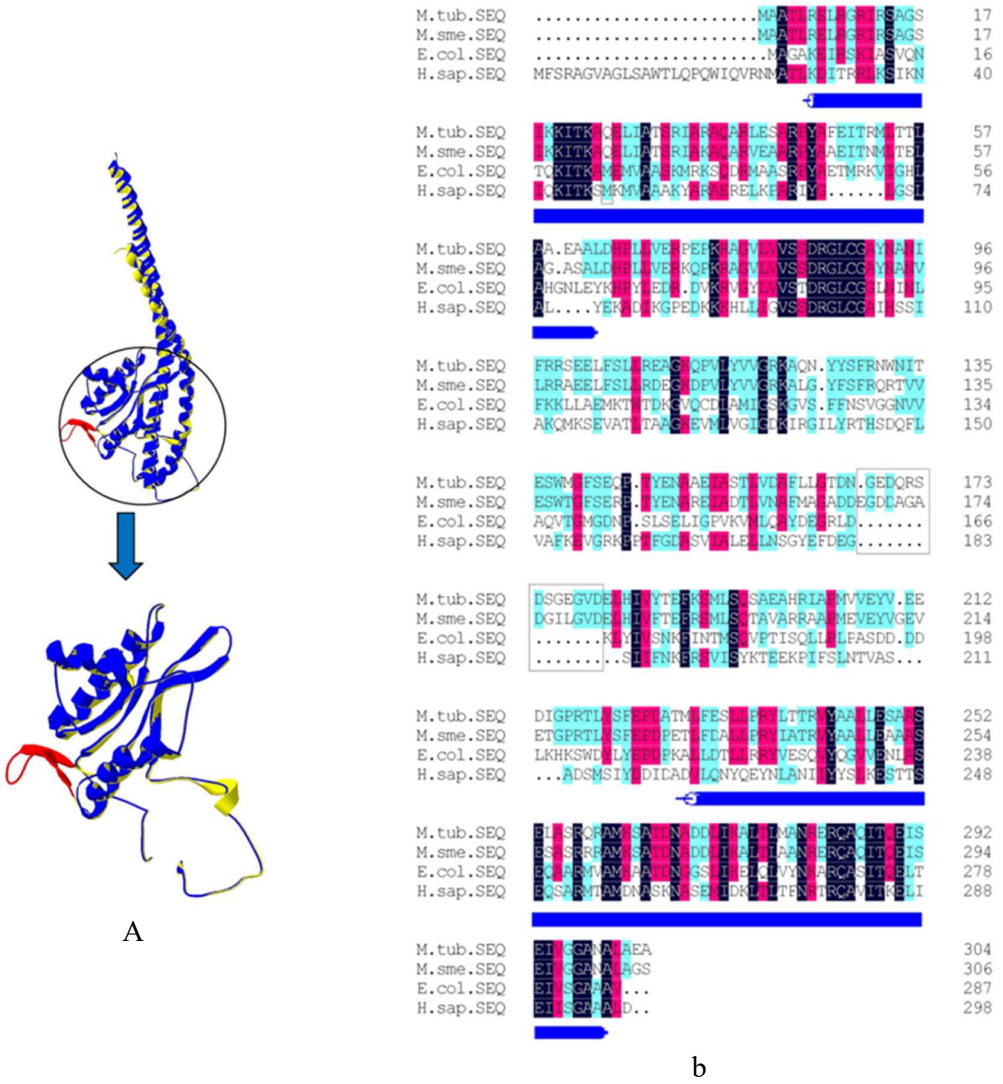

Figure 2.1 Homology model for the *Mtb* subunit γ (yellow) superimposed on the *E. coli.* subunit γ homolog (blue). Lower part: expansion of the mixed helical/sheet domain with the unique 13 amino acid residues in *Mtb* (red loop). (a), and amino acid sequence of γ subunit, comparing between M.tub (*Mtb*), M.sme (*M. smegmatis*), E. coli (*Escherichia coli*), B.ps3 (*Bacillus* PS3), and H.sap (*Homo sapiens*). Blue rods below the sequences indicate the coiled-coil α-helices. The boxed region highlights the *Mtb* unique γ-loop.[5] Reprinted from Lu, P. *et al.* Biochim. Biophys. Acta. Bioenerg. **2014,** *1837* (7), 1208-1218. Copyright (2021), reprinted with permission from Elsevier.

The γ-loop deletion of the F-ATP synthase of inversed membrane vesicle (IMV) experiments in *M. smegmatis* (*M. smeg.*) recently demonstrated a 46% decrease in ATP synthesis and 34% increase in ATP hydrolysis.[6] Thus, the mutation in this region to avoid the impact of an inhibitor would lead to greater ATP consumption than its synthesis and eventually eliminate the mycobacteria. Furthermore, the acceleration of ATP hydrolysis would also activate the H^+ pump of the F-ATP synthase, consequentially disrupting the membrane potential, resulting in cell respiration failure. Hence, the γ subunit globular region could be a possible inhibitor target for growth inhibition and killing of *Mtb* while preventing mycobacterial mutation and with no effect on human or other bacterial F-ATP synthases.

2.1.2 GaMF1; the mycobacterial F-ATP synthase γ subunit inhibitor

GaMF1 was discovered by *in-silico* screening at the *Mtb* γ subunit. The computed binding site was proposed to be the interface between the γ subunit and the *c*-ring with two hydrogen bonds from amide N-H and ethyl amine N-H to E212 (Glutamic acid) as the key interactions, shown in Figure 2.2.[7] Furthermore, this molecule fits with Lipinski's rule of five by possessing drug-like characteristics, as shown in Table 2.1.[7]

Table 2.1 GaMF1 drug likeliness analysis toward Lipinski's rule of five

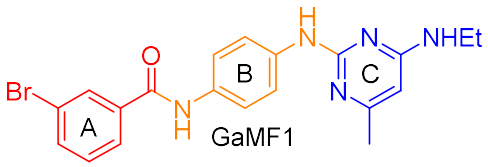

Properties	Lipinski's rule of five[7]	GaMF1[8]
Molecular mass	< 500 g/mol	426.3 g/mol
XlogP3	≤ 5.00[9]	4.7
Number of hydrogen bond donors	≤ 5	3
Number of hydrogen bond acceptors	≤ 10	5
Number of rotatable bonds[10]	≤ 10	6

The metabolic stability of GaMF1 was initially hypothesized to be problematic as a result of the *in vivo* oxidation of the 1,4-phenylenediamine moiety to form a conjugated imine species (Scheme 2.1).[11] The Michael acceptor of the conjugated imine could cause protein degradation through 1,4-addition of nucleophilic side chains of amino acids. However, the metabolic stability examination by the mouse liver microsomes experiment showed that GaMF1 had good *in vivo* stability ($T_{1/2}$ with or without NADPH of 47.5 min and 68 min, respectively; Cl_{int} of 14.6 μLmin^{-1}mg of protein^{-1}). Hence, this ceased to be a concern.

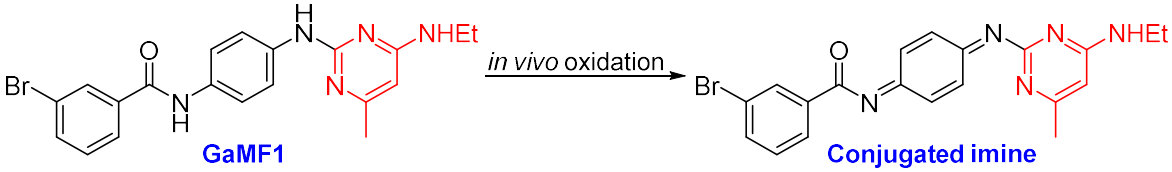

Scheme 2.1 *in vivo* oxidation of GaMF1

ATP synthesis inhibition experiments in *M. smeg.* IMV demonstrated that GaMF1 inhibits bacterial ATP synthesis with half-maximum inhibitory concentration (IC_{50}) of 0.3 μM and suppressed ATP hydrolysis by 52% at 100 μM of GaMF1.[8] These findings are consistent with many ATP synthase inhibitors (such as BDQ, quercetin, and 4-chloro-7-nitrobenzofurazan), which suggest that GaMF1 probably targets the F-ATP synthase as well.

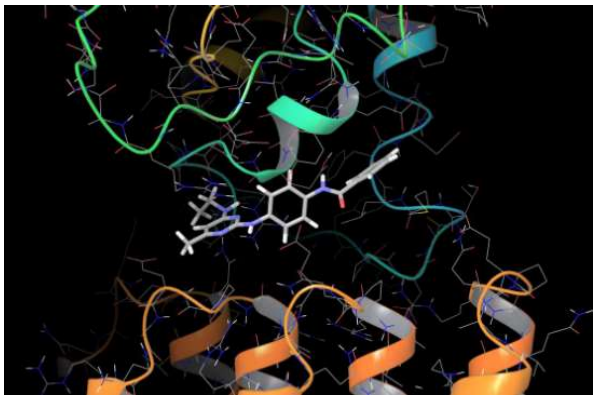

Figure 2.2 *In-silico* screening model of GaMF1 interacting with the interface between γ subunit and *c*-ring.[8]

These results are also consistent with minimum inhibitory concentrations (MIC_{50s}) inhibiting 50% growth of *M. smeg.* and *Mtb*, which are 11 and 33 μM, respectively.[8] Furthermore, GaMF1 has a synergistic effect with BDQ against *M. smeg.*, allowing for lower doses of both BDQ and GaMF1, which is possible to develop a combination drug.[8] Nevertheless, GaMF1 has a low water solubility with a saturated concentration at around 23.8 μM in a pH 7.4 solution at room temperature.[8] Normally, acidification should improve GaMF1 solubility, but the solubility was lower at 7.7 μM and 2.0 μM in pH 6.0 and 2.0 solutions, respectively.[8] Hence, this limitation would provide a problem for future research on this species.

The preliminary structure-activity relationship (SAR) of GaMF1 was studied by Hotra, A. *et al.*[8] to increase its enzymatic and bacterial growth inhibitory activities by focusing on substituents and their positions on ring A and C. Overall, GaMF1 remains the most effective molecule in the series in inhibiting *M. smeg.* IMV ATP synthesis and *M. smeg.* growth inhibition. Although the substituents on ring A have little influence on enzymatic inhibition, bromide is suggested for its bacterial growth inhibition. The enzymatic activity can be retained by a short alkyl group (methyl or ethyl) on the pyrimidine ring C. The secondary amine of ethyl amine is crucial for activity, whereas the methyl group on the ring C is not necessary for potency, as shown in Figure 2.3.[8]

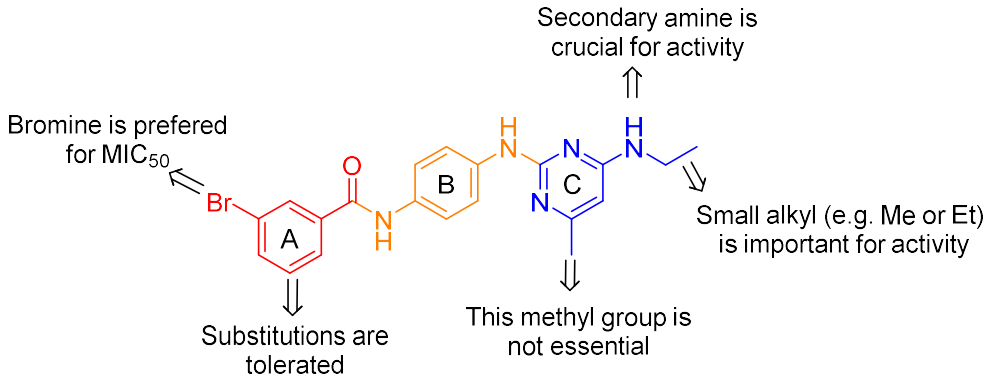

Figure 2.3 Summary of GAMF1 SAR by Hotra *et al.*[8]

2.1.3 Previously reported synthesis of GaMF1

GaMF1 was successfully synthesized by a five-step sequence in 26% overall yield, starting from *m*-bromobenzoic acid **2.1** and 2,4-dichloro-6-methylpyrimidine **2.5**.[8] The synthesis began with amidation between *m*-bromobenzoic acid **2.1** and *p*-nitroaniline **2.2**, followed by selective hydrogenation to produce aniline **2.4**. Nucleophilic Aromatic Substitution (NAS) of 2,4-dichloro-6-methylpyrimidine **2.5** with ethylamine formed pyrimidine **2.6**. However, this reaction lacked regioselectivity, resulting in the formation of pyrimidine **2.7** as a by-product. This issue and purification difficulties resulted in a low isolated

yield of **2.6** of 33%. Finally, the second NAS between aniline **2.4** and pyridine **2.6** gave GaMF1 in high yield (Scheme 2.2).[8]

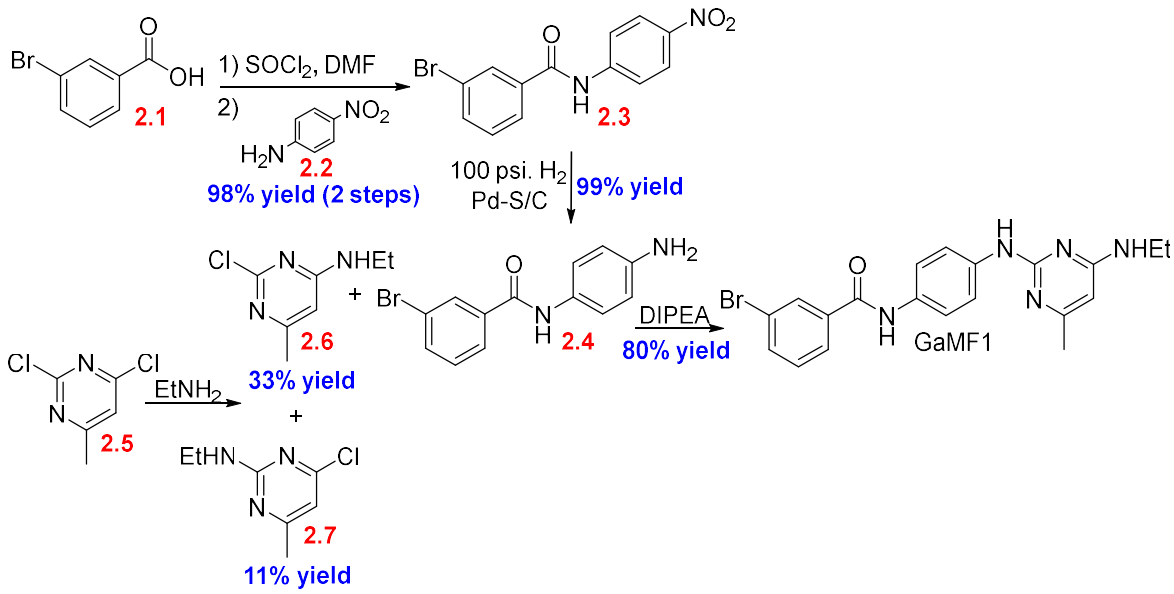

Scheme 2.2 Synthesis of GaMF1 by Hotra *et al.*[8]

2.2 Drugs design of the next generation of GaMF1

In Hotra's SAR,[8] only ring A and C were investigated, and the ring C examples were also limited to only pyrimidine analogs. Furthermore, even though Hotra's SAR study generated a batch of GaMF1 analogs, they remain water-insoluble. Therefore, in this work, SAR investigation on ring B, which was not mentioned in Hotra's research, and further ring C SAR would be studied, as well as the prospect of improving water solubility.

Based on the Hotra's SAR pattern, the methyl on the pyrimidine ring C was not required for mycobacterial ATP synthesis inhibition.[8] This finding was consistent with the *in silico* screening model, which demonstrated that the ring C methyl group does not have any significant interaction with the mycobacterial F-ATP synthase binding site.[8] Hence, replacing the methyl group with a polar substituent should improve the water solubility and help in understanding SAR on ring C.

In this work, a 1,3,5-triazine was considered to replace the pyrimidine (ring C) since the 1,3,5-triazine has an extra nitrogen atom to benefit the water solubility and is well-known to show antimicrobial properties.[12] Additionally, the use of a 1,3,5-triazine will likewise benefit the analog synthesis (discussed in 2.3.1), which will enable the study of different polar substituents. Moreover, the investigation of ring B SAR, which has not been investigated yet, would be studied by varying the chemical structure of ring B to be a cyclic or linear alkane or a *m*-phenylene diamine. Length between the two nitrogen atoms would be explored by adjusting the number of carbons on the structure (Figure 2.4).

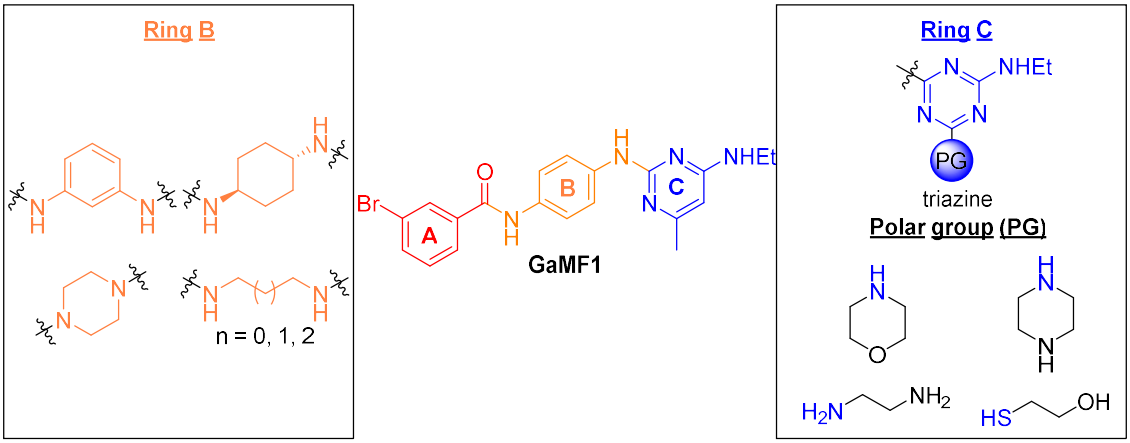

Figure 2.4 Modification of ring B and ring C on GaMF1

2.3 Synthesis of GaMF1 analogs for SAR investigation

GaMF1 analogs approach could be modified from GaMF1 synthesis by Hotra's strategy[8], beginning with amidation between *m*-bromobenzoic acid (ring A) and diamine derivatives (ring B). The subsequent product would then be coupled with triazine or pyrimidine (ring C) to yield GaMF1 analogs (Scheme 2.3).

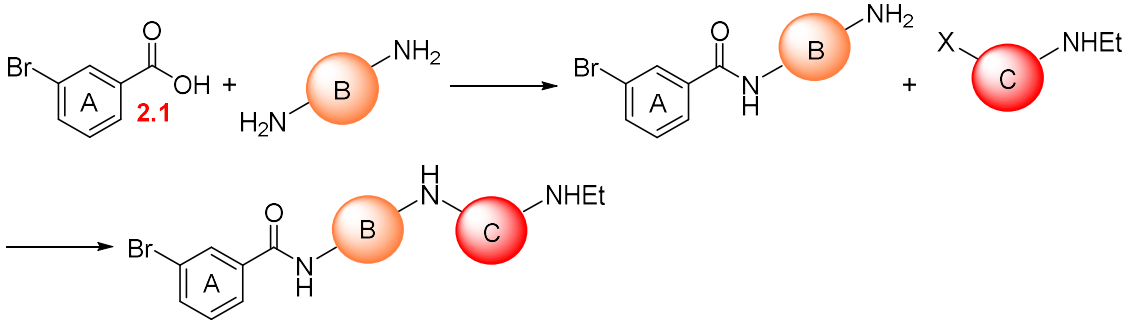

Scheme 2.3 Plan for our GaMF1 analogs synthesis

2.3.1 Synthesis of triazine GaMF1 analogs

All triazine analogs could be synthesized in three steps of NAS, starting from cyanuric chloride **2.8**. Because of the symmetrical structure of 1,3,5-triazine, none of these NASs have the regioselectivity problem as found in the previously reported GaMF1 synthesis. The final NAS of the chlorotriazine **2.10** could allow us to couple to different kinds of nucleophiles containing a polar group to access our triazine analogs (Scheme 2.4).

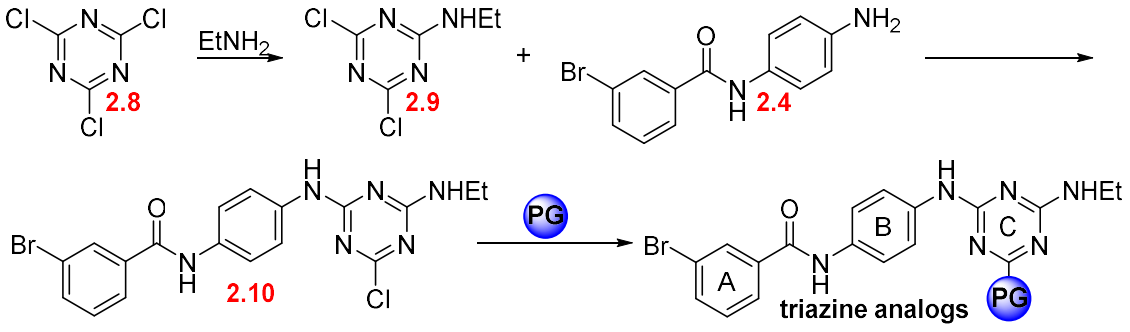

Scheme 2.4 Synthetic plan of triazine analogs; PG means the polar group

2.3.1.1 Synthesis of triazine analogs with the polar moiety

The approach began with coupling between ring A and ring B. The aniline **2.4** was synthesized by a three-step sequence from Hotra's strategy.[8] *m*-Bromobenzoic acid **2.1** was converted to the acid chloride using oxalyl chloride and dimethylformamide as a catalyst, followed by a reaction with *p*-nitro aniline **2.2** in the presence of K_2CO_3[13] to produce nitro-amide **2.3** in 96% yield over two steps. Common Pd/C hydrogenation under normal atmospheric pressure of H_2 is an effective method to convert nitro groups to amines in high yield. However, this results in dehalogenation, as reported by Richey *et al.*[14] Thus, selective hydrogenation with sulfided Pd/C under 100 psi. H_2 at 100 °C was used to prevent debromination,[14] giving rise to aniline **2.4** in 99% yield (Scheme 2.5).[8]

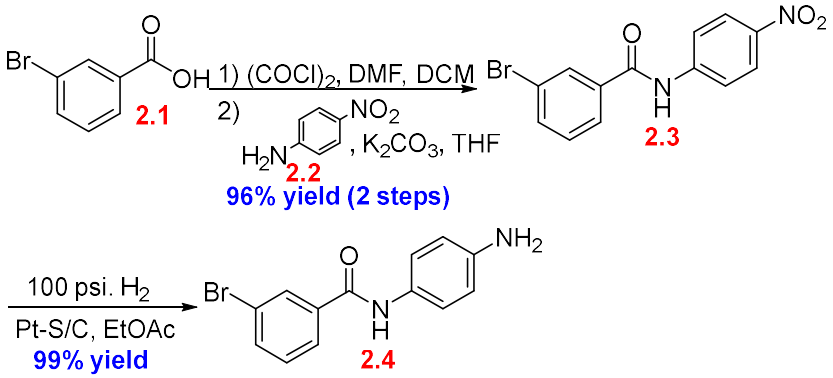

Scheme 2.5 Synthesis of *N*-(4-aminophenyl)-3-bromobenzamide **2.4**

The chloro-triazine **2.10** was produced in a two-step sequence. The NAS reaction between cyanuric chloride (**2.8**) and ethylamine provided 2,4-dichlorotriazine **2.9** in 76% yield.[15] The reaction temperature was strictly controlled at 0 °C to avoid side products from multiple substitutions. The second NAS coupled between aniline **2.4** and 2,4-dichlorotriazine **2.9** in dioxane at reflux[8] generated chloro-triazine **2.10** in an excellent yield of 88% (Scheme 2.6).

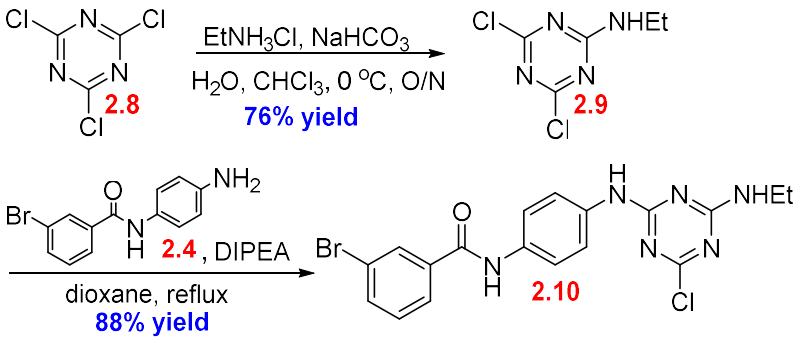

Scheme 2.6 Synthesis of chlorotriazine **2.10**

NAS between chlorotriazine **2.10** and different nucleophiles afforded 12 triazine analogs (**2.11**–**2.22**) in moderate to high yield (41–92% yield), as summarized in Table 2.2.[8] The reaction conditions were selected depending on the kind of nucleophiles. For the amine nucleophiles, the amine was used in excess (> 2 eq.) so that the amines function as both base and nucleophile. However, Cs_2CO_3 was necessary as a base for non-basic nucleophiles, e.g., thiols (Entry 11-12) and salt species (Entry 8).

Table 2.2 Nucleophilic Aromatic Substitution of polar moiety into triazine ring

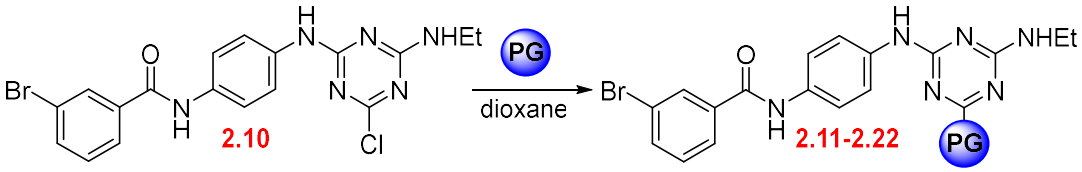

Entry	Equivalents of substrate	Substrate	Temperature	Product (PG)	% yield
1	2.5	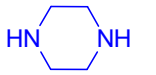	RT	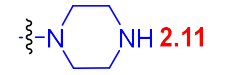	82%
2	5	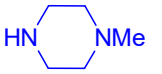	RT	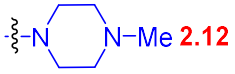	89%
3	2.5	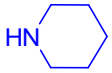	RT	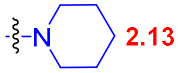	73%
4	7.5	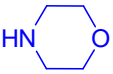	RT to 80 °C	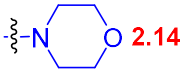	92%
5	2.5	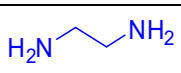	RT to 50 °C	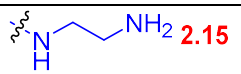	86%
6	2.5	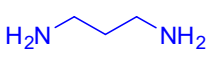	RT	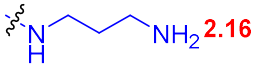	77%
7	5	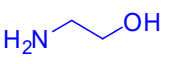	RT to 50 °C	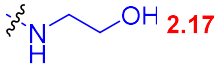	86%
8[a]	4	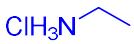	80 °C	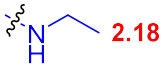	81%
9	10	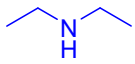	80 °C	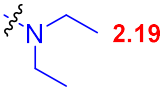	41%
10	5	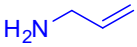	80 °C	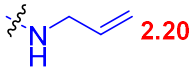	91%
11[b]	2	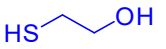	80 °C	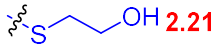	79%
12[b]	4		80 to 100 °C	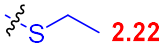	63%

[a] Cs_2CO_3 (2 eq.) was used as a base

[b] Cs_2CO_3 (1 eq.) was used as a base

2.3.1.2 Synthesis of 2-(piperazin-1-yl)-1,3,5-triazine GaMF1 analogs

Several 2-(piperazin-1-yl)-1,3,5-triazines (e.g., compounds **2.23** and **2.24**) have recently shown antibacterial and anti-TB micromolar activities with minimum inhibitory concentrations at the micromolar level (5 – 40 μM).[16, 17] According to the biological activities of our triazine series (**2.11**–**2.22**, discussed in 2.6.1), 2-(4-methylpiperazin-1-yl)-1,3,5-triazine (**2.12**), which is structurally related to **2.23**/**2.24**, was the most effective analog in this series. Therefore, understanding SAR on the piperazine ring could lead to further modifications to GaMF1 for greater efficacy. The designed molecules in the piperazine series are shown in Figure 2.5.

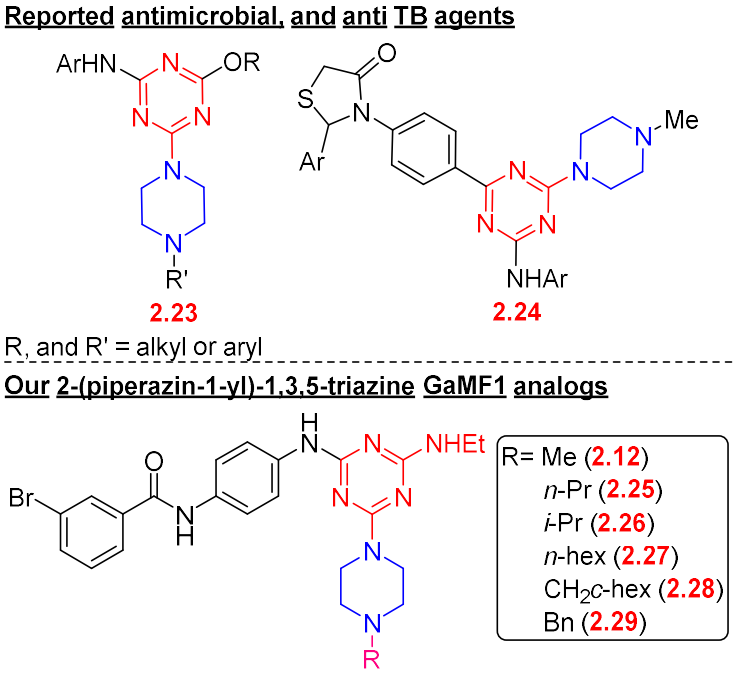

Figure 2.5 Examples of 2-(piperazin-1-yl)-1,3,5-triazines with antimicrobial and anti TB properties, and our 2-(piperazin-1-yl)-1,3,5-triazines GaMF1 analogs

The synthesis of 2-(piperazin-1-yl)-1,3,5-triazines GaMF1 analogs could be synthesized by a four-step sequence, in which NAS between the chlorotriazine **2.10** and piperazines, containing the desired alkyl group (**2.32**–**2.36**) was a key step. The approach began

with mono-Boc protection of piperazine **2.30**, which resulted in a 74% yield of Boc-protected piperazine (**2.31**).[18] The remaining free amino group of Boc-piperazine (**2.31**) was subjected to reductive amination with aldehydes using sodium acetate as a water absorber to promote the generation of imine intermediates, which were reduced immediately by H_2 with a Pd catalyst to generate the Boc-protected alkylated piperazines **2.32–2.36**.[19] The Boc group was deprotected using 50% trifluoroacetic acid in DCM, followed by NAS with compound **2.10**, using Cs_2CO_3 as a base, as described in Table 2.3.

Table 2.3 Reductive amination and NAS to obtain piperazine derivatives

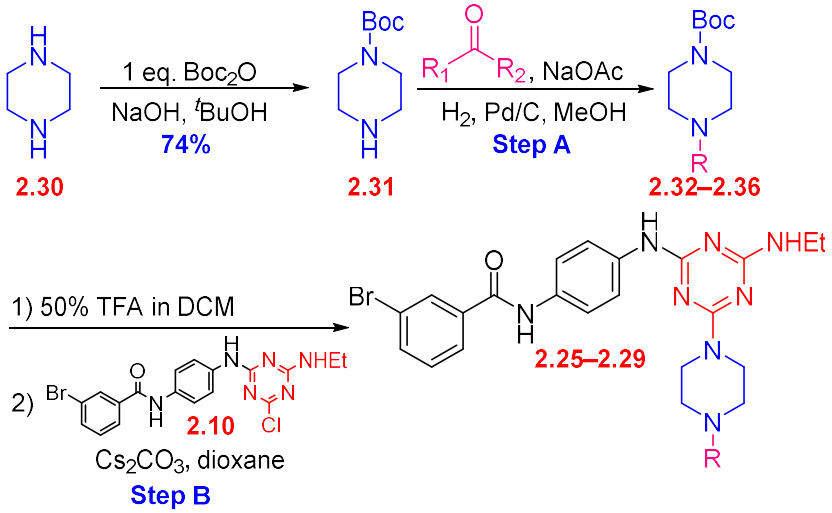

Entry	Aldehyde	Product (R)	% yield of Step A	% yield of Step B
1	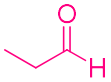	*n*-Pr (**2.25**)	Quantitative yield	71%
2		*i*-Pr (**2.26**)	91%	36%
3	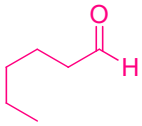	*n*-hex (**2.27**)	54%	77%
4	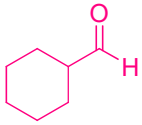	*c*-hexCH_2 (**2.28**)	47%	80%
5	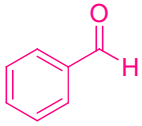	Bn (**2.29**)	47%	62%

2.3.1.3 Synthesis of triazine-hydride (2.37)

In this section, the impact of the triazine ring alone on the biological activities of GaMF1 was examined by comparing the bioactivities of the triazine-hydride GaMF1 analog **2.37** to those of pyrimidine analog **2.38** (Scheme 2.7). As reported by Hotra *et al.*,[8] the pyrimidine analog **2.38** was synthesized and found to have the IC_{50} of *M. smeg.* IMV and MIC_{50} against *M. smeg.* at 1.03 and 16.82 µM, respectively,[8] while the triazine-hydride **2.37** was a new compound that had not been reported before. Therefore, in this work, this compound (**2.37**) must be synthesized and evaluated for those bioactivities.

The strategy to obtain triazine-hydride **2.37** could begin with synthesizing the chlorotriazine **2.39**, starting from *p*-nitroaniline **2.2** and 2,4-dichlorotriazine **2.9**. Then, the dechlorination of the chlorotriazine **2.39** could be a key step to producing triazine-hydride **2.40**, which would then be amidated with the *m*-bromobenzoyl moiety to furnish the target triazine **2.37** (Scheme 2.7).

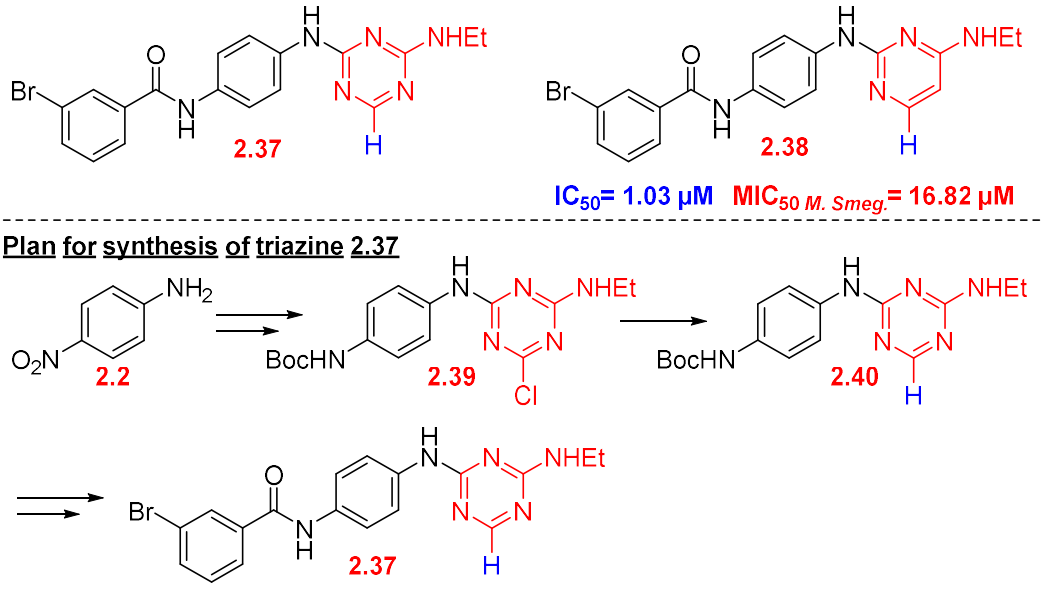

Scheme 2.7 Structures of compound **2.37** and **2.38**, and synthetic plan of triazine **2.37**

In the synthesis, di-Boc protection of *p*-nitroaniline **2.2**, followed by selective Boc deprotection, was performed to provide Boc-protected *p*-nitroaniline **2.42** in 45% yield over two steps.[20] The nitrobenzene **2.42** was subsequently transformed to aniline **2.43** by standard hydrogenation in 99% yield. NAS with triazine **2.9** then gave the key intermediate chlorotriazine **2.40** in 92% yield. The dechlorination step[14] was carried out in the presence of hydrogen gas with Pd/C as a catalyst and K_2CO_3 as the base to generate triazine-hydride **2.41** in 32%. Finally, Boc-protected aniline **2.41** was deprotected in DCM with 50% TFA and amidated in the presence of K_2CO_3 with *m*-bromobenzoyl chloride[13] to generate target **2.37** in 59% yield over three steps (Scheme 2.8).

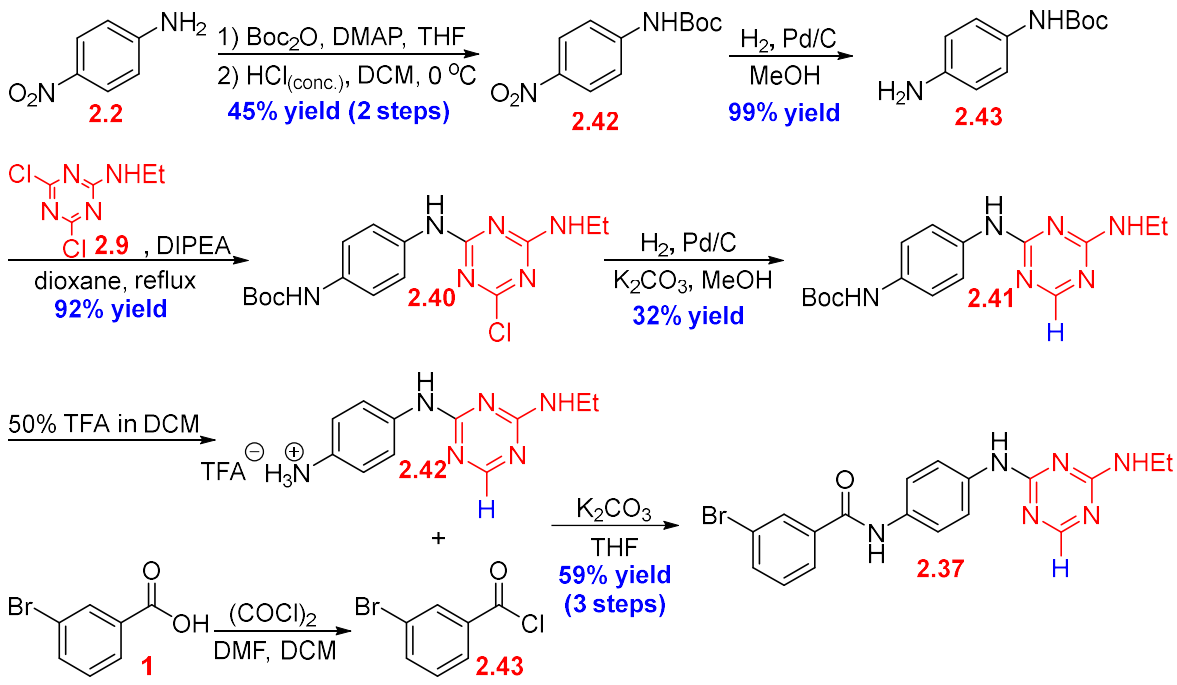

Scheme 2.8 Synthesis of triazine **2.37** from *p*-nitroaniline **2.2**

2.3.2 Synthesis of ring B analogs

The influence of the middle ring (ring B) on ATP synthesis inhibition and mycobacterial growth inhibition was investigated by varying ring B to be *m*-phenylene diamine, cyclic, or linear alkane. Furthermore, the inhibitory effect of ring B was examined together with the effect of ring C by comparing ring B analogs with the original pyrimidine ring C and ring B analogs with the 4-methylpiperazine-triazine ring C (the best IC_{50} and MIC_{50} in the triazine series). In this section, the synthesis of all ring B analogs (Figure 2.6) is explained. The synthetic strategy for ring B GaMF1 analogs was modified from Hotra's approach[8] by coupling between rings A and B, after which ring C would be attached (discussed in section 2.3, scheme 2.3).

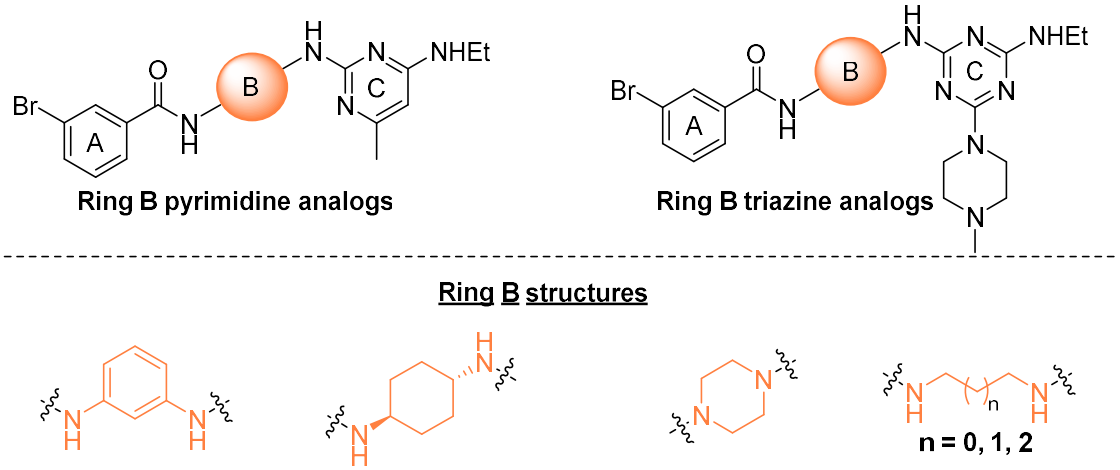

Figure 2.6 Ring B GaMF1 analogs

The aniline **2.46** was synthesized by using the same procedure as compound **2.4**. It starts with amide formation between *m*-bromobenzoic acid (**2.1**) and *m*-nitroaniline (**2.44**)[13] to obtain amide **2.45** in 91% yield over two steps, followed by medium pressure hydrogenation using sulfided Pd/C as the catalyst[8] to yield aniline **2.46** in 52% (Scheme 2.9).

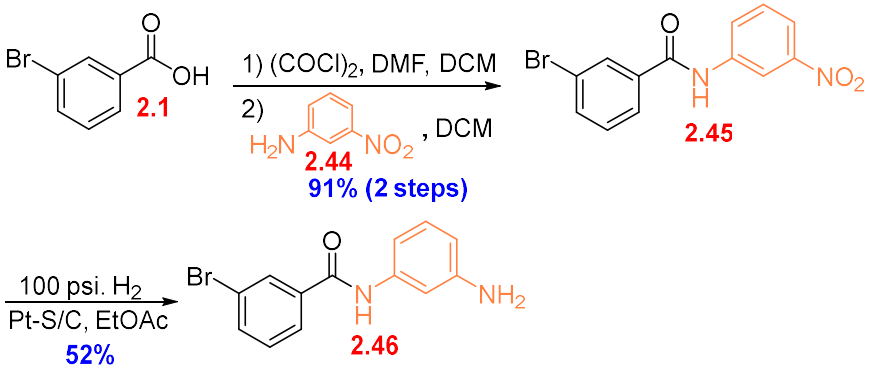

Scheme 2.9 Synthesis of aniline **2.46** from *m*-bromobenzoic acid **2.1**

Other amides (**2.47**–**2.49**) required the monoamidation of *m*-bromobenzoic acid (**2.1**) and diamine (**2.50**–**2.52**). All results are summarized in Table 2.4. The core problem encountered in this reaction is the undesirable side reaction of diamidation of diamines forming bis(3-bromobenzamide). Attempting to suppress this side reaction using an excess of diamine resulted in low yields of **2.47**-**2.49** (14–23%).

Table 2.4 Monoamidation between *m*-bromobenzoic acid and diamine

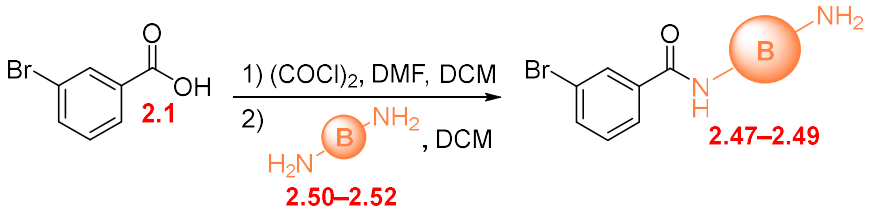

Entry	Eq. of diamine	Structure of diamine	Product (ring B)	%isolated yield
1	4 eq.	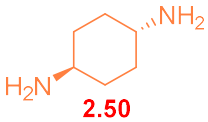 2.50	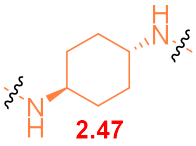 2.47	22%
2	10 eq.	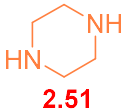 2.51	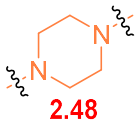 2.48	14%
3	4 eq.	 2.52	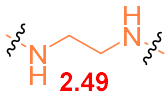 2.49	23%

Boc protection proved to be a reliable method for curbing the diamidation. Thus, the monoBoc-protected amines (**2.55**–**2.57**) were produced in 50–91% yield by treating an excess of the diamine with Boc_2O.[21] Finally, amidation between *m*-bromobenzoic acid **2.1** through converting to the acid chloride by oxalyl chloride and amines (**2.55**–**2.57**) furnished amide **2.58**–**2.60** in 27–32% yield, as summarized in Table 2.5.

Table 2.5 MonoBoc protection following by amidation

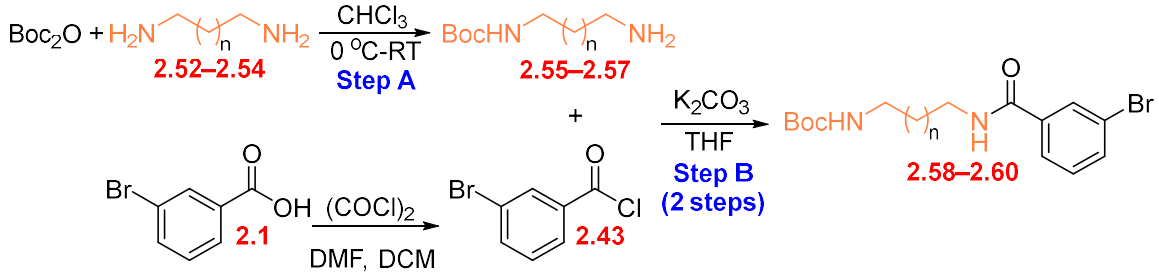

Entry	n	Starting material[a]	product	% yield of Step A	% yield of Step B
1	0	diamine **2.52**	Boc-amine **2.58**	50%	32%
2	1	diamine **2.53**	Boc-amine **2.59**	74%	27%
3	2	diamine **2.54**	Boc-amine **2.60**	91%	31%

[a] 10 eq. of diamines (**43**, **47-48**) were used

To synthesize the ring B analogs with the original pyrimidine ring C, the pyrimidine **2.6** was prepared by Hotra's method.[8] The NAS of 2,4-dichloro-6-methylpyrimidine **2.5** with $EtNH_2$, which was generated from $EtNH_3Cl$ salt in the presence of DIPEA, furnished the pyrimidine **2.6** in 33% yield. As reported by Hotra *et al.*, the second NAS of amines to the pyrimidine **2.6** in the presence of DIPEA in dioxane (boiling point: 101 °C) at reflux required a lengthy 2–5 days to complete.[8] Thus, a higher temperature was applied to shorten the time for the reaction to reach completion. The reaction involved NAS between **2.6** and **2.48** with DIPEA and DMF heated at 120 °C in a sealed tube, which yielded **2.63** in 71% with a reaction time of 2 days (Table 2.6, Entry 3).

Another approach to shortening the reaction time was the microwave irradiation condition. The reactions were performed at a high temperature (220 °C) using DIPEA as the base. However, the Boc-protected linear amines needed to be deprotected before NAS. Therefore, even though the target **2.61**–**2.66** was successfully synthesized and the reaction time was decreased to 30 minutes to 1.5 hours, this harsh condition (at 160-220 °C) resulted in

burning, leading to low yields, as shown in Table 2.6 (Entry 1 and 5). All results are shown in Table 2.6.

Table 2.6 Synthesize target **2.61-2.66** starting from 2,4-dichloro-6-methylpyrimidine **2.5**

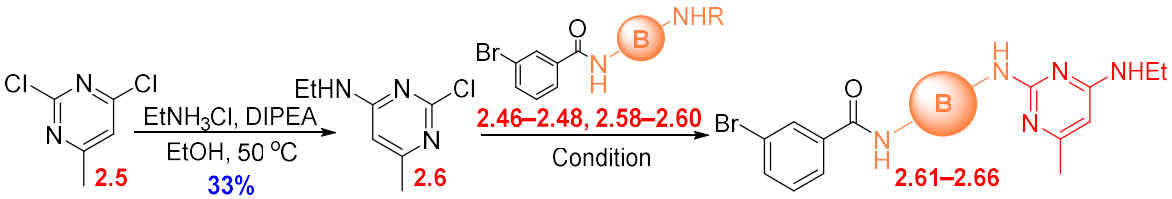

Entry	Structure of substrate	Condition[a]	Product (ring B)	Temperature	% isolated yield
1	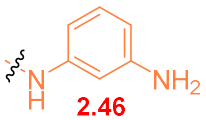 2.46	A	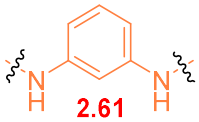 2.61	220 °C	26%
2	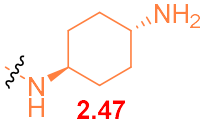 2.47	A	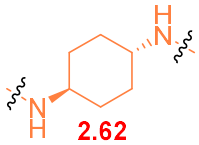 2.62	220 °C	63%
3	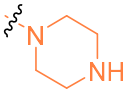 2.48	B	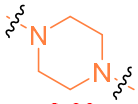 2.63	120 °C	71%
4	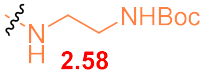 2.58	C	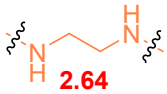 2.64	160 °C	62%
5	 2.59	C	 2.65	160 °C	28%
6	 2.60	C	 2.66	160 °C	56%

[a] Condition A: 1 eq. pyrimidine, 1 eq. amine or aniline, 1 eq. DIPEA, microwave, dioxane;
Condition B: 1 eq. pyrimidine, 1 eq. amine, 1 eq. DIPEA, sealed tube, DMF;
Condition C: 50% TFA in DCM (v/v) was treated with 1 eq. Boc-protected amine, then 1 eq. pyrimidine, 2.5 eq. DIPEA, microwave, dioxane;

The synthesis of the ring B analogs with the triazine ring-containing methyl piperazine was followed by the same strategy to synthesize the triazine GaMF1 analogs (discussed in 2.3.1.1). The monoamides **2.46**, **2.47**, and **2.49** were subjected to NAS with triazine **2.9** in the presence of DIPEA in dioxane at reflux[8] to obtain **2.67**–**2.69** in 54–84% yield. The subsequent NAS was performed on methyl piperazine to give **2.70**–**2.72** in 42–92% yield, as shown in Table 2.7.

Table 2.7 Synthesis of **2.70**–**2.72** starting from monoamide species

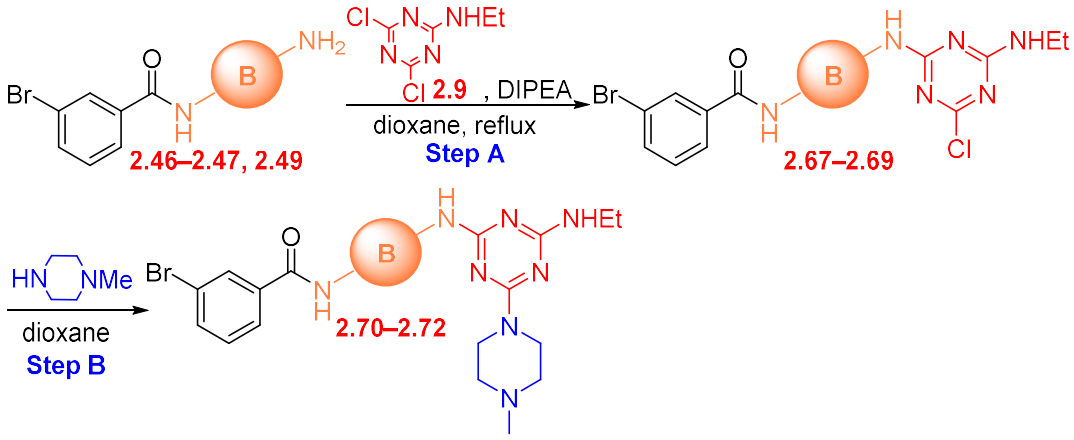

Entry	Substrate	Product (ring B)	% yield of Step A	% yield of Step B
1	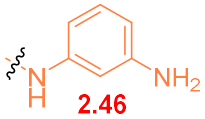 2.46	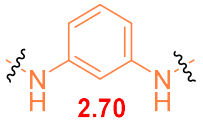 2.70	54%	92%
2	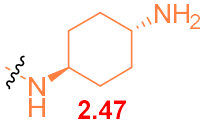 2.47	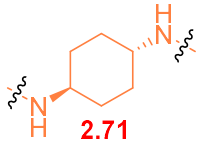 2.71	83%	84%
3	 2.49	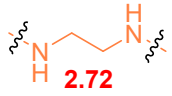 2.72	84%	42%

2.4 Biological activity evaluation

All GaMF1 analogs' ATP synthesis and mycobacterial growth inhibitions (**2.4**, **2.11**–**2.22, 2.25**–**2.29**, **2.37**, **2.61**–**2.66**, **2.70**–**2.72**) were evaluated by our collaborators from the Experimental Drug Development Centre (EDDC); the Agency for Science, Technology, and Research, Singapore (A*star), and the National University of Singapore (NUS). For safety purposes, since *Mtb* is a harmful pathogen that causes severe disease, which must be handled with special biosafety equipment (Biosafety level 3)[22], the less harmful organism *M. smeg*., which is a well-known pathogen often used as a representative of *Mtb* in many *Mtb* studies[23], was employed in this research instead.

Basically, the series of ETC enzymes and ATP synthase are embedded in the inner cell membrane, restricting the direct measurement of the ATP synthesis activity. Therefore, in this work, the inverted membrane vesicle (IMV) strategy, which can flip the inner side of the cell membrane out, was applied to allow all analogs (**2.4**, **2.11**–**2.22, 2.25**–**2.29**, **2.37**, **2.61**–**2.66, 2.70**–**2.72**) to inhibit the ATP synthesis directly.[24] The inverted membrane vesicle (IMV) would be prepared by disrupting the *M. smeg.* cell membrane in the French press or the microfluidizer (The procedure is described in section 2.10).[25] The ATP synthesis evaluation was performed by treating *M. smeg.* IMV with the inhibitors (**2.4**, **2.11**–**2.22, 2.25**–**2.29**, **2.37**, **2.61**–**2.66, 2.70**–**2.72**). The ATP synthesis was measured by the chemiluminescence of the reaction between Luciferin and ATP in the presence of Luciferase enzyme, magnesium ion, and oxygen in the air (Scheme 2.10).[8] The intensity of light emission, quantified by relative light unit (RLU), is proportional to the concentration of ATP in the system.[8] The ATP synthesis inhibition was presented as the concentrations of molecules to inhibit 50% of ATP synthesis, termed IC_{50} (done by Umayal Lakshmanan[26])

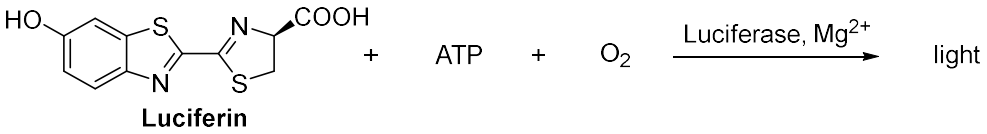

Scheme 2.10 Chemiluminescence of the reaction between Luciferin and ATP

Conversely, the bacterial growth inhibition assay was conducted by treating *M. smeg.* directly with the inhibitors (**2.4**, **2.11**–**2.22, 2.25**–**2.29**, **2.37**, **2.61**–**2.66, 2.70**–**2.72**) and then measuring the optical density value (loss of light intensity from light scattering) in the studied cell culture.[7] The bacterial growth inhibition was reported as the concentration of analogs to inhibit bacteria growth by half, termed MIC_{50} (done by Jickky Palmae Sarathy[27]).

2.4.1 Investigation of the substituent on triazine derivatives

The triazine analogs (**2.11**–**2.22**) were designed based on Hotra's SAR and the *in silico* screening model of GaMF1 in Figure 2.2, as discussed in Section 2.1.2, so that modification of the methyl group on the pyrimidine ring C, as well as replacing the pyrimidine ring with the triazine, should have no effect on enzymatic inhibition.[8] However, the IC_{50} and MIC_{50} values of the triazine analogs (**2.11**–**2.22**) were found to be higher than that of GaMF1, which revealed that the compounds were less effective in inhibiting ATP synthesis and *M. smeg.* bacterial growth as compared to the original GaMF1, as shown in Graph 2.1. These IC_{50} results show that the triazine ring, or the investigated substituents, influence ATP synthesis property that is unexpected based on the computational model (Figure 2.2, Section 2.1.2). Similarly, the MIC_{50} results reflected that the majority of triazine analogs totally lose the mycobacterial growth inhibition property. Only two analogs (**2.12** and **2.16**) showed activities against *M. smeg.* in the study concentration range (100 μM); however, both were still significantly lower in potency than GaMF1.

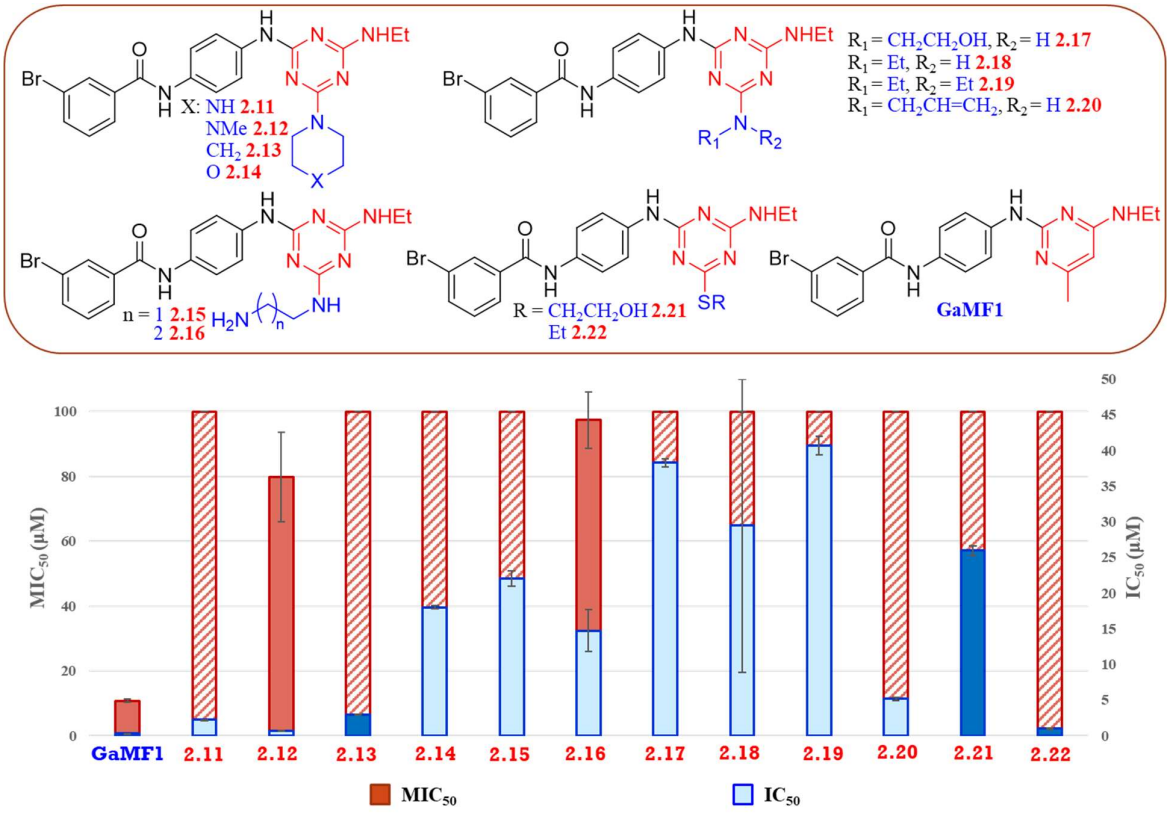

Graph 2.1 IC_{50}s and MIC_{50}s of GaMF1, and the triazine analogs **2.11**–**2.22**; IMV experiment was done by U. Lakshmanan[26]; *M. smeg.* growth inhibition experiment was done by J. P. Sarathy[27]; the experiments were performed in triplicate; deep blue bars indicate incomplete inhibition curve (**2.13**, and **2.21**–**2.22**); pattern red bars exhibit MIC_{50} above studying range at 100 μM; provided error is the standard error of the mean (SEM).

According to the IC_{50} inhibitory curves, compounds **2.13** and **2.21**–**2.22** show only 40 – 60% ATP synthesis inhibition at high concentrations (incomplete inhibition), as shown in Figure 2.7a. This pattern could be caused by ineffective molecular binding to the target or poor water solubility in the testing media at high concentrations,[28] whereas the rest of the analogs remained with their complete IC_{50} curves. The analog **2.12**'s IC_{50} curve is shown in Figure 2.7b as a representative of this series of analogs. Nonetheless, only piperazine-containing analogs **2.11** and **2.12** have IC_{50} values (2.2 μM for **2.11** and 0.7 μM for **2.12**) close to the original

molecule (GaMF1, 0.328 μM). Thus, the SAR investigation of piperazine ring analogs was further studied.

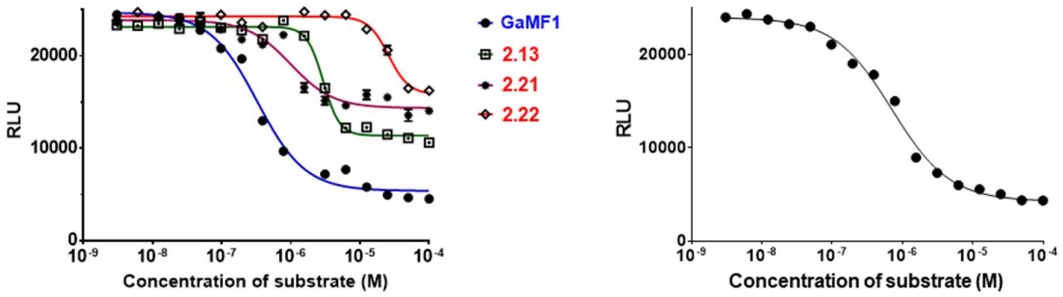

Figure 2.7 inhibitory curves of GaMF1 as compared to **2.13** and **2.21**–**2.22** (a), and the inhibitory curve of **2.12** (b).

2.4.2 Investigation of the piperazine derivatives

Recently, some triazines containing piperazine compounds (Figure 2.5 in 2.3.1.2) were reported to inhibit *Mtb* growth with 90–95% inhibition at 5–40 μM concentration[16, 17], and the *N*-substituent on the piperazine ring was observed to influence the potency (more detail was discussed in 2.3.1.2).[16] Hence, SAR studies on the *N*-substituent on the piperazine ring of the piperazine analogs could improve mycobacterial growth inhibition (Graph 2).

ATP synthesis inhibition experiment revealed that a small alkyl group (e.g., methyl) on the piperazine ring tended to increase potency, as methyl piperazine analog **2.12** had a three-fold lower IC_{50} than non-alkylated piperazine **2.11**. However, the larger size of the alkyl chain (compound **2.25**–**2.29**) led to less potency to inhibit ATP synthesis, especially the high steric hindrance of cyclohexyl methyl (**2.28**) and benzyl groups (**2.29**), which displayed incomplete inhibitory curves, presumably due to weak binding affinity to the enzyme target (Graph 2.2). The *M. smeg.* growth inhibition of the piperazine analogs with MIC_{50} above 75 μM was significantly less efficient than the original GaMF1 (MIC_{50} = 11 μM).

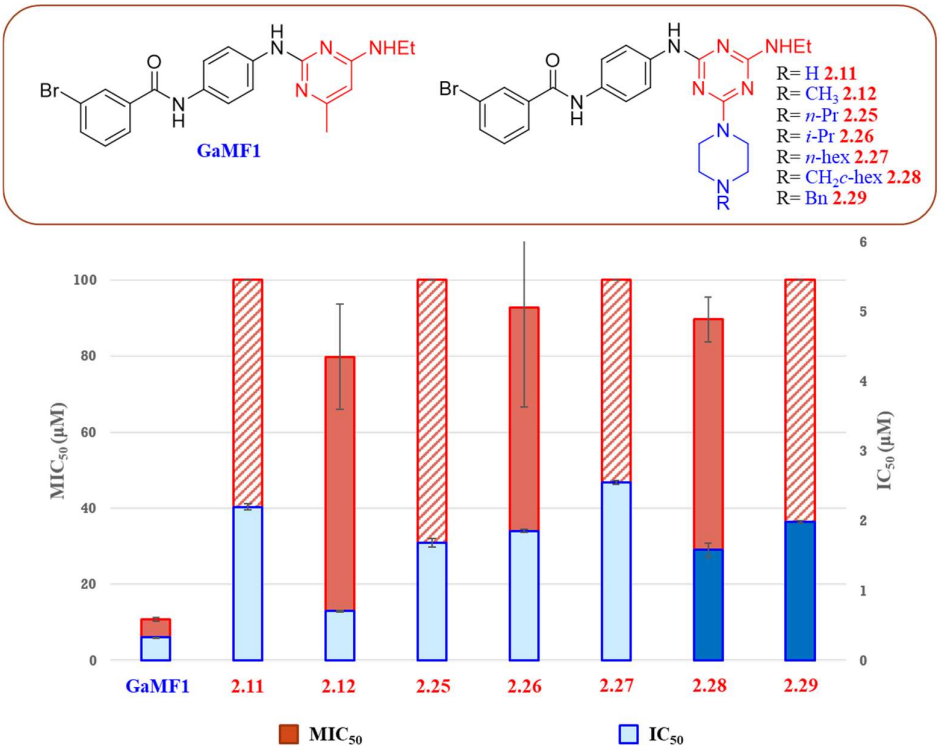

Graph 2.2 IC_{50}s and MIC_{50}s of GaMF1, analog **2.11**–**2.12**, and **2.25**–**2.29**; IMV experiment was done by U. Lakshmanan[26]; *M. smeg.* growth inhibition experiment was done by J. P. Sarathy[27]; the experiments were performed in triplicate; deep blue bars indicate incomplete inhibitory curve (**2.28**–**2.29**); pattern red bars exhibit MIC_{50}s above studying range at 100 μM; provided error is the standard error of the mean (SEM).

2.4.3 Investigation of the effect of ring C

In this section, the influence of the triazine ring on the ATP synthesis inhibition and *M. smeg.* growth inhibition was discussed in comparison to the original pyrimidine ring. In section 2.6.1, ring C was verified to be essential for the potency as *N*-(4-aminophenyl)-3-bromobenzamide **2.4** lost both IC_{50} and MIC_{50} inhibitions. Furthermore, triazine **2.37** exhibited no inhibition in both IC_{50} and MIC_{50} assays, whereas pyrimidine **2.38** had IC_{50} and MIC_{50} in the same range as GaMF1.[8] This finding indicated that ring C of GaMF1 is a crucial moiety for ATP inhibitory effect and that even adding one nitrogen atom can wholly change the potency (Graph 2.3).

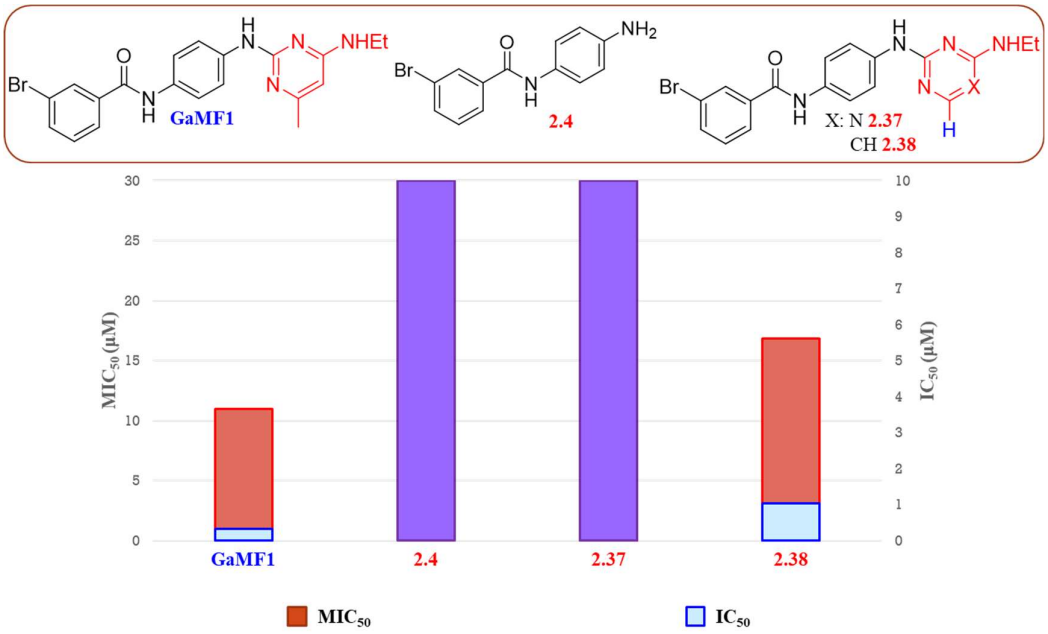

Graph 2.3 IC_{50}s and MIC_{50}s of GaMF1, analog **2.4**, and **2.37**–**2.38**; IMV experiment was done by U. Lakshmanan[26]; *M. smeg.* growth inhibition experiment was done by J. P. Sarathy[27]; the experiments were performed in triplicate; purple bars indicate IC_{50}s and MIC_{50}s above the studying range at 100 μM (**2.37**–**2.38**).

2.4.4 Investigation of ring B

The ATP synthesis and *M. smeg.* growth inhibitory effects of ring B analogs (**2.61**–**2.66** and **2.70**–**2.72**) were investigated. The results are shown in Graph 2.4. In both ATP synthesis inhibition and bacterial growth assays, all ring B analogs (**2.12**, **2.61**–**2.66, 2.70**–**2.72**) had less potency than the original GaMF1. Nonetheless, despite the fact that the variation of the ring B analogs had largely different molecular structures, the IC_{50} and MIC_{50} results of aromatic and cyclic linkage in both pyrimidine (**2.61**–**2.62**) and triazine analogs (**2.70**–**2.71**) did not show significantly different activities from the original GaMF1, indicating significant variation in ring B is quite well-tolerated.

The ATP synthesis inhibition property of the piperazine linker (**2.63**) was poorer than that of GaMF1, and this could reflect that one of the two N-H on the linker has a crucial interaction with the binding area or that the linker's range is insufficient. Nonetheless, only the linear linkage in both pyrimidine (**2.64**–**2.66**) and triazine analogs (**2.72**) showed a significantly lower ATP synthesis inhibitory effect than other analogs in the series (**2.12**, **2.61**–**2.62, 2.70**–**2.71**) and completely lost *M. smeg.* growth inhibition, presumably due to the linear linkages, led the molecules (**2.64**–**2.66, 2.72**) to be highly flexible, which resulted in difficulty fitting the inhibitors into the binding site. By comparing the activities of pyrimidine (**2.61**–**2.63**) and triazine analogs (**2.70**–**2.71**), both IC_{50} and MIC_{50} assays showed insignificantly different inhibitory effects. However, only the *p*-phenylene diamine linker (GaMF1 versus **2.12**) showed a significant difference in bacterial growth inhibition, which remains inexplicable.

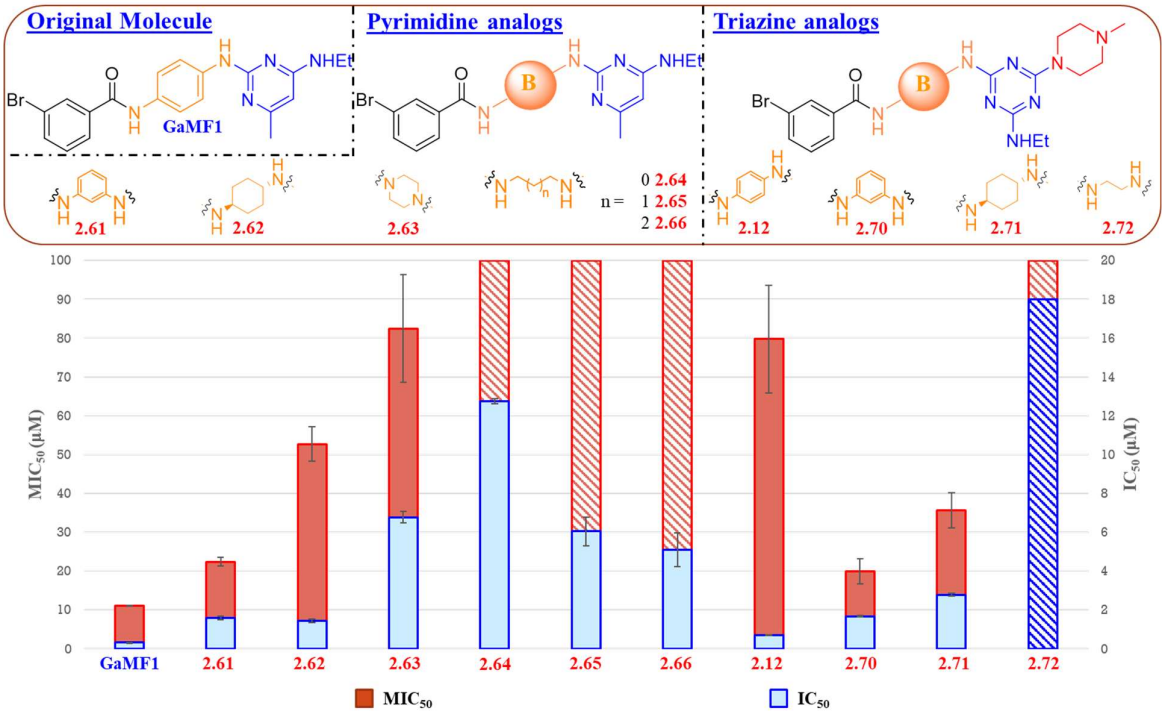

Graph 2.4 IC_{50}s and MIC_{50}s of GaMF1, analog **2.12**, **2.61**–**2.66**, and **2.70**–**2.72**; IMV experiment was done by U. Lakshmanan[26]; *M. smeg.* growth inhibition experiment was done by J. P. Sarathy[27]; the experiments were performed in triplicate; a blue pattern bar (**2.72**) represents that the IC_{50} value was 74.3 μM.; pattern red bars exhibit MIC_{50}s above the studying range at 100 μM; provided error is the standard error of the mean (SEM).

2.5 ^{1}H-^{15}N HSQC-NMR titration molecular modeling analysis

^{1}H-^{15}N HSQC-NMR titration is a technique to determine the binding area between the targeted enzyme and the inhibitor. The binding interactions of each ^{15}N-labeled amino acid residue in the protein sequence to the inhibitor result in distinct changes in the chemical shift position of the inhibitor-bound protein to the pure protein, which can assign the interacting ^{15}N-labeled amino acid residue.[29] Therefore, the NMR titration experiment was used to experimentally determine the GaMF1 binding site at the *Mtb* γ subunit.

The HSQC-NMR titration was performed by Priya Ragunathan[30] and analyzed by Joon Shin[31]. The molecular model (Figure 2.2) was then simulated based on the NMR titration outcome done by Amaravadhi Harikishore[32]. The NMR titration experiment suggested a binding site between the γ-loop and the globular component of the *Mtb* γ subunit (Figure 2.8a)., which was different from the *in-silico* screening model's originally hypothesized binding site at the interface between the subunit and the *c*-ring.

The pyrimidine ring (ring C) interacted with the *Mtb* γ globular region by hydrogen bonding from the amine at the ethyl amine group to R71 (Arginine), and the π-anion interaction between the pyrimidine ring and E70 (Glutamic acid). The main interactions with the *Mtb* γ-loop were the π-anion interaction from the *p*-phenylene ring (the middle ring) to R169 (Arginine) and hydrogen bonding from the carbonyl on the amide linkage to Q171 (Glutamine), where the N-H amide had the hydrogen bonding to D64 (Aspartic acid), as shown in Figure 2.8b.

According to the recent model based on the HSQC-NMR titration experiment,[30-32] the ring C of GaMF1 became a key component in interacting with the enzyme and fitting into the binding pocket (Figure 2.8b). This explained the loss of enzymatic activity caused by the ring C substituent modification, as the steric hindrance from the substituent tends to clash with the globular component of the subunit at the binding site. However, the model was unable to explain the loss of activity caused by replacing the pyrimidine ring with a triazine ring. The middle ring B modification could influence the π interaction from the phenylene ring and two hydrogen bonding from the amide linkage, which explains the lower efficacy in *m*-phenylene and *trans*-cyclohexyl linkers.

Therefore, the model from the HSQC-NMR titration experiment can be used to explain the experimental SAR results in this work, demonstrating that the utilization of that computational modeling based on the experimental data is valuable and useful as a supporting tool to understand the experimental results.

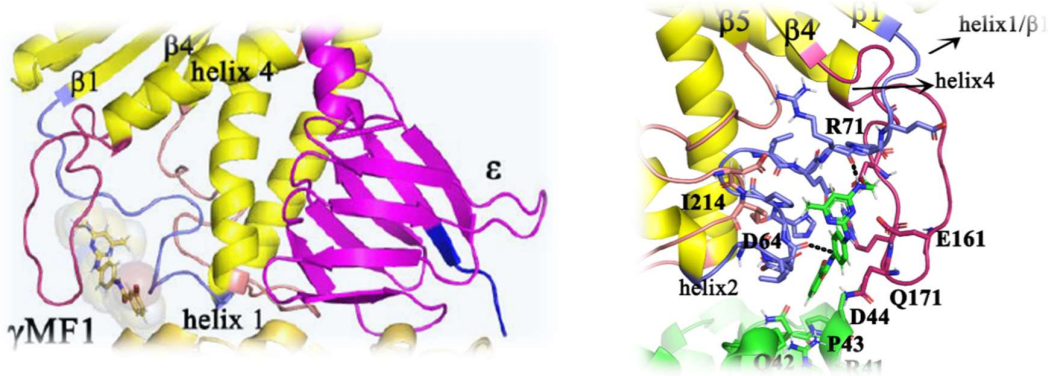

a b

Figure 2.8 Recent modeling of GaMF1 binding to γ subunit of F-ATP synthase (a), detailed interaction between GaMF1 and the enzyme (b)

2.6 Future work

In this work, the SAR investigation reveals that ring C modification affects the enzymatic inhibition by decreasing the activity, whereas ring B is quite well-tolerated for modification. However, the effects of two N-Hs on ring B remain unclear. Thus, the methylated N-H analogs (**2.79**–**2.81**) will be synthesized to perform further SAR investigation.

According to the model from the HSQC-NMR titration experiment (Figure 2.8), the additional substituent on ring B, such as carboxylic acid, hydroxy, or amine, or replacing the phenylene moiety with a heterocyclic aromatic component, could increase the interaction of ring B to the enzyme. Therefore, ring B analogs (**2.82**–**2.85**) will be made and studied.

The SAR investigation into ring A will be studied by replacing the *m*-bromo phenyl with a cyclic alkane and extending the ring A by naphthalene or a larger group. Thus, analogs (**2.73**–**2.75**) become interesting for further studies. According to Hotra's SAR investigation on

ring A,[8] the Br substituent caused the water solubility problem by having a highly lipophilic atom. In contrast, the F substituent on ring A led to lower bacterial growth inhibition.[8] Hence, the Cl substituent on ring A, which has not been studied yet, could improve the water solubility and retain the bacterial growth inhibition property. Thus, the Cl substituent ring A analogs (**2.76**–**2.78**) will be synthesized and SAR studied (Figure 2.9).

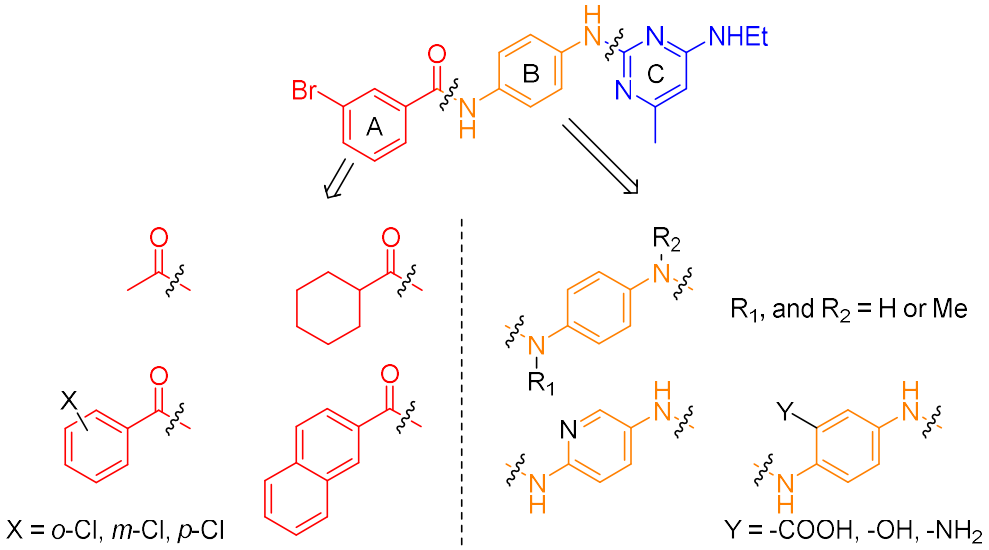

Figure 2.8 Proposed future work

2.7 Conclusion

In conclusion, 28 GaMF1 analogs (**2.4**, **2.11**–**2.22, 2.25**–**2.29**, **2.37**, **2.61**–**2.66**, and **2.70**–**2.72**) were synthesized by a modification of Hotra's approach.[8] By the ring C SAR investigation, bulky substituents on 1,3,5-triazine analogs (**2.11**–**2.22**, and **2.25**–**2.29**) tend to decrease both ATP synthesis and *M. smeg.* growth inhibitions, which are correlated with the recent HSQC-NMR titration molecular modeling. The original pyrimidine ring C is crucial for both inhibitory properties as removal of ring C (**2.4**) and replacing the original pyrimidine ring C with 1,3,5-triazine (**2.37**) result in complete loss of potency. However, modification of the middle ring B is quite well-tolerated, and aromatic (**2.12**, **2.61**, and **2.70**) or cyclic alkanes (**2.62** and **2.71**) are favored for efficacy, as shown in Figure 2.10.

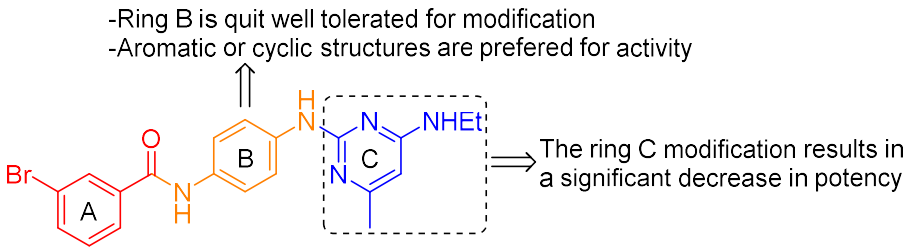

Figure 2.9 Summary of SAR results

2.8 Experimental section

Biological assays

Preparation of *M. smeg.* Inverted membrane vesicle (IMV)

The IMV preparation was done according to Koul *et al.*'s method[33] and was done by Priya Ragunathan[30]. Briefly, *M. smeg.* cells (5 g wet weight) were resuspended in 10 mL of the 50 mM MOPS buffer solution and 2 mM $MgCl_2$ at pH 7.5, containing an EDTA-free protease inhibitor cocktail (1 tablet/20 mL buffer, cOmplete^{TM}, Roche-USA) and 1.2 mg/mL of lysozyme. The suspension was stirred at room temperature for 45 minutes and added with 150 µL of 1 M aqueous $MgCl_2$ and 25 µL DNAse I (Thermo Fischer, USA), which was stirred continually for another 15 minutes at room temperature. All the subsequent steps were performed on ice. The cells were lysed by four passages through a pre-cooled Model M-110L Microfluidizer processor at 18,000 psi. The resulting suspension was centrifuged at 4,200 x g for 20 minutes at 4 °C. Supernatant liquor containing the membrane fraction was put through ultracentrifugation at 4,500 x g at 4 °C for 1 hour. The supernatant was discarded and precipitated membrane fractions were resuspended in the buffer of 15% glycerol, aliquoted, snap-frozen, and kept at -80 °C. The concentration of the protein in the vesicles was quantified by the BCA assay,[33] for which BCA reagent was available in kit form from Pierce (Rockford, IL, USA). The membrane fraction solution was diluted, and the optical density was measured at 562 nm against a blank in triplicates. The resulting OD_{562} was fitted into the standard calibration curve at 50–250 µg/mL, and the concentration was calculated.

ATP synthesis inhibition assay

The ATP synthesis inhibition of all inhibitors (**2.4**, **2.11**–**2.22, 2.25**–**2.29**, **2.37**, **2.61**–**2.66, 2.70**–**2.72**) in this work was evaluated in terms of IC_{50} by chemoluminescence.[6] The assay was performed in the flat-bottom white microtiter 96 or 384 well plates (Corning USA). A solution of 10 μM ADP, 250 μM Pi, and 1 mM NADH in the buffer of 50 mM MOPS and 10 mM $MgCl_2$ at pH 7.5 was prepared. The Pi concentration was adjusted by the solution of 100 mM KH_2PO_4. The inverted membrane vesicles at the final concentration of 5 μg/mL were added to initialize the ATP synthesis. The mixed solution was incubated at room temperature for 30 minutes, followed by adding 50 μL CellTiterglow reagent and incubating for another 10 minutes in the dark at room temperature. Luminescence correlates to the amount of synthesized ATP, which was determined by Tecan plate reader Infinite 200 Pro (Tecan USA) using the following parameters: luminescence, integration time of 500 msec, attenuation none, settle time 0. Synthesis of ATP.

Antimycobacterial activity and minimum inhibitory concentration determination

The *M. smeg.* growth inhibition dose-response assay was carried out using the broth microdilution method as described previously.[34] Briefly, clear 96-well flat-bottom Costar cell culture plates (Corning) were filled with 100 μL of complete 7H9 medium in each well. Each compound (**2.4**, **2.11**–**2.22, 2.25**–**2.29**, **2.37**, **2.61**–**2.66, 2.70**–**2.72**) was added to the first well in each row to create two times the desired highest final concentration. Subsequently, a 10-point, 2-fold serial dilution was carried out starting from the first well in each row. The mycobacterial strains used for the assay were grown to the mid-log phase and subsequently diluted to an OD_{600} of 0.1. 100 μL of the diluted culture was added to each well to create a final OD_{600} of 0.05 in all wells. For *M. smegmatis* strains, the plates were incubated at 37 °C on an orbital shaker set at 110 rpm for 1 day. At the end of the incubation period, the culture in all

wells was manually resuspended, and the OD_{600} was read using a TECAN Infinite Pro 200 plate reader. The MIC_{50} reported represents the concentration that inhibits 50% of growth compared to the untreated culture.

Table 2.8 IC_{50} and MIC_{50} values of GaMF1 analogs in this work

Compound	IC_{50} (μM)[a]	MIC_{50} (μM)[a]
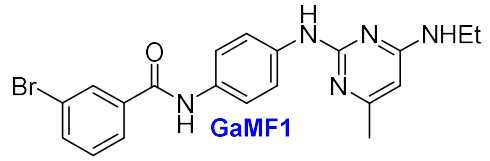 GaMF1	0.328[8]	10.8[8]
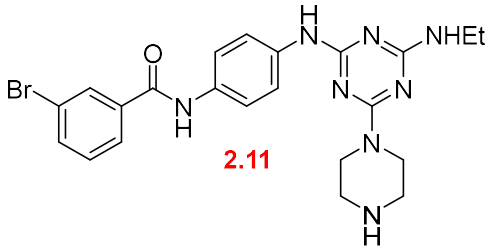 2.11	2.20 ± 0.04	>100[c]
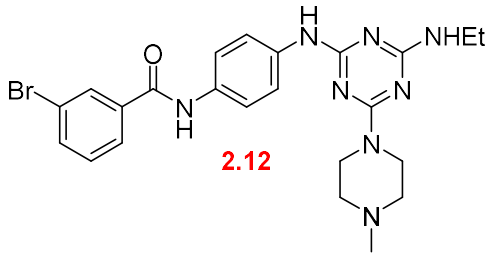 2.12	0.708 ± 0.011	79.8 ± 13.9
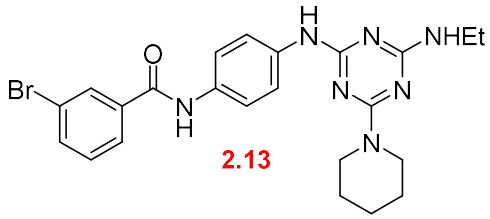 2.13	2.94 ± 0.03[b]	>100[c]
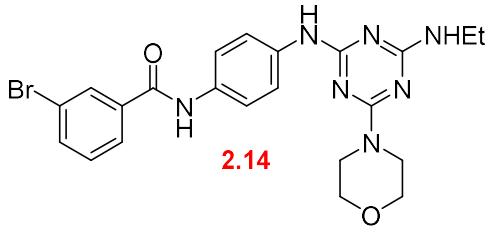 2.14	18.0 ± 0.2	>100[c]
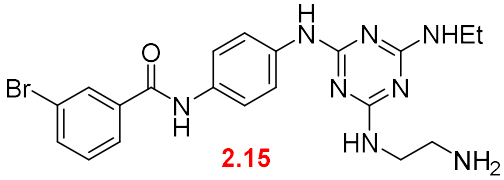 2.15	22.0 ± 1.1	>100[c]

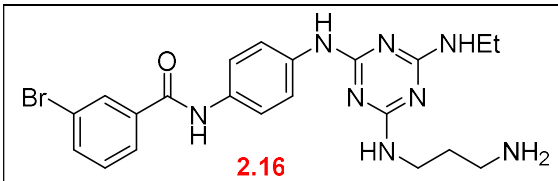 2.16	14.7 ± 2.9	97.4 ± 8.7
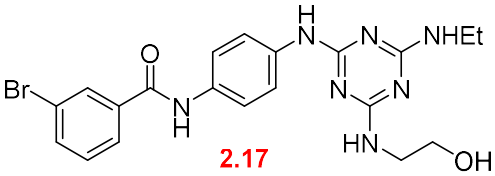 2.17	38.3 ± 0.6	>100[c]
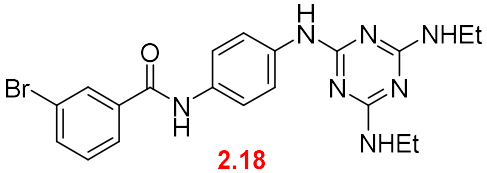 2.18	29.4 ± 2.6	>100[c]
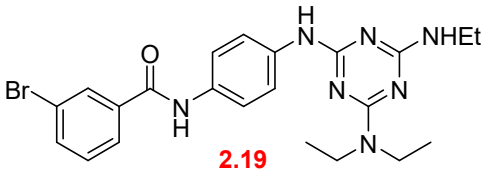 2.19	40.7 ± 1.3	>100[c]
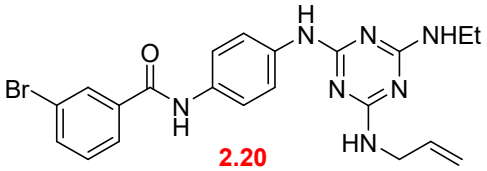 2.20	5.15 ± 0.25	>100[c]
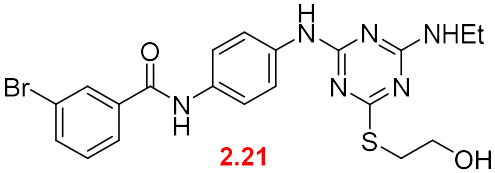 2.21	26.0 ± 0.7[b]	>100[c]
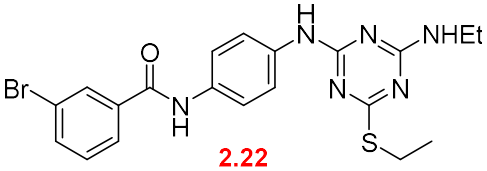 2.22	0.993 ± 0.106[b]	>100[c]
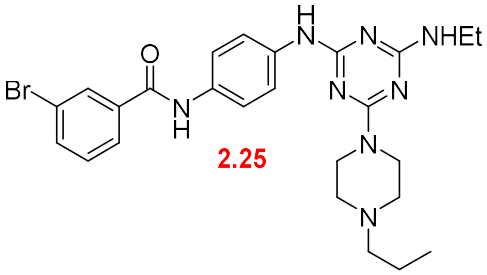 2.25	1.69 ± 0.06	>100[c]

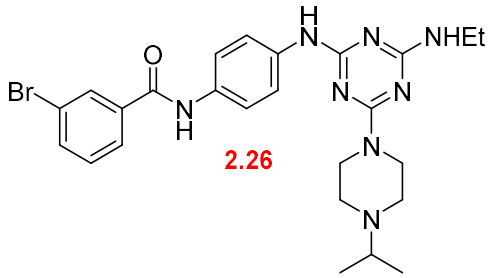 2.26	1.86 ± 0.02	92.7 ± 26.2
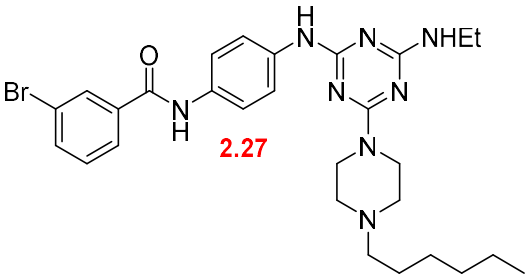 2.27	2.55 ± 0.02	>100[c]
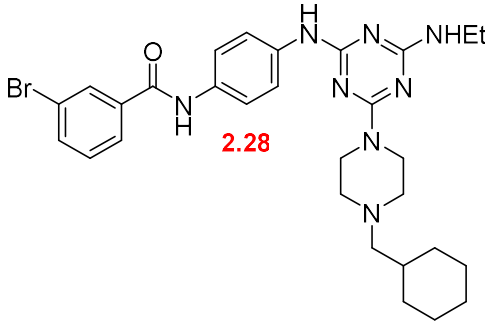 2.28	1.58 ± 0.10[b]	89.6 ± 5.9
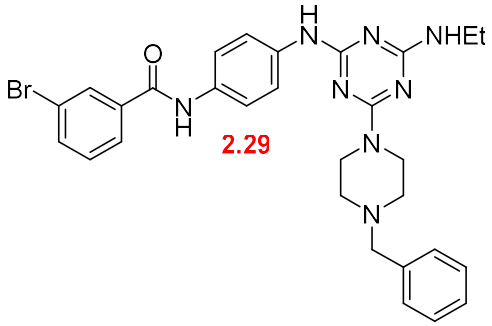 2.29	1.99 ± 0.02[b]	>100[c]
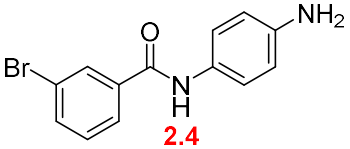 2.4	> 100[c]	>100[c]
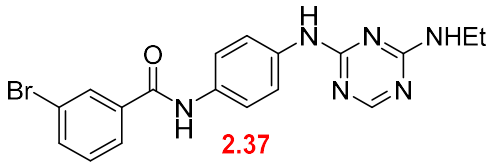 2.37	> 100[c]	>100[c]

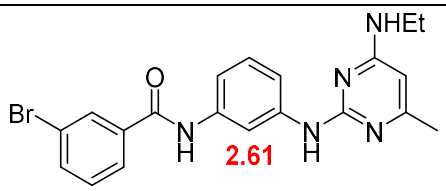 2.61	1.28 ± 0.09	22.4 ± 1.1
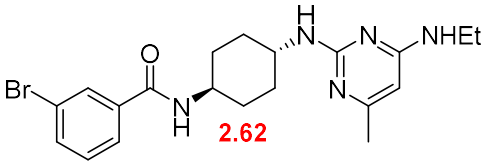 2.62	3.41 ± 0.08	52.7 ± 4.5
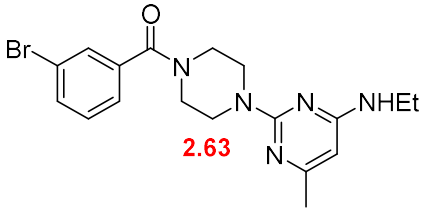 2.63	6.78 ± 0.28	82.4 ± 13.9
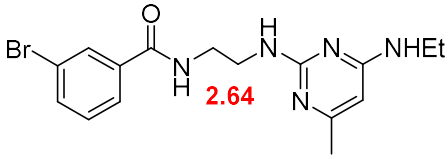 2.64	12.7 ± 0.1	>100[c]
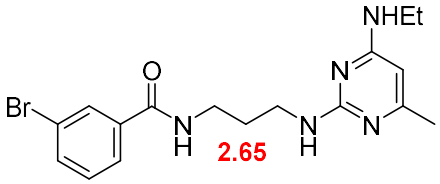 2.65	5.89 ± 0.73	>100[c]
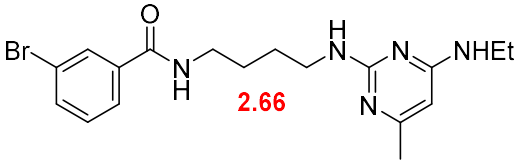 2.66	5.09 ± 0.87	>100[b]
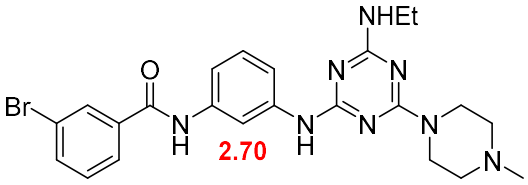 2.70	1.67 ± 0.04	19.9 ± 3.3
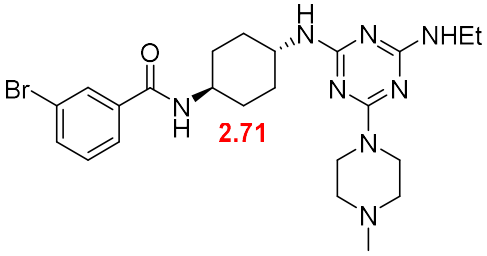 2.71	2.79 ± 0.08	35.7 ± 4.5

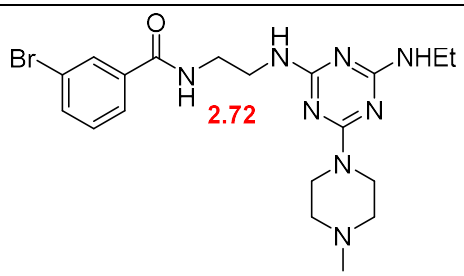	74.3 ± 29.1	>100[c]

[a] All experiments were performed in triplicate

[b] Subinhibitory concentrations were determined (the curve showed an incomplete curve)

[c] IC_{50}s or MIC_{50}s were above the studying range at 100 μM

Synthetic procedures

All moisture-sensitive reactions were carried out under a nitrogen atmosphere using oven-dried glassware (120 ºC), which was cooled under vacuum. Syringes and needles were dried under vacuum for at least 30 minutes before use. Anhydrous THF was freshly distilled from sodium metal with benzophenone under a nitrogen atmosphere before use, while Anhydrous DCM was distilled from CaH_2 under nitrogen. Anhydrous DMF was distilled under reduced pressure from CaH_2 under nitrogen and stored under 4Å molecular sieves. All other solvents and reagents were used as received. Flash column chromatography was performed on 230–400 mesh particle-sized silica gel.

All synthetic compounds in this research were structurally elucidated by ^{1}H-NMR, ^{13}C-NMR, IR spectroscopy, or mass spectrometry. The minimum purity of target compounds (**2.4**, **2.11**–**2.22, 2.25**–**2.29**, **2.37**, **2.61**–**2.66, 2.70**–**2.72**) for biological assays was accepted at 90%, and the purity was confirmed by ^{1}H- and ^{13}C- NMR spectroscopy. All supporting spectra information (^{1}H- and ^{13}C-NMR spectra) for this chapter were shown in Appendix A.

^{1}H- and ^{13}C- NMR spectra were recorded in deuterated solvents ($CDCl_3$ or DMSO-d6) at 400 MHz and 100 MHz, respectively, using JEOL ECA 400 and ECA 400SL spectrometers. Chemical shifts are reported in part per million (ppm), and coupling constants are recorded in Hertz (Hz). Infrared spectra were recorded using Spectrum 100 ATR-IR spectrometer (Perkin-

Elmer) and reported in cm^{-1}. Molecular weights were recorded using a high-resolution mass spectrometer equipped with Waters acquity UPLC (Waters Xeco G2-X2 MS) or a low-resolution mass spectrometer (Thermo Scientific LTQ XL MS). Melting points were recorded using Optimelt.

General Procedure 1: Synthesis of *N*-(4-nitrophenyl)benzamides[13]

To the corresponding benzoic acid (1 eq.) in dichloromethane (1 mL/1 mmol of benzoic acid) was added dropwise oxalyl chloride (1.2 eq) in the presence of a catalytic amount of dimethylformamide. The mixture was stirred at room temperature for 1 hour and then concentrated. The residue was taken up in THF (2.5 mL/1 mmol of benzoic acid). 4-Nitroaniline (1 eq) and K_2CO_3 (2 eq) were added, and the mixture was stirred for 16 hours at room temperature. The product was filtered and washed with water and hexane.

3-Bromo-*N*-(4-nitrophenyl)benzamide (2.3)

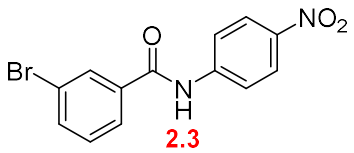

2.3

General procedure 1 was followed using m-bromobenzoic acid **2.1** (4.02 g, 20 mmol), oxalyl chloride (2.15 mL, 24 mmol), and anhydrous DMF (150 µL) in anhydrous DCM (20 mL). The resulting acid chloride was coupled to 4-nitroaniline (**2.2**; 2.77 g, 20 mmol) using K_2CO_3 (5.54 g, 40 mmol) in anhydrous THF (30 mL). After completion, as indicated by TLC (hexanes:EtOAc 1:1; UV), THF was evaporated, and an aqueous solution of 2 M HCl was added to the crude reaction. The precipitate **2.3** was collected by filtration, followed by washing with water to obtain 3-bromo-*N*-(4-nitrophenyl)benzamide **2.3** as a yellow solid (6.19 g, 96% yield). ^{1}H NMR (396 MHz, DMSO-d6) δ 10.85 (s, 1H), 8.25 (d, J = 9.0 Hz, 2H), 8.16 (s, 1H), 8.04 (d, J = 9.0 Hz, 2H), 7.97 (d, J = 7.7 Hz, 1H), 7.82 (d, J = 7.8 Hz, 1H), 7.52 (t, J = 7.9 Hz,

1H); ^{13}C NMR (100 MHz, DMSO-d6) δ 165.22, 145.70, 143.17, 136.88, 135.37, 131.26, 130.99, 127.66, 125.28, 122.27, 120.49, 100.00. The analytical data are in agreement with those reported before.[8]

_N_-(4-Aminophenyl)-3-bromobenzamide (2.4)

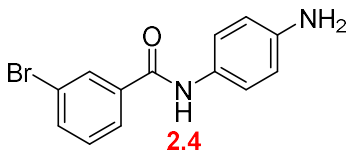

2.4

3-Bromo-*N*-(4-nitrophenyl)benzamide (**2.3**; 6.19 g, 19.3 mmol) was hydrogenated in EtOAc (50 mL) with sulfur poisoned platinum on carbon (10% wt), for two days under 100 psi of H_2 at 100°C. The reaction mixture was filtered through celite, and the solvent was evaporated under reduced pressure. *N*-(4-Aminophenyl)-3-bromobenzamide **2.4** was obtained as a yellow solid (5.58 g, 99% yield). ^{1}H NMR (396 MHz, DMSO-d6) δ 9.97 (s, 1H), 8.10 (t, J = 1.8 Hz, 1H), 7.92 (ddd, J = 8.0, 2.0, 1.0 Hz, 1H), 7.75 (ddd, J = 8.0, 2.0, 1.0 Hz, 1H), 7.47 (t, J = 7.9 Hz, 1H), 7.37 d, J = 8.8 Hz, 2H), 6.57 – 6.51 (d, J = 8.8 Hz, 2H), 4.96 (s, 2H); HRMS calcd for $C_{13}H_{12}N_2O^{79}Br$ ($M+H^+$) 291.0133; found 291.0126; IR (KBr, cm^{-1}) υ_{max} 3267, 3063, 1643, 1535, 1516; mp: dec. The analytical data are in agreement with those reported before.[8]

4,6-Dichloro-*N*-ethyl-1,3,5-triazin-2-amine (2.9)

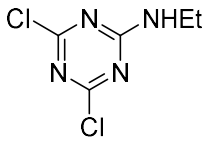

2.9

A solution of cyanuric chloride (**2.8**; 1.02 g, 5.4 mmol) in $CHCl_3$ (40 mL) was added dropwise to a solution of $NaHCO_3$ (1.37 g, 16.3 mmol) and ethylamine hydrochloride (1.33 g, 16.3 mmol) in water (20 mL) at 0 °C. The mixture was stirred vigorously at 0 °C for 21 hours. After completion, as monitored by TLC (hexanes:EtOAc 1:4; UV), the organic layer was then

separated and washed with water twice and with brine. The $CHCl_3$ was evaporated under reduced pressure to afford 4,6-dichloro-*N*-ethyl-1,3,5-triazin-2-amine **2.9** as a colorless solid (794 mg, 76% yield). ^{1}H NMR (400 MHz, $CDCl_3$) δ 5.90 (s, 1H), 3.53 (qd, *J* = 7.3, 6.0 Hz, 1H), 1.26 (t, *J* = 7.3 Hz, 1H). The ^{1}H NMR is in agreement with those reported before.[15]

3-Bromo-*N*-(4-((4-chloro-6-(ethylamino)-1,3,5-triazin-2-yl)amino)phenyl)benzamide (2.10)

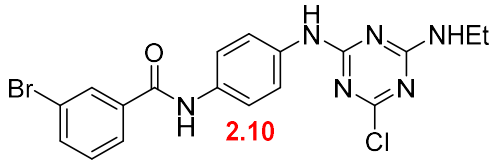

A solution of *N*-(4-aminophenyl)-3-bromobenzamide **2.4** (2.92 g, 10 mmol), 4,6-dichloro-N-ethyl1,3,5-triazin-2-amine **2.9** (1.93 g, 10 mmol), and di-isopropylethylamine (1.75 mL, 10 mmol) in dioxane (50 mL) was heated at reflux under nitrogen for 3 hours. The reaction was monitored by TLC (hexanes:EtOAc 1:1; UV). After the completion, water was added to the reaction mixture. The mixture was filtered and the precipitate was washed with a solution of 5% 2-methoxyethanol in EtOAc to afford 3-bromo-*N*-(4-((4-chloro-6-(ethylamino)-1,3,5-triazin-2-yl)amino)phenyl) benzamide **2.10** as a colorless solid (2.83 g, 63% yield). ^{1}H NMR[a] (396 MHz, DMSO-d6) δ 10.30 (s, 1H), 10.05 and 9.91 (2 br s, 1H, rotamer), 9.91 (s, 1H), 8.13 (s, 2H), 7.95 (d, *J* = 7.6 Hz, 1H), 7.84 – 7.57 (m, 4H), 7.49 (t, *J* = 7.8 Hz, 1H), 3.52 – 3.10 (m, 2H), 1.67 – 0.95 (m, 3H); ^{13}C NMR[a] (100 MHz, DMSO-d6) δ 168.4, 167.7, 165.2, 163.6, 163.1, 137.1, 135.0, 134.2, 134.0, 130.6, 130.2, 126.8, 121.7, 120.8, 120.3, 35.4, 35.2, 14.6, 14.2; HRMS calcd for $C_{18}H_{17}N_6O^{35}Cl^{79}Br$ ($M+H^+$) 477.0336; found 477.0327; IR (KBr) 3433, 3333, 3260, 3121, 2982, 1678, 1639, 1585, 1551, 1512, 1420 cm^{-1}; mp: dec.

[a]The compound exists as a mixture of rotamers.

General Procedure 2: Nucleophilic aromatic substitution of chlorotriazine **2.10** with nucleophiles

The chlorotriazine (1 eq.) and the nucleophile (2.5 – 10 eq.) were dissolved in dioxane (7 mL /1 mmol of chlorotriazine). The reaction was stirred and heated at the indicated temperature. After completion, the mixture was poured into water. The desired product was collected by filtration and washed with water.

3-Bromo-*N*-(4-((4-(ethylamino)-6-(piperizin-1-yl)-1,3,5-triazin-2-yl)amino)phenyl) benzamide (2.11)

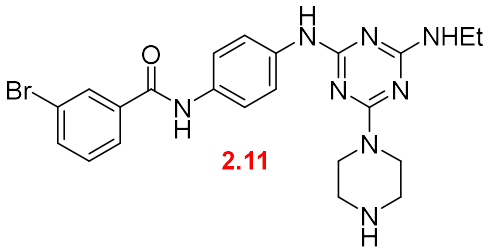

2.11

General procedure 2 was followed using piperazine hexahydrate (164 mg, 0.84 mmol) and 3-bromo-*N*-(4-((4-chloro-6-(ethylamino)-1,3,5-triazin-2-yl)amino)phenyl)benzamide **2.10** (150 mg, 0.34 mmol) in dioxane (2 mL). After stirring at room temperature for 1 day, the reaction was monitored by TLC (hexanes:EtOAc 2:3; UV). 3-Bromo-*N*-(4-((4-(ethylamino)-6-(piperizin-1-yl)- 1,3,5-triazin-2-yl)amino)phenyl)benzamide **2.11** was obtained as a colorless solid (137 mg, 82% yield). ^{1}H NMR[a] (396 MHz, DMSO-d6) δ 10.21 (s, 1H), 8.97, and 8.82 (2 br s, 1H, rotamer), 8.13 (t, J = 1.7 Hz, 1H), 7.94 (d, J = 7.9 Hz, 1H), 7.78 (d, J = 7.9 Hz, 1H), 7.70 (d, J = 9.0 Hz, 2H), 7.61 (d, J = 8.9 Hz, 2H), 7.49 (t, J = 7.9 Hz, 1H), 6.82 (br s, 1H), 3.63 (br s, 4H), 3.40 – 3.25 (m, 2H), 2.69 (br s, 4H), 1.11 (t, J = 7.2 Hz, 3H); ^{13}C NMR (100 MHz, DMSO-d6) δ 165.6, 164.6, 164.0, 163.5, 137.2, 136.9, 134.1, 132.4, 130.6, 130.1, 126.7, 121.7, 120.7, 119.5, 45.6, 44.0, 34.8, 15.1; HRMS calcd for $C_{22}H_{26}N_8O^{79}Br$ ($M+H^+$) 497.1413; found

497.1417; IR (KBr, cm^{-1}) υ_{max} 3418, 3300, 3066, 2968, 2927, 2857, 1654, 1582, 1543, 1508, 1420; mp: dec.

[a]The compound exists as a mixture of rotamers.

3-Bromo-*N*-(4-((4-(ethylamino)-6-(4-methylpiperizin-1-yl)-1,3,5-triazin-2-yl)amino) phenyl)benzamide (2.12)

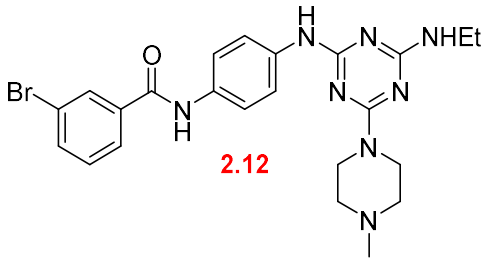

2.12

General procedure 2 was followed using 1-methylpiperazine (160 µL, 1.4 mmol) and 3-bromo-*N*-(4-((4-chloro-6-(ethylamino)-1,3,5-triazin-2-yl)amino)phenyl)benzamide **2.10** (125 mg, 0.28 mmol) in dioxane (2 mL). After stirring at room temperature for 1 day, the reaction was monitored by TLC (hexanes:EtOAc 2:3; UV). 3-Bromo-*N*-(4-((4-(ethylamino)-6-(4-methylpiperizin-1-yl)-1,3,5-triazin-2-yl)amino)phenyl)benzamide **2.12** was obtained as a colorless solid (127 mg, 0.25 mmol, 89% yield). ^{1}H NMR[a] (400 MHz, DMSO-d6) δ 10.21 (s, 1H), 9.00, and 8.85 (2 br s, 1H, rotamer), 8.13 (s, 1H), 7.95 (s, 1H), 7.87 – 7.31 (m, 6H), 6.87 (br s, 1H), 3.70 (s, 4H), 3.45 – 3.20 (m, 2H), 2.31 (s, 4H), 2.19 (s, 3H), 1.11 (s, 3H); ^{13}C NMR (100 MHz, DMSO-d6) δ 165.5, 164.5, 164.0, 163.5, 137.2, 136.9, 134.1, 132.5, 130.6, 130.1, 126.7, 121.7, 120.7, 119.5, 54.5, 45.9, 42.6, 34.8, 15.1; HRMS calcd for $C_{23}H_{28}N_8O^{79}Br$ ($M+H^+$) 511.1569; found 511.1564; IR (KBr, cm^{-1}) υ_{max} 3422, 3321, 3075, 2936, 2801, 1651, 1582, 1543, 1508, 1420; mp: dec.

[a]The compound exists as a mixture of rotamers.

3-Bromo-*N*-(4-((4-(ethylamino)-6-(piperidin-1-yl)-1,3,5-triazin-2-yl)amino)phenyl) benzamide (2.13)

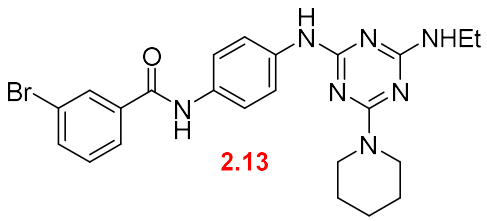

General procedure 2 was followed using piperidine (110 µL, 1.1 mmol) and 3-bromo-*N*-(4-((4-chloro-6-(ethylamino)-1,3,5-triazin-2-yl)amino)phenyl)benzamide **2.10** (100 mg, 0.22 mmol) in dioxane (1.5 mL). After stirring at room temperature for 2 hours, the reaction was monitored by TLC (hexanes:EtOAc 2:3; UV). 3-Bromo-*N*-(4-((4-(ethylamino)-6-(piperidin-1-yl)-1,3,5-triazin-2-yl)amino)phenyl)benzamide **2.13** was obtained as a colorless solid (80.5 mg, 73% yield). ^{1}H NMR[a] (396 MHz, DMSO-d6) δ 10.21 (s, 1H), 8.87 (2 br s, 1H, rotamer), 8.13 (s, 1H), 7.94 (d, *J* = 7.8 Hz, 1H), 7.78 (d, *J* = 8.2 Hz, 1H), 7.71 (d, *J* = 8.9 Hz, 2H), 7.60 (d, *J* = 8.7 Hz, 2H), 7.49 (t, *J* = 7.9 Hz, 1H), 6.81 (s, 1H), 3.70 (s, 4H), 3.45 – 3.25 (m, 2H), 1.62 (s, 2H), 1.51 (m, 4H), 1.11 (t, *J* = 7.1 Hz, 3H); ^{13}C NMR[a] (100 MHz, DMSO-d6) δ 165.7, 165.5, 164.4, 164.3, 164.1, 163.5, 137.2, 137.0, 134.1, 132.4, 130.6, 130.1, 126.7, 121.7, 120.7, 119.4, 43.5, 34.8, 25.4, 24.5, 15.1; HRMS calcd for $C_{23}H_{27}N_7O^{79}Br$ (M+ H^+) 496.1460; found 496.1458; IR (KBr, cm^{-1}) υ_{max} 3437, 3294, 2936, 2855, 1651, 1593, 1508, 1423; mp: dec.

[a]The compound exists as a mixture of rotamers.

3-Bromo-*N*-(4-((4-(ethylamino)-6-morpholino-1,3,5-triazin-2-yl)amino)phenyl) benzamide (2.14)

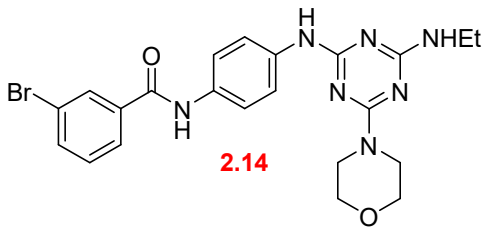

2.14

General procedure 2 was followed using morpholine (216 µL, 2.5 mmol) and 3-bromo-*N*-(4-((4-chloro-6-(ethylamino)-1,3,5-triazin-2-yl)amino)phenyl)benzamide **2.10** (150 mg, 0.34 mmol) in dioxane (2 mL). After stirring at 80 °C for 1 day, the reaction was monitored by TLC (hexanes:EtOAc 1:1; UV). 3-Bromo-*N*-(4-((4-(ethylamino)-6-morpholino-1,3,5-triazin-2-yl)amino)phenyl)benzamide **2.14** was obtained as a colorless solid (154 mg, 92% yield). ^{1}H NMR[a] (396 MHz, DMSO-d6) δ 10.21 (s, 1H), 9.03, and 8.88 (2 br s, 1H, rotamer), 8.13 (s, 1H), 7.94 (d, J = 7.9 Hz, 1H), 7.78 (d, J = 7.8 Hz, 1H), 7.70 (d, J = 8.9 Hz, 2H), 7.61 (d, J = 8.8 Hz, 2H), 7.49 (t, J = 7.9 Hz, 1H), 6.87 (br s, 1H), 3.68 (s, 4H), 3.62 (s, 4H), 3.40 – 3.25 (m, 2H), 1.11 (t, J = 7.1 Hz, 3H); ^{13}C NMR (100 MHz, DMSO-d6) δ 165.6, 164.8, 163.9, 163.5, 137.2, 136.8, 134.1, 132.6, 130.6, 130.1, 126.7, 121.7, 120.7, 119.6, 66.0, 43.3, 34.8, 14.9; HRMS calcd for $C_{22}H_{25}N_7O_2{}^{79}Br$ (M+ H^+) 498.1253; found 498.1252; IR (KBr, cm^{-1}) υ_{max} 3321, 3065, 2968, 1680, 1562, 1501; mp: dec.

[a]The compound exists as a mixture of rotamers.

***N*-(4-((4-((2-Aminoethyl)amino)-6-(ethylamino)-1,3,5-triazin-2-yl)amino)phenyl)-3-bromobenzamide (2.15)**

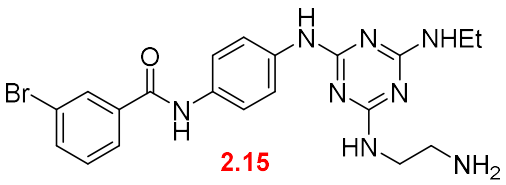

2.15

General procedure 2 was followed using ethylenediamine (56 µL, 0.84 mmol) and 3-bromo-*N*-(4-((4-chloro-6-(ethylamino)-1,3,5-triazin-2-yl)amino)phenyl)benzamide **2.10** (151 mg, 0.34 mmol) in dioxane (2 mL). After stirring at 50 °C for 2 days, the reaction was monitored by TLC (hexanes:EtOAc 2:3; UV). *N*-(4-((4-((2-Aminoethyl)amino)-6-(ethylamino)-1,3,5-triazin-2-yl)amino)phenyl)-3-bromobenzamide **2.15** was obtained as a colorless solid (138 mg, 0.29 mmol, 86% yield). ^{1}H NMR[a] (396 MHz, DMSO-d6) δ 10.20 (s, 1H), 8.95, 8.83, and 8.72 (3 br s, 1H), 8.13 (s, 1H), 7.94 (d, *J* = 7.6 Hz, 1H), 7.83 – 7.69 (m, 3H), 7.60 (d, *J* = 8.2 Hz, 2H), 7.49 (t, *J* = 7.8, 1H), 6.90 – 6.49 (m, 2H), 3.50 – 3.00 (m, 4H), 2.68 (s, 2H), 1.10 (t, *J* = 6.4 Hz, 3H); ^{13}C NMR (100 MHz, DMSO-d6) δ 165.8, 165.5, 163.9, 163.4, 137.2, 137.1, 134.1, 132.3, 130.6, 130.1, 126.7, 121.6, 120.7, 119.4, 43.6, 41.4, 34.7, 15.1; HRMS calcd for $C_{20}H_{24}N_8O^{79}Br$ (M+ H^+) 471.1256; found 471.1262; IR (KBr, cm^{-1}) υ_{max} 3418, 3294, 3065, 2970, 2929, 2872, 1654, 1564, 1423; mp: dec.

[a]The compound exists as a mixture of rotamers.

***N*-(4-((4-((3-Aminopropyl)amino)-6-(ethylamino)-1,3,5-triazin-2-yl)amino)phenyl)-3-bromobenzamide (2.16)**

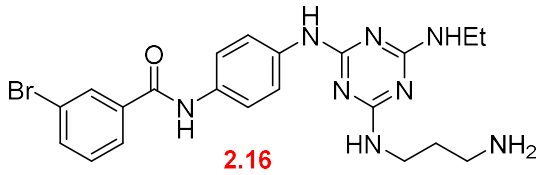

2.16

General procedure 2 was followed using 1,3-diaminopropane (70 µL, 0.84 mmol) and 3-bromo-*N*-(4-((4-chloro-6-(ethylamino)-1,3,5-triazin-2-yl)amino)phenyl)benzamide **2.16** (150 mg, 0.34 mmol) in dioxane (2 mL). After stirring at 50 °C for 2 days, the reaction was monitored by TLC (hexanes:EtOAc 2:3; UV). *N*-(4-((4-((3-Aminopropyl)amino)-6-(ethylamino)-1,3,5-triazin-2-yl)amino)phenyl)-3-bromobenzamide **2.16** was obtained as a colorless solid (126 mg, 77% yield). ^{1}H NMR[a] (396 MHz, DMSO-d6) δ 10.19 (s, 1H), 8.91, and 8.77 (2 br s, 1H), 8.13 (s, 1H), 7.94 (d, J = 7.9 Hz, 1H), 7.83 – 7.68 (m, 3H), 7.60 (d, J = 8.9 Hz, 2H), 7.49 (t, J = 7.9 Hz, 1H), 6.74 (br s, 1H), 3.63 – 3.45 (m, 4H), 3.40 – 3.24 (m, 2H), 1.18 – 1.06 (m, 5H); ^{13}C NMR (100 MHz, DMSO-d6) δ 165.6, 163.9, 163.4, 137.2, 137.1, 134.1, 132.3, 130.6, 130.1, 126.7, 121.7, 120.7, 119.4, 37.8, 37.6, 34.7, 33.0, 15.1; HRMS calcd for $C_{21}H_{26}N_8O^{79}Br$ ($M+H^+$) 485.1413; found 485.1409; IR (KBr, cm^{-1}) υ_{max} 3415, 3294, 3065, 2970, 1651, 1564, 1512; mp: dec.

[a]The compound exists as a mixture of rotamers.

3-Bromo-*N*-(4-((4-(ethylamino)-6-((2-hydroxyethyl)amino)-1,3,5-triazin-2-yl)amino) phenyl)benzamide (2.17)

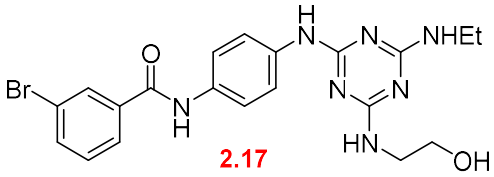

2.17

General procedure 2 was followed using ethanolamine (140 μL, 2.2 mmol) and 3-bromo-*N*-(4-((4- chloro-6-(ethylamino)-1,3,5-triazin-2-yl)amino)phenyl)benzamide **2.10** (201 mg, 0.45 mmol) in dioxane (2 mL). After stirring at 50 °C for 2 day, the reaction was monitored by TLC (hexanes:EtOAc 2:3; UV). 3-Bromo-*N*-(4-((4-(ethylamino)-6-((2-hydroxyethyl)amino)-1,3,5-triazin-2-yl)amino)phenyl)benzamide (**2.17**) was obtained as a colorless solid (183 mg, 0.39 mmol, 86% yield). ^{1}H NMR[a] (396 MHz, DMSO-d6) δ 10.20 (s, 1H), 8.95, 8.85, and 8.72 (3 br s, 1H, rotamer), 8.13 (t, *J* = 1.7 Hz, 1H), 7.94 (d, *J* = 7.9 Hz, 1H), 7.84 – 7.70 (m, 3H), 7.60 (d, *J* = 8.8 Hz, 2H), 7.49 (t, *J* = 7.9 Hz, 1H), 7.00 – 6.38 (m, 2H), 4.67 (br s, 1H), 3.51 (s, 2H), 3.34 – 3.20 (m, 4H), 1.10 (t, *J* = 7.0 Hz, 3H); ^{13}C NMR (100 MHz, DMSO-d6) δ 165.8, 165.5, 163.9, 163.4, 137.2, 137.0, 134.1, 132.4, 130.6, 130.1, 126.7, 121.7, 120.7, 119.4, 60.2, 42.8, 34.7, 15.1; HRMS calcd for $C_{20}H_{23}N_7O_2{}^{79}Br$ (M+ H^+) 472.1097; found 472.1090; IR (KBr, cm^{-1}) υ_{max} 3428, 3321, 2930, 1651, 1543, 1514; mp: dec.

[a]The compound exists as a mixture of rotamers.

3-Bromo-*N*-(4-((4-(diethylamino)-6-(ethylamino)-1,3,5-triazin-2-yl)amino)phenyl) benzamide (2.19)

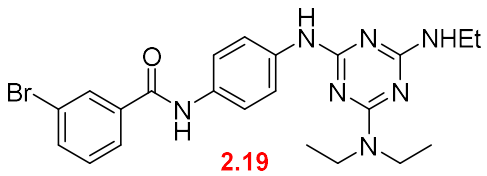

2.19

General procedure 2 was followed using diethylamine (240 µL, 2.2 mmol) and 3-bromo-N-(4-((4-chloro-6-(ethylamino)-1,3,5-triazin-2-yl)amino)phenyl)benzamide **2.10** (101 mg, 0.22 mmol) in dioxane (1.5 mL). After stirring at 80 °C for 5 days, the reaction was monitored by ^{1}H NMR spectroscopy. 3-Bromo-*N*-(4-((4-(diethylamino)-6-(ethylamino)-1,3,5-triazin-2-yl)amino)phenyl) benzamide **2.19** was obtained as a brown solid (43.4 mg, 41% yield). ^{1}H NMR[a] (396 MHz, DMSO-d6) δ 10.19 (s, 1H), 8.84 (2 br s, 1H, rotamer), 8.13 (t, *J* = 1.7 Hz, 1H), 7.94 (d, *J* = 7.9 Hz, 1H), 7.82 – 7.67 (m, 3H), 7.60 (d, *J* = 8.9 Hz, 2H), 7.49 (t, *J* = 7.9 Hz, 1H), 6.75 (br s, 1H), 3.64 – 3.43 (m, 4H), 3.34 – 3.27 (m, 2H), 1.18 – 1.07 (m, 9H); ^{13}C NMR (100 MHz, DMSO-d6) δ 164.1, 163.9, 163.4, 137.2, 137.1, 134.1, 132.3, 130.6, 130.1, 126.7, 121.6, 120.6, 119.2, 34.7, 15.1, 13.4; HRMS calcd for $C_{22}H_{27}N_7O^{79}Br$ (M+ H^+) 484.1460; found 484.1467; IR (KBr, cm^{-1}) υ_{max} 3426, 3294, 2972, 2930, 1653, 1618, 1585, 1543, 1510; mp: dec.

[a]The compound exists as a mixture of rotamers.

***N*-(4-((4-(Allylamino)-6-(ethylamino)-1,3,5-triazin-2-yl)amino)phenyl)-3-bromobenzamide (2.20)**

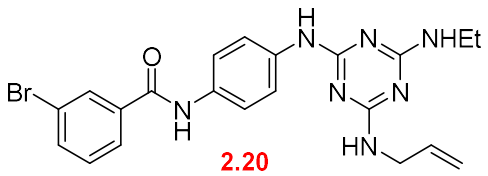

2.20

General procedure 2 was followed using allylamine (170 µL, 2.2 mmol) and 3-bromo-*N*-(4-((4-chloro-6-(ethylamino)-1,3,5-triazin-2-yl)amino)phenyl)benzamide **2.10** (202 mg, 0.44 mmol) in dioxane (2.5 mL). After stirring at 80 °C for 3 days, the reaction was monitored by TLC (hexanes:EtOAc 2:3; UV). *N*-(4-((4-(Allylamino)-6-(ethylamino)-1,3,5-triazin-2-yl)amino) phenyl)-3-bromobenzamide **2.20** was obtained as a colorless solid (188 mg, 0.40 mmol, 91% yield). ^{1}H NMR (396 MHz, DMSO-d6) δ 10.20 (s, *J* = 18.5 Hz, 1H), 9.09 – 8.61 (m, 1H), 8.13 (t, *J* = 1.7 Hz, 1H), 7.94 (d, *J* = 7.9 Hz, 1H), 7.83 – 7.68 (m, 3H), 7.60 (d, *J* = 8.9 Hz, 2H), 7.49 (t, *J* = 7.9 Hz, 1H), 7.14 – 6.56 (m, 2H), 5.90 (ddd, *J* = 22.1, 10.3, 5.2 Hz, 1H), 5.15 (d, *J* = 17.2 Hz, 1H), 5.05 (dd, *J* = 10.3, 1.6 Hz, 1H), 3.90 (s, 2H), 3.37 – 3.23 (m, 2H), 1.10 (t, *J* = 7.1 Hz, 3H); ^{13}C NMR (100 MHz, DMSO-d6) δ 165.6, 165.5, 164.0, 163.4, 137.2, 137.0, 136.4, 134.1, 132.4, 130.6, 130.1, 126.7, 121.6, 120.6, 119.4, 114.5, 42.4, 34.7, 15.1; HRMS calcd for $C_{21}H_{23}N_7O^{79}Br$ ($M+H^+$) 468.1147; found 468.1146; IR (KBr, cm^{-1}) υ_{max} 3429, 3397, 3277, 3179, 2934, 1645, 1608, 1578, 1543, 1491; mp: dec.

General Procedure 3: Nucleophilic aromatic substitution of chlorotriazine **2.10** with nucleophiles using Cs_2CO_3

The chlorotriazine (1 eq.) and the nucleophile (2 – 4 eq.) were dissolved in dioxane (7 mL/1 mmol of chlorotriazine). Cs_2CO_3 (1 eq.) was added to the solution. The mixture was stirred at the indicated temperature. After the completion, the reaction mixture was poured into water. The desired product was collected by filtration, washing with a suitable solvent, as indicated below.

***N*-(4-((4,6-Bis(ethylamino)-1,3,5-triazin-2-yl)amino)phenyl)-3-bromobenzamide (2.18)**

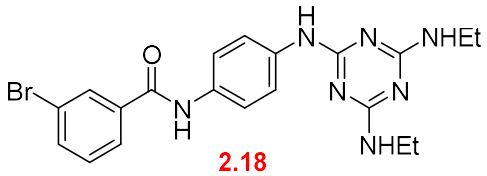

2.18

General procedure 3 was followed using ethylamine hydrochloride (74.5 mg, 0.91 mmol), 3-bromo-*N*-(4-((4-chloro-6-(ethylamino)-1,3,5-triazin-2-yl)amino)phenyl)benzamide **2.10** (101 mg, 0.22 mmol), and Cs_2CO_3 (151 mg, 0.44 mmol) in dioxane (1.5 mL). After stirring at 50 °C for 2 days, the reaction was monitored by TLC (hexanes:EtOAc 2:3; UV). *N*-(4-((4,6-Bis(ethylamino)-1,3,5-triazin-2-yl)amino)phenyl)-3-bromobenzamide **2.18** was obtained as a colorless solid (81.0 mg, 0.18 mmol, 81% yield). ^{1}H NMR (396 MHz, DMSO-d6) δ 10.19 (s, 1H), 9.13 – 8.55 (m, 1H), 8.13 (s, 1H), 7.94 (d, J = 7.8 Hz, 1H), 7.85 – 7.67 (m, 3H), 7.59 (d, J = 8.7 Hz, 2H), 7.49 (t, J = 7.9 Hz, 1H), 6.97 – 6.51 (m, 2H), 3.35 – 3.21 (m, 4H), 1.10 (t, J = 6.8 Hz, 6H); ^{13}C NMR (100 MHz, DMSO-d6) δ 165.6, 165.4, 164.0, 163.4, 137.2, 137.1, 134.1, 132.3, 130.6, 130.1, 126.7, 121.6, 120.7, 119.4, 34.7, 15.1; HRMS calcd for $C_{20}H_{23}N_7O^{79}Br$ (M+ H^+) 456.1147; found 456.1146; IR (KBr, cm^{-1}) υ_{max} 3397, 3275, 2972, 2932, 1645, 1611, 1578, 1510; mp: dec.

3-Bromo-*N*-(4-((4-(ethylamino)-6-((2-hydroxyethyl)thio)-1,3,5-triazin-2-yl)amino)phenyl)benzamide (2.21)

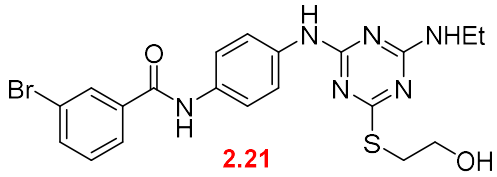

2.21

General procedure 3 was followed using 2-mercaptoethanol (42 µL, 0.60 mmol), 3-bromo-*N*-(4-((4-chloro-6-(ethylamino)-1,3,5-triazin-2-yl)amino)phenyl)benzamide **2.10** (134 mg, 0.30 mmol), and Cs_2CO_3 (98.3 mg, 0.30 mmol) in dioxane (2 mL). After stirring at 80 °C for 2 days, the reaction was monitored by TLC (hexanes:EtOAc 2:3; UV). 3-Bromo-*N*-(4-((4-(ethylamino)-6-((2-hydroxyethyl)thio)-1,3,5-triazin-2-yl)amino)phenyl)benzamide **2.21** was obtained as a colorless solid (116 mg, 0.24 mmol, 79% yield). ^{1}H NMR[a] (396 MHz, DMSO-d6) δ 10.26 (s, 1H), 9.53, and 9.42 (2 br s, 1H), 8.13 (s, 1H), 7.95 (d, J = 7.8 Hz, 1H), 7.77 (d, J = 7.8 Hz, 1H), 7.74 – 7.60 (m, 4H), 7.50 (t, J = 7.9 Hz, 1H), 4.94 – 4.89 (m, 1H), 3.68 – 3.60 (m, 2H), 3.39 – 3.28 (m, 2H), 3.15 (t, J = 6.6 Hz, 2H), 2.87 – 2.76 (m, 1H), 1.19 – 1.07 (m, 3H); ^{13}C NMR[a] (100 MHz, DMSO-d6) δ 178.7, 178.2, 163.9, 163.7, 163.6, 162.5, 162.2, 137.2, 135.8, 134.1, 133.3, 130.6, 130.2, 126.8, 121.7, 120.7, 120.0, 34.9, 23.4, 23.2, 15.1, 14.8, 14.5; HRMS calcd for $C_{20}H_{22}N_6O_2S^{79}Br$ ($M+ H^+$) 489.0708; found 489.0704; IR (KBr, cm-1) υ_{max} 3277, 3059, 2968, 2930, 1686, 1655, 1578, 1560, 1508; mp: dec.

[a]The compound exists as a mixture of rotamers.

3-Bromo-*N*-(4-((4-(ethylamino)-6-(ethylthio)-1,3,5-triazin-2-yl)amino)phenyl)benzamide (2.22)

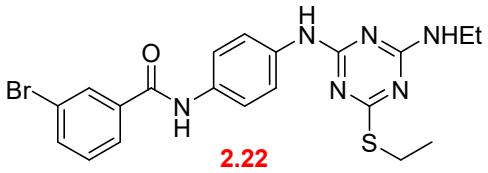

2.22

General procedure 3 was followed using ethanethiol (64 μL, 0.88 mmol), 3-bromo-*N*-(4-((4-chloro-6-(ethylamino)-1,3,5-triazin-2-yl)amino)phenyl)benzamide **2.10** (101 mg, 0.22 mmol), and Cs_2CO_3 (80 mg, 0.22 mmol) in dioxane (1.5 mL). After stirring at 80 °C for 5 days, the reaction was monitored by TLC (hexanes:EtOAc 1:1; UV). 3-Bromo-*N*-(4-((4-(ethylamino)-6-(ethylthio)-1,3,5-triazin-2-yl)amino)phenyl)benzamide **2.22** was obtained as a colorless solid (65.7 mg, 0.14 mmol, 63% yield). ^{1}H NMR[a] (396 MHz, DMSO-d6) δ 10.26 (s, 1H), 9.52, and 9.41 (2 br s, 1H), 8.14 (s, 1H), 7.95 (d, J = 7.9 Hz, 1H), 7.78 (d, J = 8.1 Hz, 1H), 7.75 – 7.60 (m, 4H), 7.49 (t, J = 7.9 Hz, 1H), 3.38 – 3.27 (m, 2H), 3.08 – 3.00 (m, 2H), 1.31 (q, J = 7.2 Hz, 3H), 1.13 (q, J = 7.1 Hz, 3H); ^{13}C NMR[a] (100 MHz, DMSO-d6) δ 164.1, 163.9, 163.8, 162.6, 162.4, 137.4, 136.0, 136.0, 134.4, 133.6, 133.5, 130.8, 130.4, 127.0, 121.9, 120.9, 120.2, 60.5, 41.4, 35.1, 32.1, 31.9, 15.0, 14.8; HRMS calcd for $C_{20}H_{22}N_6OS^{79}Br$ (M+ H^+) 473.0759; found 473.0768; IR (KBr, cm^{-1}) υ_{max} 3397, 3273, 3138, 2970, 2928, 1643, 1616, 1547, 1510; mp: dec.

[a]The compound exists as a mixture of rotamers.

***tert*-Butyl piperazine-1-carboxylate (2.31)**

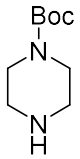

2.31

An aqueous solution of NaOH (2 M, 12.5 mL) was added dropwise to a solution of piperazine hexahydrate **2.30** (12.16 g, 62.5 mmol) and di-*tert*-butyl dicarbonate (Boc_2O; 4.86 g, 25 mmol) in *tert*-butyl alcohol (75 mL). The mixture was stirred at ambient temperature for 12 hours. Volatiles were evaporated under reduced pressure. Water was added, solids were removed by filtration, and the filtrate was extracted with DCM 3 times. The combined organic layers were dried (Na_2SO_4) and evaporated under reduced pressure to give *tert*-butyl piperazine-1-carboxylate **2.31** as a white solid (3.45 g, 18.5 mmol, 74% yield). ^{1}H NMR (400 MHz, $CDCl_3$) δ 3.56 – 3.28 (m, 4H), 2.92 – 2.70 (m, 4H), 1.46 (s, 9H). The ^{1}H NMR is in agreement with those reported before.[18]

General procedure 4: reductive amination of *tert*-butyl piperazine-1-carboxylate with aldehydes

tert-butyl piperazine-1-carboxylate **2.31** (1 eq.), and the aldehyde (1 – 4 eq.) were dissolved in MeOH (2 mL/1 mmol of **2.31**). NaOAc (2.2 eq.) and 10% Pd/C (10% wt of starting material) were added. The mixture was stirred under hydrogen (1 atm) at ambient temperature. After the completion, the mixture was filtered through celite. The filtrate was evaporated under reduced pressure. Water was added, and the solution was basified to pH 10 with a 2 M aqueous NaOH solution. The solution was extracted with DCM 3 times. The combined organic layers were washed with water and brine, followed by evaporation under reduced pressure.

***tert*-Butyl 4-propylpiperazine-1-carboxylate (2.32)**

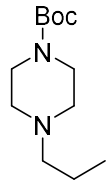

2.32

General procedure 4 was followed using *tert*-butyl piperazine-1-carboxylate **2.31** (378 mg, 2 mmol), propionaldehyde (0.290 mL, 4 mmol), 10% Pd/C (38.4 mg), and anhydrous NaOAc (366 mg, 4.4 mmol) in MeOH (4 mL). After stirring at ambient temperature under hydrogen for 2 days, the reaction was monitored by TLC (EtOAc; $KMnO_4$). *tert*-Butyl 4-propylpiperazine-1-carboxylate **2.32** was obtained as yellow liquid (477 mg, quantitative). ^{1}H NMR (400 MHz, $CDCl_3$) δ 3.47 – 3.37 (m, 4H), 2.42 – 2.33 (m, 4H), 2.32 – 2.25 (m, 2H), 1.53 (sex, J = 7.6 Hz, 2H), 1.46 (s, 9H), 0.90 (t, J = 7.4 Hz, 3H). The ^{1}H NMR is in agreement with those reported before.[35]

***tert*-Butyl 4-isopropylpiperazine-1-carboxylate (2.33)**

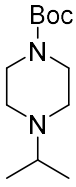

2.33

General procedure 4 was followed using *tert*-butyl piperazine-1-carboxylate **2.31** (378 mg, 2 mmol), acetone (300 µL, 4 mmol), 10% Pd/C (40.0 mg), and anhydrous NaOAc (366 mg, 4.4 mmol) in MeOH (4 mL). After stirring at ambient temperature under hydrogen for 2 days, the reaction was monitored by TLC (EtOAc; $KmnO_4$). *tert*-Butyl 4-isopropylpiperazine-1-carboxylate **2.33** was obtained as yellow liquid (417 mg, 91% yield). ^{1}H NMR (400 MHz, $CDCl_3$) δ 3.46 – 3.36 (m, 4H), 2.70 (sep, J = 6.5 Hz, 1H), 2.52 – 2.37 (m, 4H), 1.46 (s, 9H), 1.04 (d, J = 6.5 Hz, 6H); ^{13}C NMR (100 MHz, $CDCl_3$) δ 154.8, 79.6, 54.7, 48.5, 44.0, 28.5,

18.4; HRMS calcd for $C_{12}H_{25}N_2O_2$ (M+ H^+) 229.1916; found 229.1920; IR (ATR, cm^{-1}) υ_{max} 3266, 2973, 2933, 2862, 2814, 1695.

tert-Butyl 4-hexylpiperazine-1-carboxylate (2.34)

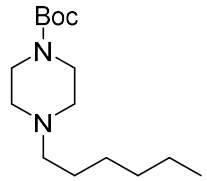

2.34

General procedure 4 was followed using *tert*-butyl piperazine-1-carboxylate **2.31** (377 mg, 2 mmol), *n*-hexanal (250 µL, 2 mmol), 10% Pd/C (39.0 mg), and anhydrous NaOAc (365 mg, 4.4 mmol) in MeOH (4 mL). After stirring at ambient temperature under hydrogen for 2 days, the reaction was monitored by TLC (EtOAc; $KMnO_4$). The crude mixture was purified by column chromatography on silica gel using EtOAc as an isocratic eluent to afford *tert*-butyl 4-hexylpiperazine-1-carboxylate **2.34** as yellow liquid (294 mg, 1.1 mmol, 55% yield). ^{1}H NMR (400 MHz, $CDCl_3$) δ 3.48 – 3.38 (m, 4H), 2.42 – 2.28 (m, 6H), 1.52 – 1.47 (m, 2H), 1.46 (s, 9H), 1.34 – 1.24 (m, 6H), 0.88 (t, J = 6.8 Hz, 3H); ^{13}C NMR (100 MHz, $CDCl_3$) δ 154.8, 79.6, 58.9, 53.1, 43.6, 31.8, 28.5, 27.3, 26.8, 22.6, 14.1; HRMS calcd for $C_{15}H_{31}N_2O_2$ (M+ H^+) 271.2386; found 271.2401; IR (ATR, cm^{-1}) υ_{max} 2957, 2929, 2810, 2774, 1696.

***tert*-Butyl 4-(cyclohexylmethyl)piperazine-1-carboxylate (2.35)**

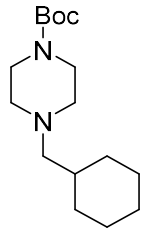

2.35

General procedure 4 was followed using *tert*-butyl piperazine-1-carboxylate **2.31** (374 mg, 2 mmol), cyclohexanecarboxaldehyde (225 mg, 2 mmol), 10% Pd/C (39.8 mg), and anhydrous NaOAc (368 mg, 4.4 mmol) in MeOH (4 mL). After stirring at ambient temperature under hydrogen for 2 days, the reaction was monitored by TLC (EtOAc; KMnO4). The crude mixture was purified by column chromatography on silica gel using EtOAc as an isocratic eluent to afford *tert*-butyl 4-(cyclohexylmethyl)piperazine-1-carboxylate **2.35** as yellow liquid (268 mg, 47% yield). ^{1}H NMR (400 MHz, $CDCl_3$) δ 3.55 – 3.33 (m, 4H), 2.45 – 2.25 (m, 4H), 2.14 (d, *J* = 7.0 Hz, 2H), 1.83 – 1.59 (m, 5H), 1.46 (s, 9H), 1.33 – 1.11 (m, 4H), 1.01 – 0.77 (m, 2H); ^{13}C NMR (100 MHz, $CDCl_3$) δ 155.0, 79.7, 65.7, 53.6, 43.8, 35.0, 32.0, 28.6, 26.9, 26.3; HRMS calcd for $C_{16}H_{31}N_2O_2$ (M+ H^+) 283.2386; found 283.2376; IR (ATR, cm^{-1}) υ_{max} 2973, 2921, 2854, 2806, 2770, 1694.

***tert*-Butyl 4-benzylpiperazine-1-carboxylate (2.36)**

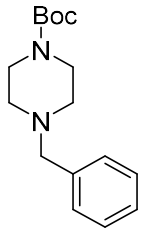

2.36

General procedure 4 was followed using *tert*-butyl piperazine-1-carboxylate **2.31** (373 mg, 2 mmol), benzaldehyde (205 mL, 2 mmol), 10% Pd/C (37.0 mg), and anhydrous NaOAc (363 mg, 4.4 mmol) in MeOH (4 mL). After stirring at ambient temperature under hydrogen for 2 days, the reaction was monitored by TLC (EtOAc; $KMnO_4$). The crude mixture was purified by column chromatography on silica gel using EtOAc as an isocratic eluent to afford *tert*-butyl 4-(cyclohexylmethyl)piperazine-1-carboxylate **2.36** as a yellow liquid (261 mg, 47% yield). ^{1}H NMR (396 MHz, $CDCl_3$) δ 7.37 (d, J = 4.6 Hz, 2H), 7.32 (m, 3H), 3.51 (s, 2H), 3.46 – 3.37 (m, 4H), 2.44 – 2.33 (m, 4H), 1.45 (s, 9H). The ^{1}H NMR is in agreement with those reported before.[36]

General procedure 5: nucleophilic aromatic substitution of chlorotriazine with Boc-protected alkyl piperazine

Boc-protected alkyl piperazine **2.32** – **2.36** (1.5 eq.) was dissolved in TFA/DCM (1:1, 0.5 mL/1 mmol of Boc-protected alkyl piperazine). The solution was stirred for 1 hour, followed by evaporation to dryness to give the TFA salt. The residue was redissolved together with 3-bromo-*N*-(4-((4-chloro-6-(ethylamino)-1,3,5-triazin-2-yl)amino)phenyl)benzamide **2.10** (1 eq.) in dioxane (6.5 mL/1 mmol of **2.10**). Cs_2CO_3 (3 – 4 eq.) was added to the solution. The reaction was stirred at room temperature. After the completion, the reaction mixture was poured into water, followed by filtration to collect the desired product.

3-Bromo-*N*-(4-((4-(ethylamino)-6-(4-propylpiperizin-1-yl)-1,3,5-triazin-2-yl)amino)phenyl)benzamide (2.25)

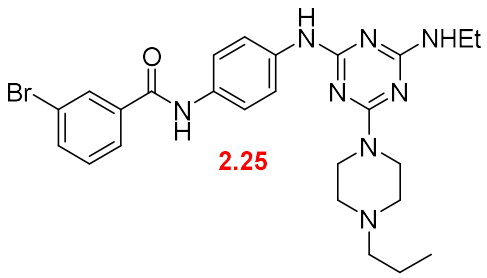

General procedure 5 was followed using *tert*-butyl 4-propylpiperazine-1-carboxylate **2.32** (81.9 mg, 0.33 mmol) and TFA/DCM (1:1, 1 mL). After evaporation to dryness, the coupling step was performed using the residue, 3-bromo-*N*-(4-((4-chloro-6-(ethylamino)-1,3,5-triazin-2-yl)amino)phenyl)benzamide **2.10** (103 mg, 0.22 mmol), and Cs_2CO_3 (295 mg, 0.91 mmol) in dioxane (1.5 mL). The mixture was stirred at room temperature for 2 days. The reaction was indicated the completion by TLC (hexanes:EtOAc 1:1; UV) to afford 3-bromo-*N*-(4-((4-(ethylamino)-6-(4-propylpiperizin-1-yl)-1,3,5-triazin-2-yl)amino)phenyl)benzamide **2.25** as a colorless solid (85.5 mg, 71% yield). ^{1}H NMR[a] (396 MHz, DMSO-d6) δ 10.23 (s, 1H), 8.98, and 8.83 (2 br s, 1H, rotamer), 8.11 (s, 1H), 7.93 (d, J = 7.4 Hz, 1H), , 7.77 (d, J = 7.8 Hz, 1H), 7.69 (d, J = 8.7 Hz, 2H), 7.60 (d, J = 8.5 Hz, 2H), 7.48 (t, J = 7.7 Hz, 1H), 6.83 (br s, 1H), 3.69 (s, 4H), 3.29 (s, 2H), 2.37 (s, 4H), 2.25 (t, J = 7.3 Hz, 2H), 1.45 (sextet, J = 7.3 Hz, 2H), 1.10 (t, J = 7.0 Hz, 3H), 0.85 (t, J = 7.3 Hz, 3H); ^{13}C NMR[a] (100 MHz, DMSO-d6) δ 165.9, 165.7, 164.8, 164.7, 164.3, 164.2, 164.0, 137.4, 137.1, 134.5, 132.7, 131.0, 130.4, 127.0, 122.0, 121.2, 119.9, 60.1, 52.8, 42.8, 35.1, 19.5, 15.3, 12.1; HRMS calcd for $C_{25}H_{32}N_8O^{79}Br$ (M+ H^+) 539.1882; found 539.1890; IR (KBr, cm^{-1}) υ_{max} 3418, 3294, 3067, 2955, 2928, 2859, 1655, 1585, 1543, 1508, 1420; mp: dec.

[a]The compound exists as a mixture of rotamers.

3-Bromo-*N*-(4-((4-(ethylamino)-6-(4-isopropylpiperizin-1-yl)-1,3,5-triazin-2-yl)amino)phenyl)benzamide (2.26)

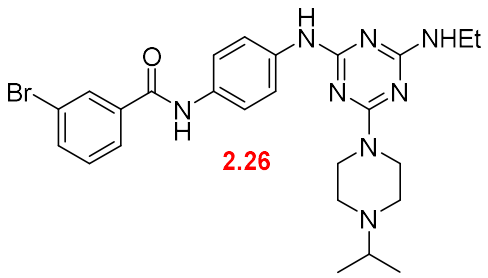

General procedure 5 was followed using *tert*-butyl 4-isopropylpiperazine-1-carboxylate **2.33** (77.6 mg, 0.33 mmol) and TFA/DCM (1:1, 1 mL). After evaporation to dryness, the coupling step was performed using the residue, 3-bromo-*N*-(4-((4-chloro-6-(ethylamino)-1,3,5-triazin-2- yl)amino)phenyl)benzamide **2.10** (101 mg, 0.22 mmol), and Cs_2CO_3 (299 mg, 0.92 mmol) in dioxane (1.5 mL). The mixture was stirred at room temperature for 2 days. The reaction was indicated the completion by TLC (hexanes:EtOAc 1:1; UV) to afford 3-bromo-*N*-(4-((4-(ethylamino)-6-(4-isopropylpiperizin-1-yl)-1,3,5-triazin-2-yl)amino)phenyl)benzamide **2.26** as a colorless solid (42.7 mg, 36% yield). ^{1}H NMR (396 MHz, $CDCl_3$) δ 8.06 (s, 1H), 7.94 (s, 1H), 7.71 (d, J = 6.6 Hz, 1H), 7.59 (d, J = 7.1 Hz, 1H), 7.49 (s, 4H), 7.36 – 6.96 (m, 2H), 5.04 (br s, 1H), 3.78 (s, 4H), 3.38 (s, 2H), 2.68 (s, 1H), 2.50 (s, 4H), 1.15 (s, 3H), 1.04 (s, 6H); ^{13}C NMR (100 MHz, $CDCl_3$) δ 166.1, 164.9, 164.4, 137.1, 136.7, 134.7, 132.2, 130.3, 125.8, 122.9, 121.2, 120.4, 54.7, 48.7, 43.5, 35.7, 18.6, 15.2; HRMS calcd for $C_{25}H_{32}N_8O^{79}Br$ ($M+ H^+$) 539.1882; found 539.1870; IR (KBr, cm^{-1}) υ_{max} 3422, 3298, 2967, 2932, 2924, 1655, 1582, 1543, 1508, 1420; mp: dec.

3-Bromo-*N*-(4-((4-(ethylamino)-6-(4-hexylpiperizin-1-yl)-1,3,5-triazin-2-yl)amino)phenyl)benzamide (2.27)

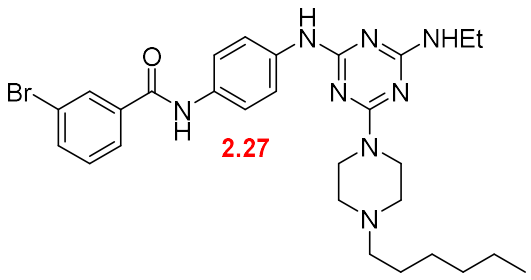

General procedure 5 was followed using *tert*-butyl 4-hexylpiperazine-1-carboxylate **2.34** (94.3 mg, 0.33 mmol) and TFA/DCM (1:1, 1 mL). After evaporation to dryness, the coupling step was performed using the residue, 3-bromo-*N*-(4-((4-chloro-6-(ethylamino)-1,3,5-triazin-2-yl)amino)phenyl)benzamide **2.10** (104 mg, 0.22 mmol), and Cs_2CO_3 (298 mg, 0.92 mmol) in dioxane (1.5 mL). The mixture was stirred at room temperature for 2 days. The reaction was indicated the completion by TLC (hexanes:EtOAc 1:1; UV) to afford 3-bromo-*N*-(4-((4-(ethylamino)-6-(4-hexylpiperizin-1-yl)-1,3,5-triazin-2-yl)amino)phenyl)benzamide **2.27** as a colorless solid (100 mg, 77% yield). ^{1}H NMR[a] (396 MHz, DMSO-d6) δ 10.23 (s, 1H), 8.96, and 8.82 (2 br s, 1H, rotamer), 8.10 (s, 1H), 7.94 (d, J = 7.9 Hz, 1H), 7.77 (d, J = 8.1 Hz, 1H), 7.69 (d, J = 8.9 Hz, 2H), 7.59 (d, J = 8.7 Hz, 2H), 7.48 (t, J = 7.9 Hz, 1H), 6.82 (br s, 1H), 3.68 (s, 4H), 3.36 – 3.19 (m, 2H), 2.36 (s, 4H), 2.27 (t, J = 7.3 Hz, 2H), 1.33 – 1.16 (m, 8H), 1.09 (t, J = 7.1 Hz, 3H), 0.84 (t, J = 6.6 Hz, 3H); ^{13}C NMR[a] (100 MHz, DMSO-d6) δ 165.9, 165.8, 164.9, 164.8, 164.3, 164.1, 137.4, 137.2, 134.5, 132.7, 131.0, 130.4, 127.0, 122.0, 121.2, 119.9, 66.7, 61.0, 58.3, 52.9, 51.8, 42.8, 35.1, 31.5, 26.9, 26.3, 22.4, 15.3, 14.3; HRMS calcd for $C_{28}H_{38}N_8O^{79}Br$ (M+ H^+) 581.2352; found 581.2333; IR (KBr, cm^{-1}) υ_{max} 3418, 3294, 3067, 2955, 2928, 2859, 1655, 1585, 1543, 1508, 1420; mp: dec.

[a]The compound exists as a mixture of rotamers.

3-Bromo-*N*-(4-((4-(4-(cyclohexylmethyl)piperizin-1-yl)-6-(ethylamino)-1,3,5-triazin-2-yl)amino)phenyl)benzamide (2.28)

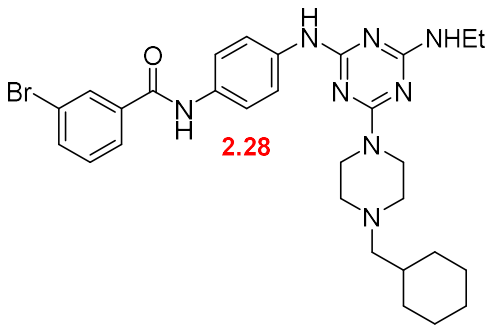

General procedure 5 was followed using *tert*-butyl 4-(cyclohexylmethyl)piperazine-1-carboxylate **2.35** (94.3 mg, 0.33 mmol) and TFA/DCM (1:1, 1 mL). After evaporation to dryness, the coupling step was performed using the residue, 3-bromo-*N*-(4-((4-chloro-6-(ethylamino)-1,3,5-triazin-2-yl)amino)phenyl)benzamide **2.10** (100 mg, 0.22 mmol), and Cs_2CO_3 (300 mg, 0.92 mmol) in dioxane (1.5 mL). The mixture was stirred at room temperature for 4 days. The reaction was indicated the completion by TLC (hexanes:EtOAc 1:1; UV) to afford 3-bromo-*N*-(4-((4-(4- (cyclohexylmethyl)piperizin-1-yl)-6-(ethylamino)-1,3,5-triazin-2-yl)amino)phenyl) benzamide **2.28** as a colorless solid (106 mg, 81% yield). ^{1}H NMR (396 MHz, $CDCl_3$) δ 8.04 (s, 1H), 7.97 (s, 1H), 7.74 (d, J = 5.5 Hz, 1H), 7.62 (d, J = 6.5 , 1H), 7.52 (s, 4H), 7.36 – 7.22 (m, 1H), 7.16 (s, 1H), 5.03 (br s, 1H), 3.78 (s, 4H), 3.32 (s, 2H), 2.39 (s, 4H), 2.29 – 2.02 (m, 2H), 1.97 – 1.59 (m, 5H), 1.40 – 1.02 (m, 7H), 1.02 – 0.76 (m, 2H); ^{13}C NMR (100 MHz, $CDCl_3$) δ 166.1, 165.0, 164.4, 137.2, 136.7, 134.7, 132.1, 130.3, 125.7, 122.9, 121.2, 120.3, 65.9, 53.7, 43.3, 35.7, 35.1, 32.0, 26.9, 26.3, 15.2; HRMS calcd for $C_{29}H_{38}N_8O^{79}Br$ (M+ H^+) 593.2352; found 593.2344; IR (KBr, cm^{-1}) υ_{max} 3429, 2924, 2851, 1655, 1585, 1543, 1508, 1420; mp: dec.

***N*-(4-((4-(4-Benzylpiperizin-1-yl)-6-(ethylamino)-1,3,5-triazin-2-yl)amino)phenyl)-3-bromobenzamide (2.29)**

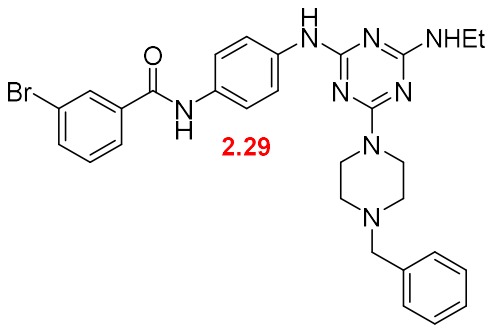

General procedure 5 was followed using *tert*-butyl 4-benzylpiperazine-1-carboxylate **2.36** (96.6 mg, 0.33 mmol) and TFA/DCM (1:1, 1 mL). After evaporation to dryness, the coupling step was performed using the residue, 3-bromo-*N*-(4-((4-chloro-6-(ethylamino)-1,3,5-triazin-2-yl)amino)phenyl)benzamide **2.10** (100 mg, 0.22 mmol), and Cs_2CO_3, (219 mg, 0.67 mmol) in dioxane (1.5 mL). The mixture was stirred at room temperature for 4 days. The reaction was indicated the completion by TLC (hexanes:EtOAc 1:1; UV) to afford *N*-(4-((4-(4-benzylpiperizin-1-yl)-6-(ethylamino)-1,3,5-triazin-2-yl)amino)phenyl)-3-bromobenzamide **2.29** as a colorless solid (81.0 mg, 62% yield). ^{1}H NMR (396 MHz, $CDCl_3$) δ 8.22 (s, 1H), 7.93 (s, 1H), 7.70 (d, *J* = 7.6 Hz, 1H), 7.57 (d, *J* = 7.8 Hz, 1H), 7.47 (s, 4H), 7.41 – 7.16 (m, 7H), 5.15 (br s, 1H), 3.78 (s, 4H), 3.51 (s, 2H), 3.38 (quin, *J* = 6.6 Hz, 2H), 2.44 (s, 4H), 1.15 (t, *J* = 7.1 Hz, 3H); ^{13}C NMR (100 MHz, $CDCl_3$) δ 166.0, 164.9, 164.5, 164.2, 137.8, 137.0, 136.7, 134.6, 132.1, 130.4, 130.2, 129.4, 128.4, 127.3, 125.8, 122.8, 121.3, 120.3, 63.2, 53.0, 43.2, 35.7, 15.1; HRMS calcd for $C_{29}H_{32}N_8O^{79}Br$ (M+ H^+) 587.1882; found 587.1870. IR (KBr, cm^{-1}) υ_{max} 3418, 3294, 2970, 2932, 2812, 2770, 1655, 1582, 1543, 1508, 1420; mp: dec.

***tert*-Butyl (4-nitrophenyl)carbamate (2.42)**

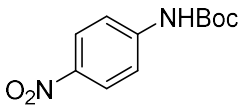

2.42

Di-*tert*-butyl decarbonate **2.2** (5.70 g, 26.1 mmol) was added gradually to a solution of *p*-nitroaniline (1.38 g, 10 mmol) and *N*,*N*-dimethylaminopyridine (126 mg, 1 mmol) in THF (50 mL). The mixture was stirred at ambient temperature for 4 days. Volatiles were evaporated under reduced pressure. The residue was redissolved in DCM and filtered through silica. The filtrate was evaporated to dryness. The residue was redissolved in DCM (50 mL), and concentrated HCl solution (35% wt/v, 2 mL) was added dropwise at 0 °C. The mixture was stirred at 0 °C for 3 hours. After completion, as indicated by TLC (hexanes:EtOAc 3:1; UV), the mixture was washed with 0.1 M aqueous HCl twice. The combined organic layers were dried over Na_2SO_4 and evaporated. The residue was purified by column chromatography on silica gel using DCM/hexanes (1:1) as isocratic eluent to afford *tert*-butyl (4-nitrophenyl)carbamate **2.42** as a yellow solid (1.06 g, 44% yield). ^{1}H NMR (400 MHz, DMSO-d6) δ 10.08 (s, 1H), 8.14 (d, *J*= 9.3 Hz, 2H), 7.65 (d, *J* = 9.3 Hz, 2H), 1.46 (s, 9H). The ^{1}H NMR is in agreement with those reported before.[20]

***tert*-Butyl (4-aminophenyl)carbamate (2.43)**

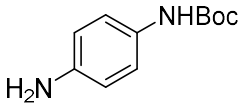

2.43

A mixture of *tert*-butyl (4-nitrophenyl)carbamate **2.42** (959 mg, 4.03 mmol) and 10% Pd/C (97.9 mg) in MeOH (20 mL) was stirred vigorously under hydrogen at ambient temperature for 12 hours. The reaction was monitored by TLC (hexanes:EtOAc 1:1; UV). The mixture was filtered through celite, and the MeOH was evaporated to afford *tert*-butyl (4-aminophenyl)

carbamate **2.43** as a red solid (827 mg, 99% yield). ^{1}H NMR (400 MHz, DMSO-d6) δ 8.76 (s, 1H), 7.05 (d, *J* = 7.5 Hz, 2H), 6.45 (d, *J* = 8.7 Hz, 2H), 4.72 (s, 2H), 1.43 (s, 9H). The ^{1}H NMR is in agreement with those reported before.[37]

General procedure 6: reaction of anilines with dichlorotriazine

A solution of the *N*-(4-aminophenyl)benzamide (1 eq.), 4,6-dichloro-*N*-ethyl1,3,5-triazin-2-amine **2.9** (1 eq.), and *N*,*N*-Diisopropylethylamine (DIPEA, 1 eq.) was heated at reflux in dioxane (5 mL/1 mmol of **2.9**) for 1.5-2 hours. When TLC indicated completion, the mixture was allowed to cool to room temperature, then filtered to give the product.

***tert*-Butyl (4-((4-chloro-6-(ethylamino)-1,3,5-triazin-2-yl)amino)phenyl)carbamate (2.40)**

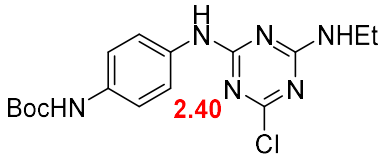

General procedure 6 was followed using *tert*-butyl (4-aminophenyl)carbamate **2.43** (301 mg, 1.44 mmol), 4,6-dichloro-*N*-ethyl-1,3,5-triazin-2-amine **2.9** (278 mg, 1.44 mmol), and DIPEA (250 µL, 1.44 mmol) in dioxane (5 mL). After stirring at ambient temperature for 1.5 hours, the reaction was proceeded to completion as indicated by TLC (hexanes:EtOAc 1:1; UV). After the filtration, the precipitate was washed with water to afford *tert*-butyl (4-((4-chloro-6-(ethylamino)-1,3,5-triazin-2-yl)amino)phenyl)carbamate **2.40** as a beige solid (485 mg, 92% yield). ^{1}H NMR[a] (400 MHz, DMSO-d6) δ 10.09, 9.92 and 9.77 (3 br s, 1H, rotamer), 9.30 – 9.18 (m, 1H), 8.08 and 7.97 (2 br s, 1H, rotamer), 7.79 – 7.16 (m, 4H), 3.50 – 3.08 (m, 2H), 1.46 (s, 9H), 1.17 – 1.00 (m, 3H); ^{13}C NMR[a] (100 MHz, DMSO-d6) δ 168.4, 167.6, 165.2, 164.9, 163.7, 163.4, 163.1, 152.8, 135.4, 134.8, 133.4, 132.6, 121.5, 120.7, 120.4, 118.3, 78.9, 66.4, 35.7, 35.4, 35.1, 28.2, 14.6, 14.2, 13.8; HRMS calcd for $C_{16}H_{22}N_6O_2{}^{35}Cl$ (M+ H^+)

365.1493; found 365.1476; IR (ATR, cm^{-1}) υ_{max} 3262, 3117, 2980, 2933, 1691, 1678, 1580, 1512, 1412; mp: dec.

[a] This compound exists as a mixture of rotamers.

***tert*-Butyl (4-((4-(ethylamino)-1,3,5-triazin-2-yl)amino)phenyl)carbamate (2.41)**

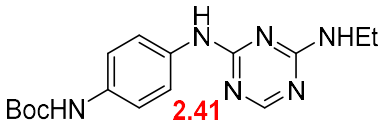

10% Pd/C (97.9 mg) and K_2CO_3 (136 mg) were added to solution of *tert*-butyl (4-((4-chloro-6- (ethylamino)-1,3,5-triazin-2-yl)amino)phenyl)carbamate **2.40** (351 mg, 0.96 mmol) in MeOH (10 mL). The mixture was stirred vigorously under hydrogen at ambient temperature. After completion as indicated by TLC (hexanes:EtOAc 1:1; UV), the mixture was filtered through celite and the volatiles were evaporated. The residue was redissolved in EtOAc and washed with water 3 times and brine. The organic phase was dried over Na_2SO_4 and evaporated under reduced pressure. The crude mixture was purified by column chromatography on silica gel using gradient eluent starting from hexanes:EtOAc (3:7) to MeOH to afford *tert*-butyl (4-((4-(ethylamino)-1,3,5-triazin-2-yl)amino)phenyl)carbamate **2.41** as a dull white solid (98.2 mg, 32% yield). ^{1}H NMR[a] (396 MHz, DMSO-d6) δ 9.40 and 9.30 (2 br s, 1H, rotamer), 9.18 (br s, 1H), 8.16 and 8.06 (2 br s, 1H, rotamer), 7.59 (br s, 2H), 7.33 (br s, 2H), 3.40 – 3.12 (m, 2H), 1.46 and 1.44 (2 s, 9H), 1.30 – 0.97 (m, 3H); ^{13}C NMR[a] (100 MHz, DMSO-d6) δ 165.8, 165.4, 164.6, 163.4, 163.1, 152.9, 134.2, 120.5, 118.4, 78.8, 34.9, 34.8, 28.2, 14.8, 14.4; HRMS calcd for $C_{16}H_{23}N_6O_2$ (M+ H^+) 331.1882; found 331.1873. IR (ATR, cm^{-1}) υ_{max} 3262, 3116, 2981, 2933, 1693, 1620, 1580, 1535, 1514, 1412; mp: dec.

[a] This compound exists as a mixture of rotamers.

3-Bromo-*N*-(4-((4-(ethylamino)-1,3,5-triazin-2-yl)amino)phenyl)benzamide (2.37)

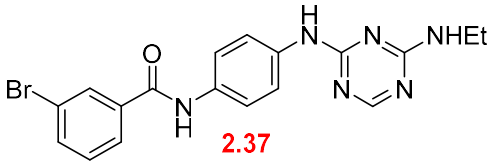

2.37

tert-Butyl (4-((4-(ethylamino)-1,3,5-triazin-2-yl)amino)phenyl)carbamate **2.41** (60.2 mg, 0.18 mmol) was dissolved in TFA/DCM (1:1, 1 mL). The solution was stirred for 30 minutes followed by evaporation to dryness to give the TFA salt. The residue was redissolved in anhydrous THF (1.5 mL). In separate container, *m*-bromobenzoic acid (36.5 mg, 0.18 mmol) was suspended in anhydrous DCM (1 mL). Anhydrous DMF was then added (0.05 mL) following by dropwise addition of oxalyl chloride (20 µL, 0.22 mmol) over 15 minutes. The mixture was stirred at room temperature for 1 hour with exclusion of moisture. The volatiles were evaporated under reduced pressure. The crude mixture was redissolved in anhydrous THF (2 mL) and added together with K_2CO_3 (77.8 mg, 0.55 mmol) to the solution of the TFA salt. The mixture was stirred at ambient temperature with exclusion of moisture for 1 day. After completion as indicated by TLC (hexanes:EtOAc 1:1; UV), the volatiles were evaporated and water was added. The mixture was filtered and the precipitate was washed with THF to afford 3-bromo-*N*-(4-((4-(ethylamino)-1,3,5-triazin-2-yl)amino)phenyl)benzamide **2.37** as a colorless solid (44.1 mg, 59% yield). ^{1}H NMR[a] (400 MHz, DMSO-d6) δ 10.28 (s, 1H), 9.55, and 9.46 (2 br s, 1H, rotamer), 8.27 – 8.04 (m, 2H), 7.95 (d, J = 7.6 Hz, 1H), 7.79 (d, J = 7.9 Hz, 1H), 7.72 (d, J = 8.5 Hz, 2H), 7.66 (d, J = 8.7 Hz, 2H), 7.60 (br s, 1H), 7.50 (t, J = 7.8 Hz, 1H), 3.50 – 3.15 (m, 2H), 1.17 – 1.08 (m, 3H); ^{13}C NMR[a] (100 MHz, DMSO-d6) δ 165.8, 165.4, 164.7, 164.6, 163.6, 163.4, 163.1, 137.2, 135.8, 134.1, 133.3, 130.6, 130.2, 126.8, 121.7, 120.7, 120.0, 34.9, 34.8, 14.8, 14.4; HRMS calcd for $C_{18}H_{18}N_6O^{79}Br$ (M+ H^+) 413.0725; found 413.0728; IR (ATR, cm^{-1}) υ_{max} 3273, 3238, 3096, 3016, 2977, 2874, 1641, 1547, 1514, 1421, 1403; mp: dec.

[a] This compound exists as a mixture of rotamers.

3-Bromo-*N*-(3-nitrophenyl)benzamide (2.45)

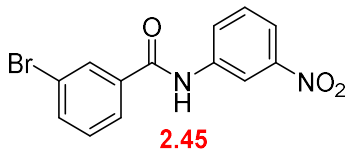

2.45

General procedure 1 was followed using *m*-bromobenzoic acid **2.1** (1.61 g, 8 mmol), oxalyl chloride (850 µL, 9.6 mmol), and anhydrous DMF (50 µL) in anhydrous DCM (8 mL). The resulting acid chloride was coupled to *m*-nitroaniline **2.44** (1.11 g, 8 mmol) using K_2CO_3 (2.22 g, 16 mmol) in anhydrous THF (12 mL). After completion, as indicated by TLC (hexanes:EtOAc 1:1; UV), THF was evaporated and aqueous solution of 2 M HCl was added to the crude reaction. The precipitate **2.45** was collected by filtration, following by washing with water to obtain 3-bromo-*N*-(3-nitrophenyl)benzamide **2.45** as a yellow solid (2.34 g, 91% yield). ^{1}H NMR (396 MHz, DMSO-d6) δ 10.74 (s, 1H), 8.76 (s, 1H), 8.29 – 8.05 (m, 2H), 8.02 – 7.94 (m, 2H), 7.80 (d, J = 7.5 Hz, 1H), 7.63 (t, J = 8.2 Hz, 1H), 7.51 (t, J = 7.9 Hz, 1H); ^{13}C NMR (100 MHz, DMSO-d6) δ 164.4, 147.8, 140.1, 136.3, 134.7, 130.7, 130.3, 130.0, 127.0, 126.2, 121.8, 118.3, 114.4; HRMS calcd for $C_{13}H_{10}N_2O_3{}^{79}Br$ (M+ H^+) 320.9875; found 320.9844; IR (ATR, cm^{-1}) υ_{max} 3314, 3084, 1655, 1594, 1522, 1486, 1349, 1324, 1302; mp: 173 – 174 °C.

***N*-(3-Aminophenyl)-3-bromobenzamide (2.46)**

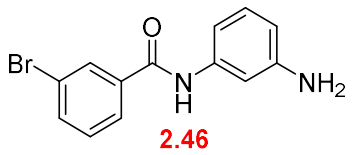

2.46

3-Bromo-*N*-(3-nitrophenyl)benzamide (**2.45**; 2.21 g, 6.87 mmol) was hydrogenated in EtOAc (15 mL) with sulfur poisoned platinum on carbon (10% wt, 221 mg), for two days under 100

psi of H_2 at 100 °C. The reaction was monitored by TLC (hexanes:EtOAc 1:1; UV). After work up, the crude mixture was purified by column chromatography on silica gel using hexanes:EtOAc (1:1) as isocratic eluent to afford *N*-(3-aminophenyl)-3-bromobenzamide **2.46** as an orange solid (1.04 g, 52% yield). ^{1}H NMR (400 MHz, DMSO-d6) δ 10.06 (s, 1H), 8.11 (t, *J* = 1.7 Hz, 1H), 7.93 (d, *J* = 8.3 Hz, 1H), 7.76 (ddd, *J* = 8.0, 2.0, 0.9 Hz, 1H), 7.47 (t, *J* = 7.9 Hz, 1H), 7.12 (t, *J* = 1.9 Hz, 1H), 6.98 (t, *J* = 7.9, 1H), 6.87 (d, *J* = 8.0 Hz, 1H), 6.35 (ddd, *J* = 7.9, 2.2, 1.0 Hz, 1H), 5.15 (br s, 2H); ^{13}C NMR (100 MHz, DMSO-d6) δ 163.7, 149.0, 139.5, 137.4, 134.0, 130.5, 130.2, 128.8, 126.8, 121.6, 110.0, 108.4, 106.2; HRMS calcd for $C_{13}H_{12}N_2O^{79}Br$ ($M+H^+$) 291.0133; found 291.0139; IR (ATR, cm^{-1}) υ_{max} 3449, 3358, 3247, 3211, 3139, 3068, 1647, 1609, 1585, 1542, 1492, 1454, 1440; mp: 154 – 156 °C.

General Procedure 7: amidation between benzoic acid and diamine species

To the corresponding benzoic acid (1 eq.) in DCM (1 mL/1 mmol of benzoic acid) was added dropwise oxalyl chloride (1.2 eq) in the presence of a catalytic amount of DMF. The mixture was stirred at room temperature for 1 hour, and the organic solvent was evaporated under reduced pressure. The residue was taken up in DCM (6 mL/1 mmol of benzoic acid). The solution of diamine species (4-10 eq.) in DCM (4 mL/1 mmol of **1**) was added dropwise by using a dropping funnel into the solution of the crude mixture, and the mixture was stirred for 16 hours at room temperature.

_N_-((_1r_,_4r_)-4-Aminocyclohexyl)-3-bromobenzamide (2.47)

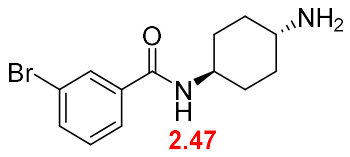

2.47

General procedure 7 was followed using *m*-bromobenzoic acid **2.1** (1.01 g, 5 mmol), oxalyl chloride (520 µL, 6 mmol), and anhydrous DMF (50 µL) in anhydrous DCM (5 mL). The resulting acid chloride was coupled to *trans*-1,4-diaminocyclohexane **2.50** (2.40 g, 20 mmol) in anhydrous DCM (50 mL). After stirring for 1 day, the mixture was washed with 2M aqueous NaOH, water (twice) and brine. The combined organic layers were dried (Na_2SO_4) and evaporated to give *N*-((*1r*,*4r*)-4-aminocyclohexyl)-3-bromobenzamide **2.47** as an orange solid (331 mg, 22% yield). ^{1}H NMR (400 MHz, DMSO-d6) δ 8.29 (d, *J* = 7.6 Hz, 1H), 7.98 (s, 1H), 7.80 (d, *J* = 7.8 Hz, 1H), 7.65 (d, *J* = 8.0 Hz, 1H), 7.37 (t, *J* = 7.9 Hz, 1H), 3.73 – 3.59 (m, 1H), 3.08 – 2.23 (m, 3H), 2.02 – 1.54 (m, 4H), 1.32 (q, *J* = 12.1 Hz, 2H), 1.07 (q, *J* = 11.7 Hz, 2H); ^{13}C NMR (100 MHz, DMSO-d6) δ 163.9, 136.9, 133.7, 130.4, 129.9, 126.4, 121.6, 49.7, 48.3, 35.0, 31.0; HRMS calcd for $C_{13}H_{18}N_2O^{79}Br$ ($M+ H^+$) 297.0602; found 297.0626; IR (ATR, cm^{-1}) υ_{max} 3290, 3076, 2937, 2862, 1629, 1540, 1471, 1451; mp: 147 – 149 °C.

(3-Bromophenyl)(piperizin-1-yl)methanone (2.48)

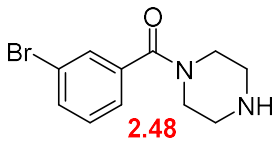

2.48

General procedure 7 was followed using *m*-bromobenzoic acid **2.1** (1.01 g, 5 mmol), oxalyl chloride (520 µL, 6 mmol), and anhydrous DMF (100 µL) in anhydrous DCM (5 mL). The resulting acid chloride was coupled to piperazine hexahydrate **2.51** (9.72 g, 50 mmol) in anhydrous DCM (50 mL). After stirring for 1 day, the mixture was washed with an aqueous solution of 2 M HCl. The aqueous phase was basified by concentrated $NaHCO_3$ solution and

extracted with EtOAc 3 times. The combined organic layers were washed with water twice, and brine followed by drying (Na_2SO_4) and evaporated to obtain (3-bromophenyl)(piperizin-1-yl)methanone **2.48** as a colorless solid (187 mg, 14% yield). ^{1}H NMR[a] (400 MHz, $CDCl_3$) δ 7.72 – 7.45 (m, 2H), 7.39 – 7.27 (m, 2H), 3.73 and 3.37 (2 br s, 4H, rotamer), 2.92 and 2.81 (2 br s, 4H, rotamer); ^{13}C NMR[a] (100 MHz, $CDCl_3$) δ 168.7, 137.9, 132.7, 130.2, 130.1, 125.6, 122.7, 49.0, 46.5, 45.9, 43.3; HRMS calcd for $C_{11}H_{14}N_2O^{79}Br$ (M+ H^+) 269.0289; found 269.0282; IR (ATR, cm^{-1}) υ_{max} 3302, 3088, 3064, 3008, 2953, 2917, 2818, 2751, 1620, 1562, 1432, 1412; mp: 80 – 82 °C.

[a] This compound exists as a mixture of rotamers

***N*-(2-Aminoethyl)-3-bromobenzamide (2.49)**

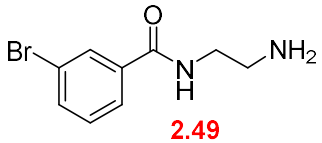

2.49

General procedure 7 was followed using *m*-bromobenzoic acid **2.1** (501 mg, 2.5 mmol), oxalyl chloride (260 µL, 3 mmol), and anhydrous DMF (50 µL) in anhydrous DCM (2.5 mL). The resulting acid chloride was coupled to ethylenediamine **2.52** (840 µL, 10 mmol) in anhydrous DCM (30 mL). After stirring for 1 day, the reaction mixture was washed with aqueous solution of 2 M NaOH, water (twice), and brine. The combined organic phase was dried over Na_2SO_4 and evaporated to obtain *N*-(2-aminoethyl)-3-bromobenzamide **2.49** as a colorless solid (142 mg, 23% yield). ^{1}H NMR[a] (396 MHz, DMSO-d6) δ 8.74 (br s, 1H), 8.03 (br s, 1H), 7.84 (br s, 1H), 7.71 (br s, 1H), 7.42 (br s, 1H), 6.60 (br s, 1H), 3.30 (br s, 2H), 3.12, and 2.74 (2 br s, 2H, rotamer); ^{13}C NMR[a] (100 MHz, DMSO-d6) δ 164.9, 164.7, 159.2, 136.8, 133.8, 130.5, 129.9, 126.4, 121.6, 42.1, 40.6; HRMS calcd for $C_9H_{12}N_2O^{79}Br$ (M+ H^+) 243.0133; found 243.0139; IR (ATR, cm^{-1}) υ_{max} 3350, 3290, 3064, 2937, 2877, 2552, 2481, 1633, 1595, 1538, 1474, 1452; mp: 135 – 138 °C.

[a] This compound exists as a mixture of rotamers.

General Procedure 8: Boc protection of diamine species

To the corresponding diamine species (10 eq.) in dichloromethane (10 mL/1 mmol of Boc_2O) was added dropwise di-*tert*-butyl dicarbonate (Boc_2O; 1 eq.) in chloroform (3 mL/1 mmol of Boc_2O) at 0 °C. The mixture was stirred at 0 °C, which was allowed to warm up to room temperature overnight. Then, the reaction was washed with water 8 times to remove an excessive amount of diamine. The organic phase was dried over Na_2SO_4 and evaporated.

***tert*-Butyl (2-aminoethyl)carbamate (2.55)**

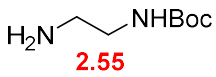

2.55

General procedure 8 was followed using ethylenediamine (**2.52**; 2.01 mL, 30 mmol) and di-*tert*-butyl dicarbonate (Boc_2O; 656 mg, 3 mmol) to obtain *tert*-butyl (2-aminoethyl)carbamate **2.55** as colorless liquid (239 mg, 50% yield). ^{1}H NMR (396 MHz, $CDCl_3$) δ 4.85 (br s, 1H), 3.17 (q, J = 5.8 Hz, 2H), 2.80 (t, J = 5.9 Hz, 2H), 1.45 (s, 9H), 1.34 (br s, 2H). The ^{1}H NMR is in agreement with those reported before.[38]

***tert*-Butyl (3-aminopropyl)carbamate (2.56)**

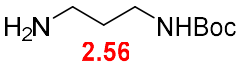

2.56

General procedure 8 was followed using propylenediamine (**2.53**; 2.50 mL, 30 mmol) and di-*tert*-butyl dicarbonate (Boc_2O; 658 mg, 3 mmol) to obtain *tert*-butyl (3-aminopropyl)carbamate **2.56** as colorless liquid (389 mg, 74% yield). ^{1}H NMR (396 MHz, $CDCl_3$) δ 4.88 (br s, 1H), 3.22 (q, J = 6.1 Hz, 2H), 2.77 (t, J = 6.6 Hz, 2H), 1.61 (quin, J = 6.6 Hz, 2H), 1.44 (s, 11H). The ^{1}H NMR is in agreement with those reported before.[39]

***tert*-Butyl (4-aminobutyl)carbamate (2.57)**

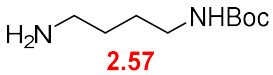

2.57

General procedure 8 was followed using 1,4-diaminobutane (**2.54**; 3.02 mL, 30 mmol) and di-*tert*-butyl dicarbonate (Boc_2O; 657 mg, 3 mmol) to obtain *tert*-butyl (4-aminobutyl)carbamate **2.57** as colorless liquid (512 mg, 91% yield). ^{1}H NMR (396 MHz, $CDCl_3$) δ 4.65 (br s, 1H), 3.13 (q, J = 5.8 Hz, 2H), 2.71 (t, J = 6.7 Hz, 1H), 1.59 – 1.46 (m, 4H), 1.44 (s, 9H), 1.30 (br s, 2H). The ^{1}H NMR is in agreement with those reported before.[40]

***tert*-Butyl (2-(3-bromobenzamido)ethyl)carbamate (2.58)**

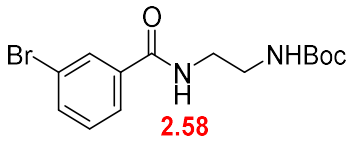

2.58

General procedure 1 was followed using *m*-bromobenzoic acid **2.1** (204 mg, 1 mmol), oxalyl chloride (105 µL, 1.2 mmol), and anhydrous DMF (150 µL) in anhydrous DCM (1 mL). The resulting acid chloride was coupled to *tert*-butyl (4-aminobutyl)carbamate **2.55** (161 mg, 1 mmol) using K_2CO_3 (275 mg, 2 mmol) in anhydrous THF (5 mL). After completion as indicated by TLC (EtOAc:MeOH 4:1 with a few drops of concentrated aqueous NH_3 solution; $KMnO_4$), THF was evaporated and water was added to the crude reaction. The precipitate was collected by filtration, following by washing with water to obtain *tert*-butyl (2-(3-bromobenzamido)ethyl)carbamate **2.58** as a colorless solid (111 mg, 32% yield). ^{1}H NMR (396 MHz, $CDCl_3$) δ 7.98 (s, 1H), 7.75 (d, J = 7.9 Hz, 1H), 7.61 (d, J = 7.8 Hz, 1H), 7.36 – 7.27 (m, 2H), 4.97 (br s, 1H), 3.60 – 3.51 (m, 2H), 3.47 – 3.37 (m, 2H), 1.44 (s, 9H); ^{13}C NMR (100 MHz, $CDCl_3$) δ 166.5, 157.9, 136.3, 134.5, 130.4, 130.1, 125.8, 122.8, 80.2, 42.5, 39.9, 28.5; HRMS calcd for $C_{14}H_{19}N_2O_3{}^{23}Na^{79}Br$ (M+ Na^+) 365.0477; found 365.0482; IR (ATR, cm^{-1}) υ_{max} 3358, 3282, 3059, 2977, 2929, 1700, 1649, 1534, 1469, 1443; mp: 118 – 119 °C.

***tert*-Butyl (3-(3-bromobenzamido)propyl)carbamate (2.59)**

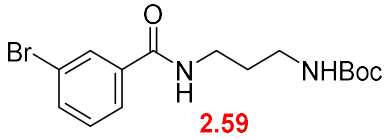

2.59

General procedure 1 was followed using *m*-bromobenzoic acid **2.1** (206 mg, 1 mmol), oxalyl chloride (105 µL, 1.2 mmol), and anhydrous DMF (150 µL) in anhydrous DCM (1 mL). The resulting acid chloride was coupled to *tert*-butyl (4-aminobutyl)carbamate **2.56** (174 mg, 1 mmol) using K_2CO_3 (276 mg, 2 mmol) in anhydrous THF (5 mL). After completion as indicated by TLC (EtOAc:MeOH 4:1 with a few drops of concentrated aqueous NH_3 solution; $KMnO_4$), THF was evaporated and water was added to the crude reaction. The precipitate was collected by filtration, following by washing with water to obtain *tert*-butyl (3-(3-bromobenzamido)propyl)carbamate **2.59** as a collourless solid (97.0 mg, 0.27 mmol, 27% yield). ^{1}H NMR (396 MHz, $CDCl_3$) δ 8.04 (s, 1H), 7.77 (d, J = 7.4 Hz, 1H), 7.62 (d, J = 7.7 Hz, 1H), 7.38 (br s, 1H), 7.32 (t, J = 7.9 Hz, 1H), 4.86 (br s, 1H), 3.56 – 3.44 (m, 2H), 3.32 – 3.18 (m, 2H), 1.79 – 1.65 (m, 2H), 1.46 (s, 9H); ^{13}C NMR (100 MHz, $CDCl_3$) δ 166.2, 157.2, 136.7, 134.4, 130.5, 130.2, 125.6, 122.8, 79.8, 37.2, 36.3, 30.2, 28.5; HRMS calcd for $C_{15}H_{21}N_2O_3{}^{23}Na^{79}Br$ (M+ Na^+) 379.0633; found 379.0663; IR (ATR, cm^{-1}) υ_{max} 3354, 3318, 2985, 2949, 2877, 1680, 1631, 1522, 1477; mp: 120 °C.

***tert*-Butyl (4-(3-bromobenzamido)butyl)carbamate (2.60)**

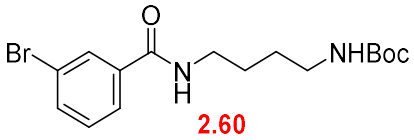

2.60

General procedure 1 was followed using *m*-bromobenzoic acid **2.1** (204 mg, 1 mmol), oxalyl chloride (0.105 mL, 1.2 mmol), and anhydrous DMF (0.150 mL) in anhydrous DCM (1 mL). The resulting acid chloride was coupled to *tert*-butyl (4-aminobutyl)carbamate **2.57** (188 mg,

1 mmol) using K_2CO_3 (280 mg, 2 mmol) in anhydrous THF (5 mL). After completion as indicated by TLC (EtOAc:MeOH 4:1 with a few drops of concentrated aqueous NH_3 solution; $KMnO_4$), THF was evaporated and water was added to the crude reaction. The precipitate was collected by filtration, following by washing with water to obtain *tert*-butyl (4-(3-bromobenzamido)butyl)carbamate **2.60** as a white solid (117 mg, 0.32 mmol, 32% yield). ^{1}H NMR (396 MHz, $CDCl_3$) δ 7.96 (s, 1H), 7.74 (s, 1H), 7.61 (s, 1H), 7.37 – 7.27 (m, 1H), 6.62 (br s, 1H), 4.64 (br s, 1H), 3.50 (s, 2H), 3.17 (s, 2H), 1.77 – 1.56 (m, 4H), 1.45 (s, 9H); ^{13}C NMR (100 MHz, $CDCl_3$) δ 166.3, 156.4, 136.7, 134.3, 130.4, 130.1, 125.8, 122.7, 79.4, 40.0, 28.5, 28.0, 26.3; HRMS calcd for $C_{16}H_{23}N_2O_3{}^{23}Na^{79}Br$ (M+ Na^+) 393.0790; found 393.0810; IR (ATR, cm^{-1}) υ_{max} 3350, 3318, 2981, 2945, 2877, 1680, 1631, 1520, 1477; mp: 120 – 121 °C.

2-Chloro-*N*-ethyl-6-methylpyrimidin-4-amine (2.6)

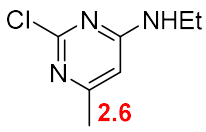

Ethylamine hydrochloride (2.45 g, 30 mmol), 2,4-dichloro-6-methylpyrimidine **2.5** (4.89 g, 30 mmol), and DIPEA (10.5 mL, 60 mmol) were dissolved into EtOH (60 mL). The mixture was stirred at 50 °C for 1 day. After completion, as monitored by TLC (hexanes:EtOAc 9:1; UV), the mixture was evaporated under reduced pressure and purified by column chromatography on silica gel using gradient eluent starting from hexanes:EtOAc 9:1 to hexanes:EtOAc 1:1 to afford 2-chloro-*N*-ethyl-6-methylpyrimidin-4-amine **2.6** as a colorless solid (1.71 g, 33% yield). ^{1}H NMR (400 MHz, $CDCl_3$) δ 6.06 (s, 1H), 5.13 (s, 1H), 3.32 (br s, 2H), 2.33 (s, 3H), 1.25 (t, J = 7.2 Hz, 3H). The ^{1}H NMR is in agreement with those reported before.[8]

3-Bromo-*N*-(3-((4-(ethylamino)-6-methylpyrimidin-2-yl)amino)phenyl)benzamide (2.61)

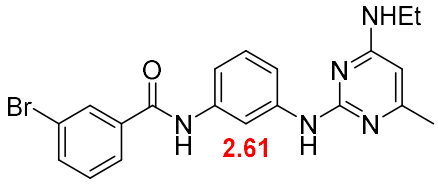

N-(3-Aminophenyl)-3-bromobenzamide **2.46** (80.0 mg, 0.30 mmol), 2-chloro-*N*-ethyl-6-methylpyrimidin-4-amine **2.6** (47.5 mg, 0.30 mmol), and DIPEA (48 µL, 0.30 mmol) were dissolved in dioxane (2 mL). The mixture was stirred at 220 °C for 1 hour using microwave synthesizer. After completion as indicated by TLC (hexanes:EtOAc 1:4; UV), the mixture was poured into water. The precipitate was collected by filtration and purified by column chromatography on silica gel using hexanes:EtOAc (1:4) as isocratic eluent to afford 3-bromo-*N*-(3-((4-(ethylamino)-6-methylpyrimidin-2-yl)amino)phenyl)benzamide **2.61** as an orange solid (28.0 mg, 0.07 mmol, 26% yield). ^{1}H NMR (396 MHz, $CDCl_3$) δ 8.10 (s, 1H), 8.03 – 7.85 (m, 2H), 7.75 (d, J = 7.4 Hz, 1H), 7.65 (d, J = 7.6 Hz, 1H), 7.55 (br s, 1H), 7.43 – 7.28 (m, 3H), 5.70 (s, 1H), 5.01 (br s, 1H), 3.34 (s, 2H), 2.51 (br s, 1H), 2.26 (s, 3H), 1.23 (t, J = 7.1 Hz, 3H); ^{13}C NMR (100 MHz, $CDCl_3$) δ 165.3, 164.4, 163.5, 159.0, 141.1, 138.2, 137.3, 134.8, 130.5, 130.4, 129.4, 125.7, 123.0, 115.5, 113.8, 110.9, 94.2, 36.5, 23.6, 14.8; HRMS calcd for $C_{20}H_{21}N_5O^{79}Br$ (M+ H^+) 426.0929; found 426.0891; IR (ATR, cm^{-1}) υ_{max} 3401, 3278, 3135, 3064, 2969, 2925, 2870, 1650, 1591, 1532, 1468, 1409; mp: dec.

3-Bromo-*N*-((*1r*,*4r*)-4-((4-(ethylamino)-6-methylpyrimidin-2-yl)amino)cyclohexyl) benzamide (2.62)

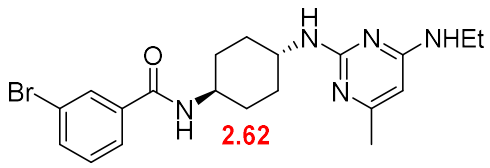

N-((*1r*,*4r*)-4-Aminocyclohexyl)-3-bromobenzamide **2.47** (51.0 mg, 0.17 mmol), 2-chloro-*N*-ethyl-6-methylpyrimidin-4-amine **2.6** (29.1 mg, 0.17 mmol), and DIPEA (30 µL, 0.17 mmol) were dissolved in dioxane (2 mL). The mixture was stirred at 220 °C for 1.5 hours using a microwave synthesizer. After completion as indicated by TLC (hexanes:EtOAc 1:4; UV), the reaction mixture was poured into water. The precipitate was collected by filtration to afford 3-bromo-*N*-((*1r*,*4r*)-4-((4-(ethylamino)-6-methylpyrimidin-2-yl)amino)cyclohexyl) benzamide **2.62** as a brown solid (46.8 mg, 63% yield). ^{1}H NMR (396 MHz, $CDCl_3$) δ 7.88 (s, 1H), 7.67 (s, 1H), 7.61 (s, 1H), 7.28 (s, 1H), 6.01 (s, 1H), 5.56 (s, 1H), 4.69 (s, 1H), 4.60 (s, 1H), 3.95 (s, 1H), 3.77 (s, 1H), 3.28 (s, 2H), 2.46 – 1.87 (m, 7H), 1.36 (s, 4H), 1.22 (s, 3H); ^{13}C NMR (100 MHz, $CDCl_3$) δ 166.1, 165.5, 163.8, 161.7, 137.0, 134.4, 130.3, 130.2, 125.6, 122.8, 92.2, 49.0, 48.8, 36.2, 32.0, 31.9, 24.1, 15.0; HRMS calcd for $C_{20}H_{27}N_5O^{79}Br$ ($M+ H^+$) 432.1399; found 432.1396; IR (ATR, cm^{-1}) υ_{max} 3416, 3298, 3063, 2933, 2858, 1634, 1589, 1519, 1473, 1447 cm^{-1}; mp: dec.

(3-Bromophenyl)(4-(4-(ethylamino)-6-methylpyrimidin-2-yl)piperizin-1-yl)methanone (2.63)

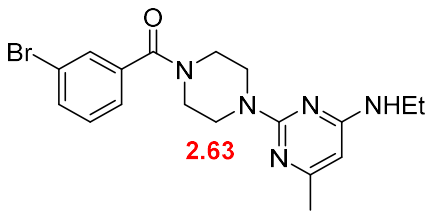

A solution of (3-bromophenyl)(piperizin-1-yl)methanone **2.48** (80.3 mg, 0.30 mmol), 2-chloro-*N*-ethyl-6-methylpyrimidin-4-amine **2.6** (51.4 mg, 0.30 mmol), and DIPEA (0.052 mL, 0.30 mmol) in DMF (1.5 mL) was heated at 120 °C in a sealed tube with stirring for 2 days. After completion as indicated by TLC (hexanes:EtOAc 1:1; UV), the mixture was poured into water. The precipitate was collected by filtration to afford (3-bromophenyl)(4-(4-(ethylamino)-6-methylpyrimidin-2-yl)piperizin-1-yl)methanone **2.63** as a brown solid (85.2 mg, 71% yield). ^{1}H NMR (396 MHz, $CDCl_3$) δ 7.86 – 7.46 (m, 2H), 7.46 – 7.20 (m, 2H), 5.59 (s, 1H), 4.59 (br s, 1H), 4.07 – 3.01 (m, 10H), 2.20 (s, 3H), 1.21 (t, J = 6.9 Hz, 3H); ^{13}C NMR (100 MHz, $CDCl_3$) δ 168.9, 166.0, 163.5, 161.7, 137.9, 132.9, 130.2, 125.7, 122.8, 92.8, 47.8, 44.3, 43.8, 42.4, 36.1, 24.3, 14.9; HRMS calcd for $C_{18}H_{23}N_5O^{79}Br$ (M+ H^+) 404.1086; found 404.1079; IR (ATR, cm^{-1}) υ_{max} 3326, 3170, 3051, 2973, 2921, 2862, 1624, 1581, 1564, 1479, 1431; mp: dec.

3-Bromo-*N*-(2-((4-(ethylamino)-6-methylpyrimidin-2-yl)amino)ethyl)benzamide (2.64)

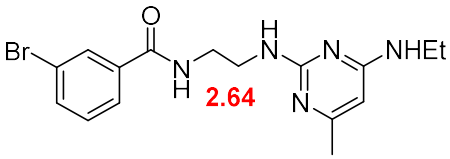

tert-Butyl (2-aminoethyl)carbamate **2.58** (68.6 mg, 0.20 mmol) was dissolved in TFA/CH_2Cl_2 (1:1, 1 mL) and stirred at ambient temperature for 30 minutes, followed by evaporation to dryness to give the TFA salt. The residue, 2-chloro-*N*-ethyl-6-methylpyrimidin-4-amine **2.6** (34.4 mg, 0.20 mmol), and DIPEA (90 µL, 0.50 mmol) were dissolved in dioxane (2 mL). The

mixture was stirred at 160 °C for 1 hour using a microwave synthesizer. After completion as indicated by TLC (hexanes:EtOAc 1:1; UV), the reaction mixture was poured into water and extracted with EtOAc 3 times. Combined organic phase was washed with brine, dried over Na_2SO_4, and evaporated. The crude mixture was purified by column chromatography on silica gel using 2% Et_3N in EtOAc as isocratic eluent to afford 3-bromo-*N*-(2-((4-(ethylamino)-6-methylpyrimidin-2-yl)amino) ethyl)benzamide **2.64** as a colorless solid (41.5 mg, 62% yield). ^{1}H NMR (396 MHz, $CDCl_3$) δ 8.26 (br s, 1H), 7.78 (s, 1H), 7.68 (d, *J* = 7.7 Hz, 1H), 7.57 (d, *J* = 7.8 Hz, 1H), 7.31 – 7.16 (m, 1H), 5.64 (s, 1H), 5.32 (br s, 1H), 4.60 (br s, 1H), 3.69 – 3.63 (m, 2H), 3.62 – 3.57 (m, 2H), 3.38 – 3.12 (m, 2H), 2.20 (s, 3H), 1.19 (t, *J* = 7.2 Hz, 3H); ^{13}C NMR (100 MHz, $CDCl_3$) δ 166.6, 165.9, 163.6, 163.1, 137.2, 134.2, 130.2, 130.1, 126.1, 122.6, 93.4, 44.1, 40.3, 36.3, 24.1, 14.9; HRMS calcd for $C_{16}H_{21}N_5O^{79}Br$ (M+ H^+) 378.0929; found 378.0907; IR (ATR, cm^{-1}) υ_{max} 3338, 3310, 3251, 3072, 2981, 2965, 2937, 2874, 1650, 1607, 1585, 1528, 1496, 1462, 1421; mp: 161 – 162 °C.

3-Bromo-*N*-(3-((4-(ethylamino)-6-methylpyrimidin-2-yl)amino)propyl)benzamide (2.65)

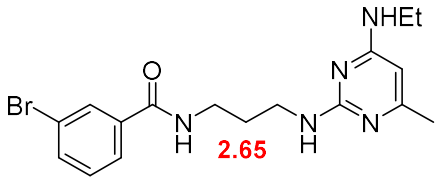

tert-Butyl (3-aminopropyl)carbamate **2.59** (71.4 mg, 0.20 mmol) was dissolved in TFA/CH_2Cl_2 (1:1, 1 mL) and stirred at ambient temperature for 30 minutes followed by evaporation to dryness to give TFA salt. The residue, 2-chloro-*N*-ethyl-6-methylpyrimidin-4-amine **2.6** (34.2 mg, 0.20 mmol), and DIPEA (90 µL, 0.50 mmol) were dissolved in dioxane (2 mL). The reaction mixture was stirred at 160 °C for 2 hours by using microwave synthesizer. After completion as indicated by TLC (EtOAc with a few drops of Et_3N; UV), the reaction mixture was poured into water and extracted with EtOAc 3 times. Combined organic phase was washed

with brine, dried over Na_2SO_4, and evaporated. The crude mixture was purified by column chromatography on silica gel using 2% Et_3N in EtOAc as isocratic eluent to afford 3-bromo-*N*-(3-((4-(ethylamino)-6-methylpyrimidin-2-yl)amino)propyl)benzamide **2.65** as yellow syrup (21.6 mg, 28% yield). ^{1}H NMR (400 MHz, $CDCl_3$) δ 7.96 (t, *J* = 1.4 Hz, 1H), 7.88 (br s, 1H), 7.77 (d, *J* = 7.7 Hz, 1H), 7.61 (d, *J* = 8.1 Hz, 1H), 7.30 (t, *J* = 7.9 Hz, 1H), 5.56 (s, 1H), 4.96 (br s, 1H), 4.51 (br s, 1H), 3.62 – 3.45 (m, 4H), 3.34 – 3.11 (m, 2H), 2.11 (s, 3H), 1.77 (quin, *J* = 6.0 Hz, 1H), 1.16 (t, *J* = 7.2 Hz, 1H); ^{13}C NMR (100 MHz, $CDCl_3$) δ 166.4, 166.1, 163.6, 162.9, 137.8, 134.2, 130.3, 130.2, 126.0, 122.7, 92.5, 37.8, 36.3, 36.2, 30.8, 24.2, 14.9; HRMS calcd for $C_{17}H_{23}N_5O^{79}Br$ ($M+H^+$) 392.1086; found 392.1097; IR (ATR, cm^{-1}) υ_{max} 3302, 3064, 2929, 2870, 1638, 1589, 1522, 1431.

3-Bromo-*N*-(4-((4-(ethylamino)-6-methylpyrimidin-2-yl)amino)butyl)benzamide (2.66)

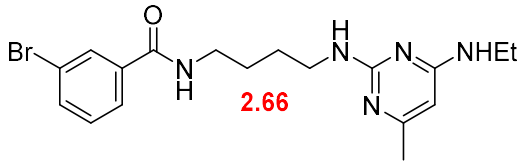

tert-Butyl (4-aminobutyl)carbamate **2.60** (74.3 mg, 0.20 mmol) was dissolved in TFA/CH_2Cl_2 (1:1, 1 mL) and stirred at ambient temperature for 30 minutes followed by evaporation to dryness to give TFA salt. The residue, 2-chloro-*N*-ethyl-6-methylpyrimidin-4-amine **2.6** (34.5 mg, 0.20 mmol), and DIPEA (90 µL, 0.50 mmol) were dissolved in dioxane (2 mL). The reaction mixture was stirred at 160 °C for 1 hours by using microwave synthesizer. After completion as indicated by TLC (hexanes:EtOAc 1:1; UV), the reaction mixture was poured into water and extracted with EtOAc 3 times. Combined organic phase was washed with brine, dried over Na_2SO_4, and evaporated. The crude mixture was purified by column chromatography on silica gel using 2% Et_3N in EtOAc as isocratic eluent to afford 3-bromo-*N*-(4-((4-(ethylamino)-6-methylpyrimidin-2-yl)amino)butyl)benzamide **2.66** as yellow syrup

(45.5 mg, 56% yield). ^{1}H NMR (400 MHz, $CDCl_3$) δ 7.92 (t, *J* = 1.8 Hz, 1H), 7.68 (d, *J* = 7.8 Hz, 1H), 7.59 (dd, *J* = 8.0, 1.9 Hz, 1H), 7.33 – 7.21 (m, 1H), 6.76 (br s, 1H), 5.55 (s, 1H), 4.95 (br s, 1H), 4.69 (br s, 1H), 3.47 (q, *J* = 6.5 Hz, 2H), 3.40 (q, *J* = 6.3 Hz, 2H), 3.29 – 3.16 (m, 2H), 2.14 (s, 3H), 1.74 – 1.55 (m, 4H), 1.18 (t, *J* = 7.2 Hz, 3H); ^{13}C NMR (100 MHz, $CDCl_3$) δ 166.3, 165.9, 163.7, 162.4, 136.9, 134.3, 130.3, 130.1, 125.7, 122.8, 92.3, 40.7, 40.1, 36.1, 27.7, 26.6, 24.0, 14.9; HRMS calcd for $C_{18}H_{25}N_5O^{79}Br$ (M+ H^+) 406.1242; found 406.1257; IR (ATR, cm^{-1}) υ_{max} 3306, 3068, 2929, 2862, 1638, 1589, 1561, 1544, 1473, 1431.

3-Bromo-*N*-(3-((4-chloro-6-(ethylamino)-1,3,5-triazin-2-yl)amino)phenyl)benzamide (2.67)

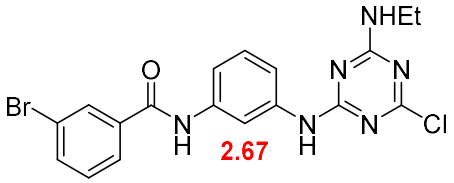

General procedure 6 was followed using *N*-(3-aminophenyl)-3-bromobenzamide **2.46** (121 mg, 0.42 mmol), 4,6-dichloro-*N*-ethyl-1,3,5-triazin-2-amine **2.9** (80.0 mg, 0.42 mmol), and diisopropylethylamine (DIPEA; 72 µL, 0.42 mmol) in dioxane (2 mL) for 2 hours. The reaction was monitored by TLC (hexanes:EtOAc 1:1; UV). After the filtration, the precipitate was washed with water to afford 3-bromo-*N*-(3-((4-chloro-6-(ethylamino)-1,3,5-triazin-2-yl)amino)phenyl)benzamide **2.67** as a light brown solid (101 mg, 54% yield). ^{1}H NMR[a] (400 MHz, DMSO-d6) δ 10.34 (s, 1H), 10.07 and 9.94 (2 br s, 1H, rotamer), 8.20 – 8.04 (m, 2H), 8.00 – 7.90 (m, 1H), 7.80 (d, *J* = 8.5 Hz, 1H), 7.50 (t, *J* = 7.9 Hz, 1H), 7.42 (d, *J* = 7.3 Hz, 1H), 7.36 – 7.20 (m, 2H), 3.47 – 3.23 (m, 2H), 1.15 – 1.03 (m, 3H); ^{13}C NMR[a] (100 MHz, DMSO-d6) δ 168.6, 167.8, 165.2, 163.9, 163.8, 163.5, 139.2, 139.1, 139.0, 138.9, 137.13, 137.0, 134.3, 130.7, 130.2, 128.5, 126.9, 121.7, 116.7, 115.9, 115.6, 113.4, 113.0, 35.3, 35.2, 14.6, 14.3;

HRMS calcd for $C_{18}H_{23}N_6O^{35}Cl^{79}Br$ (M+ H^+) 453.0805; found 453.0804; IR (ATR, cm^{-1}) υ_{max} 3266, 3159, 3131, 2933, 2858, 1625, 1589, 1567, 1536, 1492, 1442; mp: dec.

[a] This compound exists as a mixture of rotamers.

3-Bromo-*N*-((*1r*,*4r*)-4-((4-chloro-6-(ethylamino)-1,3,5-triazin-2-yl)amino)cyclohexyl) benzamide (2.68)

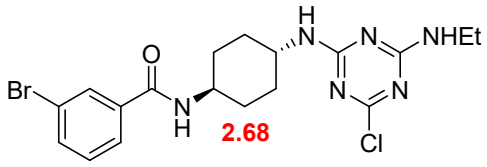

General procedure 6 was followed using *N*-((*1r*,*4r*)-4-aminocyclohexyl)-3-bromobenzamide **2.47** (124 mg, 0.42 mmol), 4,6-dichloro-*N*-ethyl-1,3,5-triazin-2-amine **2.9** (80.0 mg, 0.42 mmol), and DIPEA (72 μL, 0.42 mmol) in dioxane (2 mL) for 1.5 hours. The reaction was monitored by TLC (hexanes:EtOAc 1:1; UV). After the filtration, the precipitate was washed with water to afford 3-bromo-*N*-((*1r*,*4r*)-4-((4-chloro-6-(ethylamino)-1,3,5-triazin-2-yl)amino)cyclohexyl) benzamide **2.68** as a light brown solid (156 mg, 83% yield). ^{1}H NMR[a] (396 MHz, DMSO-d6) δ 8.57 – 8.23 (m, 1H), 8.09 – 7.98 (m, 1H), 7.96 – 7.77 (m, 2H), 7.77 – 7.62 (m, 2H), 7.43 (t, *J* = 7.9 Hz, 1H), 3.82 – 3.60 (m, 2H), 3.29 – 3.10 (m, 3H), 2.00 – 1.71 (m, 4H), 1.52 – 1.18 (m, 4H), 1.16 – 0.99 (m, 3H); ^{13}C NMR[a] (100 MHz, DMSO-d6) δ 168.2, 168.2, 167.6, 165.4, 165.2, 164.9, 164.6, 164.2, 164.0, 163.9, 136.9, 136.8, 133.8, 130.4, 129.9, 126.5, 121.6, 49.0, 48.4, 48.3, 48.0, 47.9, 35.1, 35.0, 34.9, 31.1, 30.9, 30.7, 14.9, 14.7, 14.4, 14.3; HRMS calcd for $C_{18}H_{23}N_6O^{35}Cl^{79}Br$ (M+ H^+) 453.0805; found 453.0804; IR (ATR, cm^{-1}) υ_{max} 3266, 3159, 3131, 2933, 2858, 1625, 1589, 1567, 1536, 1492, 1442; mp: dec.

[a] This compound exists as a mixture of rotamers.

3-Bromo-*N*-(2-((4-chloro-6-(ethylamino)-1,3,5-triazin-2-yl)amino)ethyl)benzamide (2.69)

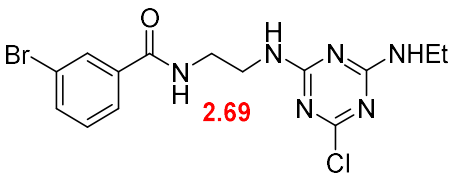

General procedure 3 was followed using *N*-(2-aminoethyl)-3-bromobenzamide **2.49** (102 mg, 0.42 mmol), 4,6-dichloro-*N*-ethyl-1,3,5-triazin-2-amine **2.9** (80.6 mg, 0.42 mmol), and DIPEA (72 µL, 0.42 mmol) in dioxane (2 mL) for 1.5 hours. The reaction was monitored by TLC (hexanes:EtOAc 1:1; UV). After the filtration, the precipitate was washed with water to afford 3-bromo-*N*-(2-((4-chloro-6-(ethylamino)-1,3,5-triazin-2-yl)amino)ethyl)benzamilde **2.69** as a colorless solid (139 mg, 84% yield). ^{1}H NMR (396 MHz, DMSO-d6) δ 8.63 (s, 1H), 8.01 (s, 1H), 7.91 – 7.65 (m, 4H), 7.42 (t, *J* = 7.3 Hz, 1H), 3.58 – 3.36 (m, 4H), 3.29 – 3.11 (m, 2H), 1.06 (s, 3H); ^{13}C NMR[a] (100 MHz, DMSO-d6) δ 168.2, 168.1, 167.6, 165.8, 165.6, 165.3, 165.1, 165.0, 165.0, 164.8, 136.8, 133.8, 130.5, 129.9, 126.4, 121.6, 38.8, 35.0, 34.9, 14.8, 14.6, 14.4, 14.3; HRMS calcd for $C_{14}H_{17}N_6O^{35}Cl^{79}Br$ (M+ H+) 399.0336; found 399.0344; IR (ATR, cm^{-1}) υ_{max} 3258, 3104, 2977, 2941, 1636, 1538, 1432, 1402; mp: 200 – 203 °C.

[a] This compound exists as a mixture of rotamers.

3-Bromo-*N*-(3-((4-(ethylamino)-6-(4-methylpiperizin-1-yl)-1,3,5-triazin-2-yl)amino) phenyl)benzamide (2.70)

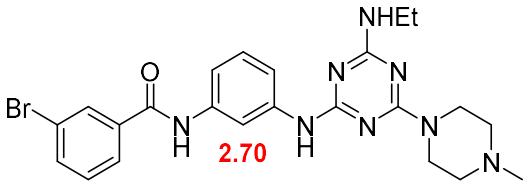

General procedure 2 was follow using 3-bromo-*N*-(3-((4-chloro-6-(ethylamino)-1,3,5-triazin-2-yl)amino)phenyl)benzamide **2.46** (65.5 mg, 0.15 mmol) and 1-methylpiperizine (85 µL, 0.73

mmol) in dioxane (1 mL). After stirring at room temperature for 2 day, the reaction was monitored by TLC (hexanes:EtOAc 1:1; UV). 3-Bromo-*N*-(3-((4-(ethylamino)-6-(4-methylpiperizin-1-yl)-1,3,5-triazin-2-yl)amino)phenyl)benzamide **2.70** was obtained as a colorless solid (68.5 mg, 92% yield). ^{1}H NMR[a] (396 MHz, $CDCl_3$) δ 8.09 (s, 1H), 8.02 (br s, 1H), 7.95 (s, 1H), 7.71 (d, *J* = 6.6 Hz, 1H), 7.63 (d, *J* = 7.6 Hz, 1H), 7.43 – 6.91 (m, 5H), 5.27, and 5.02 (2 br s, 1H, rotamer), 3.82 (s, 4H), 3.40 (br s, 2H), 2.42 (s, 4H), 2.31 (s, 3H), 1.16 (br s, 3H); ^{13}C NMR[a] (100 MHz, $CDCl_3$) δ 166.1, 165.0, 164.3, 140.5, 138.1, 137.1, 134.8, 130.4, 129.3, 125.7, 123.0, 116.1, 114.2, 111.8, 55.1, 46.3, 43.2, 35.7, 15.1; HRMS calcd for $C_{18}H_{18}N_6O^{79}Br$ (M+ H^+) 511.1569; found 511.1575; IR (ATR, cm^{-1}) υ_{max} 3412, 3286, 2973, 2937, 2854, 2802, 1654, 1612, 1584, 1539, 1496, 1482, 1421; mp: dec.

[a] This compound exists as a mixture of rotamers.

3-Bromo-*N*-((*1r*,*4r*)-4-((4-(ethylamino)-6-(4-methylpiperazin-1-yl)-1,3,5-triazin-2-yl)amino)cyclohexyl)benzamide (2.71)

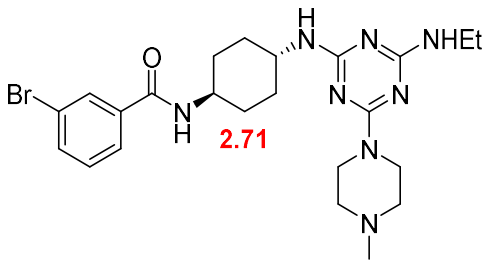

General procedure 2 was follow using 3-bromo-*N*-((*1r*,*4r*)-4-((4-chloro-6-(ethylamino)-1,3,5-triazin-2-yl)amino)cyclohexyl) benzamide **2.68** (88.9 mg, 0.20 mmol) and 1-methylpiperazine (110 µL, 1 mmol) in dioxane (1.5 mL). After stirring at room temperature for 1 day, the reaction was monitored by TLC (hexanes:EtOAc 1:1; UV). 3-Bromo-*N*-((*1r*,*4r*)-4-((4-(ethylamino)-6-(4-methylpiperazin-1-yl)-1,3,5-triazin-2-yl)amino)cyclohexyl)benzamide **2.71** was obtained as a light brown solid (85.2 mg, 84% yield). ^{1}H NMR (396 MHz, $CDCl_3$) δ 7.88 (s, 1H), 7.67 (d, *J* = 6.4 Hz, 1H), 7.61 (d, *J* = 6.5 Hz, 1H), 7.29 (s, 1H), 6.07 (s, 1H), 4.75 (br s, 2H), 4.14 –

3.53 (m, 6H), 3.38 (br s, 2H), 2.71 – 2.22 (m, 7H), 2.13 (s, 4H), 1.54 – 1.24 (m, 4H), 1.17 (s, 3H); ^{13}C NMR (100 MHz, $CDCl_3$) δ 166.2, 165.5, 165.1, 136.9, 134.4, 130.2, 130.1, 125.6, 122.8, 55.0, 48.7, 46.3, 43.0, 35.6, 31.9, 15.2; HRMS calcd for $C_{23}H_{34}N_8O^{79}Br$ (M+ H^+) 517.2039; found 517.2031; IR (ATR, cm^{-1}) υ_{max} 3416, 3298, 3063, 2933, 2858, 1634, 1589, 1519, 1473, 1447; mp: dec.

3-Bromo-*N*-(2-((4-(ethylamino)-6-(4-methylpiperizin-1-yl)-1,3,5-triazin-2-yl) amino) ethyl) benzamide (2.72)

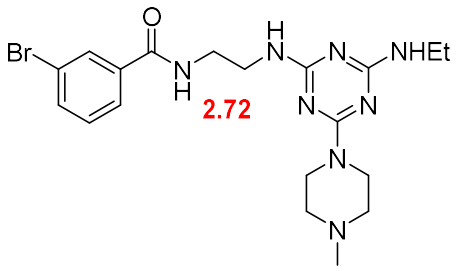

3-Bromo-*N*-(2-((4-chloro-6-(ethylamino)-1,3,5-triazin-2-yl)amino)ethyl)benzamide **2.49** (80.3 mg, 0.20 mmol) and 1-methylpiperazine (0.110 mL, 1 mmol) were dissolved in dioxane (1.5 mL). The reaction was stirred and heated at the indicated temperature for 2 days. After completion as indicated by TLC (hexanes:EtOAc 1:1; UV), the mixture was poured into water and extracted with EtOAc 3 times. Combined organic layers were washed with 2 M aqueous NaOH, water (twice) and brine. The organic layer was dried (Na_2SO_4) and evaporated to afford 3-bromo-*N*-(2-((4-(ethylamino)-6-(4-methylpiperizin-1-yl)-1,3,5-triazin-2-yl)amino)ethyl)benzamide **2.72** as a colorless solid (38.6 mg, 42% yield). ^{1}H NMR (396 MHz, $CDCl_3$) δ 7.83 (s, 1H), 7.72 – 7.49 (m, 2H), 7.34 – 7.12 (m, 1H), 5.41 (br s, 1H), 4.91 (br s, 1H), 4.12 – 3.47 (m, 8H), 3.38 (s, 2H), 2.77 (s, 1H), 2.58 – 2.16 (m, 7H), 1.16 (s, 3H); ^{13}C NMR (100 MHz, $CDCl_3$) δ 167.2, 166.8, 166.5, 165.7, 164.8, 136.8, 134.3, 130.3, 130.1, 125.8, 122.7, 55.1, 54.9, 46.3, 43.1, 39.6, 35.7, 15.1; HRMS calcd for $C_{19}H_{28}N_8O^{79}Br$ (M+ H^+)

463.1565; found 463.1567; IR (ATR, cm^{-1}) υ_{max} 3409, 3258, 3175, 2937, 2854, 1646, 1614, 1544, 1496, 1461, 1435, 1415; mp: 138 – 140 °C.

2.9 References

1. Priya, R.; Biuković, G.; Manimekalai, M. S. S.; Lim, J.; Rao, S. P. S.; Grüber, G. *J. Bioenerg. Biomembr.* **2013,** *45* (1), 121-129.

2. Abrahams, J. P.; Leslie, A. G. W.; Lutter, R.; Walker, J. E. *Nature* **1994,** *370* (6491), 621-628.

3. Cingolani, G.; Duncan, T. M. *Nat. Struct. Mol. Biol.* **2011,** *18* (6), 701-707.

4. Gibbons, C.; Montgomery, M. G.; Leslie, A. G.; Walker, J. E. *Nat. Struct. Biol.* **2000,** *7* (11), 1055-61.

5. Lu, P.; Lill, H.; Bald, D. *Biochim. Biophys. Acta. Bioenerg.* **2014,** *1837* (7), 1208-1218.

6. Hotra, A.; Suter, M.; Biuković, G.; Ragunathan, P.; Kundu, S.; Dick, T.; Grüber, G. *FEBS. J.* **2016,** *283* (10), 1947-1961.

7. Lipinski, C. A.; Lombardo, F.; Dominy, B. W.; Feeney, P. J. *Adv. Drug Deliv. Rev.* **2001,** *46* (1), 3-26.

8. Hotra, A. Design of Novel F-ATP Synthase Inhibitors of Mycobacterium Tuberculosis Nanyang Technological University, Singapore, Unpublished doctoral dissertation, 2018.

9. Pathania, S.; Singh, P. K. *Expert Opin. Drug Metab. Toxicol.* **2021,** *17* (4), 351-354.

10. Veber, D. F.; Johnson, S. R.; Cheng, H.-Y.; Smith, B. R.; Ward, K. W.; Kopple, K. D. *J. Med. Chem.* **2002,** *45* (12), 2615-2623.

11. Zanoni, T. B.; Hudari, F.; Munnia, A.; Peluso, M.; Godschalk, R. W.; Zanoni, M. V. B.; den Hartog, G. J. M.; Bast, A.; Barros, S. B. M.; Maria-Engler, S. S.; Hageman, G. J.; de Oliveira, D. P. *Toxicol. Lett.* **2015,** *239* (3), 194-204.

12. Singh, S.; Mandal, M. K.; Masih, A.; Saha, A.; Ghosh, S. K.; Bhat, H. R.; Singh, U. P. *Arch. Pharm. (Weinheim)* **2021,** *354* (6), e2000363.

13. Boger, D. L.; Zarrinmayeh, H. *J. Org. Chem.* **1990,** *55* (4), 1379-1390.

14. Richey, R. N.; Yu, H. *Org. Process Res. Dev.* **2009,** *13* (2), 315-320.

15. A. Brewer, S.; T. Burnell, H.; Holden, I.; G. Jones, B.; R. Willis, C. *J. Chem. Soc., Perkin trans. 2* **1999,** (6), 1231-1234.

16. Mewada, N. S.; Shah, D. R.; Lakum, H. P.; Chikhalia, K. H. J. *Assoc. Arab Univ. Basic Appl. Sci.* **2016,** *20* (1), 8-18.

17. Patel, R. V.; Kumari, P.; Rajani, D. P.; Chikhalia, K. H. *Eur. J. Med. Chem.* **2011,** *46* (9), 4354-65.

18. Biannic, B.; Bozell, J. J.; Elder, T. *Green Chem.* **2014,** *16* (7), 3635-3642.

19. Kanaya, N.; Ishihara, H.; Kimura, Y.; Ishiyama, T.; Ochiai, Y. Pyrazole Derivative. EP1591443, 25 Aug 2010.

20. Wensbo, D.; Annby, U.; Gronowitz, S. *Tetrahedron* **1995,** *51* (37), 10323-10342.

21. Muller, D.; Zeltser, I.; Bitan, G.; Gilon, C. *J. Org. Chem.* **1997,** *62* (2), 411-416.

22. Geneva: *World Health Organization, Tuberculosis laboratory biosafety manual*; 2012.

23. Singh, A. K.; Reyrat, J.-M. *Curr. Protoc. Microbiol.* **2009,** *14* (1), 10C.1.1-10C.1.12.

24. Koul, A.; Arnoult, E.; Lounis, N.; Guillemont, J.; Andries, K. *Nature* **2011,** *469* (7331), 483-490.

25. Koul, A.; Vranckx, L.; Dendouga, N.; Balemans, W.; Van den Wyngaert, I.; Vergauwen, K.; Göhlmann, H.; Willebrords, R.; Poncelet, A.; Guillemont, J.; Bald, D.; Andries, K. *J. Biol. Chem.* **2008,** *283*, 25273-80.

26. Umayal Lakshmanan; Drug Development Centre (EDDC); the Agency for Science, Technology, and Research, Singapore (A*star).

27. Jickky Palmae Sarathy; National University of Singapore (NUS).

28. Shoichet, B. K. *J. Med. Chem.* **2006,** *49* (25), 7274-7277.

29. Billur, R.; Ban, D.; Sabo, T. M.; Maurer, M. C. *Biochemistry* **2017,** *56* (48), 6343-6354.

30. Priya Ragunathan; School of Biological Science (SBS), Nanyang Technological University (NTU).

31. Joon Shin; School of Biological Science (SBS), Nanyang Technological University (NTU).

32. Amaravadhi Harikishore; School of Biological Science (SBS), Nanyang Technological University (NTU).

33. Koul, A.; Dendouga, N.; Vergauwen, K.; Molenberghs, B.; Vranckx, L.; Willebrords, R.; Ristic, Z.; Lill, H.; Dorange, I.; Guillemont, J.; Bald, D.; Andries, K. *Nat. Chem. Biol.* **2007,** *3* (6), 323-4.

34. Madhavi Sastry, G.; Adzhigirey, M.; Day, T.; Annabhimoju, R.; Sherman, W. *J. Comput. Aided Mol. Des.* **2013,** *27* (3), 221-234.

35. Chandrika, N. T.; Shrestha, S. K.; Ngo, H. X.; Garneau-Tsodikova, S. *Bioorg. Med. Chem.* **2016,** *24* (16), 3680-3686.

36. Huang, H.; Kang, J. Y. *J. Org. Chem.* **2017,** *82* (13), 6604-6614.

37. Mofford, D. M.; Reddy, G. R.; Miller, S. C. *J. Am. Chem. Soc.* **2014,** *136* (38), 13277-13282.

38. Abbas, A.; Xing, B.; Loh, T.-P. *Angew. Chem. Int. Ed.* **2014,** *53* (29), 7491-7494.

39. Kalia, D.; Malekar, P. V.; Parthasarathy, M. *Angew. Chem. Int. Ed.* **2016,** *55* (4), 1432-1435.

40. Scheiner, M.; Hoffmann, M.; He, F.; Poeta, E.; Chatonnet, A.; Monti, B.; Maurice, T.; Decker, M. *J. Med. Chem.* **2021,** *64* (13), 9302-9320.

Chapter 3

Synthesis and investigation of *Mycobacterium tuberculosis* F-ATP synthase inhibitors with epigallocatechin gallate (EGCG)

CHAPTER 3: Synthesis and investigation of *Mycobacterium tuberculosis* F-ATP synthase inhibitors with epigallocatechin gallate (EGCG)

3.1 Introduction

As discussed in the GaMF1 project, the γ subunit of F-ATP synthase has been confirmed to be a promising drug target. However, the mycobacterial ε subunit is a crucial moiety in the ATP synthesis from ATP synthase, which has been investigated to show many different features from other organisms. This subunit has been discovered to be one of the key binding sites for a potent MDR-TB drug, BDQ, suggesting that the ε subunit may be a potential drug target for our next drug generation.

3.1.1 Epsilon subunit of the mycobacterial F-ATP synthase: An interesting binding site for the next drug generation

F-ATP synthase is the main ATP synthesis site for the entire organism. The key mechanism involves rotation of the *c*-ring, which proceeds through ATP hydrolysis and H^+ pumping from subunits *a*-*c*. The *c*-Ring rotation then initiates conformational changes to γ and ε subunits, connecting to the main synthesis site at the $\alpha_3\beta_3$ hexamer to generate ATP.[1, 2] The detailed mechanism and role of each subunit are not yet fully understood.

The ε subunit is known to be a crucial element in regulating the ATP hydrolysis activity, consisting of an N-terminal β-barrel connecting to two α-helices, which can either align in a compact form (called the hairpin state) or stretch into an extended form as shown in Figure 3.1a.[2-4] The conformational interconversion is reported to control ATP hydrolysis. The activity is suppressed when the C-terminal helix is in the expanded conformation to engage with the central cavity of the $\alpha_3\beta_3$ hexamer.[5] In mycobacteria, the excess ATP consumption by ATP hydrolysis must be exceptionally strict as *Mtb* has to survive a hypoxia environment (low oxygen level) in granulomas;[6] consequently, the *Mtb* ε subunit may play a vital role in handling the environment encountered in the human host[5].

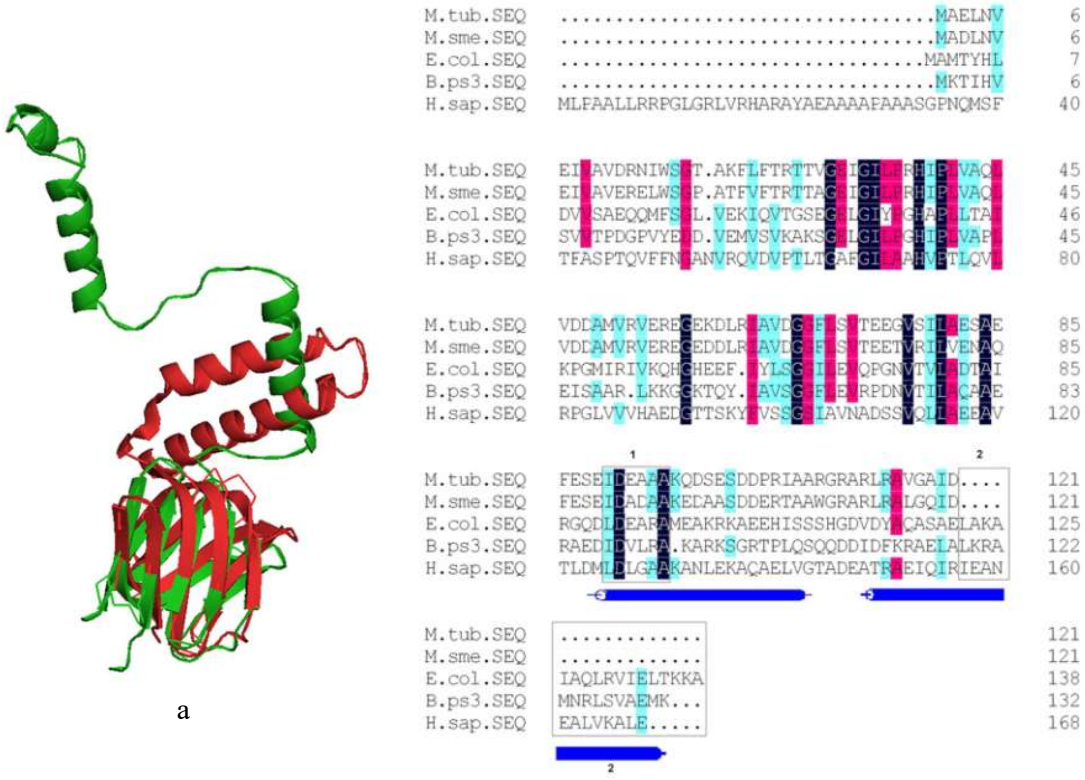

Figure 3.1 Structure of mycobacterial ε subunit in a compact form (red) as compared to an extended form (green) from the protein data bank (a) and amino acid sequence of ε subunit, comparing between M.tub (*Mtb*), M.sme (*Mycobacterium smegmatis*), *E. coli* (*Escherichia coli*), B.ps3 (*Bacillus* PS3) and H.sap (*Homo sapiens*). Blue rods below the sequence indicate the amino acid sequence in the *C*-terminal *α*-helix.[5] Reprinted from Lu, P. *et al.* Biochim. Biophys. Acta. Bioenerg. **2014,** *1837* (7), 1208-1218. Copyright (2021), reprinted with permission from Elsevier.

In most species, the intercellular ATP level in the organism affects the ATP hydrolysis activity of ATP synthase toward stabilization of the hairpin conformer by contact with an ATP molecule.[7, 8] This phenomenon allows fine-tuning of the ATP synthase activity to meet the physiological demands of each species. However, the mycobacterial ε subunit is reported to be incapable of binding to ATP,[9] indicating that this mechanism cannot regulate ATP hydrolysis

in mycobacterial species, and the *Mtb* ATP hydrolysis suppression is observed to be caused by a difference in the catalytic core compared to other organisms[10].

Significant differences in the features of ATP synthase regulation of mycobacterial species by ε subunit compared to most other organisms indicates a large distinction in the protein and amino acid structure. Mycobacterial species have shorter peptide units in the N-terminal β-barrel than in the human ε subunit, and the mycobacterial C-terminal helix is likewise shorter than other species.[9] *Mycobacterium* species (*Mtb* and *M. smeg.*) have peptide sequences that are more than 80% distinct from other organisms *(E. coli*, *Bacillus PS3*, and *Homo sapiens*).[5] Thus, the unique mycobacterial ε subunit could be an interesting target for drug design that could specifically inhibit mycobacterial ATP synthase without interfering with host bacteria in humans or inhibiting human ATP synthesis.[5]

3.1.2 Bedaquiline targets *Mtb* ε subunit

Bedaquiline (BDQ) is an effective MDR-TB medication with a high treatment success rate. The widely accepted mechanism of action is to inhibit the *Mtb* F-ATP synthase by binding at the *c*-ring subunit[11] or ε subunit[12], as discussed in 1.4.3.5. Since the *c*-ring is composed of identical copies of *c* subunits, more than one BDQ molecule is required for BDQ activity at this binding site.[11] However, the BDQ binding site at the *Mtb* ε subunit requires only a single BDQ molecule for activity.[12] Therefore, inhibitors that specifically bind to the ε subunit could be more effective than BDQ.

Molecular modeling based on the NMR titration data provides a good starting point to utilize the computational screening approach to find interesting candidates for developing inhibitors specifically targeting the *Mtb* ε subunit. The model shows that BDQ binds to the β-barrel component of the *Mtb* ε subunit. Hydrogen bonding from the quinoline moiety to R13 (arginine), as well as the hydrophobic interaction with A84 (alanine) and F86 (phenylalanine). The aromatic moiety of W16 (tryptophan) has a π-π interaction with the naphthalene ring,

which is further stabilized by the hydrophobic interaction of S17 (serine).[12] The phenyl moiety interacts with W16 (Tryptophan) *via* face-to-face stacking and with F86 *via* edge-to-face aromatic contact (Phenylalanine). *N,N*-Dimethyl amine moiety has hydrogen bonding with N14 (Asparagine). In addition, there is hydrogen bonding between the hydroxyl group and I15 (Isoleucine) (Figure 3.2).[12]

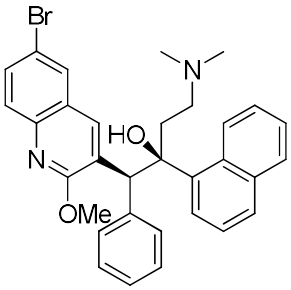

a

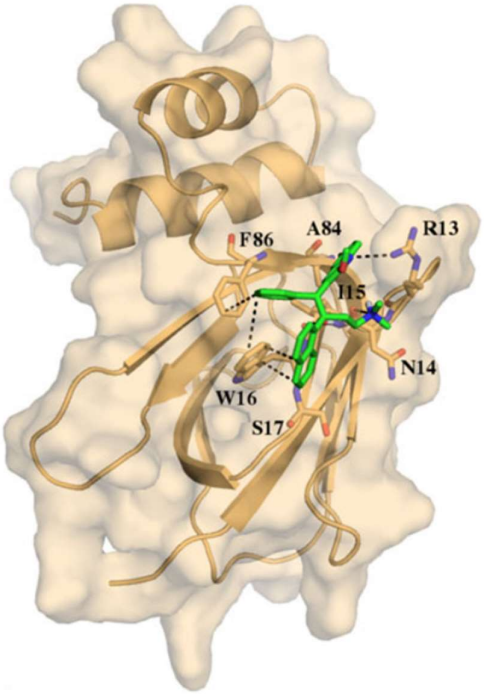

B

Figure 3.2 Structure of BDQ (a) and Molecular interaction between BDQ and ε subunit from NMR titration experiments (b).[12] Reprinted with permission from Joon, S. *et al.* FEBS J. **2018,** *285* (6), 1111-1128. Copyright 2021 FEBS J.

3.1.3 Interesting candidate for the *Mtb* ε subunit inhibitor

In-silico screening at the BDQ ε subunit binding site, done by Amaravadhi Harikishore,[13] suggested that epigallocatechin gallate (EGCG, Figure 3.3a) can bind to the *Mtb* ε subunit. The experimental results reveal that EGCG inhibits NADH-driven ATP synthesis of *M. smeg.* inversed membrane vesicles (IMVs) with a half-maximal inhibitory concentration (IC_{50}) at 155.6 ± 1.2 nM and *M. bovis.* IMV with an IC_{50} at 2.2 ± 0.3 μM,[13] which was correlated with computational modeling.

The binding site of EGCG was experimentally tested. EGCG has the capability to inhibit ATP production in *M. smeg.* IMVs in the presence of succinate, indicating that EGCG did not inhibit the NADH dehydrogenase. HSQC-NMR titration was used to validate the EGCG binding site at the *Mtb* ε subunit.[13] The molecular model based on the NMR data suggests that EGCG binds to the *Mtb* ε subunit, however, with a distinct binding site from BDQ, which is at the interface of the N-terminal β-barrel and C-terminal α-helices. Hydrogen bondings from 7-OH to D66 (Aspartic acid), 3-OH on 2-phenyl substituent to both D48 (Aspartic acid) and A116 (Alanine), and 3', 4'-OHs on gallate ester to D60 (Aspartic acid) provide key interactions. Moreover, hydrophobic interactions from chromane and gallate ester rings to A64 (Alanine), I90 (Isoleucine), and A112 (Alanine) also stabilize this binding site (Figure 3.3b).[13] This experimental data support the hypothesis that EGCG can bind to the *Mtb* ε subunit. By the HSQC NMR titration modeling, both the gallocatechin and gallate moieties are required for ATP inhibitory action, which the 7-hydroxy group on the chromane, the 3-hydroxy group on the 2-phenyl ring, and the 3', 4'-hydroxy groups on the gallate ester are crucial substituents to bind to the *Mtb* ε subunit.[13]

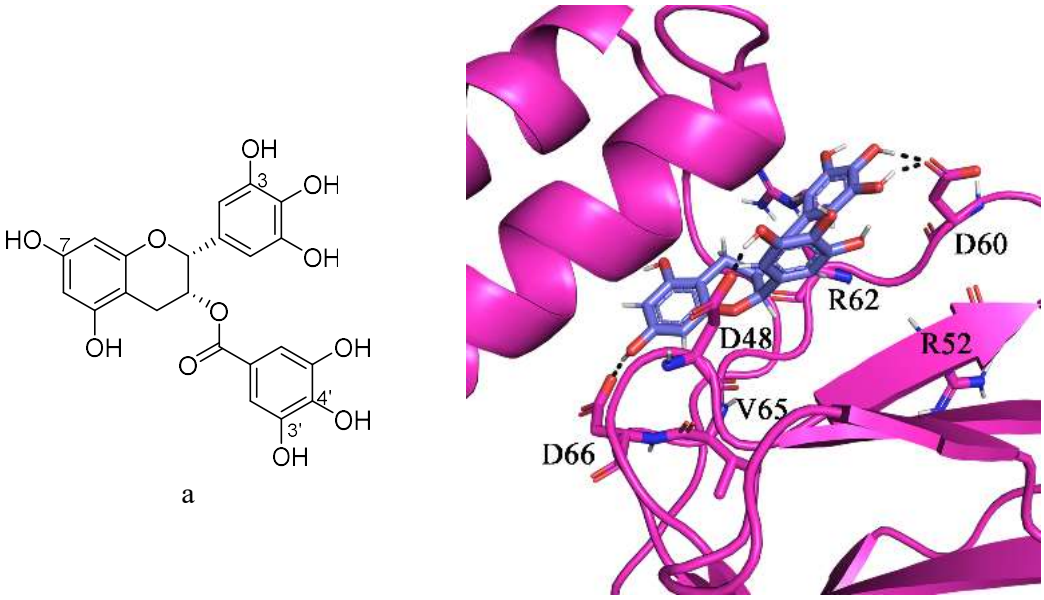

Figure 3.3 Structure of Epigallocatechin gallate (a) and Molecular interaction between EGCG and ε subunit from NMR titration experiments (b).[13] Reprinted with permission from Saw, W.-G. *et al. Scientific Reports* **2019,** *9* (1), 16759. Copyright © 2019 by Saw, W.-G. *et al.*

Furthermore, EGCG inhibited ATP production of *M. smeg.* IMV with the BDQ mutant I66M on the *c*-ring, with the same IC_{50} value as wide type *M. smeg.* IMV.[13] However, BDQ inhibited I66M ring *c* mutant *M. smeg.* IMVs with 10-times less effective than wide-type IMVs.[13] Notably, EGCG did not show the uncoupler effect, which is the main problem of BDQ (discussed in 1.4.3.5).[13] Thus, EGCG has the potential to be developed into compounds, being capable of curing MDR-TB or even BDQ resistant TB without the BDQ severe side effect of Arrhythmia.

Despite showing promising activity in IMV experiments, EGCG does not have any bacterial growth inhibition properties against *M. smeg.*[13] In this work, we were interested in synthesizing EGCG analogs to solve the bacterial growth inhibition problem and understanding the structure-activity relationship of EGCG to inhibit *Mycobacterium* ATP synthesis.

3.1.4 Epigallocatechin Gallate (EGCG)

EGCG (Figure 3.3a) is a natural product of the flavonoid and polyphenol class. It is usually isolated in high quantities from green tea and white tea leaves but only in small quantities from black tea.[14] This is because it is oxidized during the tea fermentation process. Moreover, EGCG is found in trace amounts in apple skin, hazelnuts, plums, carob, and pecans.[14] EGCG is a well-known commercial supplement that is claimed to have numerous health benefits such as antioxidant,[15] anti-inflammatory,[16] advantages to heart and blood circulation,[17, 18] and body weight reduction[19]. Many medical features, for instance, anti-allergic,[20] anti-carcinogenic,[21] anti-cancer,[22] and anti-diabetic[23], are still under drug development. Furthermore, EGCG has been reported to have antimicrobial properties against various kinds of pathogens that cause food poisoning, oral and gastrointestinal infections.[24-28] However, EGCG is required at very high doses to inhibit bacterial growth, and the mechanisms of action are varied, as shown in Table 3.1. Therefore, EGCG appears to be promiscuous in medical applications.

Table 3.1 EGCG mechanism of action to kill bacterial species

Organism	Proposed mechanism of action
Escherichia coli (MIC_{50} > 200 μM)[24] *Staphylococcus aureus* (MIC_{50} = 62.5 μg/mL)[25]	1) Oxidative stress condition from the generation of hydrogen peroxide from EGCG[25] 2) Interactions of EGCG with bacterial cell wall compartment, in which the exact targets depend on species[24] 3) Disruption of cell division and alerting the bacterial cell morphology[26]
Bacillus cereus (MIC_{50} = 621 μg/mL)[26]	Affecting to cell division and the bacterial cell morphology[26]
Gram-negative bacteria (MIC_{50} >800 μg/mL; *Klebsiella pneumonia, Proteus mirabilis, Pseudomonas aeruginosa, Serratia marcescens*)[27] *Salmonella typhi* (MIC_{50} >100 μg/mL)[27]	Binding to bacterial cell wall compartment[27]
Helicobacter Pylori (MIC_{90} = 100 μg/mL)[28]	Blocking Toll-like receptor 4 (TLR4) glycosylation to inhibit bacterial adhesion to human cell[29]

Various medicinal properties have been claimed for EGCG, and its derivatives, such as gallocatechin gallate (GCG) and epicatechin gallate (ECG) (Figure 3.4).[30, 31] In general, EGCG derivatives exhibit similar properties to the original EGCG. For example, gallocatechin gallate (GCG) is an epimer of EGCG, showing higher anti-allergenic potency than EGCG and other catechin analogs.[32] Epicatechin gallate (ECG) inhibited *Staphylococcus aureus* more effectively than EGCG.[33]

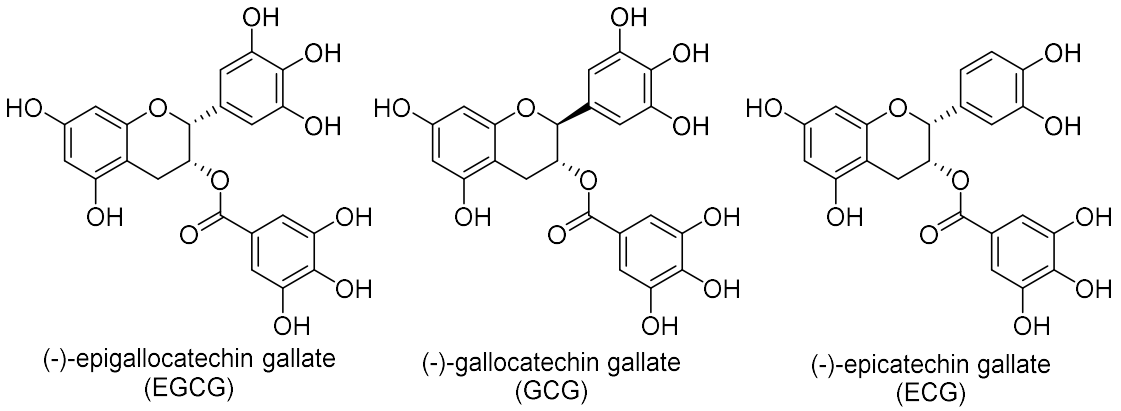

Figure 3.4 Structure of Epigallocatechin gallate (EGCG) and EGCG derivatives

Even though EGCG and its derivatives have many medicinal properties, high concentration is still necessary for their effectiveness. This results from low absorption,[29] poor membrane permeability,[29] blood iron chelation property,[34] and metabolic instability[29]. Stability problems in medical applications are reported to involve oxidation with O_2 *in vivo*.[29]

3.1.5 Epigallocatechin Gallate (EGCG) and EGCG derivatives' stability

EGCG and its derivatives are reported to decompose in the presence of light[35], oxidizing agents[36], and at high temperature[36]. Epimerization and autooxidation are the main mechanisms.[36] At high temperature or under UV light, epimerization is known to convert the less stable *cis* isomer of EGCG to a more stable *trans*-geometry (GCG, Figure 3.4). Under thermal conditions, the electron-rich ring **C** donates electrons from its *p*-hydroxyl group to form **Int-A.**[37] The generated phenonium anion reattacks the sp^2 carbon center, allowing rearrangement to the *trans*-geometrical isomer (Scheme 3.1).[37] On the other hand, UV irradiation of EGCG results in homolytic cleavage at the weakest carbon-oxygen bond on the tetrahydro-pyran ring **B**.[35] The diradical species (**Int-B**) then undergoes photo-induced electron transfer, followed by nucleophilic attack from phenolate to the carbocation to become GCG (Scheme 3.1).[35]

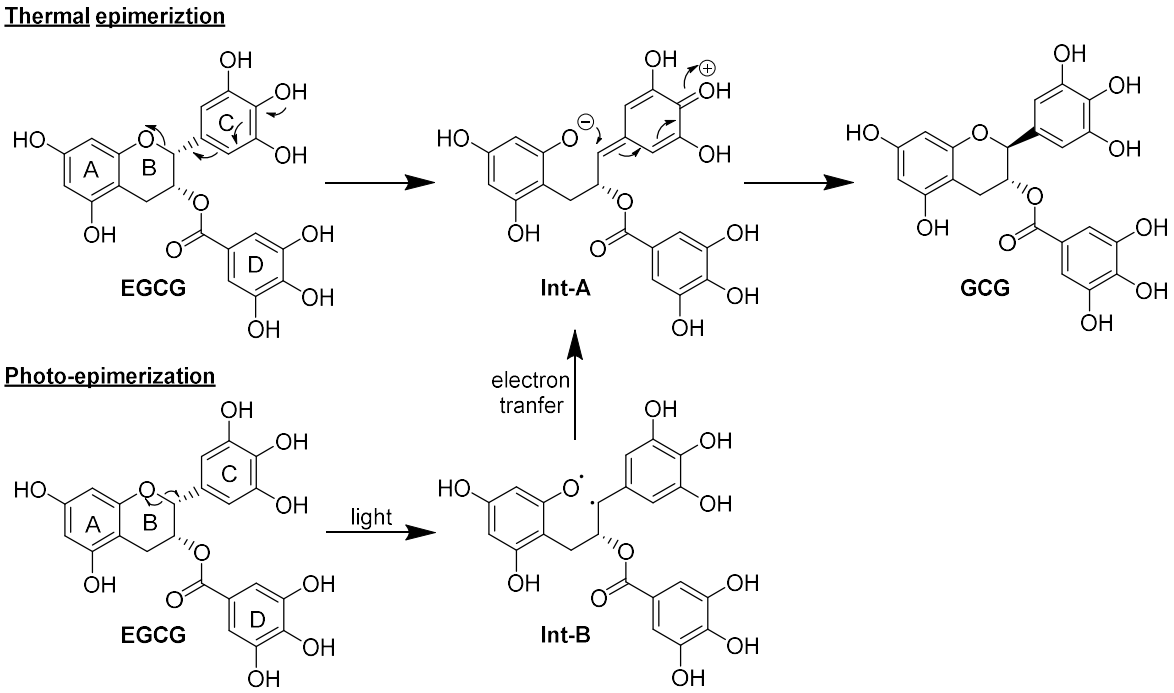

Scheme 3.1 Thermal epimerization and Photo-epimerization of EGCG

Auto-oxidation degrades EGCG to Theasinensin A and D.[38] This process can occur at any temperature in the presence of oxidants, e.g., oxygen, with higher pH and temperature accelerating the process.[39] This decomposition begins with oxidation to convert the catechol group in ring C to *o*-quinone (**Int-C**).[40] The unstable **Int-C** immediately reacts with another EGCG molecule. The highly electron-rich ring C of EGCG undergoes Michael addition to the 2-carbon of the *o*-quinone *via* electrophilic aromatic substitution (EAS).[38] Finally, rearomatization takes place to generate Theasinensins A and D, which differ only in the stereochemistry of the biaryl union (Scheme 3.2).

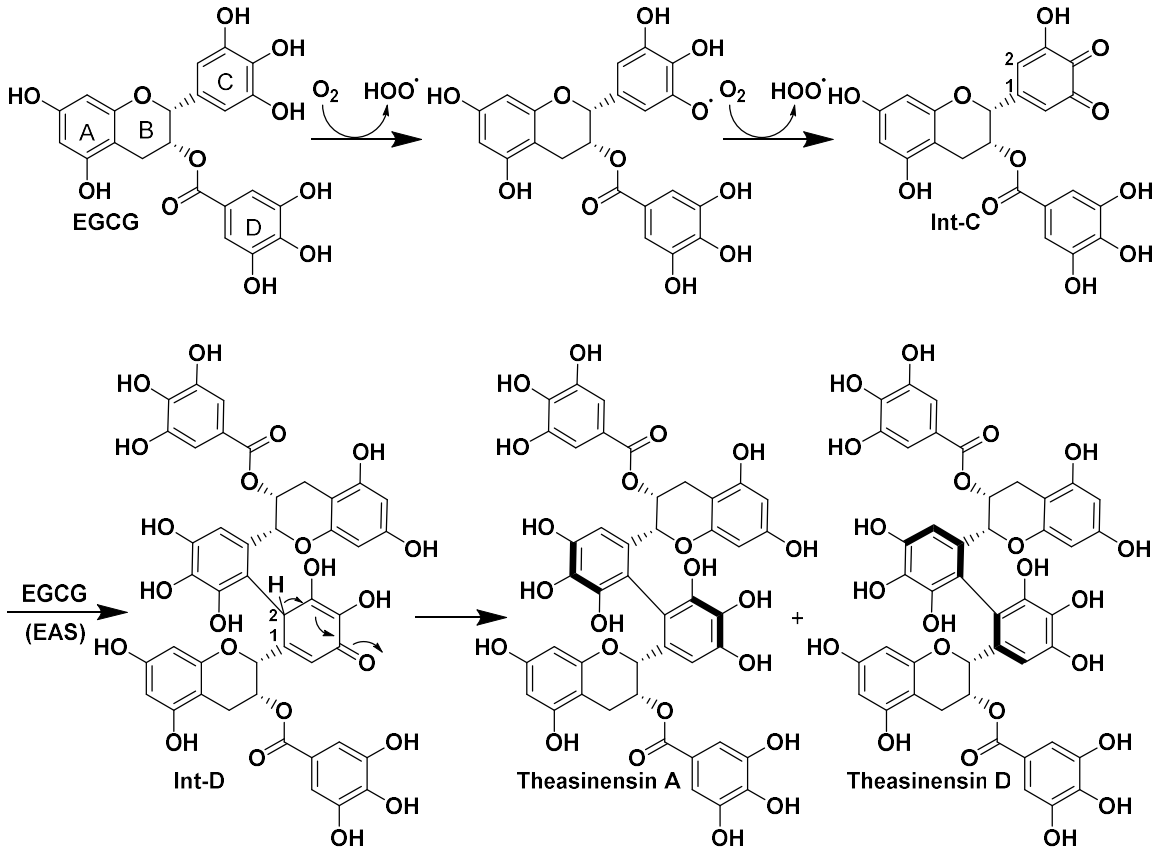

Scheme 3.2 Auto-oxidation of EGCG

3.2 Drug design to target *Mtb* ε subunit of the next generation of EGCG

EGCG has promising activity in inhibiting ATP synthesis of *M. smeg.*, I66M ring *c* mutant *M. smeg.*, and *M. bovis.* IMVs without uncoupler effect,[13] suggesting that it might be possible to develop potent compounds to treat MDR-TB or even BDQ-resistant TB without the severe side effects found in BDQ. However, the lack of bacterial growth inhibition is problematic since it was hypothesized to be caused by EGCG's metabolic instability or membrane impermeability.[29]

EGCG metabolic instability is not only a problem in our research but also one of the main reasons for the high dose needed for other medicinal properties.[29, 34] As EGCG decomposition is driven by the electron-rich ring C, as discussed in 3.1.5, modification to decrease the electron density on this ring could improve the stability.

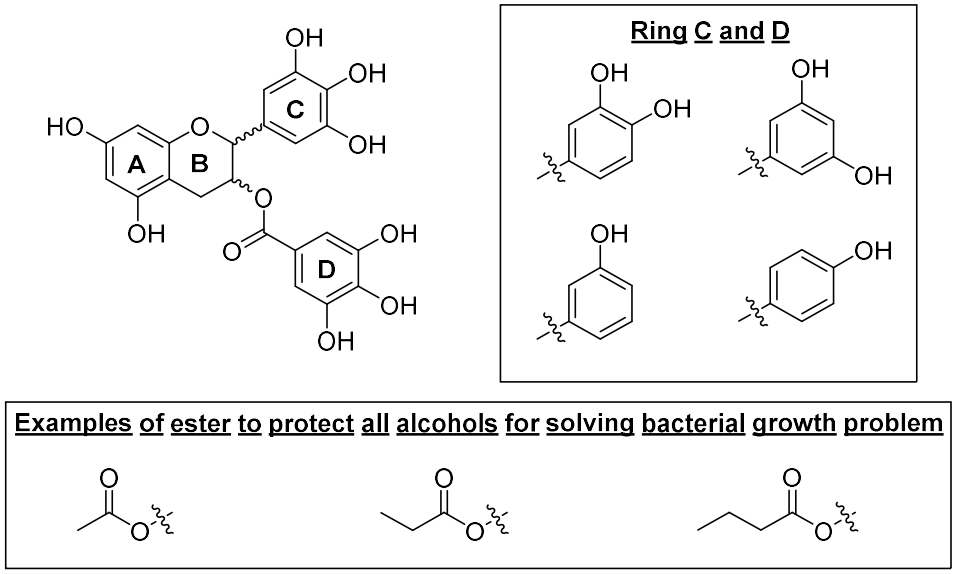

Figure 3.5 Drug design for EGCG modification

In this work, we aim to understand the structure-activity relationship (SAR) of EGCG in inhibiting mycobacterial ATP synthesis. Our strategy was to remove each hydroxy group from the EGCG to determine which is crucial for the mycobacterial ATP synthesis inhibition, focusing on ring C, and D, as well as the stereoisomer chemistry of the chromane structure (Figure 3.5). This study could decrease unimportant hydroxyls, which would address the stability problem and lower the numbers of hydrogen bond donors and acceptors, resulting in improved drug likeliness as recommended by Lipinski's rule[41], shown in Table 3.2.

Table 3.2 EGCG drug likeliness analysis toward Lipinski's rule of five

Properties	Lipinski's rule of five[41]	EGCG
Molecular mass	< 500 g/mol	458.4 g/mol
ClogP	≤ 5.00	1.49[a]
Number of hydrogen bond donors	≤ 5	8
Number of hydrogen bond acceptors	≤ 10	11
Number of rotatable bonds[42]	≤ 10	4

[a] ClogP was calculated by Chemdraw

A lack of membrane penetration is one of the main problems in TB drug development due to the unique lipophilic cell wall.[43] Therefore, most successful TB drugs are lipophilic compounds with ClopP greater than 5, which does not follow the guidance of Lipinski's rules.[44] EGCG is relatively polar with 8 hydroxy groups. Esterification of each hydroxyl (Figure 3.5) would be expected to improve MIC_{50} by allowing compounds to penetrate through the lipophilic *Mtb* cell wall, while the ester groups would be rapidly cleaved within the cell.[45]

3.3 Previously reported the synthesis of EGCG

The previously reported total syntheses of EGCG are reviewed as a guide to designing our EGCG analogs' synthetic route.

3.3.1 The first total synthesis of EGCG by Li *et al.*

The first total synthesis of EGCG was reported by Li *et al.* in 2001.[46] Racemic EGCG (***rac*-EGCG**) was successfully synthesized in a nine-step sequence in 23% overall yield, starting from 3,5-bis(benzyloxy)phenol (**3.1**) and (*E*)-3-(3,4,5-tris(benzyloxy)phenyl)prop-2-en-1-ol (**3.2**).[46] A crucial coupling step involved Friedel-craft alkylation of phenol **3.1** with cinnamyl alcohol **3.2**. The ortho ester cyclization was carried out in a three-step synthesis, beginning with the synthesis of racemic diol rac-**3.4**, followed by cyclization and hydrolysis to obtain racemic gallocatechin ***rac*-3.5** in good yield with high stereoselectivity (*trans* : *cis* = 9:1) (Scheme 3.3).[46]

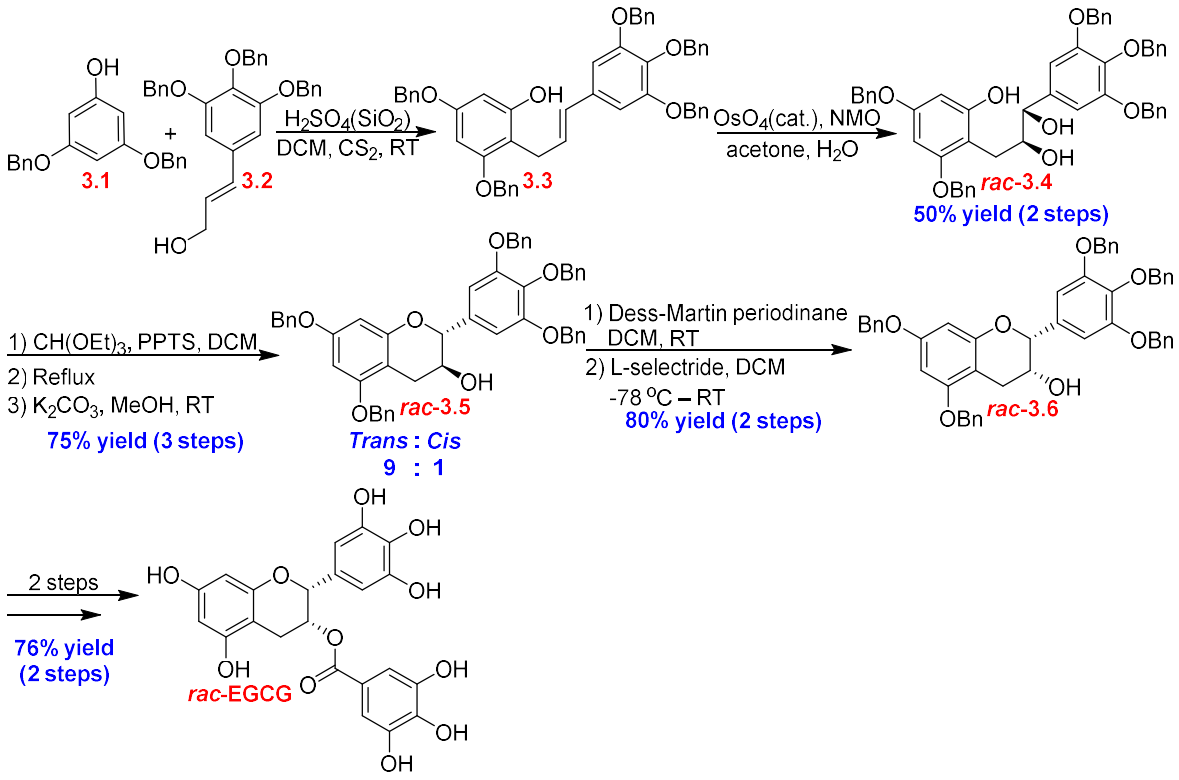

Scheme 3.3 Synthesis of racemic EGCG starting from phenol **3.1**

Epimerization of racemic gallocatechin ***rac*-3.5** by Dess-Martin oxidation, followed by reduction from the less hindered site using the bulky reducing agent of L-selectride, produced racemic epigallocatechin ***rec*-3.6** in excellent yield over 2 steps.[46] Esterification and global debenzylation were then performed to produce racemic EGCG (*rac*-EGCG) in high yield (Scheme 3.3).[46] This route was utilized to synthesize enantiomerically pure EGCG by conducting asymmetric Sharpless dihydroxylation after the Friedel-craft alkylation step (Scheme 3.4).[46] The enantiomeric purity of the synthetic EGCG synthesized by this approach was confirmed to be high by the identical values of specific rotation to a commercially available EGCG sample.[46]

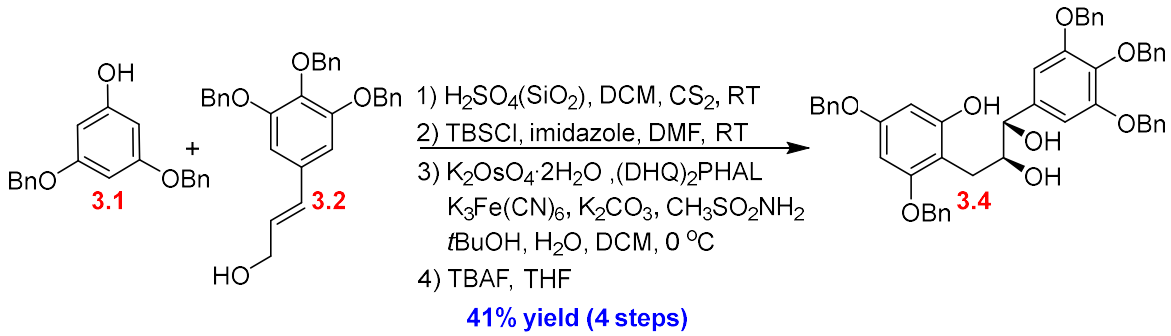

Scheme 3.4 Asymmetric Synthesis of EGCG by Li *et al.*

3.3.2 Total synthesis of EGCG by Zaveri *et al.*

Zaveri *et al.* developed another strategy to synthesize a racemic EGCG derivative (***rac*-3.22**).[47] This approach achieved the synthesis of EGCG derivatives in a 12-step sequence in 5% overall yield. The key intermediate in this approach is ***rac*-3.5**, having aldol condensation between methyl ketone **3.7** and aldehyde **3.8** as a key coupling reaction. The intramolecular cyclization of α,β-unsaturated ketone **3.9** toward $NaBH_4$ reduction with Michael addition and, subsequently, hydroboration-oxidation yielded ***trans*-*rac*-3.5** in good yield (Scheme 3.5).[47] The stereochemistry of the racemic gallocatechin (***trans*-*rac*-3.5**) was installed during the hydroboration step with high selectivity to generate *trans*-isomer (*trans* : *cis* = more than 95:5) due to the steric hindrance from the 2-aryl substituent, in which the regioselectivity was controlled by the electronic effect from the chromane aromatic ring.[47]

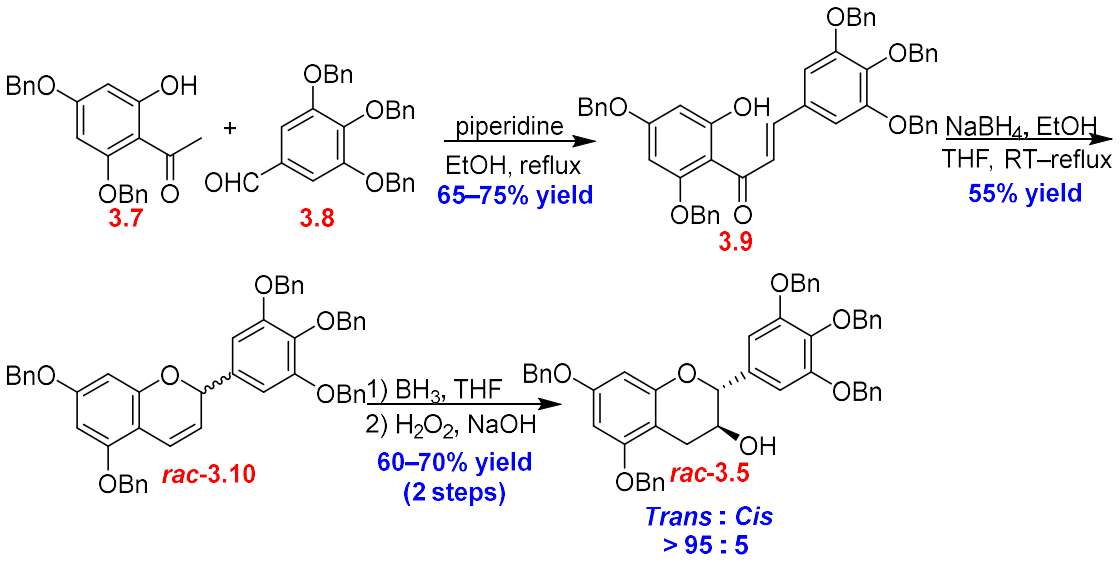

Scheme 3.5 Synthesis of racemic *trans*-benzopyran ***rac*-3.5** starting from **3.7** and **3.8**

3.3.3 Total synthesis of GC and EGCG by Suzuki's research group.

Suzuki's group developed a different approach to epigallocatechin. Starting from trifluorobenzene, EGCG was obtained in an 11-step sequence with an overall yield of 10 to 15%.[48] The key steps in the synthesis were an S_NAr reaction to couple fluorobenzene **3.11** and epoxy alcohol **3.12**, obtaining two diastereomers **3.13a** and **3.13b** in 39% and 37% isolated yield, respectively.[48] The precise stereochemistry of **3.13a/b** was unspecified. Epoxides **3.13a/b** were regioselectively ring-opened with Li_2NiBr_4 as a soft nucleophilic bromide source, followed by alcohol protection with a triethylsilyl (TES) group to produce **3.14a/b** (97% yield from **3.14a** and 91% yield **3.14b**).[48] The cyclization *via* the sulfonyl-metal exchange provided **3.15** (81% and 62% yield starting from **3.15a** and **3.15b**, respectively)**.** Desilylation, EDCI esterification, and global debenzylation were then performed to furnish EGCG (Scheme 3.6).[48]

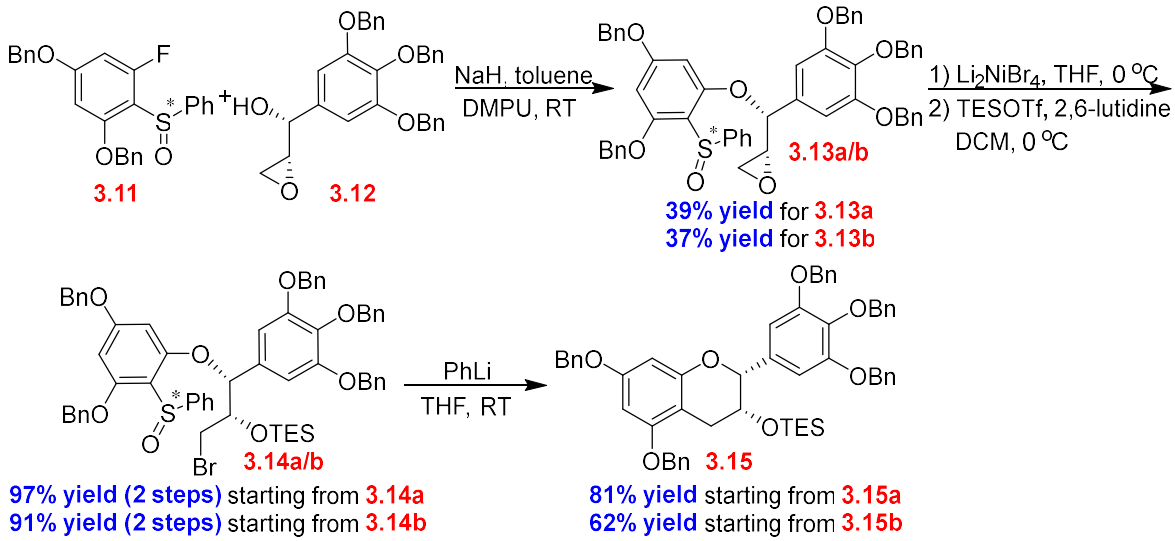

Scheme 3.6 Synthesis of EGCG from fluorobenzene **3.11** and epoxy alcohol **3.12**

The three approaches outlined above; all connect ring A and ring C in the first few steps, requiring numerous steps afterward to obtain the target compound. These are considered early-stage couplings between rings A and C. As a result, all the stated methodologies are inefficient for synthesizing ring C analogs for SAR study because there are only a few co-intermediates on each analog. All distinct intermediates in a long linear synthesis must be synthesized to generate a large batch of ring C analogs. These routes will, therefore, be material and time-consuming. In contrast, the late-stage coupling (Scheme 3.7) uses the same precursor in the final few stages to produce end products. The late-stage ring C synthesis allows large-scale reactions to synthesize a crucial precursor prior to ring C coupling, which may then be distributed to numerous final products. To the best of our knowledge, no reports of the ring C late-stage pathway have been made. Hence, we intend to develop this late-stage synthesis for SAR research, focusing on ring C.

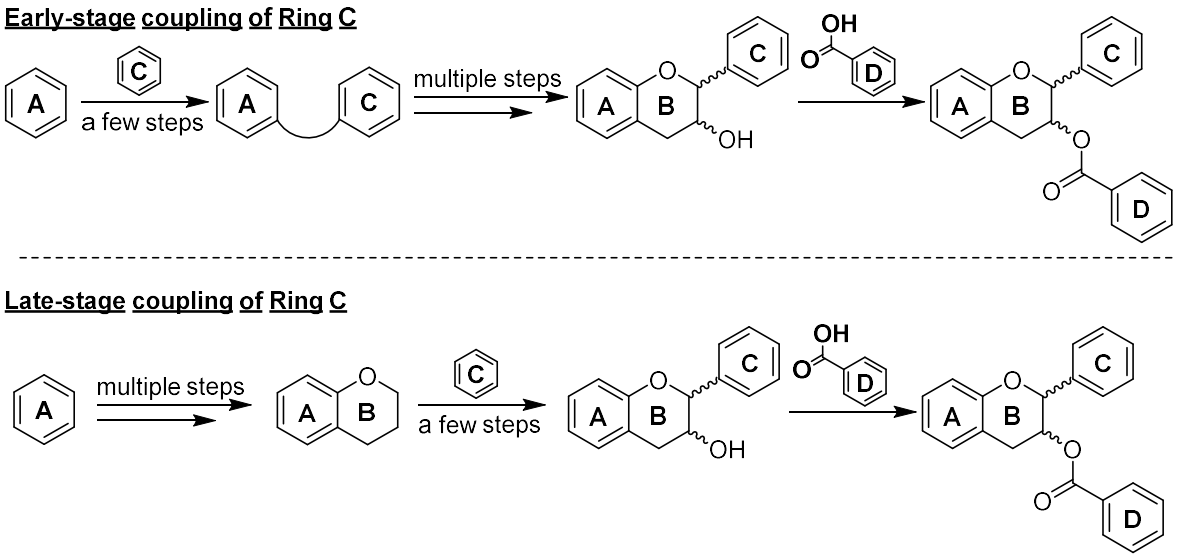

Scheme 3.7 comparison between early-stage and late-stage coupling of ring C EGCG analogs

3.4 Aims of this research

In this work, we aim to:

1) develop a new late-stage coupling pathway for EGCG and analogs' synthesis.
2) synthesize EGCG analogs to understand the structure-activity relationship (SAR) to inhibit mycobacterial ATP synthesis activity.
3) synthesize EGCG derivatives to solve the inability to inhibit mycobacterial growth inhibition.

3.5 Retrosynthetic analysis and synthetic plan of the next generation of EGCG

Retrosynthetic analysis of a new late-stage coupling synthetic route began with disconnecting the ester linkage between benzylated gallic acid derivatives (**3.16**) and catechin moiety **3.6**. Benzylated catechin **3.6** can be formed *via* the reaction between chromene **3.17** and iodobenzene **3.18** (Scheme 3.8).

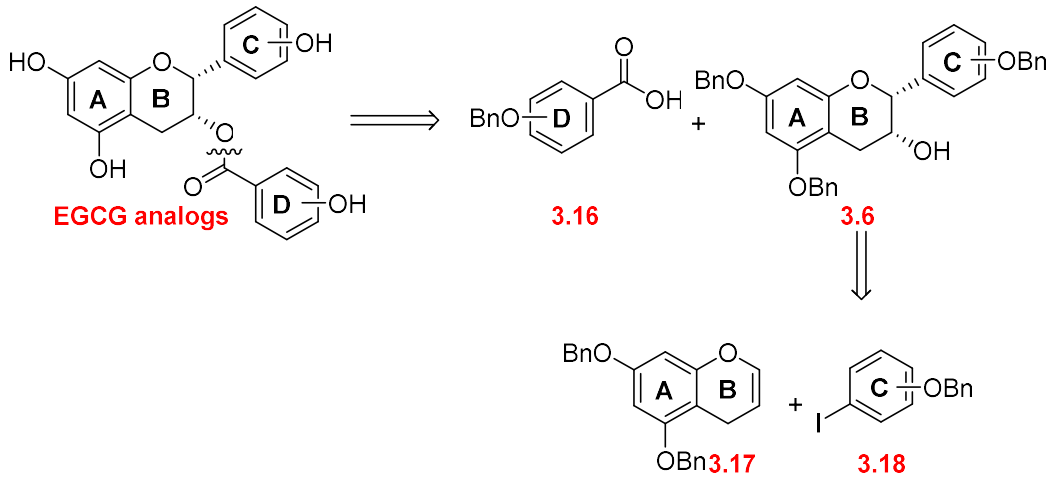

Scheme 3.8 Retrosynthetic analysis of EGCG analogs

3.6 Investigation of a new late-stage coupling pathway for EGCG and analogs' synthesis

The synthetic plan began with the chromene **3.17** synthesis, starting from 3,5-bis(benzyloxy)phenol **3.1** by a known procedure.[49] Diacetate **3.19** might be produced by dihydroxylation of the chromene **3.17**, followed by acetylation. Nucleophilic substitution of **3.19** with Lewis acidic organometallic reagent **3.20** could produce compound **3.21** with *cis* selectivity by axial attack *via* the favored transition state (TS).[50, 51] Finally, acetate hydrolysis, esterification, and global debenzylation would be expected to generate EGCG analogs (Scheme 3.9).

Our late-stage coupling strategy as described above could also be developed for asymmetric synthesis by using Sharpless asymmetric dihydroxylation[52] of the chromene **3.17**, which should provide enantiomerically enriched diacetate **3.19**. After the nucleophilic substitution of the enantiomerically enriched diacetate **3.19** to generate **3.21**, the following three-step sequence could be produced enantiomerically pure EGCG or EGCG analogs.

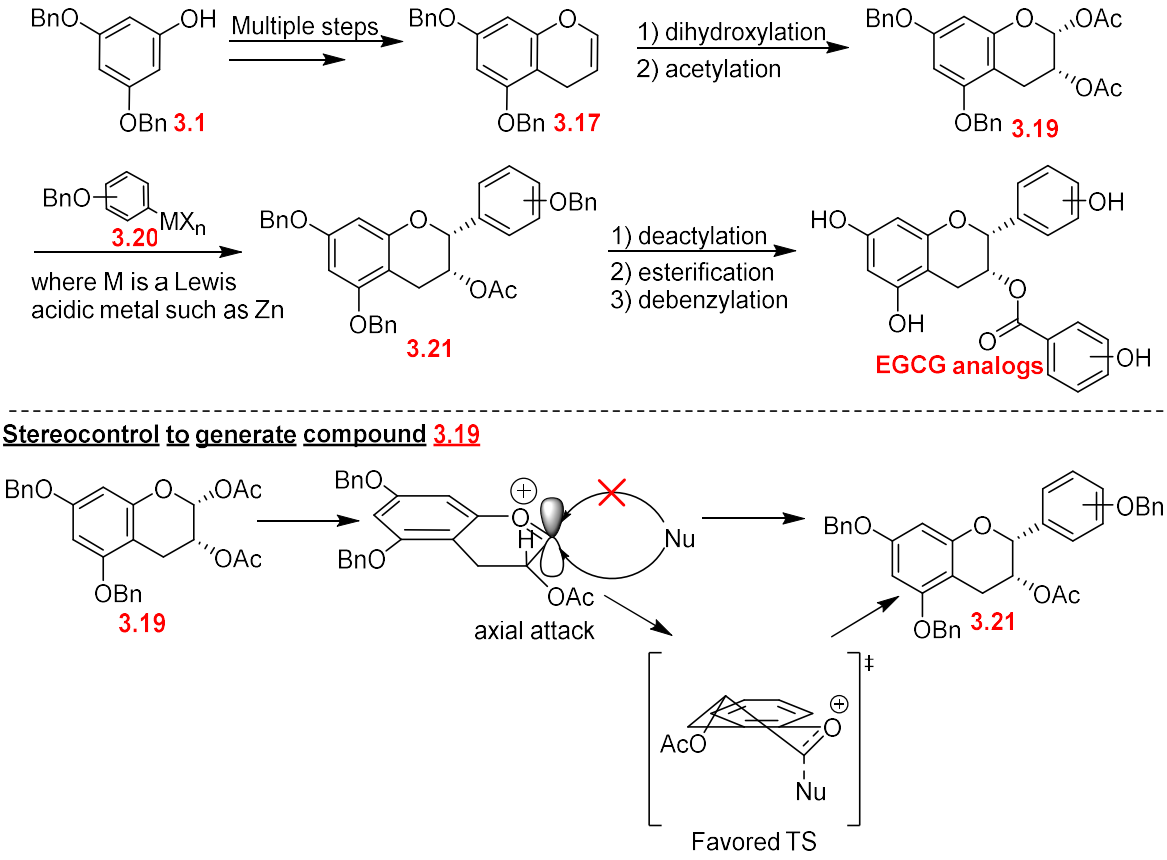

Scheme 3.9 Our late-stage coupling synthesis of EGCG analogs

3.6.1 Synthesis of 3,5-bis(benzyloxy)phenol (3.1)

3,5-Bis(benzyloxy)phenol (**3.1**) was a key precursor to produce chromene **3.17**. In this work, three synthetic routes to produce 3,5-bis(benzyloxy)phenol (**3.1**) were investigated to optimize product yield.

3.6.1.1 Direct dibenzylation of phloroglucinol (3.22)

A single-step dibenzylation of Phloroglucinol (**3.22**) using 2 equivalents of benzyl bromide (BnBr) and K_2CO_3 as a base[53] produced a mixture of multiple compounds based on TLC analysis. After flash column chromatography, only a small amount of a mixture of 1,3,5-tris(benzyloxy)benzene (**3.23**) and *C*-benzylation by-product **3.24** was isolated and identified. The *C*-benzylation behavior was consistent with Deme's report.[54] The remaining fractions were

inseparable mixtures, which were hypothesized to consist of mono and dibenzylation products together with *C*-benzylation by-products (Scheme 3.10).

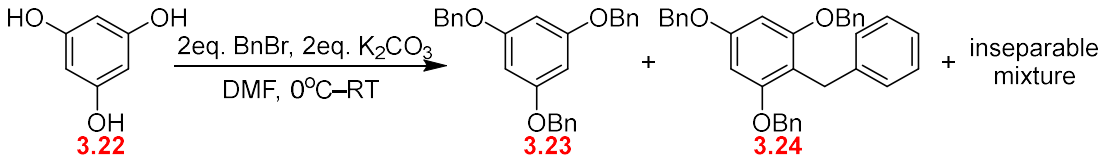

Scheme 3.10 Direct dibenzylation of Phloroglucinol (**3.22**)

3.6.1.2 Tribenzylation of Phloroglucinol (3.22) with selective monodebenzylation

Due to the complications and purification difficulties of the product of direct dibenzylation, the tribenzylation of **3.22** followed by selective debenzylation[55] was an alternative strategy (Scheme 3.11).

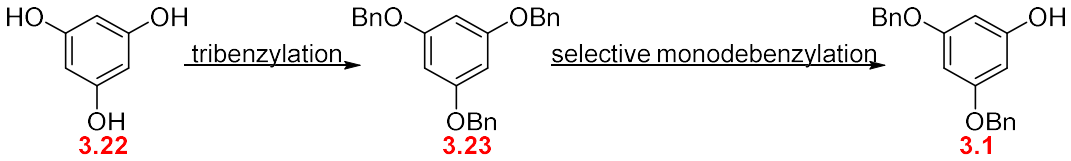

Scheme 3.11 The synthetic plan for 3,5-bis(benzyloxy)phenol **3.1** through tribenzylation of **3.22** and selective monodebenzylation

Tribenzylation of phloroglucinol **3.22** was performed by increasing the number of equivalents of BnBr and K_2CO_3 from 2 equivalents to 3 equivalents.[53] The expected 1,3,5-tris(benzyloxy)benzene (**3.23**) was observed in high conversion, based on ^{1}H NMR analysis. However, the formation of the *C*-benzylated by-product **3.24** was still evident. After purification, the tribenzylated **3.23** was obtained in 14–17% isolated yield (Scheme 3.12). The majority of the desired product was lost during recrystallization to remove by-product **3.24**. To improve the yield of **3.23**, our strategy was to suppress *C*-benzylation.

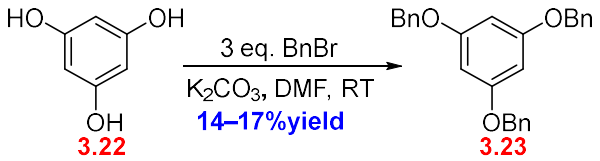

Scheme 3.12 Tribenzylation of phloroglucinol **3.22**

The *C*-benzylation to form the by-product **3.24** was promoted due to the high electron density of the aromatic ring caused by the three strong electron-donating hydroxyl groups. Therefore, decreasing the electron density by using fully esterified hydroxyls of **3.22** could avoid this side reaction, becoming our alternative approach. The standard acetylation of **3.22** gave fully acetylated phloroglucinol **3.25** in 84–93% yield.[56] The following step involved *in situ* generation of NaOH in precisely 3 equivalents from the reaction of sodium hydride and 3 equivalents of water. Acetate groups of **3.25** were hydrolyzed slowly with limited NaOH, which allowed phenolate to be formed gradually and benzylated immediately with benzyl chloride (BnCl) to obtain 1,3,5-tris(benzyloxy)benzene (**3.23**)[57] in high yield (73–75% yield) (Scheme 3.13). Even though the extra step of acetylation was required to improve yield, this method resulted in 61–70% overall yield over 2 steps. Therefore, this acetylation protocol was more efficient than the 14–17% yield from single-step tribenzylation.

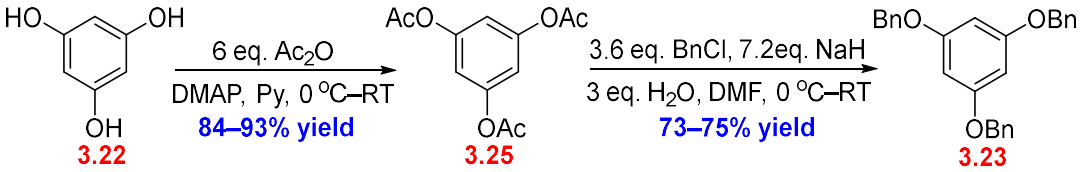

Scheme 3.13 Tribenzylation of **3.22** with selective monodebenzylation

Selective monodebenzylation of **3.23**[55] was next performed. The mechanism for selectivity has not yet been clearly described. We hypothesized that hydrogenolysis of **3.23** took place on the palladium metal surface under H_2. The initially formed phenol was promptly

deprotonated, which disturbed the adsorption on the metal surface and discontinued the following second debenzylation. Selective monodebenzylation of **3.23** then gave the desired 3,5-bis(benzyloxy)phenol (**3.1**)[55] in excellent yield (94–99% yield). The synthesis of phenol **3.1** from phloroglucinol (**3.22**) toward acetylation is summarized in Scheme 3.14.

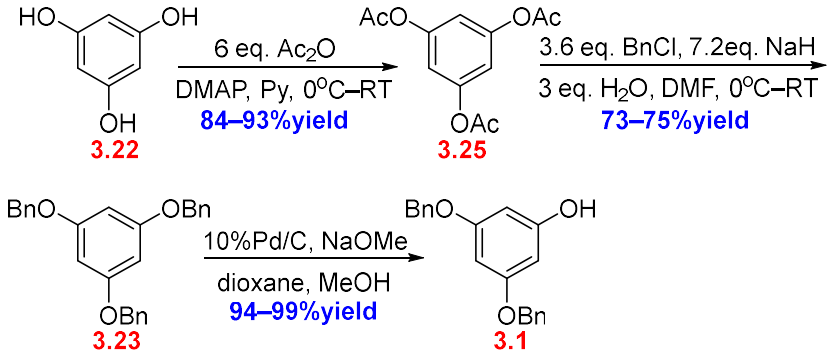

Scheme 3.14 Synthesis of 3,5-bis(benzyloxy)phenol **3.1** from phloroglucinol (**3.22**) towards acetylation

3.6.2 Synthesis of 5,7-bis(benzyloxy)-4*H*-chromene (3.17)

A five-step synthesis of chromene **3.17** starting from phenol **3.1** has been reported by Machado, *et al.*[49] Herein, the shorter synthesis *via* a three-step sequence utilizing Pt(II)-catalyzed cyclization was proposed**.**

3.6.2.1 Proposed chromene synthesis by Pt catalyzed cyclization strategy

The desired chromene **3.17** could be furnished by a three-step synthesis. Phenol **3.1** would be propargylated, followed by Nevado's platinum(II) cyclization,[58] which would probably result in a mixture of 2*H*-chromenes (**3.27**) and 4*H*-chromene (**3.17**). Therefore, isomerization to convert 2*H*-chromene (**3.27**) to 4*H*-chromene (**3.17**) could be required to improve the product yield (Scheme 3.15).

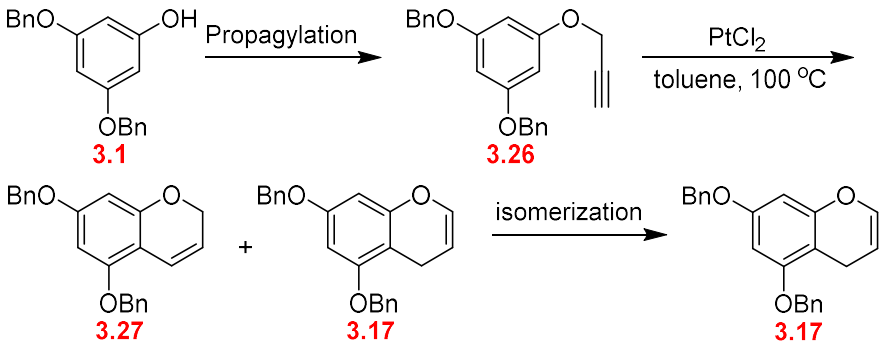

Scheme 3.15 Plan to synthesize chromene **3.17**

Phenol **3.1** was propargylated with propargyl bromide in the presence of K_2CO_3 under reflux to give **3.26** in quantitative yield. Platinum(II)-catalyzed cyclization with platinum (II) chloride ($PtCl_2$) at 100 °C[58] produced a mixture of 2*H*-chromene **3.27** and 4*H*-chromene **3.17** in 23% yield (Scheme 3.16).

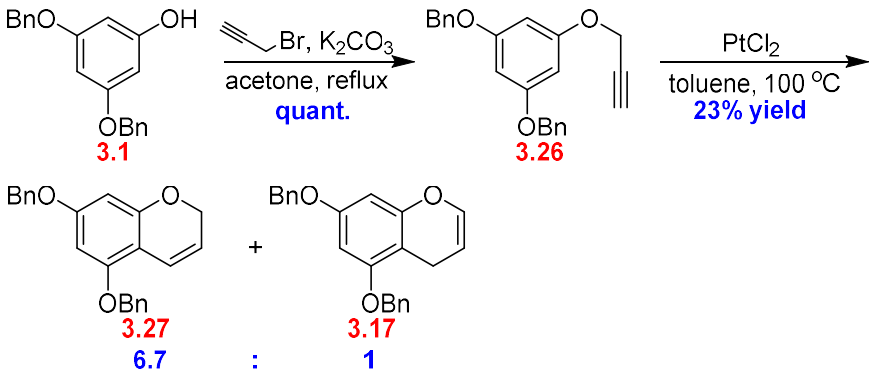

Scheme 3.16 Synthesis of chromene **3.17** and **3.27** starting from phenol **3.1**

The mole ratio between **3.27** and **3.17** was determined to be 6.5 : 1, based on ^{1}H NMR spectroscopy by calculating the signal integration ratio between 2*H*-Chromene (**3.27**) at 6.75 ppm and 4*H*-chromene (**3.17**) at 3.23 ppm from the isolated product (Figure 3.6). The 2*H*-chromene **3.27** likely undergoes *in situ* isomerization to give the desired chromene **3.17**.

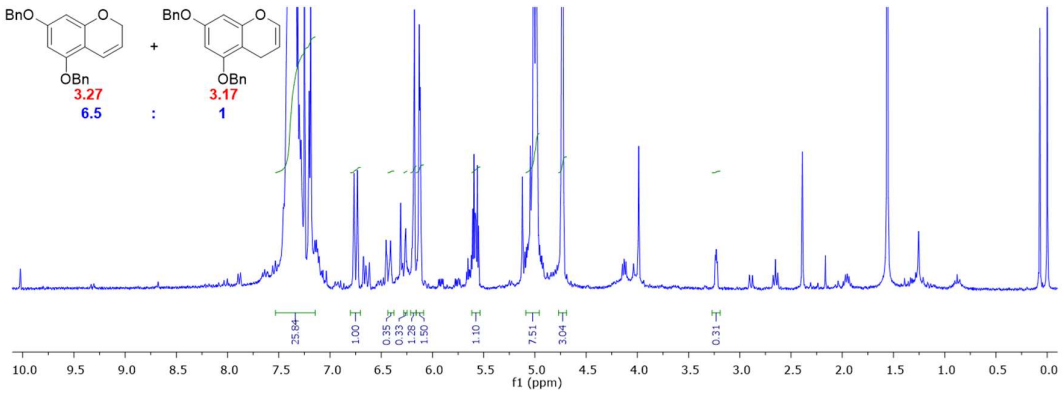

Figure 3.6 ^{1}H NMR spectrum of a mixture of 2*H*-chromene **3.27** and 4*H*-chromene **3.17** from Platinum (II)-catalyzed cyclization of compound **3.26**

Rhodium(I) species are known to be effective catalysts for olefin isomerization.[59] Rh(diphos)BF_4 was reported by Bergens *et al.* to result in the isomerization of allyl alcohol to give prop-1-en-1-ol under very mild conditions.[60] To perform the isomerization, Rh(diphos)BF_4 was pre-formed by the reaction of Rh(COD)BF_4 with 1,2-bis(diphenylphosphino)ethane (diphos). The mixture between 2*H*-chromene **3.27** and the desired 4*H*-chromene **3.17** in 6.7 : 1 mol ratio (calculated by ^{1}H NMR spectroscopy) was then added to the preformed Rh(I) catalyst solution. The temperature and reaction time were examined, as shown in Table 3.3.

Table 3.3 Rhodium (I)-catalyzed isomerization of a chromene mixture **3.27** and **3.17**

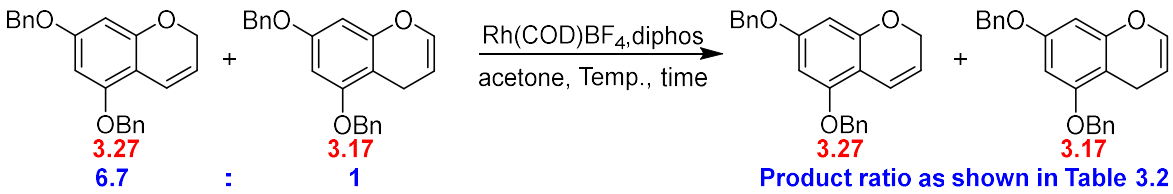

Temperature	Time	Mole ratio between 3.27 and 3.17[a]
RT (25 °C)	2 days	4.3 : 1
Refluxing temperature[b]	8 hours	3.2 : 1
Refluxing temperature[b]	24 hours	Complex mixture (product decomposition)

[a] Mole ratios were determined by ^{1}H-NMR

[b] Bath temperature was set at 60 °C

This isomerization strategy was able to convert 2*H*-chromene **3.27** to the desired 4*H*-chromene **3.17** as the proportion of product **3.17** was increased at room temperature (see Table 3.3). The amount of **3.17** was improved by refluxing for 8 hours. However, after extended 24-hour reflux, both chromene **3.27** and **3.17** were degraded to a complex mixture. Therefore, this approach was ineffective for synthesizing chromene **3.17** due to its inability to completely convert chromene **3.27** to chromene **3.17**, in which the desired chromene **3.17** was observed as a minor component in a mixture with chromene **3.27**.

3.6.2.2 Modified chromene synthesis from Machado's strategy

The second synthetic route to **3.17** was adapted from Machado's procedure[49]. This strategy involved a three-step synthesis of diene **3.28** from 3,5-bis(benzyloxy)phenol **3.1**. Ring-closing metathesis of **3.28** then gives chromene **3.17**[49] (Scheme 3.17). Even though this route is reported by Machado *et al.*,[49] the synthetic procedure would require reinvestigating as Machado *et al.* only provided a synthetic scheme in the main paper without a detailed procedure.[49]

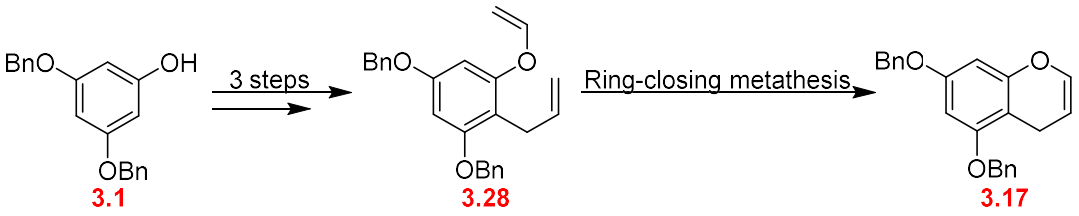

Scheme 3.17 Synthetic plan for 4*H*-chromene **3.17** through the synthesis of diene **3.28** and ring-closing metathesis

Phenol **3.1** was allylated with allyl bromide in the presence of K_2CO_3 under reflux to furnish allyl phenyl ether **3.29** in 75–81% yield. Claisen rearrangement by heating **3.29** neat at 200 °C produced allyl benzene **3.30** in 67–73% yield through a [3,3]–sigmatropic rearrangement. 2-Allylphenol **3.30** was then alkylated with 1,2-dibromethane using Cs_2CO_3 as a base under reflux, followed by elimination with potassium *tert*-butoxide to give diene **3.28** in 55–61% yield over 2 steps, as shown in Scheme 3.18.

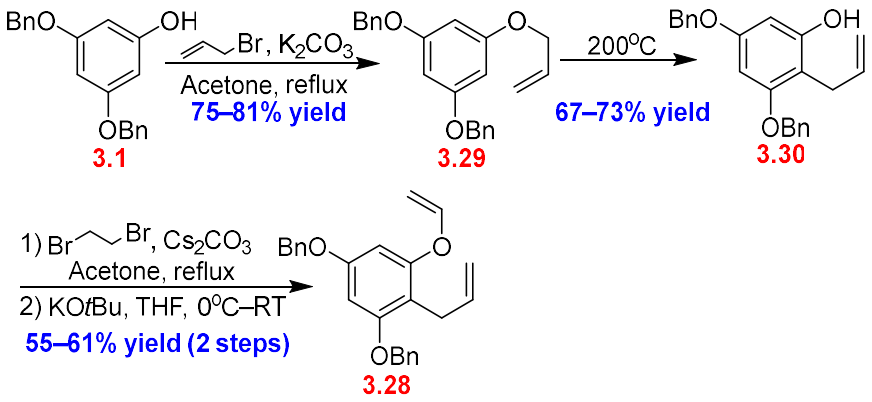

Scheme 3.18 Synthesis of diene **3.28** from 3,5-bis(benzyloxy)phenol **3.1**

Ring-closing metathesis, using Grubbs' second-generation catalyst (**Grubbs II**) at 60 °C, generated the desired chromene **3.17**. The ^{1}H NMR spectrum of **3.17** (Figure 7B-a) correlated to the previous report.[49] However, this compound **3.17** was found to decompose during solvent evaporation (toluene) under reduced pressure (about 30 psi) at 55 °C (Figure 7B-c). A similar degradation was also observed during storage of **3.17** at room temperature or even at -20 °C under an ambient atmosphere for 6 days (Figure 7B-d and e). This decomposition is postulated to occur by air oxidation at any temperature.

Thus, the entire experiment for this reaction was optimized by handling under nitrogen or under air-limited conditions to prevent air oxidation of chromene **3.17**. For instance, toluene was evaporated by cold finger distillation at 0.5–1 psi pressure at room temperature or by blowing dry under a nitrogen stream. This gave rise to chromene **3.17** in excellent yield (92–96% yield) (Figure 3.7A). ^{1}H NMR spectroscopy was used to determine the quality (Figure 3.7B-b). The resulting chromene **3.17** was used in the next step immediately.

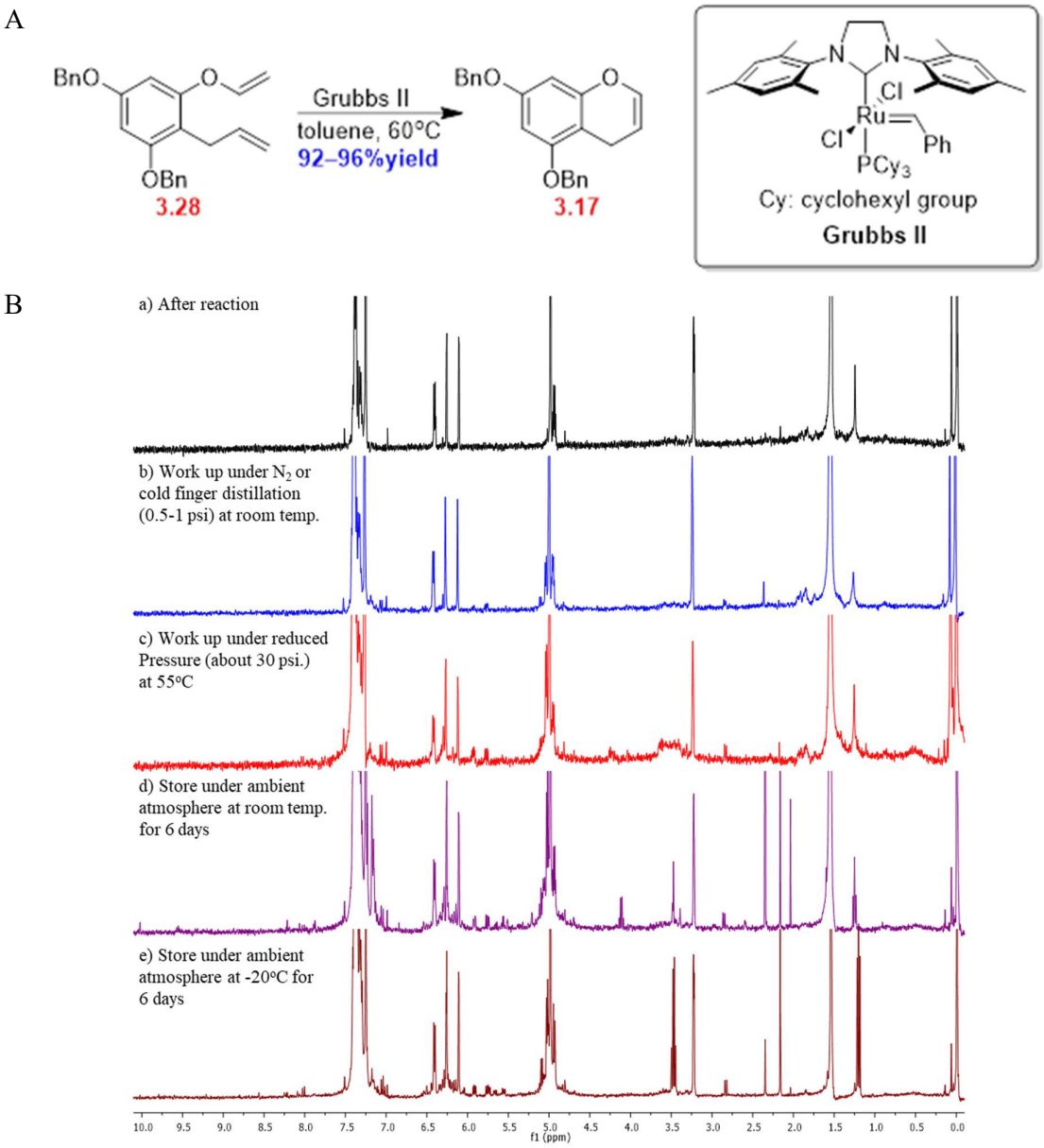

Figure 3.7 Ring-closing metathesis of diene **3.28** (A) ^{1}H NMR spectra of chromene **3.17** (B) after reaction (a), after working up under nitrogen or cold finger distillation (0.5–1 psi.) at room temperature (b), after working up under reduced pressure (about 30 psi.) at 55 °C (c), after storage under an ambient atmosphere at room temperature for 6 days (d), and after storage under an ambient atmosphere at -20 °C for 6 days (e)

The observed decomposition of chromene **3.17** could involve hydrogen atom abstraction by oxygen in the air to generate the chromene radical **Int-E**. This radical species is stabilized by resonance effects from conjugated alkene to form the resonance structure **Int-F**, as well as by the aromatic ring A (Scheme 3.19). The resulting radical species could undergo further reactions, becoming multiple by-products.

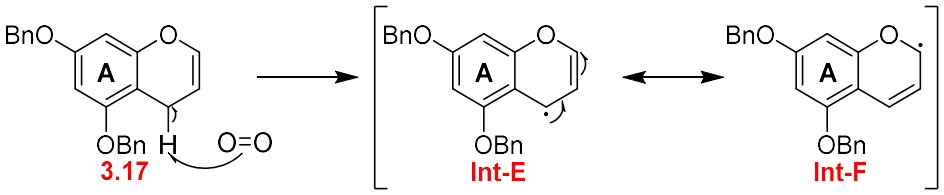

Scheme 3.19 Proposed decomposition mechanism of chromene **3.17**

3.6.3 Synthesis of 5,7-bis(benzyloxy)chromane-2,3-diyl diacetate (3.19)

To obtain diacetate **3.19**, dihydroxylation and then acetylation would be conducted, as shown in Scheme 3.20. Two well-known dihydroxylations reported by Tsuji[61] and Upjohn[62] research groups were investigated. Tetrahydropyran-2,3-diol **3.31** was hypothesized to be able to decompose during purification by silica gel column chromatography.[63] Thus, our strategy was to immediately acetylate the crude mixture from dihydroxylation to generate a more stable diacetate **3.19** before further purification.

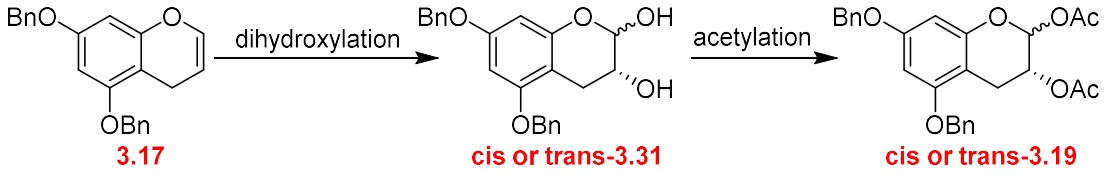

Scheme 3.20 Synthetic plan for diacetate **3.19** through dihydroxylation and acetylation

3.6.3.1 Tsuji dihydroxylation strategy

Tsuji dihydroxylation uses potassium osmate (K_2OsO_4) as a pre-catalyst, which is oxidized by a co-oxidant $K_3Fe(CN)_6$ to generate the key catalyst osmium tetroxide (OsO_4).[61] In general, alkenes with OsO_4 undergo oxidation in the presence of water and K_2CO_3 to furnish diol species. The chromene **3.17** was subjected to racemic dihydroxylation under Tsuji's condition[61] and then immediately protected with acetyl groups by standard acetylation[64]. However, a mixture of multiple compounds was observed based on TLC analysis. After purification, only conjugated ester **3.32** and aldehyde **3.33** were isolated (Scheme 3.21).

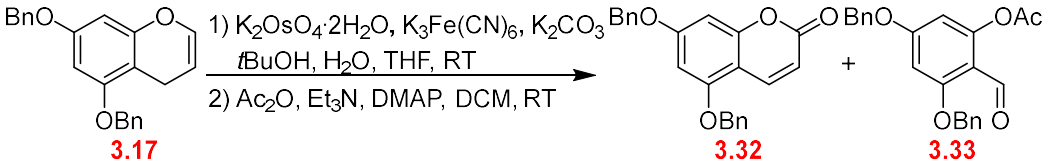

Scheme 3.21 Tsuji dihydroxylation with acetylation of chromene **3.17**

The conversion of chromene **3.17** to both conjugated ester **3.32** and aldehyde **3.33** could involve overoxidation of the desired diol **3.31** to form α-hydroxy ester (**Int-G**), which could then undergo elimination to produce ester **3.32**. The generated alkene might be able to undergo dihydroxylation to become the intermediate **Int-H**. Oxidation with oxidative cleavage would result in aldehyde **Int-I**. After the following step of acetylation, acetate **3.33** was obtained (Scheme 3.22).

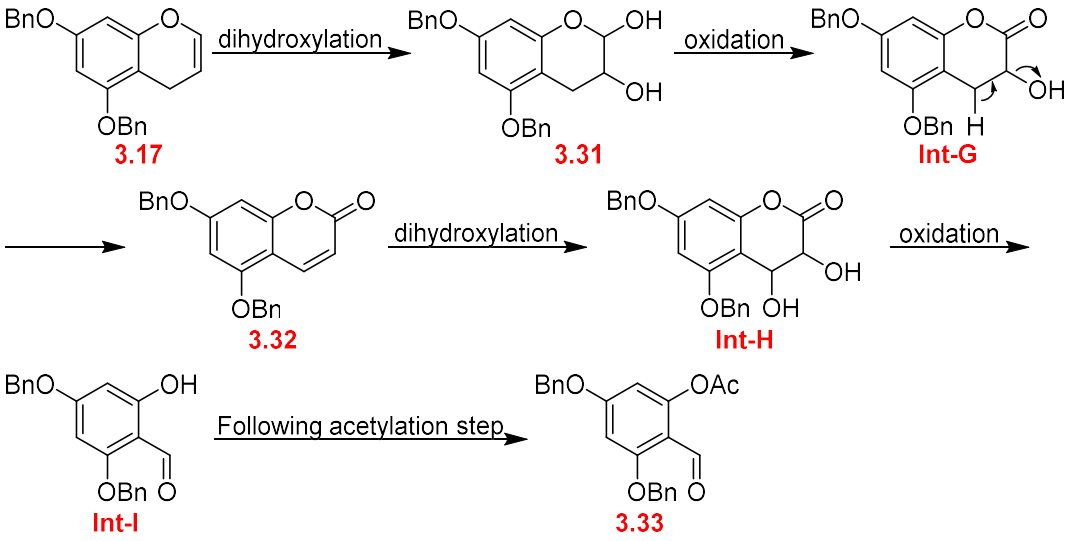

Scheme 3.22 Proposed mechanism to converse chromene **3.17** to both conjugated ester **3.32** and aldehyde **3.33**

Based on the proposed mechanism, $K_3Fe(CN)_6$ is the possible oxidant that causes overoxidation of the desired diol **3.31** to generate by-product **3.32** and **3.33**. As a single-electron oxidant, it may not be an innocent co-oxidant when the substrate is highly sensitive to radical reactions. Therefore, the Upjohn method[62] became an alternative since it uses *N*-methylmorpholine-*N*-oxide (NMO) as a co-oxidant instead of $K_3Fe(CN)_6$.

3.6.3.2 Upjohn dihydroxylation strategy

Upjohn dihydroxylation is reported to work well with a wide range of alkene substrates, requiring less than 5 mol% of K_2OsO_4 and 1.1–1.5 equivalent co-oxidant NMO to provide diol products.[62, 65] Upjohn dihydroxylation, followed by acetylation of chromene **3.17**, was performed. However, two diastereomers of diacetate **3.19** and triacetate **3.34** were obtained in low isolated yields of 21% and 10%, respectively. The unexpected triacetate formation could form through benzylic oxidation in the presence of water, having a similar pattern to the benzylic oxidation of catechin as reported by Es-Safi *et al.*[66] OsO_4 or NMO was postulated to be an oxidant, leading to the benzylic oxidation of diol **3.31** (Scheme 3.23).

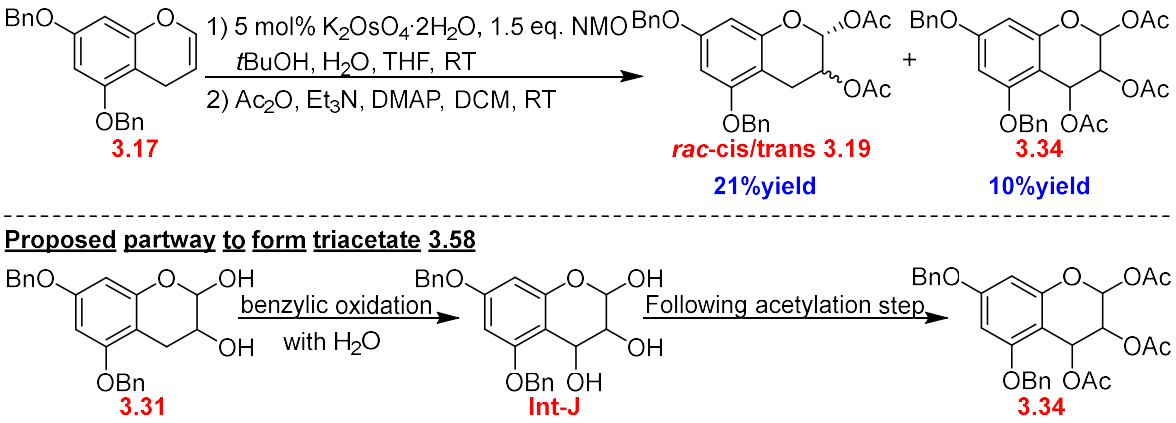

Scheme 3.23 Upjohn dihydroxylation with acetylation of chromene **3.17** and proposed pathway for triacetate **3.34** formation

To suppress benzylic oxidation, the number of equivalents of NMO was decreased from 1.5 to 1.05 equivalents. The resulting product was a diastereomeric mixture of diacetates ***rac-cis* 3.19** and ***rac-trans* 3.19** in 85% yield over 2 steps, as outlined in Scheme 3.24A. The mole proportion between these two diastereomers was estimated to be 2 : 3.1 (*cis* : *trans*) by calculating the signal integration ratio between ***rac-cis* 3.19** at 2.73 ppm and ***rac-trans* 3.19** at 2.92 ppm from the crude mixture in Scheme 3.24B. The relative stereochemistry of each diastereomer was determined by the Karplus relationship[67].

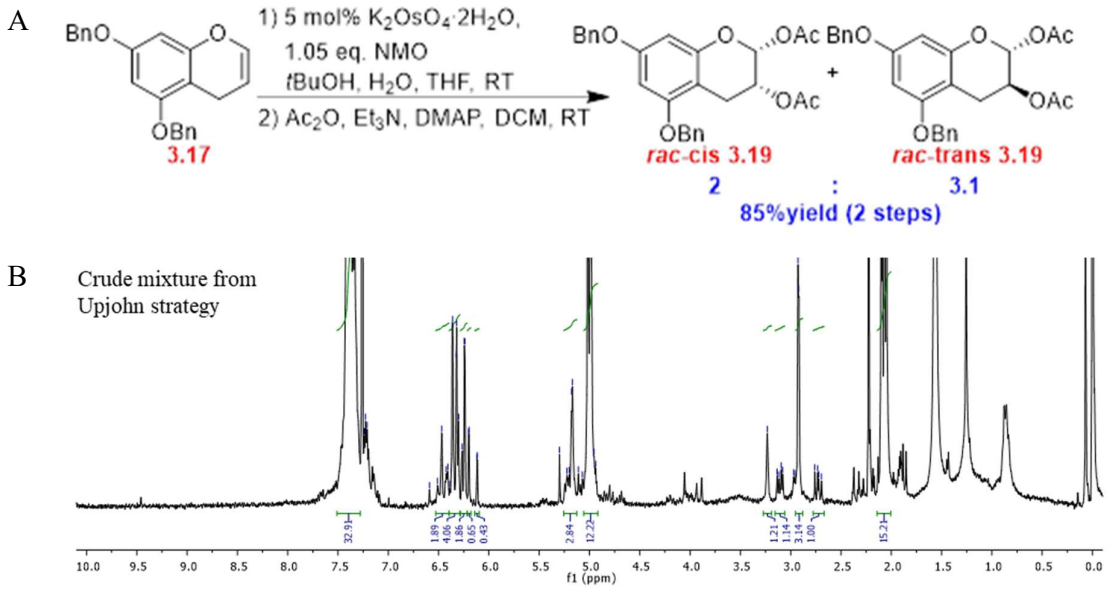

Scheme 3.24 Optimization of Upjohn dihydroxylation with acetylation (A) and ^{1}H NMR spectra of the crude mixture from Upjohn strategy (B)

The Karplus relationship was used to establish the relative stereoisomer of the major product. By dihedral angle analysis on the C3–C4 bond, the bond angle between the C3 equatorial proton (H_{eq}, 5.17 ppm) and H_{eq} on C4 (2.96 – 2.88 ppm) was about 90 degrees, which was consistent with the absence of an observed coupling constant between those 2 protons (0 Hz). The estimated dihedral angle between the C3 proton and the axial proton (H_{ax}, 2.96 – 2.88 ppm) on C4 was 30 approximately degrees (see Figure 3.8), which is consistent with an observed 6.4 Hz coupling. The coupling from H_{eq} on C3 and H_{eq} on C2 (6.36 ppm) was 3.1 Hz, while coupling was not observed between geminal protons (H_{ax} and H_{eq}) on C4, which displayed a similar chemical shift. Thus, the major isomer was assigned to ***rac-trans* 3.19**, as shown in Figure 3.8.

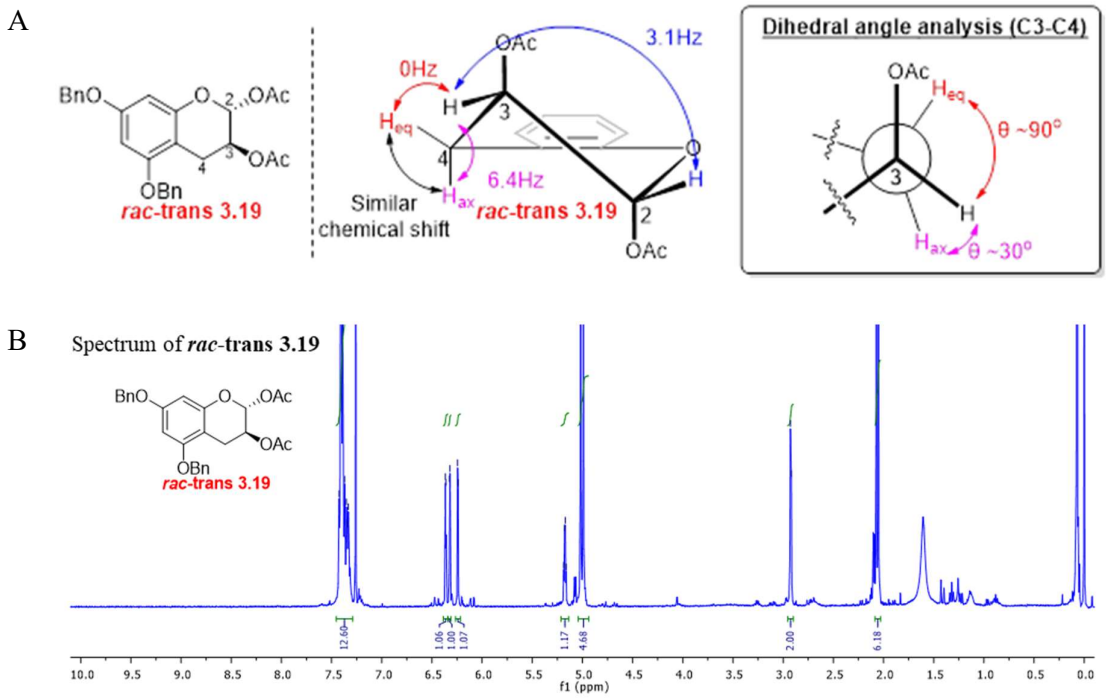

Figure 3.8 Analysis of the major diacetate by Karplus relationship (A; Benzyloxy groups were omitted for clarity), and ^{1}H NMR spectrum of ***rac-trans* 3.19** (B)

A similar analysis was carried out on the minor product. The dihedral angle between H_{ax} on C3 (5.23 ppm) and C4 H_{ax} (2.73 or 3.11 ppm) is estimated to be 160 degrees, being consistent with the 10.9 Hz coupling (see Figure 3.9). The approximated angle between C3 H_{ax} and C4 H_{eq} (2.73 or 3.11 ppm) was roughly 30 degrees, agreeing with the observed 6.4 Hz. The couplings from C2 H_{eq} and C3 H_{ax} was 2.5 Hz, and the geminal coupling on C4 (H_{ax} and H_{eq} on C4) was found at 15.6 Hz. The analysis showed a good match with ***rac-cis* 3.19** (Figure 3.9).

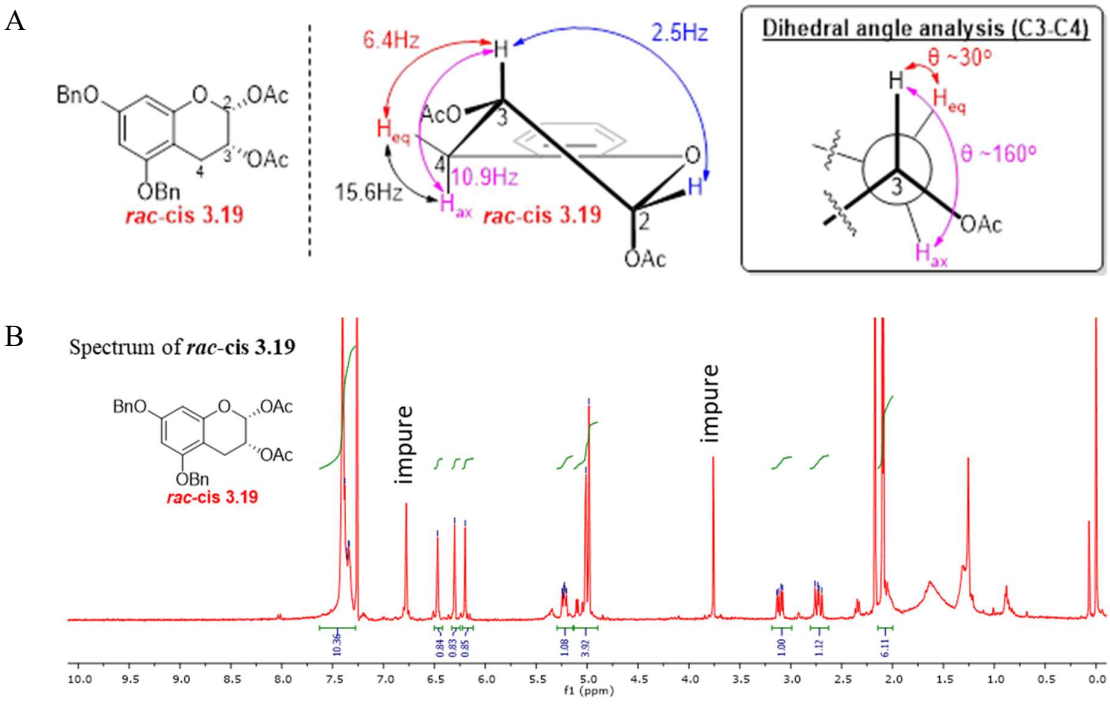

Figure 3.9 Analysis of the minor diacetate by Karplus relationship (A; Benzyloxy groups were omitted for clarity), and ^{1}H NMR spectrum of ***rac-cis* 3.19** (B)

The *trans*-diacetate **3.19** was formed as the major component, which was unlikely to be directly produced by OsO_4 dihydroxylation (*cis* selectivity).[65] The formation of ***rac-trans* 3.19** began with dihydroxylation of chromene **3.17**, generating *cis* diol **3.31**. The anomeric site of *cis* diol **3.31** could undergo ring-opening to form **Int-K**. Ring closure of **Int-K** then gives rise to *trans* diol **3.31**, which is acetylation to give diacetate ***rac-trans* 3.19** (Scheme 3.25).

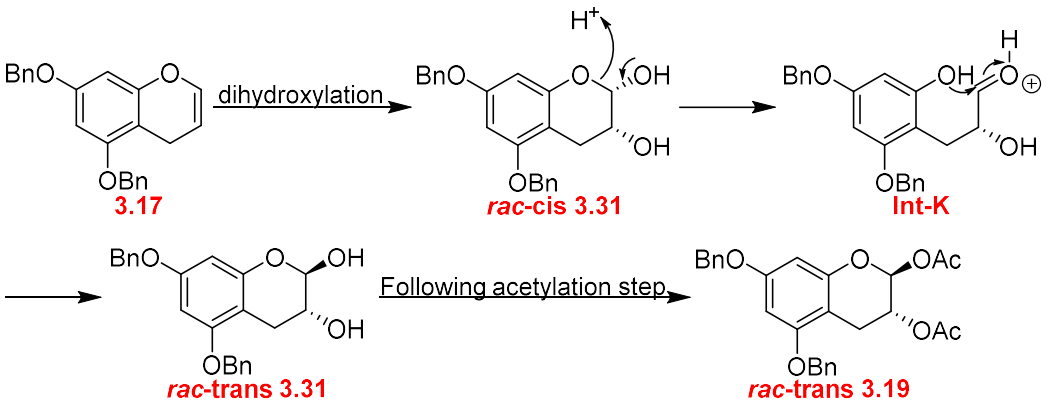

Scheme 3.25 Proposed mechanism for transformation from chromene **3.17** to ***rac-trans* 3.19**

Due to the purification difficulty in isolating ***rac-cis* 3.19** and ***rac-trans* 3.19** from each other, the diacetate **3.19** was carried through as the starting material for the next step in the diastereomeric mixture form. Moreover, both diacetate ***rac-cis* 3.19** and ***rac-trans* 3.19** could generate the same product in the next step by the S_N1 mechanism involving oxonium ion formation as discussed in 3.6.4. Therefore, the diastereomeric mixture between ***rac-cis* 3.19** and ***rac-trans* 3.19** would not give a different result from the diacetate **3.19** in diastereomerically pure form.

3.6.4 Synthesis of 5,7-bis(benzyloxy)-2-(aryl)chroman-3-yl acetate compounds

This step aimed to replace an acetate at the anomeric site of the diacetate **3.19** with an aryl group. In this work, the nucleophilic substitution of the diacetate **3.19** with Lewis acidic organometallic aryl reagent, and the electrophilic aromatic substitution of the diacetate **3.19** with an electron-rich aromatic compound were considered because electron donation from the pyran oxygen atom may convert both ***rac-cis* 3.19** and ***rac-trans* 3.19** to the identical oxonium ion. *Cis* selectivity by axial attack *via* the preferred transition state (TS) was expected to result in racemic catechin acetate, as shown in Scheme 3.26.

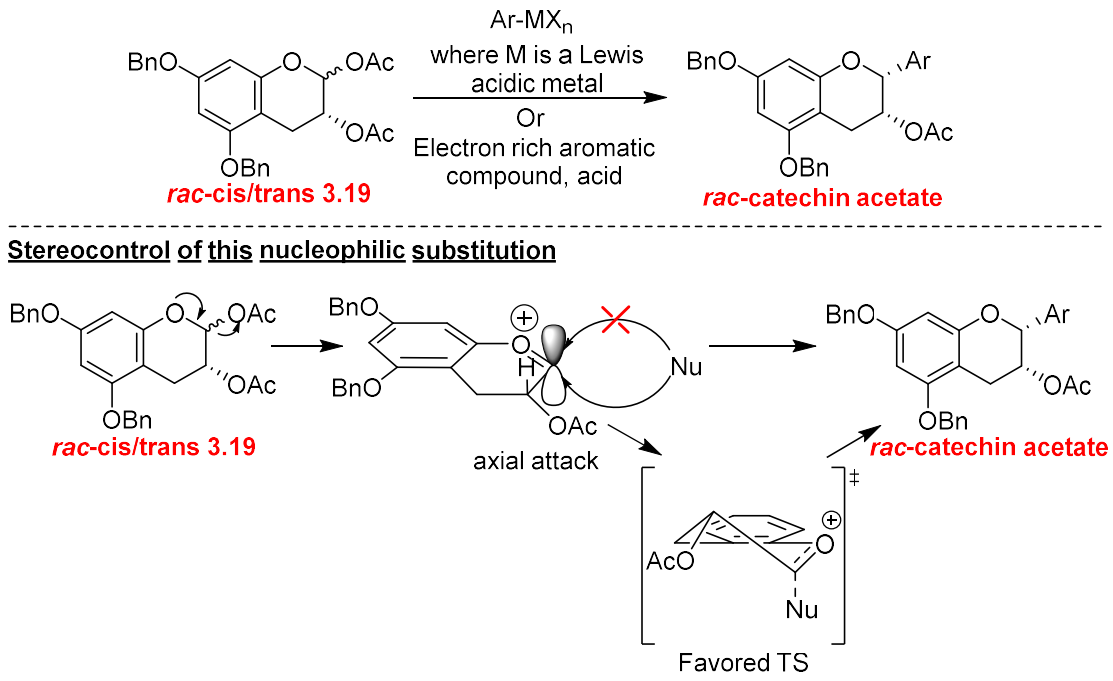

Scheme 3.26 Nucleophilic substitution of ***rac-cis/trans* 3.19**

3.6.4.1 Nucleophilic substitution with Organozinc reagent

The nucleophilic substitution of the diacetate **3.19** with Lewis acidic organometallic aryl reagent was expected to allow for the replacement of acetate at the anomeric position of **3.19** with an ally group from organometallic reagent. This strategy could be useful for researching SAR on ring C (detail in 3.2) as organometallic reagents with different aryl groups could be treated with the diacetate **3.19** in this step to generate a large number of ring C catechin acetate analogs.

Brown *et al.* studied nucleophilic substitution of 2-phenylsulfonyl-piperidines (**3.35**) with *in situ* produced organozinc reagents from *trans*-metalation between organolithium or Grignard reagents and $ZnBr_2$ to obtain substitution products (**3.36**) in moderate to excellent yield (Scheme 3.27).[68] This concept was applied to the synthesis of Asperidine B by Waddell *et al.*[50] The nucleophilic substitution of the diastereomeric mixture of piperidine diacetates **3.37a/b** (3.6:1) was a key step in substituting benzyl organozinc at the hemiaminal carbon to

yield **3.38** in 39% isolated yield.[50] Therefore, the nucleophilic substitution of the diastereomeric mixture ***rac-cis* 3.19** and ***rac-trans* 3.19** with *in situ* generated organozinc ally reagents could show high diastereoselectivity to provide racemic epigallocatechin acetate ***rac*-3.21** (Scheme 3.27).

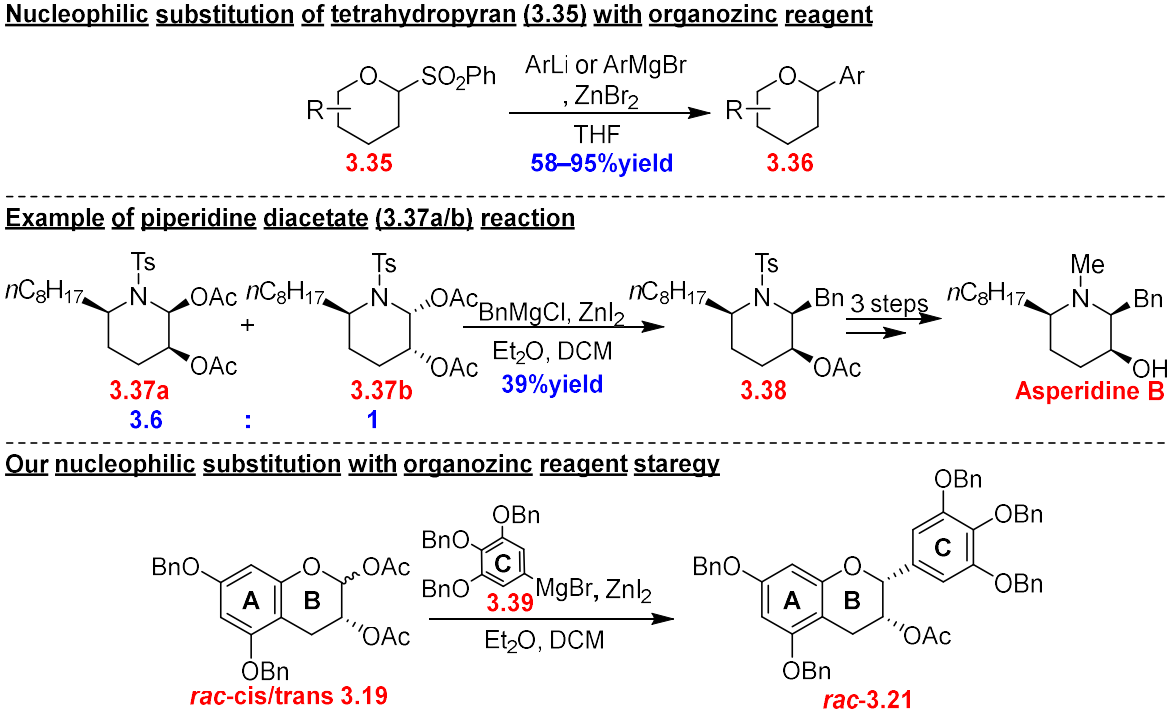

Scheme 3.27 Nucleophilic substitution with organozinc reagent and our synthetic strategy to synthesize ***rac*-3.21**

The nucleophilic substitution of the diastereomeric mixture of diacetates ***rac*-cis/trans 3.19** was studied with a simple organozinc reagent, (4-methoxyphenyl)zinc iodide. The organozinc reagent was *in situ* generated by transmetalation between ZnI_2 and (4-methoxyphenyl)magnesium iodide (**3.41**). The Grignard reagent (**3.41**) was prepared by heating *p*-iodoanisole (**3.40**) in THF at reflux with magnesium metal. Conditions and outcomes are summarized in Table 3.4.

Table 3.4 Studying of Nucleophilic substitution of ***rac-cis/trans* 3.19** with organozinc reagent

Grignard reagent preparation

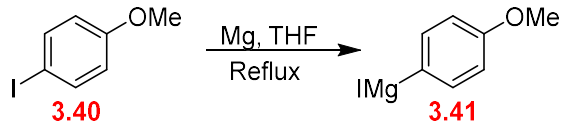

Preliminary Investigation of Nucleophilic substitution with Organozinc

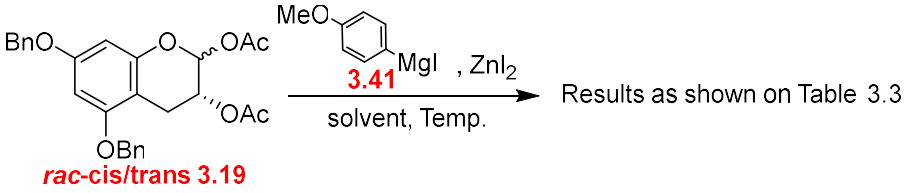

Entry[a]	Solvent[a]	Temperature	Results[b]
1	THF/Et_2O/DCM	Room temperature	No reaction
2		45 °C	No reaction
3		65 °C (Reflux)	No reaction
4	THF/Et_2O/DCE	Room temperature	No reaction
5		65 °C	No reaction
6		85 °C (Reflux)	Complex mixture (decomposition)

[a] Condition: ***rac-cis/trans* 3.19** (1 eq., 0.11 mmol), Grignard **3.41** (2 eq., 0.22 mmol), and ZnI_2 (2 eq., 0.22 mmol) in 3 mL of mixed solvent

[b] Solvent proportion was 3 : 2 : 8 (THF : Et_2O : DCM/DCE)

[c] Results were analyzed by ^{1}H NMR spectroscopy

Waddell's conditions using DCM as the major solvent at room temperature[50] (Entry 1) were examined for synthesizing racemic epigallocatechin acetate ***rac*-3.21**. However, only starting material was observed, as interpreted by ^{1}H NMR spectroscopy. Even after increasing the temperature to 45 °C and 65 °C (reflux), respectively (Entry 2 and 3), no conversion to the desired ***rac*-3.21**, as analyzed by ^{1}H NMR spectroscopy, was observed. We postulated that the reaction temperature of the mixed solvent, having DCM as a major solvent (boiling point = 40 °C), could be too low to activate the reaction. Therefore, DCE (boiling point = 83 °C) was investigated as an alternative. At room temperature and 65 °C (Entry 4 and 5), the outcomes were similar to those observed in the DCM condition. However, reaction at 85 °C (Entry 6) led

to starting material decomposition without any catechin product formation, as analyzed by ^{1}H NMR spectroscopy.

The problem was postulated to be due to the substrate. In Waddell's work,[50] the electron donation from the nitrogen atom on the piperidine ring and the steric hindrance from the tosyl group of piperidine diacetates **3.37a/b** (Scheme 3.27) were proposed as the key driving force for iminium ion formation.[50] Whereas the diacetate ***rac*-3.19** in our work could have only the electron donation from oxygen on the tetrahydropyran ring to drive the substitution, which could be insufficient to initiate the reaction, resulting in no conversion at room temperature to 65 °C. Nevertheless, the diacetate ***rac*-3.19** could not tolerate a high temperature (85 °C), leading to decomposition.

3.6.4.2 Nucleophilic substitution by Electrophilic Aromatic Substitution

Electrophilic aromatic substitution of diacetate ***rac*-3.19** with the electron-rich aromatic compound was an option since it does not require any modification to the aromatic nucleophile and can be varied to promote oxonium formation with different types of strong Lewis acid. Tetrahydrofuran acetate and tetrahydropyran acetate derivatives were demonstrated as examples of achieving electrophilic aromatic substitution with electron-rich aromatic in the presence of Lewis acid at low temperature in excellent yield with high stereoselectivity.[69-72] This reaction between diacetate ***rac*-3.19** and 1,2-bis(benzyloxy)benzene (**3.42**) could produce catechin derivatives based on the target compounds from the SAR investigation on ring C (detail in 3.2), as shown in Scheme 3.28.

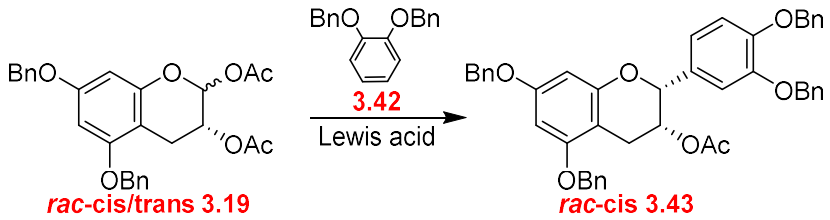

Scheme 3.28 Our plan for Electrophilic aromatic substitution between ***rac-cis/trans* 3.19** and **3.42**

The study began with dibenzylation of catechol (**3.44**) to furnish 1,2-bis(benzyloxy)benzene (**3.42**) in 87% yield. Electrophilic Aromatic Substitution was studied with 2 equivalents of **3.42** and different Lewis acids, given in Table 3.5. At 1.1 equivalents of Lewis acids, $Sc(OTf)_3$, $Ti(OiPr)_4$, $SnCl_4$, and $BF_3{\cdot}OEt_2$ resulted in no conversion as analyzed by ^1H NMR spectroscopy (Table 3.5; Entry 1 to 4). However, ***rac*-3.19** was observed to decompose without catechin product formation with 3.3 equivalents of BF_3 (Entry 6).

Table 3.5 Investigation of Electrophilic Aromatic Substitution between ***rac*-3.19** and **3.42**

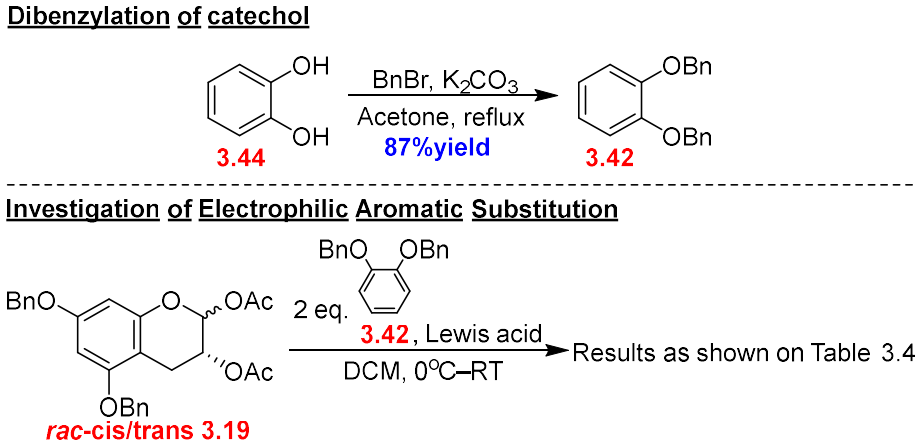

Entry[a]	Lewis acid	Equivalents of Lewis acid	Results[b]
1	$Sc(OTf)_3$	1.1	No reaction
2	$Ti(OiPr)_4$	1.1	No reaction
3	$SnCl_4$	1.1	No reaction
4	$BF_3{\cdot}Et_2O$	1.1	No reaction
5		2.2	No reaction
6		3.3	Complex mixture (decomposition)

[a] Conditions: ***rac-cis*/*trans* 3.19** (1 eq., 0.11 mmol), **3.42** (2eq, 0.22 mmol), and Lewis (as indicated in the table) in 1.5 mL of DCM

[b] Results were analysed by ^1H NMR spectroscopy

The anomeric acetate of **3.19** was found to be unusually stable compared to other anomeric acetates[69-72]. The observed decomposition of ***rac-cis/trans* 3.19** upon treatment with a high number of equivalents of BF_3 was hypothesized to be involved with the cleavage of the benzyl protecting groups[73] on ***rac-cis/trans* 3.19**. Therefore, the benzyls would be deprotected, and the benzyl carbocation was generated before the acetate group was expelled to form an oxonium ion. The resultant reactive carbocation then reacted at random to become a source of decomposition, leading to the complex mixture (Scheme 3.29).

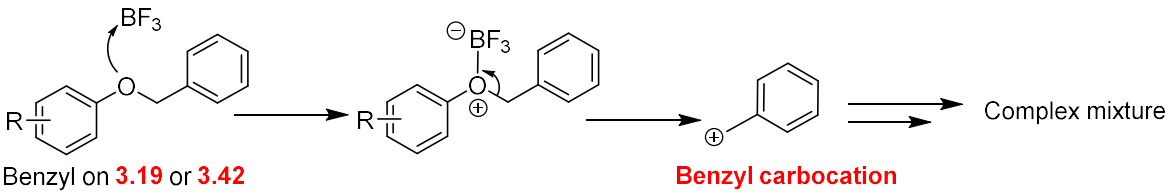

Scheme 3.29 Proposed decomposition mechanism of Electrophilic aromatic substitution between ***rac-cis/trans* 3.19** and **3.42** under excess BF_3

3.6.5 Tebbe strategy: An alternative pathway

Our next approach, inspired by Nicolaou's Tebbe reaction,[74] was to convert the olefinic ester directly to a cyclic enol ether. This route would begin with the esterification of intermediate **3.30**, using the method outlined earlier in 3.6.2.2. The ester **3.45** could then be treated with Tebbe reagent[75] to furnish chromene **3.46** *via* methylenation and ring-closing metathesis (RCM) in a single step. The resulting chromene **3.46** could be subjected to hydroboration-oxidation to provide gallocatechin (***rac-trans* 3.5**), as shown in Scheme 3.30.

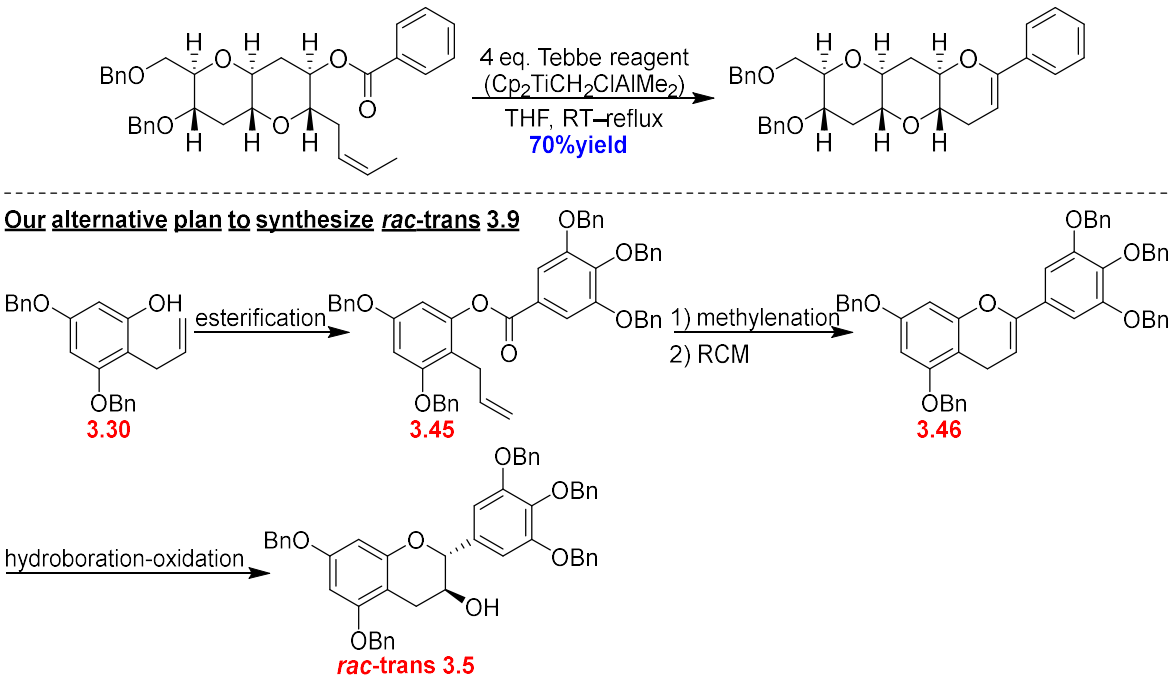

Scheme 3.30 Direct conversion of olefinic ester to cyclic enol ether by Nicolaou *et al.* and our synthetic plan for ***rac-trans* 3.5** through chromene **3.46**

Benzylated gallic acid **3.16** was prepared by global benzylation of gallic acid **3.47** with an excess of BnBr, followed by hydrolysis with NaOH in 50% EtOH in water at reflux[76] to provide **3.16** in 98% yield over 2 steps. The resulting benzoic acid **3.16** was converted to acid chloride by oxalyl chloride with a DMF catalyst and then esterified with phenol **3.30** under standard conditions[46] to furnish ester **3.45** in quantitative yield over 2 steps (Scheme 3.31).

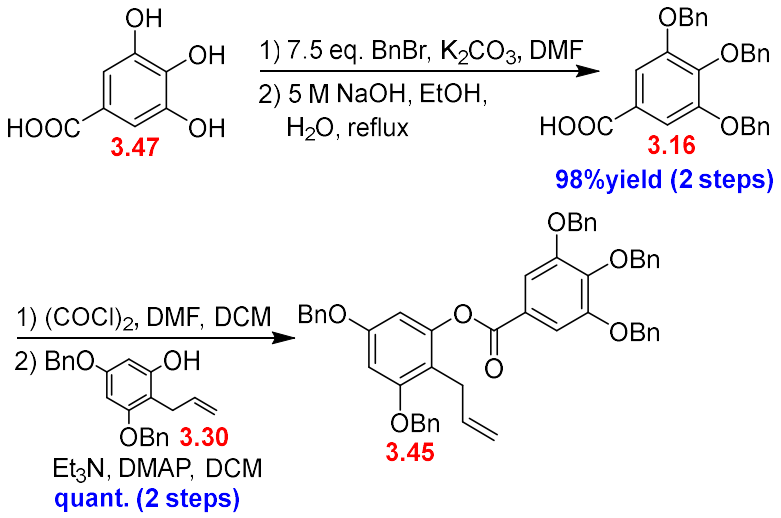

Scheme 3.31 Synthesis of olefinic ester **3.45** from gallic acid **3.47**

The Tebbe reaction was performed by treating olefinic ester **3.45** with 6 equivalents of Tebbe reagent at -20 °C to room temperature. The ester **3.45** was completely consumed as analyzed by ^{1}H NMR spectroscopy. However, the resulting product was too sensitive to handle, and elucidation of the structure was difficult since the product was unstable under air and decomposed during workup (Scheme 3.32).

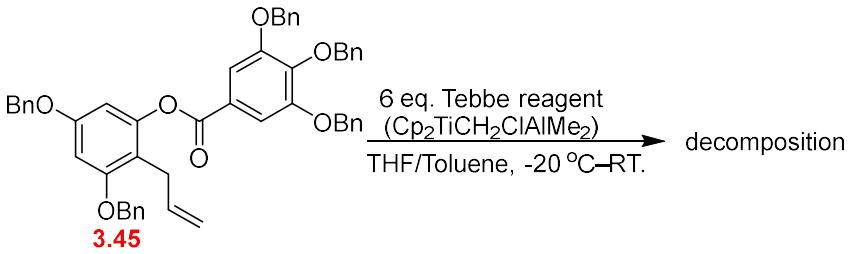

Scheme 3.32 Tebbe reaction of olefinic ester **3.45**

The expected chromene **3.46** could similarly decompose to chromene **3.17**, as discussed in 3.6.2.2 (Scheme 3.19). By comparison between the radical intermediates from the starting chromenes **3.17** and **3.46**, the **3.46-rad Int** could be more stable than the **3.17-rad Int** by the resonance stabilization from the additional aromatic ring C (Figure 3.10). Therefore, the chromene **3.46** should be less stable than the chromene **3.17**, which is correlated with the experimental results from the Tebbe reaction of the ester **3.45**.

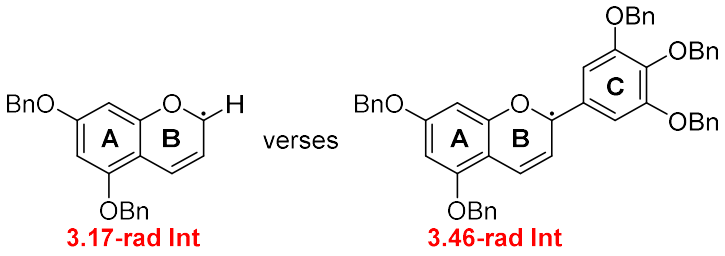

Figure 3.10 Comparison between radical intermediates **3.17-rad Int** and **3.46-rad Int**

3.7 Synthesis of EGCG derivatives for Structure-Activity Relationship (SAR)

The SAR investigation began with the synthesis of EGCG analogs. As discussed in section 3.2, ring C and ring D were our focus. Since our proposed synthetic routes failed to furnish targets as discussed in 3.6, the modified pathway from Li *et al.*[46] was employed to prepare our analogs.

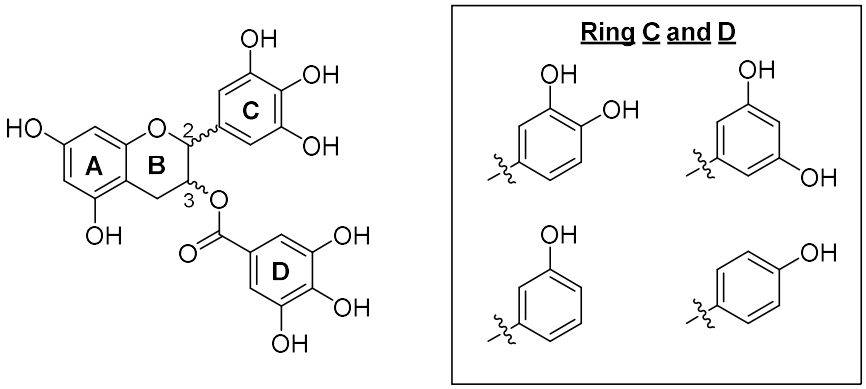

Figure 3.11 Targeted EGCG analogs for SAR investigation

3.7.1 Synthesis of EGCG analogs for SAR of Ring D

This section aims to synthesize analogs to understand the influence of each hydroxy group on ring D, as well as the stereochemistry of C2 and C3 to ATP inhibition activity (Figure 3.11). Our synthetic strategy was to esterify the commercially available catechin and gallic acid derivatives because this method involved a short pathway. Due to the chemical cost economy, catechin was chosen as a core instead of gallocatechin or epigallocatechin.

The approach was to benzylate catechin **3.48a** to give compound **3.49**, which would be isomerized by Li's method[46] to obtain epicatechin **3.50**. Both benzylated species **3.49/3.50** would be subjected to esterification with gallic acid derivatives and global debenzylation to yield ring D analogs (Scheme 3.33).

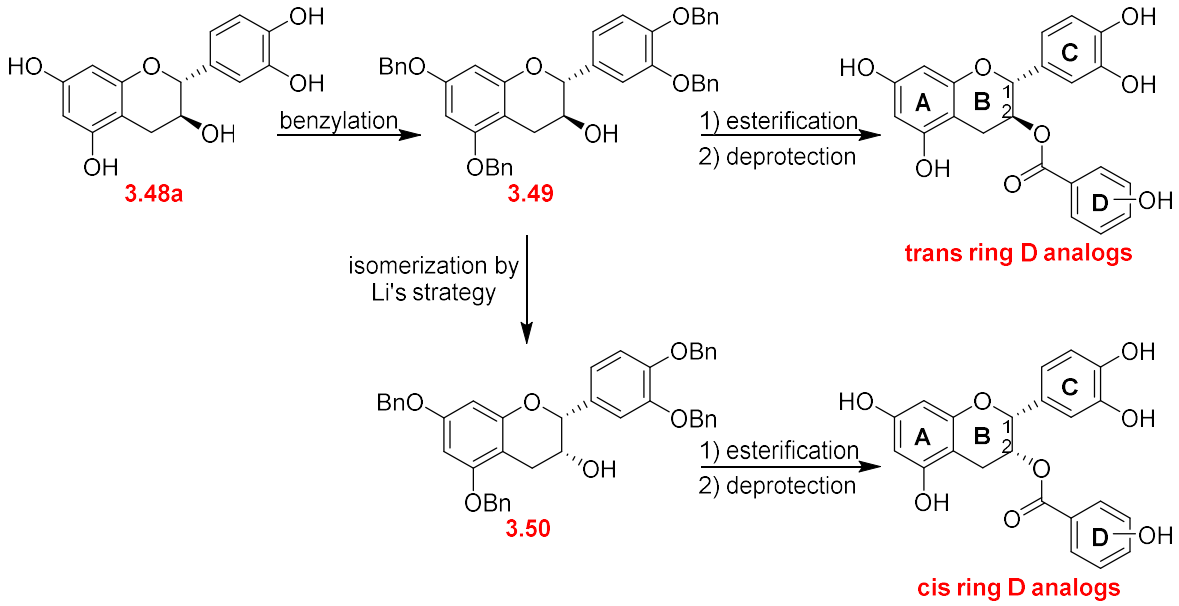

Scheme 3.33 Our plan to synthesize *cis*/*trans* ring D analogs

The phenols of catechin **3.48a** were benzylated on reaction with excess BnBr in the presence of K_2CO_3. KI was added to generate BnI *in situ* to accelerate the reaction, producing benzylated catechin **3.49** in 76–78% yield. The resulting **3.49** was oxidized by the Dess-Martin periodinane to furnish ketone **3.51**, which was then reduced without further purification using

K-Selectride.[46] The steric bulk of the aryl group of ketone **3.51** blocks access of K-Selectride to the same site as those allyl group and allow it to react only on the opposite side to yield catechin **3.50** stereospecifically in 47–52% yield (Scheme 3.34).

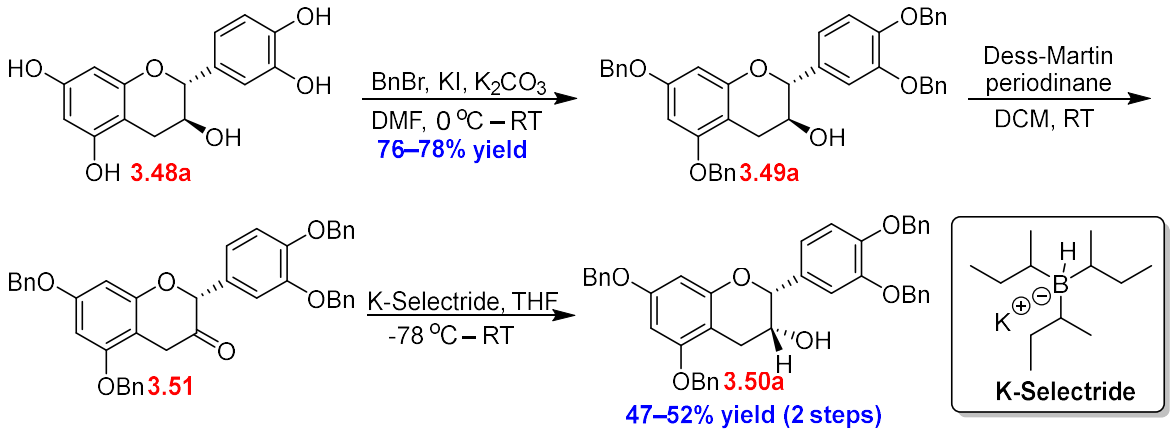

Scheme 3.34 Synthesis of *cis*/*trans* benzylated catechin **3.49** and **3.50** from catechin **3.48a**

The hydroxybenzoic acids (**3.47b–f**) were fully benzylated on reaction with excess BnBr and K_2CO_3, followed by hydrolysis with NaOH in 50% EtOH in water at reflux to yield benzylated benzoic acid and derivatives (**3.16b–f**) in excellent yield (90–98% yield) (Scheme 3.35).[76] The esterification[47] was studied for both catechin (**3.49a**) and epicatechin (**3.50a**) by coupling to acid **3.16e**. The benzoic acid **3.16e** was converted to acid chloride by oxalyl chloride in the presence of the DMF catalyst. Acid chlorides reacted with catechin (**3.49a** or **3.50a**) using Et_3N as a base and DMAP as a catalyst, as shown in Table 3.6.

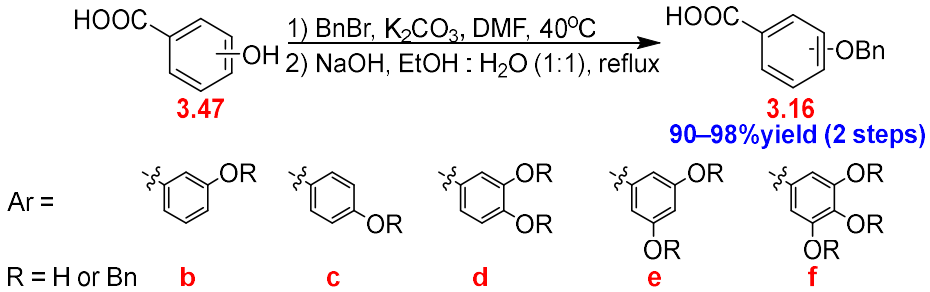

Scheme 3.35 Synthesis of benzylated gallic acid **3.16**

Even though the reaction was stirred for longer than 2 days (Entry 1 and 2), the common esterification[47] (condition A in Table 3.6) could not proceed to completion as analyzed by ^{1}H NMR spectroscopy. Furthermore, epicatechin (**3.50a**) showed lower conversion than catechin **3.49a**, as shown in Table 3.6. This result was correlated with the bulkiness of the β substituent (allyl group) to the alcohol reaction center. The *cis* stereochemistry of epicatechin (**3.50a**) has a greater effect on decreasing the nucleophilicity of the alcohol than the *trans* relationship of catechin (**3.49a**).

Table 3.6 Investigation of esterification between catechins and gallic acid derivatives

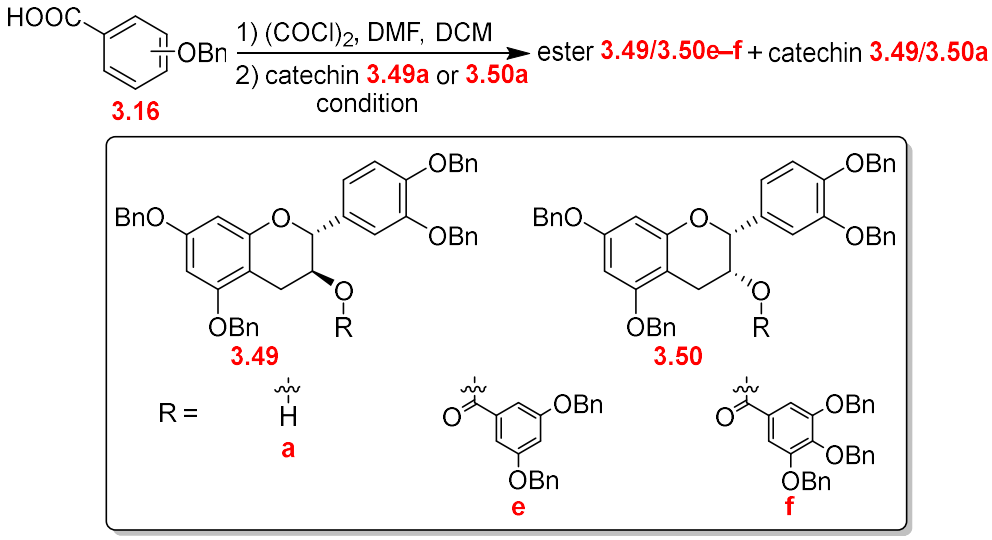

Entry	Catechin	Benzoic acid	Condition[a]	Time	%Conversion[b]
1	Catechin (**3.49a**)	**3.76e**	Condition A	2 days	79% (**3.77e**)
2	Epicatechin (**3.50a**)	**3.76e**	Condition A	7 days	43% (**3.78e**)
3	Epicatechin (**3.50a**)	**3.76f**	Condition B	1 day	100% (**3.78f**)

[a] Condition A: 1 eq. catechin, 1.2 eq. benzoic acid, 6 eq. Et_3N, 10 mol% DMAP in DCM[47]; Condition B: 1 eq. catechin, 1.2 eq. benzoic acid, 2.5 eq. DMAP in DCM[46]

[b] %Conversion was estimated by ^{1}H NMR spectroscopy, calculating from signal integration ratio between ester product **3.77** (at 2.83 ppm) or **3.78** (at 4.71 ppm) and catechin starting material **3.59** (at 2.64 ppm) or **3.74** (at 4.71 ppm).

To improve the conversion from the common esterification[47] (condition A in Table 3.6), a superstoichiometric quantity of DMAP (2.5 equivalents) was used as both catalyst and base instead of Et_3N[46] (condition B in Table 3.6). This method resulted in full conversion of the reaction between epicatechin **3.50a** and the bulkiest acid in the series **3.16f** after stirring for 24 hours (Table 3.6, Entry 3).

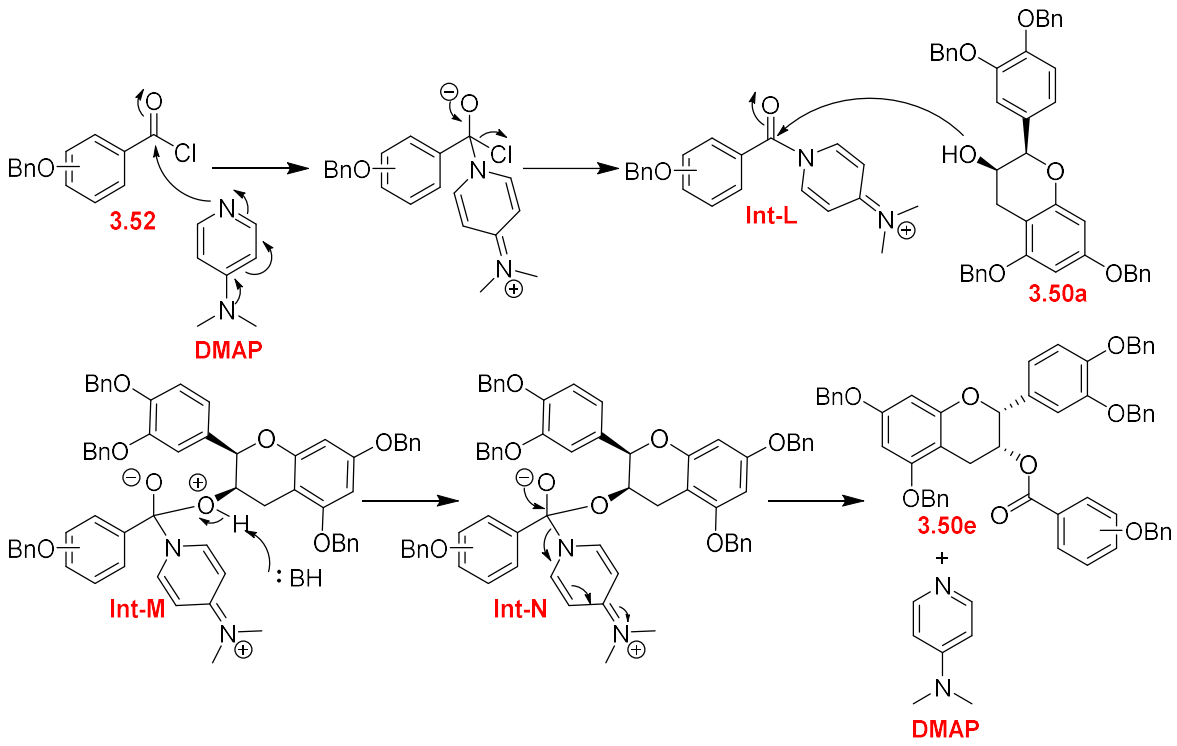

Scheme 3.36 Mechanism of DMAP activated esterification

The improvement by the DMAP condition (condition B in Table 3.6) could be described by the mechanism shown in Scheme 3.36. Acid chloride **3.52** underwent nucleophilic acyl substitution with DMAP activator to generate **Int-L** as a key intermediate. Catechin **3.50a** was then added into carbonyl to yield **Int-M**, which was deprotonated by the base in the system. Finally, DMAP was eliminated from **Int-N** to obtain ester **3.50e** (Scheme 3.36). The excessive quantity of DMAP (condition B) could increase the **Int-L** concentration and accelerate the

catechin addition step, resulting in better conversion than the common esterification (condition A).

Table 3.7 Synthesis of ester **3.49d–f** and **3.50d–f** by DMAP esterification[77]

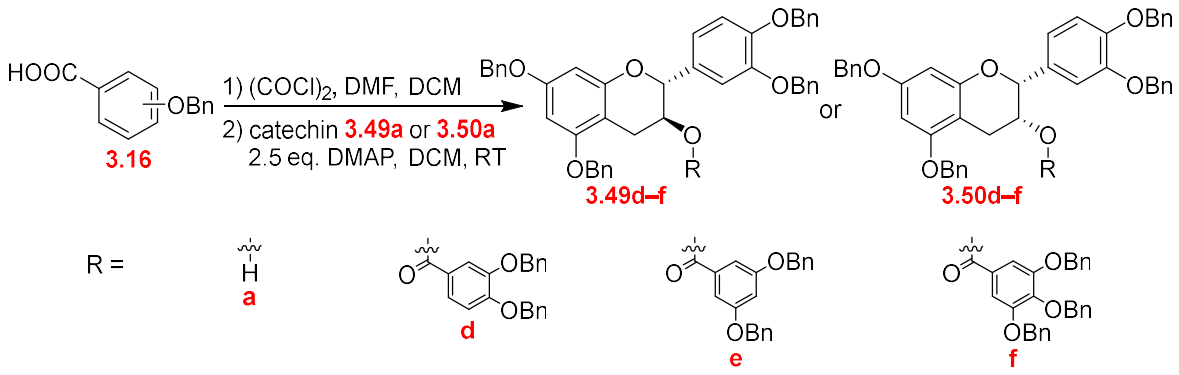

Entry	Catechin	%Isolated yield over 2 steps
1	Catechin (**3.49a**)	48% (**3.77d**)
2	Catechin (**3.49a**)	58% (**3.77e**)
3	Catechin (**3.49a**)	65% (**3.77f**)
4	Epicatechin (**3.50a**)	58% (**3.78d**)
5	Epicatechin (**3.50a**)	52% (**3.78e**)
6	Epicatechin (**3.50a**)	56% (**3.78f**)

The DMAP procedure was used to prepare **3.49/3.50d–f** in moderate yields (48–65% yield over 2 steps, Table 3.7). Both catechin **3.49a** and epicatechin **3.50a** provided ester products with insignificantly different percentage yields (*trans* ester **3.49d–f**: 48–65% yield versus *cis* ester **3.50d–f**: 52–58% yield), indicating that this strategy was able to overcome the bulkiness of the β substituent in alcohol to synthesize benzylated catechin ester and might be a good option for the synthesis of other esters with bulky starting materials.

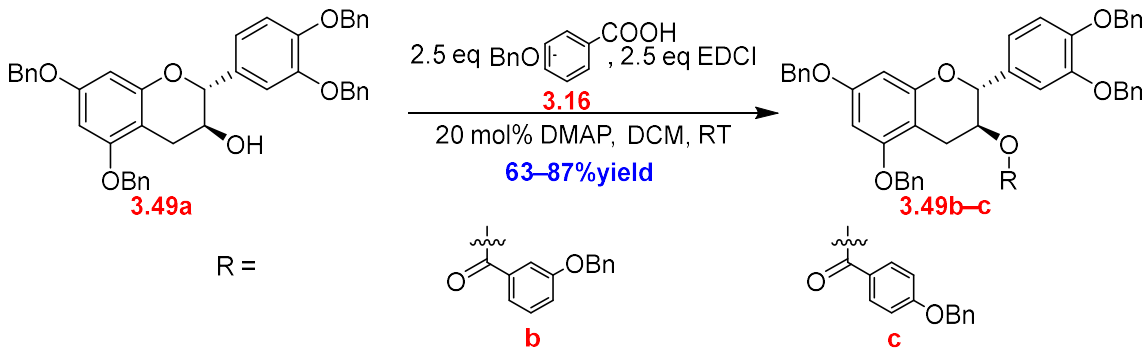

Scheme 3.37 EDCI esterification to synthesize **3.49b/c**

The single-step esterification between catechin **3.49a** and acid **3.16** with EDCI-activated benzoic acid[48] (Scheme 3.37) was studied as a shorter and more convenient route than the acid halide esterification approach. The EDCI esterification was able to esterify catechin **3.49a** with acid **3.16** to produce *trans* ester **3.49b–c** in good yield (Scheme 3.37). Finally, all benzylated ester **3.49b–f**, **3.50a**, and **3.50d–f** were debenzylated with $Pd(OH)_2$ under H_2 to provide 9 ring D analogs ***trans* 3.48b–f**, ***cis* 3.53a**, and ***cis* 3.53 d–f** in 66–93% yield (Scheme 3.38). In conclusion, ***trans* 3.48b–f** were synthesized by a 6-step sequence in 22–46% overall yield. Compounds ***cis* 3.53a** and ***cis* 3.53d–f** were furnished in an 8-steps synthesis in 11–21% overall yield.

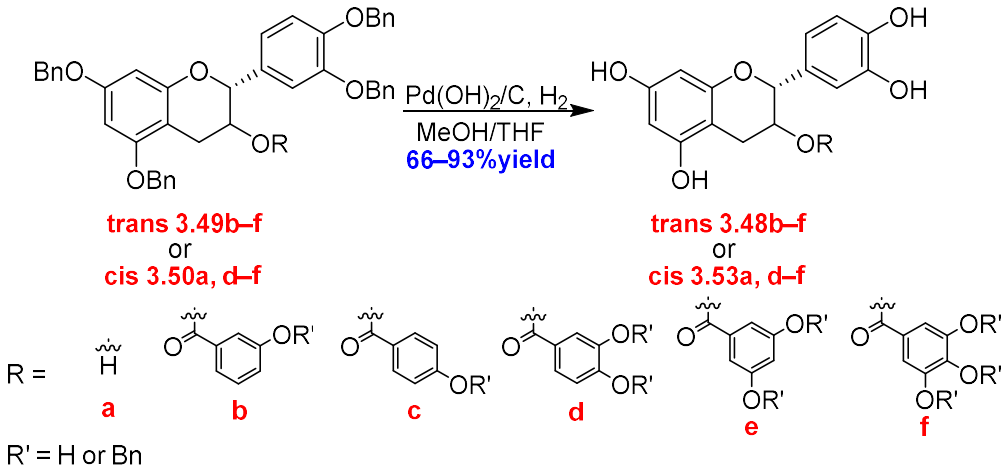

Scheme 3.38 Global debenzylation of cis/trans ester **3.49b–f** and **3.50a, 3.50d–f**

3.7.2 Synthesis of EGCG analogs for SAR of Ring C

A modification of Li's strategy[46] was utilized to synthesize EGCG analogs in racemic form for SAR investigation to analyze the influence of each hydroxy group on ring C to ATP inhibition activity. This approach involved Friedel-Crafts alkylation between allylic alcohol **3.54** or ***rac*-3.55** and phenol **3.1**, followed by dihydroxylation to yield diol ***rac*-3.56**. The resulting diol ***rac*-3.56** would cyclize through an ortho ester intermediate, followed by hydrolysis, producing racemic catechin product ***rac*-3.57**. Esterification and global debenzylation would furnish the target ***rac*-3.58** (Scheme 3.39).

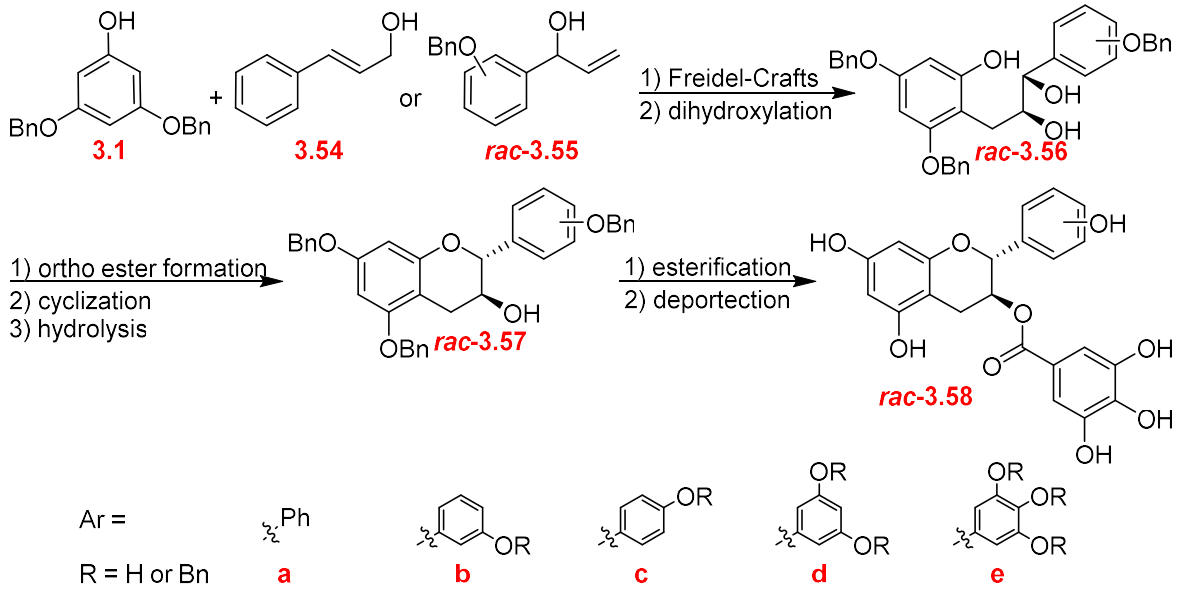

Scheme 3.39 Synthetic plan for ***rac*-3.58a–e**

The approach began with the synthesis of racemic *sec*-allylic alcohol ***rac*-3.55**. The Schotten–Baumann reaction[78] of acid **3.16** furnished Weinreb amides **3.59b–e** in good yield over 2 steps. The resulting amide was reduced by DIBAL to give the corresponding aldehydes in excellent yield, followed by Grignard reaction with vinyl magnesium bromide to obtain racemic **3.55b–e** in 97%–quantitative yield (Scheme 3.40).

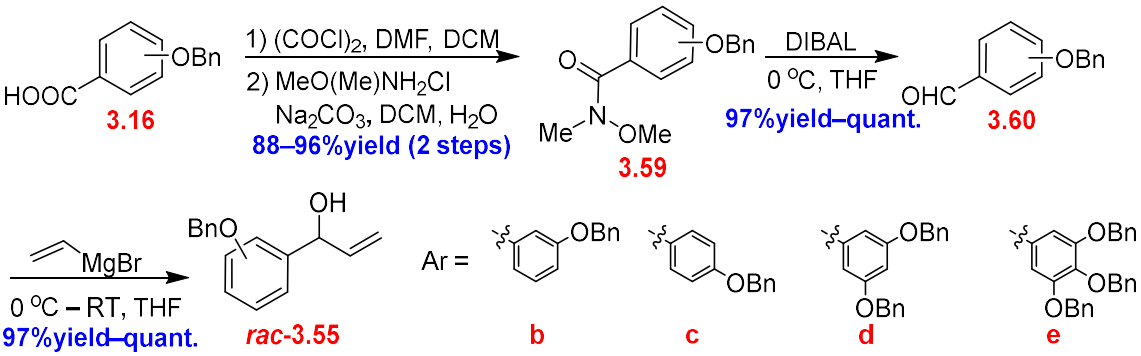

Scheme 3.40 Synthesis of ***rac*-3.55b–e**

The following Friedel-Crafts alkylation of **3.1** with allylic alcohol **3.54** or ***rac*-3.55b–e**[79] provided inseparable mixtures. After OsO_4 dihydroxylation, the racemic diols ***rac*-3.56a–e** were obtained in 21–31% yield over 2 steps (Scheme 3.41). The poor overall isolated yields were hypothesized to be due to multiple side reactions such as multiple alkylations on **3.1** or oligomerization during the Friedel-Crafts alkylation step.

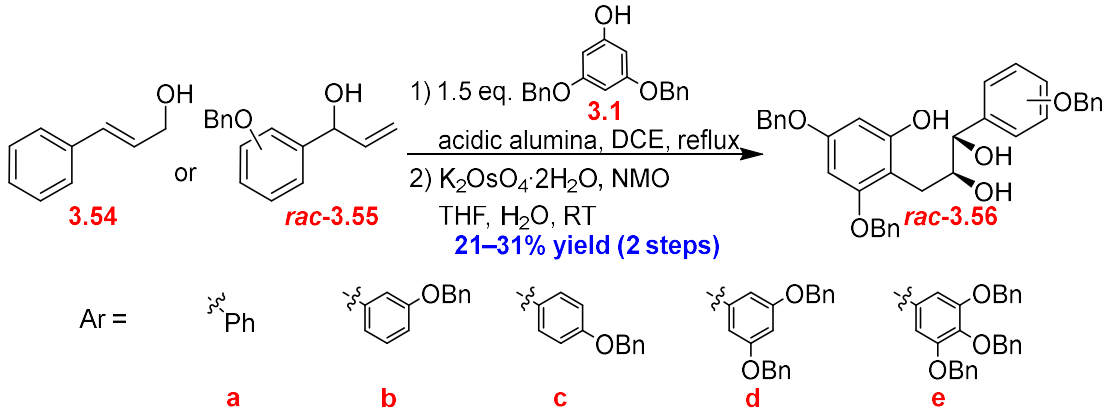

Scheme 3.41 Synthesis of ***rac*-3.56a–e**

The racemic benzylated catechin derivatives ***rac*-3.57a–e** were synthesized by a three-step sequence from racemic diol ***rac*-3.56a–e**. The approach began with ortho ester formation of racemic diol ***rac*-3.56a–e** with triethyl orthoformate ($MeC(OEt)_3$) under catalysis by pyridinium *p*-toluenesulfonate (PPTS),[46] which was continued the next step after completion,

as analyzed by TLC without further purification. The resulting mixture was then treated with BF_3, followed by hydrolysis with LiOH[46] to obtain racemic catechin derivatives ***rac*-3.57a–e** in 90% to quantitative yield over 3 steps with *trans* selectivity. The subsequent EDCI esterification produced racemic ester ***rac*-3.61a–e** in 30–53% yield, followed by global debenzylation to obtain ***rac*-3.58a–e** in 51–77% yield (Scheme 3.42). In summary, 5 ring C analogs (***rac*-3.58a–e**) were obtained in an 11-step synthesis in 2.3–12% overall yield, starting from 3,5-bis(benzyloxy)phenol (**3.1**) and benzylated gallic acid derivatives (**3.47**).

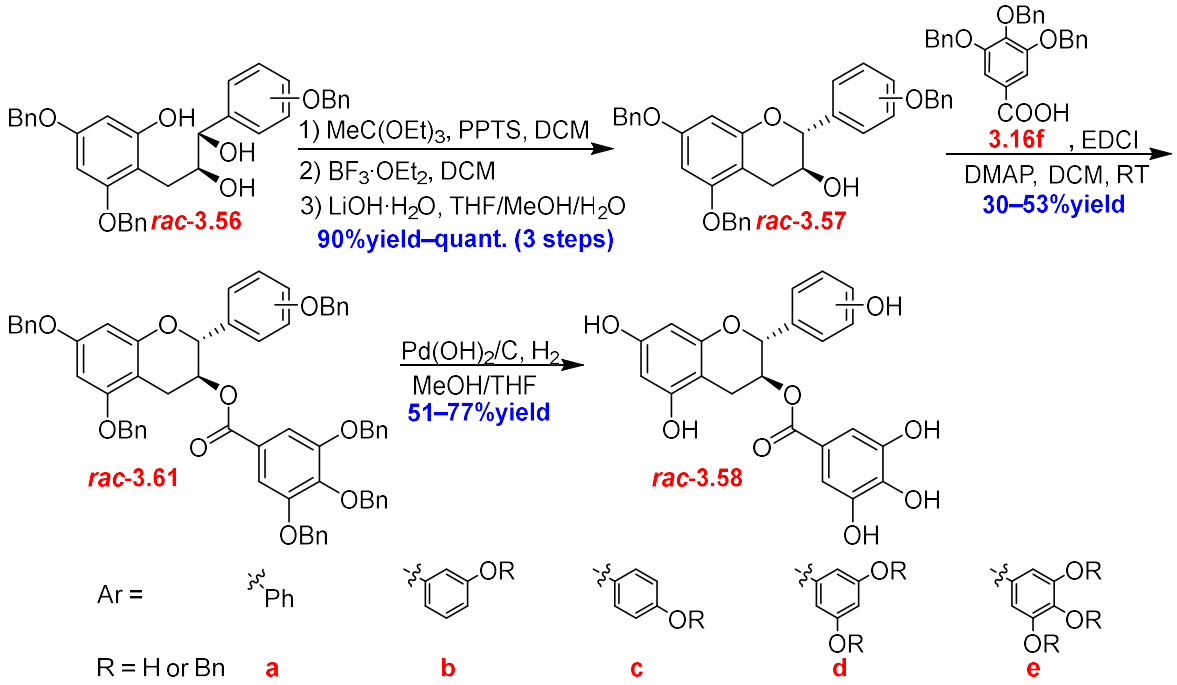

Scheme 3.42 Synthesis of ***rac*-3.58a–e** from ***rac*-3.56a–e**

3.8 Structure-Activity Relationship (SAR) of EGCG and EGCG analogs

Analogs **3.48a–f**, **3.53a**, **3.53d–f**, ***rac*-3.58a–e**, and **3.16f** were evaluated for ATP synthesis inhibition of *M. smeg.* IMVs,[80] done by Priya Ragunathan[81]. Overall, the synthetic EGCG analogs **3.48a–f**, **3.53a**, **3.53d–f**, ***rac*-3.58a–e**, and **3.16f** were less potent in inhibiting ATP synthesis of *M. smeg.* IMVs than the original **EGCG**. Only analogs **3.48d** (0.59 μM), **3.48f** (1.36 μM), and **3.53d** (0.87 μM) showed about the same ATP synthesis inhibitory effect

as the original compound (**EGCG**; 0.155 μM). By the comparison between IC_{50} of **3.48a/3.53a**, **3.48f/3.53f**, and **3.16f** (Graph 3.1), both catechin and gallate ester moieties were necessary for the activity of both catechin gallate (**3.48a–f**) and epicatechin gallate derivatives (**3.53a**, and **3.53d–f**).

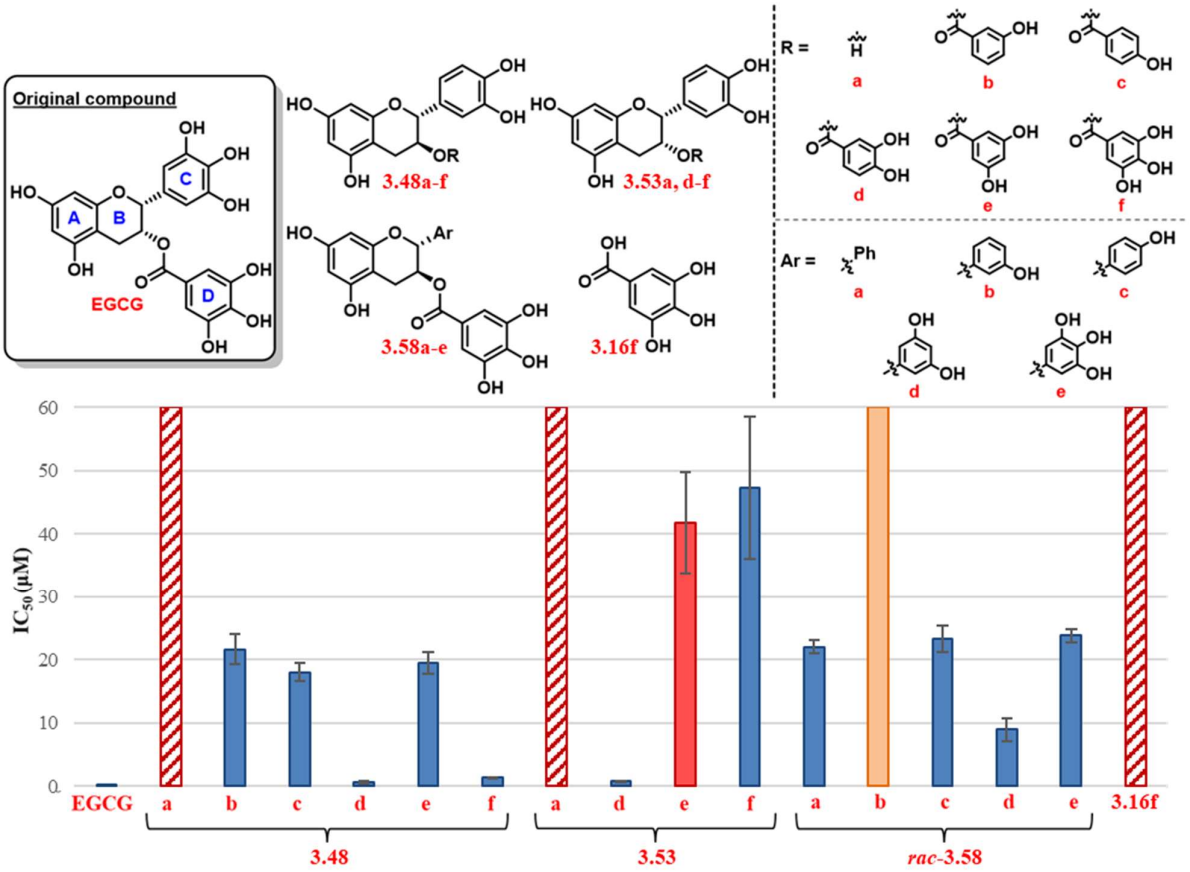

Graph 3.1 IC_{50} of EGCG and enantiomeric pure **3.48a–f**, **3.53a**, **3.53d–f**, racemic mixture of ***rac*-3.58a–e**, and **3.16f**; The IMV experiments were done by P. Ragunathan[81]; The experiments were performed in duplicate; Pattern red indicated above studying range at 100 μM; Solid red showed incomplete inhibition curve at the studied concentration range; orange bar exhibited the inhibition profile could not fit the inhibition curve; provided error is the standard error of the mean (SEM).

3.9 HSQC-NMR titration molecular modeling analysis

According to molecular modeling based on HSQC-NMR titration data between EGCG and the *Mtb* ε subunit by Saw *et al.*, as discussed in Section 3.1.3,[13] both gallocatechin and gallate moieties are needed to interact with the *Mtb* ε subunit, which agreed with our SAR results when **3.53a**, **3.53f**, and **3.16f** were compared. Notably, Saw *et al.* model also established that the 3-hydroxy group on a 2-phenyl substituent is an important component in interacting with the *Mtb* ε subunit.[13] However, the ATP synthesis inhibition of epicatechin gallate **3.53f** by removing this 3-hydroxy group greatly reduced potency (384 times less effective than EGCG), which was not correlated with the Saw *et al.* modeling[13]. This might support the hypothesis that the catechin and gallocatechin series have different binding sites. Nonetheless, the number of *cis*-isomer analogs in this work was insufficient to fully understand the SAR trend of *cis*-stereoisomer analogs to validate the Saw *et al.* modeling, as discussed in Section 3.1.3.

The HSQC-NMR titration between EGCG and the *Mtb* ε subunit by Saw *et al.*[13] showed that EGCG had significant interaction at multiple locations (Figure 3.13). An explanation for this promiscuity could be based upon non-specific binding by EGCG. It is known that EGCG is readily oxidized to an ortho-quinone, as discussed in Scheme 3.2. It may be noted that many of the locations in the ε subunit where EGCG interacts have arginine residues (R) in proximity. It can, therefore, be suggested that binding is through nucleophilic trapping of the oxidized form of EGCG by arginine. This would imply that EGCG acts as a covalent inhibitor. This would also explain why EGCG has been observed to have so many forms of biological activities.

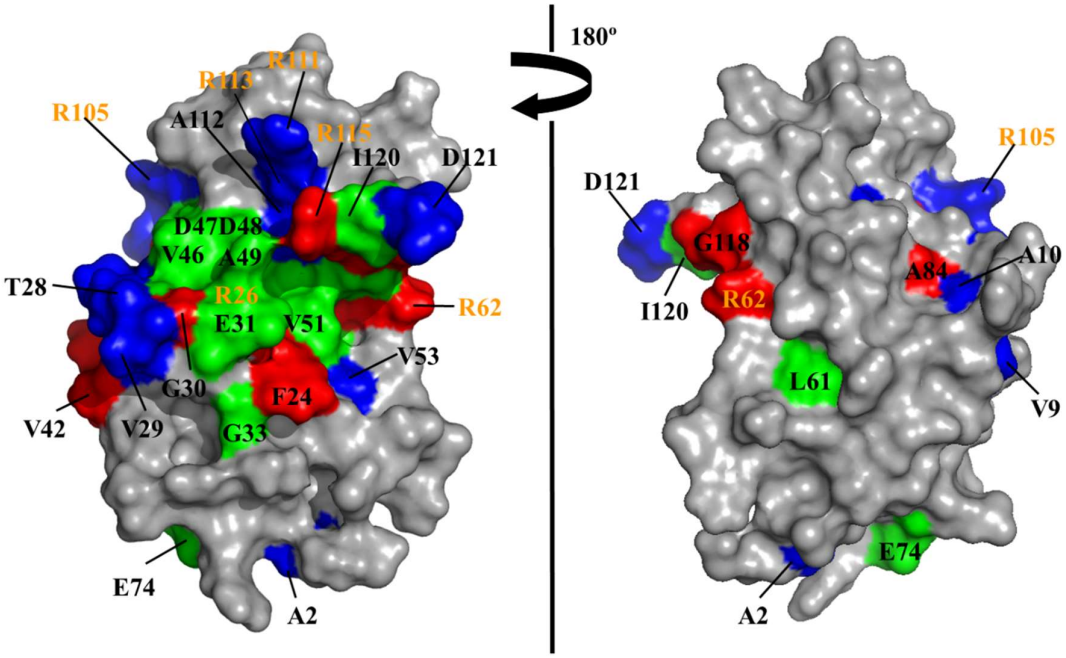

Figure 3.13 Mapping of the EGCG binding surface to the *Mtb* ε subunit and conformational changes by chemical shift perturbation (CSP) results; The residues revealing more than 0.1 ppm are represented in *red*, while those showing CSP between 0.05 and 0.1 ppm and disappeared are displayed in *blue* and *green,* respectively.[13] Reprinted with permission from Saw, W.-G. *et al. Sci. Rep.***2019,** *9* (1), 16759. Copyright © 2019 by Saw, W.-G. *et al.*

The HSQC-NMR titration between catechin ester **3.48d** and the *Mtb* ε subunit was performed by Priya Ragunathan[81] and analyzed by Joon Shin[82]. However, no significant chemical shift perturbation values were observed. For ester **3.48d**, the largest chemical shift perturbation was approximately 0.03 Δppm, as shown in Graph 3.2. In comparison, for EGCG, perturbations greater than 0.1 Δppm were observed. This confirms that EGCG and ester **3.48d** do behave quite differently in this context. This information suggested that the most active compound **3.48d** in the catechin ester series does not have the *Mtb* ε subunit as a binding site, and it also supported the hypothesis that catechin gallate analogs could have distinct binding sites from gallocatechin gallate analogs.

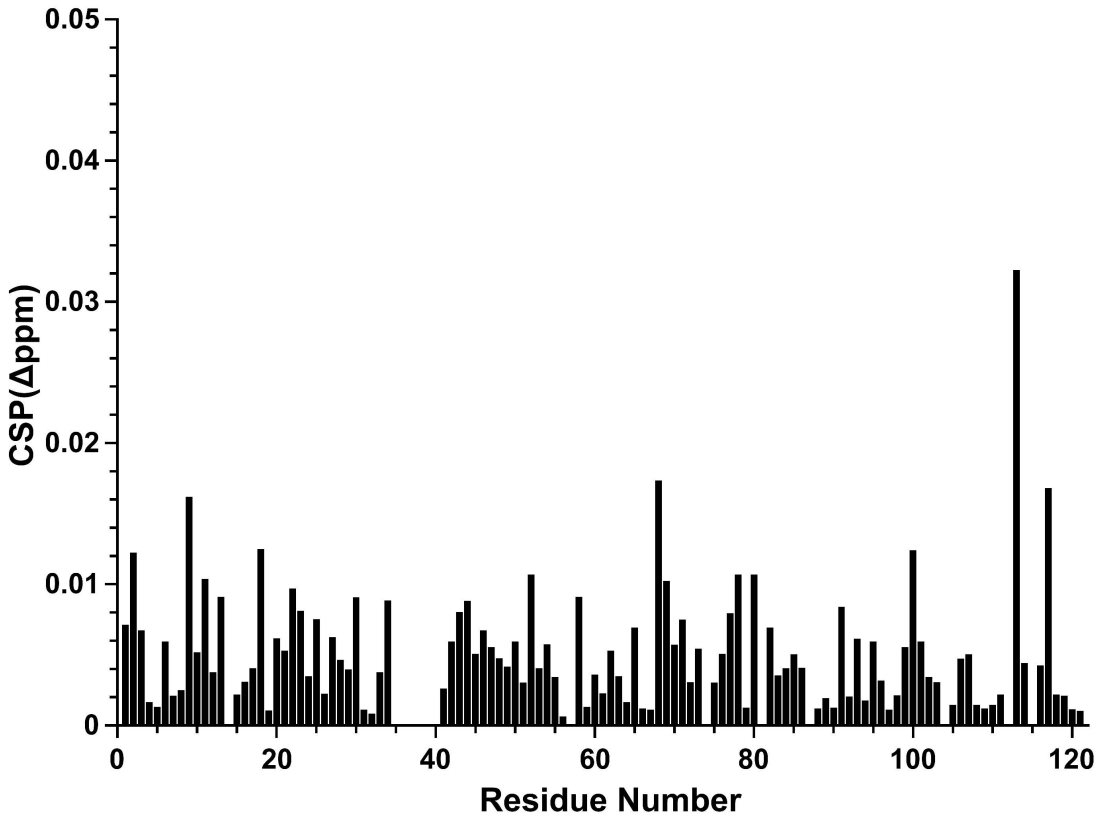

Graph 3.2 Plot of CSP based on the ^{1}H-^{15}N HSQC spectra of *Mtb* epsilon with/without drug at a 1:2 molar ratio. Weighted CSP values were calculated by the formula Δppm = $[(\Delta N/5)^2 + (\Delta HN)^2]^{0.5}$

3.10 Investigation of Bacterium growth inhibition property of EGCG analogs

The bacterial growth inhibition against *M. smeg.*[83] was investigated and performed by Priya Ragunathan[81]. Catechin/epicatechin gallates **3.48a–f/3.53a** and **3.53d–f** had no inhibitory effect on *M. smeg.* growth. This was correlated to the EGCG property that EGCG shows ATP synthesis inhibition against *M. smeg.* IMVs, however, it does not inhibit *M. smeg.* growth as reported by Saw *et al*[13]. We postulated that inadequate membrane penetration and inhibitors elimination *via* efflux pumping are possible causes.

3.10.1 Investigation of membrane penetration hypothesis

Due to the unique lipophilic cell wall of *Mtb*, drug penetration is one of the main problems in TB drug development.[43, 84] The majority of successful TB medicines are lipophilic compounds with ClopP of more than 5,[44] which ClogPs of the original EGCG, and the active analogs (**3.48d**, **3.48f**, and **3.53d**) were between 1.49–2.78, supporting the membrane impermeability hypothesis.

In this work, fluorescence confocal imaging, which has been reported to be utilized in transportation across the membrane study,[85] was considered to experimentally confirm our hypothesis. In general, the technique could show the location of the fluorescence active species inside the cell. However, the selected catechin gallate (**3.48d**) from the most active SAR series showed ultraviolet (UV)-visible absorption property in the UV range as shown in Graph 3.3, which was correlated to EGCG optical properties,[86] and was in the same range as cell components' optical absorption.[87] This demonstrated that the fluorescence confocal technique cannot be adopted to confirm the membrane penetration hypothesis for catechin gallate (**3.48d**), EGCG, and our EGCG analogs.

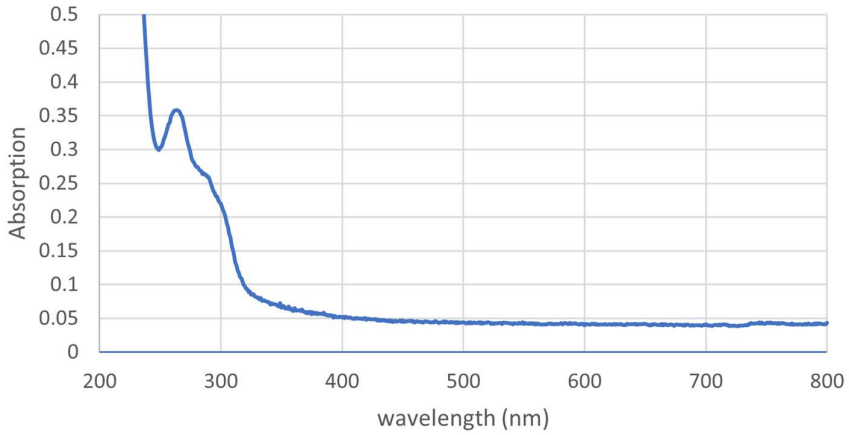

Graph 3.2 UV-visible spectrum of catechin gallate (**3.48d**) at 0.02 mM concentration

To date, the pro-drug concept has been employed to solve the problem of membrane penetration. Lipophilic ester pro-drugs have been found to promote cell membrane permeability, intracellular breakdown, and the release of active species within the cell.[45] This approach was used in mycobacterial examples to enhance the growth inhibition of pyrazinamide.[88]

Herein, the selected catechin gallate (**3.48d**) was fully esterified with acid anhydrides (**3.62a–e**) to form corresponding esters (**3.63a–e**) with different ClogP in between 1.90–14.60 in moderate to good yield, as shown in Scheme 3.43. This strategy is predicted to not only address the bacterial growth inhibition problem by increasing the lipophilicity to allow the molecule to penetrate through the mycobacterial cell wall but also increase the stability of catechin gallate (**3.48d**) from oxidation of catechol (discussed in 3.1.5). However, all synthetic esters **3.63a–e** exhibited no enzymatic inhibition to ATP synthesis of *M. smeg.* IMV, as well as no *M. smeg.* growth inhibition. In the enzymatic inhibition assay, the hydroxyl groups on catechin gallate (**3.48d**) were confirmed to be crucial for activity. However, the lipophilic ester could not solve the membrane penetration problem. The hydrophilic of original **3.48d** and acetate **3.63a** could be too high to allow molecules to penetrate through the waxy cell wall. In contrast, the rest of the esters **3.63b–e** were water-insoluble, leading to no growth inhibition observed.

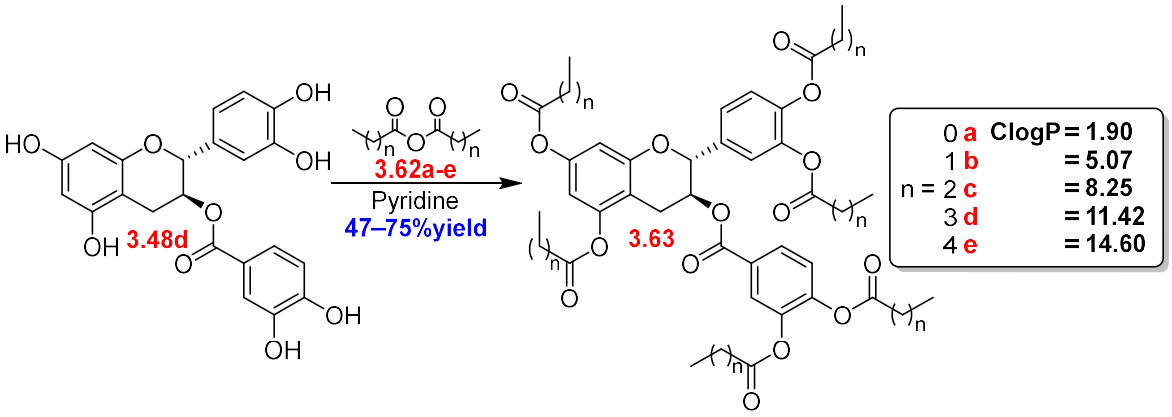

Scheme 3.43 Esterification of **3.48d** to produce **3.63a–e**, ClogPs were calculated by Chemdraw

3.10.2 Investigation of efflux pumping hypothesis

One mechanism for drug resistance is through the action of efflux pumps, expelling the drug molecules from the organism to avoid the drug effect.[89] Recently, it was shown that co-administration of Verapamil (Figure 3.14), a well-known efflux pump inhibitor, restored the activity of various anti-TB drugs, enhancing bacterial growth inhibition property.[89, 90] Therefore, we decided to perform the *M. smeg.* growth inhibition of the combination between Verapamil and our compounds to determine whether efflux pump activity is the cause of the problem.

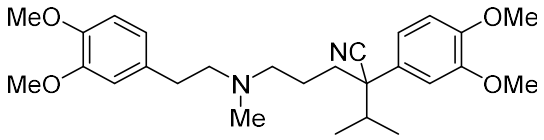

Figure 3.14 Structure of Verapamil

In this work, the quantity of Verapamil required to inhibit efflux without affecting bacterial growth was studied. Verapamil had an *M. smeg.* MIC_{50} of 1.33 mM, whereas more dilute doses of 8 µM and 24 µM had additive effects on BDQ, reducing the *M. smeg.* MIC_{50} of BDQ by 1.6 and 2.6 times, respectively. Therefore, verapamil concentrations of 8 µM and 24

μM were considered subinhibitory concentrations and employed for studies with EGCG analogs.

Our top three most active IC_{50} analogs (**3.48d**, **3.48f**, and **3.53d**) at 2 mM were studied with 24 μM of Verapamil in the slow-growing *M. bovis*, which commonly exhibits behavior closely similar to *Mtb*. However, no effect was detected for any of the EGCG analogs examined (**3.48d**, **3.48f**, and **3.53d**). Therefore, it is unlikely that the lack of activity is due to efflux pumps, although it may be noted that verapamil may not inhibit all efflux pumps.

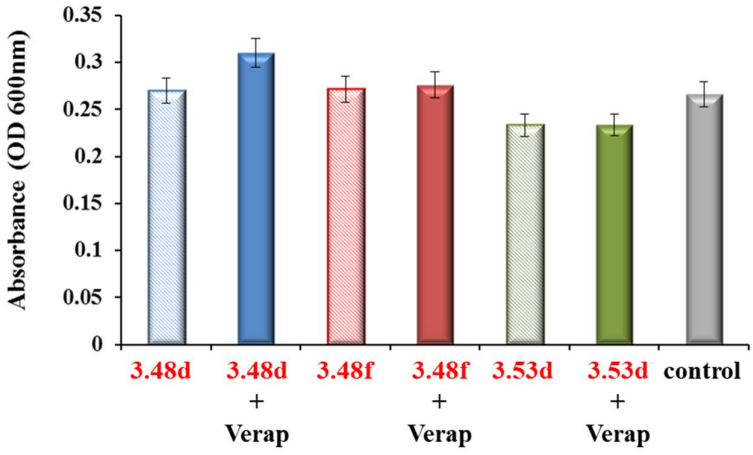

Graph 3.3 Synergistic investigation between **3.48d**, **3.48f**, and **3.53d**, and Verapamil (Verap)

3.11 Future work

In this work, the catechin series (**3.48a–f**, **3.53a**, **3.53d–f**, ***rac*-3.58a–e**, and **3.16f**) was thoroughly SAR studied. However, the number of analogs in the gallocatechin series (EGCG and ***rac*-3.58e**) and *cis*-isomer analogs (**3.53a** and **3.53d–f**) are still limited. Thus, more analogs will be synthesized using our modified Li's strategy to complete the SAR trend and validate the EGCG modeling (Figure 3.15). Additionally, the lipophilic ester strategy to solve the bacterial growth inhibition problem was met by the limited water solubility of hydrophobic esters. Therefore, partially capped ester **3.63** should address the solubility issue while the lipophilic property remains (ClogP 4.71–7.89, Figure 3.14). Furthermore, if the mycobacterial

growth inhibition problem is resolved, bacterial growth inhibition assays will be performed in the other bacteria, e.g., *E. coli,* to investigate selectivity. In addition, the target specificity of catechin ester **3.48d** should be investigated to identify the targeted enzyme involved in inhibiting mycobacterial ATP synthesis. Finally, experiments should be designed to determine whether EGCG is a covalent inhibitor.

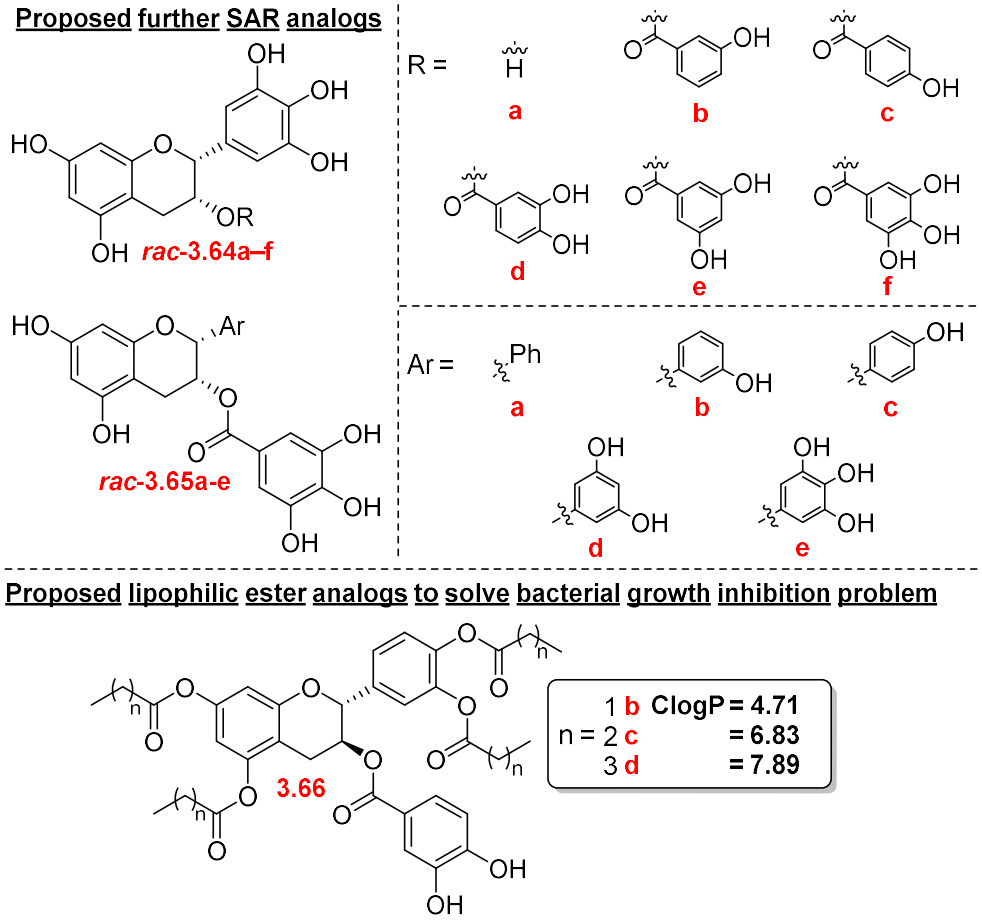

Figure 3.15 Proposed future works

3.12 Conclusion

The new late-stage coupling strategy involving the nucleophilic substitution of the diacetate **3.19** was proposed to synthesize EGCG analogs. The key intermediate, 5,7-bis(benzyloxy)chromane-2,3-diyl diacetate (***rac*-3.19**), was synthesized in a 10-step sequence in 12–20% overall yield, beginning with phloroglucinol. However, subsequent nucleophilic substitution failed to produce catechin derivatives. Using the modified Li's strategy,[46] fourteen EGCG analogs (**3.48b–f**, **3.53a**, **3.53d–f**, and ***rac*-3.58a–e**) for SAR investigation were successfully synthesized.

The SAR study by IMV experiments revealed that both catechin and gallate ester moieties were required for mycobacterial ATP synthesis inhibition. However, catechin gallate (**3.48f** and **3.53f**) and gallocatechin gallate derivatives (EGCG and ***rac*-3.58e**) revealed different SAR patterns as the *trans* stereoisomer had significantly higher potency than the *cis*-isomer in the catechin series. While epigallocatechin gallate (EGCG) exhibited better activity than trans relationships, Moreover, catechol ester can improve the effectiveness of inhibiting ATP synthesis in catechin analogs.

The bacterial growth inhibition assay demonstrated that EGCG and its analogs had no *M. smeg.* growth inhibition. The high hydrophilicity was postulated to result in a lack of membrane penetration. The lipophilic ester-protected catechin gallate (**3.63a–e**), which was synthesized from the most active analog (**3.48d**) based on the SAR investigation, could not dissolve in water, resulting in the inability to inhibit the mycobacterial growth. The efflux pumping hypothesis was examined by studying the bacterial growth inhibition assay of the combination between our top three enzymatic active EGCG analogs (**3.48d**, **3.48f,** and **3.53d**) and verapamil against *M. smeg.*, which exhibit no additive effect and can not address the bacterial growth problem.

3.13 Experimental section

Biological assays

Preparation of *M. smeg.* Inverted membrane vesicle (IMV),[91] ATP synthesis inhibition,[80] and antimycobacterial activity[83] assays were followed the procedures as discussed in 2.8 in the biological assays section.

Table 3.8 IC_{50} and MIC_{50} values of EGCG analogs in this work

Compound	IC_{50} (μM)[a]
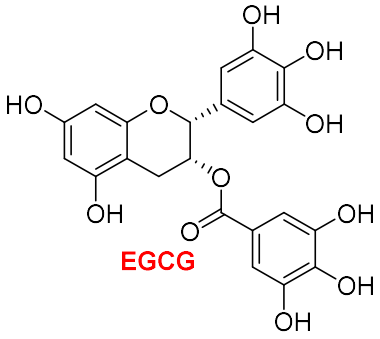 EGCG	0.156[c, 13]
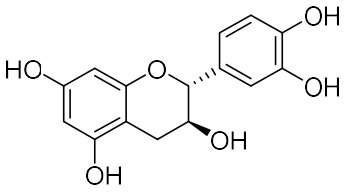 3.48a	> 100[b, c]
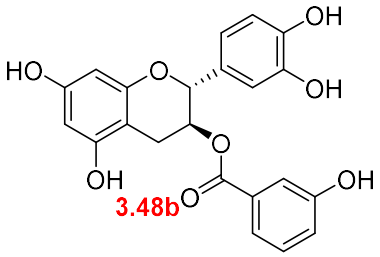 3.48b	21.7 ± 2.4
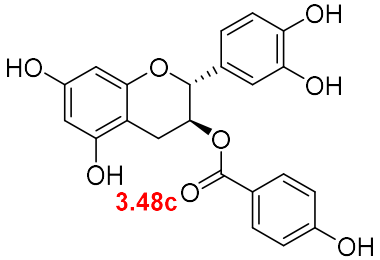 3.48c	18.0 ± 1.4

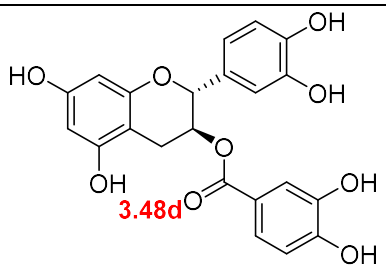 3.48d	0.593 ± 0.154[c]
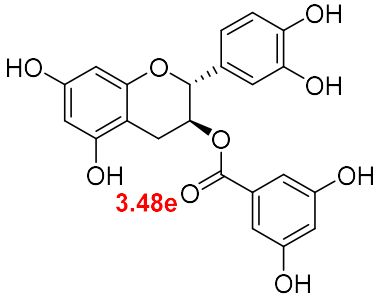 3.48e	19.5 ± 1.7[c]
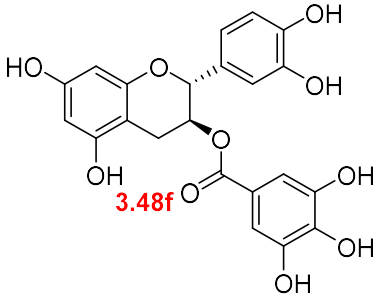 3.48f	1.36 ± 0.01[c]
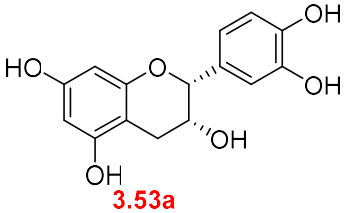 3.53a	> 100[b, c]
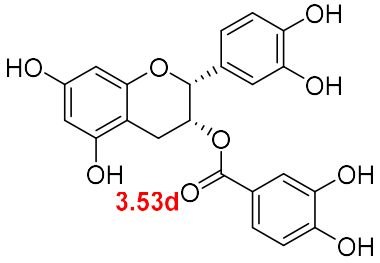 3.53d	0.866 ± 0.013[c]
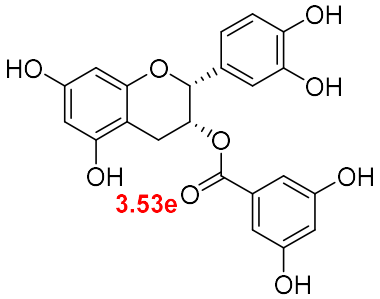 3.53e	41.8 ± 8.0[c]

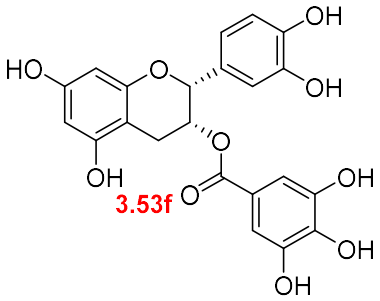 3.53f	47.3 ± 11.2[c]
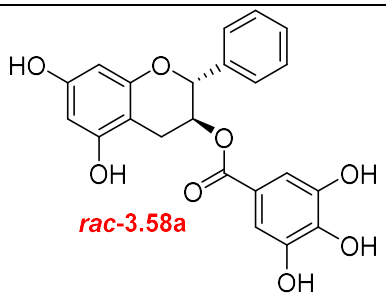 *rac*-3.58a	22.0 ± 1.1
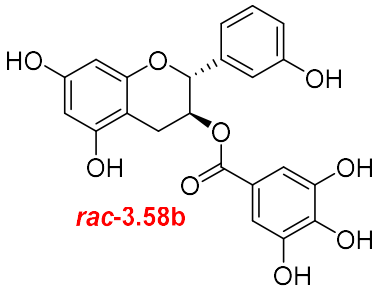 *rac*-3.58b	N. A.[d]
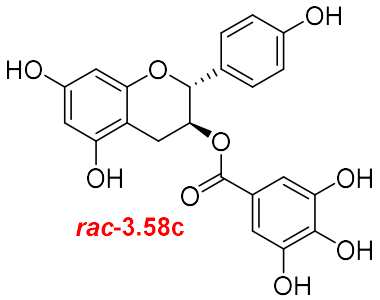 *rac*-3.58c	23.4 ± 2.1
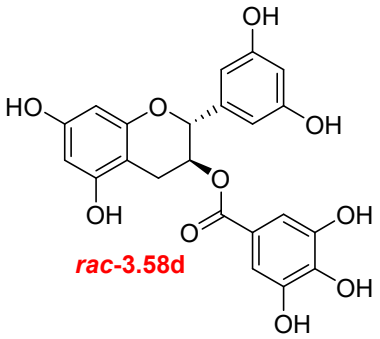 *rac*-3.58d	8.9 ± 1.9

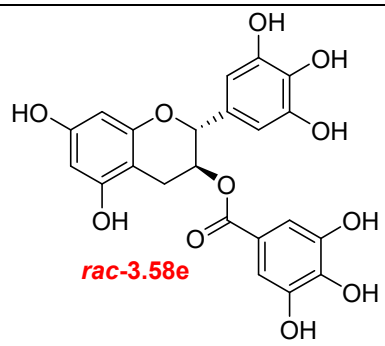 *rac*-3.58e	23.8 ± 1.1
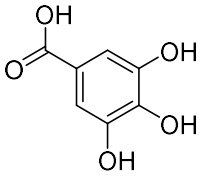 3.16f	> 100[b, c]
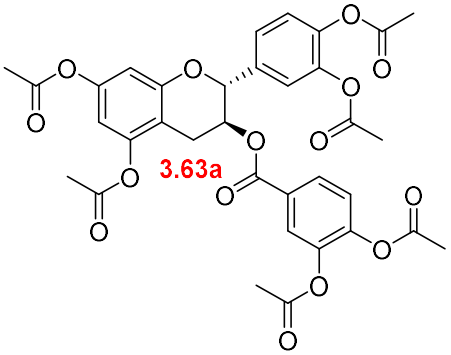 3.63a	> 100[b, c]
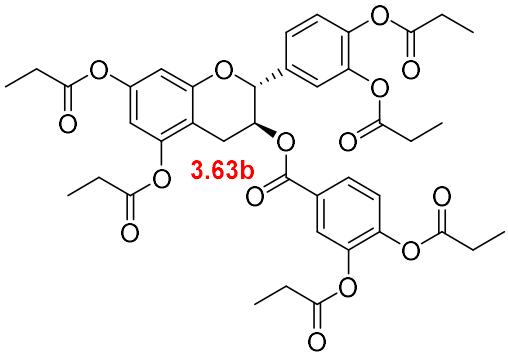 3.63b	> 100[b, c]
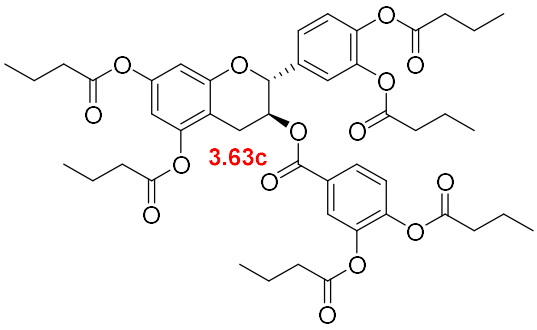 3.63c	> 100[b, c]

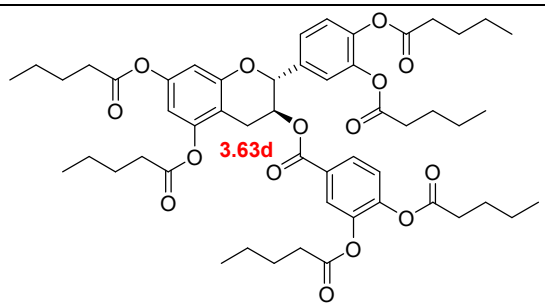 3.63d	> 100[b, c]
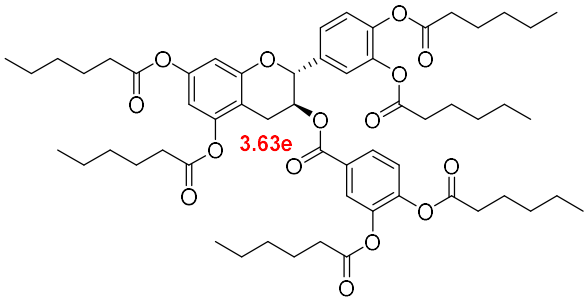 3.63e	> 100[b, c]

[a] All experiments were performed in duplicate
[b] IC_{50}s were above the studying range at 100 μM
[c] MIC_{50}s were measured to be above the studying range at 100 μM
[d] The inhibition profile could not fit the inhibition curve

Synthetic procedures

All moisture-sensitive reactions were carried out under a nitrogen atmosphere using oven-dried glassware (120 ºC), which was cooled under vacuum. Syringes and needles were dried under vacuum before use. Anhydrous diethyl ether, THF, and toluene were fleshly distilled from sodium metal with benzophenone under a nitrogen atmosphere before use, while Anhydrous DCM and DCE were distilled from CaH_2 under nitrogen. Anhydrous DMF was distilled under reduced pressure from CaH_2 under nitrogen and stored under 4Å molecular sieves. All other solvents and reagents were used as received. Flash column chromatography was performed on 230–400 mesh particle-sized silica gel.

All synthetic compounds in this research were structurally elucidated by ^{1}H-NMR, ^{13}C-NMR, IR spectroscopy, or mass spectrometry. The minimum purity of target compounds (**3.48a–f**, **3.53a**, **3.53d–f**, ***rac*-3.58a–e**, **3.16f**, and **3.63a–e**) for biological assays was accepted at 90%, and the purity was confirmed by ^{1}H-, and ^{13}C- NMR spectroscopy. All supporting spectra information (^{1}H- and ^{13}C-NMR spectra) for this chapter were shown in Appendix B.

^{1}H- and ^{13}C- NMR spectra were recorded in deuterated solvents ($CDCl_3$ or DMSO-d6) at 400 MHz and 100 MHz, respectively, using JEOL ECA 400 and ECA 400SL spectrometers. Chemical shifts are reported in part per million (ppm), and coupling constants are recorded in Hertz (Hz). Infrared spectra were recorded using Spectrum 100 ATR-IR spectrometer (Perkin-Elmer) and reported in cm^{-1}. Molecular weights were recorded using a high-resolution mass spectrometer equipped with Waters acquity UPLC (Waters Xeco G2-X2 MS) or a low-resolution mass spectrometer (Thermo Scientific LTQ XL MS). Melting points were recorded using Optimelt. Optical rotation was measured and recorded using a P-1030 polarimeter (Jasco).

Benzene-1,3,5-triyl triacetate (3.25)

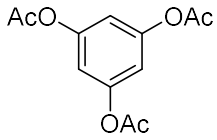

3.25

To the phloroglucinol (6.31g, 50 mmol) in pyridine (35 mL) was added dropwise acetic anhydride (18.9 mL, 200 mmol) in the presence of 4-dimethylaminopyridine (306 mg, 2.5 mmol). The mixture was stirred at room temperature for 1 day. The reaction was monitored by TLC (hexanes:EtOAc 3:1; UV). The reaction mixture was diluted with EtOAc, washed with an aqueous solution of 2 M HCl, water, and a saturated aqueous solution of $NaHCO_3$. The organic layer was evaporated under reduced pressure to obtain benzene-1,3,5-triyl triacetate (**2.25**) as a colorless solid (11.70g, 93% yield). ^{1}H NMR (400 MHz, $CDCl_3$) δ 6.84 (s, 3H), 2.28 (s, 9H). The ^{1}H NMR is in agreement with those reported before.[92]

1,3,5-Tris(benzyloxy)benzene (3.23)

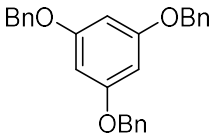

3.23

To the benzene-1,3,5-triyl triacetate **3.25** (6.03 g, 23.9 mmol), benzyl chloride (9.9 mL, 86.1 mmol), 60% w/w NaH in mineral oil (6.89 g, 172 mmol) in anhydrous DMF (70 mL) was added dropwise water (1.3 mL, 71.8 mmol) at 0 °C under nitrogen atmosphere. The mixture was stirred at 0 °C, which was allowed to warm up to room temperature for 2 days. The reaction was monitored by TLC (hexanes:EtOAc 3:1; UV). Water was added and extracted with EtOAc 3 times. The combined organic phase was washed with water and brine, followed by evaporation under reduced pressure. The residue was recrystallized in hot MeOH. 1,3,5-Tris(benzyloxy)benzene (**3.23**) was obtained as a colorless solid (7.15 g, 75% yield). ^{1}H NMR (400 MHz, $CDCl_3$) δ 7.54 – 7.28 (m, 15H), 6.27 (s, 3H), 5.00 (s, 6H). The ^{1}H NMR is in agreement with those reported before.[57]

3,5-Bis(benzyloxy)phenol (3.1)

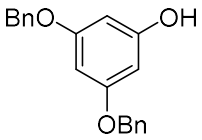

3.1

The suspension of 1,3,5-tris(benzyloxy)benzene **3.23** (3.57g, 9 mmol) and 10% Pd/C (178 mg) in the mixture between 80 mL of MeOH and 20 mL of dioxane was charged with 10 mL of 1.5 M NaOMe in MeOH. The reaction was stirred under hydrogen (1 atm) at room temperature, which was monitored closely by TLC (hexanes:EtOAc 9:1; UV). After the completion (after stirring for 45 minutes), the mixture was filtered through celite. The filtrate was evaporated under reduced pressure. The residue was added with an aqueous solution of 2 M HCl and then

extracted with DCM 3 times. The combined organic phase was dried over Na_2SO_4 and then evaporated to give 3,5-bis(benzyloxy)phenol **3.1** as a brown solid (2.78 g, 99% yield). ^{1}H NMR (396 MHz, $CDCl_3$) δ 7.44 – 7.28 (m, 10H), 6.24 (t, *J* = 1.8 Hz, 1H), 6.11 (d, *J* = 1.7 Hz, 2H), 5.00 (s, 4H), 4.89 (s, 1H); LRMS calcd for $C_{20}H_{19}O_3$ (M+ H^+) 307.4; found 307.0. The analytical data are in agreement with those reported before.[55]

(((5-(Prop-2-yn-1-yloxy)-1,3-phenylene)bis(oxy))bis(methylene))dibenzene (3.26)

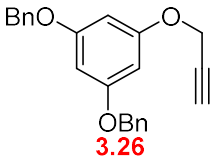

3.26

To the 3,5-bis(benzyloxy)phenol **3.1** (350 mg, 1.14 mmol) and K_2CO_3 (415 mg, 3 mmol) in acetone (5 mL) was added 80%wt propargyl bromide in toluene (419 mg, 2.8 mmol). The mixture was stirred at reflux under nitrogen atmosphere overnight. The reaction was monitored by TLC (hexanes:EtOAc 9:1; UV) and evaporated under reduced pressure. Water was added and then extracted with DCM 3 times. The combined organic phase was washed with brine, dried over Na_2SO_4, and evaporated to give (((5-(prop-2-yn-1-yloxy)-1,3-phenylene)bis(oxy))bis(methylene)) dibenzene **3.26** as yellow liquid (398 mg, quantitative). ^{1}H NMR (400 MHz, $CDCl_3$) δ 7.44 – 7.25 (m, 10H), 6.28 (t, *J* = 2.0 Hz, 1H), 6.24 (d, *J* = 2.0 Hz, 2H), 4.98 (s, 4H), 4.60 (d, *J* = 2.4 Hz, 2H), 2.49 (t, *J* = 2.4 Hz, 1H).

The mixture of 5,7-bis(benzyloxy)-2*H*-chromene (3.27) and 5,7-bis(benzyloxy)-4*H*-chromene (3.17)

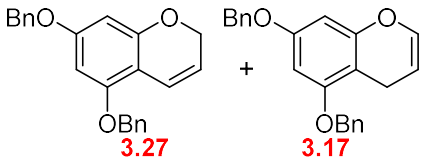

The $PtCl_2$ (13.2 mg) was suspended into the solution of (((5-(prop-2-yn-1-yloxy)-1,3-phenylene)bis(oxy))bis(methylene))dibenzene **3.26** (298 mg, 0.87 mmol) in toluene (15 mL). The mixture was stirred and refluxed under a nitrogen atmosphere for 5.5 hours. The reaction was monitored by TLC (hexanes:EtOAc 9:1; UV), and evaporated under reduced pressure. The crude mixture was purified by column chromatography on silica gel using 10% EtOAc in hexanes as an isocratic eluent to afford the mixture between 5,7-bis(benzyloxy)-2*H*-chromene **3.27** and 5,7-bis(benzyloxy)-4*H*-chromene **3.17** with 6.7:1 mole ratio as a yellow liquid (69.4 mg, 23% yield).

5,7-bis(benzyloxy)-2*H*-chromene (**3.27**) ^{1}H NMR (400 MHz, $CDCl_3$) δ 7.46 – 7.26 (m, 10H), 6.75 (dt, J = 9.9, 1.5 Hz, 1H), 6.18 (d, J = 2.2 Hz, 1H), 6.13 (d, J = 2.2 Hz, 1H), 5.58 (dt, J = 9.9, 3.7 Hz, 1H), 5.01 (s, 2H), 4.99 (s, 2H), 4.73 (dd, J = 3.7, 1.8 Hz, 2H).

5,7-bis(benzyloxy)-4*H*-chromene (**3.17**) ^{1}H NMR (396 MHz, $CDCl_3$) δ 7.53 – 7.28 (m,10H), 6.42 (dt, J = 6.3, 1.9 Hz, 1H), 6.27 (d, J = 2.3 Hz, 1H), 6.12 (d, J = 2.3 Hz, 1H), 5.02 – 4.91 (m, 4H), 3.23 (dd, J = 3.2, 2.1 Hz, 2H). The ^{1}H NMR is in agreement with those reported before.[49]

Investigation of the isomerization of 5,7-bis(benzyloxy)-2*H*-chromene (3.27)

The $Rh(diphos)BF_4$ was pre-formed by dissolving $Rh(COD)BF_4$ (1.8 mg, 4 μmol) and 1,2-Bis(diphenylphosphino)ethane (1.7 mg, 4 μmol) in DCM (0.5 mL) under nitrogen atmosphere. The solution was stirred at room temperature for 15 minutes. This resulting mixture was

canulated into 5,7-bis(benzyloxy)-2*H*-chromene **3.27** (57.2 mg, 0.17 mmol) in degassed acetone (0.5 mL). The temperature and reaction time were studied. The reaction was monitored by ^{1}H NMR spectroscopy.

(((5-(Allyloxy)-1,3-phenylene)bis(oxy))bis(methylene))dibenzene (3.29)

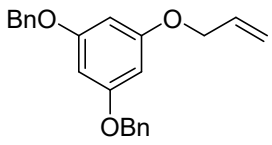

3.29

To the 3,5-bis(benzyloxy)phenol **3.1** (1.39 g, 4.5 mmol) and K_2CO_3 (2.51 g, 18.1 mmol) in anhydrous acetone (10 mL) was added a solution of 80%wt allyl bromide in toluene (2 mL, 23.1 mmol). The mixture was stirred at reflux under a nitrogen atmosphere for 1 day. After the completion, as monitored by TLC (hexanes:EtOAc 9:1; UV), the solvent was evaporated under reduced pressure. The crude mixture was redissolved in water and extracted with DCM 3 times. The combined organic phase was dried over Na_2SO_4 and removed. The crude mixture was purified by column chromatography using 5% EtOAc in hexane as an isocratic eluent system to obtain (((5-(allyloxy)-1,3-phenylene)bis(oxy))bis(methylene))dibenzene (**3.29**) as light yellow liquid (1.27 g, 81% yield). ^{1}H NMR (400 MHz, $CDCl_3$) δ 7.46 – 7.28 (m, 10H), 6.26 (t, J = 2.1 Hz, 1H), 6.20 (d, J = 2.1 Hz, 2H), 6.03 (ddt, J = 17.1, 10.6, 5.3 Hz, 1H), 5.39 (dd, J = 17.3, 1.4 Hz, 1H), 5.27 (dd, J = 10.5, 1.4 Hz, 1H), 5.00 (s, 4H), 4.48 (dt, J = 5.4, 1.4 Hz, 2H). The ^{1}H NMR is in agreement with those reported before.[49]

2-Allyl-3,5-bis(benzyloxy)phenol (3.30)

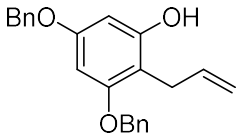

3.30

(((5-(Allyloxy)-1,3-phenylene)bis(oxy))bis(methylene))dibenzene **3.29** (1.01 g, 2.91 mmol) was heated neat for 5 hours. After the completion as monitored by TLC (hexanes:EtOAc 9:1; UV), the crude mixture was purified by column chromatography using 10% EtOAc in hexane as an isocratic eluent system to obtain 2-allyl-3,5-bis(benzyloxy)phenol **3.30** a colorless solid (738 mg, 73% yield). ^{1}H NMR (400 MHz, $CDCl_3$) δ 7.48 – 7.28 (m, 10H), 6.26 (d, J = 2.3 Hz, 1H), 6.17 (d, J = 2.3 Hz, 1H), 5.97 (ddt, J = 16.1, 10.1, 6.1 Hz, 1H), 5.18 – 5.06 (m, 3H), 5.01 (s, 2H), 4.99 (s, 2H), 3.45 (dt, J = 6.0, 1.4 Hz, 2H). The ^{1}H NMR is in agreement with those reported before.[49]

(((4-Allyl-5-(vinyloxy)-1,3-phenylene)bis(oxy))bis(methylene))dibenzene (3.28)

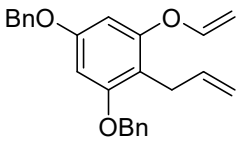

3.28

To the 2-allyl-3,5-bis(benzyloxy)phenol **3.30** (186 mg, 0.54 mmol) and Cs_2CO_3 (1.05 g, 3.22 mmol) in anhydrous acetone (5 mL) was added dibromoethane (465 µL, 5.4 mmol). The mixture was refluxed under a nitrogen atmosphere for 1 day and monitored by TLC (hexanes:EtOAc 9:1; UV). The solvent was evaporated under reduced pressure. The residue was redissolved in water and extracted with DCM 3 times. The combined organic phase was evaporated to dryness. The crude mixture was continued to the next step without further purification. The resulting residue was dissolved in anhydrous THF (2 mL). A solution of 1 M KO^{t}Bu in THF (810 µL, 0.81 mmol) was added dropwise at 0 °C under a nitrogen atmosphere.

The mixture was stirred at 0 °C for 45 minutes and monitored by TLC (hexanes:EtOAc 9:1; UV). Brine was added to quench the reaction. The organic phase was collected, and the aqueous was extracted with EtOAc twice. The combined organic phase was evaporated under reduced pressure. The residue was purified by column chromatography using 5% EtOAc and 3% Et_3N in hexane as an isocratic eluent system to obtain (((4-allyl-5-(vinyloxy)-1,3-phenylene)bis(oxy))bis(methylene))dibenzene **3.28** as colorless liquid (124 mg, 61% yield over 2 steps). ^{1}H NMR (400 MHz, $CDCl_3$) δ 7.43 – 7.28 (m, 10H), 6.56 (dd, J = 13.8, 6.1 Hz, 1H), 6.38 (d, J = 2.3 Hz, 1H), 6.29 (d, J = 2.3 Hz, 1H), 5.94 (ddt, J = 16.3, 10.0, 6.3 Hz, 1H), 5.03 (s, 2H), 4.97 – 4.90 (m, 4H), 4.66 (dd, J = 13.8, 1.7 Hz, 1H), 4.36 (dd, J = 6.1, 1.7 Hz, 1H), 3.39 (dt, J = 6.3, 1.5 Hz, 2H). The ^{1}H NMR is in agreement with those reported before.[49]

5,7-Bis(benzyloxy)-4*H*-chromene (3.17)

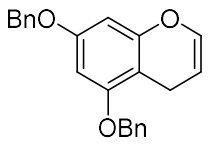

3.17

To a solution of (((4-allyl-5-(vinyloxy)-1,3-phenylene)bis(oxy))bis(methylene))dibenzene **3.28** (103 mg, 0.28 mmol) in toluene (12 mL), a solution of Grubbs' 2nd-generation Ru catalyst (11.5 mg, 0.014 mmol) in toluene (2 mL) was added dropwise under nitrogen atmosphere. The reaction was stirred at 60 °C under bubbling by nitrogen for 45 minutes and monitored by ^{1}H NMR spectroscopy. The mixture was filtrated through silica gel under flushing with nitrogen gas. The filtrate was evaporated to dryness by blowing with nitrogen to obtain 5,7-bis(benzyloxy)-4*H*-chromene **3.17** as light-yellow liquid (90.2 mg, 95% yield). ^{1}H NMR (396 MHz, $CDCl_3$) δ 7.53 – 7.28 (m,10H), 6.42 (dt, J = 6.3, 1.9 Hz, 1H), 6.27 (d, J = 2.3 Hz, 1H), 6.12 (d, J = 2.3 Hz, 1H), 5.02 – 4.91 (m, 4H), 3.23 (dd, J = 3.2, 2.1 Hz, 2H). The ^{1}H NMR is in agreement with those reported before.[49]

Tsuji dihydroxylation of 5,7-bis(benzyloxy)-4*H*-chromene (3.17)

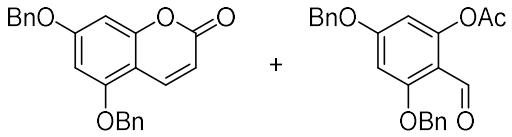

3.32 3.33

The mixture of 5,7-bis(benzyloxy)-4*H*-chromene **3.17** (82.3 mg, 0.24 mmol), K_2CO_3 (100 mg, 0.72 mmol), and $K_3Fe(CN)_6$ (237 mg, 0.72 mmol) were dissolved in the mixture of *t*BuOH, water, and THF in 2 : 2 : 3 ratio (3 mL). The catalyst $K_2OsO_4 \cdot 2H_2O$ (9.2 mg, 0.024 mmol) was added. The mixture was stirred at ambient temperature overnight and monitored by ^{1}H NMR spectroscopy. Brine was added to quench the reaction. The organic phase was collected, and the aqueous was extracted with EtOAc 3 times. The combined organic phase was evaporated under reduced pressure. The residue was redissolved in anhydrous DCM (2 mL). Acetic anhydride (90 µL, 0.96 mmol), Et_3N (170 µL, 1.2 mmol), and 4-dimethylaminopyridine (2.8 mg, 0.024 mmol) were added. The reaction was stirred at room temperature for 1 day and monitored by TLC (hexanes:EtOAc 1:1; UV). The mixture was diluted with DCM, and a saturated aqueous solution of NH_4Cl was added. The organic phase was washed with water twice, dried over Na_2SO_4, and evaporated. The crude mixture was purified by column chromatography using a gradient eluent system starting from 2% to 10% EtOAc in hexane to obtain 5,7-bis(benzyloxy)-2H-chromen-2-one (**3.32**) as a white solid and 3,5-bis(benzyloxy)-2-formylphenyl acetate (**3.33**) as a white solid.

5,7-bis(benzyloxy)-2H-chromen-2-one (**3.32**) ^{1}H NMR (400 MHz, $CDCl_3$) δ 8.02 (d, J = 9.6 Hz, 1H), 7.46 – 7.32 (m, 10H), 6.51 (d, J = 1.8 Hz, 1H), 6.45 (d, J = 2.1 Hz, 1H), 6.16 (d, J = 9.6 Hz, 1H), 5.11 (s, 2H), 5.09 (s, 2H); ^{13}C NMR (400 MHz, $CDCl_3$) 162.8, 161.6, 156.9, 156.2, 139.0, 135.9, 128.9, 128.6, 127.8, 127.7, 111.3, 104.6, 96.8, 94.3, 70.9, 70.7.

3,5-bis(benzyloxy)-2-formylphenyl acetate (**3.33**) ^{1}H NMR (396 MHz, $CDCl_3$) 10.33 (s, 1H), 7.50 – 7.29 (m, 10H), 6.52 (d, *J* = 2.2 Hz, 1H), 6.32 (d, *J* = 1.9 Hz, 1H), 5.11 (s, 2H), 5.07 (s, 2H), 2.37 (s, 3H).

Upjohn dihydroxylation of 5,7-bis(benzyloxy)-4*H*-chromene (3.17) with 1.5 eq. NMO

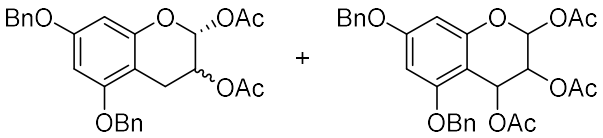

rac-cis/trans 3.19 3.34

The mixture of 5,7-bis(benzyloxy)-4*H*-chromene **3.17** (90.2 mg, 0.26 mmol) and 50%wt NMO in water (92.0 mg, 0.39 mmol) were dissolved in the mixture of *t*BuOH, water, and THF in 2 : 2 : 3 ratio (3 mL). The catalyst $K_2OsO_4{\cdot}2H_2O$ (5.0 mg, 0.013 mmol) was added. The mixture was stirred at ambient temperature overnight and monitored by ^{1}H NMR spectroscopy. Brine was added to quench the reaction. The organic phase was collected, and the aqueous was extracted with EtOAc 3 times. The combined organic phase was evaporated under reduced pressure. The residue was redissolved in anhydrous DCM (2 mL). Acetic anhydride (100 µL, 1.05 mmol), Et_3N (190 µL, 1.31 mmol) and 4-dimethylaminopyridine (3.2 mg, 0.026 mmol) were added. The reaction was stirred at room temperature for 1 day and monitored by TLC (hexanes:EtOAc 1:1; UV). The mixture was diluted with DCM, and a saturated aqueous solution of NH_4Cl was added. The organic phase was washed with water twice, dried over Na_2SO_4, and evaporated. The crude mixture was purified by column chromatography using a gradient eluent system starting from 2% to 10% EtOAc in hexane to obtain racemic *trans*-5,7-bis(benzyloxy)chromane-2,3-diyl diacetate ***rac-trans* 3.19** as a white solid (9.9 mg, 8% yield over 2 steps), racemic *cis*-5,7-bis(benzyloxy)chromane-2,3-diyl diacetate ***rac-cis* 3.19** in an inseparable mixture to ***rac-trans* 3.19**, and other unknown impurities as a white solid (15.2 mg,

13% maximum yield over 2 steps), and 5,7-bis(benzyloxy)chromane-2,3,4-triyl triacetate (**3.34**) as a white solid (13.4 mg, 10% yield over 2 steps).

Racemic *cis*-5,7-bis(benzyloxy)chromane-2,3-diyl diacetate (***rac-cis* 3.19**) ^{1}H NMR (400 MHz, $CDCl_3$) δ 7.45 – 7.28 (m, 10H), 6.46 (d, J = 2.3 Hz, 1H), 6.29 (d, J = 2.3 Hz, 1H), 6.19 (d, J = 2.2 Hz, 1H), 5.22 (ddd, J = 10.9, 6.4, 2.5 Hz, 1H), 5.02 – 4.95 (m, 4H), 3.10 (dd, J = 15.6, 6.4 Hz, 1H), 2.72 (dd, J = 15.6, 10.9 Hz, 1H), 2.09 (s, 3H), 2.08 (s, 3H).

Racemic *trans*-5,7-bis(benzyloxy)chromane-2,3-diyl diacetate (***rac-trans* 3.19**) ^{1}H NMR (400 MHz, $CDCl_3$) δ 7.46 – 7.29 (m, 10H), 6.36 (d, J = 3.1 Hz, 1H), 6.32 (d, J = 2.3 Hz, 1H), 6.24 (d, J = 2.2 Hz, 1H), 5.17 (dd, J = 6.4, 3.1 Hz, 1H), 5.02 (s, 2H), 4.99 (s, 2H), 2.96 – 2.88 (m, 2H), 2.07 (s, 3H), 2.05 (s, 3H).

5,7-bis(benzyloxy)chromane-2,3,4-triyl triacetate (**3.34**) ^{1}H NMR (400 MHz, $CDCl_3$) 7.45 – 7.29 (m, 10H), 6.52 (d, J = 4.0 Hz, 1H), 6.41 (d, J = 8.6 Hz, 1H), 6.25 (d, J = 2.1 Hz, 1H), 6.16 (d, J = 2.1 Hz, 1H), 5.27 (dd, J = 8.6, 4.1 Hz, 1H), 5.02 (s, 2H), 4.99 (s, 2H), 2.17 (s, 3H), 2.05 (s, 3H), 1.96 (s, 3H).

5,7-Bis(benzyloxy)chromane-2,3-diyl diacetate (*rac*-3.19): Upjohn dihydroxylation of 5,7-bis(benzyloxy)-4*H*-chromene (3.17) with 1.05 eq. NMO

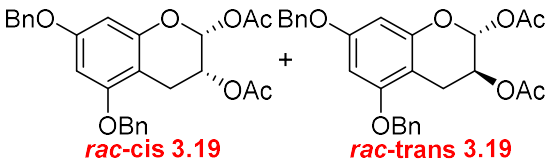

The mixture of 5,7-bis(benzyloxy)-4*H*-chromene **3.17** (162 mg, 0.47 mmol) and 50%wt NMO in water (118 mg, 0.50 mmol) were dissolved in 30% water in acetone (5 mL). The catalyst $K_2OsO_4 \cdot 2H_2O$ (9.2 mg, 0.024 mmol) was added. The mixture was stirred at ambient temperature overnight and monitored by ^{1}H NMR spectroscopy. Brine was added to quench the reaction. The organic phase was collected, and the aqueous was extracted with EtOAc 3

times. The combined organic phase was evaporated under reduced pressure. The residue was redissolved in anhydrous DCM (6 mL). Acetic anhydride (180 µL, 1.88 mmol), Et_3N (330 µL, 2.35 mmol), and 4-dimethylaminopyridine (5.6 mg, 0.047 mmol) were added. The reaction was stirred at room temperature for 1 day and monitored by TLC (hexanes:EtOAc 1:1; UV). The mixture was diluted with DCM, and a saturated aqueous solution of NH_4Cl was added. The organic phase was washed with water twice, dried over Na_2SO_4, and evaporated to obtain the mixture between racemic *cis*-5,7-bis(benzyloxy)chromane-2,3-diyl diacetate ***rac-cis* 3.19** and racemic *trans*-5,7-bis(benzyloxy)chromane-2,3-diyl diacetate ***rac-trans* 3.19** with 2 : 3.1 mole ratio as black solid (185 mg, 85% yield over 2 steps).

Racemic *cis*-5,7-bis(benzyloxy)chromane-2,3-diyl diacetate (***rac-cis* 3.19**) ^{1}H NMR (400 MHz, $CDCl_3$) δ 7.45 – 7.28 (m, 10H), 6.46 (d, *J* = 2.3 Hz, 1H), 6.29 (d, *J* = 2.3 Hz, 1H), 6.19 (d, *J* = 2.2 Hz, 1H), 5.22 (ddd, *J* = 10.9, 6.4, 2.5 Hz, 1H), 5.02 – 4.95 (m, 4H), 3.10 (dd, *J* = 15.6, 6.4 Hz, 1H), 2.72 (dd, *J* = 15.6, 10.9 Hz, 1H), 2.09 (s, 3H), 2.08 (s, 3H).

Racemic *trans*-5,7-bis(benzyloxy)chromane-2,3-diyl diacetate (***rac-trans* 3.19**) ^{1}H NMR (400 MHz, $CDCl_3$) δ 7.46 – 7.29 (m, 10H), 6.36 (d, *J* = 3.1 Hz, 1H), 6.32 (d, *J* = 2.3 Hz, 1H), 6.24 (d, *J* = 2.2 Hz, 1H), 5.17 (dd, *J* = 6.4, 3.1 Hz, 1H), 5.02 (s, 2H), 4.99 (s, 2H), 2.96 – 2.88 (m, 2H), 2.07 (s, 3H), 2.05 (s, 3H).

Investigation of the nucleophilic substitution of 5,7-bis(benzyloxy)chromane-2,3-diyl diacetate (*rac*-3.19) with (4-methoxyphenyl)zinc(II) iodide

Activated zinc (983 mg, 15 mmol) was added portion-wise to iodine (2.59 g, 10 mmol) in anhydrous diethyl ether (20 mL) and stirred for 1–2 hours at 0 °C under a nitrogen atmosphere until the solution turned clear to obtain the 0.5 M ethereal solution of ZnI_2. In a separated container, magnesium (311 mg, 12.3 mmol) and 1-iodo-4-methoxybenzene **3.40** (586 mg, 2.5 mmol) in anhydrous THF (8.4 mL) were stirred at reflux under a nitrogen atmosphere for 3

hours to produce 0.3 M (4-methoxyphenyl)magnesium iodide **3.41** in THF. The 0.75 mL of the 0.3 M Grignard **3.41** solution in THF was diluted with 1 mL DCM/DCE and then added 0.45 mL of ZnI_2 solution in ether. The mixed solution was stirred at room temperature for 10 minutes under nitrogen atmosphere, then 5,7-bis(benzyloxy)chromane-2,3-diyl diacetate ***rac*-3.19** (49.6 mg, 0.11 mmol) in DCM/DCE (1 mL). The temperature was studied. The reaction was monitored by ^{1}H NMR spectroscopy.

1,2-Bis(benzyloxy)benzene (3.42)

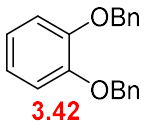

3.42

K_2CO_3 (6.91 g, 50 mmol) was suspended in the solution of pyrocatechol **3.44** (2.20 g, 20 mmol) and benzyl bromide (5.9 mL, 50 mmol) in acetone (40 mL). The mixture was refluxed under a nitrogen atmosphere for 2 days and monitored by TLC (hexanes:EtOAc 9:1; UV). The inorganic salts were removed by filtration, and then the filtrate was evaporated under reduced pressure. The residue was recrystallized in a mixture between DCM and hexanes to obtain 1,2-bis(benzyloxy)benzene **3.42 as** a colorless solid (5.04 g, 87% yield). ^{1}H NMR (396 MHz, $CDCl_3$) δ 7.45 (d, J = 7.3 Hz, 4H), 7.40 – 7.27 (m, 6H), 6.98 – 6.92 (m, 2H), 6.91 – 6.85 (m, 2H), 5.16 (s, 4H). The ^{1}H NMR is in agreement with those reported before.[93]

Investigation of the nucleophilic substitution of 5,7-bis(benzyloxy)chromane-2,3-diyl diacetate (*rac*-3.19) by electrophilic aromatic substitution

To the 5,7-bis(benzyloxy)chromane-2,3-diyl diacetate ***rac*-3.19** (30.0 mg, 0.065 mmol) and 1,2-bis(benzyloxy)benzene **3.42** (37.7 mg, 0.13 mmol) in anhydrous DCM (5 mL) was added the studied Lewis acid at 0 °C. Different Lewis acids (e.g., $Sc(OTf)_3$, $Ti(OiPr)_4$, $SnCl_4$, $BF_3{\cdot}Et_2O$) were tested, and the amount of Lewis acid investigated (1.1–3.3 eq.). The mixture was stirred

for 1 day, which was allowed to warm up to room temperature and monitored by ^{1}H NMR spectroscopy.

General procedure 1: benzylation of gallic acid derivatives **3.47**, followed by hydrolysis

To the gallic acid derivatives **3.47** (1 eq.) and K_2CO_3 (4 – 8 eq.) in DMF (4 mL/1 mmol of acid) was added benzyl bromide (4 – 7.5 eq.). After completion, water was added and then extracted with EtOAc 2 times. The combined organic phase was washed with brine, dried over Na_2SO_4, and evaporated. The crude mixture was continued to the next step without further purification. The resulting residue was charged with 5 M NaOH in the mixture between 50% EtOH in water and refluxed. After completion, EtOH was evaporated. The crude mixture was acidified by an aqueous solution of 2 M HCl to pH 2. The precipitant was filtered and recrystallized in hot MeOH.

3-(Benzyloxy)benzoic acid (3.16b)

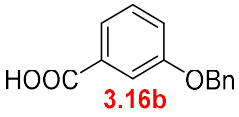

3.16b

General procedure 1 was followed using 3-hydroxybenzoic acid **3.47b** (3.45 g, 25 mmol), benzyl bromide (11.9 mL, 100 mmol), and K_2CO_3 (13.87 g, 100 mmol) in DMF (50 mL). The mixture was kept stirring at 40 °C for 3 days and monitored by TLC (hexanes:EtOAc 4:1; UV). After the aqueous work up, the resulting crude mixture was charged with 5 M NaOH in the mixture between 50% EtOH in water (50 mL) and refluxed overnight. The reaction was monitored by TLC (hexanes:EtOAc 4:1; UV). 3-(benzyloxy)benzoic acid **3.16b** was obtained as crystalline needles (5.46 g, 96% yield over 2 steps). ^{1}H NMR (396 MHz, DMSO-d6) δ 7.57 – 7.22 (m, 9H), 5.16 (s, 2H); LRMS calcd for $C_{14}H_{13}O_3$ (M+ H^+) 229.3; found 229.8. The analytical data are in agreement with those reported before.[94]

4-(Benzyloxy)benzoic acid (3.16c)

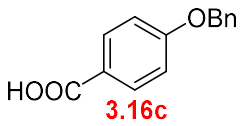

3.16c

General procedure 1 was followed using 4-hydroxybenzoic acid **3.47c** (3.45 g, 25 mmol), benzyl bromide (11.9 mL, 100 mmol), and K_2CO_3 (13.87 g, 100 mmol) in DMF (50 mL). The mixture was kept stirring at 40 °C for 3 days and monitored by TLC (hexanes:EtOAc 4:1; UV). After the aqueous work up, the resulting crude mixture was charged with 5 M NaOH in the mixture between 50% EtOH in water (50 mL) and refluxed overnight. The reaction was monitored by TLC (hexanes:EtOAc 4:1; UV). 4-(Benzyloxy)benzoic acid **3.16c** was obtained as crystalline needles (5.47 g, 96% yield over 2 steps). ^{1}H NMR (396 MHz, DMSO-d6) δ 7.94 – 7.83 (m, 2H), 7.49 – 7.43 (m, 2H), 7.43 – 7.36 (m, 2H), 7.37 – 7.30 (m, 1H), 7.14 – 6.98 (m, 2H), 5.17 (s, 2H); LRMS calcd for $C_{14}H_{13}O_3$ ($M+ H^+$) 229.3; found 229.6. The analytical data are in agreement with those reported before.[95]

3,4-Bis(benzyloxy)benzoic acid (3.16d)

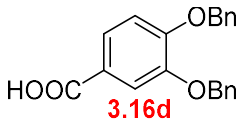

3.16d

General procedure 1 was followed using 3,4-dihydroxybenzoic acid **3.47d** (761 mg, 5 mmol), benzyl bromide (4.2 mL, 35 mmol), and K_2CO_3 (4.84 g, 35 mmol) in DMF (15 mL). The mixture was kept stirring at 40 °C for 3 days and monitored by TLC (hexanes:EtOAc 4:1; UV). After the aqueous work up, the resulting crude mixture was charged with 5 M NaOH in the mixture between 50% EtOH in water (40 mL) and refluxed overnight. The reaction was monitored by TLC (hexanes:EtOAc 4:1; UV). 3,4-Bis(benzyloxy)benzoic acid **3.16d** was obtained as crystalline needles (1.52 g, 92% yield over 2 steps). ^{1}H NMR (396 MHz, DMSO-

d6) δ 7.56 – 7.53 (m, 2H), 7.50 – 7.26 (m, 10H), 7.21 – 7.11 (m, 1H), 5.22 (s, 2H), 5.17 (s, 2H); LRMS calcd for $C_{21}H_{19}O_4$ (M+ H^+) 335.4; found 335.1. The analytical data are in agreement with those reported before.[96]

3,5-Bis(benzyloxy)benzoic acid (3.16e)

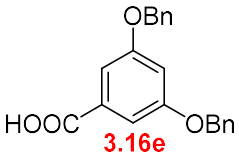

3.16e

General procedure 1 was followed using 3,5-dihydroxybenzoic acid **3.47e** (760 mg, 5 mmol), benzyl bromide (4.2 mL, 35 mmol), and K_2CO_3 (4.83 g, 35 mmol) in DMF (20 mL). The mixture was kept stirring at 40 °C for 3 days and monitored by TLC (hexanes:EtOAc 4:1; UV). After the aqueous work up, the resulting crude mixture was charged with 5 M NaOH in the mixture between 50% EtOH in water (40 mL) and refluxed overnight. The reaction was monitored by TLC (hexanes:EtOAc 4:1; UV). 3,5-Bis(benzyloxy)benzoic acid **3.16e** was obtained as crystalline needles (1.50 g, 90% yield over 2 steps). ^{1}H NMR (396 MHz, DMSO-d6) δ 7.48 – 7.29 (m, 10H), 7.15 (d, J = 2.3 Hz, 2H), 6.92 (t, J = 2.3 Hz, 1H), 5.14 (s, 4H); LRMS calcd for $C_{21}H_{19}O_4$ (M+ H^+) 335.4; found 335.6. The analytical data are in agreement with those reported before.[96]

3,4,5-Tris(benzyloxy)benzoic acid (3.16f)

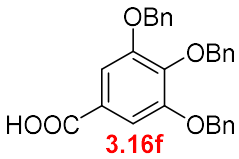

3.16f

General procedure 1 was followed using gallic acid monohydrate **3.47f** (942 mg, 5 mmol), benzyl bromide (4.5 mL, 38 mmol), and K_2CO_3 (5.19 g, 38 mmol) in DMF (20 mL). The mixture was kept stirring at 40 °C for 3 days and monitored by TLC (hexanes:EtOAc 4:1; UV).

After the aqueous work up, the resulting crude mixture was charged with 5 M NaOH in the mixture between 50% EtOH in water (40 mL) and refluxed overnight. The reaction was monitored by TLC (hexanes:EtOAc 4:1; UV). 3,4,5-Tris(benzyloxy)benzoic acid **3.16f** was obtained as crystalline needles (2.17 g, 98% yield over 2 steps). ^{1}H NMR (400 MHz, DMSO-d6) δ 7.53 – 7.21 (m, 15H), 5.18 (s, 4H), 5.04 (s, 2H); LRMS calcd for $C_{28}H_{25}O_5$ (M+ H^+) 441.5; found 441.4. The analytical data are in agreement with those reported before.[76]

2-Allyl-3,5-bis(benzyloxy)phenyl 3,4,5-tris(benzyloxy)benzoate (2.45)

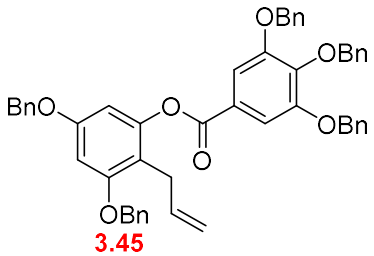

3.45

To the 3,4,5-tris(benzyloxy)benzoic acid **3.16f** (696 mg, 1.58 mmol) in DCM (9 mL) was added dropwise oxalyl chloride (170 µL, 2.05 mmol) in the presence of a catalytic amount of DMF (150 µL). The mixture was stirred at room temperature for 1 hour, fitted with a drying tube, and volatiles was evaporated under reduced pressure. The residue was taken up in DCM (12 mL). 2-Allyl-3,5-bis(benzyloxy)phenol **3.30** (520 mg, 1.5 mmol), Et_3N (630 µL, 4.5 mmol), and DMAP (18.7 mg, 0.15 mmol) were added. The mixture was stirred overnight, fitted with a drying tube, and monitored by TLC (hexanes:EtOAc 9:1; UV). The mixture was diluted with DCM and washed with a saturated aqueous solution of NH_4Cl. The aqueous phase was extracted with DCM twice. The combined organic phase was dried over Na_2SO_4 and evaporated to obtain 2-allyl-3,5-bis(benzyloxy)phenyl 3,4,5-tris(benzyloxy)benzoate **2.45** as a light-yellow solid (1.15 g, quantitative over 2 steps). ^{1}H NMR (400 MHz, $CDCl_3$) δ 7.53 (s, 2H), 7.48 – 7.23 (m, 25H), 6.55 (d, J = 2.3 Hz, 1H), 6.45 (d, J = 2.3 Hz, 1H), 5.91 – 5.78 (m, 1H), 5.17 (s, 6H), 5.06 (s, 2H), 5.00 (s, 2H), 4.91 – 4.81 (m, 2H), 3.30 (d, J = 6.3 Hz, 2H).

Investigation of the Nicolaou's Tebbe reaction of 2-allyl-3,5-bis(benzyloxy)phenyl 3,4,5-tris(benzyloxy)benzoate (2.45)

Cp_2TiCl_2 (996 mg, 4 mmol) was dissolved in 2 M $AlMe_3$ in toluene (4 mL, 8 mmol). The mixture was stirred at room temperature for 3 days to obtain a 1 M solution of $Cp_2TiCH_2ClAlMe_2$ in toluene (Tebbe reagent). 1.2 mL of the resulting Tebbe solution was added into 2-allyl-3,5-bis(benzyloxy)phenyl 3,4,5-tris(benzyloxy)benzoate **2.45** (154 mg, 0.2 mmol) in the mixture between toluene (1.2 mL) and THF (1.2 mL) at 0 °C. The reaction was stirred at 0 °C, which was allowed to warm up to room temperature for 1 day and monitored by ^{1}H NMR spectroscopy.

(*2R,3S*)-5,7-Bis(benzyloxy)-2-(3,4-bis(benzyloxy)phenyl)chroman-3-ol (3.49a)

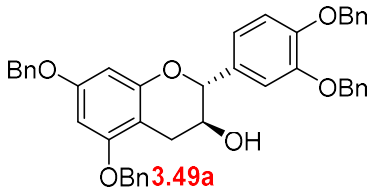

3.49a

To (+)-catechin **3.48a** (2.18 g, 7.5 mmol), KI (163 mg, 0.75 mmol), and K_2CO_3 (6.22g, 45 mmol) in degassed DMF (30 mL) was added benzyl bromide (4 mL, 33.8 mmol) at 0 °C. The mixture was kept under stirring at 0 °C, which was allowed to warm up to room temperature for 1 day and monitored by TLC (DCM; UV). Water was added and then extracted with EtOAc 3 times. The combined organic phase was washed with water, dried over Na_2SO_4, and evaporated. The crude mixture was purified by column chromatography using DCM as an isocratic eluent system to obtain (*2R,3S*)-5,7-Bis(benzyloxy)-2-(3,4-bis(benzyloxy)phenyl)chroman-3-ol **3.49a** as an orange solid (3.82 g, 78% yield). ^{1}H NMR (396 MHz, $CDCl_3$) δ 7.50 – 7.24 (m, 20H), 7.03 (s, 1H), 6.95 (s, 2H), 6.27 (d, J = 2.3 Hz, 1H), 6.21 (d, J = 2.3 Hz, 1H), 5.24 – 5.10 (m, 4H), 5.03 (s, 2H), 4.99 (s, 2H), 4.63 (d, J = 8.2 Hz,

1H), 4.04 – 3.95 (m, 1H), 3.11 (dd, *J* = 16.4, 5.7 Hz, 1H), 2.65 (dd, *J* = 16.4, 8.9 Hz, 1H); LRMS calcd for $C_{43}H_{39}O_6$ (M+ H^+) 651.8; found 651.5. The analytical data are in agreement with those reported before.[97]

(*2R,3R*)-5,7-Bis(benzyloxy)-2-(3,4-bis(benzyloxy)phenyl)chroman-3-ol (3.50a)

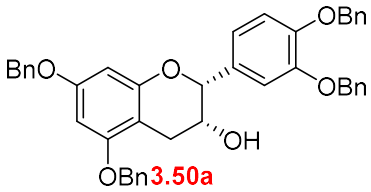

3.50a

To the suspension of Dess-Martin periodinane (3.39 g, 8 mmol) in DCM (6 mL) was added dropwise (*2R,3S*)-5,7-bis(benzyloxy)-2-(3,4-bis(benzyloxy)phenyl)chroman-3-ol **3.49a** (1.30 g, 2 mmol) in DCM (4 mL). The reaction was stirred at room temperature for 1.5 hours and monitored by TLC (hexanes:EtOAc 2:1; UV). The mixture was filtered through celite with Na_2SO_3 and $NaHCO_3$. The filtrate was washed with the mixed solution between 50%v/v of the saturated aqueous solution of Na_2SO_3 and $NaHCO_3$. The aqueous phase was extracted with DCM. The combined organic phase was washed with water, dried over Na_2SO_4, and evaporated. The residue was redissolved in THF (30 mL). The 1 M solution of K-selectride in THF (4 mL) was added dropwise at -78 °C. The reaction was stirred at -78 °C, which was allowed to warm up to room temperature overnight and monitored by TLC (hexanes:EtOAc 2:1; UV). The mixed aqueous solution of 2 M NaOH (3 mL) and 2 M H_2O_2 (3 mL) was added dropwise at 0 °C, and the mixture was stirred for 30 minutes. Brine was added, and the solution was extracted with DCM 2 times. The combined organic phase was dried over Na_2SO_4 and evaporated. The crude mixture was purified by column chromatography using 33% EtOAc in hexane as an isocratic eluent system to provide (*2R,3R*)-5,7-bis(benzyloxy)-2-(3,4-bis(benzyloxy)phenyl)chroman-3-ol (**3.50a**) as a yellow solid (676 mg, 52% yield). ^{1}H NMR (400 MHz, $CDCl_3$) δ 7.48 – 7.26 (m, 20H), 7.14 (d, *J* = 1.9 Hz, 1H), 7.00 (dd, *J* = 8.4, 1.9 Hz,

1H), 6.96 (d, *J* = 8.3 Hz, 1H), 6.27 (d, *J* = 2.3 Hz, 1H), 6.26 (d, *J* = 2.3 Hz, 1H), 5.18 (s, 2H), 5.17 (s, 2H), 5.02 (s, 2H), 5.01 (s, 2H), 4.91 (s, 1H), 4.23 – 4.18 (m, 1H), 2.99 (dd, *J* = 18.1, 2.4 Hz, 1H), 2.92 (dd, *J* = 17.2, 4.3 Hz, 1H); LRMS calcd for $C_{43}H_{39}O_6$ ($M+ H^+$) 651.8; found 651.3. The analytical data are in agreement with those reported before.[97]

General procedure 2: EDCI esterification

(*2R,3S*)-5,7-Bis(benzyloxy)-2-(3,4-bis(benzyloxy)phenyl)chroman-3-ol **3.49a** (1 eq.), benzylated gallic acid derivatives **3.16** (2.5 eq.), EDCI (2.5 eq.) and DMAP (0.2 eq.) were dissolved in DCM (75 mL/1 mmol of **49a**). After completion, the mixture was quenched with a saturated aqueous solution of NH_4Cl and extracted with DCM twice. The combined organic phase was dried over Na_2SO_4 and evaporated. The crude mixture was purified by column chromatography using DCM as an isocratic eluent system, which was then filtered through basic alumina.

(*2R,3S*)-5,7-Bis(benzyloxy)-2-(3,4-bis(benzyloxy)phenyl)chroman-3-yl 3-(benzyloxy) benzoate (3.49b)

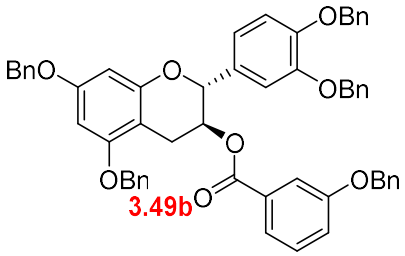

General procedure 2 was followed using (*2R,3S*)-5,7-bis(benzyloxy)-2-(3,4-bis(benzyloxy)phenyl)chroman-3-ol **3.49a** (130 mg, 0.2 mmol), 3-(benzyloxy)benzoic acid **3.16a** (116 mg, 0.5 mmol), EDCI (98.1 mg, 0.51 mmol), and DMAP (5.3 mg, 0.04 mmol) in DCM (15 mL). After stirring at room temperature under nitrogen atmosphere for 2 days, the reaction was monitored by TLC (hexanes:EtOAc 4:1; UV). (*2R,3S*)-5,7-Bis(benzyloxy)-2-

(3,4-bis(benzyloxy)phenyl) chroman-3-yl 3-(benzyloxy) benzoate **3.49b** was obtained as a colorless solid (150 mg, 87% yield). $[\alpha]_D^{23}$ = +26° (*c* = 0.52 in $CHCl_3$); ^1H NMR (396 MHz, $CDCl_3$) δ 7.62 – 7.15 (m, 28H), 7.11 (d, *J* = 8.0 Hz, 1H), 7.01 (s, 1H), 6.94 (d, *J* = 8.2 Hz, 1H), 6.86 (d, *J* = 8.3 Hz, 1H), 6.28 (s, 2H), 5.50 (q, *J* = 6.3 Hz, 1H), 5.19 – 4.90 (m, 11H), 3.05 (dd, *J* = 16.8, 5.3 Hz, 1H), 2.85 (dd, *J* = 16.8, 6.8 Hz, 1H); ^{13}C NMR (100 MHz, $CDCl_3$) δ 165.5, 159.1, 158.7, 157.9, 155.1, 149.1, 137.3, 137.2, 137.0, 136.9, 136.6, 131.4, 131.2, 129.5, 128.8, 128.7 (x2), 128.6, 128.5, 128.2, 128.1, 128.0, 127.9, 127.7, 127.6, 127.4, 122.4, 120.3, 120.0, 115.4, 115.1, 113.6, 101.5, 94.6, 93.9, 78.5, 71.5, 71.3, 70.3, 70.1, 24.4; HRMS calcd for $C_{57}H_{49}O_8$ (M+ H^+) 861.3427; found 861.3484; IR (ATR, cm^{-1}) υ_{max} 3068, 3032, 2868, 1716, 1591, 1269, 1213, 1140, 1016; mp: 84 – 86 °C.

(*2R,3S*)-5,7-bis(benzyloxy)-2-(3,4-bis(benzyloxy)phenyl)chroman-3-yl 4-(benzyloxy) benzoate (3.49c)

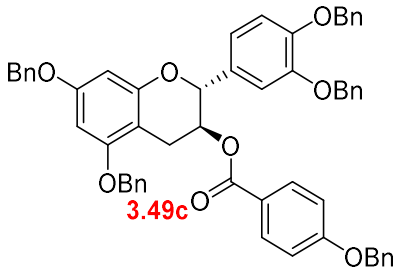

General procedure 2 was followed using (*2R,3S*)-5,7-bis(benzyloxy)-2-(3,4-bis(benzyloxy)phenyl)chroman-3-ol **3.49a** (130 mg, 0.2 mmol), 4-(benzyloxy)benzoic acid **3.16b** (114 mg, 0.5 mmol), EDCI (97.6 mg, 0.5 mmol), and DMAP (5.3 mg, 0.04 mmol) in DCM (15 mL). After stirring at room temperature under nitrogen atmosphere for 2 days, the reaction was monitored by TLC (hexanes:EtOAc 4:1; UV). (*2R,3S*)-5,7-Bis(benzyloxy)-2-(3,4-bis(benzyloxy)phenyl) chroman-3-yl 4-(benzyloxy)benzoate **3.49c** was obtained as a colorless solid (108 mg, 63% yield). $[\alpha]_D^{23}$ = +31° (*c* = 1.12 in $CHCl_3$); ^1H NMR (396 MHz, $CDCl_3$) δ 7.86 (d, *J* = 8.8 Hz, 2H), 7.48 – 7.23 (m, 25H), 7.01 (d, *J* = 1.7 Hz, 1H), 6.96 – 6.84

(m, 4H), 6.27 (s, 2H), 5.50 (q, J = 6.4 Hz, 1H), 5.18 – 4.96 (m, 11H), 3.01 (dd, J = 16.8, 5.3 Hz, 1H), 2.83 (dd, J = 16.8, 6.6 Hz, 1H); ^{13}C NMR (100 MHz, $CDCl_3$) δ 165.4, 162.7, 159.0, 157.8, 155.1, 149.0, 137.3, 137.2, 137.0, 136.9, 136.3, 131.9, 131.4, 128.8, 128.7 (x2), 128.6, 128.5, 128.3, 128.2, 128.0, 127.9, 127.7, 127.6, 127.4, 127.3, 122.7, 119.9, 115.1, 114.6, 113.6, 101.6, 94.6, 93.9, 78.5, 71.5, 71.4, 70.3, 70.2, 70.1, 69.5, 24.3; HRMS calcd for $C_{57}H_{49}O_8$ ($M+H^+$) 861.3427; found 861.3466; IR (ATR, cm^{-1}) υ_{max} 3066, 3034, 2924, 1707, 1605, 1499, 1253, 1017; mp: 91 – 94 °C.

General procedure 3: DMAP esterification

To the benzoic acid **3.16** (1.2 eq.) in DCM (15 mL/1 mmol of catechin **3.49**/**3.50**) was added dropwise oxalyl chloride (1.5 eq.) in the presence of a catalytic amount of DMF. The mixture was stirred at room temperature for 1 hour, fitted with a drying tube, and volatiles was evaporated under reduced pressure. The residue was taken up in DCM (15 mL/1 mmol of catechin **3.49**/**3.50**). Catechin **3.49/3.50** (1 eq.) and DMAP (2.5 eq.) were added. After completion, the mixture was diluted with DCM and washed with a saturated aqueous solution of NH_4Cl and water. The combined organic phase was dried over Na_2SO_4 and evaporated.

(*2R*,*3S*)-5,7-Bis(benzyloxy)-2-(3,4-bis(benzyloxy)phenyl)chroman-3-yl 3,4-bis(benzyloxy) benzoate (3.49d)

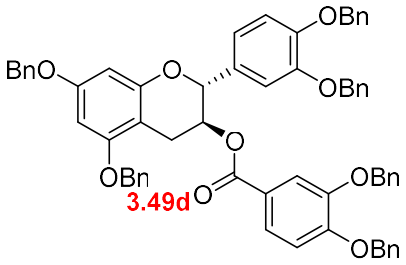

General procedure 3 was followed using 3,4-bis(benzyloxy)benzoic acid **3.16c** (140 mg, 0.42 mmol), oxalyl chloride (45 μL, 0.52 mmol), and DMF (100 μL) in DCM (3 mL). After the

chlorination step, the resulting acid chloride was reacted with (*2R,3S*)-5,7-bis(benzyloxy)-2-(3,4-bis(benzyloxy)phenyl)chroman-3-ol **3.49a** (225 mg, 0.35 mmol) in the presence of DMAP (107 mg, 0.86 mmol) in DCM (4 mL). The reaction was stirred at room temperature fitted with a drying tube overnight and monitored by TLC (hexanes:EtOAc 2:1; UV). After aqueous work up, the crude mixture was purified by trituration with *i*Pr_2O to obtain (*2R*,*3S*)-5,7-bis(benzyloxy)-2-(3,4-bis(benzyloxy)phenyl)chroman-3-yl 3,4-bis(benzyloxy) benzoate **3.49d** as a yellow solid (159 mg, 48% yield). $[\alpha]_D^{23}$ = +31° (*c* = 1.05 in $CHCl_3$); ^{1}H NMR (400 MHz, $CDCl_3$) δ 7.54 – 7.23 (m, 32H), 6.99 (s, 1H), 6.94 – 6.81 (m, 3H), 6.28 (s, 2H), 5.46 (q, *J* = 6.0 Hz, 1H), 5.23 – 4.95 (m, 13H), 3.00 (dd, *J* = 16.9, 5.5 Hz, 1H), 2.81 (dd, *J* = 17.0, 6.8 Hz, 1H); ^{13}C NMR (100 MHz, $CDCl_3$) δ 165.3, 159.0, 157.8, 155.0, 153.0, 149.0, 148.3, 137.3, 137.1, 137.0, 136.9, 136.8, 136.6, 131.3, 128.7, 128.6, 128.5, 128.2, 128.1, 128.0, 127.9, 127.7, 127.5, 127.3, 127.2, 124.2, 122.9, 120.0, 115.6, 115.0, 113.5, 113.2, 101.6, 94.5, 93.8, 78.4, 71.4, 71.3, 71.2, 70.8, 70.2, 70.0, 69.7, 24.3; HRMS calcd for $C_{64}H_{55}O_9$ (M+ H^+) 967.3846; found 967.3832; IR (ATR, cm^{-1}) υ_{max} 3066, 3034, 2940, 2861, 1701, 1595, 1499, 1269, 1213, 1127, 1014; mp: 131 – 133 °C.

(*2R*,*3S*)-5,7-Bis(benzyloxy)-2-(3,4-bis(benzyloxy)phenyl)chroman-3-yl 3,5-bis(benzyloxy) benzoate (3.49e)

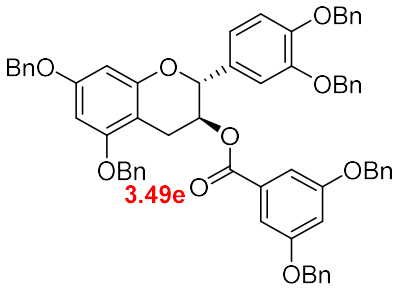

General procedure 3 was followed using 3,5-bis(benzyloxy)benzoic acid **3.16d** (139 mg, 0.42 mmol), oxalyl chloride (45 µL, 0.52 mmol), and DMF (100 µL) in DCM (3 mL). After the chlorination step, the resulting acid chloride was reacted with (*2R,3S*)-5,7-bis(benzyloxy)-2-

(3,4-bis(benzyloxy)phenyl)chroman-3-ol **3.49a** (225 mg, 0.35 mmol) in the presence of DMAP (108 mg, 0.86 mmol) in DCM (4 mL). The reaction was stirred at room temperature, fitted with a drying tube overnight and monitored by TLC (hexanes:EtOAc 2:1; UV). After aqueous work up, the crude mixture was purified by trituration with *i*Pr$_2$O to obtain (*2R*,*3S*)-5,7-bis(benzyloxy)-2-(3,4-bis(benzyloxy)phenyl)chroman-3-yl 3,5-bis(benzyloxy) benzoate **3.49e** as a colorless solid (193 mg, 58% yield). $[\alpha]_D^{22}$ = +35° (*c* = 0.97 in $CHCl_3$); ^{1}H NMR (400 MHz, $CDCl_3$) δ 7.44 – 7.21 (m, 30H), 7.14 (d, *J* = 2.4 Hz, 2H), 7.01 (d, *J* = 2.0 Hz, 1H), 6.94 (dd, *J* = 8.3, 1.9 Hz, 1H), 6.87 (d, *J* = 8.3 Hz, 1H), 6.75 (t, *J* = 2.3 Hz, 1H), 6.27 (dd, *J* = 4.8, 2.3 Hz, 2H), 5.47 (q, *J* = 6.4 Hz, 1H), 5.12 – 5.06 (m, 3H), 5.04 – 4.96 (m, 10H), 3.06 (dd, *J* = 16.7, 5.5 Hz, 1H), 2.83 (dd, *J* = 16.6, 7.1 Hz, 1H); ^{13}C NMR (100 MHz, $CDCl_3$) δ 165.4, 159.8, 159.1, 157.8, 155.1, 149.1, 137.3, 137.2, 137.0, 136.5, 132.0, 131.2, 128.8, 128.7, 128.6, 128.3, 128.1, 128.0, 127.9, 127.8, 127.7, 127.6, 127.4, 120.0, 115.1, 113.6, 108.6, 107.3, 101.5, 94.6, 94.0, 78.5, 71.4, 71.3, 70.4, 70.3, 70.1, 24.6; HRMS calcd for $C_{64}H_{55}O_9$ (M+ H^+) 967.3846; found 967.3831; IR (ATR, cm^{-1}) υ_{max} 3064, 3030, 2938, 2864, 1706, 1595, 1498, 1299, 1231, 1127, 1027; mp: 150 – 154 °C.

(*2R*,*3S*)-5,7-Bis(benzyloxy)-2-(3,4-bis(benzyloxy)phenyl)chroman-3-yl 3,4,5-tris(benzyl oxy) benzoate (3.49f)

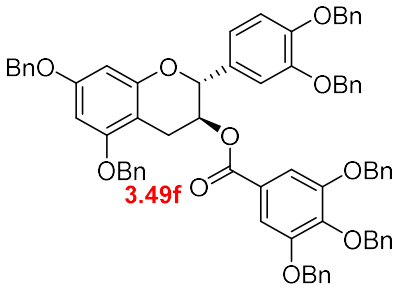

General procedure 3 was followed using 3,4,5-tris(benzyloxy)benzoic acid **3.16f** (183 mg, 0.42 mmol), oxalyl chloride (45 µL, 0.52 mmol), and DMF (100 µL) in DCM (3 mL). After the chlorination step, the resulting acid chloride was reacted with (*2R,3S*)-5,7-bis(benzyloxy)-2-

(3,4-bis(benzyloxy)phenyl)chroman-3-ol **3.49a** (226 mg, 0.35 mmol) in the presence of DMAP (106 mg, 0.86 mmol) in DCM (4 mL). The reaction was stirred at room temperature fitted with a drying tube overnight and monitored by TLC (hexanes:EtOAc 2:1; UV). After aqueous work up, the crude mixture was purified by trituration with *i*Pr$_2$O to obtain (*2R*,*3S*)-5,7-bis(benzyloxy)-2-(3,4-bis(benzyloxy)phenyl)chroman-3-yl 3,4,5-tris(benzyloxy) benzoate **3.49f** as a colorless solid (240 mg, 65% yield). ^{1}H NMR (400 MHz, $CDCl_3$) δ 7.46 – 7.16 (m, 35H), 7.00 (s, 1H), 6.94 – 6.81 (m, 2H), 6.29 (s, 2H), 5.51 – 5.40 (m, 1H), 5.16 – 4.93 (m, 15H), 3.04 (dd, *J* = 16.7, 5.1 Hz, 1H), 2.83 (dd, *J* = 16.7, 8.1 Hz, 1H); LRMS calcd for $C_{71}H_{61}O_{10}$ (M+ H^+) 1074.3; found 1074.2. The analytical data are in agreement with those reported before.[98]

(*2R*,*3R*)-5,7-Bis(benzyloxy)-2-(3,4-bis(benzyloxy)phenyl)chroman-3-yl 3,4-bis(benzyloxy) benzoate (3.50d)

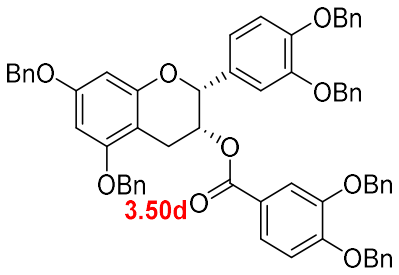

General procedure 3 was followed using 3,4-bis(benzyloxy)benzoic acid **3.16c** (139 mg, 0.42 mmol), oxalyl chloride (45 µL, 0.52 mmol), and DMF (100 µL) in DCM (3 mL). After the chlorination step, the resulting acid chloride was reacted with (*2R,3R*)-5,7-bis(benzyloxy)-2-(3,4-bis(benzyloxy)phenyl)chroman-3-ol **3.50a** (225 mg, 0.35 mmol) in the presence of DMAP (106 mg, 0.86 mmol) in DCM (4 mL). The reaction was stirred at room temperature fitted with a drying tube overnight and monitored by TLC (hexanes:EtOAc 2:1; UV). After aqueous work up, the crude mixture was purified by trituration with *i*Pr$_2$O to obtain (*2R*,*3R*)-5,7-bis(benzyloxy)-2-(3,4-bis(benzyloxy)phenyl)chroman-3-yl 3,4-bis(benzyloxy) benzoate **3.50d**

as a colorless solid (196 mg, 58% yield). $[\alpha]_D^{23}$ = -58° (*c* = 1.35 in $CHCl_3$); ^1H NMR (400 MHz, $CDCl_3$) δ 7.64 – 7.14 (m, 32H), 7.08 (s, 1H), 6.91 (d, *J* = 8.2 Hz, 1H), 6.88 – 6.72 (m, 2H), 6.33 (s, 1H), 6.29 (s, 1H), 5.61 (s, 1H), 5.21 – 4.93 (m, 11H), 4.78 (d, *J* = 11.5 Hz, 1H), 4.65 (d, *J* = 11.6 Hz, 1H), 3.18 – 2.91 (m, 2H); ^{13}C NMR (100 MHz, $CDCl_3$) δ 165.2, 158.9, 158.1, 155.8, 153.0, 149.1, 149.0, 148.2, 137.3, 137.2, 137.0, 136.9, 136.8, 136.6, 131.2, 128.7, 128.6, 128.5, 128.4, 128.1, 128.0, 127.9, 127.8, 127.7, 127.6, 127.4, 127.3, 127.3, 127.1, 124.2, 122.9, 120.1, 115.5, 114.8, 113.8, 113.2, 101.1, 94.8, 94.0, 77.8, 71.3, 71.2, 71.1, 70.8, 70.2, 70.1, 68.4, 68.3, 26.3; HRMS calcd for $C_{64}H_{55}O_9$ (M+ H^+) 967.3846; found 967.3817; IR (ATR, cm^{-1}) υ_{max} 3068, 3032, 2971, 2933, 1714, 1592, 1508, 1266, 1103, 1011; mp: 61 – 65 °C.

(*2R*,*3R*)-5,7-Bis(benzyloxy)-2-(3,4-bis(benzyloxy)phenyl)chroman-3-yl 3,5-bis(benzyloxy) benzoate (3.50e)

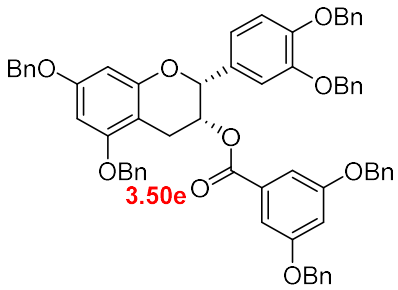

General procedure 3 was followed using 3,5-bis(benzyloxy)benzoic acid **3.16d** (139 mg, 0.42 mmol), oxalyl chloride (45 µL, 0.52 mmol), and DMF (100 µL) in DCM (3 mL). After the chlorination step, the resulting acid chloride was reacted with (*2R,3R*)-5,7-bis(benzyloxy)-2-(3,4-bis(benzyloxy)phenyl)chroman-3-ol **3.50a** (224 mg, 0.35 mmol) in the presence of DMAP (106 mg, 0.86 mmol) in DCM (4 mL). The reaction was stirred at room temperature fitted with a drying tube overnight and monitored by TLC (hexanes:EtOAc 2:1; UV). After aqueous work up, the crude mixture was purified by trituration with *i*Pr_2O to obtain (*2R*,*3R*)-5,7-bis(benzyloxy)-2-(3,4-bis(benzyloxy)phenyl)chroman-3-yl 3,5-bis(benzyloxy) benzoate **3.50e** as a colorless solid (173 mg, 52% yield). $[\alpha]_D^{23}$ = -57° (*c* = 1.17 in $CHCl_3$); ^1H NMR (396 MHz,

$CDCl_3$) δ 7.44 – 7.06 (m, 33H), 6.91 (d, *J* = 8.3 Hz, 1H), 6.84 (d, *J* = 8.2 Hz, 1H), 6.71 (d, *J* = 2.1 Hz, 1H), 6.33 (s, 1H), 6.29 (s, 1H), 5.62 (s, 1H), 5.19 – 4.89 (m, 11H), 4.86 (d, *J* = 11.7 Hz, 1H), 4.71 (d, *J* = 11.6 Hz, 1H), 3.21 – 2.93 (m, 2H); ^{13}C NMR (100 MHz, $CDCl_3$) δ 165.3, 159.8, 158.9, 158.1, 155.8, 149.2, 148.9, 143.2, 137.4, 137.3, 137.0, 136.4, 132.0, 131.2, 128.8, 128.7, 128.6, 128.5, 128.4, 128.3, 128.1, 128.0, 127.8, 127.7, 127.5, 127.4, 127.3, 120.0, 114.9, 113.6, 108.7, 107.2, 101.0, 94.9, 94.1, 77.7, 71.4, 71.2, 70.4, 70.3, 70.1, 68.9, 68.4, 26.2; HRMS calcd for $C_{64}H_{55}O_9$ (M+ H^+) 967.3846; found 967.3838; IR (ATR, cm^{-1}) υ_{max} 3066, 3032, 2940, 2870, 1717, 1592, 1497, 1296, 1218, 1027; mp: 60 – 65 °C.

(*2R*,*3R*)-5,7-Bis(benzyloxy)-2-(3,4-bis(benzyloxy)phenyl)chroman-3-yl 3,4,5-tris(benzyl oxy) benzoate (3.50f)

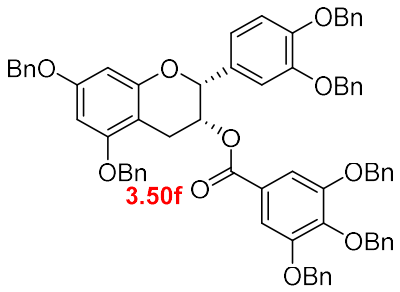

General procedure 3 was followed using 3,4,5-tris(benzyloxy)benzoic acid **3.16f** (124 mg, 0.28 mmol), oxalyl chloride (30 µL, 0.35 mmol), and DMF (100 µL) in DCM (3.5 mL). After the chlorination step, the resulting acid chloride was reacted with (*2R,3R*)-5,7-bis(benzyloxy)-2-(3,4-bis(benzyloxy)phenyl)chroman-3-ol **3.50a** (151 mg, 0.23 mmol) in the presence of DMAP (71.3 mg, 0.58 mmol) in DCM (3 mL). The reaction was stirred at room temperature fitted with a drying tube overnight and monitored by TLC (hexanes:EtOAc 2:1; UV). After aqueous work up, the crude mixture was purified by column chromatography using DCM as an isocratic eluent system to obtain (*2R*,*3R*)-5,7-bis(benzyloxy)-2-(3,4-bis(benzyloxy)phenyl)chroman-3-yl 3,4,5-tris(benzyloxy) benzoate **3.50f** as a colorless solid (138 mg, 56% yield). ^1H NMR (400 MHz, $CDCl_3$) δ 7.44 – 7.17 (m, 37H), 7.04 (d, *J* = 1.9 Hz, 1H), 6.90 (dd, *J* = 8.3, 1.9 Hz, 1H),

6.83 (d, J = 8.3 Hz, 1H), 6.37 (d, J = 2.2 Hz, 1H), 6.32 (d, J = 2.3 Hz, 1H), 5.63 – 5.58 (m, 1H), 5.12 – 4.95 (m, 13H), 4.76 (d, J = 11.6 Hz, 1H), 4.65 (d, J = 11.7 Hz, 1H), 3.11 (dd, J = 17.7, 4.3 Hz, 1H), 3.05 (dd, J = 18.0, 2.4 Hz, 1H); LRMS calcd for $C_{71}H_{61}O_{10}$ ($M+H^+$) 1074.3; found 1074.3. The analytical data are in agreement with those reported before.[97]

General procedure 4: global debenzylation of benzylated catechin benzoate ester

Benzylated catechin-3-O-benzoate derivative was hydrogenated in 50% MeOH (or EtOH) in THF (125 mL/1 mmol of benzylated catechin-3-O-benzoate derivative) with 20% $Pd(OH)_2/C$ (75% – 200%wt of ester) for overnight under H_2 atmosphere at room temperature. The reaction mixture was filtered through celite, and the solvent was evaporated under reduced pressure. The residue was purified by column chromatography using 30% DCM in EtOAc as an isocratic eluent system.

(*2R*,*3S*)-2-(3,4-Dihydroxyphenyl)-5,7-dihydroxychroman-3-yl 3-hydroxybenzoate (3.48b)

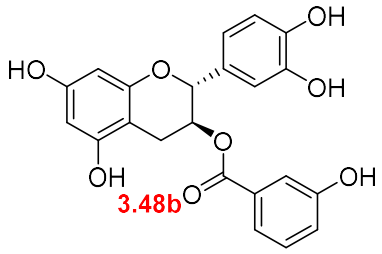

General procedure 4 was followed using (*2R,3S*)-5,7-bis(benzyloxy)-2-(3,4-bis(benzyloxy)phenyl) chroman-3-yl 3-(benzyloxy) benzoate **3.49b** (40.8 mg, 0.047 mmol) and 20% $Pd(OH)_2/C$ (80.8 mg) in 50% MeOH in THF (8 mL). (*2R,3S*)-2-(3,4-Dihydroxyphenyl)-5,7-dihydroxychroman-3-yl 3-hydroxybenzoate **3.48b** was obtained as a yellow solid (16.4 mg, 84% yield). $[\alpha]_D^{23}$ = 50° (c = 0.56 in MeOH); ^{1}H NMR (396 MHz, CD_3OD) δ 7.37 (d, J = 7.7 Hz, 1H), 7.31 (d, J = 1.5 Hz, 1H), 7.22 (t, J = 7.9 Hz, 1H), 6.97 (dd, J = 8.1, 2.6 Hz, 1H), 6.86 (s, 1H), 6.80 – 6.63 (m, 2H), 5.97 (d, J = 2.1 Hz, 1H), 5.95 (d, J =

2.2 Hz, 1H), 5.41 (q, J = 6.0 Hz, 1H), 5.06 (d, J = 6.4 Hz, 1H), 2.90 (dd, J = 16.5, 5.2 Hz, 1H), 2.74 (dd, J = 16.5, 6.6 Hz, 1H); ^{13}C NMR (100 MHz, CD_3OD) δ 167.2, 158.6, 158.2, 157.6, 156.6, 146.3, 132.5, 131.3, 130.5, 121.7, 121.3, 119.4, 117.0, 116.2, 114.6, 99.6, 96.5, 95.6, 79.5, 71.7, 24.7; HRMS calcd for $C_{22}H_{19}O_8$ (M+ H^+) 411.1080; found 411.1089; IR (ATR, cm^{-1}) υ_{max} 3290, 1695, 1603, 1520, 1280, 1062; mp: dec.

(*2R*,*3S*)-2-(3,4-Dihydroxyphenyl)-5,7-dihydroxychroman-3-yl 4-hydroxybenzoate (3.48c)

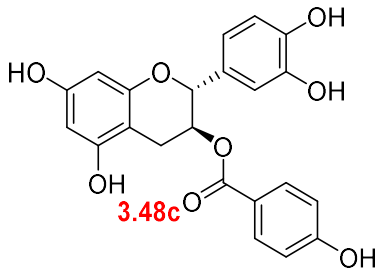

General procedure 4 was followed using (*2R*,*3S*)-5,7-bis(benzyloxy)-2-(3,4-bis(benzyloxy)phenyl) chroman-3-yl 4-(benzyloxy)benzoate **3.49c** (63.7 mg, 0.074 mmol) and 20% $Pd(OH)_2/C$ (121 mg) in 50% MeOH in THF (15 mL). (*2R*,*3S*)-2-(3,4-Dihydroxyphenyl)-5,7-dihydroxychroman-3-yl 4-hydroxybenzoate **3.48c** was obtained as a yellow solid (28.3 mg, 93% yield). $[\alpha]_D^{23}$ = 54° (c = 0.53 in MeOH); ^{1}H NMR (396 MHz, CD_3OD) δ 7.75 (d, J = 8.7 Hz, 2H), 6.86 (s, 1H), 6.81 – 6.68 (m, 4H), 5.98 (d, J = 2.2 Hz, 1H), 5.95 (d, J = 1.7 Hz, 1H), 5.37 (q, J = 6.0 Hz, 1H), 5.03 (d, J = 6.6 Hz, 1H), 2.91 (dd, J = 16.4, 5.3 Hz, 1H), 2.73 (dd, J = 16.4, 6.8 Hz, 1H); ^{13}C NMR (100 MHz, CD_3OD) δ 167.3, 163.5, 158.1, 157.6, 156.6, 146.3, 132.8, 131.4, 122.2, 119.4, 116.2, 116.1, 114.6, 99.8, 96.5, 95.6, 79.6, 71.4, 25.0; HRMS calcd for $C_{22}H_{19}O_8$ (M+ H^+) 411.1080; found 411.1068; IR (ATR, cm^{-1}) υ_{max} 3307, 1684, 1605, 1515, 1265, 1013; mp: dec.

(*2R*,*3S*)-2-(3,4-Dihydroxyphenyl)-5,7-dihydroxychroman-3-yl 3,4-dihydroxybenzoate (2.48d)

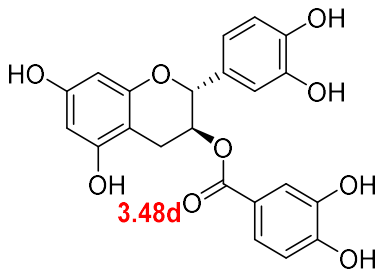

General procedure 4 was followed using (*2R*,*3S*)-5,7-bis(benzyloxy)-2-(3,4-bis(benzyloxy)phenyl)chroman-3-yl 3,4-bis(benzyloxy) benzoate **3.49d** (150 mg, 0.15 mmol) and 20% $Pd(OH)_2/C$ (302 mg) in 50% MeOH in THF (20 mL). (*2R*,*3S*)-2-(3,4-Dihydroxyphenyl)-5,7-dihydroxychroman-3-yl 3,4-dihydroxybenzoate **3.48d** was obtained as a colorless solid (49.7 mg, 77% yield). $[\alpha]_D^{23}$ = 56° (*c* = 0.97 in MeOH); ^{1}H NMR (396 MHz, CD_3OD) δ 7.37 – 7.27 (m, 2H), 6.85 (s, 1H), 6.79 – 6.64 (m, 3H), 5.97 (s, 1H), 5.95 (s, 1H), 5.37 (q, *J* = 5.9 Hz, 1H), 5.05 (d, *J* = 6.2 Hz, 1H), 2.87 (dd, *J* = 16.4, 5.0 Hz, 1H), 2.72 (dd, *J* = 16.4, 6.3 Hz, 1H); ^{13}C NMR (100 MHz, CD_3OD) δ 167.4, 158.1, 157.6, 156.5, 151.8, 146.3, 146.2, 146.0, 131.4, 123.8, 122.5, 119.3, 117.4, 116.2, 115.8, 114.5, 99.7, 96.5, 95.6, 79.5, 71.3, 24.7; HRMS calcd for $C_{22}H_{19}O_9$ ($M+H^+$) 427.1029; found 427.1046; IR (ATR, cm^{-1}) υ_{max} 3304, 1684, 1603, 1520, 1280, 1011; mp: dec.

(*2R*,*3S*)-2-(3,4-Dihydroxyphenyl)-5,7-dihydroxychroman-3-yl 3,5-dihydroxybenzoate (2.48e)

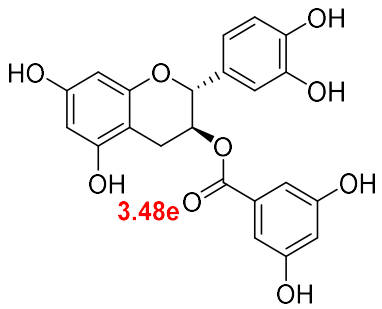

General procedure 4 was followed using (*2R*,*3S*)-5,7-bis(benzyloxy)-2-(3,4-bis(benzyloxy)phenyl)chroman-3-yl 3,5-bis(benzyloxy) benzoate **3.49e** (150 mg, 0.15 mmol) and 20% $Pd(OH)_2/C$ (300 mg) in 50% MeOH in THF (25 mL). (*2R*,*3S*)-2-(3,4-Dihydroxyphenyl)-5,7-dihydroxychroman-3-yl 3,5-dihydroxybenzoate **3.48e** was obtained as a light-yellow solid (44.1 mg, 66% yield). $[\alpha]_D^{24}$ = 17° (*c* = 0.86 in MeOH); ^{1}H NMR (400 MHz, CD_3OD) δ 6.92 – 6.75 (m, 3H), 6.72 (d, *J* = 0.8 Hz, 2H), 6.43 (t, *J* = 2.2 Hz, 1H), 5.96 (d, *J* = 2.3 Hz, 1H), 5.94 (d, *J* = 2.2 Hz, 1H), 5.40 (q, *J* = 5.8 Hz, 1H), 5.06 (d, *J* = 6.1 Hz, 1H), 2.85 (dd, *J* = 16.6, 5.2 Hz, 1H), 2.73 (dd, *J* = 16.5, 6.1 Hz, 1H); ^{13}C NMR (100 MHz, CD_3OD) δ 167.2, 159.7, 158.2, 157.6, 156.5, 146.3, 133.0, 131.4, 129.7, 119.3, 116.2, 114.5, 108.9, 108.4, 99.6, 96.5, 95.6, 79.3, 71.6, 24.4; HRMS calcd for $C_{22}H_{19}O_9$ ($M+ H^+$) 427.1029; found 427.1034; IR (ATR, cm^{-1}) υ_{max} 3303, 1693, 1600, 1519, 1238, 997; mp: dec.

(*2R*,*3S*)-2-(3,4-Dihydroxyphenyl)-5,7-dihydroxychroman-3-yl 3,4,5-trihydroxybenzoate (2.48f)

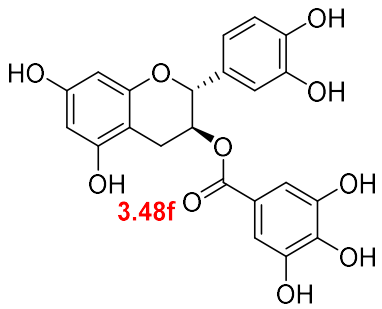

General procedure 4 was followed using (*2R*,*3S*)-5,7-bis(benzyloxy)-2-(3,4-bis(benzyloxy)phenyl)chroman-3-yl 3,4,5-tris(benzyloxy) benzoate **3.49f** (151 mg, 0.14 mmol) and 20% $Pd(OH)_2/C$ (300 mg) in 50% MeOH in THF (25 mL). (*2R*,*3S*)-2-(3,4-Dihydroxyphenyl)-5,7-dihydroxychroman-3-yl 3,4,5-trihydroxybenzoate **3.48f** was obtained as an orange solid (44.0 mg, 71% yield). ^{1}H NMR (400 MHz, CD_3OD) δ 6.96 (s, 2H), 6.83 (s, 1H), 6.72 (d, *J* = 0.8 Hz, 2H), 5.96 (d, *J* = 2.3 Hz, 1H), 5.94 (d, *J* = 2.3 Hz, 1H), 5.37 (q, *J* = 5.7 Hz, 1H), 5.06 (d, *J* = 5.9 Hz, 1H), 2.82 (dd, *J* = 16.5, 5.0 Hz, 1H), 2.71 (dd, *J* = 16.5, 6.0 Hz, 1H); LRMS calcd for $C_{22}H_{19}O_{10}$ ($M+ H^+$) 443.4; found 443.3. The analytical data are in agreement with those reported before.[99]

(*2R*,*3R*)-2-(3,4-Dihydroxyphenyl)chromane-3,5,7-triol (3.53a)

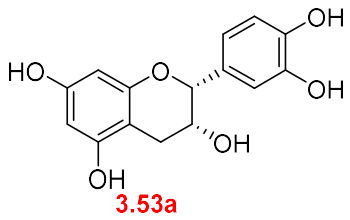

General procedure 4 was followed using (*2R,3R*)-5,7-bis(benzyloxy)-2-(3,4-bis(benzyloxy)phenyl)chroman-3-ol **3.50a** (150 mg, 0.23 mmol) and 20% $Pd(OH)_2/C$ (115 mg) in 50% MeOH in THF (30 mL). (*2R*,*3R*)-2-(3,4-Dihydroxyphenyl)chromane-3,5,7-triol **3.53a** was obtained as an orange solid (59.0 mg, 88% yield). ^{1}H NMR (400 MHz, CD_3OD) δ 7.02 (s, 1H), 6.82 (s, 2H), 6.04 (d, *J* = 2.2 Hz, 1H), 5.94 (d, *J* = 2.2 Hz, 1H), 4.87 (s, 1H), 2.84 (dd, *J* = 16.6, 4.5 Hz, 1H), 2.68 (dd, *J* = 16.8, 3.3 Hz, 1H); LRMS calcd for $C_{22}H_{19}O_{10}$ ($M+ H^+$) 291.3; found 291.2. The analytical data are in agreement with those reported before.[99]

(*2R*,*3R*)-2-(3,4-Dihydroxyphenyl)-5,7-dihydroxychroman-3-yl 3,4-dihydroxybenzoate (3.53d)

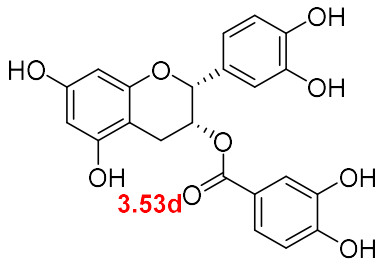

General procedure 4 was followed using (*2R*,*3R*)-5,7-bis(benzyloxy)-2-(3,4-bis(benzyloxy)phenyl)chroman-3-yl 3,4-bis(benzyloxy) benzoate **3.50d** (150 mg, 0.15 mmol) and 20% $Pd(OH)_2/C$ (302 mg) in 50% MeOH in THF (20 mL). (*2R*,*3R*)-2-(3,4-Dihydroxyphenyl)-5,7-dihydroxychroman-3-yl 3,4-dihydroxybenzoate **3.53d** was obtained as a yellow solid (55.3 mg, 86% yield). $[\alpha]_D^{24}$ = -129° (*c* = 0.95 in MeOH); ^{1}H NMR (396 MHz, CD_3OD) δ 7.39 – 7.21 (m, 2H), 6.94 (s, 1H), 6.84 – 6.62 (m, 3H), 5.97 (s, 2H), 5.53 (s, 1H),

5.04 (s, 1H), 3.00 (dd, J = 17.3, 4.3 Hz, 1H), 2.87 (d, J = 17.2 Hz, 1H); ^{13}C NMR (100 MHz, CD_3OD) δ 167.5, 157.9, 157.8, 157.3, 151.7, 145.9, 131.5, 123.9, 122.6, 119.3, 117.5, 116.0, 115.8, 115.1, 99.4, 96.5, 95.8, 78.6, 70.1, 26.8; HRMS calcd for $C_{22}H_{19}O_9$ (M+ H^+) 427.1029; found 427.1027; IR (ATR, cm^{-1}) υ_{max} 3267, 1683, 1603, 1518, 1281, 1227, 1015; mp: dec.

(*2R*,*3R*)-2-(3,4-Dihydroxyphenyl)-5,7-dihydroxychroman-3-yl 3,5-dihydroxybenzoate (3.53e)

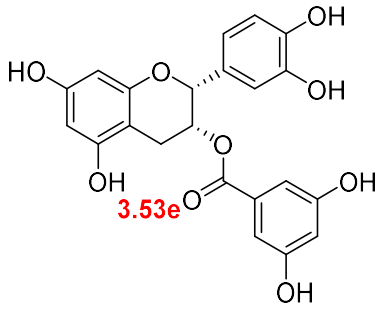

General procedure 4 was followed using (*2R*,*3R*)-5,7-bis(benzyloxy)-2-(3,4-bis(benzyloxy)phenyl)chroman-3-yl 3,5-bis(benzyloxy) benzoate **3.50e** (140 mg, 0.14 mmol) and 20% $Pd(OH)_2/C$ (282 mg) in 50% MeOH in THF (16 mL). (*2R*,*3R*)-2-(3,4-Dihydroxyphenyl)-5,7-dihydroxychroman-3-yl 3,5-dihydroxybenzoate **3.53e** was obtained as a light-green solid (50.1 mg, 84% yield). $[\alpha]_D^{23}$ = -129° (*c* = 1.45 in MeOH); ^{1}H NMR (396 MHz, CD_3OD) δ 6.94 (d, J = 1.4 Hz, 1H), 6.89 – 6.74 (m, 3H), 6.71 (d, J = 8.2 Hz, 1H), 6.41 (t, J = 1.4 Hz, 1H), 5.97 (s, 2H), 5.56 (s, 1H), 5.04 (s, 1H), 3.02 (dd, J = 17.4, 4.4 Hz, 1H), 2.87 (d, J = 16.1 Hz, 1H); ^{13}C NMR (100 MHz, CD_3OD) δ 167.3, 159.6, 157.9, 157.8, 157.2, 146.0, 133.1, 131.4, 119.3, 116.0, 115.0, 108.9, 108.3, 99.3, 96.6, 95.9, 78.5, 70.4, 26.8; HRMS calcd for $C_{22}H_{19}O_9$ (M+ H^+) 427.1029; found 427.1026; IR (ATR, cm^{-1}) υ_{max} 3293, 1695, 1600, 1517, 1234, 1140, 1004; mp: dec.

(*2R*,*3R*)-2-(3,4-Dihydroxyphenyl)-5,7-dihydroxychroman-3-yl 3,4,5-trihydroxybenzoate (3.53f)

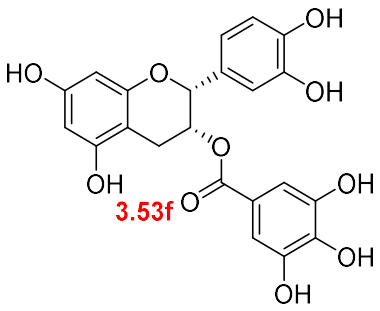

General procedure 4 was followed using (*2R*,*3R*)-5,7-bis(benzyloxy)-2-(3,4-bis(benzyloxy)phenyl)chroman-3-yl 3,4,5-tris(benzyloxy) benzoate **3.50f** (100 mg, 0.093 mmol) and 20% $Pd(OH)_2/C$ (101 mg) in 50% MeOH in THF (12 mL). (*2R*,*3R*)-2-(3,4-Dihydroxyphenyl)-5,7-dihydroxychroman-3-yl 3,4,5-trihydroxybenzoate **3.53f** was obtained as a green solid (31.0 mg, 75% yield). ^{1}H NMR (396 MHz, CD_3OD) δ 6.98 – 6.90 (m, 3H), 6.81 (dd, *J* = 8.3, 1.8 Hz, 1H), 6.69 (d, *J* = 8.2 Hz, 1H), 5.96 (s, 2H), 5.55 – 5.51 (m, 1H), 5.03 (s, 1H), 3.00 (dd, *J* = 17.6, 4.4 Hz, 1H), 2.85 (d, *J* = 17.6 Hz, 1H); LRMS calcd for $C_{22}H_{19}O_{10}$ ($M+ H^+$) 443.4; found 443.3. The analytical data are in agreement with those reported before.[99]

General procedure 5: Weinreb amides formation by the Schotten–Baumann strategy

To the corresponding benzoic acid (1 eq.) in dichloromethane (2 mL/1 mmol of benzoic acid) was added dropwise oxalyl chloride (1.2 eq) in the presence of a catalytic amount of dimethylformamide. The mixture was stirred at room temperature for 1 hour and then concentrated. The residue was taken up in a mixture between 50% DCM and water (8 mL/1 mmol of benzoic acid). *N*,*O*-Dimethylhydroxylamine *hydrochloride* (2 eq) and Na_2CO_3 (3 eq) were added and the reaction was stirred at room temperature overnight. After completion, the mixture was diluted with DCM and washed with a saturated aqueous solution of NH_4Cl and water. The organic phase was dried over Na_2SO_4 and evaporated under reduced pressure.

3-(Benzyloxy)-*N*-methoxy-*N*-methylbenzamide (3.59b)

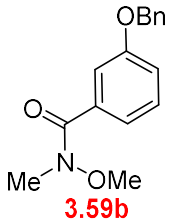

3.59b

General procedure 5 was followed using 3-(benzyloxy)benzoic acid 3.16a (1.37 g, 6 mmol), oxalyl chloride (620 µL, 7.2 mmol), and DMF (100 µL) in DCM (20 mL). After the chlorination step, the resulting acid chloride was reacted with *N*,*O*-dimethylhydroxylamine *hydrochloride* (1.17 g, 12 mmol) in the presence of Na_2CO_3 (1.91 g, 18 mmol) in the mixture of 50% DCM and water (50 mL). The reaction was stirred at room temperature, fitted with a drying tube overnight, and monitored by TLC (hexanes:EtOAc 3:1; UV). After aqueous work up, 3-(benzyloxy)-*N*-methoxy-*N*-methylbenzamide **3.59b** was obtained as a yellow oil (1.46 g, 94% yield). ^{1}H NMR (396 MHz, $CDCl_3$) δ 7.50 – 7.14 (m, 8H), 7.07 (ddd, J = 8.1, 2.5, 1.1 Hz, 1H), 5.09 (s, 2H), 3.53 (s, 3H), 3.34 (s, 3H). The analytical data are in agreement with those reported before.[100]

4-(Benzyloxy)-*N*-methoxy-*N*-methylbenzamide (3.59c)

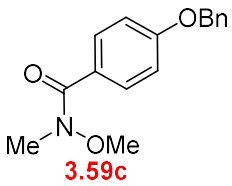

3.59c

General procedure 5 was followed using 4-(benzyloxy)benzoic acid **3.16b** (1.37 g, 6 mmol), oxalyl chloride (620 µL, 7.2 mmol), and DMF (100 µL) in DCM (20 mL). After the chlorination step, the resulting acid chloride was reacted with *N*,*O*-dimethylhydroxylamine *hydrochloride* (1.17 g, 12 mmol) in the presence of Na_2CO_3 (1.91 g, 18 mmol) in the mixture of 50% DCM and water (50 mL). The reaction was stirred at room

temperature, fitted with a drying tube overnight, and monitored by TLC (hexanes:EtOAc 3:1; UV). After aqueous work up, 4-(benzyloxy)-*N*-methoxy-*N*-methylbenzamide **3.59c** was obtained as a colorless solid (1.36 g, 88% yield). ^{1}H NMR (396 MHz, $CDCl_3$) δ 7.73 (d, *J* = 8.8 Hz, 2H), 7.47 – 7.30 (m, 5H), 6.98 (d, *J* = 8.9 Hz, 2H), 5.10 (s, 2H), 3.56 (s, 3H), 3.35 (s, 3H). The analytical data are in agreement with those reported before.[101]

3,5-Bis(benzyloxy)-*N*-methoxy-*N*-methylbenzamide (3.59d)

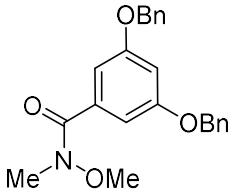

3.59d

General procedure 5 was followed using 3,5-bis(benzyloxy)benzoic acid **3.16d** (2.00 g, 6 mmol), oxalyl chloride (620 µL, 7.2 mmol), and DMF (100 µL) in DCM (20 mL). After the chlorination step, the resulting acid chloride was reacted with *N*,*O*-dimethylhydroxylamine *hydrochloride* (1.17 g, 12 mmol) in the presence of Na_2CO_3 (1.91 g, 18 mmol) in the mixture of 50% DCM and water (50 mL). The reaction was stirred at room temperature, fitted with a drying tube overnight and monitored by TLC (hexanes:EtOAc 3:1; UV). After aqueous work up, 3,5-bis(benzyloxy)-*N*-methoxy-*N*-methylbenzamide **3.59d** was obtained as a yellow solid (1.96 g, 90% yield). ^{1}H NMR (396 MHz, $CDCl_3$) δ 7.46 – 7.28 (m, 10H), 6.89 (d, *J* = 2.2 Hz, 2H), 6.71 (t, *J* = 2.3 Hz, 1H), 5.05 (s, 4H), 3.51 (s, 3H), 3.31 (s, 3H); ^{13}C NMR (100 MHz, $CDCl_3$) δ 169.6, 159.6, 136.7, 136.1, 128.7, 128.2, 127.6, 107.3, 104.8, 70.3, 61.2; HRMS calcd for $C_{23}H_{24}NO_4$ (M+ H^+) 378.1705; found 378.1687; IR (ATR, cm^{-1}) υ_{max} 3068, 3007, 2931, 2873, 1636, 1584, 1496, 1310, 1202, 1167, 1042; mp: 91 – 93 °C.

3,4,5-Tris(benzyloxy)-*N*-methoxy-*N*-methylbenzamide (3.59e)

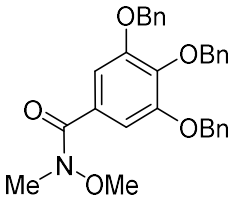

3.59e

General procedure 5 was followed using 3,4,5-tris(benzyloxy)benzoic acid **3.16f** (2.11 g, 4.8 mmol), oxalyl chloride (520 µL, 6 mmol), and DMF (100 µL) in DCM (15 mL). After the chlorination step, the resulting acid chloride was reacted with *N*,*O*-dimethylhydroxylamine *hydrochloride* (979 mg, 10 mmol) in the presence of Na_2CO_3 (1.59 g, 15 mmol) in the mixture of 50% DCM and water (40 mL). The reaction was stirred at room temperature, fitted with a drying tube overnight and monitored by TLC (hexanes:EtOAc 3:1; UV). After aqueous work up, 3,4,5-tris(benzyloxy)-*N*-methoxy-*N*-methylbenzamide **3.59e** was obtained as a yellow solid (2.23 g, 96% yield). ^{1}H NMR (396 MHz, $CDCl_3$) δ 7.47 – 7.18 (m, 15H), 5.12 (s, 4H), 5.11 (s, 2H), 3.39 (s, 3H), 3.27 (s, 3H); ^{13}C NMR (100 MHz, $CDCl_3$) δ 169.1, 152.3, 140.6, 137.7, 137.0, 129.0, 128.7, 128.6, 128.3, 128.1, 128.0, 127.6, 108.6, 75.3, 71.3, 61.0; HRMS calcd for $C_{30}H_{30}NO_5$ (M+ H^+) 484.2124; found 484.2106; IR (ATR, cm^{-1}) υ_{max} 3064, 3030, 2934, 1636, 1579, 1452, 1421, 1318, 1241, 1104, 1077; mp: 79 – 80 °C.

General procedure 6: DIBAL reduction of Weinreb amides

To the Weinreb amides **3.59** (1 eq.) in anhydrous THF (5 mL/1 mmol of **3.59**) was added dropwise 1 M DIBAL in cyclohexane (1.2 eq.) at 0 °C. The mixture was stirred at 0 °C under a nitrogen atmosphere. After completion, a saturated aqueous solution of NH_4Cl was added at 0 °C to quench the reaction. The precipitant was filtered, and the filtrate was evaporated under reduced pressure.

3-(Benzyloxy)benzaldehyde (3.60b)

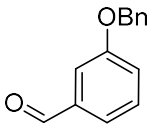

3.60b

General procedure 6 was followed using 3-(benzyloxy)-*N*-methoxy-*N*-methylbenzamide **3.59b** (1.09 g, 4 mmol) and 1 M DIBAL solution in cyclohexane (4.8 mL, 4.8 mmol) in anhydrous THF (20 mL) at 0 °C under nitrogen atmosphere. After stirring at 0 °C under a nitrogen atmosphere for 1 hour, the reaction was monitored by TLC (hexanes:EtOAc 3:1; UV). 3-(Benzyloxy)benzaldehyde **3.60b** was obtained as a colorless solid (877 mg, quantitative). ^1H NMR (396 MHz, $CDCl_3$) δ 9.97 (s, 1H), 7.55 – 7.29 (m, 8H), 7.29 – 7.20 (m, 1H), 5.12 (s, 2H); LRMS calcd for $C_{14}H_{13}O_2$ ($M+ H^+$) 213.3; found 213.2. The analytical data are in agreement with those reported before.[102]

4-(Benzyloxy)benzaldehyde (3.60c)

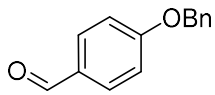

3.60c

General procedure 6 was followed using 3-(benzyloxy)-*N*-methoxy-*N*-methylbenzamide **3.60c** (1.09 g, 4 mmol) and 1 M DIBAL solution in cyclohexane (4.8 mL, 4.8 mmol) in anhydrous THF (20 mL) at 0 °C under nitrogen atmosphere. After stirring at 0 °C under a nitrogen atmosphere for 1 hour, the reaction was monitored by TLC (hexanes:EtOAc 3:1; UV). 4-(Benzyloxy)benzaldehyde **3.60c** was obtained as a colorless solid (837 mg, 99% yield). ^{1}H NMR (396 MHz, $CDCl_3$) δ 9.89 (s, 1H), 7.84 (d, J = 8.7 Hz, 2H), 7.52 – 7.30 (m, 5H), 7.08 (d, J = 8.6 Hz, 2H), 5.15 (s, 2H); LRMS calcd for $C_{14}H_{13}O_2$ (M+ H^+) 213.3; found 213.1. The analytical data are in agreement with those reported before.[103]

3,5-Bis(benzyloxy)benzaldehyde (3.60d)

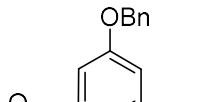

3.60d

General procedure 6 was followed using 3,5-bis(benzyloxy)-*N*-methoxy-*N*-methylbenzamide **3.59d** (1.51 g, 4 mmol) and 1 M DIBAL solution in cyclohexane (4.8 mL, 4.8 mmol) in anhydrous THF (20 mL) at 0 °C under nitrogen atmosphere. After stirring at 0 °C under a nitrogen atmosphere for 1 hour, the reaction was monitored by TLC (hexanes:EtOAc 3:1; UV). 3,5-Bis(benzyloxy)benzaldehyde **3.60d** was obtained as a colorless solid (1.26 g, 99% yield). ^{1}H NMR (396 MHz, $CDCl_3$) δ 9.90 (s, 1H), 7.47 – 7.28 (m, 10H), 7.11 (d, J = 2.3 Hz, 2H), 6.87 (t, J = 2.3 Hz, 1H), 5.09 (s, 4H); LRMS calcd for $C_{21}H_{19}O_3$ (M+ H^+) 319.4; found 319.2. The analytical data are in agreement with those reported before.[104]

3,4,5-Tris(benzyloxy)benzaldehyde (3.60e)

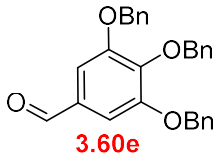

3.60e

General procedure 6 was followed using 3,4,5-tris(benzyloxy)-*N*-methoxy-*N*-methylbenzamide **3.59e** (1.52 g, 3.14 mmol) and 1 M DIBAL solution in cyclohexane (3.8 mL, 3.8 mmol) in anhydrous THF (30 mL) at 0 °C under nitrogen atmosphere. After stirring at 0 °C under a nitrogen atmosphere for 1 hour, the reaction was monitored by TLC (hexanes:EtOAc 3:1; UV). 3,4,5-Tris(benzyloxy)benzaldehyde **3.60e** was obtained as an orange solid (1.29 g, 97% yield). ^{1}H NMR (400 MHz, $CDCl_3$) δ 9.80 (s, 1H), 7.49 – 7.21 (m, 15H), 7.19 (s, 2H), 5.17 (s, 6H); LRMS calcd for $C_{28}H_{25}O_4$ (M+ H^+) 425.5; found 425.1. The analytical data are in agreement with those reported before.[105]

General procedure 7: Vinylation of benzaldehyde derivatives **3.60**

To the aldehyde **3.60** (1 eq.) in anhydrous THF (5 mL/1 mmol of **3.59**) was added dropwise 1 M vinylmagnesium bromide in THF (2 eq.) at 0 °C. The mixture was stirred at 0 °C under a nitrogen atmosphere overnight, which was allowed to warm up to room temperature. After completion, a saturated aqueous solution of NH_4Cl was added at 0 °C to quench the reaction, stirred for 30 minutes, and extracted with EtOAc 3 times. The combined organic phase was washed with water and brine, followed by evaporation under reduced pressure.

Racemic 1-(3-(benzyloxy)phenyl)prop-2-en-1-ol (*rac*-3.55b)

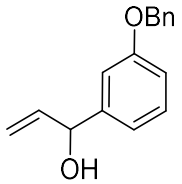

rac-3.55b

General procedure 7 was followed using 3-(benzyloxy)benzaldehyde **3.60b** (877 mg, 4 mmol) and 1 M vinylmagnesium bromide in THF (8 mL, 8 mmol) in anhydrous THF (20 mL) at 0 °C under nitrogen atmosphere. Racemic 1-(3-(benzyloxy)phenyl)prop-2-en-1-ol ***rac*-3.55b** was obtained as yellow oil (935 mg, 97% yield). ^{1}H NMR (396 MHz, $CDCl_3$) δ 7.44 – 7.17 (m, 6H), 7.00 (t, *J* = 2.6 Hz, 1H), 6.93 (d, *J* = 7.6 Hz, 1H), 6.87 (ddd, *J* = 8.2, 2.6, 0.9 Hz, 1H), 5.99 (ddd, *J* = 17.1, 10.3, 6.0 Hz, 1H), 5.31 (dt, *J* = 17.1, 1.4 Hz, 1H), 5.16 (dt, *J* = 10.3, 1.3 Hz, 1H), 5.12 (d, *J* = 6.0 Hz, 1H), 5.02 (s, 2H); ^{13}C NMR (100 MHz, $CDCl_3$) δ 159.1, 144.4, 140.2, 137.0, 129.7, 128.7, 128.1, 127.6, 119.0, 115.3, 114.2, 112.9, 75.2, 70.1; HRMS calcd for $C_{16}H_{16}O_2{}^{23}Na$ (M+ Na^+) 263.1048; found 263.1039; IR (ATR, cm^{-1}) υ_{max} 3378, 3068, 3037, 2983, 2873, 1584, 1257, 1153, 1025;

Racemic 1-(4-(benzyloxy)phenyl)prop-2-en-1-ol (*rac*-3.55c)

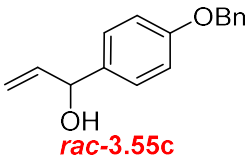

rac-3.55c

General procedure 7 was followed using 4-(benzyloxy)benzaldehyde **3.60c** (758 mg, 3.57 mmol) and 1 M vinylmagnesium bromide in THF (7.1 mL, 7.1 mmol) in anhydrous THF (15 mL) at 0 °C under nitrogen atmosphere. Racemic 1-(4-(benzyloxy)phenyl)prop-2-en-1-ol ***rac*-3.55c** was obtained as a yellow solid (846 mg, 99% yield). ^{1}H NMR (396 MHz, $CDCl_3$) δ 7.49 – 7.17 (m, 7H), 6.96 (dd, *J* = 8.5, 1.7 Hz, 2H), 6.05 (ddd, *J* = 16.2, 10.2, 5.9 Hz, 1H), 5.34 (d,

J = 17.2 Hz, 1H), 5.23 – 5.12 (m, 2H), 5.07 (s, 2H); LRMS calcd for $C_{16}H_{17}O_2$ (M+ H^+) 241.3; found 241.2. The analytical data are in agreement with those reported before.[106]

Racemic 1-(3,5-bis(benzyloxy)phenyl)prop-2-en-1-ol (*rac*-3.55d)

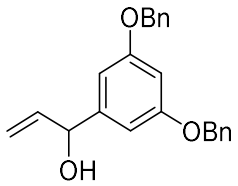

rac-3.55d

General procedure 7 was followed using 3,5-bis(benzyloxy)benzaldehyde **3.60d** (1.26 g, 3.95 mmol) and 1 M vinylmagnesium bromide in THF (8 mL, 8 mmol) in anhydrous THF (20 mL) at 0 °C under nitrogen atmosphere. Racemic 1-(3,5-bis(benzyloxy)phenyl)prop-2-en-1-ol ***rac*-3.55d** was obtained as a colorless solid (1.35 g, 99% yield). ^{1}H NMR (396 MHz, $CDCl_3$) δ 7.50 – 7.27 (m, 10H), 6.64 (d, *J* = 2.2 Hz, 2H), 6.54 (t, *J* = 2.2 Hz, 1H), 6.01 (ddd, *J* = 16.5, 10.3, 6.0 Hz, 1H), 5.35 (d, *J* = 17.1 Hz, 1H), 5.19 (d, *J* = 10.3 Hz, 1H), 5.12 (d, *J* = 2.7 Hz, 1H), 5.02 (s, 4H), 1.95 (d, *J* = 3.0 Hz, 1H); ^{13}C NMR (100 MHz, $CDCl_3$) δ 160.3, 145.3, 140.0, 136.9, 128.7, 128.2, 127.7, 115.5, 105.5, 101.5, 75.5, 70.3; HRMS calcd for $C_{23}H_{23}O_3$ (M+ H^+) 347.1647; found 347.1631; IR (ATR, cm^{-1}) υ_{max} 3326, 3075, 3032, 2980, 2870, 1592, 1453, 1290, 1156, 1021; mp: 94 – 96 °C.

Racemic 1-(3,4,5-tris(benzyloxy)phenyl)prop-2-en-1-ol (*rac*-3.55e)

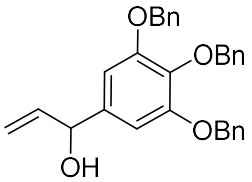

rac-3.55e

General procedure 7 was followed using 3,4,5-tris(benzyloxy)benzaldehyde **3.60e** (851 mg, 2 mmol) and 1 M vinylmagnesium bromide in THF (4 mL, 4 mmol) in anhydrous THF (10 mL) at 0 °C under nitrogen atmosphere. Racemic 1-(3,4,5-tris(benzyloxy)phenyl)prop-2-en-1-ol ***rac*-3.55e** was obtained as a yellow solid (886 mg, quantitative). ^{1}H NMR (396 MHz, $CDCl_3$) δ 7.63 – 7.14 (m, 15H), 6.68 (s, J = 9.2 Hz, 2H), 5.97 (ddd, J = 17.0, 10.3, 6.0 Hz, 1H), 5.30 (d, J = 17.1 Hz, 1H), 5.23 – 4.93 (m, 8H), 2.01 (br s, 1H); ^{13}C NMR (100 MHz, $CDCl_3$) δ 153.0, 140.1, 138.4, 138.0, 137.2, 128.7, 128.6, 128.5, 128.3, 128.0, 127.9, 127.7, 127.6, 127.5, 115.4, 106.1, 75.3, 71.4; HRMS calcd for $C_{30}H_{29}O_4$ (M+ H^+) 453.2066; found 453.2045; IR (ATR, cm^{-1}) υ_{max} 3311, 3068, 3031, 2924, 2873, 1595, 1507, 1428, 1230, 1128, 1028; mp: 88 – 90 °C.

General procedure 8: Synthesis of racemic diol ***rac*-3.56** *via* Friedel-craft alkylation, followed by dihydroxylation

The acidic alumina (2 g/1 mmol of alcohol **3.54** or **3.55**) was suspended in the solution of cinnamyl alcohol **3.54** or secondary allylic alcohol **3.55** (1 eq.) and 3,5-bis(benzyloxy)phenol **3.1** (1.5 eq.) in anhydrous DCE (15 mL/1 mmol of alcohol **3.54** or **3.55**). The mixture was refluxed under a nitrogen atmosphere. After completion, the alumina was filtered off, and the filtrate was evaporated under reduced pressure. The residue was redissolved in the solution of 33% water in THF (15 mL/1 mmol of alcohol **3.54** or **3.55**). 50%wt NMO in water (1.5 eq.) and $K_2OsO_4{\cdot}2H_2O$ (5 mol%) were added, and the reaction was stirred at room temperature. After completion, brine was added and extracted with EtOAc 3 times. The combined organic

phase was dried over Na_2SO_4 and evaporated under reduced pressure. The crude mixture was purified by column chromatography using 25% EtOAc in hexane as an isocratic eluent system.

Racemic *cis*-3-(2,4-bis(benzyloxy)-6-hydroxyphenyl)-1-phenylpropane-1,2-diol (*rac*-3.56a)

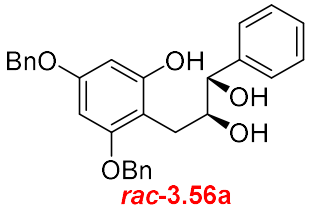

rac-3.56a

General procedure 8 was followed using cinnamyl alcohol **3.54** (136 mg, 1 mmol), 3,5-bis(benzyloxy)phenol **3.1** (459 mg, 1.5 mmol), and acidic alumina (2.00 g) in anhydrous DCE (15 mL). After heating at reflux while stirring under nitrogen atmosphere for 1 day, the reaction was monitored by ^{1}H NMR spectroscopy. After the Friedel-craft alkylation step, the resulting residue was dihydroxylated with 50%wt NMO in water (353 mg, 1.5 mmol) and $K_2OsO_4 \cdot 2H_2O$ (18.3 mg, 0.05 mmol) in 33% water in THF (15 mL). Racemic *cis*-3-(2,4-bis(benzyloxy)-6-hydroxyphenyl)-1-phenylpropane-1,2-diol ***rac*-3.56a** was obtained as a light-yellow solid (142 mg, 31% yield). ^{1}H NMR (396 MHz, $CDCl_3$) δ 8.00 (s, 1H), 7.45 – 7.20 (m, 13H), 7.12 (dd, J = 6.5, 2.9 Hz, 2H), 6.27 (d, J = 2.3 Hz, 1H), 6.20 (d, J = 2.3 Hz, 1H), 5.00 (s, 2H), 4.87 (d, J = 11.8 Hz, 1H), 4.83 (d, J = 11.7 Hz, 1H), 4.55 (dd, J = 6.6, 4.1 Hz, 1H), 4.07 – 3.97 (m, 1H), 3.30 (s, 1H), 2.92 (dd, J = 14.7, 3.3 Hz, 1H), 2.74 (dd, J = 14.7, 8.4 Hz, 1H), 2.46 (d, J = 4.2 Hz, 1H); LRMS calcd for $C_{29}H_{29}O_5$ (M+ H^+) 457.5; found 457.1. The analytical data are in agreement with those reported before.[107]

Racemic *cis*-1-(3-(benzyloxy)phenyl)-3-(2,4-bis(benzyloxy)-6-hydroxyphenyl)propane-1,2-diol (*rac*-3.56b)

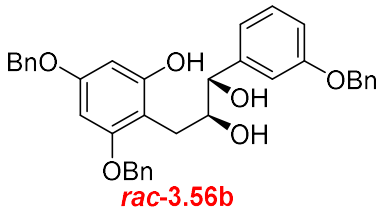

rac-3.56b

General procedure 8 was followed using racemic 1-(3-(benzyloxy)phenyl)prop-2-en-1-ol ***rac*-3.55b** (242 mg, 1 mmol), 3,5-bis(benzyloxy)phenol **3.1** (462 mg, 1.5 mmol), and acidic alumina (2.00 g) in anhydrous DCE (15 mL). After heating at reflux while stirring under nitrogen atmosphere for 1 day, the reaction was monitored by ^{1}H NMR spectroscopy. After the Friedel-craft alkylation step, the resulting residue was dihydroxylated with 50%wt NMO in water (359 mg, 1.5 mmol) and $K_2OsO_4 \cdot 2H_2O$ (18.9 mg, 0.05 mmol) in 33% water in THF (15 mL). After stirring at room temperature for 2 days, the reaction was monitored by ^{1}H NMR spectroscopy. Racemic *cis*-1-(3-(benzyloxy)phenyl)-3-(2,4-bis(benzyloxy)-6-hydroxyphenyl)propane-1,2-diol ***rac*-3.56b** was obtained as a colorless solid (131 mg, 23% yield). ^{1}H NMR (396 MHz, $CDCl_3$) δ 7.99 (s, 1H), 7.60 – 7.21 (m, 13H), 7.21 – 7.05 (m, 3H), 6.94 (s, 1H), 6.88 (d, J = 7.5 Hz, 1H), 6.85 (d, J = 8.2 Hz, 1H), 6.27 (s, 1H), 6.20 (d, J = 2.2 Hz, 1H), 5.11 – 4.90 (m, 4H), 4.91 – 4.77 (m, 2H), 4.52 (s, 1H), 4.01 (s, 1H), 3.23 (s, 1H), 2.94 (dd, J = 14.5, 3.1 Hz, 1H), 2.77 (dd, J = 14.7, 8.2 Hz, 1H), 2.50 (br s, 1H); LRMS calcd for $C_{36}H_{35}O_6$ ($M+H^+$) 563.7; found 563.1. The analytical data are in agreement with those reported before.[108]

Racemic *cis*-1-(4-(benzyloxy)phenyl)-3-(2,4-bis(benzyloxy)-6-hydroxyphenyl)propane-1,2-diol (*rac*-3.56c)

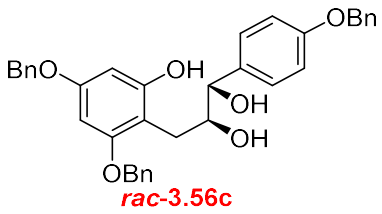

rac-3.56c

General procedure 8 was followed using racemic 1-(4-(benzyloxy)phenyl)prop-2-en-1-ol ***rac*-3.55c** (241 mg, 1 mmol), 3,5-bis(benzyloxy)phenol **3.1** (460 mg, 1.5 mmol) and acidic alumina (2.00 g) in anhydrous DCE (15 mL). After heating at reflux while stirring under nitrogen atmosphere for 1 day, the reaction was monitored by ^{1}H NMR spectroscopy. After the Friedel-craft alkylation step, the resulting residue was dihydroxylated with 50%wt NMO in water (358 mg, 1.5 mmol) and $K_2OsO_4 \cdot 2H_2O$ (18.9 mg, 0.05 mmol) in 33% water in THF (15 mL). After stirring at room temperature for 2 days, the reaction was monitored by ^{1}H NMR spectroscopy. Racemic *cis*-1-(4-(benzyloxy)phenyl)-3-(2,4-bis(benzyloxy)-6-hydroxyphenyl)propane-1,2-diol ***rac*-3.56c** was obtained as a colorless solid (173 mg, 31% yield). ^{1}H NMR (396 MHz, $CDCl_3$) δ 8.19 (br s, 1H), 7.50 – 7.24 (m, 13H), 7.20 (d, J = 8.5 Hz, 2H), 7.11 (d, J = 7.1 Hz, 2H), 6.83 (d, J = 8.3 Hz, 2H), 6.27 (d, J = 1.8 Hz, 1H), 6.20 (d, J = 2.0 Hz, 1H), 4.99 (s, 2H), 4.94 (s, 2H), 4.87 (d, J = 12.0 Hz, 1H), 4.81 (d, J = 11.8 Hz, 1H), 4.47 (d, J = 7.2 Hz, 1H), 4.00 (td, J = 7.9, 3.1 Hz, 1H), 3.51 (br s, 1H), 2.91 (dd, J = 14.7, 3.1 Hz, 1H), 2.71 (dd, J = 14.7, 8.4 Hz, 1H), 2.47 (br s, 1H); ^{13}C NMR (100 MHz, $CDCl_3$) δ 159.2, 158.9, 157.9, 157.7, 137.1, 137.0, 136.9, 132.8, 128.8, 128.7, 128.6, 128.3, 128.2, 128.1, 127.8, 127.6, 127.0, 115.0, 106.3, 96.1, 93.5, 70.2, 70.1, 70.0, 26.5; HRMS calcd for $C_{36}H_{35}O_6$ (M+ H^+) 563.2434; found 563.2419; IR (ATR, cm^{-1}) υ_{max} 3224, 3066, 3037, 2922, 2886, 1615, 1585, 1514, 1454, 1248, 1216, 1027; mp: 150 – 151 °C.

Racemic *cis*-3-(2,4-bis(benzyloxy)-6-hydroxyphenyl)-1-(3,5-bis(benzyloxy)phenyl)propane-1,2-diol (*rac*-3.56d)

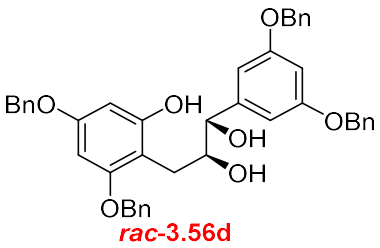

***rac*-3.56d**

General procedure 8 was followed using racemic 1-(3,5-bis(benzyloxy)phenyl)prop-2-en-1-ol ***rac*-3.55d** (324 mg, 0.93 mmol), 3,5-bis(benzyloxy)phenol **3.1** (428 mg, 1.4 mmol), and acidic alumina (1.86 g) in anhydrous DCE (15 mL). After heating at reflux while stirring under nitrogen atmosphere for 2 days, the reaction was monitored by ^{1}H NMR spectroscopy. After the Friedel-craft alkylation step, the resulting residue was dihydroxylated with 50%wt NMO in water (328 mg, 1.4 mmol) and $K_2OsO_4 \cdot 2H_2O$ (17.1 mg, 0.05 mmol) in 33% water in THF (15 mL). After stirring at room temperature for 1 day, the reaction was monitored by ^{1}H NMR spectroscopy. Racemic *cis*-3-(2,4-bis(benzyloxy)-6-hydroxyphenyl)-1-(3,5-bis(benzyloxy)phenyl)propane-1,2-diol ***rac*-3.56d** was obtained as an orange solid (134 mg, 21% yield). ^{1}H NMR (396 MHz, $CDCl_3$) δ 8.02 (br s, 1H), 7.47 – 7.19 (m, 18H), 7.14 (d, J = 6.8 Hz, 2H), 6.56 (d, J = 2.2 Hz, 2H), 6.50 (t, J = 2.2 Hz, 1H), 6.26 (d, J = 2.3 Hz, 1H), 6.19 (d, J = 2.3 Hz, 1H), 5.05 – 4.78 (m, 8H), 4.47 (d, J = 6.0 Hz, 1H), 3.99 (ddd, J = 8.1, 6.1, 3.9 Hz, 1H), 3.22 (br s, 1H), 2.95 (dd, J = 14.7, 3.8 Hz, 1H), 2.80 (dd, J = 14.7, 8.2 Hz, 1H), 2.63 (br s, 1H); ^{13}C NMR (100 MHz, $CDCl_3$) δ 160.2, 159.3, 158.0, 157.5, 143.0, 137.1, 137.0, 136.8, 128.7, 128.6, 128.2, 128.1, 127.8, 127.7, 126.8, 106.2, 106.0, 102.0, 96.1, 93.6, 77.0, 70.2, 70.1, 26.7; HRMS calcd for $C_{43}H_{41}O_7$ (M+ H^+) 669.2852; found 669.2878; IR (ATR, cm^{-1}) υ_{max} 3344, 3061, 3032, 2931, 2868, 1592, 1498, 1449, 1294, 1040; mp: 130 – 132 °C.

Racemic *cis*-3-(2,4-bis(benzyloxy)-6-hydroxyphenyl)-1-(3,4,5-tris(benzyloxy)phenyl) propane-1,2-diol (*rac*-3.56e)

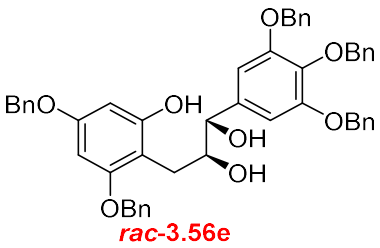

rac-3.56e

General procedure 8 was followed using racemic 1-(3,4,5-tris(benzyloxy)phenyl)prop-2-en-1-ol ***rac*-3.55e** (341 mg, 0.8 mmol), 3,5-bis(benzyloxy)phenol **3.1** (367 mg, 1.2 mmol), and acidic alumina (1.62 g) in anhydrous DCE (12 mL). After heating at reflux while stirring under nitrogen atmosphere for 1 day, the reaction was monitored by ^{1}H NMR spectroscopy. After the Friedel-craft alkylation step, the resulting residue was dihydroxylated with 50%wt NMO in water (286 mg, 1.2 mmol) and $K_2OsO_4 \cdot 2H_2O$ (14.7 mg, 0.04 mmol) in 33% water in THF (12 mL). After stirring at room temperature for 2 days, the reaction was monitored by ^{1}H NMR spectroscopy. Racemic *cis*-3-(2,4-bis(benzyloxy)-6-hydroxyphenyl)-1-(3,4,5-tris(benzyloxy)phenyl) propane-1,2-diol ***rac*-3.56e** was obtained as a colorless solid (155 mg, 25% yield). ^{1}H NMR (396 MHz, $CDCl_3$) δ 7.80 (br s, 1H), 7.47 – 7.12 (m, 25H), 6.61 (s, 2H), 6.27 (d, J = 2.3 Hz, 1H), 6.21 (d, J = 2.4 Hz, 1H), 5.05 – 4.95 (m, 8H), 4.89 (s, 2H), 4.47 (dd, J = 5.5, 4.6 Hz, 1H), 3.99 – 3.86 (m, 1H), 3.02 (br s, 1H), 2.91 (dd, J = 14.7, 3.7 Hz, 1H), 2.76 (dd, J = 14.7, 8.2 Hz, 1H), 2.44 (br s, 1H); LRMS calcd for $C_{36}H_{35}O_6$ (M+ H^+) 775.9; found 776.0. The analytical data are in agreement with those reported before.[46]

General procedure 9: Cyclization of diol **3.56** *via* ortho ester formation strategy

Pyridinium *p*-toluene sulfonate (1 mol%) was suspended in the solution of racemic *cis* diol **3.56** (1 eq.), and triethyl orthoacetate (1.5 – 2 eq.) in DCM (15 mL/1 mmol of **3.56**) and the mixture was stirred at room temperature. After completion, $BF_3{\cdot}OEt_2$ (1 eq.) was then added, and the reaction was stirred at room temperature, which was monitored closely by TLC. After the cyclization was completed, volatiles was evaporated under reduced pressure. The residue was redissolved in the mixture of THF, water, and MeOH in 4 : 2 : 1 ratio (14 mL/1 mmol of **3.56**) and $LiOH{\cdot}H_2O$ (10 eq.) was added. The reaction was then kept stirring overnight. After the hydrolysis finished, brine was added and extracted with DCM 3 times. The combined organic layer was washed with water and brine, dried over Na_2SO_4, and evaporated under reduced pressure.

Racemic *trans*-5,7-bis(benzyloxy)-2-phenylchroman-3-ol (*rac*-3.57a)

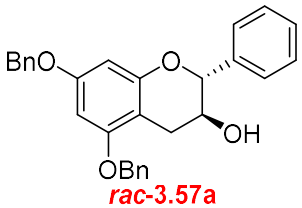

rac-3.57a

General procedure 8 was followed using racemic *cis*-3-(2,4-bis(benzyloxy)-6-hydroxyphenyl)-1-phenylpropane-1,2-diol ***rac*-3.56a** (129 mg, 0.28 mmol), triethyl orthoacetate (95 µL, 0.52 mmol) and pyridinium *p*-toluene sulfonate (0.7 mg, 0.003 mmol) in DCM (5 mL). After stirring at room temperature for 45 minutes, the reaction was monitored by TLC (hexanes:EtOAc 3:1; UV). After the ortho ester formation step, the resulting intermediate was then cyclized with $BF_3{\cdot}OEt_2$ (35 µL, 0.28 mmol). After completion by stirring at room temperature for 30 minutes as monitored by TLC (hexanes:EtOAc 3:1; UV), the crude mixture was hydrolyzed with $LiOH{\cdot}H_2O$ (118 mg, 2.8 mmol) in the mixture of THF, water, and MeOH in 4 : 2 : 1 ratio (14 mL). Racemic *trans*-5,7-bis(benzyloxy)-2-phenylchroman-3-ol ***rac*-3.57a** was obtained as a

colorless solid (110 mg, 90% yield over 3 steps). ^{1}H NMR (396 MHz, $CDCl_3$) δ 7.52 – 7.13 (m, 15H), 6.28 (d, *J* = 2.2 Hz, 1H), 6.25 (d, *J* = 2.2 Hz, 1H), 5.03 (s, 2H), 5.00 (s, 2H), 4.79 (d, *J* = 7.9 Hz, 1H), 4.18 – 4.07 (m, 1H), 3.10 (dd, *J* = 16.5, 5.5 Hz, 1H), 2.71 (dd, *J* = 16.4, 8.6 Hz, 1H); LRMS calcd for $C_{29}H_{27}O_4$ (M+ H^+) 439.5; found 439.1. The analytical data are in agreement with those reported before.[107]

Racemic *trans*-5,7-bis(benzyloxy)-2-(3-(benzyloxy)phenyl)chroman-3-ol (*rac*-3.57b)

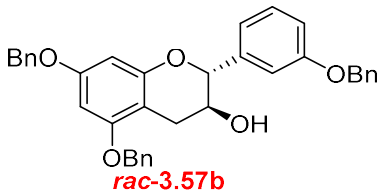

rac-3.57b

General procedure 8 was followed using racemic *cis*-1-(3-(benzyloxy)phenyl)-3-(2,4-bis(benzyloxy)-6-hydroxyphenyl)propane-1,2-diol ***rac*-3.56b** (124 mg, 0.22 mmol), triethyl orthoacetate (50 μL, 0.28 mmol) and pyridinium *p*-toluene sulfonate (0.7 mg, 0.002 mmol) in DCM (5 mL). After stirring at room temperature for 45 minutes, the reaction was monitored by TLC (hexanes:EtOAc 3:1; UV). After the ortho ester formation step, the resulting intermediate was then cyclized with $BF_3{\cdot}OEt_2$ (28 μL, 0.22 mmol). After completion by stirring at room temperature for 30 minutes as monitored by TLC (hexanes:EtOAc 3:1; UV), the crude mixture was hydrolyzed with $LiOH{\cdot}H_2O$ (92.3 mg, 2.2 mmol) in the mixture of THF, water, and MeOH in 4 : 2 : 1 ratio (11 mL). Racemic *trans*-5,7-bis(benzyloxy)-2-(3-(benzyloxy)phenyl)chroman-3-ol ***rac*-3.57b** was obtained as an orange solid (116 mg, 97% yield over 3 steps). ^{1}H NMR (396 MHz, $CDCl_3$) δ 7.47 – 7.28 (m, 16H), 7.07 (d, *J* = 1.9 Hz, 1H), 7.03 (d, *J* = 7.6 Hz, 1H), 6.97 (dd, *J* = 8.1, 2.2 Hz, 1H), 6.27 (d, *J* = 2.2 Hz, 1H), 6.24 (d, *J* = 2.2 Hz, 1H), 5.07 (s, 2H), 5.02 (s, 2H), 5.00 (s, 2H), 4.75 (d, *J* = 7.8 Hz, 1H), 4.13 – 4.04 (m, 1H), 3.09 (dd, *J* = 16.4, 5.5 Hz, 1H), 2.69 (dd, *J* = 16.4, 8.6 Hz, 1H), 1.73 (br s, 1H); LRMS

calcd for $C_{36}H_{33}O_5$ (M+ H^+) 545.7; found 545.5. The analytical data are in agreement with those reported before.[109]

Racemic *trans*-5,7-bis(benzyloxy)-2-(4-(benzyloxy)phenyl)chroman-3-ol (*rac*-3.57c)

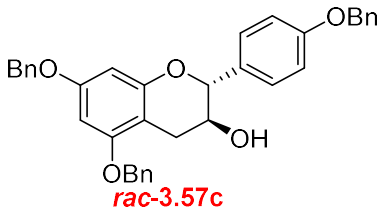

rac-3.57c

General procedure 8 was followed using racemic *cis*-1-(4-(benzyloxy)phenyl)-3-(2,4-bis(benzyloxy)-6-hydroxyphenyl)propane-1,2-diol ***rac*-3.56c** (153 mg, 0.27 mmol), triethyl orthoacetate (62 µL, 0.34 mmol), and Pyridinium *p*-toluene sulfonate (0.8 mg, 0.003 mmol) in DCM (5 mL). After stirring at room temperature for 45 minutes, the reaction was monitored by TLC (hexanes:EtOAc 3:1; UV). After the ortho ester formation step, the resulting intermediate was then cyclized with $BF_3{\cdot}OEt_2$ (34 µL, 0.27 mmol). After completion by stirring at room temperature for 30 minutes as monitored by TLC (hexanes:EtOAc 3:1; UV), the crude mixture was hydrolyzed with $LiOH{\cdot}H_2O$ (116 mg, 2.8 mmol) in the mixture of THF, water, and MeOH in 4 : 2 : 1 ratio (13 mL). Racemic *trans*-5,7-bis(benzyloxy)-2-(4-(benzyloxy)phenyl)chroman-3-ol ***rac*-3.57c** was obtained as an orange solid (146 mg, 99% yield over 3 steps). ^{1}H NMR (396 MHz, $CDCl_3$) δ 7.49 – 7.28 (m, 17H), 7.02 (d, J = 8.5 Hz, 2H), 6.27 (d, J = 2.0 Hz, 1H), 6.22 (d, J = 2.1 Hz, 1H), 5.09 (s, 2H), 5.03 (s, 2H), 4.99 (s, 2H), 4.70 (d, J = 8.1 Hz, 1H), 4.14 – 4.03 (m, 1H), 3.15 (dd, J = 16.3, 5.5 Hz, 1H), 2.68 (dd, J = 16.3, 8.8 Hz, 1H); LRMS calcd for $C_{36}H_{33}O_5$ (M+ H^+) 545.7; found 546.1. The analytical data are in agreement with those reported before.[110]

Racemic *trans*-5,7-bis(benzyloxy)-2-(3,5-bis(benzyloxy)phenyl)chroman-3-ol (*rac*-3.57d)

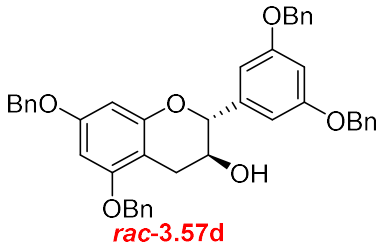

rac-3.57d

General procedure 8 was followed using racemic *cis*-3-(2,4-bis(benzyloxy)-6-hydroxyphenyl)-1-(3,5-bis(benzyloxy)phenyl)propane-1,2-diol ***rac*-3.56d** (95.1 mg, 0.14 mmol), triethyl orthoacetate (54 µL, 0.29 mmol), and Pyridinium *p*-toluene sulfonate (0.8 mg, 0.003 mmol) in DCM (3 mL). After stirring at room temperature for 45 minutes, the reaction was monitored by TLC (hexanes:EtOAc 3:1; UV). After the ortho ester formation step, the resulting intermediate was then cyclized with $BF_3 \cdot OEt_2$ (18 µL, 0.14 mmol). After completion by stirring at room temperature for 30 minutes as monitored by TLC (hexanes:EtOAc 3:1; UV), the crude mixture was hydrolyzed with $LiOH \cdot H_2O$ (59.2 mg, 1.4 mmol) in the mixture of THF, water, and MeOH in 4 : 2 : 1 ratio (7 mL). Racemic *trans*-5,7-bis(benzyloxy)-2-(3,5-bis(benzyloxy)phenyl)chroman-3-ol ***rac*-3.57d** was obtained as a light-yellow solid (99.9 mg, quantitative over 3 steps). ^{1}H NMR (396 MHz, $CDCl_3$) δ 7.46 – 7.23 (m, 20H), 6.68 (d, J = 2.1 Hz, 2H), 6.60 (t, J = 2.1 Hz, 1H), 6.26 (d, J = 2.1 Hz, 1H), 6.23 (d, J = 2.1 Hz, 1H), 5.05 – 4.94 (m, 8H), 4.67 (d, J = 7.8 Hz, 1H), 4.08 – 3.96 (m, 1H), 3.07 (dd, J = 16.4, 5.5 Hz, 1H), 2.66 (dd, J = 16.4, 8.6 Hz, 1H); ^{13}C NMR (100 MHz, $CDCl_3$) δ 160.3, 158.9, 157.9, 155.2, 140.5, 137.0, 137.0, 136.7, 128.7, 128.6, 128.2, 128.1, 128.0, 127.7, 127.6, 127.2, 106.3, 102.4, 102.3, 94.5, 94.0, 81.8, 70.3, 70.0, 68.2, 27.5; LRMS calcd for $C_{43}H_{39}O_6$ (M+ H^+) 651.8; found 651.2. The analytical data are in agreement with those reported before.[109]

Racemic *trans*-5,7-bis(benzyloxy)-2-(3,4,5-tris(benzyloxy)phenyl)chroman-3-ol (*rac*-3.57e)

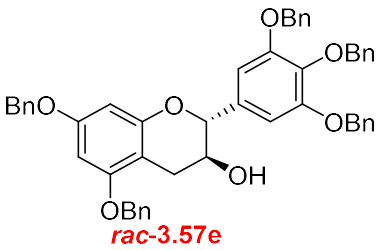

rac-3.57e

General procedure 8 was followed using racemic *cis*-3-(2,4-bis(benzyloxy)-6-hydroxyphenyl)-1-(3,4,5-tris(benzyloxy)phenyl) propane-1,2-diol ***rac*-3.56e** (161 mg, 0.21 mmol), triethyl orthoacetate (50 µL, 0.26 mmol), and pyridinium *p*-toluene sulfonate (0.5 mg, 0.002 mmol) in DCM (5 mL). After stirring at room temperature for 45 minutes, the reaction was monitored by TLC (hexanes:EtOAc 3:1; UV). After the ortho ester formation step, the resulting intermediate was then cyclized with $BF_3 \cdot OEt_2$ (26 µL, 0.21 mmol). After completion by stirring at room temperature for 30 minutes as monitored by TLC (hexanes:EtOAc 3:1; UV), the crude mixture was hydrolyzed with $LiOH \cdot H_2O$ (90.4 mg, 2.1 mmol) in the mixture of THF, water, and MeOH in 4 : 2 : 1 ratio (14 mL). Racemic *trans*-5,7-bis(benzyloxy)-2-(3,4,5-tris(benzyloxy)phenyl)chroman-3-ol ***rac*-3.57e** was obtained as a light-yellow solid (159 mg, quantitative). ^{1}H NMR (396 MHz, $CDCl_3$) δ 7.49 – 7.14 (m, 25H), 6.73 (s, 2H), 6.28 (d, J = 2.1 Hz, 1H), 6.23 (d, J = 2.2 Hz, 1H), 5.17 – 4.94 (m, 10H), 4.61 (d, J = 8.2 Hz, 1H), 3.97 (m, 1H), 3.10 (dd, J = 16.4, 5.7 Hz, 1H), 2.64 (dd, J = 16.4, 9.0 Hz, 1H); LRMS calcd for $C_{50}H_{45}O_7$ (M+ H^+) 757.9; found 758.1. The analytical data are in agreement with those reported before.[46]

General procedure 10: EDCI esterification between ***rac*-3.57** and benzylated gallic acid **3.16f**

Racemic catechin ***rac*-3.57** (1 eq.), 3,4,5-tris(benzyloxy)benzoic acid **3.16f** (5 – 6 eq.), EDCI (6 – 10 eq.), DMAP (0.2 – 0.4 eq.) and Et_3N (6 – 15 eq.) were dissolved in DCM (75 mL/1 mmol of ***rac*-3.57**). After completion, the mixture was quenched with a saturated aqueous solution of NH_4Cl and extracted with DCM twice. The combined organic phase was dried over Na_2SO_4 and evaporated. The crude mixture was purified by column chromatography using DCM as an isocratic eluent system, which was then filtered through basic alumina.

Racemic *trans*-5,7-bis(benzyloxy)-2-(3,4-bis(benzyloxy)phenyl)chroman-3-yl 3-(benzyloxy) benzoate (*rac*-3.61a)

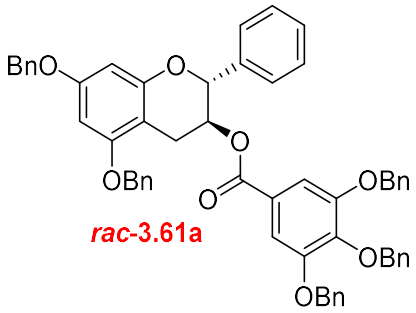

General procedure 10 was followed using racemic *trans*-5,7-bis(benzyloxy)-2-phenylchroman-3-ol ***rac*-3.57a** (80.6 mg, 0.18 mmol), 3,4,5-tris(benzyloxy)benzoic acid **3.16f** (482 mg, 1.1 mmol), EDCI (215 mg, 1.1 mmol), DMAP (9.8 mg, 0.08 mmol), and Et_3N (160 µL, 1.1 mmol) in DCM (15 mL). After stirring at room temperature under nitrogen atmosphere for 5 days, the reaction was monitored by ^1H NMR spectroscopy. Racemic *trans*-5,7-bis(benzyloxy)-2-(3,4-bis(benzyloxy)phenyl)chroman-3-yl 3-(benzyloxy) benzoate ***rac*-3.61a** was obtained as a colorless solid (47.4 mg, 30% yield). ^1H NMR (396 MHz, $CDCl_3$) δ 7.53 – 7.21 (m, 32H), 6.33 (s, 1H), 6.30 (s, 1H), 5.51 (q, J = 5.9 Hz, 1H), 5.20 (d, J = 6.4 Hz, 1H), 5.15 – 4.96 (m, 10H), 3.07 (dd, J = 16.9, 4.8 Hz, 1H), 2.86 (dd, J = 16.8, 6.5 Hz, 1H); ^{13}C NMR (100 MHz, $CDCl_3$) δ 165.3, 159.1, 157.9, 155.2, 152.5, 142.6, 138.1, 137.6, 136.9, 136.8, 128.7, 128.5, 128.3,

128.2, 128.1, 127.8, 127.7, 127.4, 126.7, 125.1, 109.2, 101.6, 94.6, 93.9, 78.8, 75.3, 71.3, 70.3, 70.2, 70.1, 24.3; HRMS calcd for $C_{57}H_{49}O_8$ ($M+H^+$) 861.3427; found 861.3477; IR (ATR, cm^{-1}) υ_{max} 3064, 3034, 2923, 2859, 1698, 1591, 1210, 1028; mp: 119 – 121 °C.

Racemic *trans*-5,7-bis(benzyloxy)-2-(3-(benzyloxy)phenyl)chroman-3-yl 3,4,5-tris(benzyl oxy)benzoate (*rac*-3.61b)

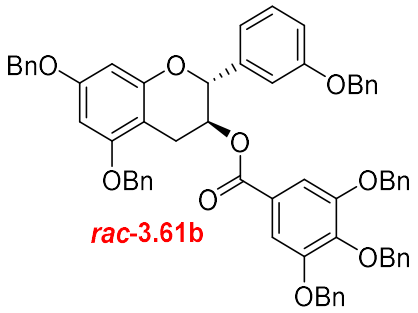

General procedure 10 was followed using racemic *trans*-5,7-bis(benzyloxy)-2-(3-(benzyloxy)phenyl)chroman-3-ol ***rac*-3.57b** (109 mg, 0.20 mmol), 3,4,5-tris(benzyloxy)benzoic acid **3.16f** (441 mg, 1.0 mmol), EDCI (293 mg, 1.5 mmol), DMAP (11.1 mg, 0.09 mmol), and Et_3N (420 µL, 3.0 mmol) in DCM (15 mL). After stirring at room temperature under nitrogen atmosphere for 4 days, the reaction was monitored by ^1H NMR spectroscopy. Racemic *trans*-5,7-bis(benzyloxy)-2-(3-(benzyloxy)phenyl)chroman-3-yl 3,4,5-tris(benzyloxy) benzoate ***rac*-3.61b** was obtained as a colorless solid (103 mg, 53% yield). ^1H NMR (396 MHz, $CDCl_3$) δ 7.57 – 7.10 (m, 33H), 7.04 (s, 1H), 6.98 (d, J = 7.4 Hz, 1H), 6.88 (d, J = 8.1 Hz, 1H), 6.32 (s, 1H), 6.30 (s, 1H), 5.54 – 5.47 (m, 1H), 5.20 (d, J = 6.1 Hz, 1H), 5.14 – 4.89 (m, 12H), 3.05 (dd, J = 16.8, 4.6 Hz, 1H), 2.86 (dd, J = 16.8, 6.2 Hz, 1H); ^{13}C NMR (100 MHz, $CDCl_3$) δ 165.3, 159.1, 157.8, 155.0, 152.5, 142.6, 139.8, 137.6, 136.9, 136.8, 136.7, 129.8, 128.8, 128.7, 128.6, 128.3, 128.2, 128.1, 128.0, 127.7, 127.4, 125.1, 119.2, 114.8, 113.2, 109.2, 101.5, 94.5, 93.9, 78.6, 75.2, 71.2, 70.3, 70.1, 70.0, 24.2; HRMS calcd for $C_{64}H_{55}O_9$

(M+ H^+) 967.3846; found 967.3870; IR (ATR, cm^{-1}) υ_{max} 3061, 3030, 2931, 2870, 1698, 1591, 1499, 1290, 1216, 1028; mp: 139 – 142 °C.

Racemic *trans*-5,7-bis(benzyloxy)-2-(4-(benzyloxy)phenyl)chroman-3-yl 3,4,5-tris(benzyloxy)benzoate (*rac*-3.61c)

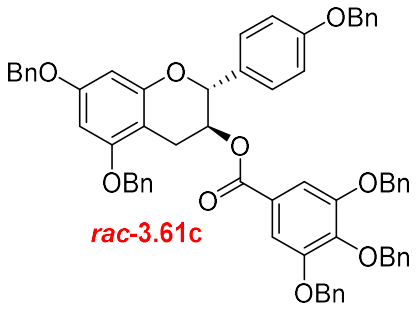

General procedure 10 was followed using racemic *trans*-5,7-bis(benzyloxy)-2-(4-(benzyloxy)phenyl)chroman-3-ol ***rac*-3.57c** (124 mg, 0.23 mmol), 3,4,5-tris(benzyloxy)benzoic acid **3.16f** (513 mg, 1.17 mmol), EDCI (337 mg, 1.76 mmol), DMAP (11.9 mg, 0.1 mmol), and Et_3N (480 µL, 3.44 mmol) in DCM (15 mL). After stirring at room temperature under nitrogen atmosphere for 4 days, the reaction was monitored by ^1H NMR spectroscopy. Racemic *trans*-5,7-bis(benzyloxy)-2-(4-(benzyloxy)phenyl)chroman-3-yl 3,4,5-tris(benzyloxy) benzoate ***rac*-3.61c** was obtained as a yellow solid (86.0 mg, 39% yield). ^1H NMR (396 MHz, $CDCl_3$) δ 7.46 – 7.14 (m, 34H), 6.92 (d, J = 8.7 Hz, 2H), 6.30 (s, 2H), 5.54 – 5.43 (m, 1H), 5.14 – 4.94 (m, 13H), 3.13 (dd, J = 16.7, 5.4 Hz, 1H), 2.84 (dd, J = 16.7, 7.1 Hz, 1H); ^{13}C NMR (100 MHz, $CDCl_3$) δ 165.3, 159.1, 158.9, 157.9, 155.3, 152.5, 142.6, 137.5, 136.9, 136.8, 130.4, 128.7, 128.6, 128.3, 128.2, 128.1, 127.7, 127.6, 127.6, 127.4, 125.1, 115.1, 109.2, 101.6, 94.6, 93.9, 78.6, 75.3, 71.3, 70.3, 70.2, 70.1, 24.7; HRMS calcd for $C_{64}H_{55}O_9$ (M+ H^+) 967.3846; found 967.3831; IR (ATR, cm^{-1}) υ_{max} 3068, 3032, 2927, 2868, 1698, 1593, 1499, 1211, 1012; mp: 116 – 117 °C.

Racemic *trans*-5,7-bis(benzyloxy)-2-(3,5-bis(benzyloxy)phenyl)chroman-3-yl 3,4,5-tris(benzyloxy)benzoate (*rac*-3.61d)

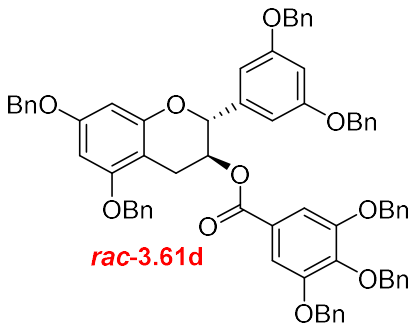

General procedure 10 was followed using racemic *trans*-5,7-bis(benzyloxy)-2-(3,5-bis(benzyloxy)phenyl)chroman-3-ol ***rac*-3.57d** (81.7 mg, 0.13 mmol), 3,4,5-tris(benzyloxy)benzoic acid **3.16f** (278 mg, 0.63 mmol), EDCI (250 mg, 1.3 mmol), DMAP (3.1 mg, 0.025 mmol), and Et_3N (265 µL, 1.9 mmol) in DCM (15 mL). After stirring at room temperature under nitrogen atmosphere for 5 days, the reaction was monitored by ^1H NMR spectroscopy. Racemic *trans*-5,7-bis(benzyloxy)-2-(3,5-bis(benzyloxy)phenyl)chroman-3-yl 3,4,5-tris(benzyloxy) benzoate ***rac*-3.61d** was obtained as a colorless solid (58.5 mg, 43% yield). ^1H NMR (396 MHz, $CDCl_3$) δ 7.46 – 7.20 (m, 37H), 6.67 (d, J = 2.0 Hz, 2H), 6.53 (t, J = 2.0 Hz, 1H), 6.32 (d, J = 2.1 Hz, 1H), 6.29 (d, J = 2.1 Hz, 1H), 5.50 (q, J = 6.0 Hz, 1H), 5.17 (d, J = 6.2 Hz, 1H), 5.08 – 4.95 (m, 10H), 4.92 (s, 4H), 3.03 (dd, J = 16.8, 5.1 Hz, 1H), 2.86 (dd, J = 16.8, 6.3 Hz, 1H); ^{13}C NMR (100 MHz, $CDCl_3$) δ 165.3, 160.2, 159.1, 157.8, 154.9, 152.5, 142.6, 140.5, 137.6, 136.9, 136.7, 136.6, 128.8, 128.7, 128.6, 128.5, 128.3, 128.1, 128.0, 127.7, 127.7, 127.3, 125.1, 109.2, 105.8, 102.0, 101.4, 94.5, 94.0, 78.5, 75.2, 71.2, 70.2, 70.1, 24.0; HRMS calcd for $C_{71}H_{61}O_{10}$ (M+ H^+) 1073.4265; found 1073.4219; IR (ATR, cm^{-1}) υ_{max} 3068, 3032, 2925, 2870, 1696, 1594, 1499, 1214, 1028; mp: 144 – 147 °C.

Racemic *trans*-5,7-bis(benzyloxy)-2-(3,4,5-tris(benzyloxy)phenyl)chroman-3-yl 3,4,5-tris(benzyloxy)benzoate (*rac*-3.61e)

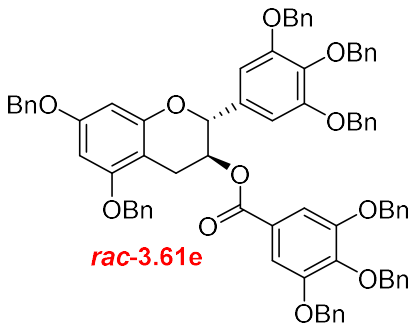

rac-3.61e

General procedure 10 was followed using Racemic *trans*-5,7-bis(benzyloxy)-2-(3,4,5-tris(benzyloxy)phenyl)chroman-3-ol ***rac*-3.57e** (163 mg, 0.22 mmol), 3,4,5-tris(benzyloxy) benzoic acid **3.16f** (238 mg, 0.54 mmol), EDCI (158 mg, 0.81 mmol), DMAP (5.3 mg, 0.04 mmol), and Et_3N (450 µL, 3.23 mmol) in DCM (15 mL). After stirring at room temperature under nitrogen atmosphere for 2 days, the reaction was monitored by ^1H NMR spectroscopy. Racemic *trans*-5,7-bis(benzyloxy)-2-(3,4,5-tris(benzyloxy)phenyl)chroman-3-yl 3,4,5-tris(benzyloxy)benzoate ***rac*-3.61e** was obtained as a colorless solid (128 mg, 50% yield). ^1H NMR (396 MHz, $CDCl_3$) δ 7.50 – 7.06 (m, 42H), 6.70 (s, 2H), 6.31 (s, 2H), 5.47 (s, 1H), 5.19 – 4.85 (m, 17H), 2.99 (d, J = 16.5 Hz, 1H), 2.86 (d, J = 11.3 Hz, 1H); ^{13}C NMR (100 MHz, $CDCl_3$) δ 165.2, 159.1, 157.8, 155.0, 153.0, 152.6, 142.8, 138.6, 137.9, 137.5, 137.0, 136.7, 133.6, 128.8, 128.7, 128.6, 128.5, 128.3, 128.2, 128.1 (x 3), 128.0, 127.9, 127.8, 127.7, 127.4, 125.1, 109.3, 106.5, 101.5, 94.5, 94.0, 78.6, 75.3, 75.2, 71.4, 71.3, 70.2, 70.1, 70.0, 24.2. The analytical data are in agreement with those reported before.[111]

Racemic *trans*-5,7-dihydroxy-2-phenylchroman-3-yl 3,4,5-trihydroxybenzoate (*rac*-3.58a)

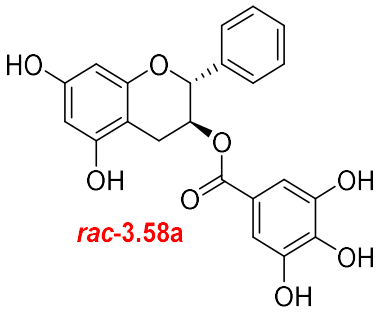

General procedure 4 was followed using racemic *trans*-5,7-bis(benzyloxy)-2-(3,4-bis(benzyloxy)phenyl)chroman-3-yl 3-(benzyloxy) benzoate ***rac*-3.61a** (47.4 mg, 0.055 mmol) and 20% $Pd(OH)_2/C$ (94.9 mg) in 50% EtOH in THF (8 mL). Racemic *trans*-5,7-dihydroxy-2-phenylchroman-3-yl 3,4,5-trihydroxybenzoate **rac-3.58a** was obtained as a colorless solid (14.0 mg, 62% yield). ^{1}H NMR (396 MHz, CD_3OD) δ 7.41 (d, J = 7.3 Hz, 2H), 7.33 (t, J = 7.3 Hz, 2H), 7.28 (d, J = 7.1 Hz, 1H), 6.96 (s, 2H), 5.97 (s, 2H), 5.42 (q, J = 5.9 Hz, 1H), 5.20 (d, J = 6.2 Hz, 1H), 2.81 (dd, J = 16.5, 5.3 Hz, 1H), 2.73 (dd, J = 16.6, 6.2 Hz, 1H); ^{13}C NMR (100 MHz, CD_3OD) δ 167.4, 158.2, 157.7, 156.4, 146.4, 140.0, 129.4, 129.1, 127.5, 121.3, 110.1, 99.6, 96.6, 95.6, 79.5, 71.2, 24.6; HRMS calcd for $C_{22}H_{19}O_8$ ($M+H^+$) 411.1080; found 411.1094; IR (ATR, cm^{-1}) υ_{max} 3331, 1686, 1608, 1525, 1303, 1239, 1215, 1058, 1019; mp: dec.

Racemic *trans*-5,7-dihydroxy-2-(3-hydroxyphenyl)chroman-3-yl 3,4,5-trihydroxy benzoate (*rac*-3.58b)

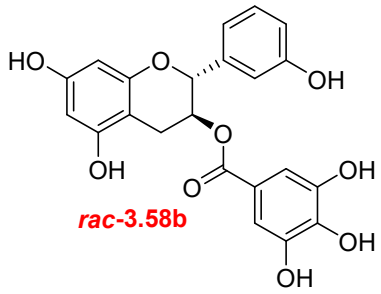

General procedure 4 was followed using racemic *trans*-5,7-bis(benzyloxy)-2-(3-(benzyloxy)phenyl)chroman-3-yl 3,4,5-tris(benzyl oxy)benzoate ***rac*-3.61b** (59.0 mg, 0.061 mmol) and 20% $Pd(OH)_2/C$ (118 mg) in 50% EtOH in THF (8 mL). Racemic *trans*-5,7-dihydroxy-2-(3-hydroxyphenyl)chroman-3-yl 3,4,5-trihydroxybenzoate **rac-3.58b** was obtained as a colorless solid (19.9 mg, 77% yield). ^{1}H NMR (396 MHz, CD_3OD) δ 7.15 (t, J = 7.8 Hz, 1H), 6.98 (s, 2H), 6.89 – 6.81 (m, 2H), 6.70 (dd, J = 8.0, 1.9 Hz, 1H), 5.98 (d, J = 2.5 Hz, 1H), 5.97 (d, J = 2.3 Hz, 1H), 5.42 (q, J = 5.3 Hz, 1H), 5.19 (d, J = 5.5 Hz, 1H), 2.74 (d, J = 5.2 Hz, 2H); ^{13}C NMR (100 MHz, CD_3OD) δ 167.6, 158.6, 158.2, 157.6, 156.3, 146.4, 141.6, 139.9, 130.5, 121.3, 118.5, 116.0, 114.0, 110.1, 99.5, 96.5, 95.6, 79.2, 71.0, 23.9; HRMS calcd for $C_{22}H_{19}O_9$ ($M+H^+$) 427.1029; found 427.1017; IR (ATR, cm^{-1}) υ_{max} 3289, 1687, 1604, 1314, 1224, 1014; mp: dec.

Racemic *trans*-5,7-dihydroxy-2-(4-hydroxyphenyl)chroman-3-yl 3,4,5-trihydroxy benzoate (*rac*-3.58c)

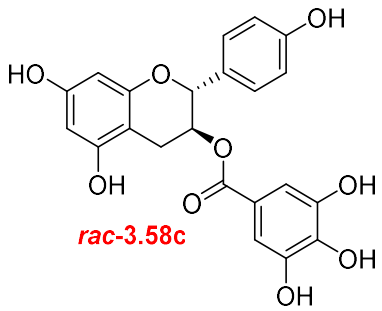

General procedure 4 was followed using racemic *trans*-5,7-bis(benzyloxy)-2-(4-(benzyloxy)phenyl)chroman-3-yl 3,4,5-tris(benzyloxy)benzoate ***rac*-3.61c** (59.9 mg, 0.062 mmol) and 20% $Pd(OH)_2/C$ (121 mg) in 50% EtOH in THF (8 mL). Racemic *trans*-5,7-dihydroxy-2-(4-hydroxyphenyl)chroman-3-yl 3,4,5-trihydroxybenzoate **rac-3.58c** was obtained as a colorless solid (13.5 mg, 51% yield). ^{1}H NMR (396 MHz, CD_3OD) δ 7.22 (d, *J* = 8.5 Hz, 2H), 6.96 (s, 2H), 6.75 (d, *J* = 8.5 Hz, 2H), 5.97 (d, *J* = 2.1 Hz, 1H), 5.94 (d, *J* = 1.9 Hz, 1H), 5.37 (q, *J* = 6.2 Hz, 1H), 5.08 (d, *J* = 6.5 Hz, 1H), 2.87 (dd, *J* = 16.5, 5.3 Hz, 1H), 2.71 (dd, *J* = 16.4, 6.6 Hz, 1H); ^{13}C NMR (100 MHz, CD_3OD) δ 167.5, 158.4, 158.2, 157.6, 156.6, 146.4, 139.9, 130.7, 128.9, 121.3, 116.2, 110.1, 99.7, 96.5, 95.6, 79.5, 71.2, 24.9; LRMS calcd for $C_{22}H_{19}O_9$ ($M+ H^+$) 427.4; found 426.9. The analytical data are in agreement with those reported before.[110]

Racemic *trans*-2-(3,5-dihydroxyphenyl)-5,7-dihydroxychroman-3-yl 3,4,5-trihydroxyben zoate (*rac*-3.58d)

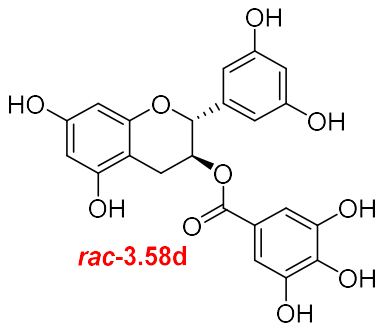

rac-3.58d

General procedure 4 was followed using Racemic *trans*-5,7-bis(benzyloxy)-2-(3,5-bis(benzyloxy)phenyl)chroman-3-yl 3,4,5-tris(benzyloxy)benzoate ***rac*-3.61d** (50.3 mg, 0.047 mmol) and 20% $Pd(OH)_2/C$ (109 mg) in 50% EtOH in THF (8 mL). Racemic *trans*-2-(3,5-dihydroxyphenyl)-5,7-dihydroxychroman-3-yl 3,4,5-trihydroxybenzoate ***rac*-3.58d** was obtained as a colorless solid (12.2 mg, 59% yield). ^{1}H NMR (396 MHz, CD_3OD) δ 6.99 (s, 2H), 6.34 (d, J = 2.0 Hz, 2H), 6.18 (t, J = 2.2 Hz, 1H), 5.97 (d, J = 2.3 Hz, 1H), 5.95 (d, J = 2.3 Hz, 1H), 5.42 (q, J = 4.8 Hz, 1H), 5.15 (d, J = 4.8 Hz, 1H), 2.75 (dd, J = 16.9, 4.8 Hz, 1H), 2.69 (dd, J = 16.8, 4.9 Hz, 1H); ^{13}C NMR (100 MHz, CD_3OD) δ 167.7, 159.7, 158.1, 157.6, 156.2, 146.4, 142.5, 139.9, 121.4, 110.2, 105.5, 103.1, 99.4, 96.4, 95.6, 79.0, 70.9, 23.3; HRMS calcd for $C_{22}H_{19}O_{10}$ ($M+H^+$) 443.0978; found 443.0956; IR (ATR, cm^{-1}) υ_{max} 3237, 1686, 1603, 1311, 1231, 1014; mp: dec.

Racemic *trans*-5,7-dihydroxy-2-(3,4,5-trihydroxyphenyl)chroman-3-yl 3,4,5-trihydroxy benzoate (*rac*-3.58e)

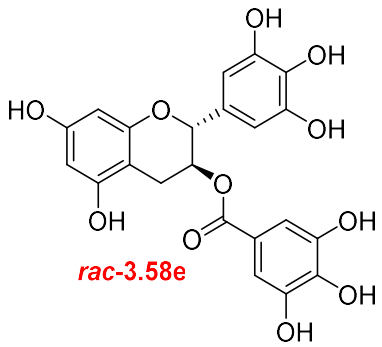

General procedure 4 was followed using racemic *trans*-5,7-bis(benzyloxy)-2-(3,4,5-tris(benzyloxy)phenyl)chroman-3-yl 3,4,5-tris(benzyloxy)benzoate ***rac*-3.61e** (77.3 mg, 0.066 mmol) and 20% $Pd(OH)_2/C$ (158 mg) in 50% EtOH in THF (15 mL). Racemic *trans*-5,7-dihydroxy-2-(3,4,5-trihydroxyphenyl)chroman-3-yl 3,4,5-trihydroxybenzoate ***rac*-3.58e** was obtained as a light-yellow solid (20.1 mg, 67% yield). ^{1}H NMR (396 MHz, CD_3OD) δ 6.97 (s, 2H), 6.40 (s, 2H), 5.95 (s, 2H), 5.38 (q, J = 5.0 Hz, 1H), 5.06 (d, J = 5.1 Hz, 1H), 2.77 (dd, J = 16.9, 5.1 Hz, 1H), 2.71 (dd, J = 17.1, 5.7 Hz, 1H); ^{13}C NMR (100 MHz, CD_3OD) δ 167.7, 158.1, 157.6, 156.4, 147.0, 146.4, 139.9, 133.9, 131.0, 121.4, 110.1, 106.3, 99.5, 96.4, 95.6, 79.2, 71.1, 23.7; LRMS calcd for $C_{22}H_{19}O_{11}$ ($M+ H^+$) 459.4; found 458.9. The analytical data are in agreement with those reported before.[99]

General procedure 11: Fully esterification of **3.48d**

To the solution of (*2R*,*3S*)-2-(3,4-dihydroxyphenyl)-5,7-dihydroxychroman-3-yl 3,4-dihydroxybenzoate **3.48d** (1 eq.) in pyridine (4 mL/1 mmol of **3.48d**) was added dropwise acid anhydride (25 eq.). The reaction was stirred at room temperature. After completion, the mixture was diluted with EA and washed with an aqueous solution of 2 M HCl, water, and a saturated aqueous solution of $NaHCO_3$.

4-((((*2R*,*3S*)-5,7-Diacetoxy-2-(3,4-diacetoxyphenyl)chroman-3-yl)oxy)carbonyl)-1,2-phenylene diacetate (3.63a)

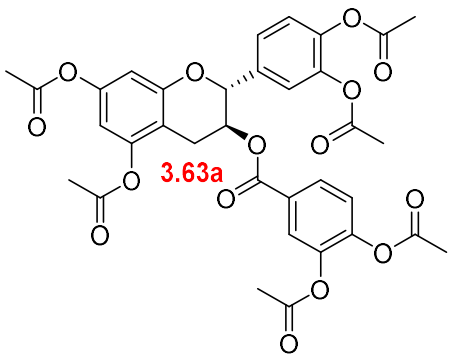

General procedure 11 was followed using (*2R*,*3S*)-2-(3,4-dihydroxyphenyl)-5,7-dihydroxychroman-3-yl 3,4-dihydroxybenzoate **3.48d** (20.1 mg, 0.047 mmol) and acetic anhydride (120 µL, 1.17 mmol) in pyridine (200 µL). After stirring at room temperature for 1 day, the reaction was monitored by TLC (hexanes:EtOAc 1:1; UV). 4-((((*2R*,*3S*)-5,7-diacetoxy-2-(3,4-diacetoxyphenyl)chroman-3-yl)oxy)carbonyl)-1,2-phenylene diacetate **3.63a** was obtained as a colorless solid (28.3 mg, 89% yield). $[\alpha]_D^{23}$ = 53° (*c* = 0.81 in CH_3Cl); ^1H NMR (396 MHz, $CDCl_3$) δ 7.92 – 7.59 (m, 2H), 7.40 – 7.06 (m, 4H), 6.69 (s, 1H), 6.63 (s, 1H), 5.56 – 5.43 (m, 1H), 5.30 (d, *J* = 5.8 Hz, 1H), 3.00 (d, *J* = 16.7 Hz, 1H), 2.79 (dd, *J* = 16.2, 5.3 Hz, 1H), 2.54 – 2.11 (m, 18H); ^{13}C NMR (100 MHz, CD_3Cl) δ 169.0, 168.5, 168.1, 167.7, 164.2, 154.5, 150.0, 149.6, 146.4, 142.3, 142.3, 142.1, 136.1, 128.5, 128.1, 125.3, 124.5, 123.9, 123.7, 121.8, 110.1, 109.0, 107.8, 77.8, 69.6, 24.1, 22.3, 21.2, 20.9, 20.8; HRMS calcd for $C_{34}H_{31}O_{15}$ (M+ H^+) 679.1663; found 679.1669; IR (ATR, cm^{-1}) υ_{max} 2938, 1765, 1724, 1594, 1506, 1261, 1110; mp: dec.

(*2R*,*3S*)-3-((3,4-Bis(propionyloxy)benzoyl)oxy)-2-(3,4-bis(propionyloxy)phenyl) chromane-5,7-diyl dipropionate (3.63b)

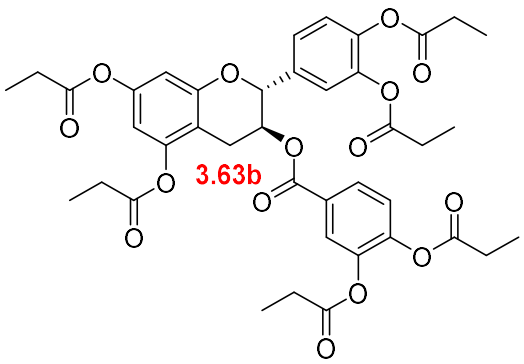

General procedure 11 was followed using (*2R*,*3S*)-2-(3,4-dihydroxyphenyl)-5,7-dihydroxychroman-3-yl 3,4-dihydroxybenzoate **3.48d** (19.9 mg, 0.047 mmol) and propionic anhydride (150 µL, 1.17 mmol) in pyridine (200 µL). After stirring at room temperature for 1 day, the reaction was monitored by TLC (hexanes:EtOAc 3:1; UV). The crude mixture was purified by column chromatography using 25% EtOAc in hexane as an isocratic eluent system to obtain (*2R*,*3S*)-3-((3,4-bis(propionyloxy)benzoyl)oxy)-2-(3,4-bis(propionyloxy)phenyl) chromane-5,7-diyl dipropionate **3.63b** as colorless liquid (24.0 mg, 67% yield). $[\alpha]_D^{23} = 44°$ (*c* = 1.05 in CH_3Cl); ^1H NMR (396 MHz, $CDCl_3$) δ 7.81 (dd, *J* = 8.5, 2.0 Hz, 1H), 7.75 (d, *J* = 2.0 Hz, 1H), 7.30 – 7.23 (m, 3H), 7.18 (d, *J* = 8.3 Hz, 1H), 6.69 (d, *J* = 2.2 Hz, 1H), 6.63 (d, *J* = 2.2 Hz, 1H), 5.48 (q, *J* = 6.0 Hz, 1H), 5.30 (d, *J* = 6.1 Hz, 1H), 2.98 (dd, *J* = 16.9, 5.1 Hz, 1H), 2.78 (dd, *J* = 16.8, 6.3 Hz, 1H), 2.63 – 2.50 (m, 12H), 1.30 – 1.20 (m, 18H); ^{13}C NMR (100 MHz, $CDCl_3$) δ 172.5, 172.0, 171.6, 171.5, 171.2, 164.3, 154.5, 150.2, 149.6, 146.6, 142.4, 142.3, 142.2, 136.0, 128.4, 128.0, 125.3, 124.3, 123.9, 123.7, 121.7, 110.0, 109.0, 107.7, 77.8, 69.6, 27.9, 27.6 (x 2), 27.5 (x 2), 24.0, 9.2, 9.1; HRMS calcd for $C_{40}H_{43}O_{15}$ ($M+H^+$) 763.2602; found 763.2617; IR (ATR, cm^{-1}) υ_{max} 2984, 2947, 2888, 1762, 1722, 1594, 1505, 1259, 1108.

(*2R*,*3S*)-3-((3,4-Bis(butyryloxy)benzoyl)oxy)-2-(3,4-bis(butyryloxy)phenyl)chromane-5,7-diyl dibutyrate (3.63c)

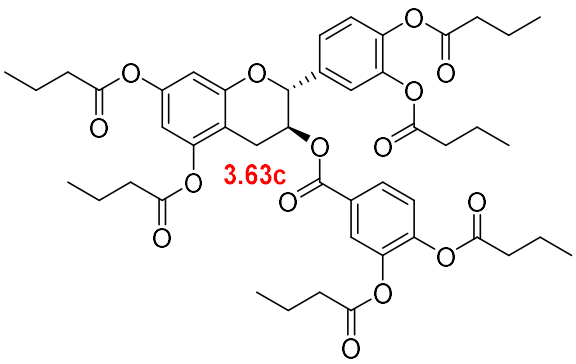

General procedure 11 was followed using (*2R*,*3S*)-2-(3,4-dihydroxyphenyl)-5,7-dihydroxychroman-3-yl 3,4-dihydroxybenzoate **3.48d** (15.6 mg, 0.037 mmol) and butyric anhydride (150 µL, 1.15 mmol) in pyridine (200 µL). After stirring at room temperature for 1 day, the reaction was monitored by TLC (hexanes:EtOAc 3:1; UV). The crude mixture was purified by column chromatography using 20% EtOAc in hexane as an isocratic eluent system to obtain (*2R*,*3S*)-3-((3,4-bis(butyryloxy)benzoyl)oxy)-2-(3,4-bis(butyryloxy)phenyl) chromane-5,7-diyl dibutyrate **3.63c** as colorless liquid (14.5 mg, 47% yield). $[\alpha]_D^{23}$ = 43° (*c* = 0.60 in CH_3Cl); ^{1}H NMR (396 MHz, $CDCl_3$) δ 7.80 (dd, *J* = 8.5, 2.0 Hz, 1H), 7.74 (d, *J* = 2.0 Hz, 1H), 7.29 – 7.21 (m, 3H), 7.17 (d, *J* = 8.4 Hz, 1H), 6.68 (d, *J* = 2.2 Hz, 1H), 6.61 (d, *J* = 2.2 Hz, 1H), 5.47 (q, *J* = 5.9 Hz, 1H), 5.30 (d, *J* = 6.1 Hz, 1H), 2.98 (dd, *J* = 16.8, 5.1 Hz, 1H), 2.77 (dd, *J* = 16.8, 6.3 Hz, 1H), 2.60 – 2.41 (m, 12H), 1.84 – 1.67 (m, 12H), 1.10 – 0.93 (m, 18H); ^{13}C NMR (100 MHz, $CDCl_3$) δ 171.7, 171.2, 170.8, 170.4, 164.3, 154.5, 150.1, 149.6, 146.6, 142.4, 142.3, 142.2, 136.1, 128.4, 128.0, 125.3, 124.4, 123.9, 123.8, 121.8, 110.0, 109.0, 107.7, 77.8, 69.6, 36.3, 36.1, 36.0 (x 2), 35.9, 24.1, 18.5, 18.4, 13.8; HRMS calcd for $C_{46}H_{55}O_{15}$ (M+ H^+) 847.3541; found 847.3502; IR (ATR, cm^{-1}) υ_{max} 2967, 2938, 2877, 1764, 1725, 1595, 1506, 1258, 1127.

(*2R*,*3S*)-3-((3,4-Bis(pentanoyloxy)benzoyl)oxy)-2-(3,4-bis(pentanoyloxy)phenyl) chromane-5,7-diyl dipentanoate (3.63d)

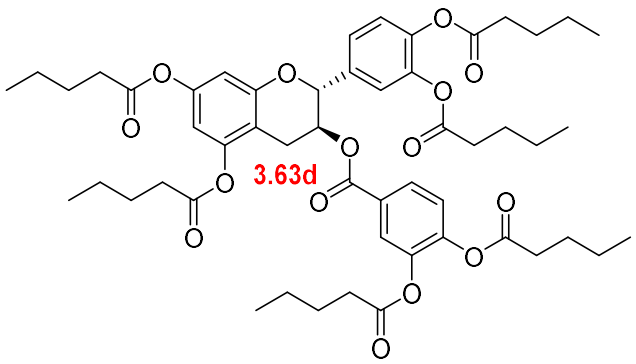

General procedure 11 was followed using (*2R*,*3S*)-2-(3,4-dihydroxyphenyl)-5,7-dihydroxychroman-3-yl 3,4-dihydroxybenzoate **3.48d** (15.0 mg, 0.035 mmol) and *Valeric anhydride* (180 µL, 0.90 mmol) in pyridine (250 µL). After stirring at room temperature for 1 day, the reaction was monitored by TLC (hexanes:EtOAc 9:1; UV). The crude mixture was purified by column chromatography using 10% to 12.5% EtOAc in hexane as a gradient eluent system and kept under reduced pressure at 60 °C for 30 minutes. (*2R*,*3S*)-3-((3,4-Bis(pentanoyloxy)benzoyl)oxy)-2-(3,4-bis(pentanoyloxy)phenyl)chromane-5,7-diyl dipentanoate **3.63d** was obtained as colorless liquid (17.4 mg, 53% yield). $[\alpha]_D^{23}$ = 36° (*c* = 1.47 in CH_3Cl); ^{1}H NMR (396 MHz, $CDCl_3$) δ 7.80 (d, *J* = 8.5 Hz, 1H), 7.74 (d, *J* = 1.6 Hz, 1H), 7.30 – 7.19 (m, 3H), 7.17 (d, *J* = 8.4 Hz, 1H), 6.67 (d, *J* = 1.6 Hz, 1H), 6.60 (d, *J* = 1.8 Hz, 1H), 5.47 (q, *J* = 5.8 Hz, 1H), 5.30 (d, *J* = 6.0 Hz, 1H), 2.97 (dd, *J* = 16.8, 4.9 Hz, 1H), 2.77 (dd, *J* = 16.8, 6.2 Hz, 1H), 2.60 – 2.46 (m, 12H), 1.80 – 1.64 (m, 12H), 1.51 – 1.34 (m, 12H), 1.03 – 0.89 (m, 18H); ^{13}C NMR (100 MHz, $CDCl_3$) δ 171.9, 171.4, 171.0, 170.6, 164.3, 154.5, 150.1, 149.6, 146.6, 142.5, 142.4, 142.2, 136.1, 128.3, 128.0, 125.3, 124.4, 123.9, 123.8, 121.8, 110.0, 109.0, 107.7, 77.8, 69.6, 34.2, 34.0, 33.9 (x 2), 33.8, 27.0, 26.9, 24.1, 22.4, 13.8; HRMS calcd for $C_{52}H_{67}O_{15}$ (M+ H^+) 931.4480; found 931.4487; IR (ATR, cm^{-1}) υ_{max} 2960, 2933, 2875, 1764, 1725, 1595, 1505, 1257, 1128.

(*2R*,*3S*)-3-((3,4-Bis(hexanoyloxy)benzoyl)oxy)-2-(3,4-bis(hexanoyloxy)phenyl)chromane-5,7-diyl dihexanoate (3.63e)

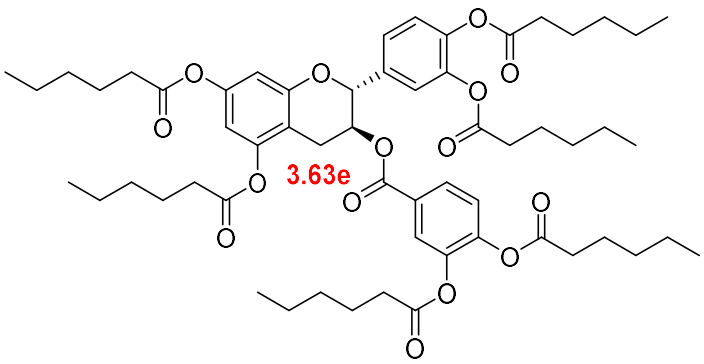

General procedure 11 was followed using (*2R*,*3S*)-2-(3,4-dihydroxyphenyl)-5,7-dihydroxychroman-3-yl 3,4-dihydroxybenzoate **3.48d** (15.0 mg, 0.035 mmol) and *hexanoic anhydride* (200 µL, 0.90 mmol) in pyridine (250 µL). After stirring at room temperature for 1 day, the reaction was monitored by TLC (hexanes:EtOAc 9:1; UV). The crude mixture was purified by column chromatography using 10% to 12.5% EtOAc in hexane as a gradient eluent system and kept under reduced pressure at 60 °C for 30 minutes. (*2R*,*3S*)-3-((3,4-Bis(hexanoyloxy)benzoyl)oxy)-2-(3,4-bis(hexanoyloxy)phenyl)chromane-5,7-diyl dihexanoate **3.63e** was obtained as colorless liquid (18.7 mg, 52% yield). $[\alpha]_D^{23} = 35°$ ($c = 0.92$ in CH_3Cl); ^1H NMR (396 MHz, $CDCl_3$) δ 7.79 (d, $J = 8.5$ Hz, 1H), 7.74 (d, $J = 1.2$ Hz, 1H), 7.29 – 7.20 (m, 3H), 7.17 (d, $J = 8.3$ Hz, 1H), 6.67 (s, 1H), 6.60 (s, 1H), 5.47 (q, $J = 5.6$ Hz, 1H), 5.29 (d, $J = 6.0$ Hz, 1H), 2.98 (dd, $J = 16.9$, 4.9 Hz, 1H), 2.77 (dd, $J = 16.8$, 6.3 Hz, 1H), 2.58 – 2.46 (m, 12H), 1.81 – 1.65 (m, 12H), 1.46 – 1.27 (m, 24H), 0.99 – 0.83 (m, 18H); ^{13}C NMR (100 MHz, $CDCl_3$) δ 171.9, 171.4, 171.0, 170.6, 164.3, 154.5, 150.1, 149.6, 146.6, 142.5, 142.4, 142.2, 136.0, 128.3, 128.0, 125.3, 124.4, 123.9, 123.8, 121.8, 110.0, 109.0, 107.7, 77.8, 69.6, 34.5, 34.3, 34.2, 34.1, 34.0, 31.4, 24.7, 24.1, 22.4, 22.3, 14.0; HRMS calcd for $C_{58}H_{79}O_{15}$ ($M+ H^+$) 1015.5419; found 1015.5449; IR (ATR, cm^{-1}) υ_{max} 2958, 2932, 2870, 1766, 1723, 1598, 1259, 1130.

3.14 References

1. von Ballmoos, C.; Wiedenmann, A.; Dimroth, P. *Annu. Rev. Biochem.* **2009,** *78*, 649-72.

2. Stock, D.; Leslie, A. G.; Walker, J. E. *Science* **1999,** *286* (5445), 1700-5.

3. Wilkens, S.; Dahlquist, F. W.; McIntosh, L. P.; Donaldson, L. W.; Capaldi, R. A. Nat. Struct. Biol. **1995,** *2* (11), 961-967.

4. Uhlin, U.; Cox, G. B.; Guss, J. M. *Structure* **1997,** *5* (9), 1219-1230.

5. Lu, P.; Lill, H.; Bald, D. *Biochim. Biophys. Acta. Bioenerg.* **2014,** *1837* (7), 1208-1218.

6. Datta, M.; Via, L. E.; Chen, W.; Baish, J. W.; Xu, L.; Barry, C. E.; Jain, R. K. *Ann. Biomed. Eng.* **2016,** *44* (4), 863-872.

7. Suzuki, T.; Murakami, T.; Iino, R.; Suzuki, J.; Ono, S.; Shirakihara, Y.; Yoshida, M. *J. Biol. Chem.* **2003,** *278* (47), 46840-46846.

8. Feniouk, B. A.; Suzuki, T.; Yoshida, M. *J. Biol. Chem.* **2007,** *282* (1), 764-772.

9. Biuković, G.; Basak, S.; Manimekalai Malathy Sony, S.; Rishikesan, S.; Roessle, M.; Dick, T.; Rao Srinivasa, P. S.; Hunke, C.; Grüber, G. *Antimicrob. Agents Chemother.* **2013,** *57* (1), 168-176.

10. Morales-Ríos, E.; De la Rosa-Morales, F.; Mendoza-Hernández, G.; Rodríguez-Zavala, J. S.; Celis, H.; Zarco-Zavala, M.; García-Trejo, J. J. *FASEB J.* **2010,** *24* (2), 599-608.

11. Preiss, L.; Langer, J. D.; Yildiz, Ö.; Eckhardt-Strelau, L.; Guillemont, J. E. G.; Koul, A.; Meier, T. *Sci. Adv.* **2015,** *1* (4), e1500106-e1500106.

12. Joon, S.; Ragunathan, P.; Sundararaman, L.; Nartey, W.; Kundu, S.; Manimekalai, M. S. S. *FEBS J.* **2018,** *285* (6), 1111-1128.

13. Saw, W.-G.; Wu, M.-L.; Ragunathan, P.; Biuković, G.; Lau, A.-M.; Shin, J.; Harikishore, A.; Cheung, C.-Y.; Hards, K.; Sarathy, J. P.; Bates, R. W.; Cook, G. M.; Dick, T.; Grüber, G. *Sci. Rep.* **2019,** *9* (1), 16759.

14. Bhagwat, S.; Haytowitz, D. B.; Holden, J. M. *USDA Database for the Flavonoid Content of Selected Foods, Release 3*; Agricultural Research Service, U.S. Department of Agriculture.: 2011.

15. Zhong, Y.; Shahidi, F. *J. Agric. Food Chem.* **2011,** *59* (12), 6526-6533.

16. Kanlaya, R.; Thongboonkerd, V. *CDN.* **2019,** *3* (9).

17. Eng, Q. Y.; Thanikachalam, P. V.; Ramamurthy, S. *J Ethnopharmacol.* **2018,** *210*, 296-310.

18. Batista Gde, A.; Cunha, C. L.; Scartezini, M.; von der Heyde, R.; Bitencourt, M. G.; Melo, S. F. *Arq. Bras. Cardiol.* **2009,** *93* (2), 128-34.

19. Vázquez Cisneros, L. C.; López-Uriarte, P.; López-Espinoza, A.; Navarro Meza, M.; Espinoza-Gallardo, A. C.; Guzmán Aburto, M. B. *Nutr. Hosp.* **2017,** *34* (3), 731-737.

20. Fujimura, Y.; Tachibana, H.; Maeda-Yamamoto, M.; Miyase, T.; Sano, M.; Yamada, K. *J. Agric. Food Chem.* **2002,** *50* (20), 5729-34.

21. Aggarwal, V.; Tuli, H. S.; Tania, M.; Srivastava, S.; Ritzer, E. E.; Pandey, A.; Aggarwal, D.; Barwal, T. S.; Jain, A.; Kaur, G.; Sak, K.; Varol, M.; Bishayee, A. *Semin. Cancer. Biol.* **2020**.

22. Chen, B.-H.; Hsieh, C.-H.; Tsai, S.-Y.; Wang, C.-Y.; Wang, C.-C. *Sci. Rep.* **2020,** *10* (1), 5163.

23. Li, X.; Li, S.; Chen, M.; Wang, J.; Xie, B.; Sun, Z. *Food Funct.* **2018,** *9* (9), 4651-4663.

24. Zhang, Y. M.; Rock, C. O. *J. Biol. Chem.* **2004,** *279* (30), 30994-1001.

25. Moreno-Vásquez, M. J.; Plascencia-Jatomea, M.; Sánchez-Valdes, S.; Tanori-Córdova, J. C.; Castillo-Yañez, F. J.; Quintero-Reyes, I. E.; Graciano-Verdugo, A. Z. *Polymers* **2021,** *13* (9), 1375.

26. Si, W.; Gong, J.; Tsao, R.; Kalab, M.; Yang, R.; Yin, Y. *J. Chromatogr. A.* **2006,** *1125*, 204–210.

27. Yoda, Y.; Hu, Z.-Q.; Shimamura, T.; Zhao, W.-H. *J. Infect. Chemother.* **2004,** *10* (1), 55-58.

28. Yanagawa, Y.; Yamamoto, Y.; Hara, Y.; Shimamura, T. *Curr. Microbiol.* **2003,** *47* (3), 244-9.

29. Das, S.; Tanwar, J.; Hameed, S.; Fatima, Z. *J. Biochem. Pharmacol. Res.* **2014,** *2*, 167-174.

30. Bae, J.; Kim, N.; Shin, Y.; Kim, S.-Y.; Kim, Y.-J. *Biomed. Dermatol.* **2020,** *4* (1), 8.

31. Taylor, P. W.; Hamilton-Miller, J. M. T.; Stapleton, P. D. *Food Sci. Technol. Bull.* **2005,** *2*, 71-81.

32. Ohmori, Y.; Ito, M.; Kishi, M.; Mizutani, H.; Katada, T.; Konishi, H. *Biol. Pharm. Bull.* **1995,** *18* (5), 683-6.

33. Hamilton-Miller, J. M.; Shah, S. *J. Antimicrob. Chemother.* **2000,** *46* (5), 852-3.

34. Brown, R. A. M.; Richardson, K. L.; Kabir, T. D.; Trinder, D.; Ganss, R.; Leedman, P. J. *Front. Oncol.* **2020,** *10*, 476-476.

35. Huang, S.-T.; Hung, Y.-A.; Yang, M.-J.; Chen, I.-Z.; Yuann, J.-M. P.; Liang, J.-Y. *Molecules (Basel, Switzerland)* **2019,** *24* (4), 787.

36. Xu, Y.-Q.; Yu, P.; Zhou, W. *J. Food Eng.* **2019,** *250*, 46-54.

37. Mehta, P. P.; Whalley, W. B. *J. Chem. Soc. (Resumed)* **1963,** (0), 5327-5332.

38. Weerawatanakorn, M.; Hung, W.-L.; Pan, M.-H.; Li, S.; Li, D.; Wan, X.; Ho, C.-T. *Food Sci. Hum. Wellness.* **2015,** *4* (4), 133-146.

39. Zhu, Q. Y.; Zhang, A.; Tsang, D.; Huang, Y.; Chen, Z.-Y. *J. Agric. Food Chem.* **1997,** *45* (12), 4624-4628.

40. Mochizuki, M.; Yamazaki, S.-i.; Kano, K.; Ikeda, T. *Biochim. Biophys. Acta - Gen. Subj.* **2002,** *1569* (1), 35-44.

41. Lipinski, C. A.; Lombardo, F.; Dominy, B. W.; Feeney, P. J. *Adv. Drug Deliv. Rev.* **2001,** *46* (1), 3-26.

42. Veber, D. F.; Johnson, S. R.; Cheng, H.-Y.; Smith, B. R.; Ward, K. W.; Kopple, K. D. *J. Med. Chem.* **2002,** *45* (12), 2615-2623.

43. Vincent, A. T.; Nyongesa, S.; Morneau, I.; Reed, M. B.; Tocheva, E. I.; Veyrier, F. J. *Front. microbiol.* **2018,** *9* (2341).

44. Piccaro, G.; Poce, G.; Biava, M.; Giannoni, F.; Fattorini, L. *J. Antibiot.* **2015,** *68* (11), 711-714.

45. Beaumont, K.; Webster, R.; Gardner, I.; Dack, K. *Curr. Drug Metab.* **2003,** *4* (6), 461-85.

46. Li, L.; Chan, T. H. *Org. Lett.* **2001,** *3* (5), 739-741.

47. Zaveri, N. T. *Org. Lett.* **2001,** *3* (6), 843-846.

48. Ohmori, K.; Yano, T.; Suzuki, K. *Org. Biomol. Chem.* **2010,** *8* (12), 2693-2696.

49. Machado, A.; Sousa, M.; Patto, D.; Azevedo, L.; Bombonato, F.; Correia, C. *Tetrahedron Lett.* **2009,** *50*, 1222.

50. Waddell, L. J. N.; Watts, O. F. B.; Saetang, P.; Rukachaisirikul, V.; Bates, R. W. *Tetrahedron Lett.* **2020,** *61* (27), 152078.

51. Bates, R. W.; Kasinathan, S. *Tetrahedron* **2013,** *69* (14), 3088-3092.

52. Heravi, M. M.; Zadsirjan, V.; Esfandyari, M.; Lashaki, T. B. *Tetrahedron: Asymmetry* **2017,** *28* (8), 987-1043.

53. Tang, Y.; Jiang, C.; Zhang, X.; Liu, C.; Lin, J.; Wang, Y.; Du, C.; Peng, X.; Li, W.; Liu, Y.; Cheng, M. *J. Org. Chem.* **2017,** *82* (20), 11102-11109.

54. Deme, E. *J. Org. Chem.* **1976,** *41* (23), 3769.

55. Lehmann, M.; Jahr, M. *Org Lett* **2006,** *8* (4), 721-3.

56. Liu, Q.; Guo, T.; Li, W.; Li, D.; Feng, Z. *Arch. Pharm.* **2012,** *345* (10), 771-783.

57. Kawamoto, H.; Nakatsubo, F.; Murakami, K. *Synth. Commun.* **1996,** *26* (3), 531-534.

58. Nevado, C.; Echavarren, A. M. *Chem. Eur. J.* **2005,** *11* (10), 3155-3164.

59. Yip, S. Y. Y.; Aïssa, C. *Angew. Chem. Int. Ed.* **2015,** *54* (23), 6870-6873.

60. Bergens, S. H.; Bosnich, B. *J. Am. Chem. Soc.* **1991,** *113* (3), 958-967.

61. Minato, M.; Yamamoto, K.; Tsuji, J. *J. Org. Chem.* **1990,** *55* (2), 766-768.

62. VanRheenen, V.; Kelly, R. C.; Cha, D. Y. *Tetrahedron Lett.* **1976,** *17* (23), 1973-1976.

63. Kasinathan, S. Application of hydroformylation for the stereoselective synthesis of piperidine alkaloids. Nanyang Technological University, Singapore, Unpublished doctoral dissertation, 2014.

64. Larson, D. P.; Heathcock, C. H. *J. Org. Chem.* **1996,** *61* (16), 5208-5209.

65. Schroeder, M. *Chem. Rev.* **1980,** *80* (2), 187-213.

66. Es-Safi, N.-E.; Ghidouche, S.; Ducrot, P. H. *Molecules* **2007,** *12* (9), 2228-2258.

67. Minch, M. J. *Concepts Magn. Reson. A: Bridg. Educ. Res.* **1994,** *6* (1), 41-56.

68. Brown, D. S.; Bruno, M.; Davenport, R. J.; Ley, S. V. *Tetrahedron* **1989,** *45* (13), 4293-4308.

69. Hamamichi, N.; Miyasaka, T. *J. Org. Chem.* **1991,** *56* (11), 3731-3734.

70. Frick, W.; Schmidt, R. R. *Carbohydr. Res.* **1991,** *209*, 101-107.

71. Cai, M.-S.; Qiu, D.-X. *Carbohydr. Res.* **1989,** *191* (1), 125-129.

72. Allevi, P.; Anastasia, M.; Ciuffreda, P.; Fiecchi, A.; Scala, A. *J. Chem. Soc., Chem. Commun.* **1987,** (16), 1245-1246.

73. Congreve, M. S.; Davison, E. C.; Fuhry, M. A. M.; Holmes, A. B.; Payne, A. N.; Robinson, R. A.; Ward, S. E. *Synlett* **1993,** *1993* (09), 663-664.

74. Nicolaou, K. C.; Postema, M. H. D.; Claiborne, C. F. *J. Am. Chem. Soc.* **1996,** *118* (6), 1565-1566.

75. Hartley, R. C.; McKiernan, G. J. *J. Chem. Soc., Perkin Trans. 1.* **2002,** 2763-2793.

76. Cheng, K.; Wang, X.; Zhang, S.; Yin, H. *Angew. Chem. Int. Ed.* **2012,** *51* (49), 12246-12249.

77. Dou, Q. P.; Chan, T.-H.; Smith, D. M. Polyphenol proteasome inhibitors, synthesis, and methods of use. 2004.

78. Kurti, L.; Czako, B., *Strategic Applications of Named Reactions in Organic Synthesis*. Academic Press: 2005.

79. Jentsch, N. G.; Zhang, X.; Magolan, J. *J. Nat. Prod.* **2020,** *83* (9), 2587-2591.

80. Hotra, A.; Suter, M.; Biuković, G.; Ragunathan, P.; Kundu, S.; Dick, T.; Grüber, G. *FEBS J.* **2016,** *283* (10), 1947-1961.

81. Priya Ragunathan; School of Biological Science (SBS), Nanyang Technological University (NTU).

82. Joon Shin; School of Biological Science (SBS), Nanyang Technological University (NTU).

83. Madhavi Sastry, G.; Adzhigirey, M.; Day, T.; Annabhimoju, R.; Sherman, W. *J. Comput. Aided Mol. Des.* **2013,** *27* (3), 221-234.

84. Ghazaei, C. *J. Res. Med. Sci.* **2018,** *23*, 63.

85. Li, S.; Hu, P.; Malmstadt, N. *Anal. Chem.* **2010,** *82* (18), 7766-7771.

86. Ibrahim, Y.A., Musa, A. and Yakasai, I.A. *Nig. Journ. Pharm. Sci.* **2017,** *16*, 25-30.

87. Bhambhani, A.; Thakkar, S.; Joshi, S. B.; Russell Middaugh, C., 2 - A formulation method to improve the physical stability of macromolecular-based drug products. In *Therapeutic Protein Drug Products*, Meyer, B. K., Ed. Woodhead Publishing: 2012; pp 13-45.

88. Pires, D.; Valente, E.; Simões, M. F.; Carmo, N.; Testa, B.; Constantino, L.; Anes, E. *Antimicrob. Agents Chemother.* **2015,** *59* (12), 7693-9.

89. Balganesh, M.; Dinesh, N.; Sharma, S.; Kuruppath, S.; Nair, A. V.; Sharma, U. *Antimicrob. Agents Chemother.* **2012,** *56* (5), 2643-2651.

90. Gupta, S.; Cohen, K. A.; Winglee, K.; Maiga, M.; Diarra, B.; Bishai, W. R. *Antimicrob. Agents Chemother.* **2014,** *58* (1), 574-576.

91. Koul, A.; Dendouga, N.; Vergauwen, K.; Molenberghs, B.; Vranckx, L.; Willebrords, R.; Ristic, Z.; Lill, H.; Dorange, I.; Guillemont, J.; Bald, D.; Andries, K. *Nat. Chem. Biol.* **2007,** *3* (6), 323-4.

92. Zhu, X.; Qian, B.; Wei, R.; Huang, J.-D.; Bao, H. *Green Chem.* **2018,** *20* (7), 1444-1447.

93. Wang, H.; Ma, Y.; Tian, H.; Yu, A.; Chang, J.; Wu, Y. *Tetrahedron* **2014,** *70* (16), 2669-2673.

94. Hartmann, M.; Huber, J.; Kramer, J. S.; Heering, J.; Pietsch, L.; Stark, H.; Odadzic, D.; Bischoff, I.; Fürst, R.; Schröder, M.; Akutsu, M.; Chaikuad, A.; Dötsch, V.; Knapp, S.; Biondi, R. M.; Rogov, V. V.; Proschak, E. *J. Med. Chem.* **2021,** *64* (7), 3720-3746.

95. Tian, Q.; Xu, S.; Zhang, C.; Liu, X.; Wu, X.; Li, Y. *J. Org. Chem.* **2021,** *86* (13), 8797-8804.

96. Bermudez, M.; Grabowski, M.; Murgueitio, M. S.; Tiemann, M.; Varga, P.; Rudolf, T.; Wolber, G.; Weindl, G.; Rademann, J. *Chem. Med. Chem.* **2020,** *15* (14), 1364-1371.

97. Huang, D.-M.; Li, H.-J.; Wang, J.-H.; Wu, Y.-C. *Org. Biomol. Chem.* **2018,** *16* (4), 585-592.

98. Saito, A.; Emoto, M.; Tanaka, A.; Doi, Y.; Shoji, K.; Mizushina, Y.; Ikawa, H.; Yoshida, H.; Matsuura, N.; Nakajima, N. *Tetrahedron* **2004,** *60* (52), 12043-12049.

99. Feng, L.; Yan, Q.; Zhang, B.; Tian, X.; Wang, C.; Yu, Z.; Cui, J.; Guo, D.; Ma, X.; James, T. D. *Chem. Commun.* **2019,** *55* (24), 3548-3551.

100. Dias, L. C.; Polo, E. C. *J. Org. Chem.* **2017,** *82* (8), 4072-4112.

101. Verhoest, P. R.; Chapin, D. S.; Corman, M.; Fonseca, K.; Harms, J. F.; Hou, X.; Marr, E. S.; Menniti, F. S.; Nelson, F.; O'Connor, R.; Pandit, J.; Proulx-LaFrance, C.; Schmidt, A. W.; Schmidt, C. J.; Suiciak, J. A.; Liras, S. *J. Med. Chem.* **2009,** *52* (16), 5188-5196.

102. Sayama, M.; Inoue, A.; Nakamura, S.; Jung, S.; Ikubo, M.; Otani, Y.; Uwamizu, A.; Kishi, T.; Makide, K.; Aoki, J.; Hirokawa, T.; Ohwada, T. *J. Med. Chem.* **2017,** *60* (14), 6384-6399.

103. Christensen, S. H.; Olsen, E. P. K.; Rosenbaum, J.; Madsen, R. *Org. Biomol. Chem.* **2015,** *13* (3), 938-945.

104. Jorgensen, W. T.; Gulliver, D. W.; Werry, E. L.; Reekie, T.; Connor, M.; Kassiou, M. *Eur. J. Med. Chem.* **2016,** *108*, 730-740.

105. Zhuravel, M. A.; Davis, N. E.; Nguyen, S. T.; Koltover, I. *J. Am. Chem. Soc.* **2004,** *126* (32), 9882-9883.

106. Latham, D. E.; Polidano, K.; Williams, J. M. J.; Morrill, L. C. *Org. Lett.* **2019,** *21* (19), 7914-7918.

107. Anderson, J. C.; McCarthy, R. A.; Paulin, S.; Taylor, P. W. *Bioorganic Med. Chem. Lett.* **2011,** *21* (23), 6996-7000.

108. Anderson, J. C.; Headley, C.; Stapleton, P. D.; Taylor, P. W. *Tetrahedron* **2005,** *61* (32), 7703-7711.

109. Anderson, J. C.; Grounds, H.; Reeves, S.; Taylor, P. W. *Tetrahedron* **2014,** *70* (21), 3485-3490.

110. Wan, S. B.; Chan, T. H. *Tetrahedron* **2004,** *60* (37), 8207-8211.

111. Wan, S. B.; Chen, D.; Ping Dou, Q.; Hang Chan, T. *Bioorg. Med. Chem.* **2004,** *12* (13), 3521-3527.

Appendix A

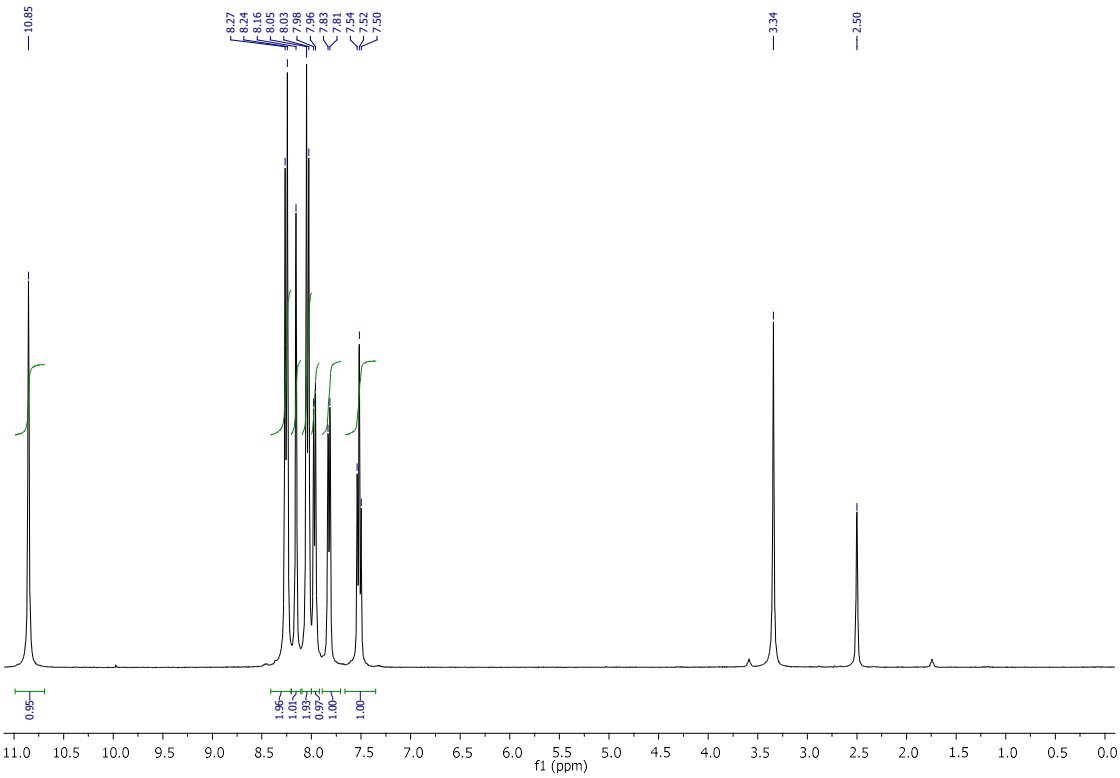

^{1}H NMR spectrum of compound **2.3**

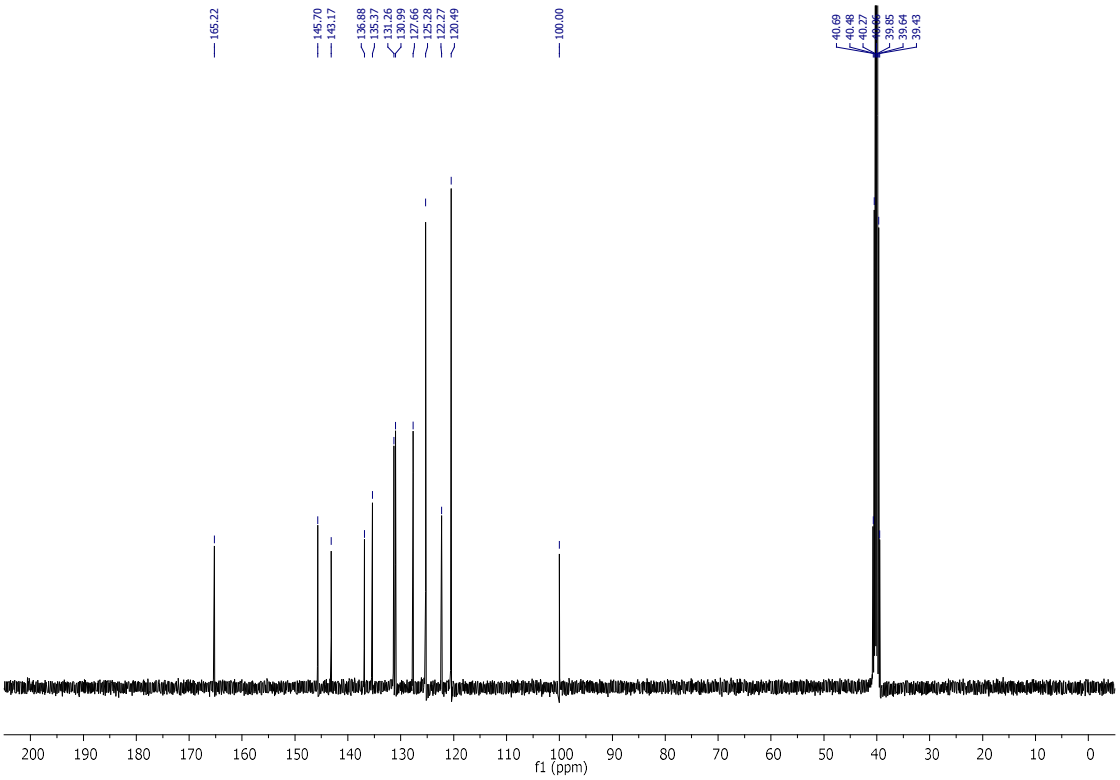

^{13}C NMR spectrum of compound **2.3**

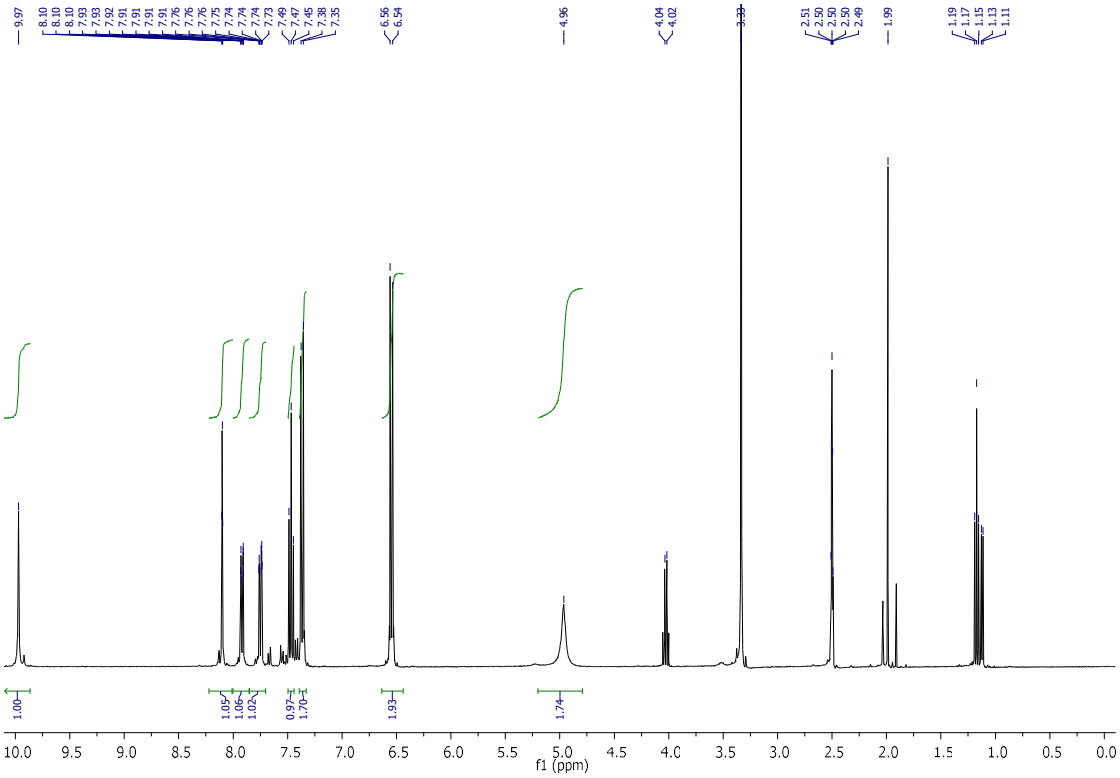

^{1}H NMR spectrum of compound **2.4**

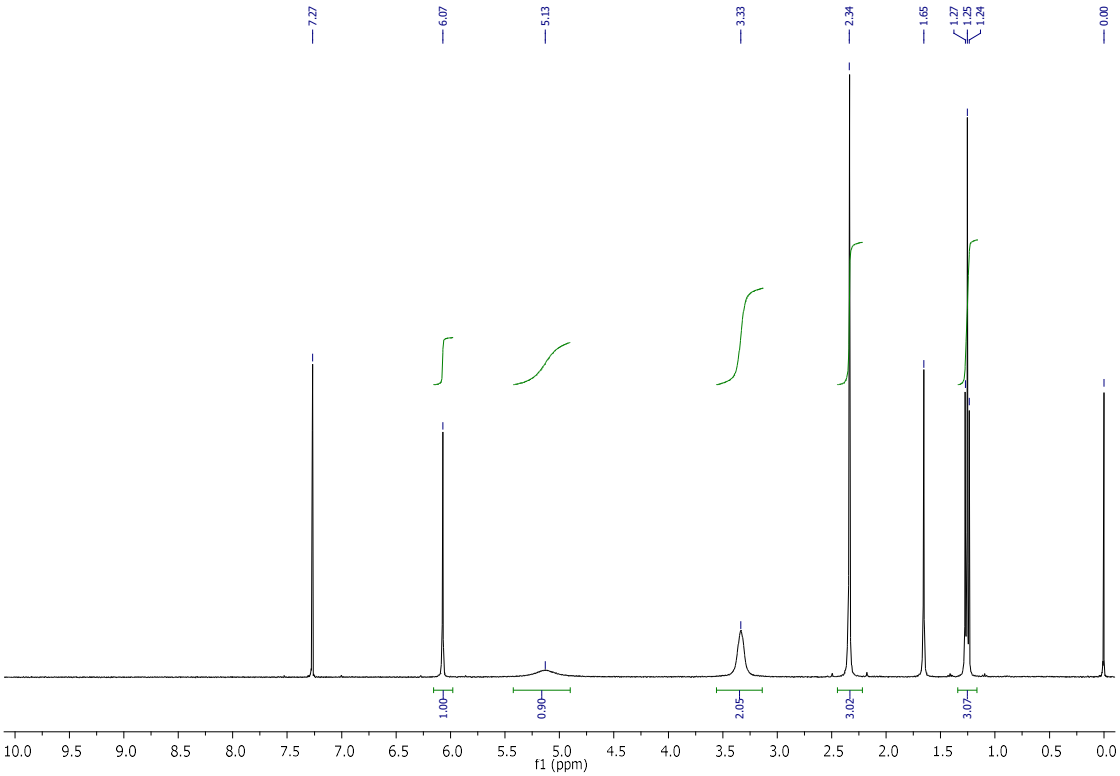

^{1}H NMR spectrum of compound **2.6**

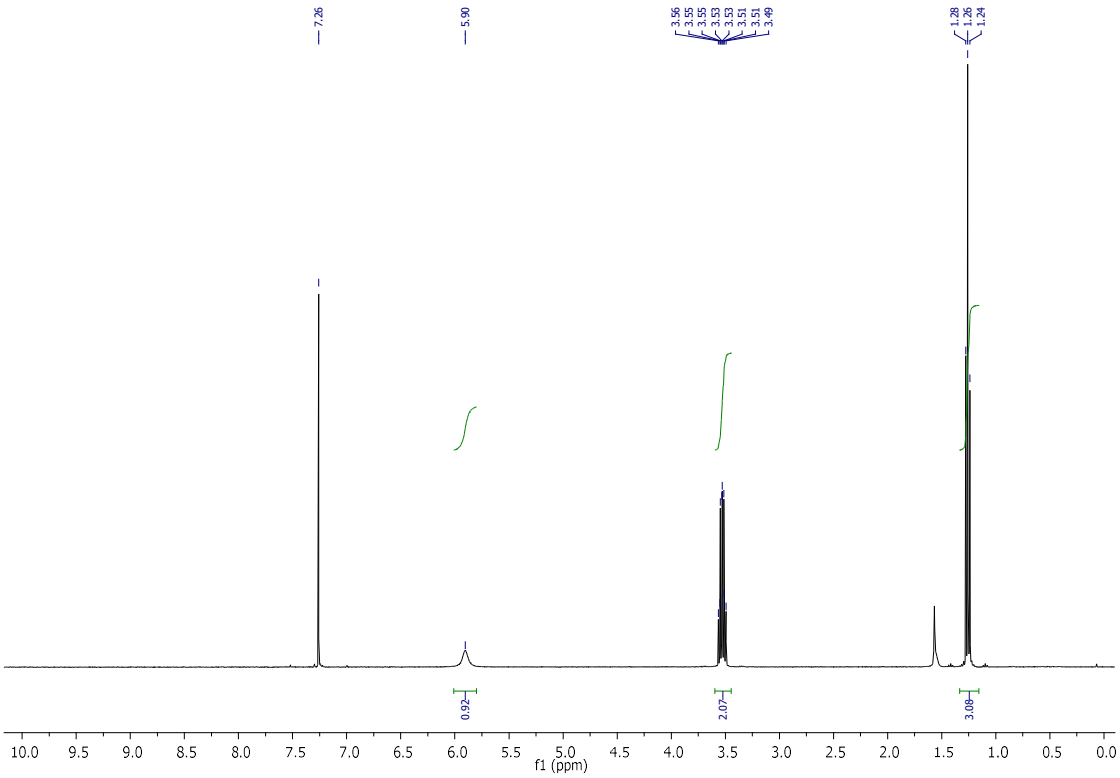

^{1}H NMR spectrum of compound **2.9**

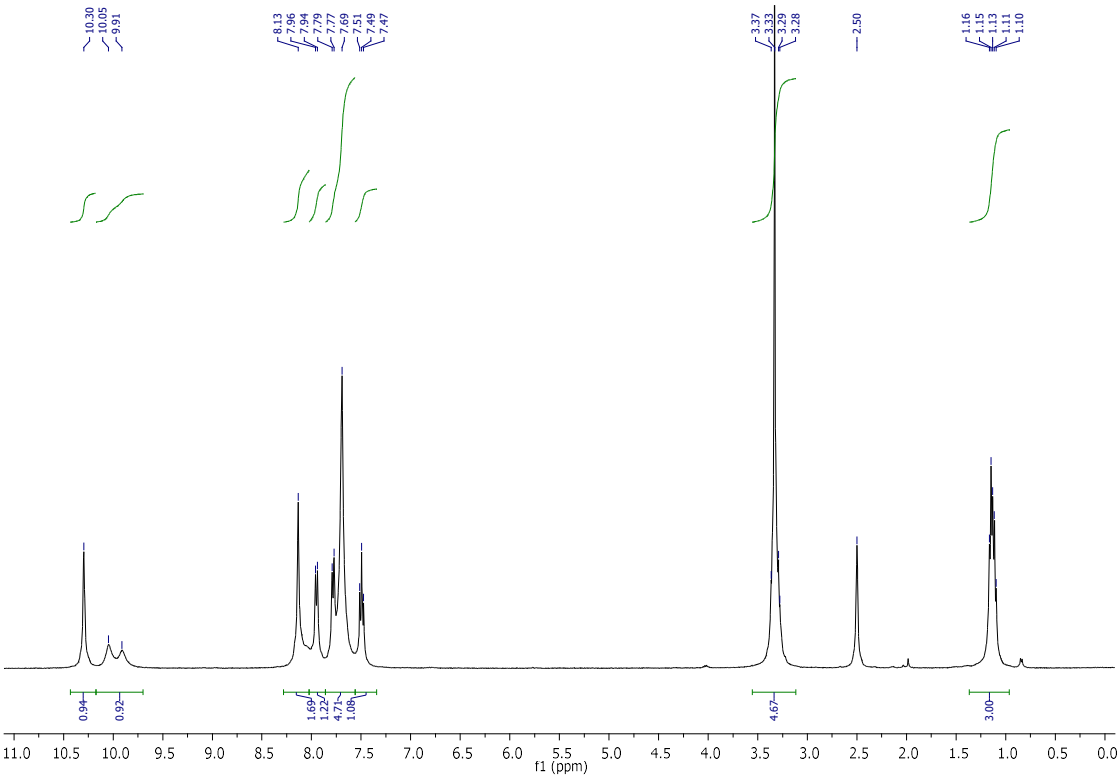

^{1}H NMR spectrum of compound **2.10**

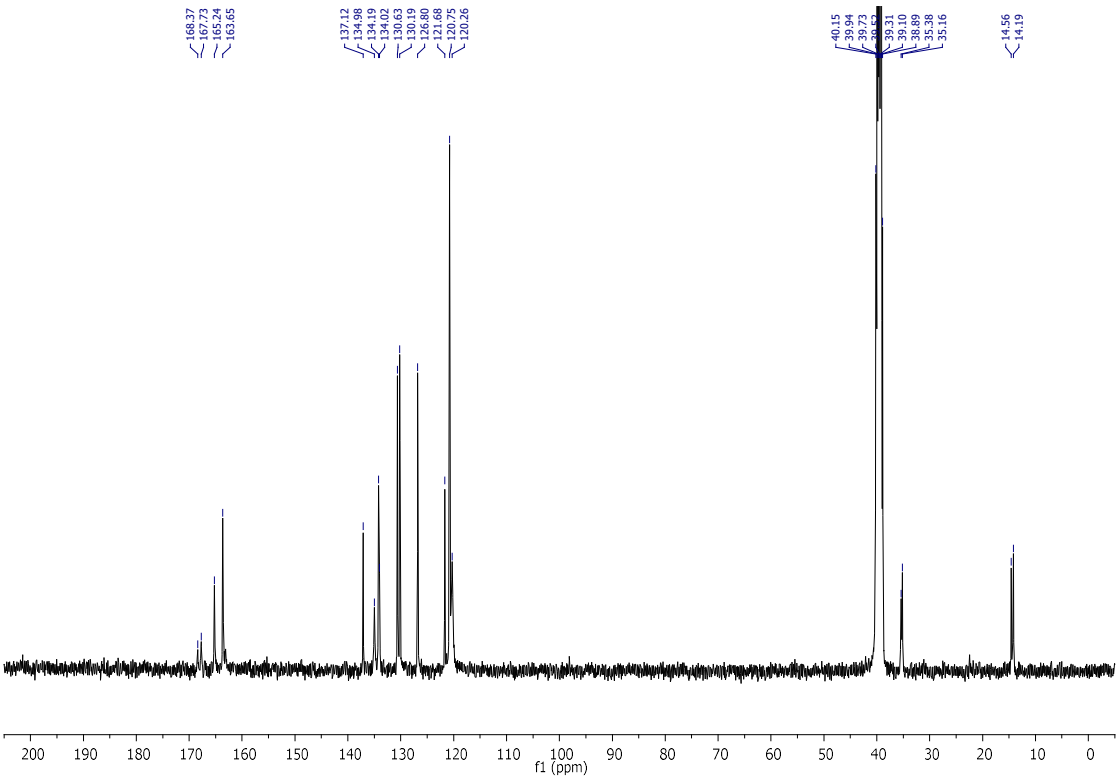

^{13}C NMR spectrum of compound **2.10**

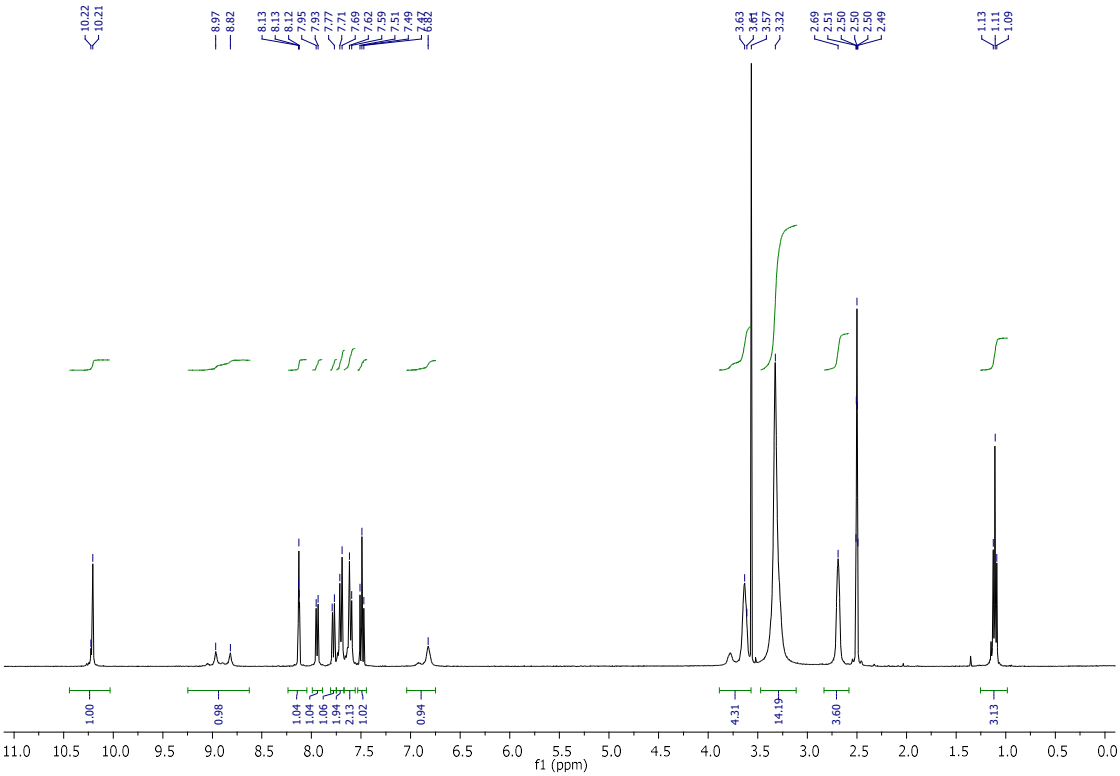

^{1}H NMR spectrum of compound **2.11**

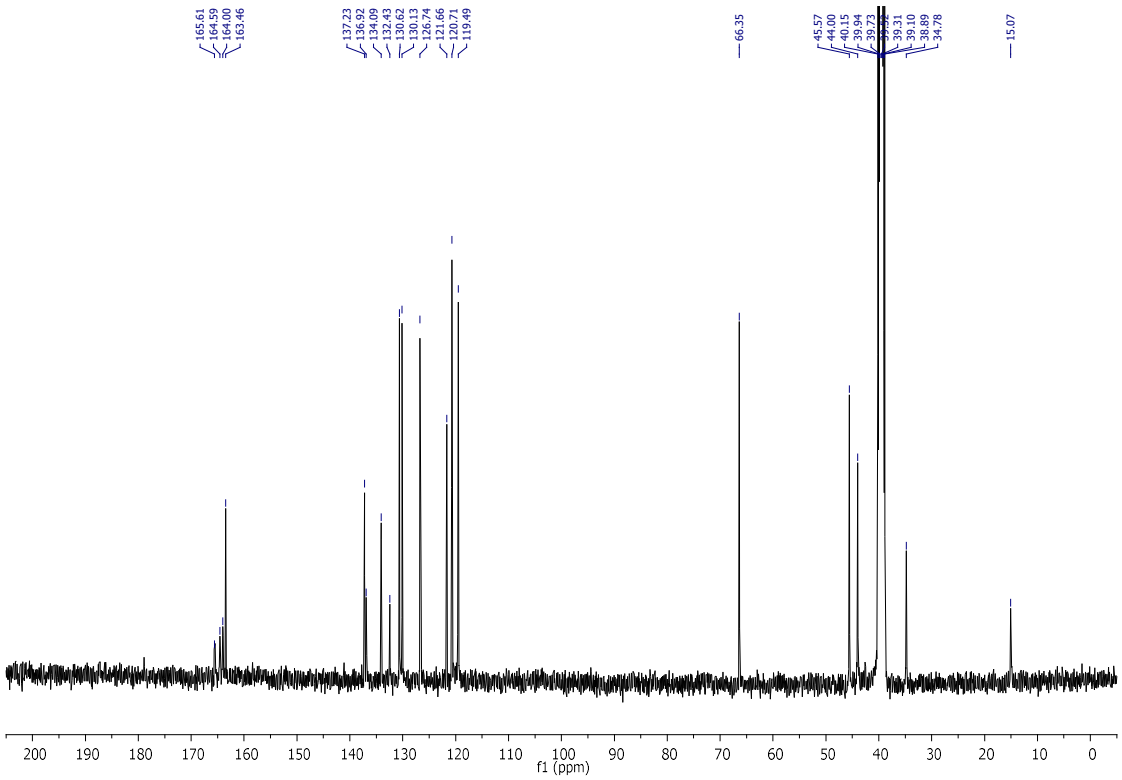

^{13}C NMR spectrum of compound **2.11**

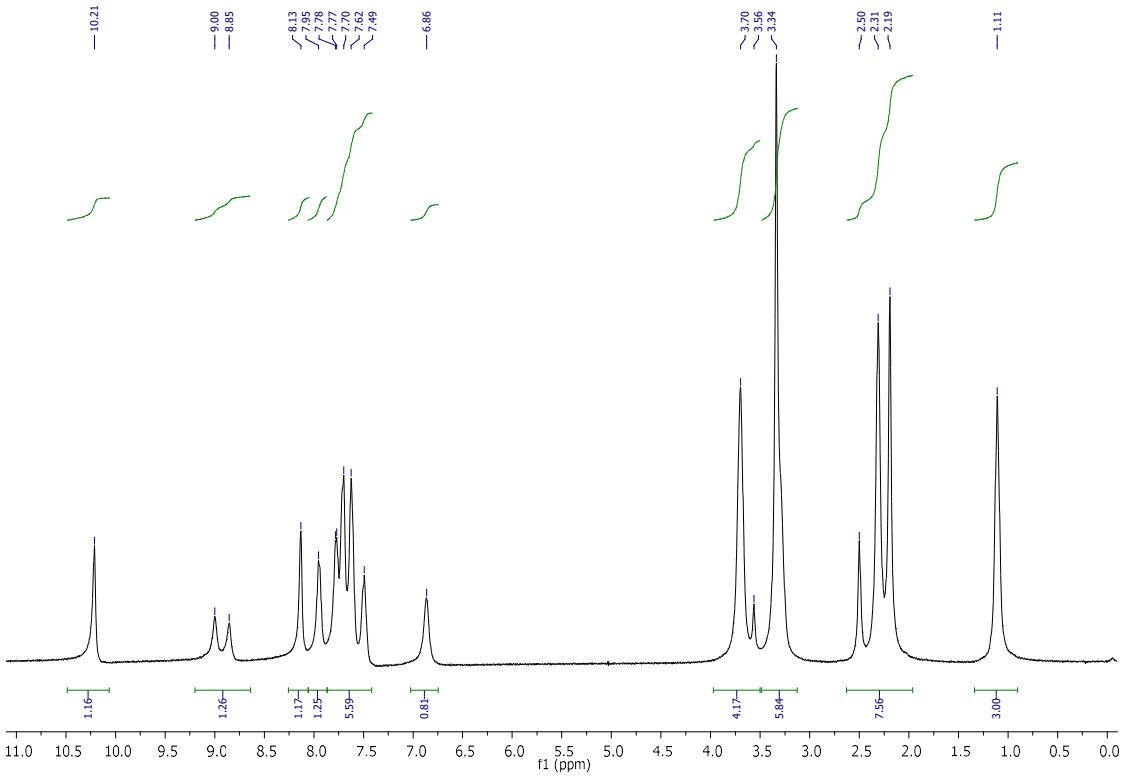

^{1}H NMR spectrum of compound **2.12**

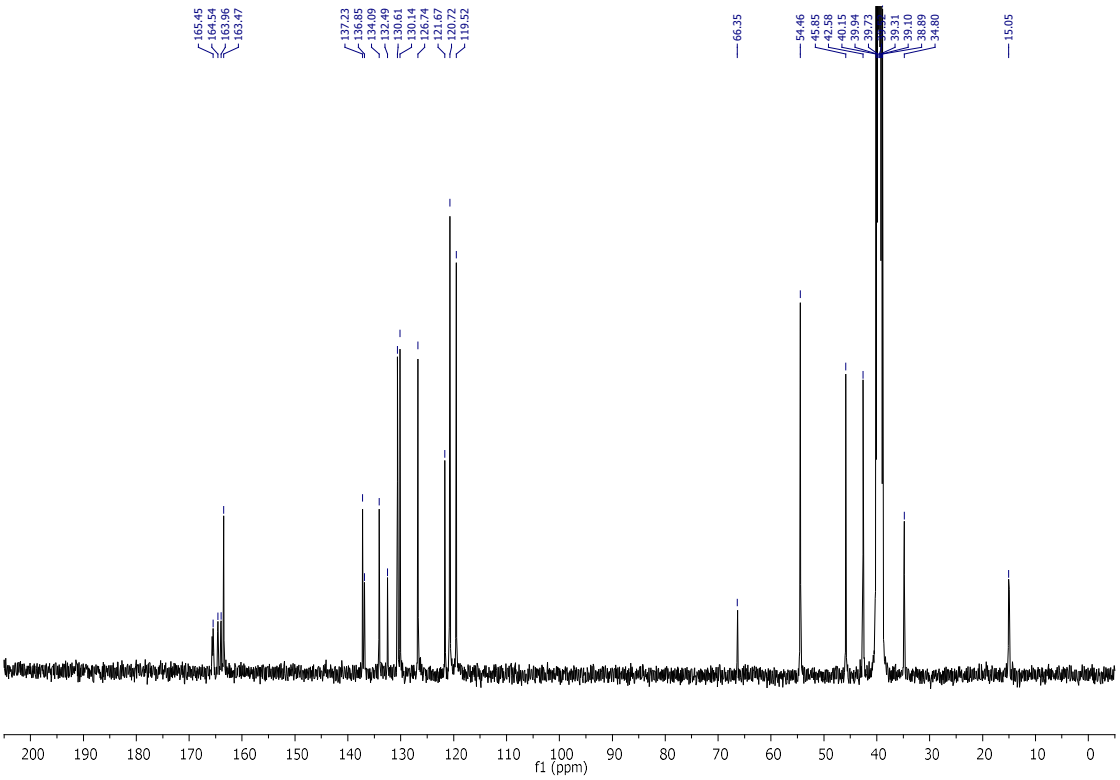

^{13}C NMR spectrum of compound **2.12**

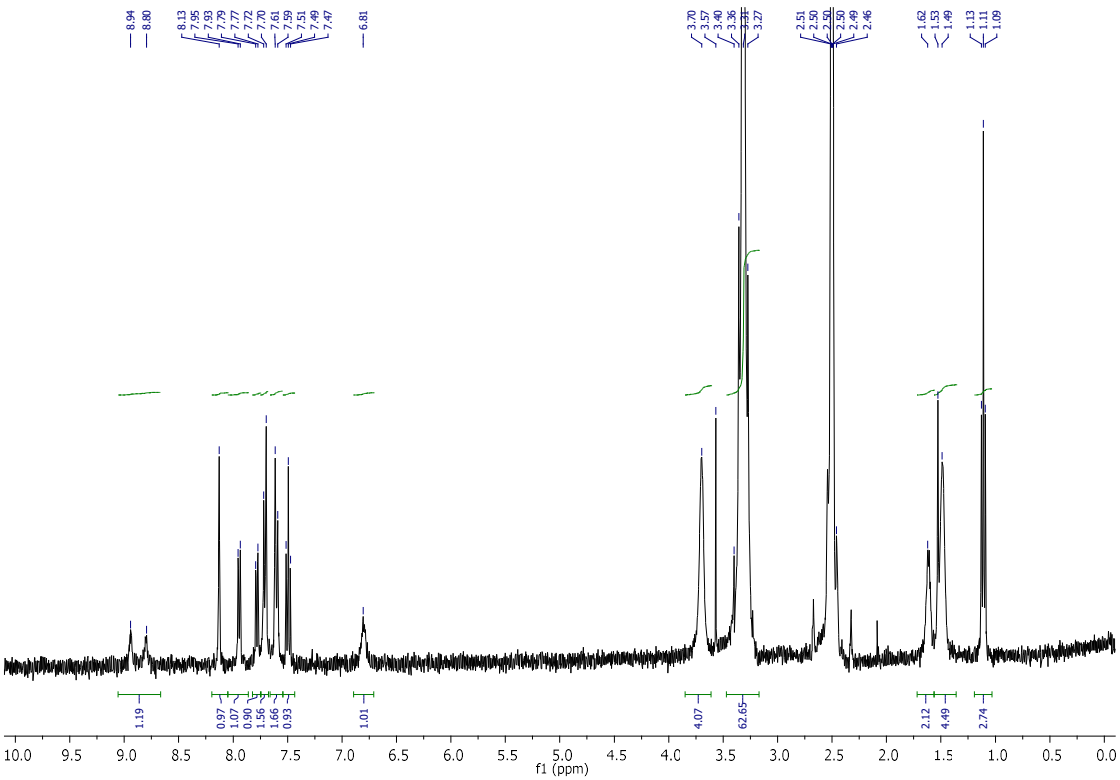

^{1}H NMR spectrum of compound **2.13**

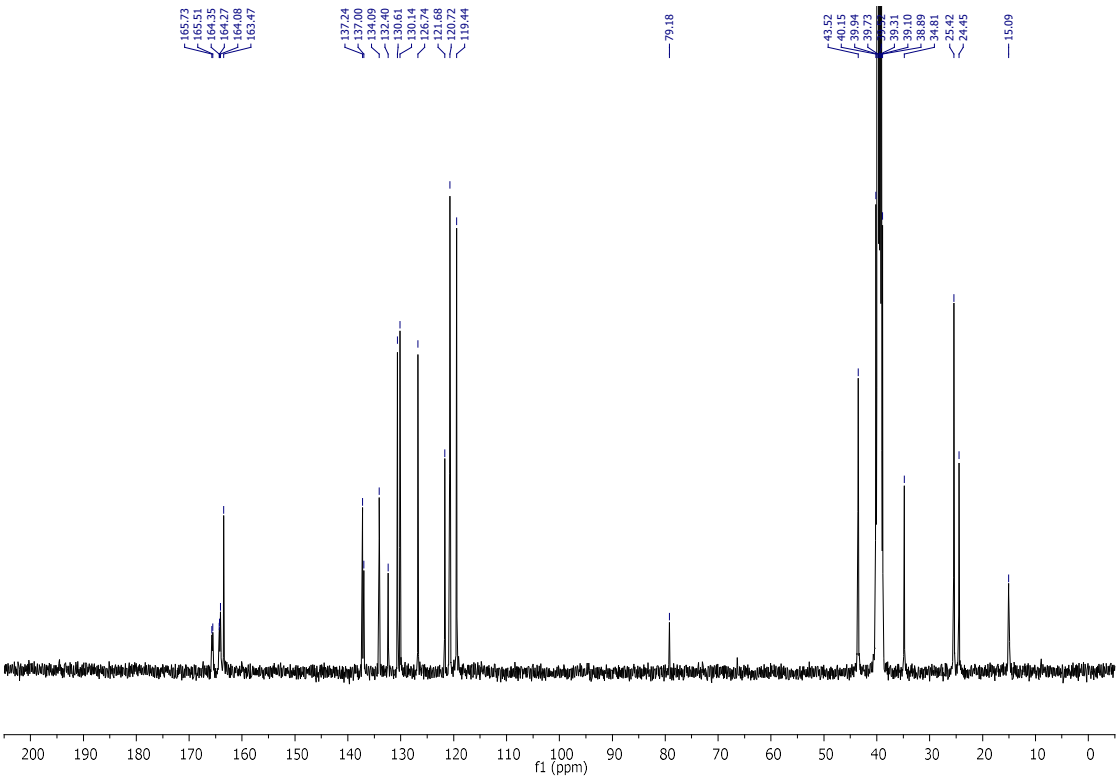

^{13}C NMR spectrum of compound **2.13**

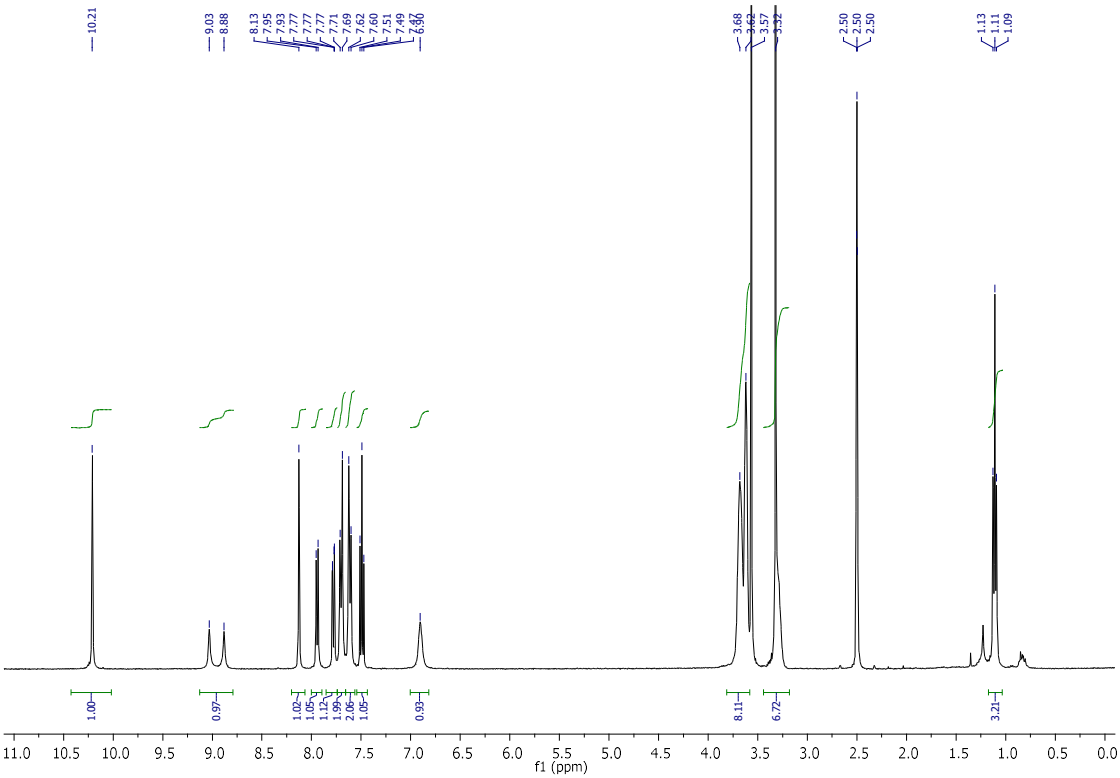

^{1}H NMR spectrum of compound **2.14**

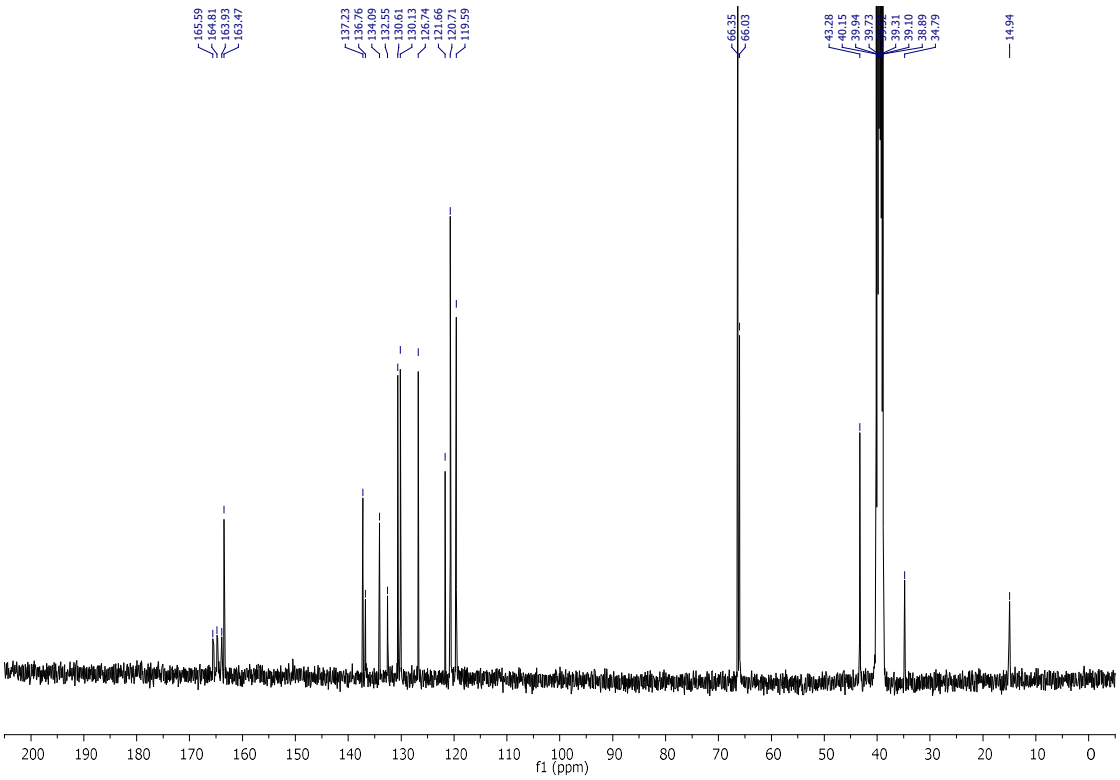

^{13}C NMR spectrum of compound **2.14**

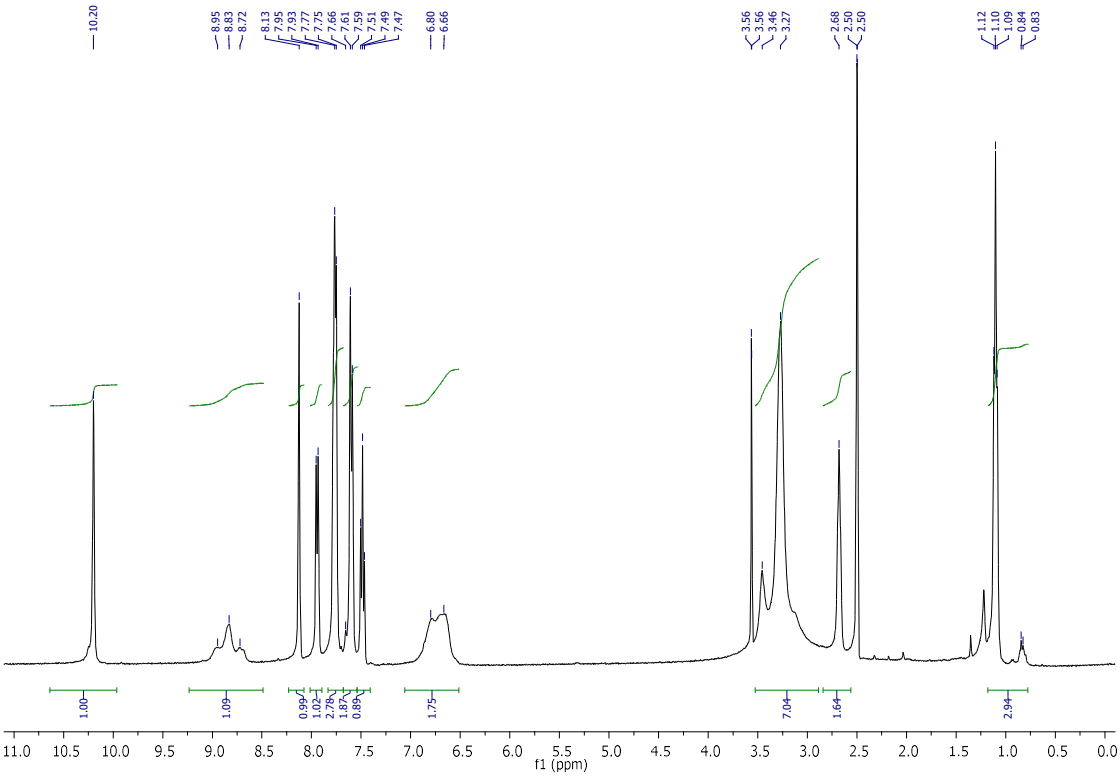

^{1}H NMR spectrum of compound **2.15**

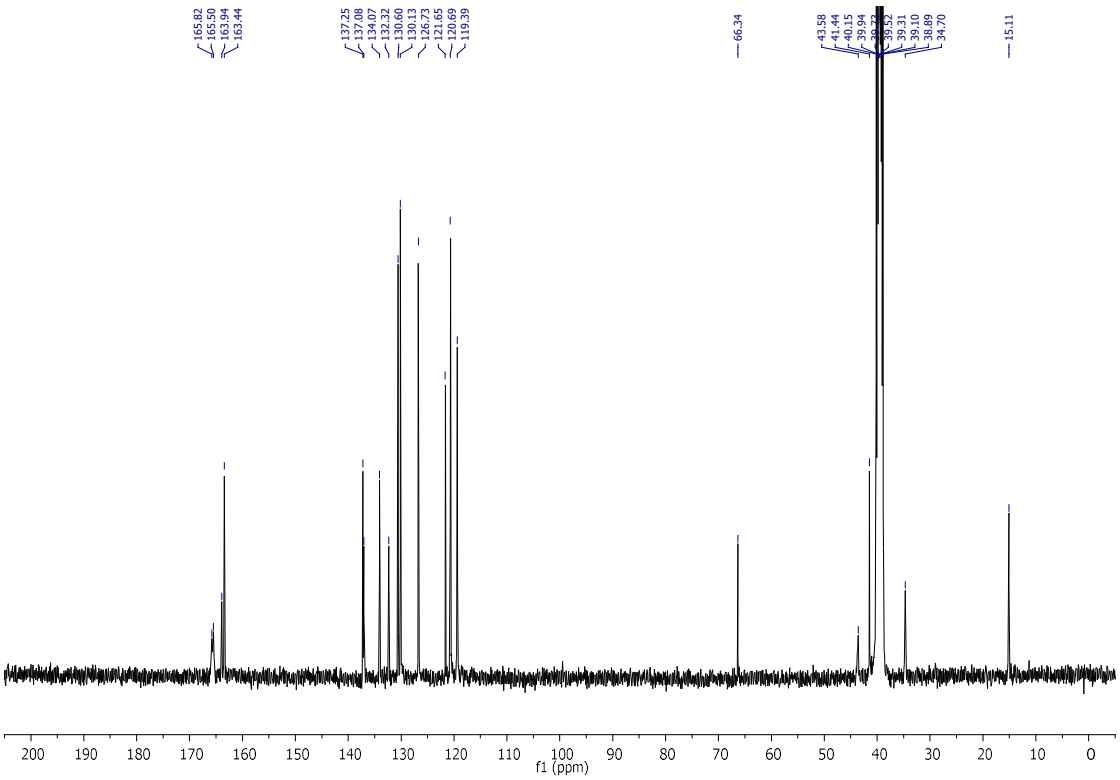

^{13}C NMR spectrum of compound **2.15**

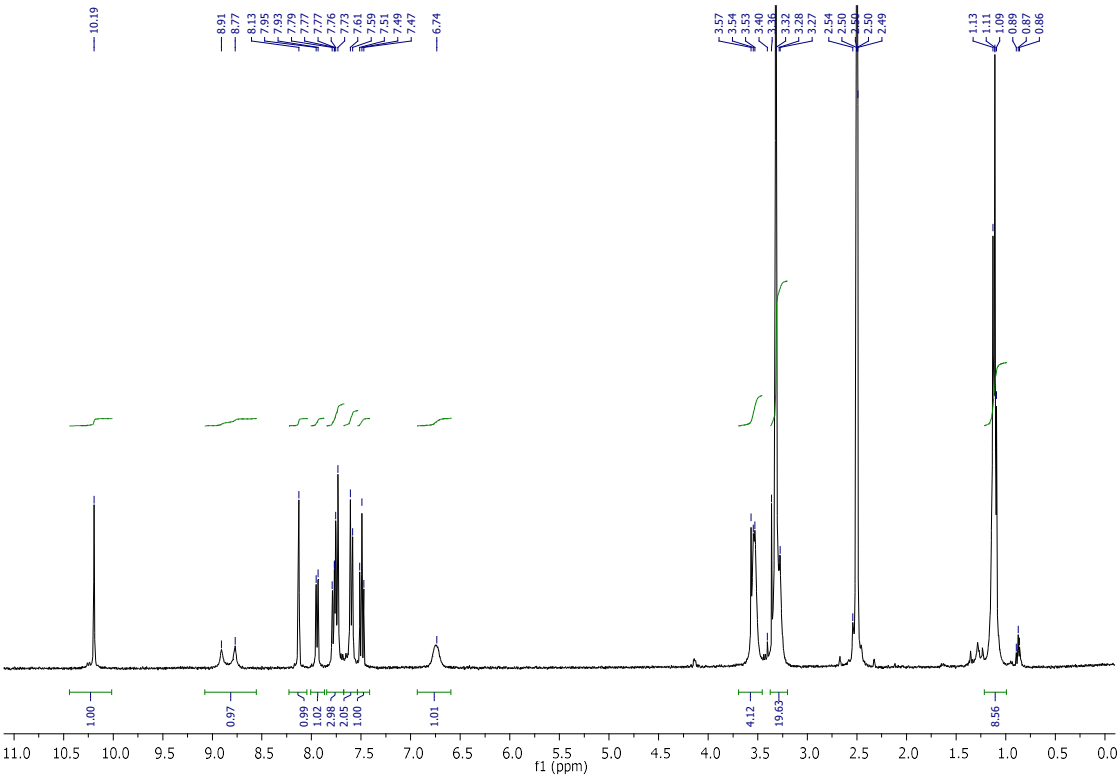

^{1}H NMR spectrum of compound **2.16**

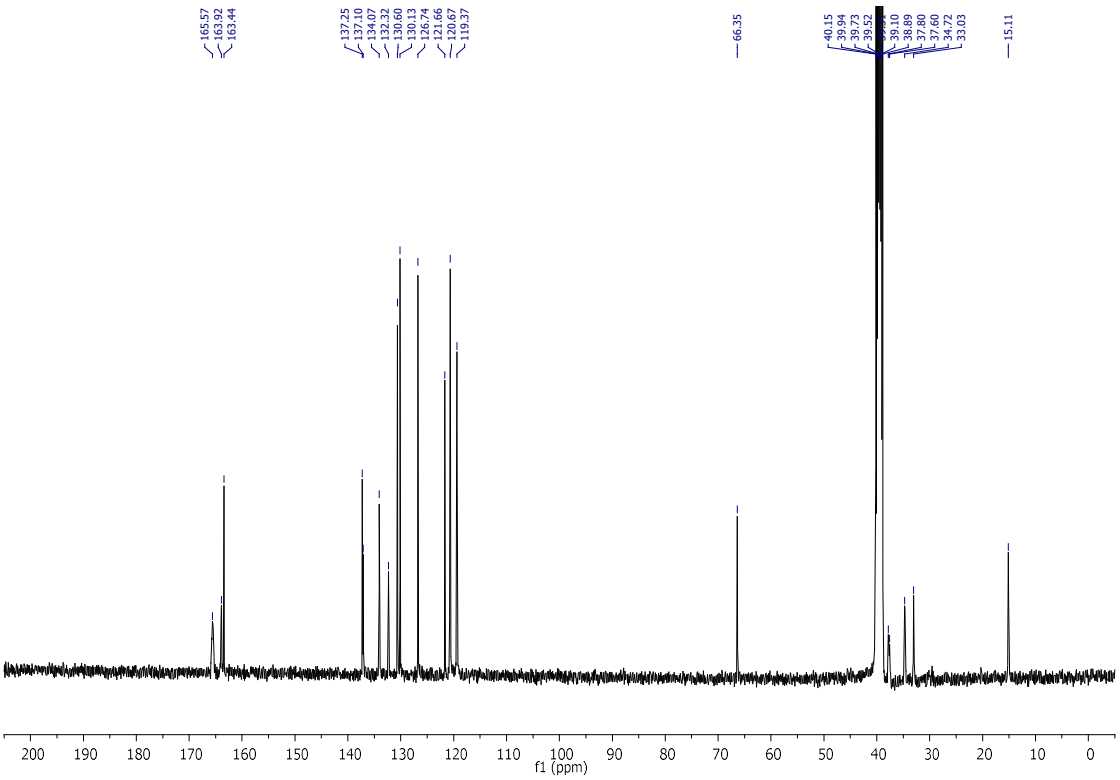

^{13}C NMR spectrum of compound **2.16**

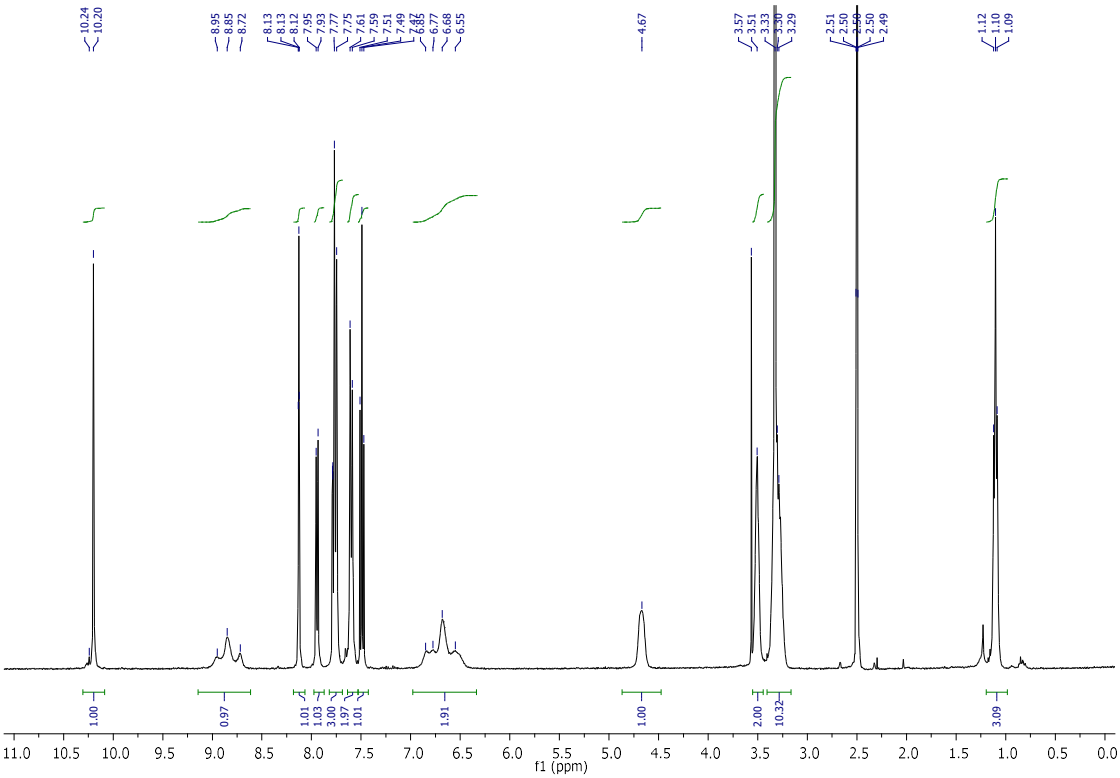

^{1}H NMR spectrum of compound **2.17**

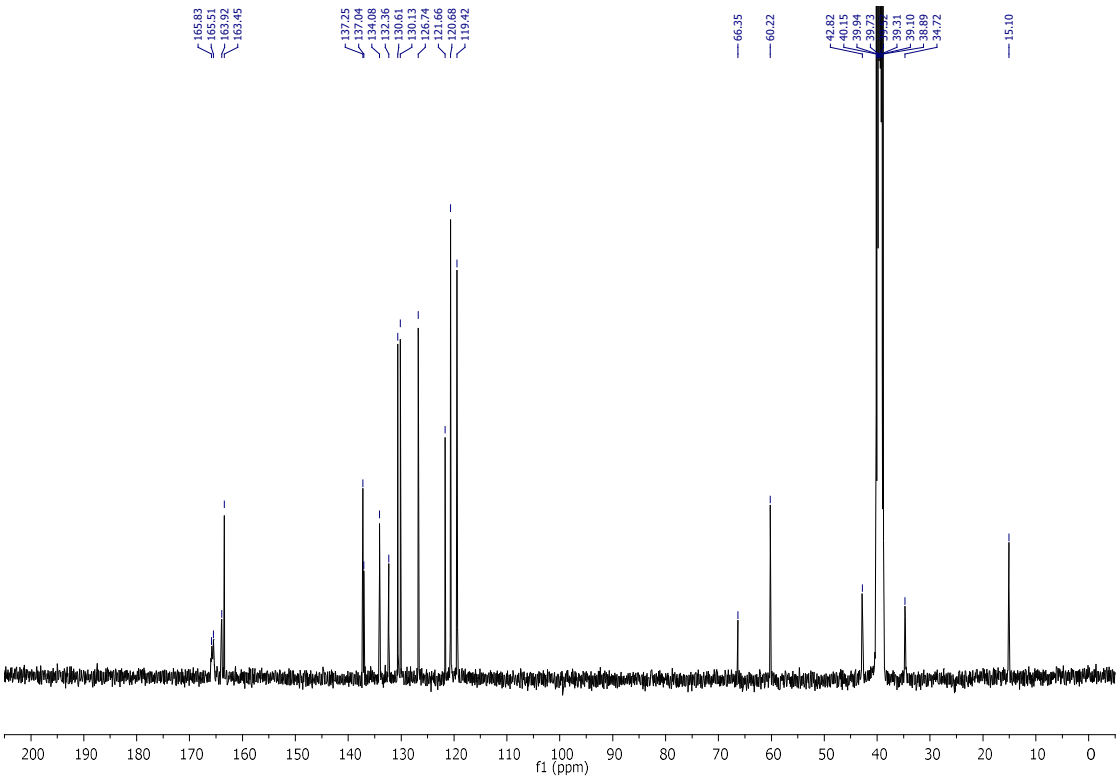

^{13}C NMR spectrum of compound **2.17**

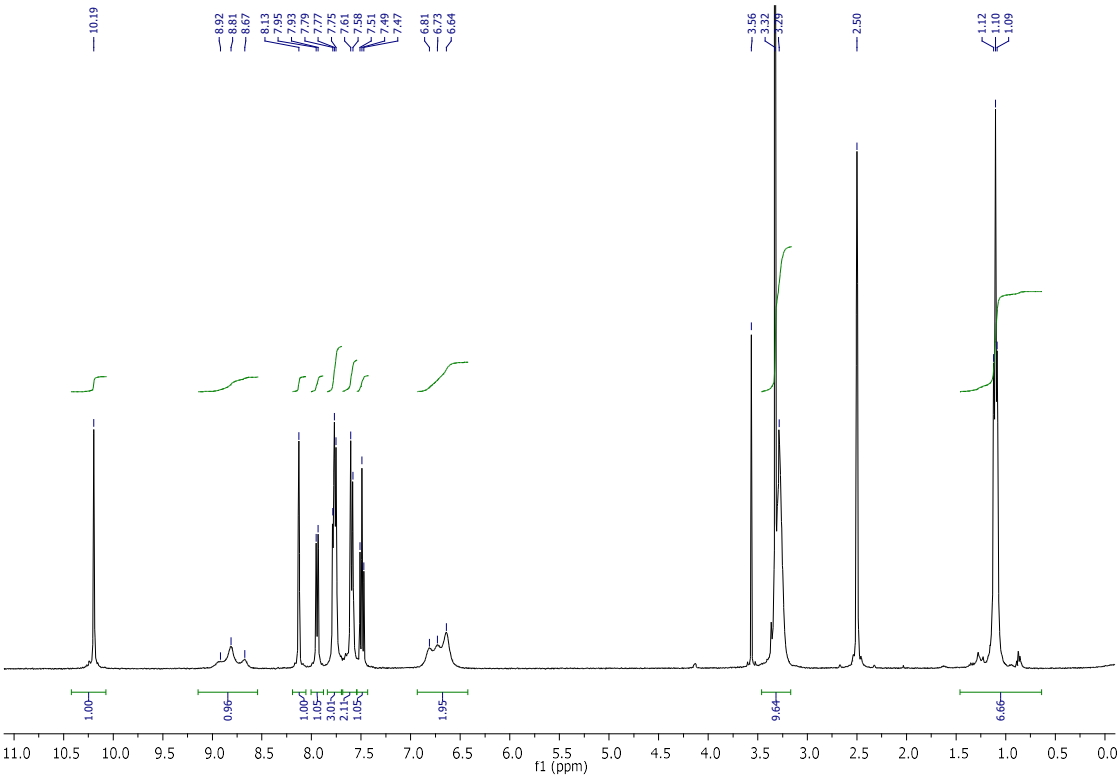

^{1}H NMR spectrum of compound **2.18**

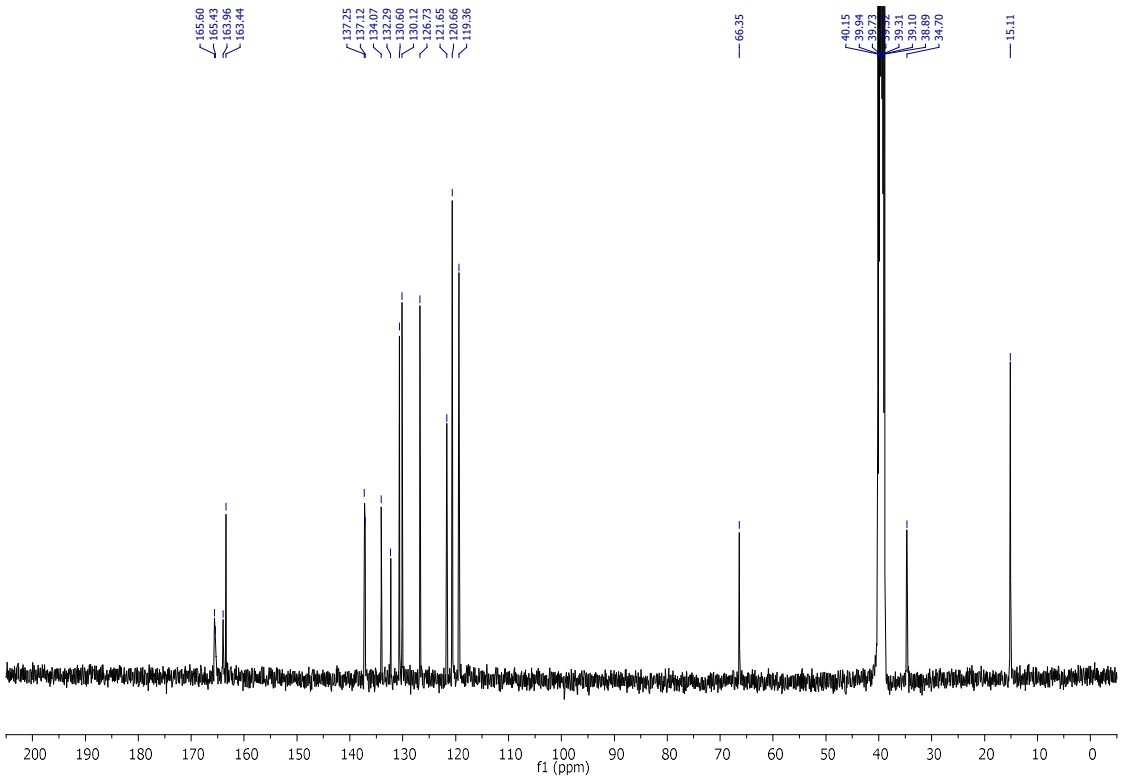

^{13}C NMR spectrum of compound **2.18**

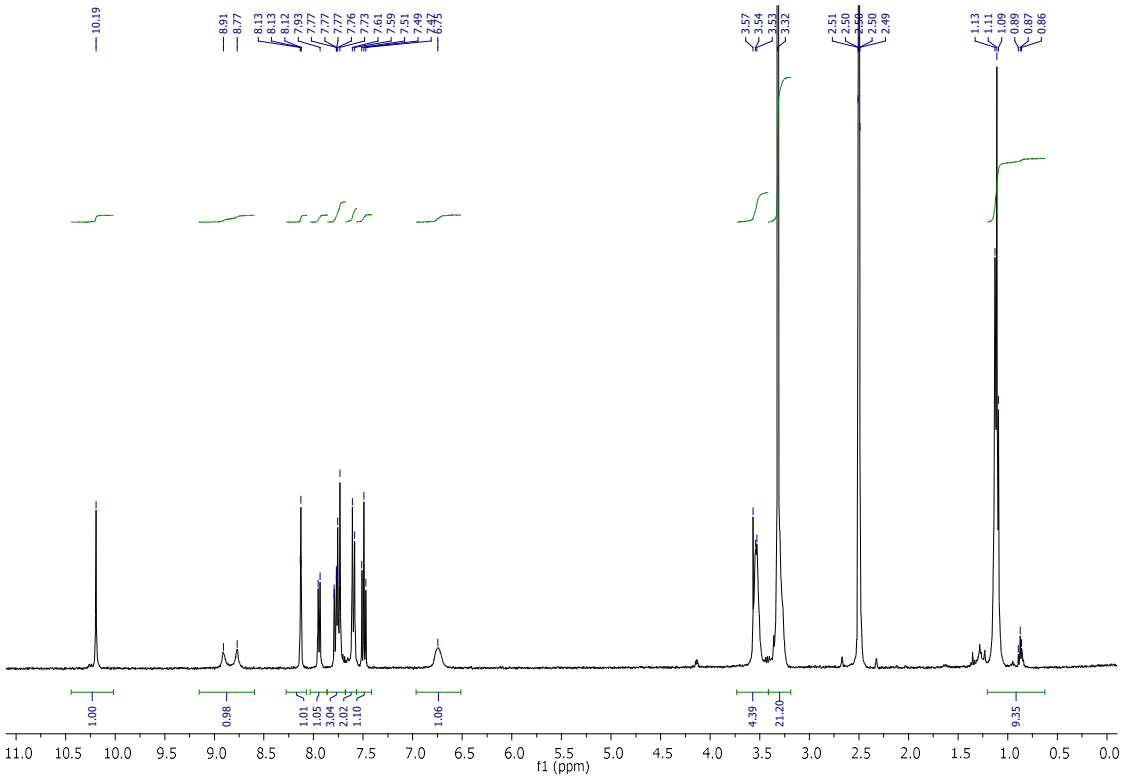

^{1}H NMR spectrum of compound **2.19**

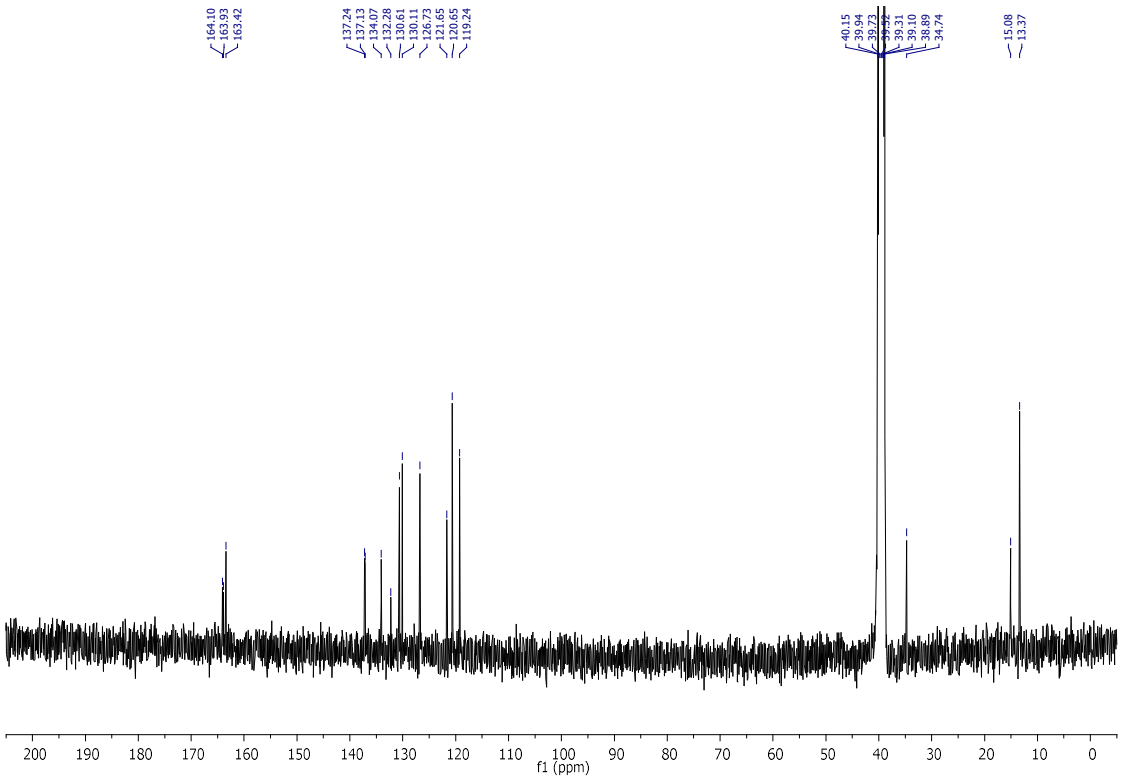

^{13}C NMR spectrum of compound **2.19**

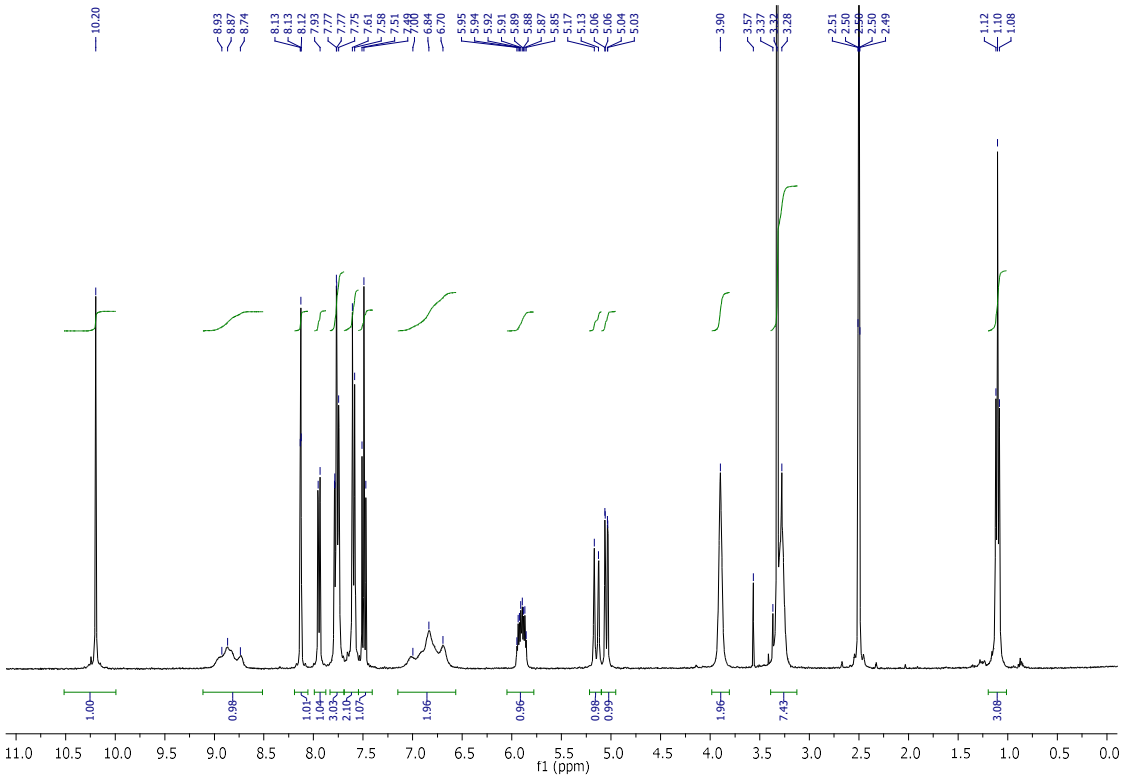

^{1}H NMR spectrum of compound **2.20**

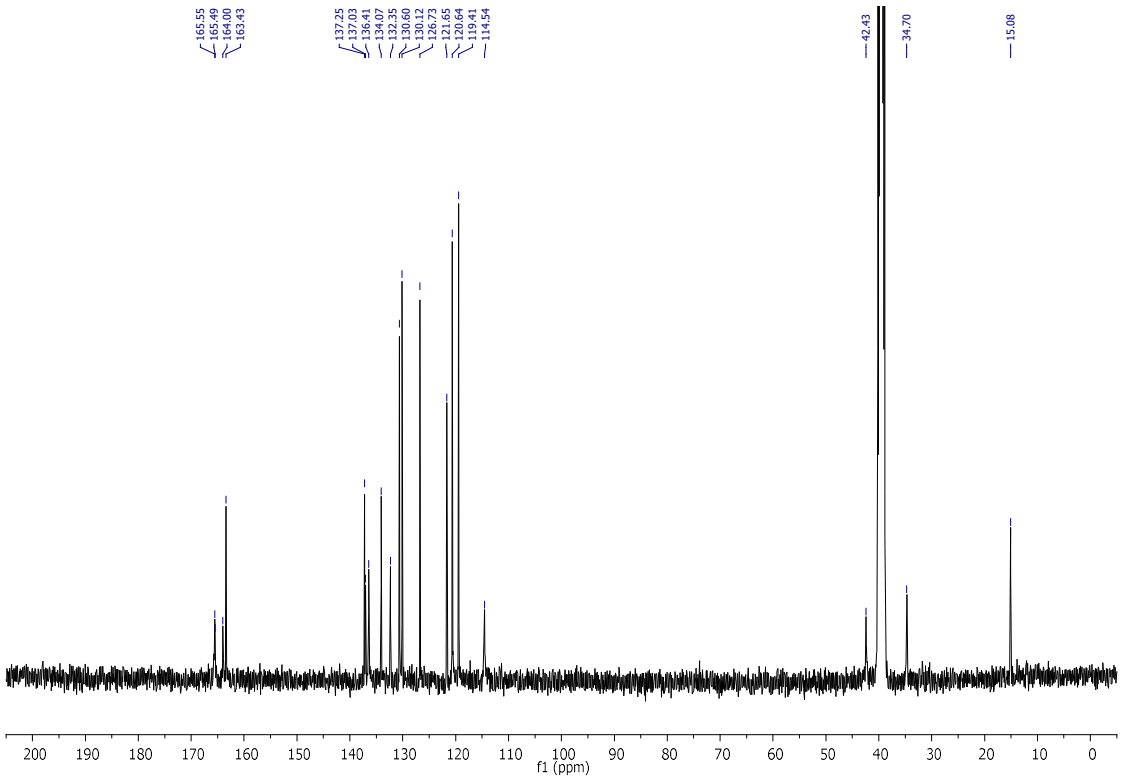

^{13}C NMR spectrum of compound **2.20**

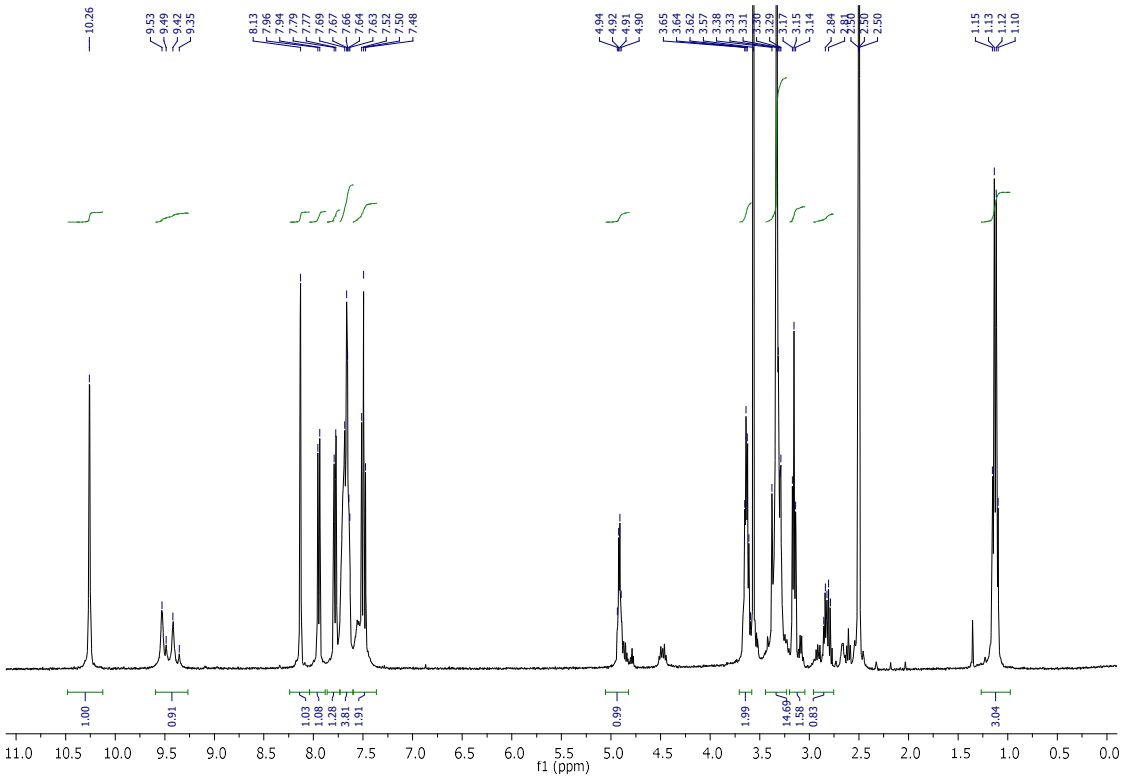

^{1}H NMR spectrum of compound **2.21**

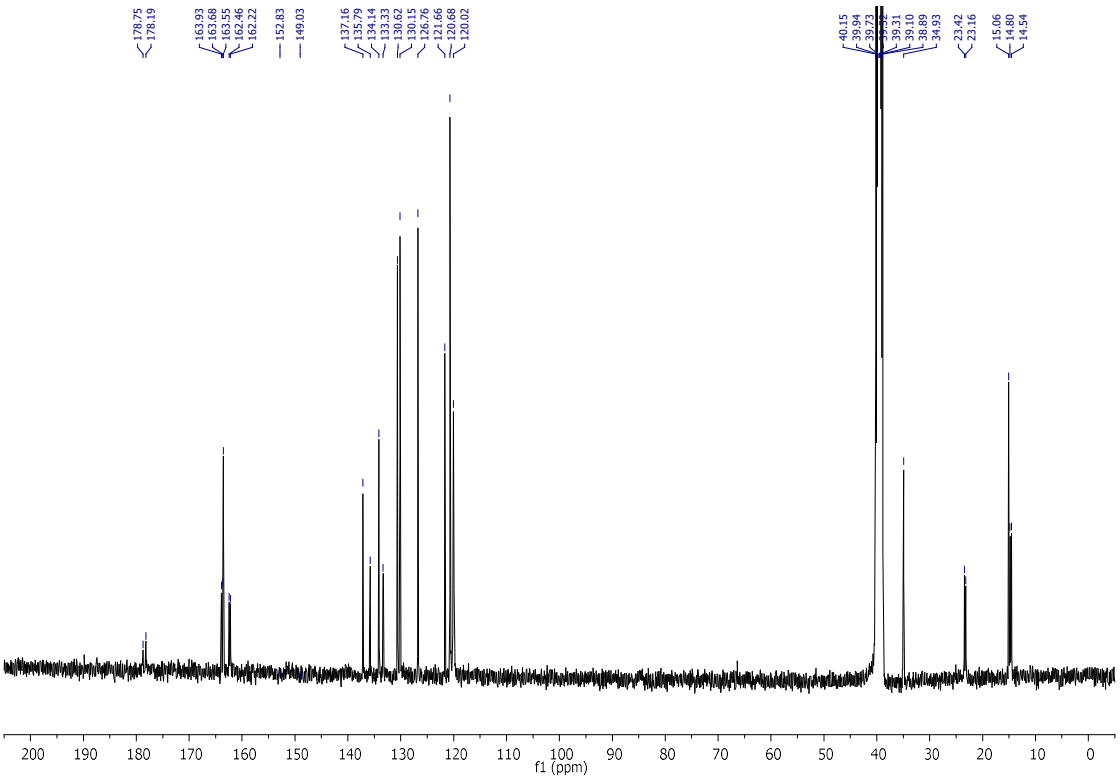

^{13}C NMR spectrum of compound **2.21**

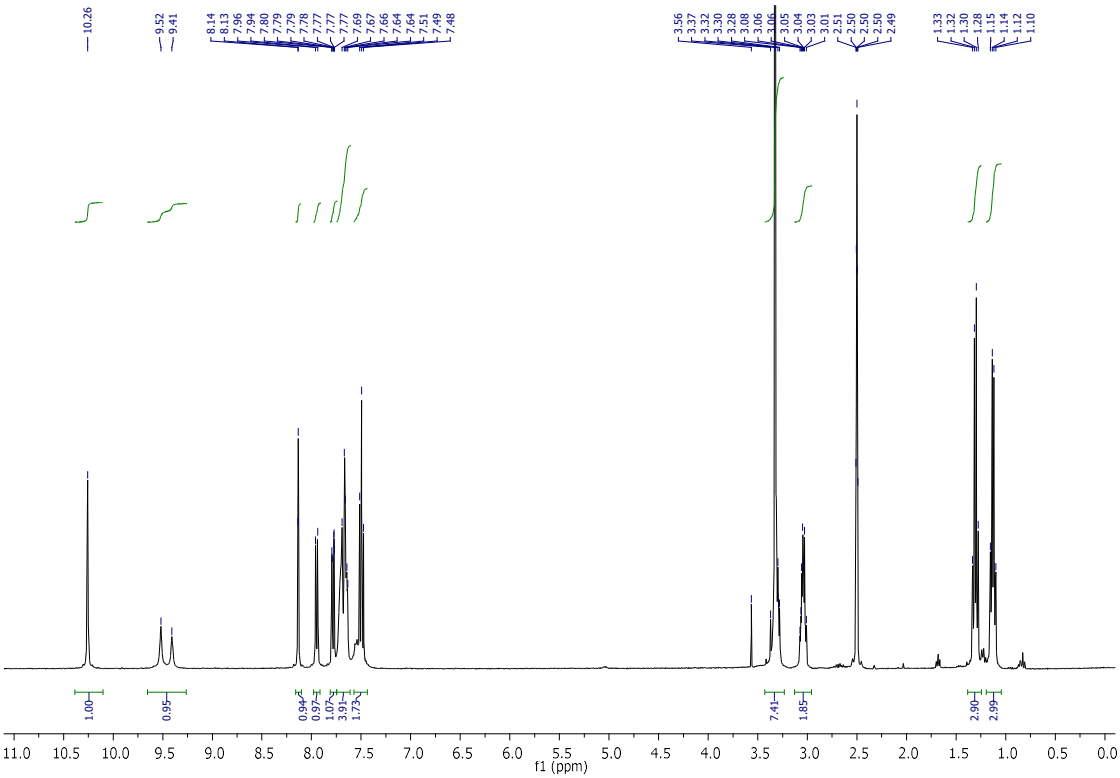

^{1}H NMR spectrum of compound **2.22**

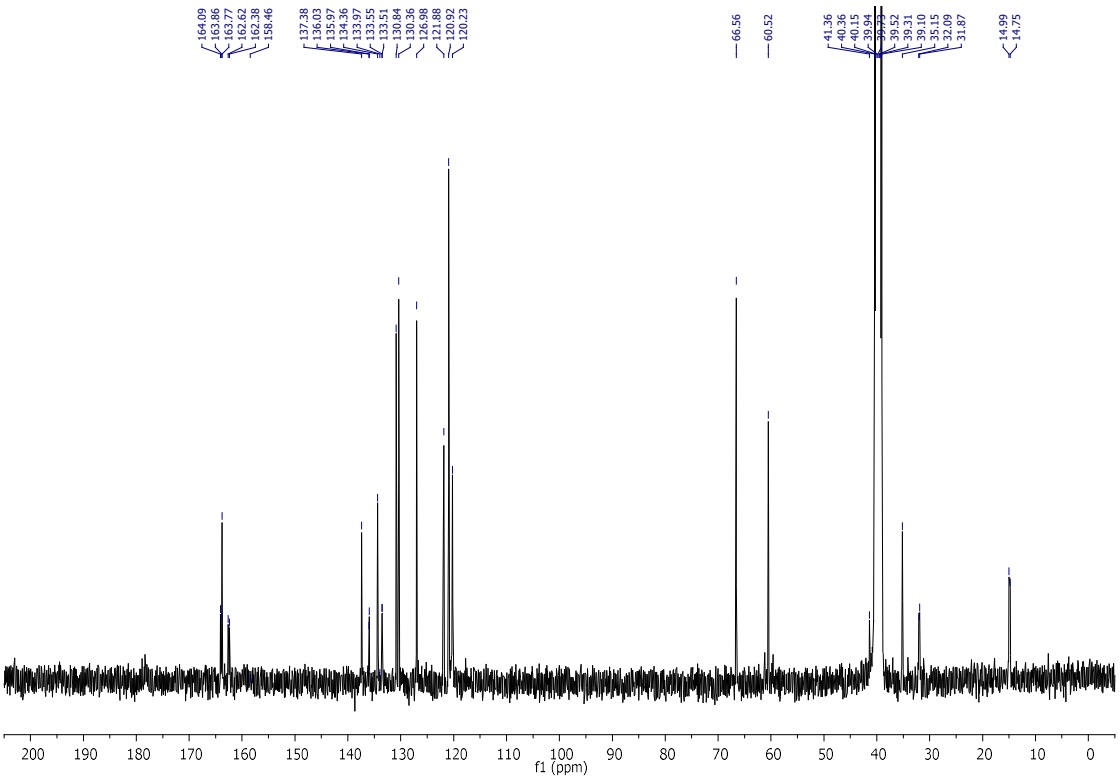

^{13}C NMR spectrum of compound **2.22**

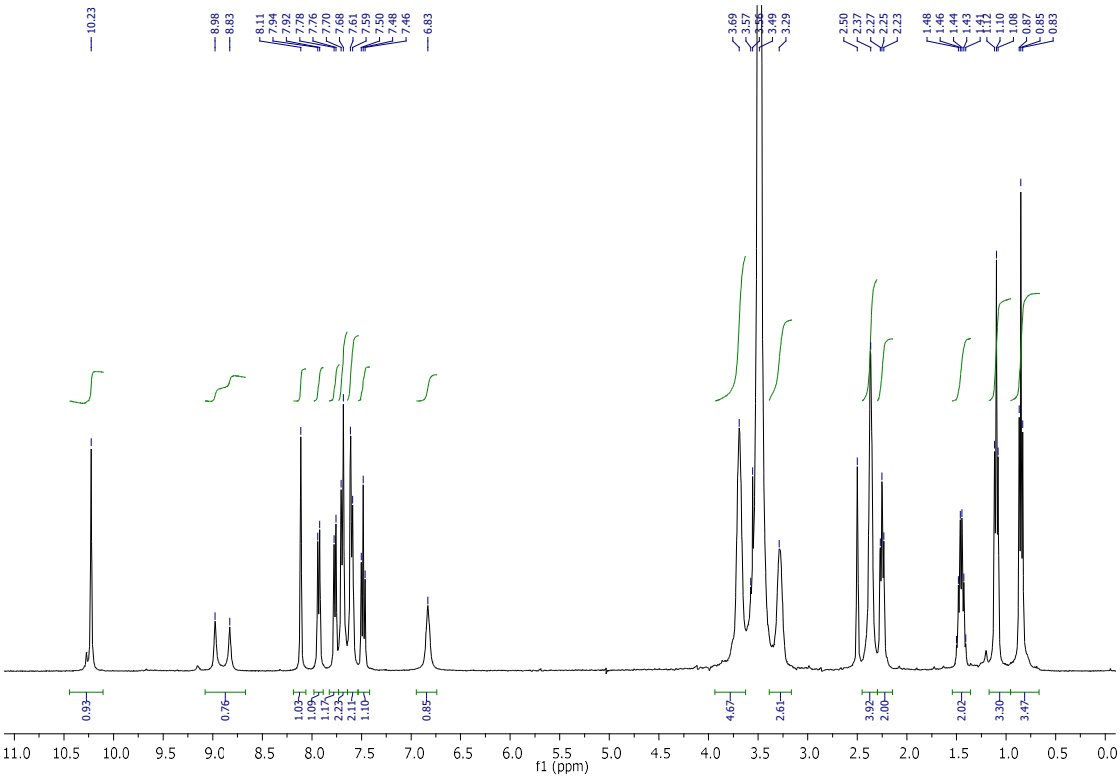

^{1}H NMR spectrum of compound **2.25**

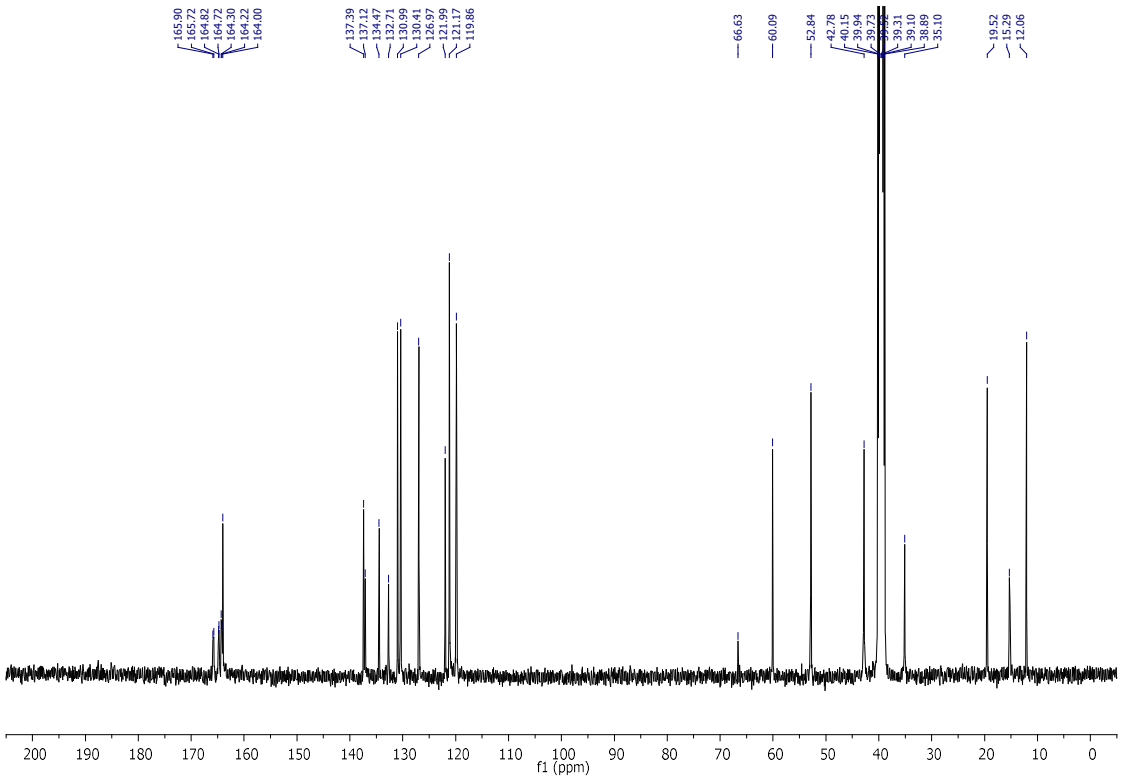

^{13}C NMR spectrum of compound **2.25**

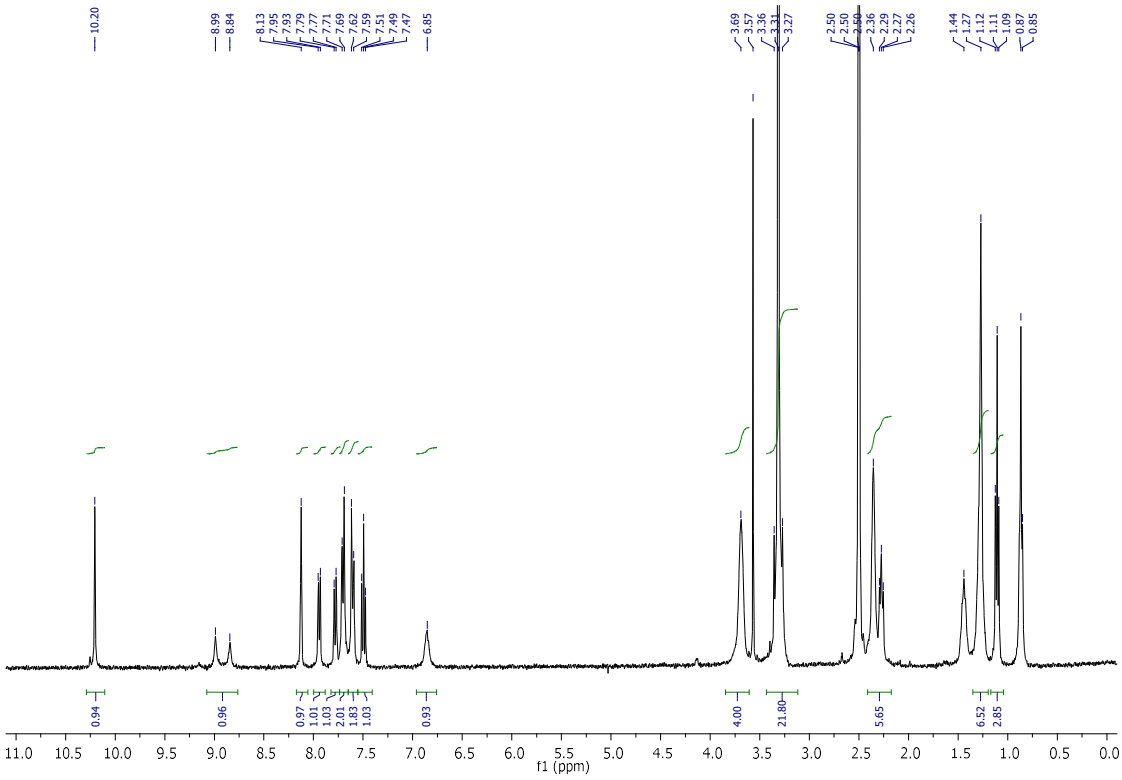

^{1}H NMR spectrum of compound **2.26**

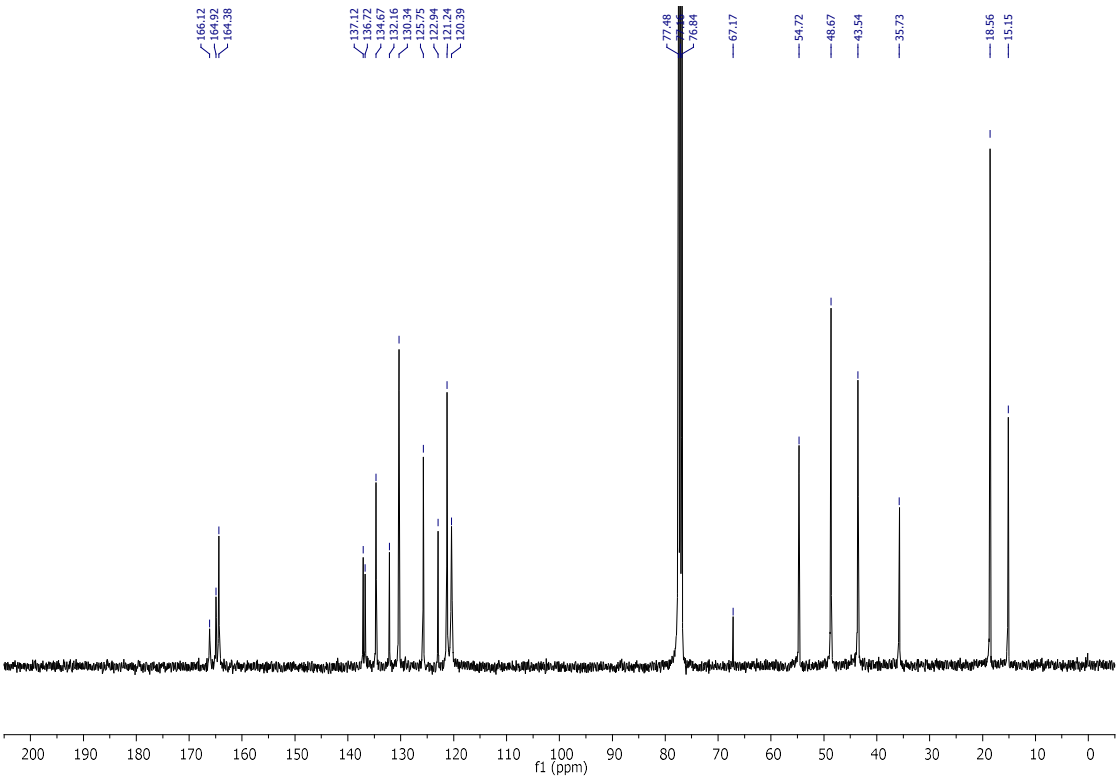

^{13}C NMR spectrum of compound **2.26**

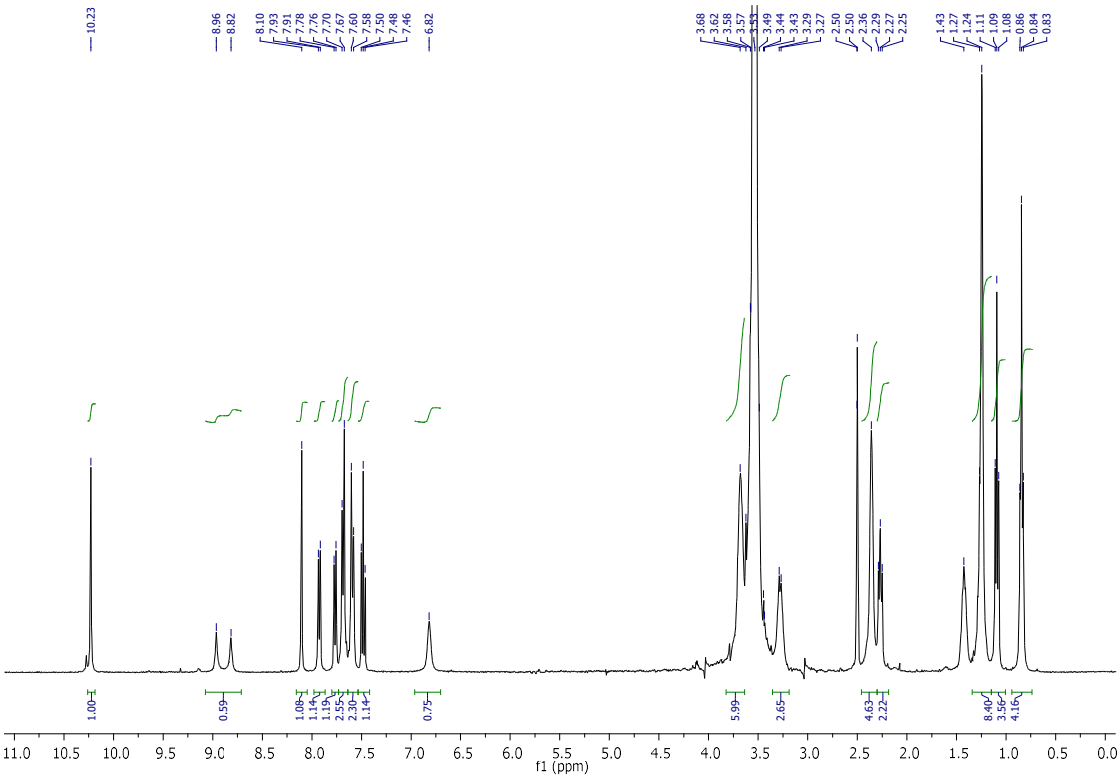

^{1}H NMR spectrum of compound **2.27**

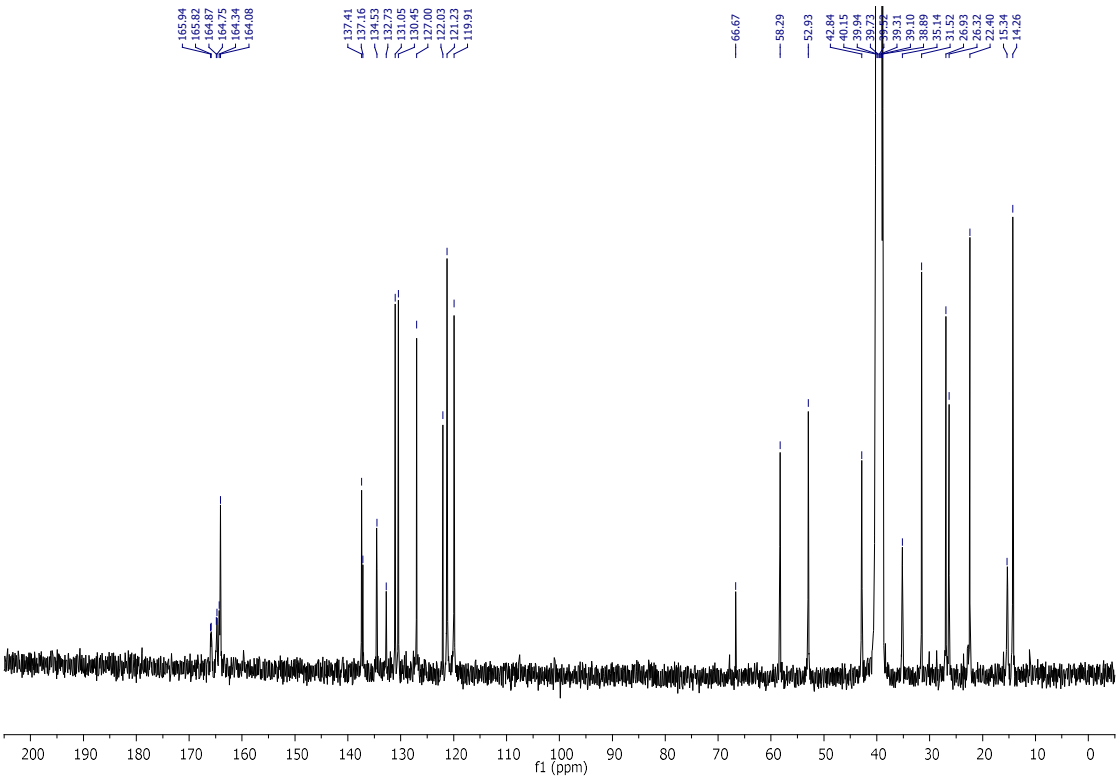

^{13}C NMR spectrum of compound **2.27**

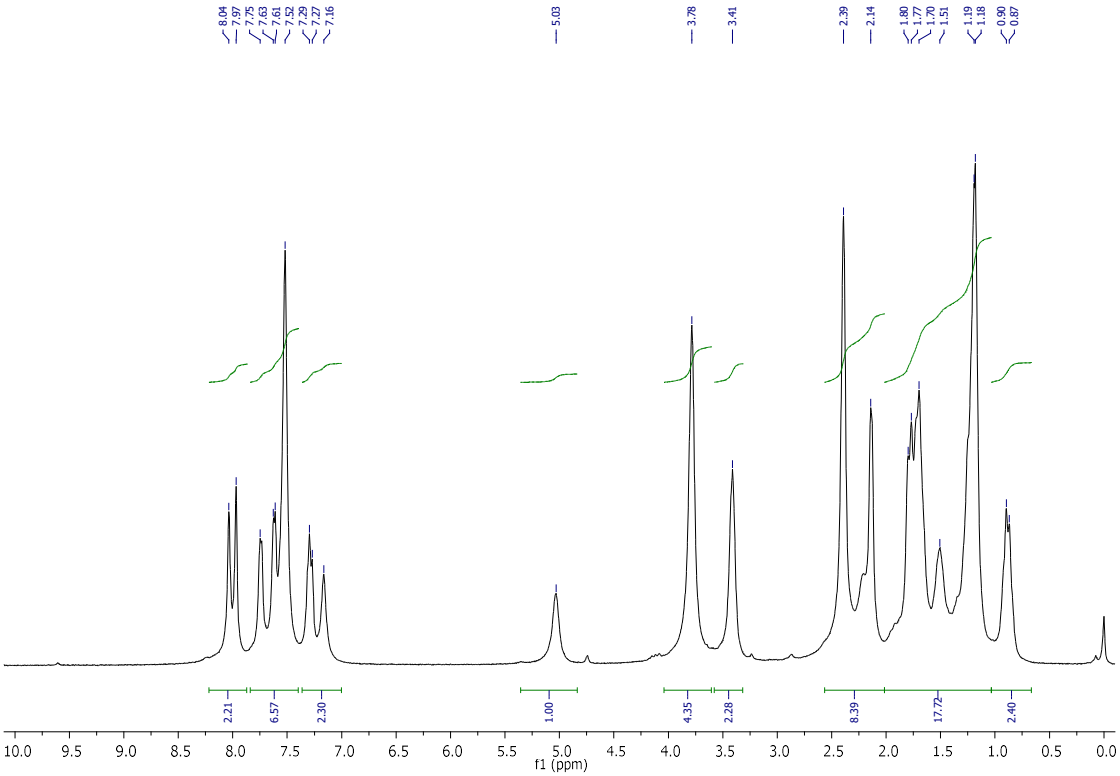

^{1}H NMR spectrum of compound **2.28**

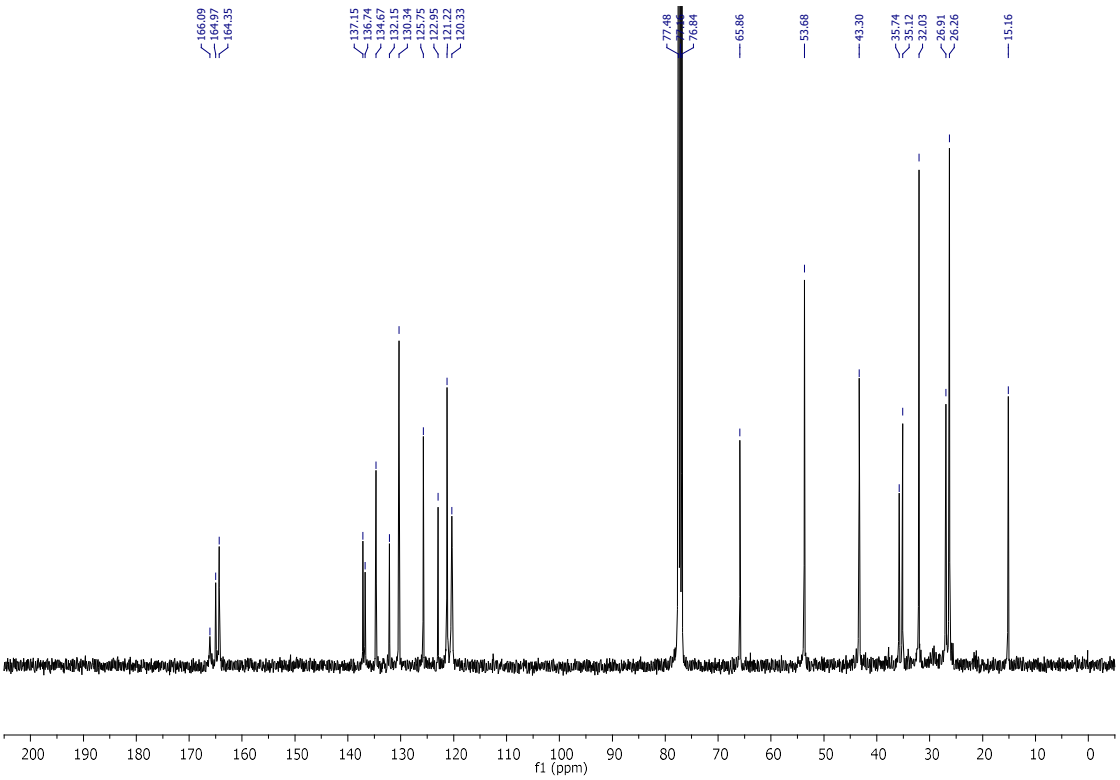

^{13}C NMR spectrum of compound **2.28**

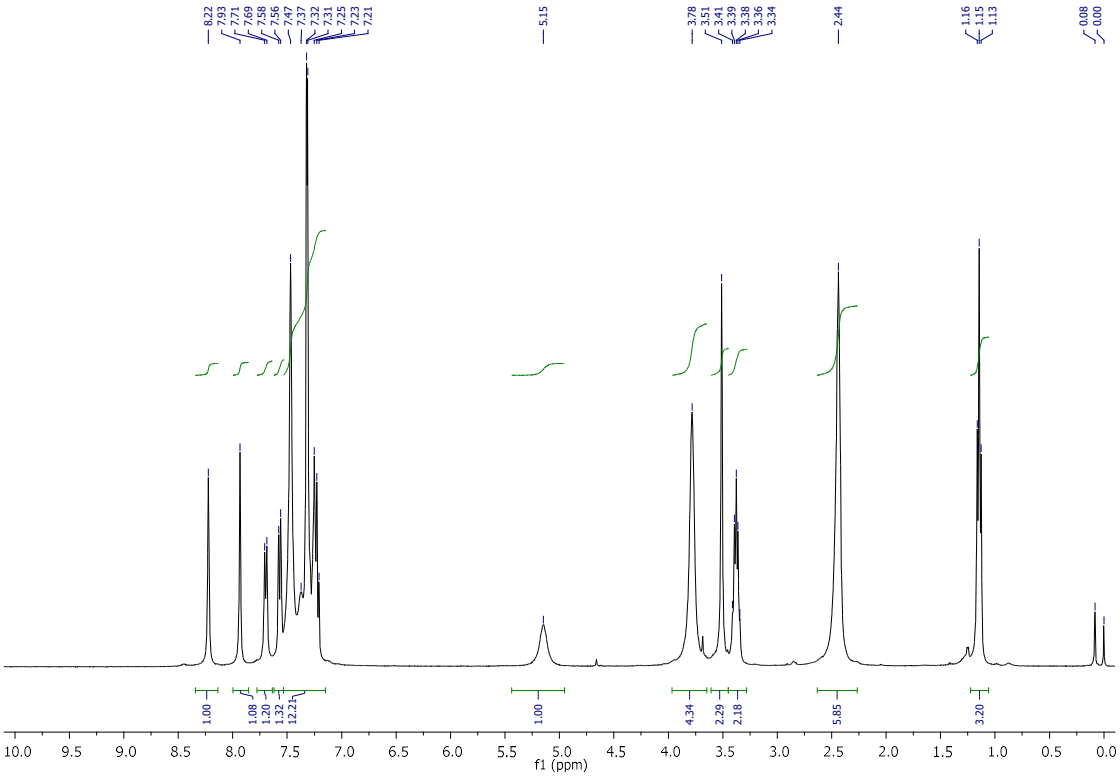

^{1}H NMR spectrum of compound **2.29**

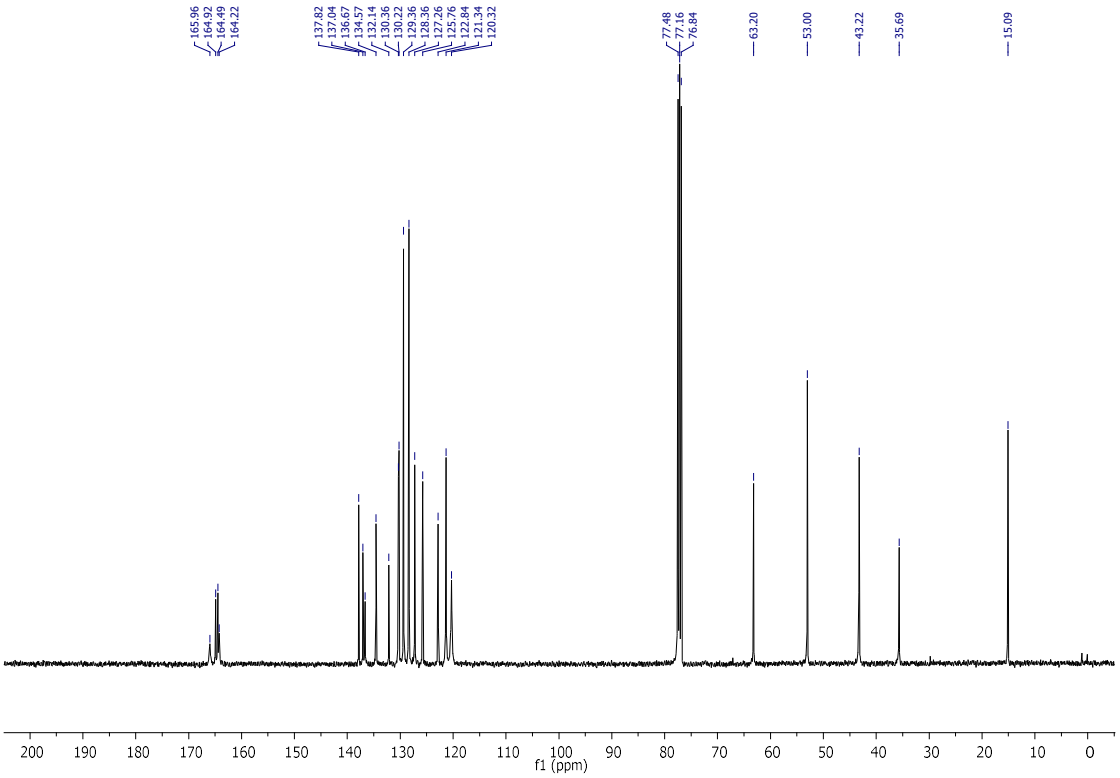

^{13}C NMR spectrum of compound **2.29**

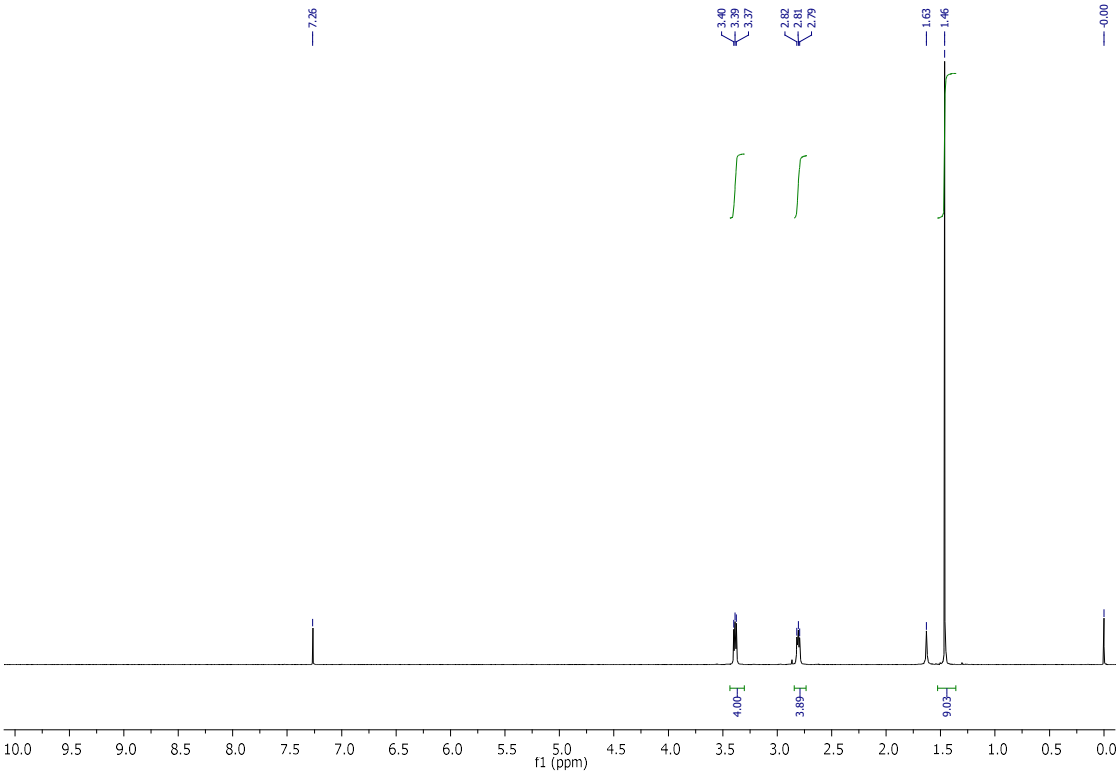

^{1}H NMR spectrum of compound **2.31**

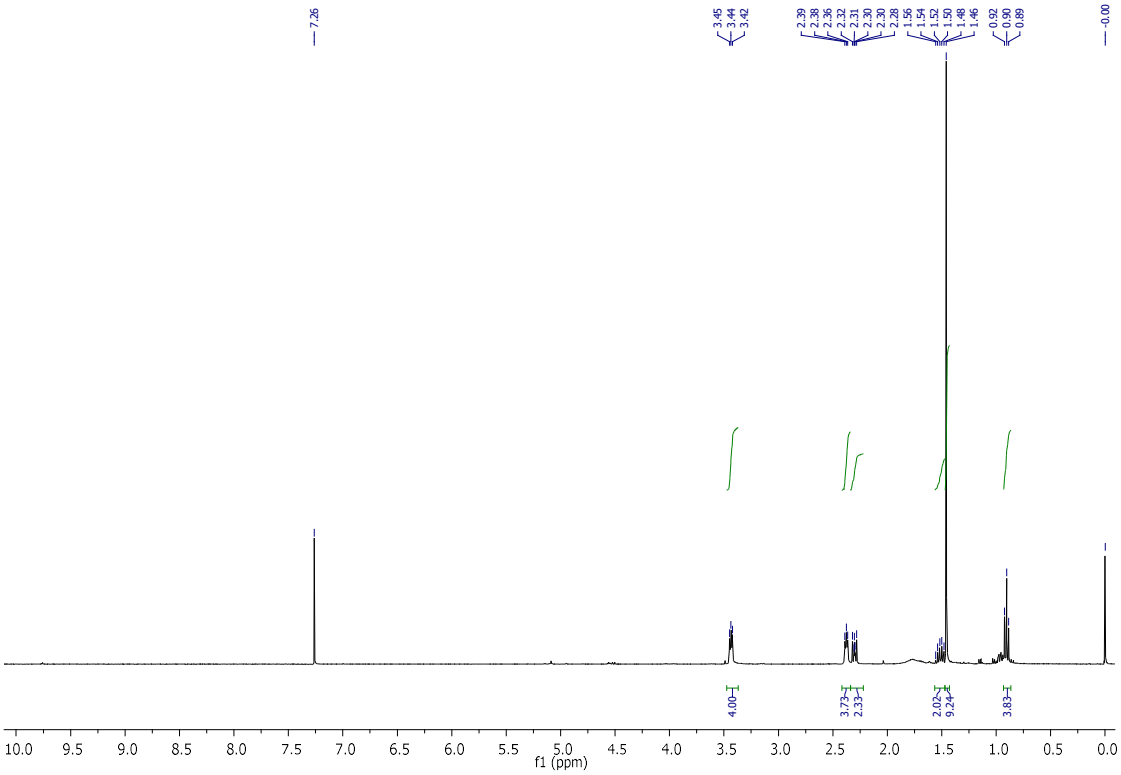

^{1}H NMR spectrum of compound **2.32**

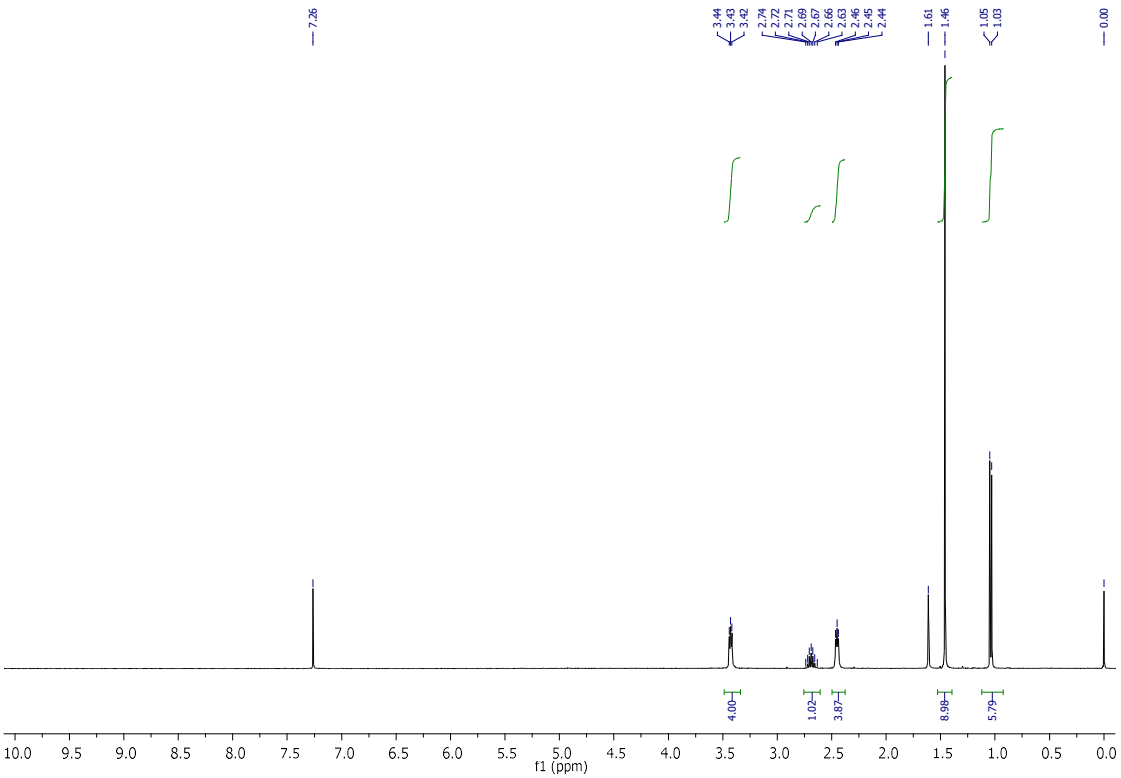

^{1}H NMR spectrum of compound **2.33**

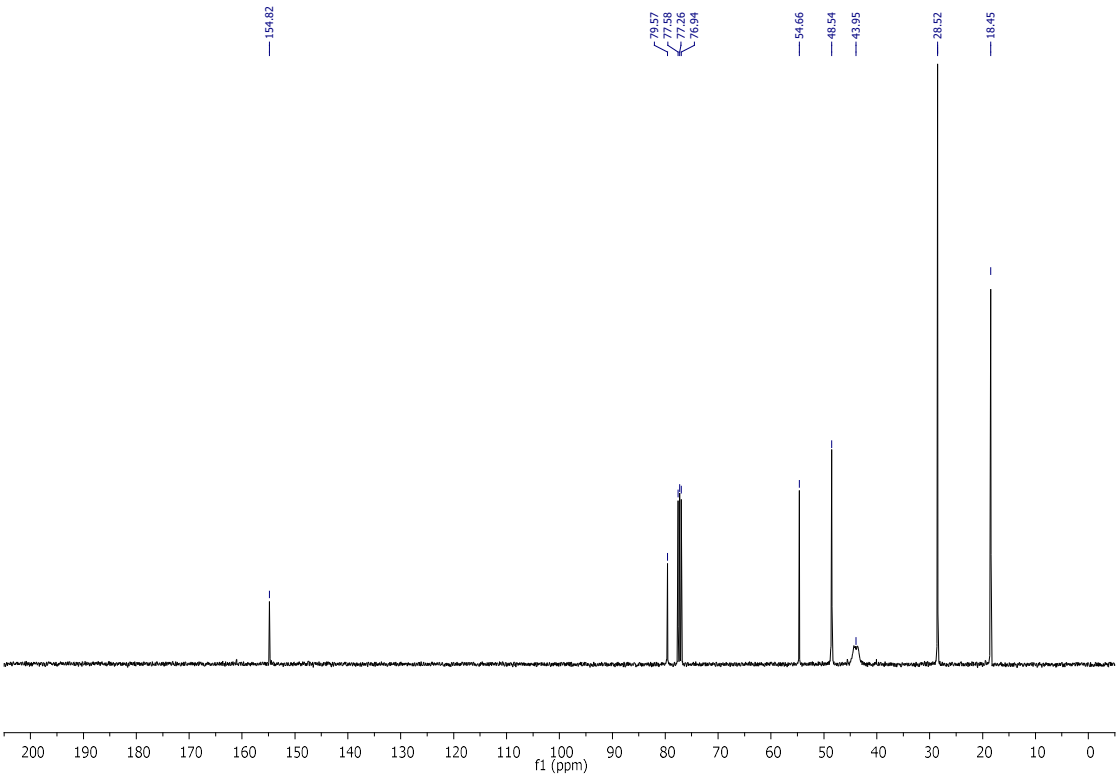

^{13}C NMR spectrum of compound **2.33**

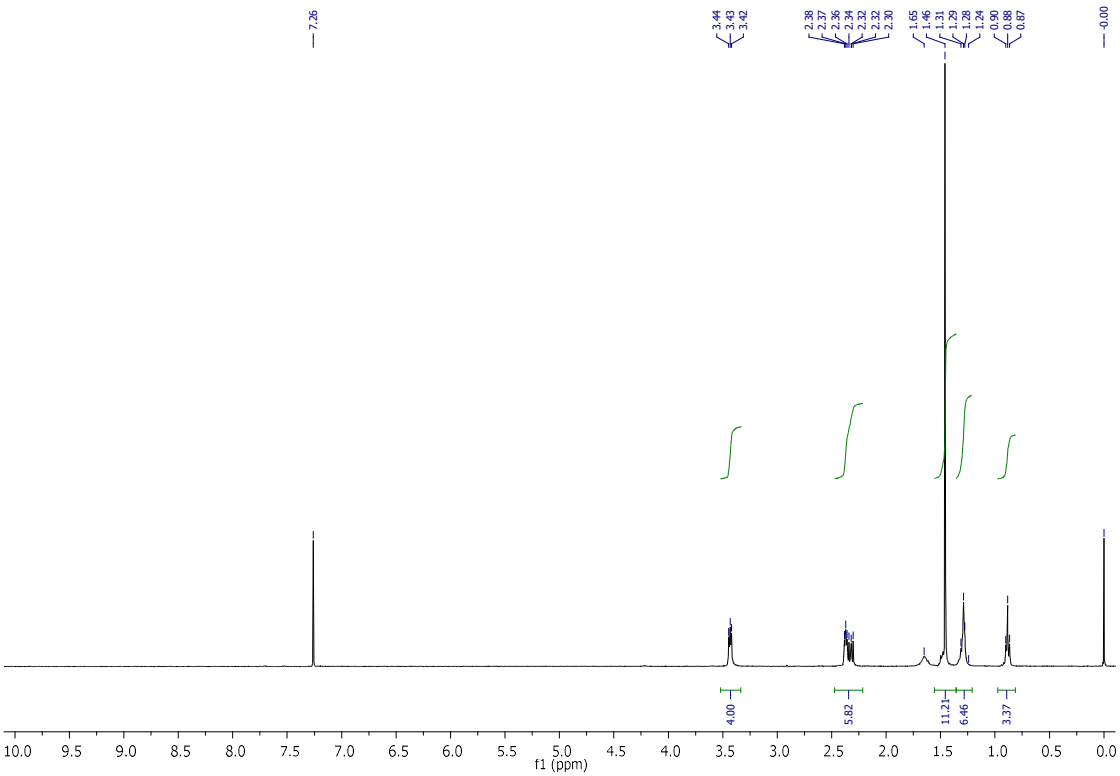

^{1}H NMR spectrum of compound **2.34**

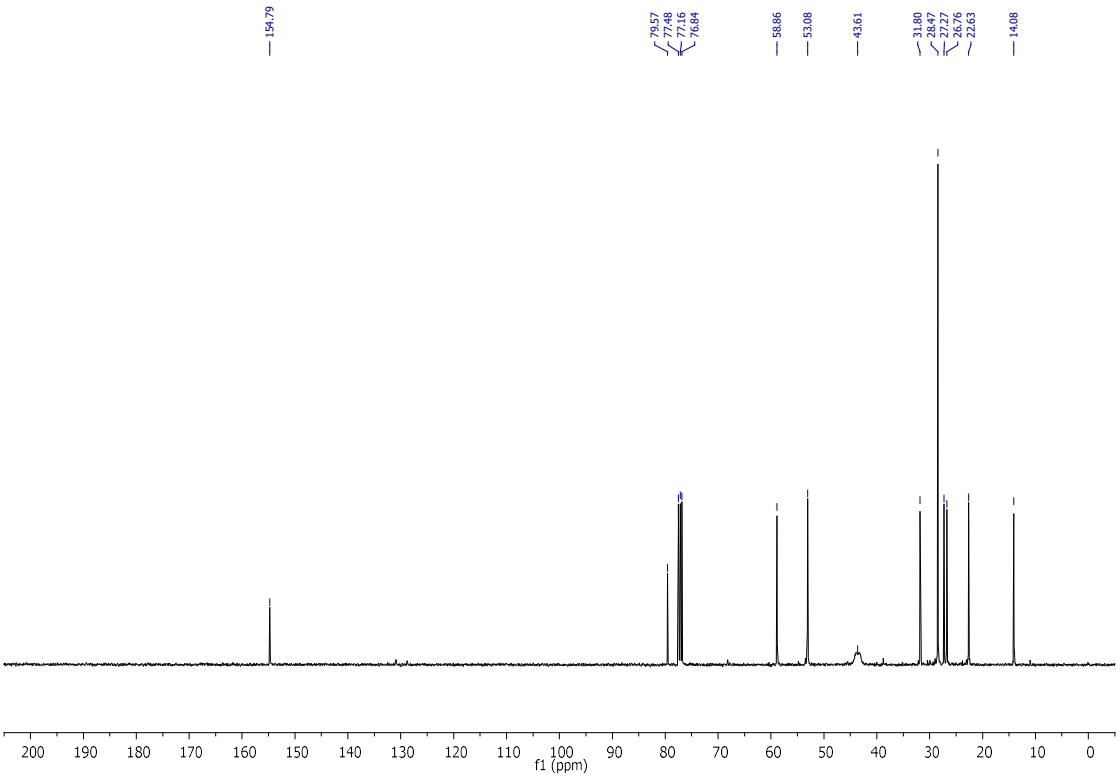

^{13}C NMR spectrum of compound **2.34**

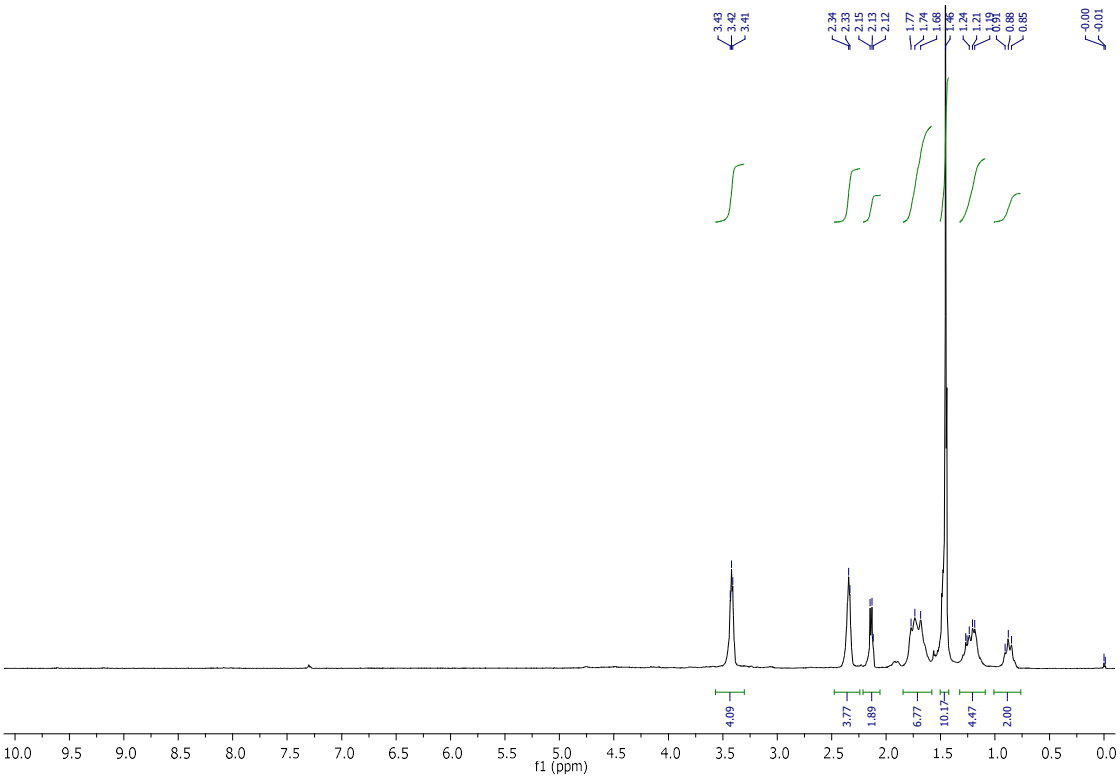

^{1}H NMR spectrum of compound **2.35**

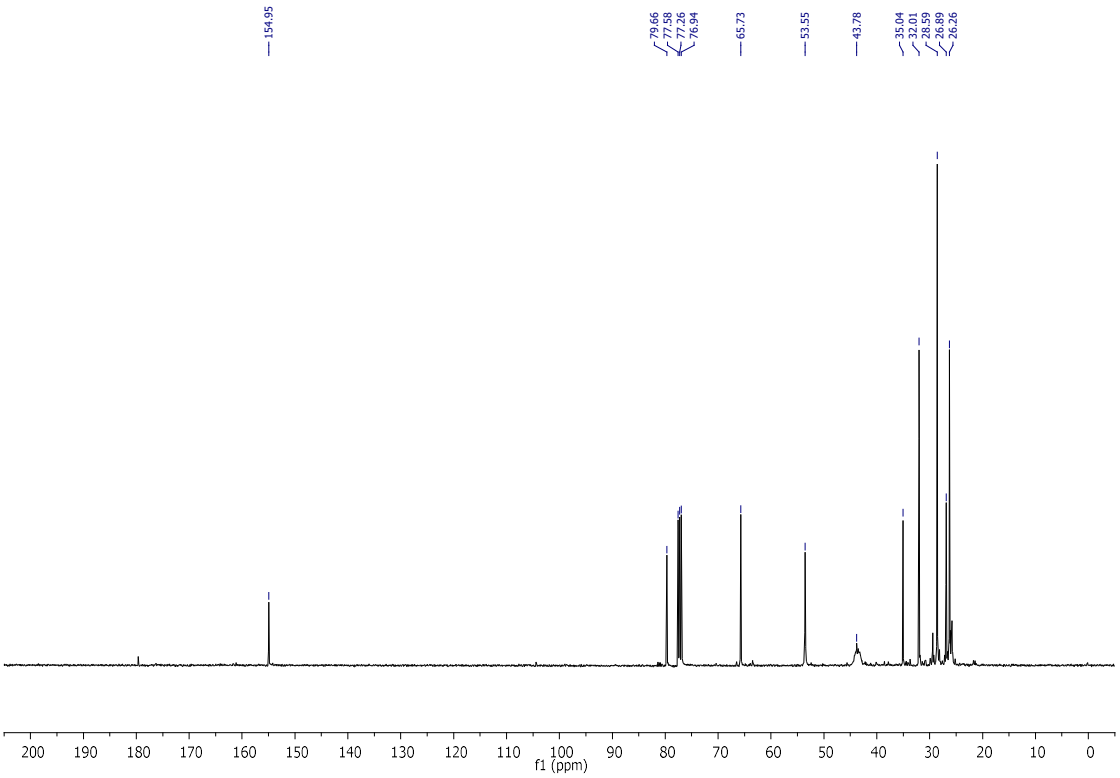

^{13}C NMR spectrum of compound **2.35**

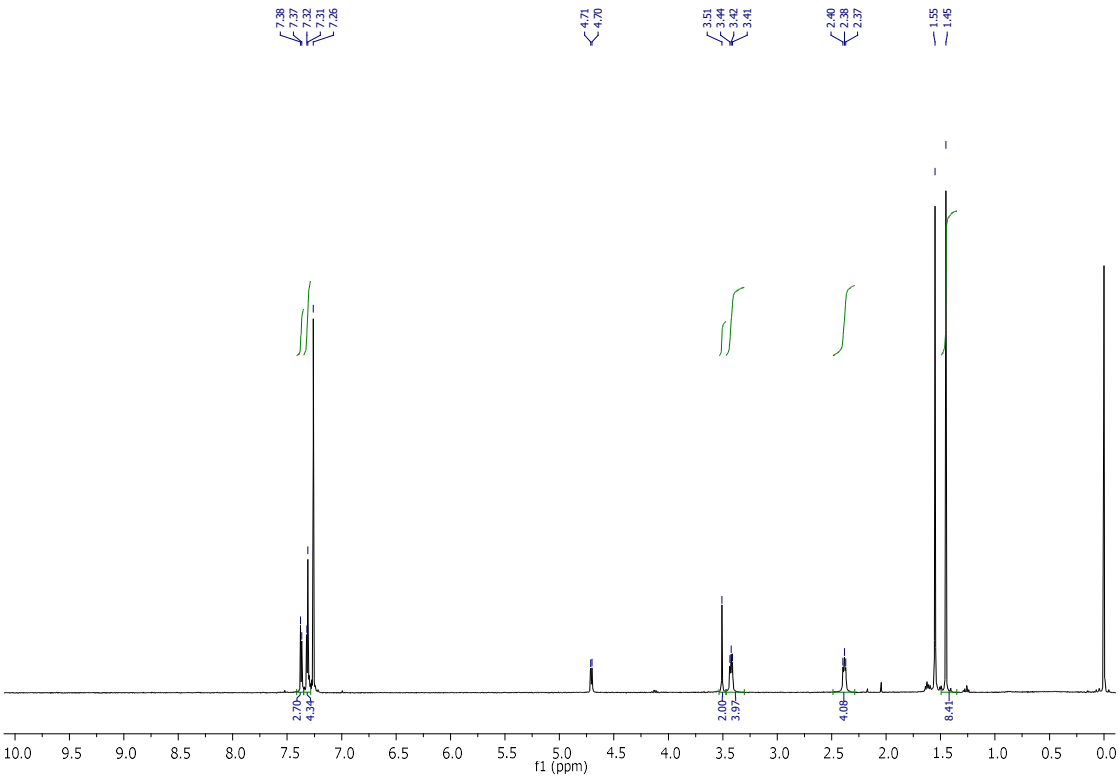

^{1}H NMR spectrum of compound **2.36**

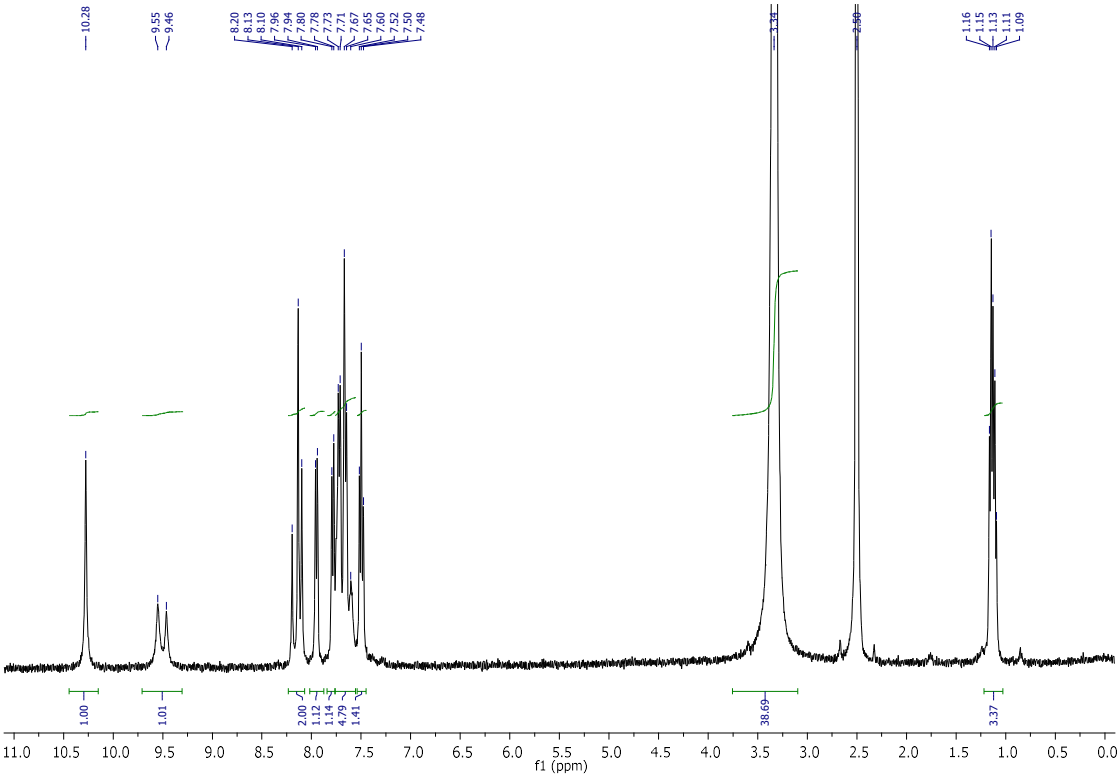

^{1}H NMR spectrum of compound **2.37**

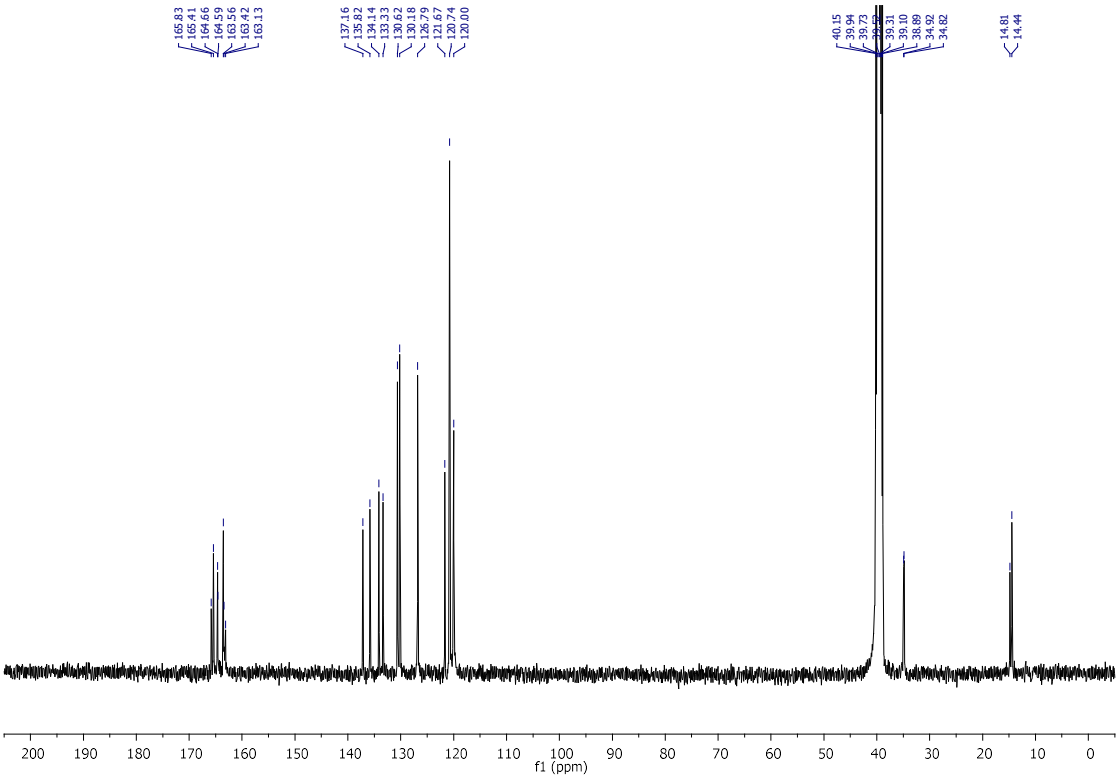

^{13}C NMR spectrum of compound **2.37**

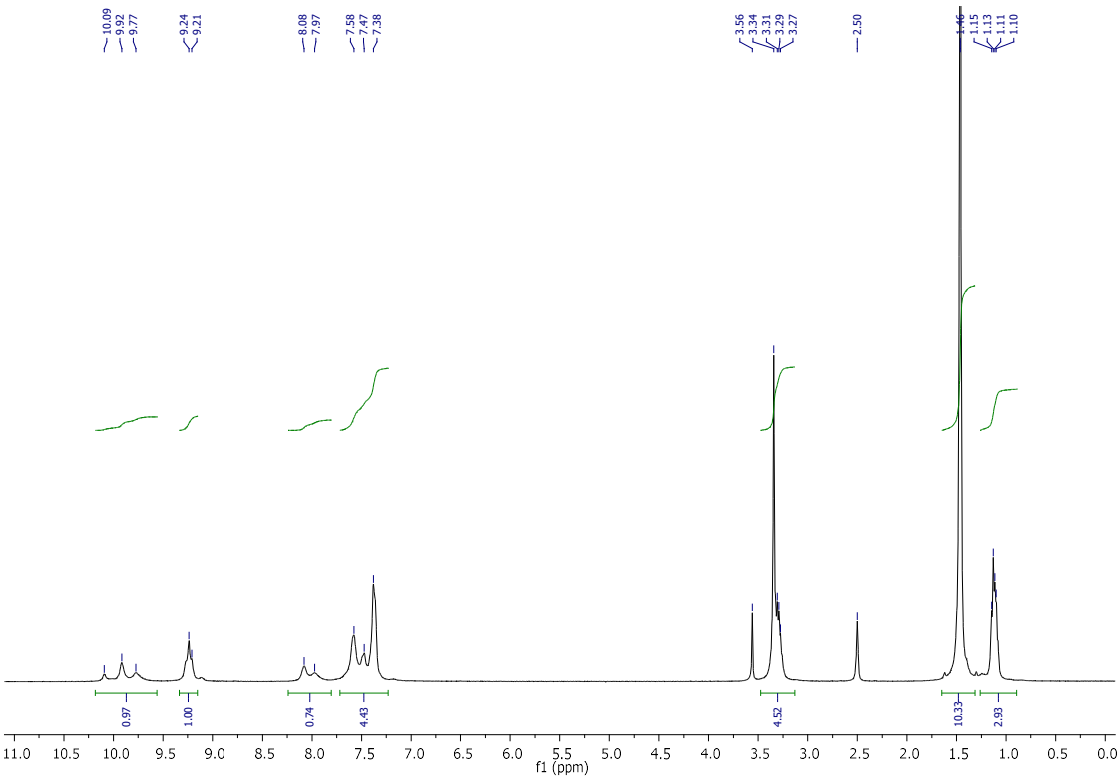

^{1}H NMR spectrum of compound **2.40**

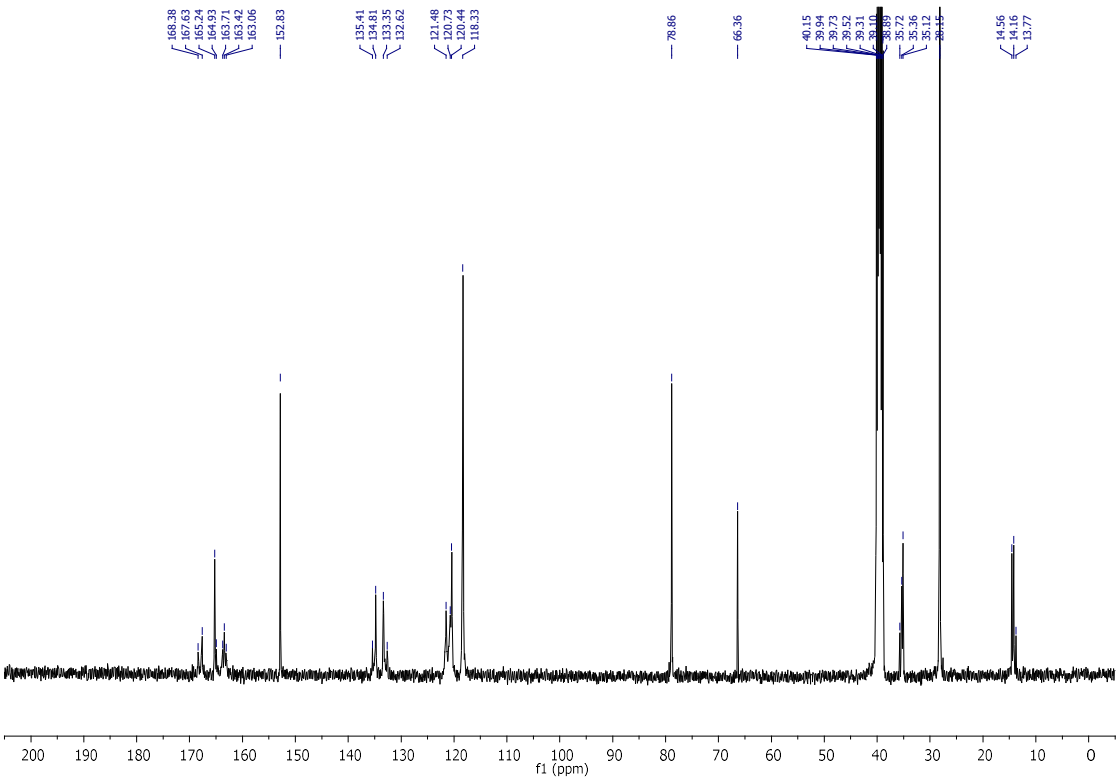

^{13}C NMR spectrum of compound **2.40**

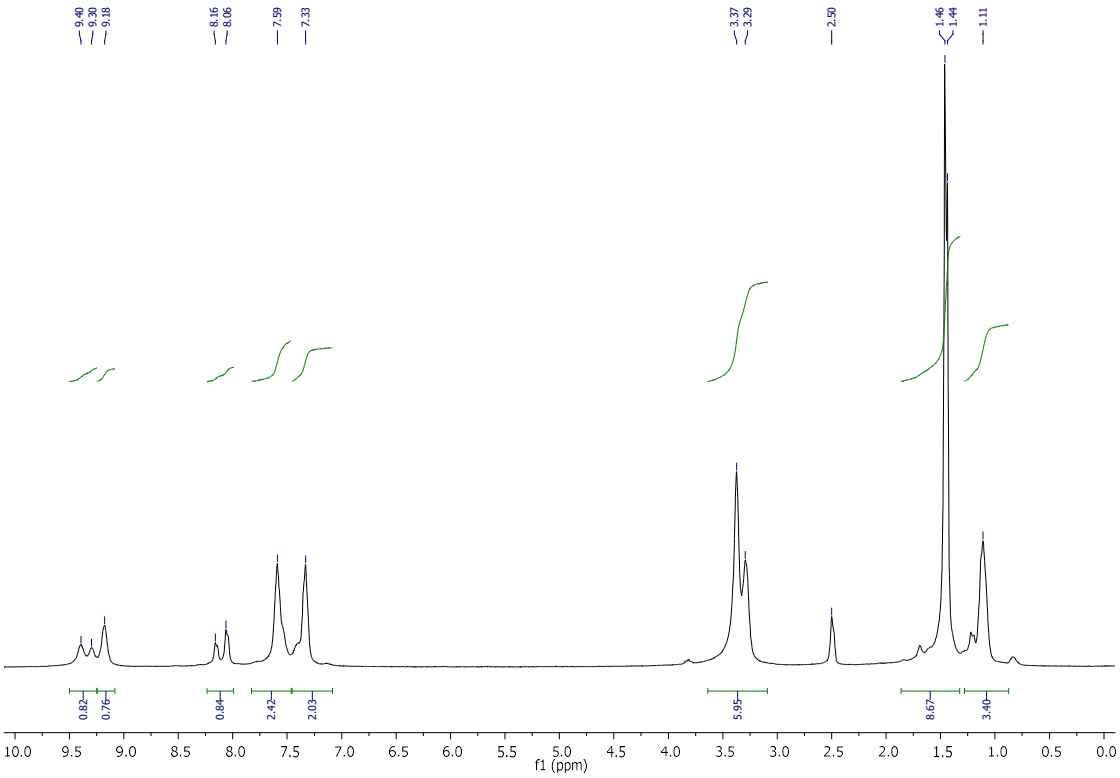

^{1}H NMR spectrum of compound **2.41**

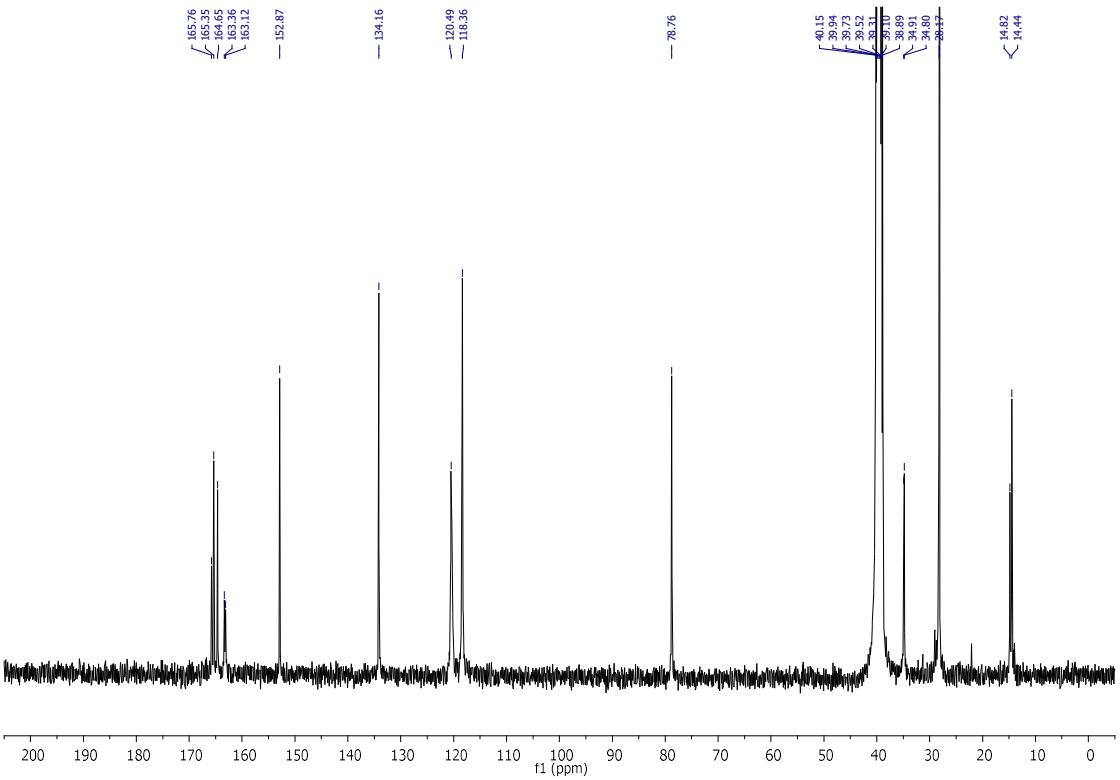

^{13}C NMR spectrum of compound **2.41**

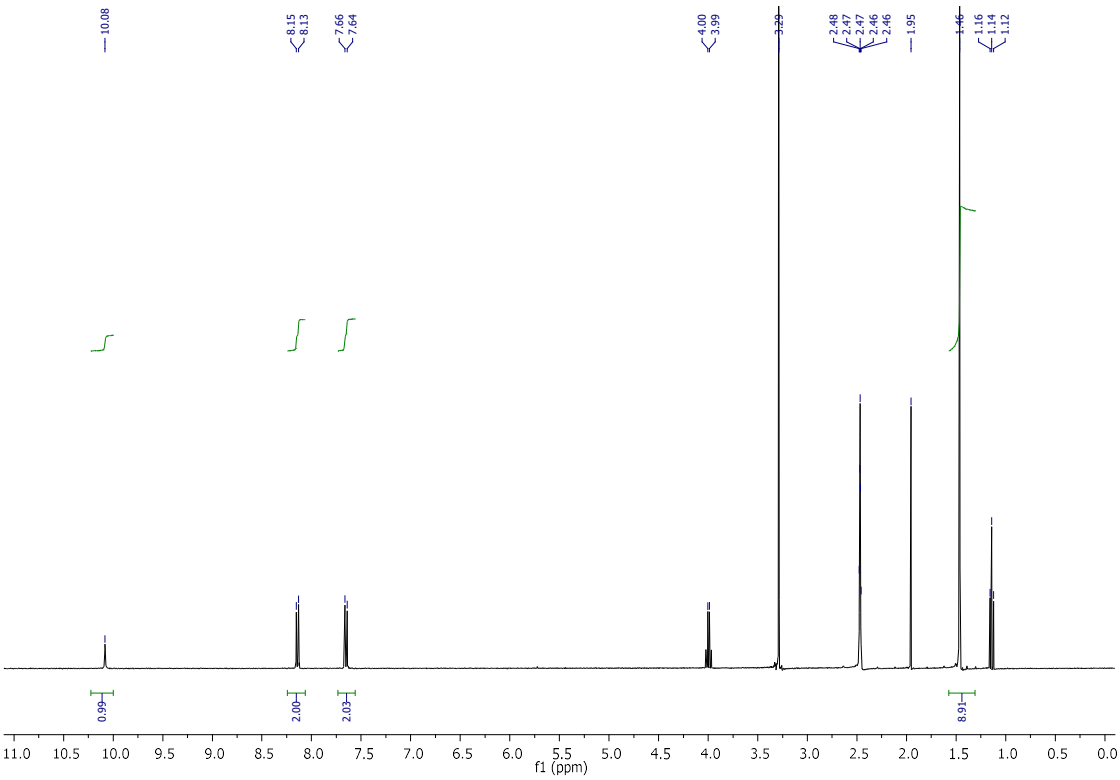

^{1}H NMR spectrum of compound **2.42**

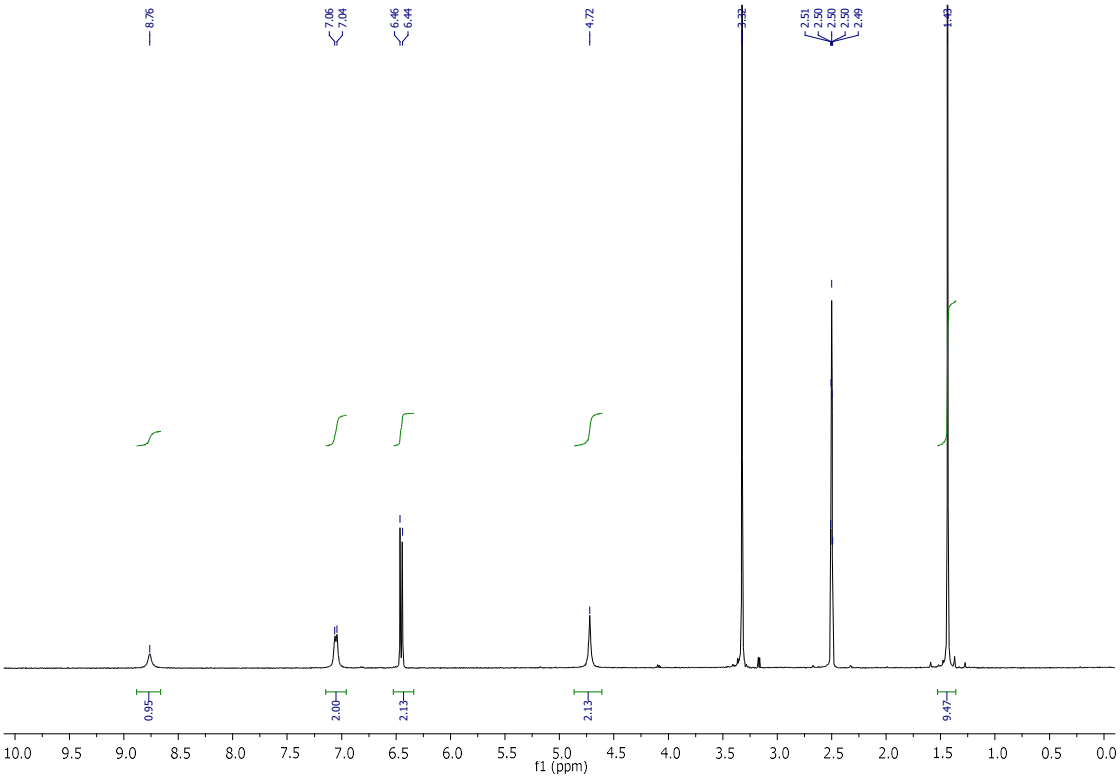

^{1}H NMR spectrum of compound **2.43**

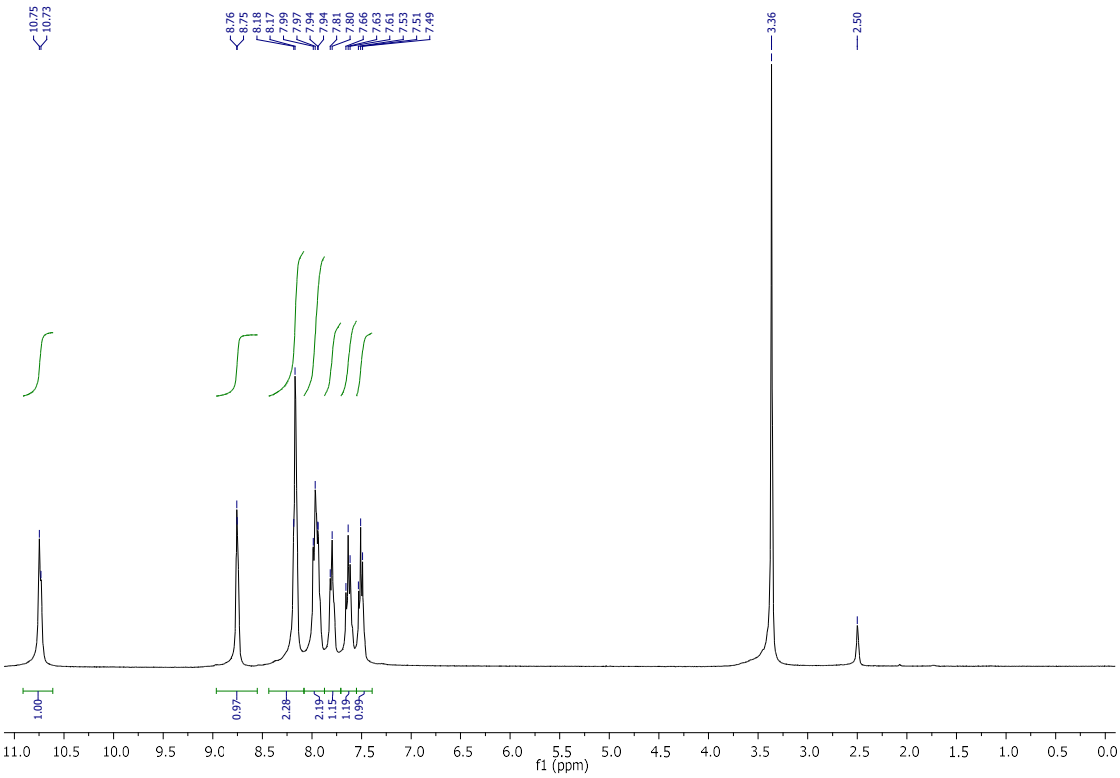

^{1}H NMR spectrum of compound **2.45**

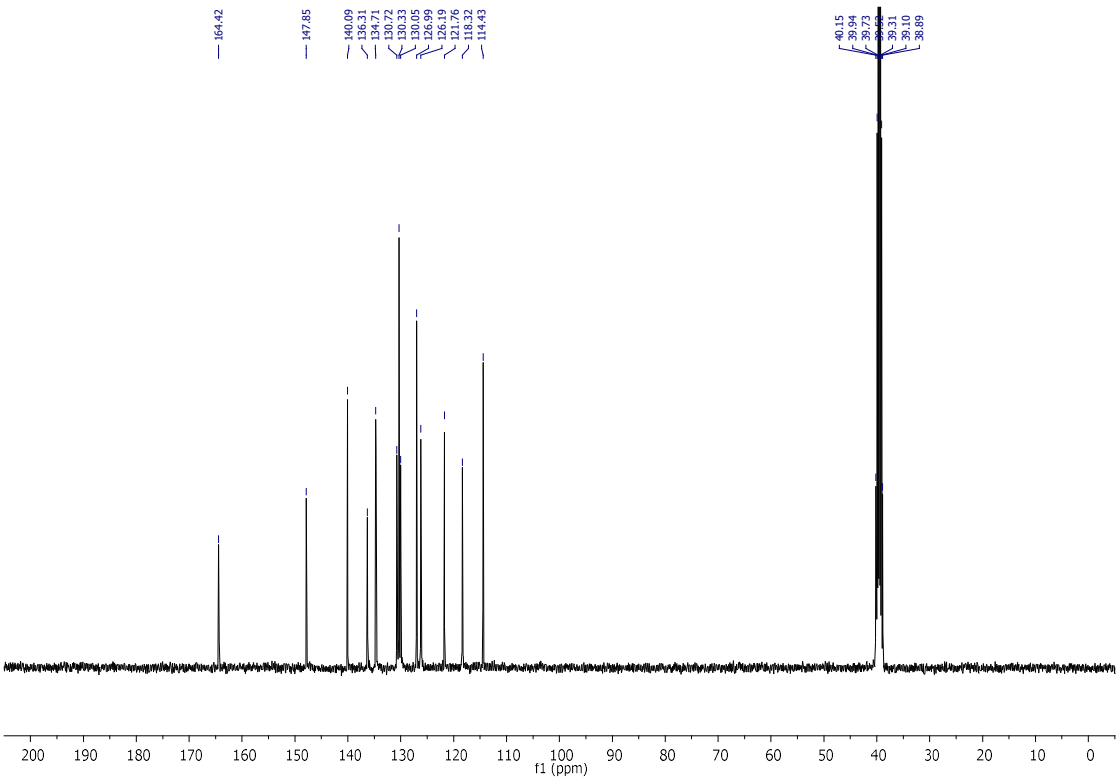

^{13}C NMR spectrum of compound **2.45**

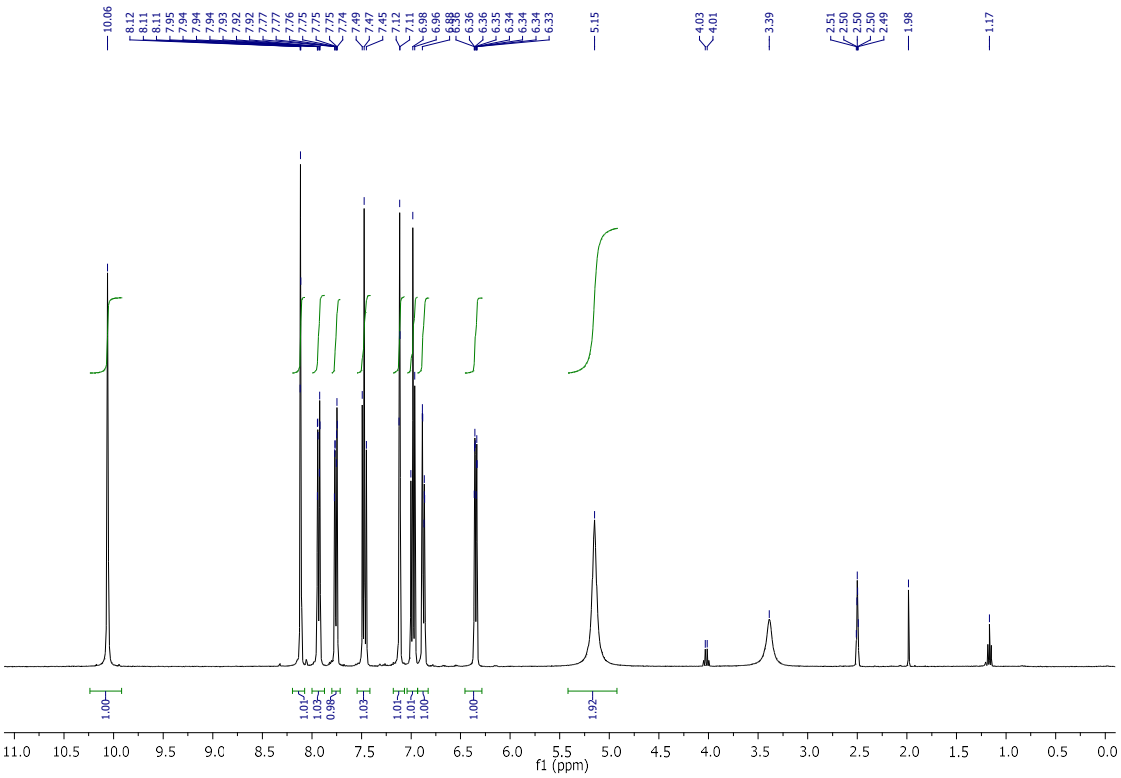

^{1}H NMR spectrum of compound **2.46**

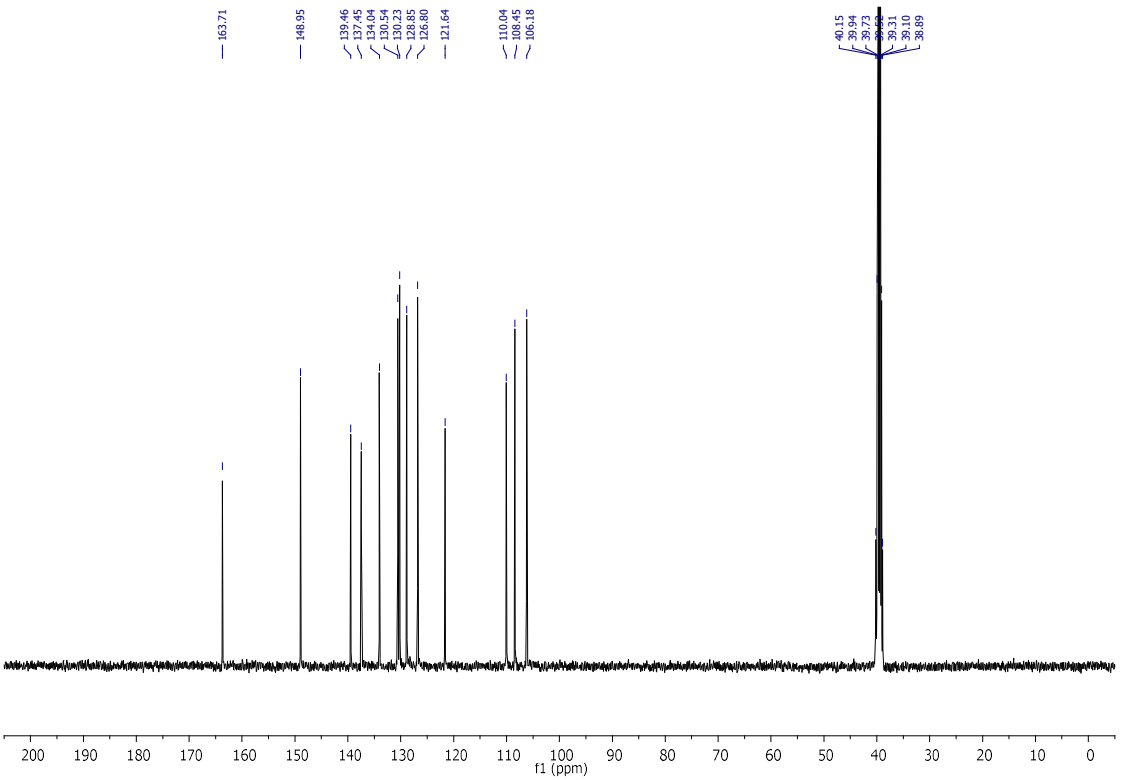

^{13}C NMR spectrum of compound **2.46**

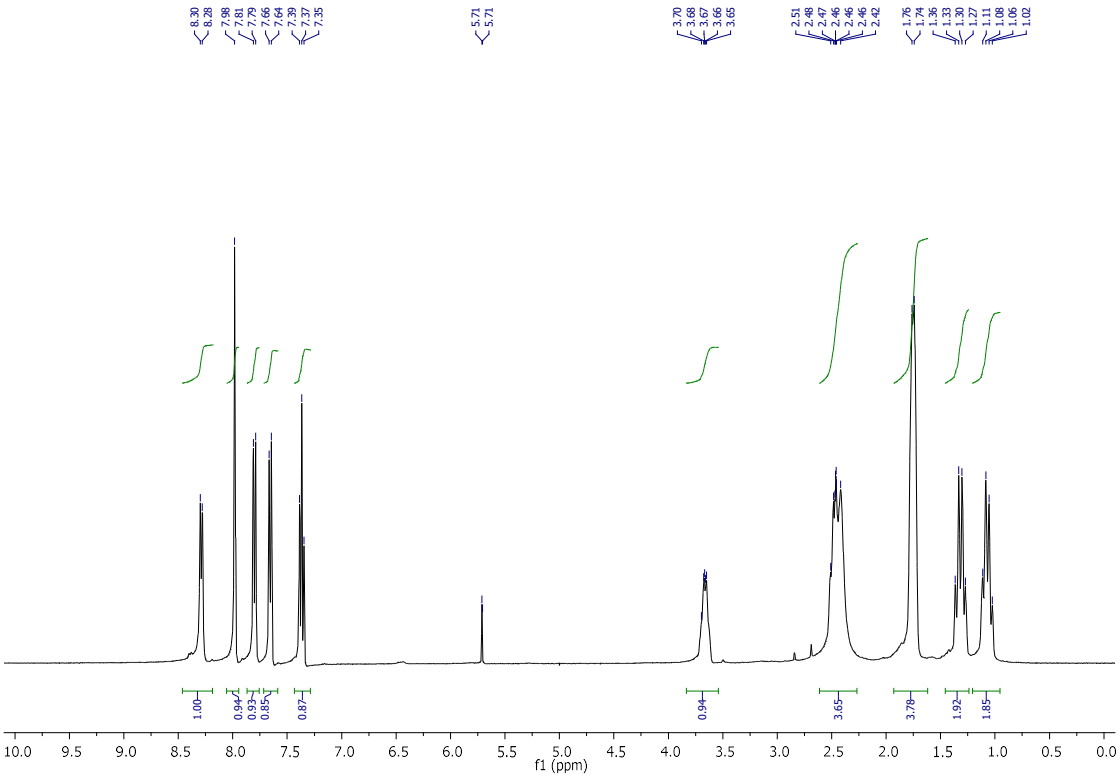

^{1}H NMR spectrum of compound **2.47**

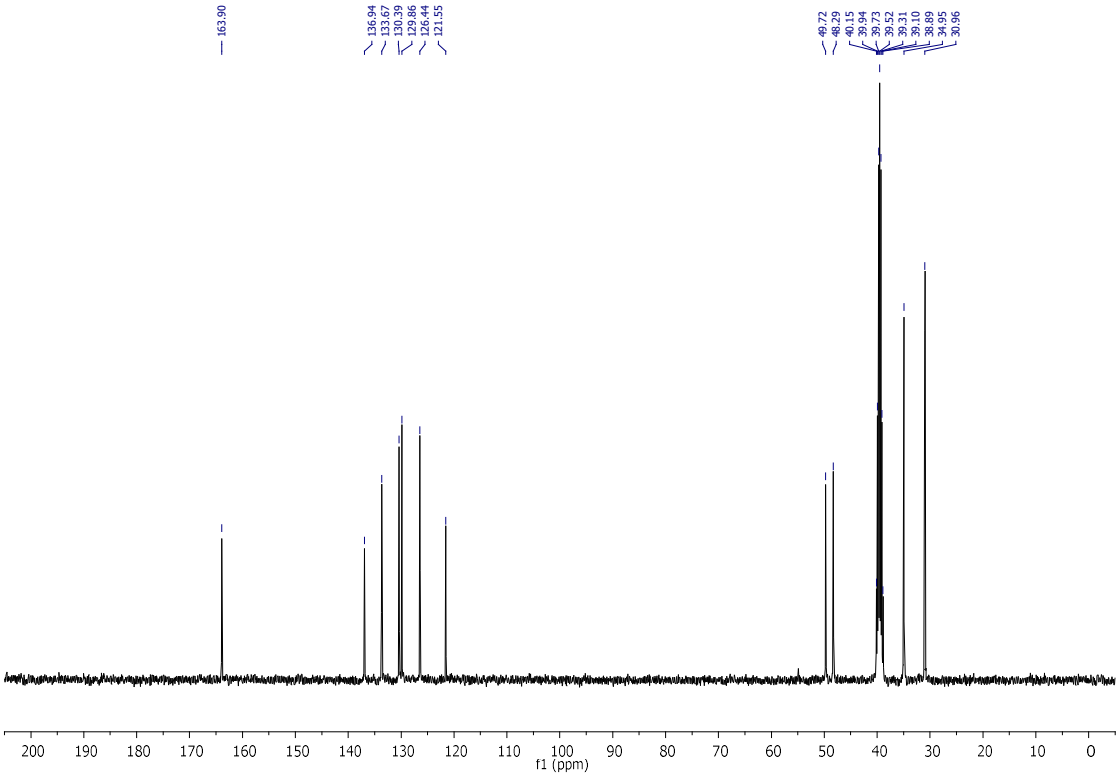

^{13}C NMR spectrum of compound **2.47**

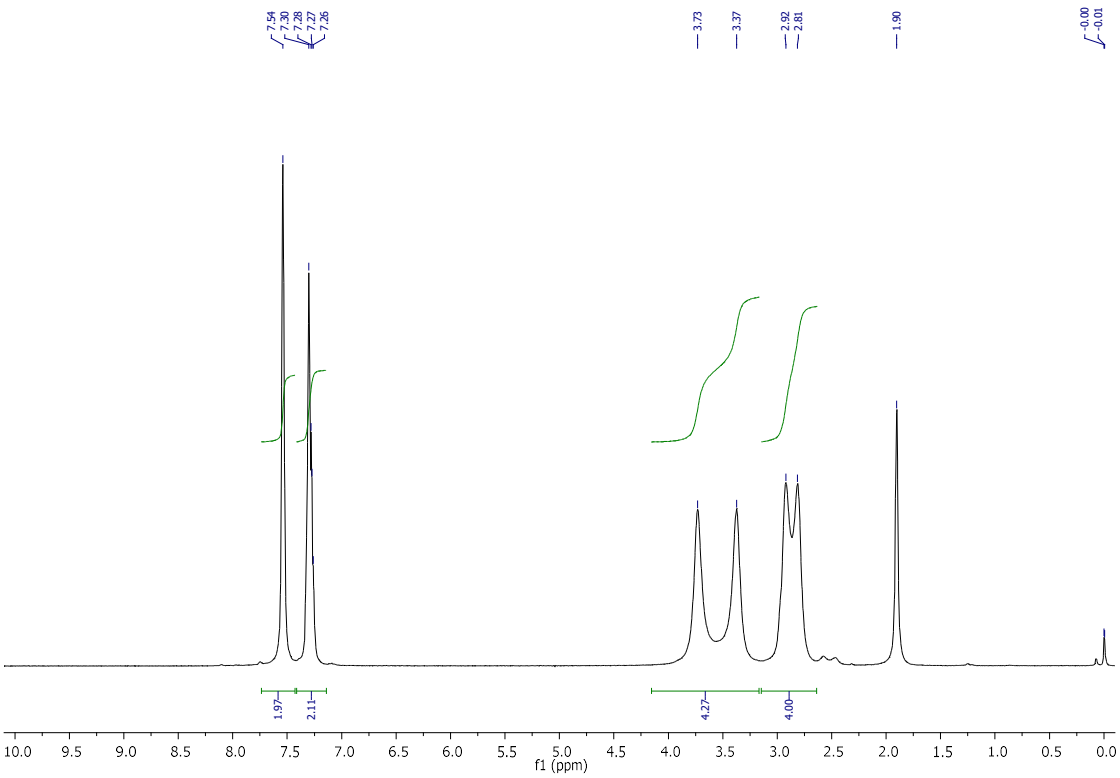

^{1}H NMR spectrum of compound **2.48**

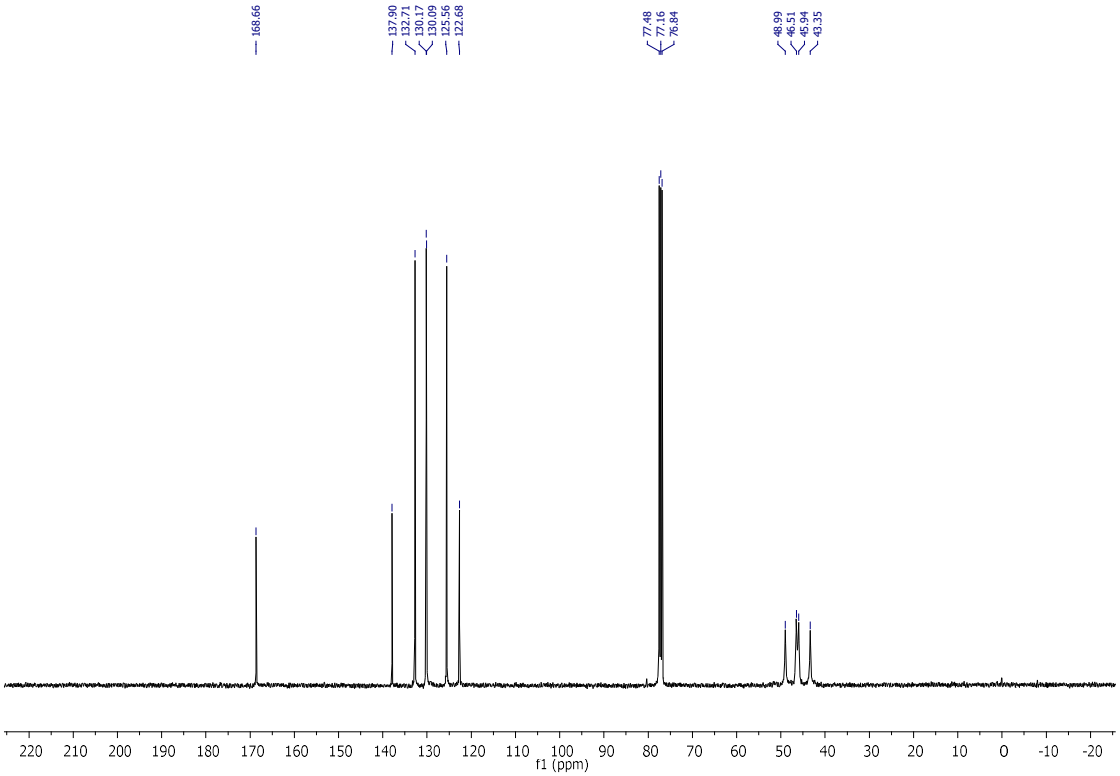

^{13}C NMR spectrum of compound **2.48**

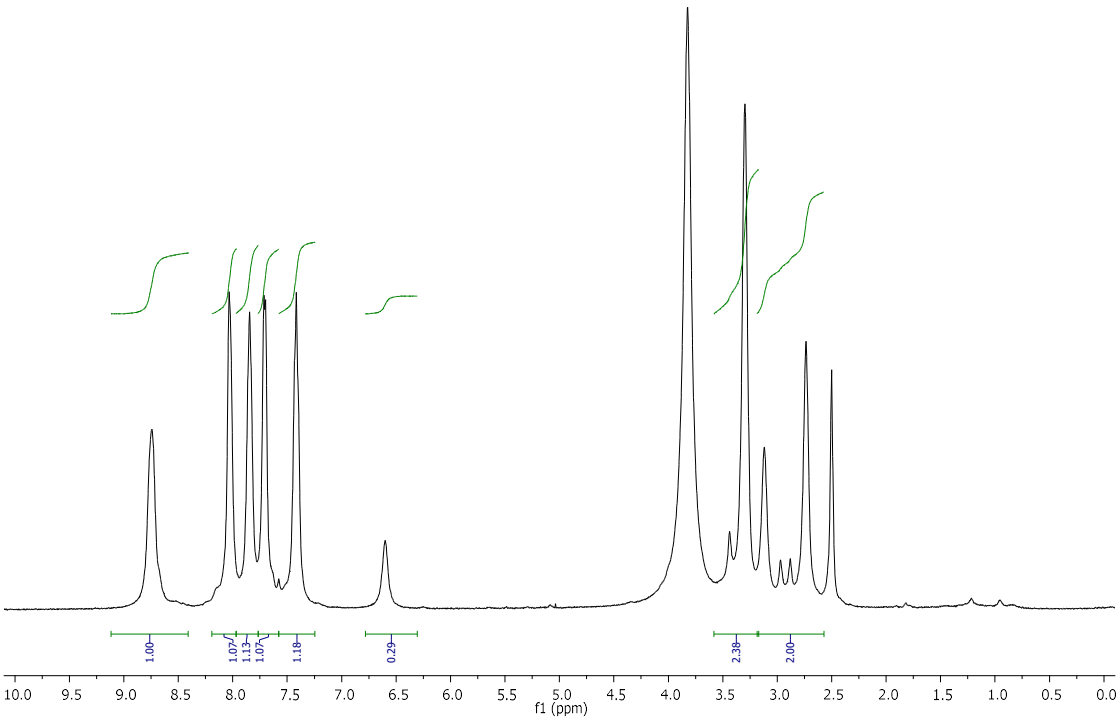

^{1}H NMR spectrum of compound **2.49**

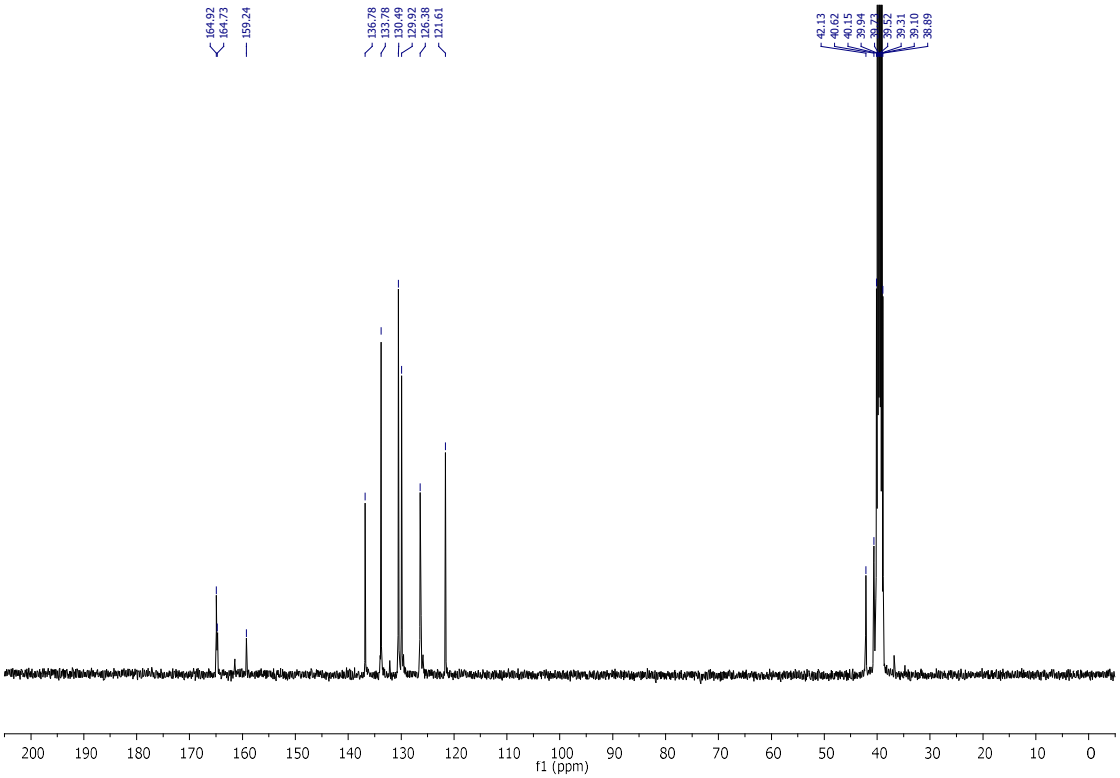

^{13}C NMR spectrum of compound **2.49**

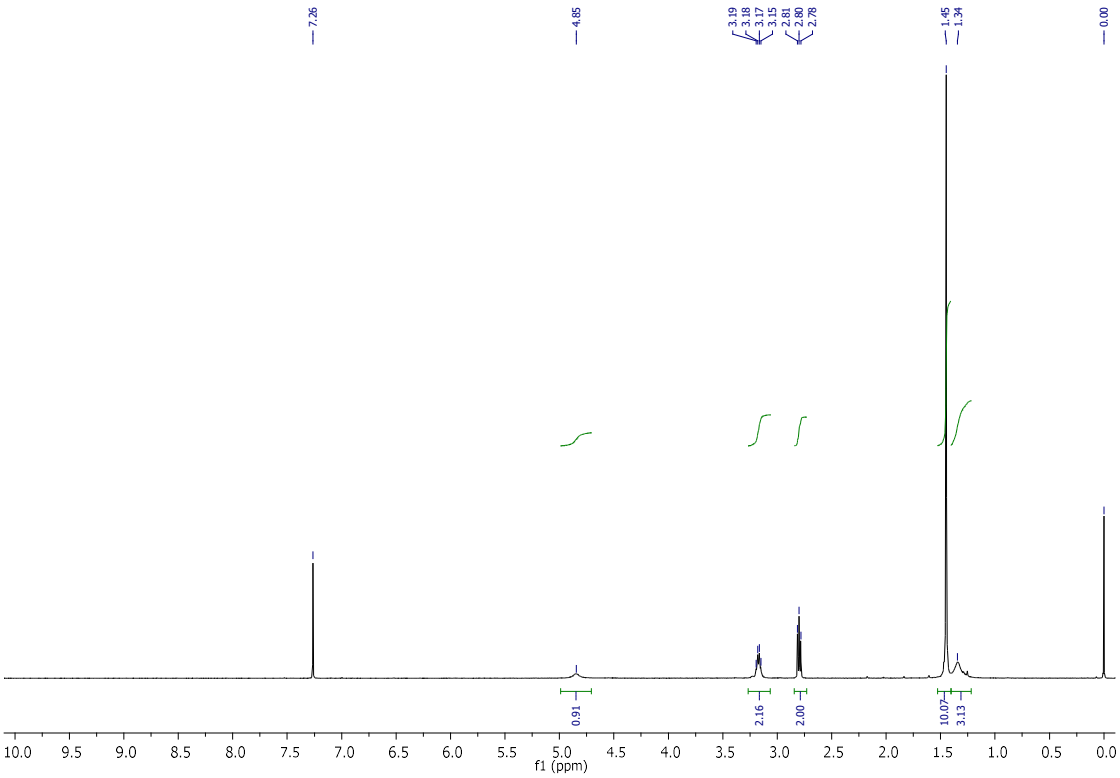

^{1}H NMR spectrum of compound **2.55**

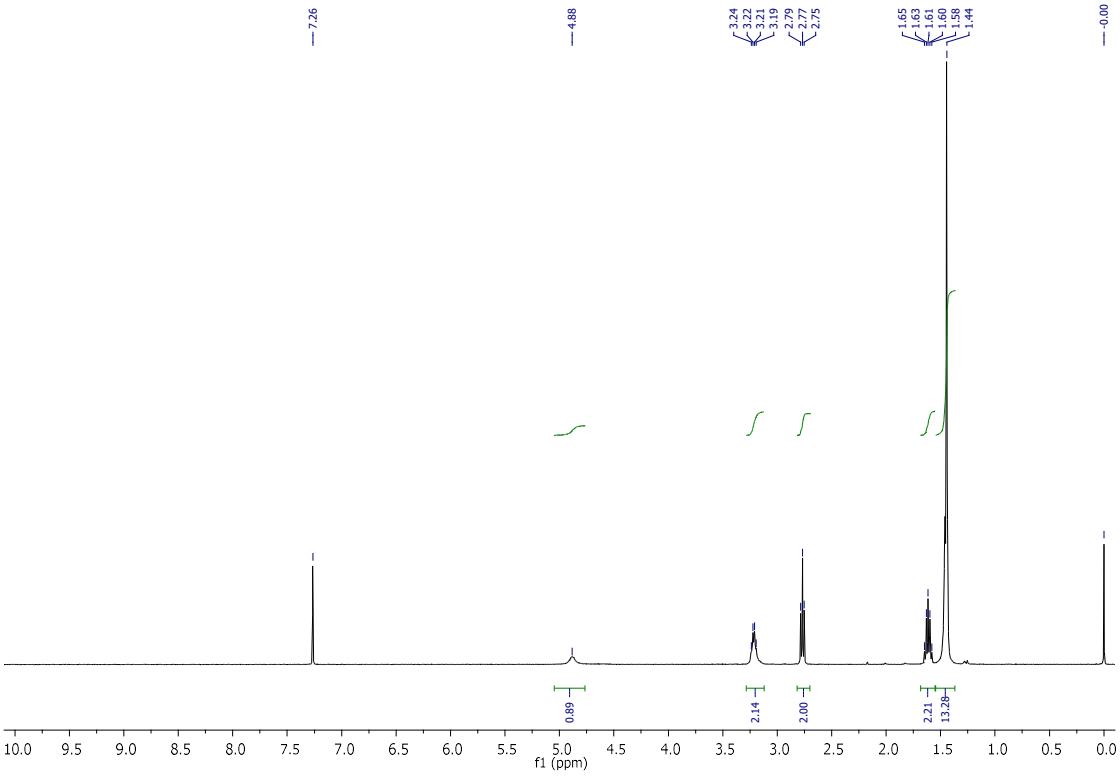

^{1}H NMR spectrum of compound **2.56**

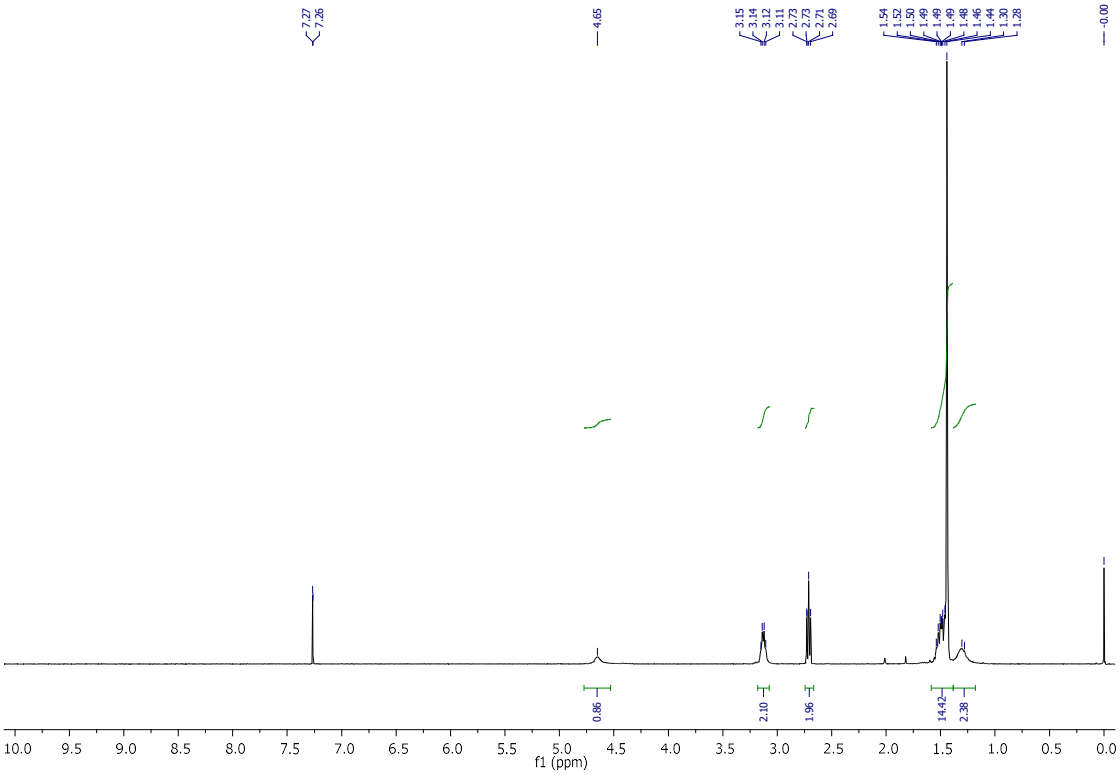

^{1}H NMR spectrum of compound **2.57**

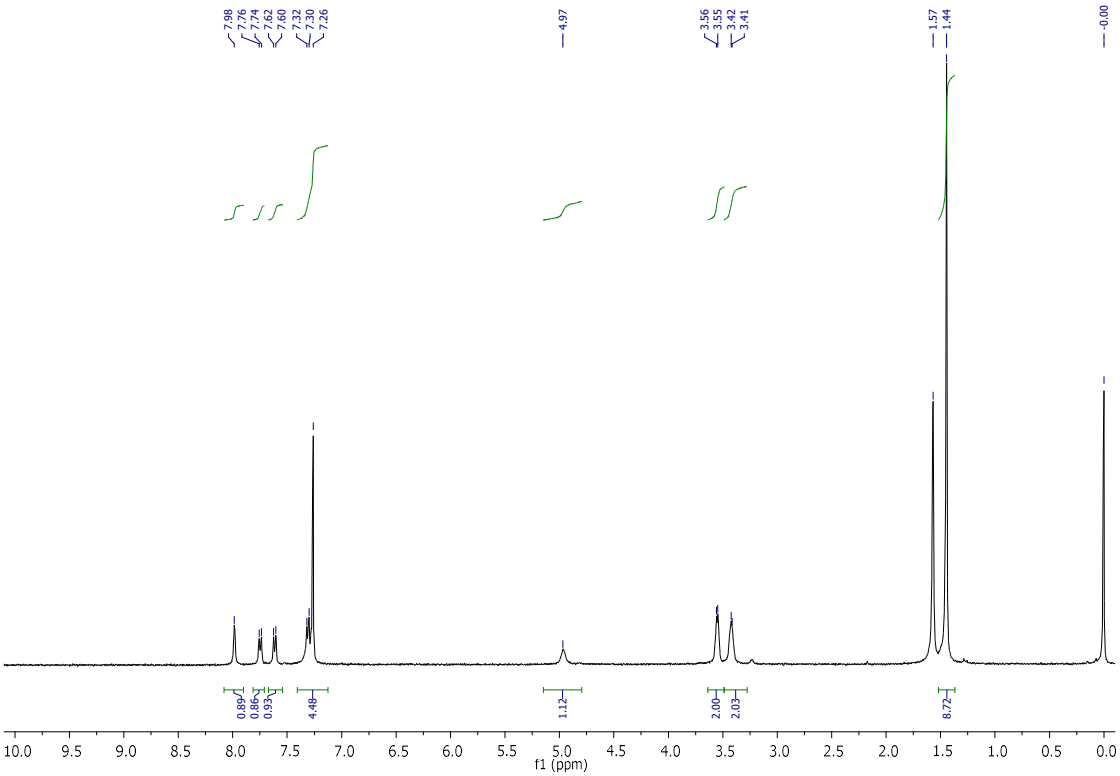

^{1}H NMR spectrum of compound **2.58**

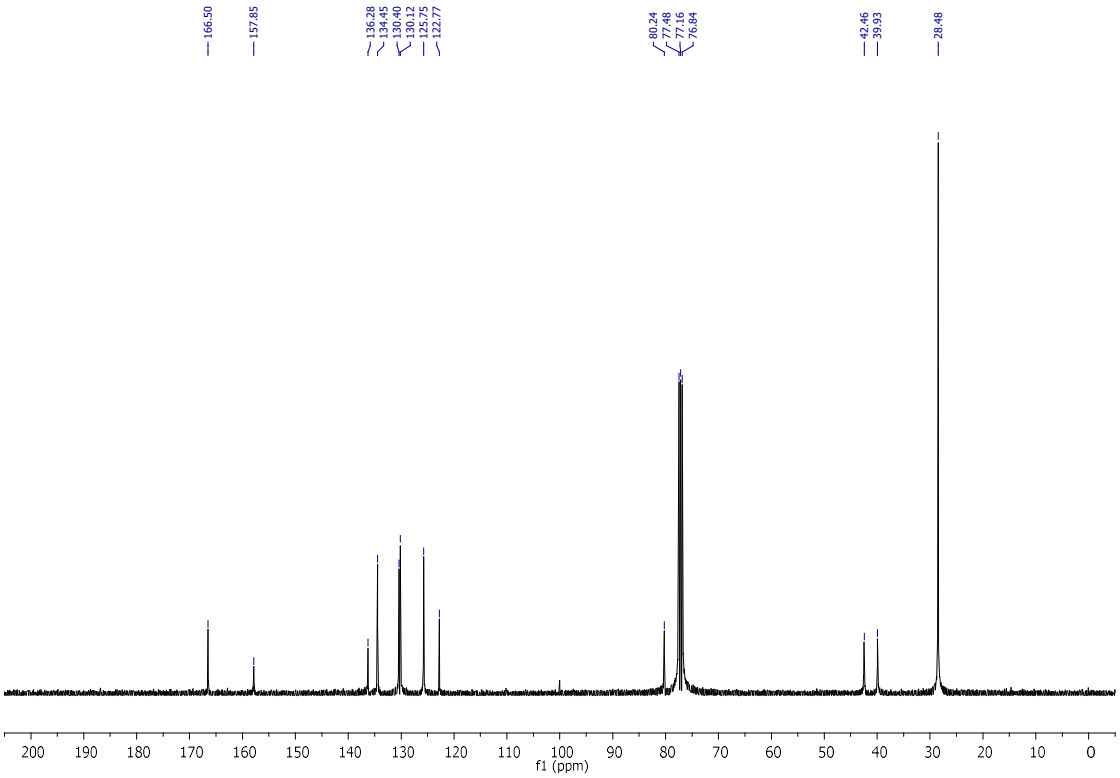

^{13}C NMR spectrum of compound **2.58**

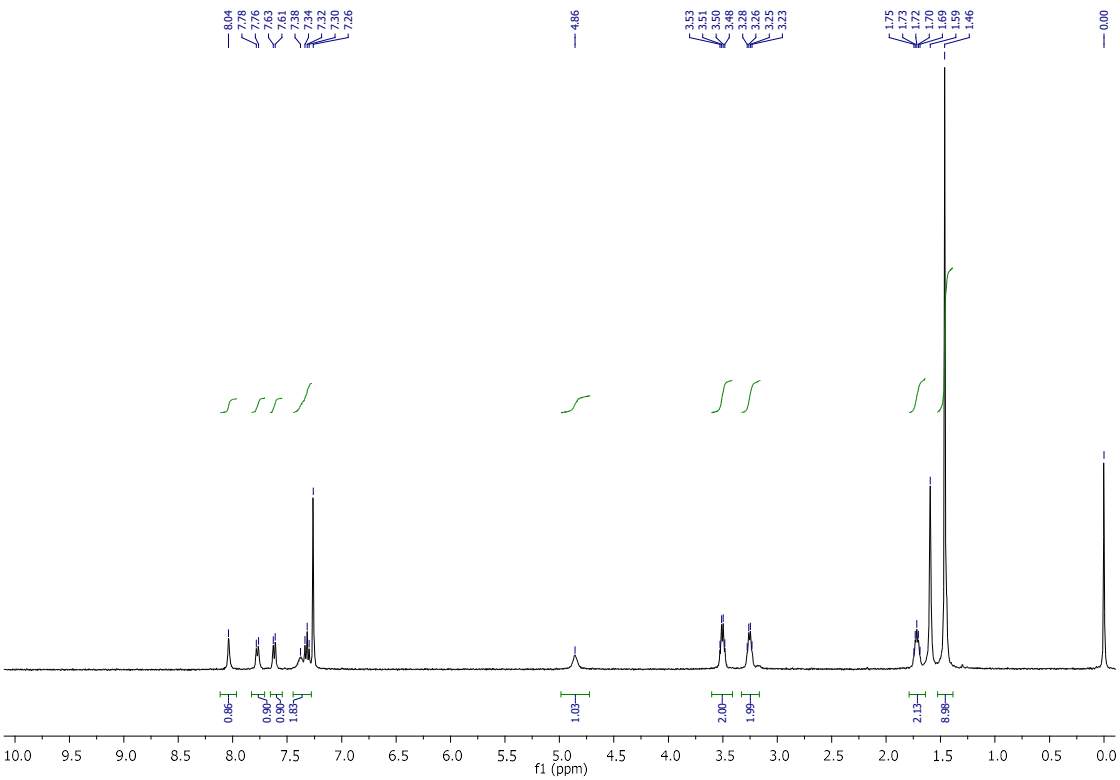

^{1}H NMR spectrum of compound **2.59**

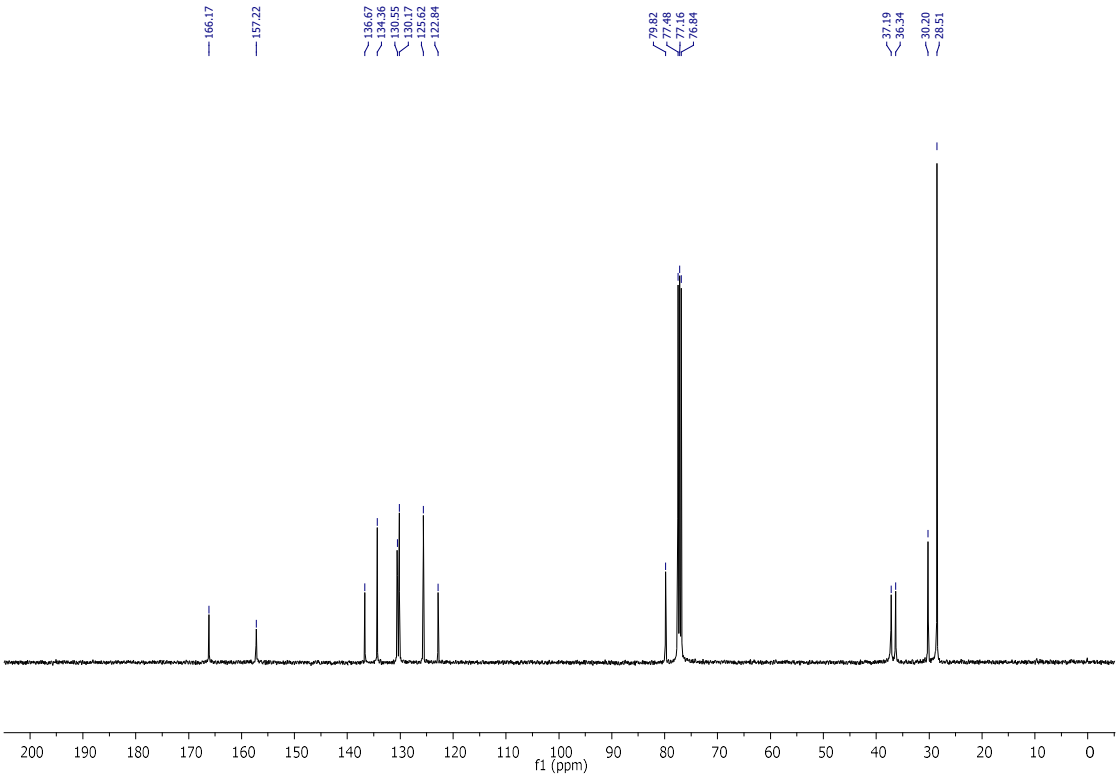

^{13}C NMR spectrum of compound **2.59**

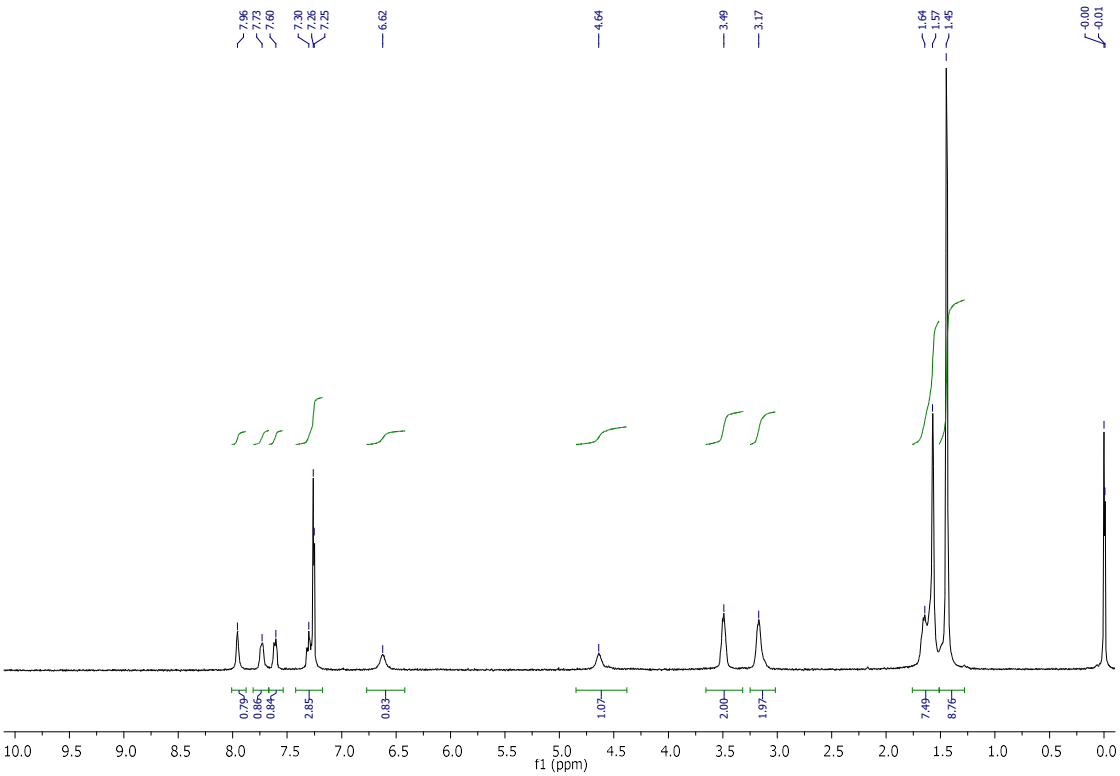

^{1}H NMR spectrum of compound **2.60**

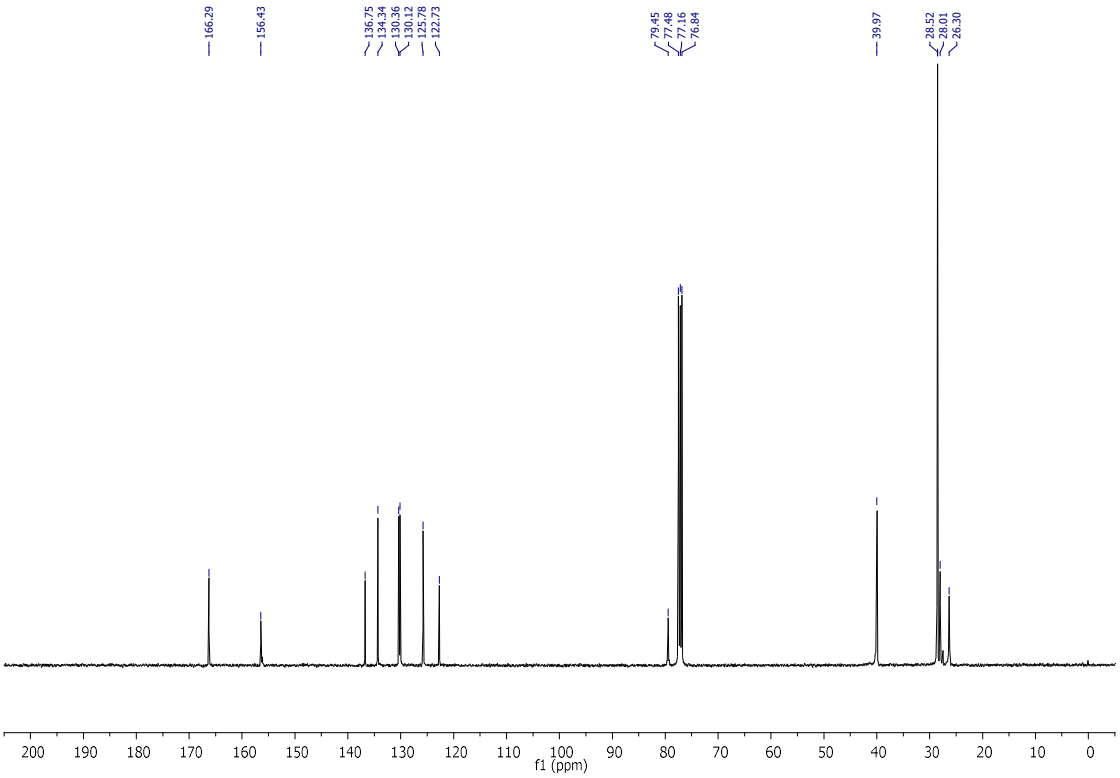

^{13}C NMR spectrum of compound **2.60**

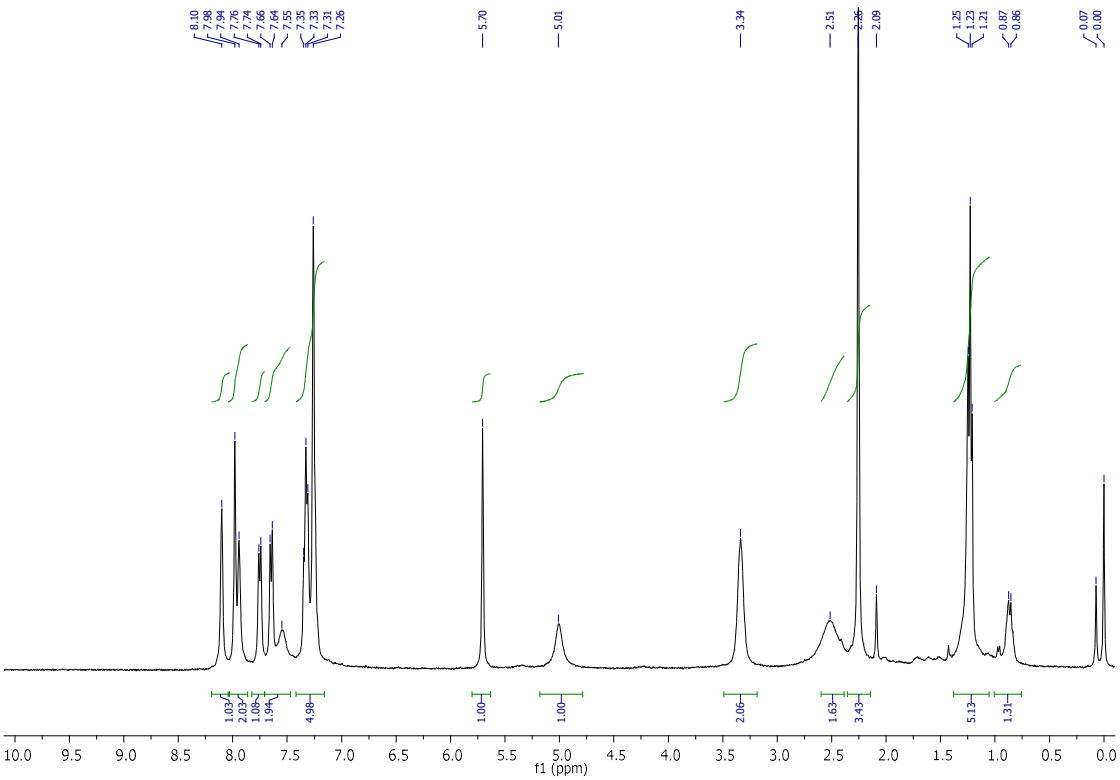

^{1}H NMR spectrum of compound **2.61**

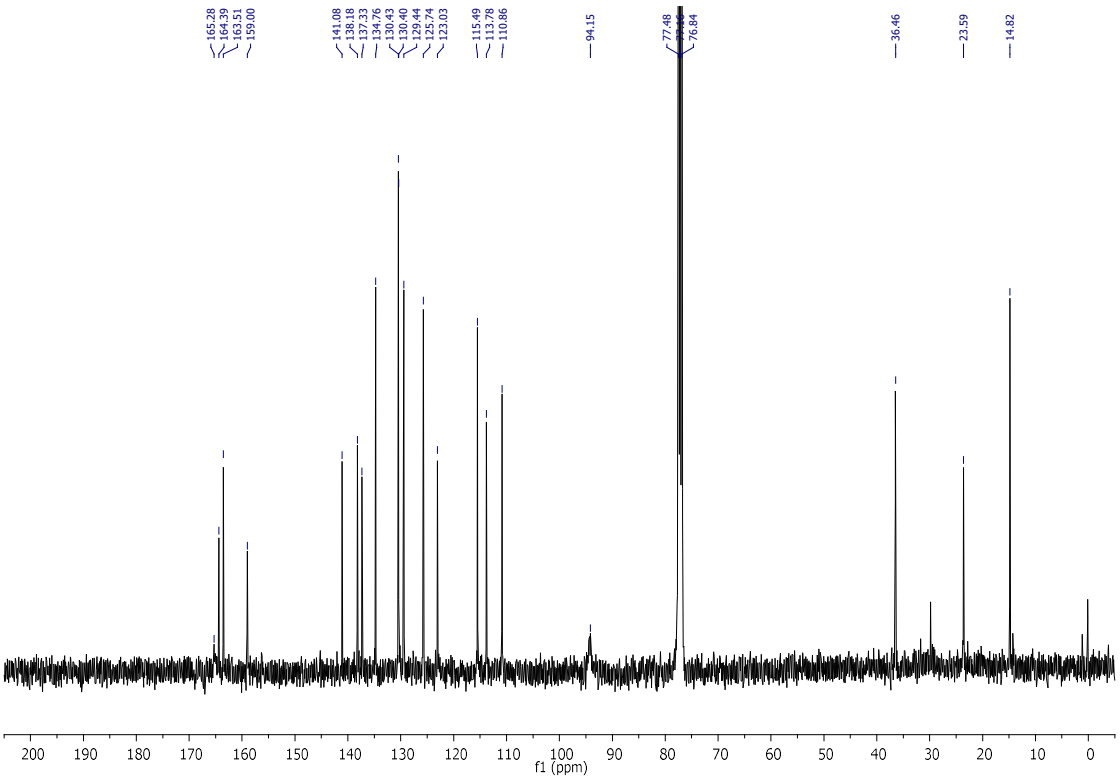

^{13}C NMR spectrum of compound **2.61**

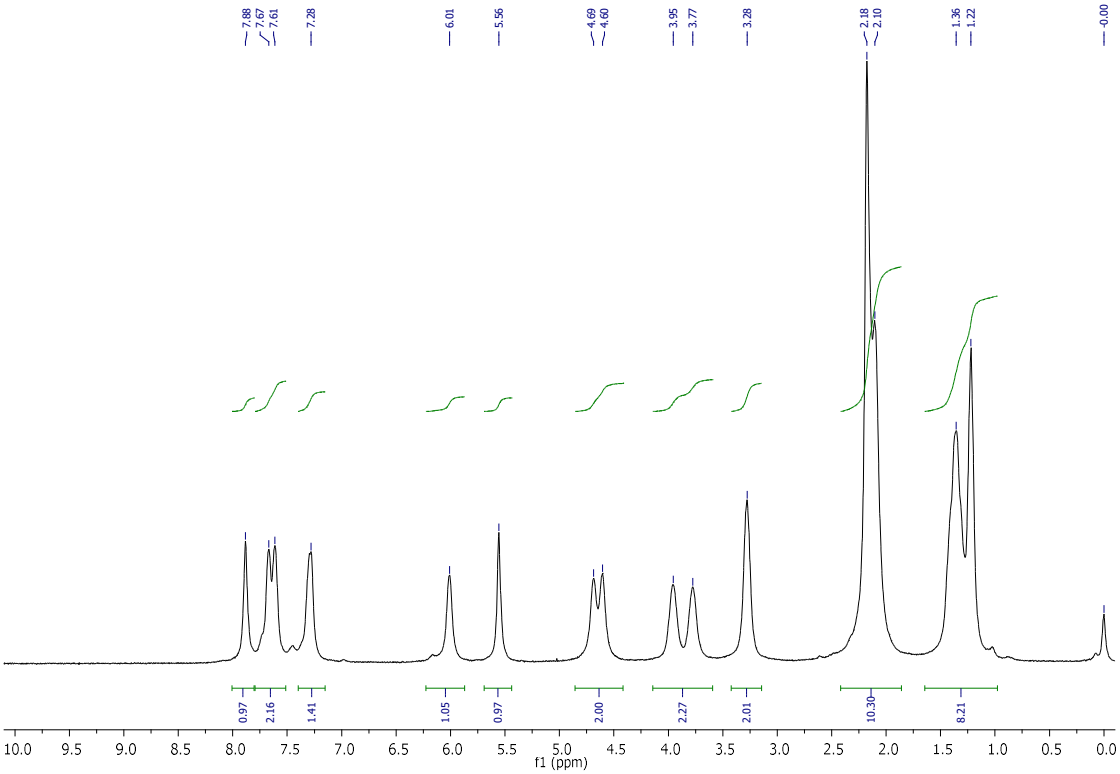

^{1}H NMR spectrum of compound **2.62**

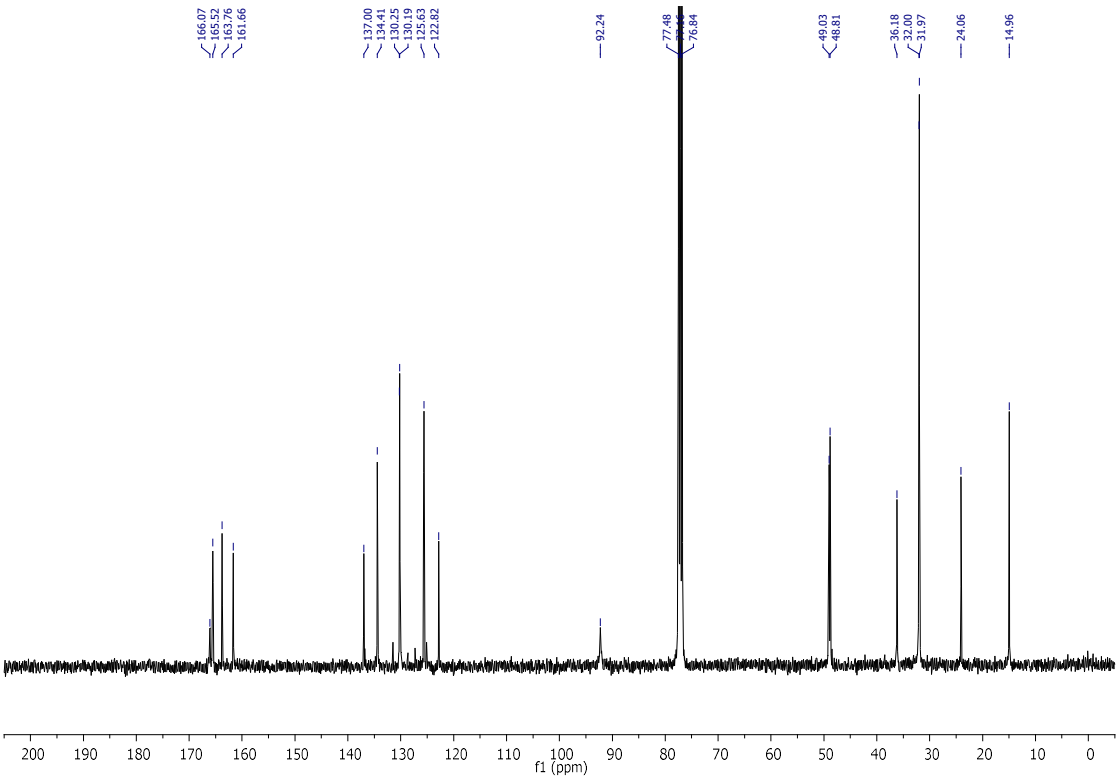

^{13}C NMR spectrum of compound **2.62**

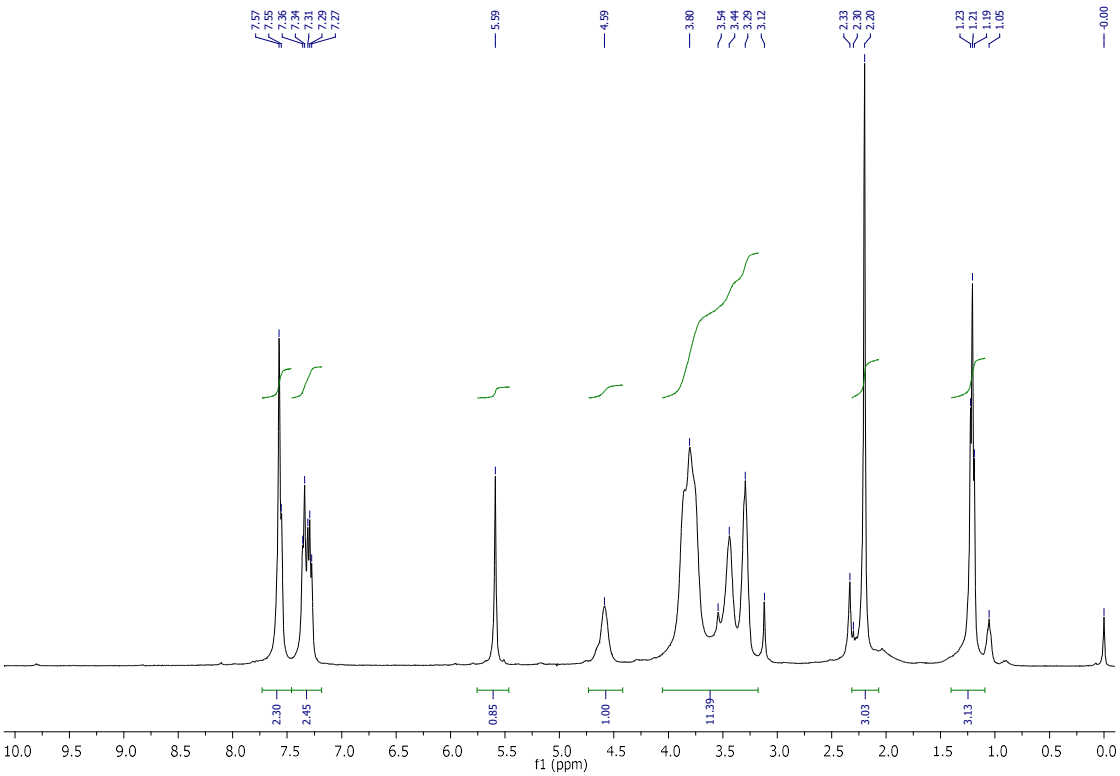

^{1}H NMR spectrum of compound **2.63**

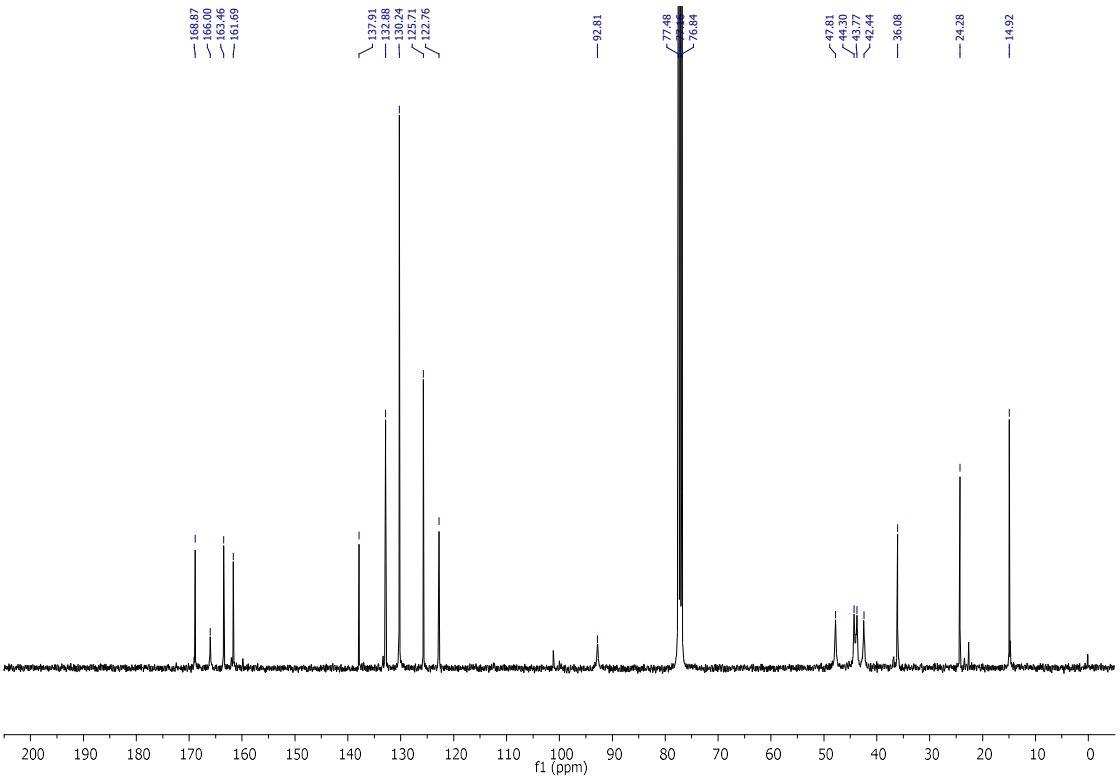

^{13}C NMR spectrum of compound **2.63**

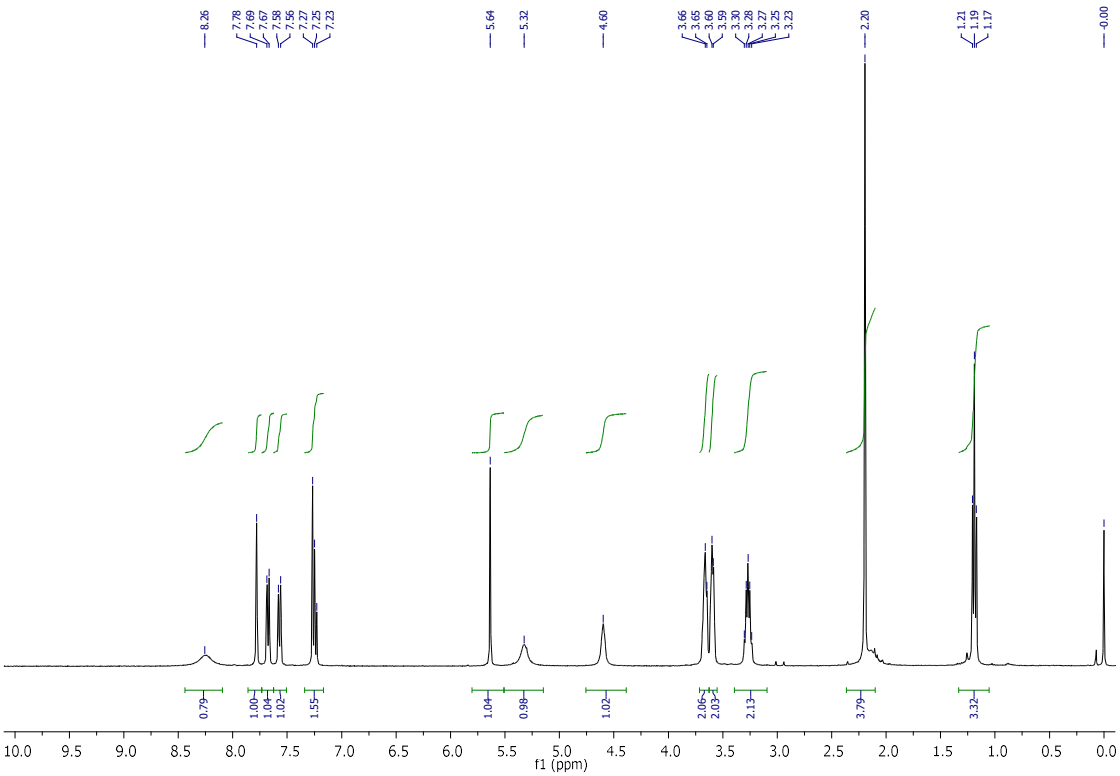

^{1}H NMR spectrum of compound **2.64**

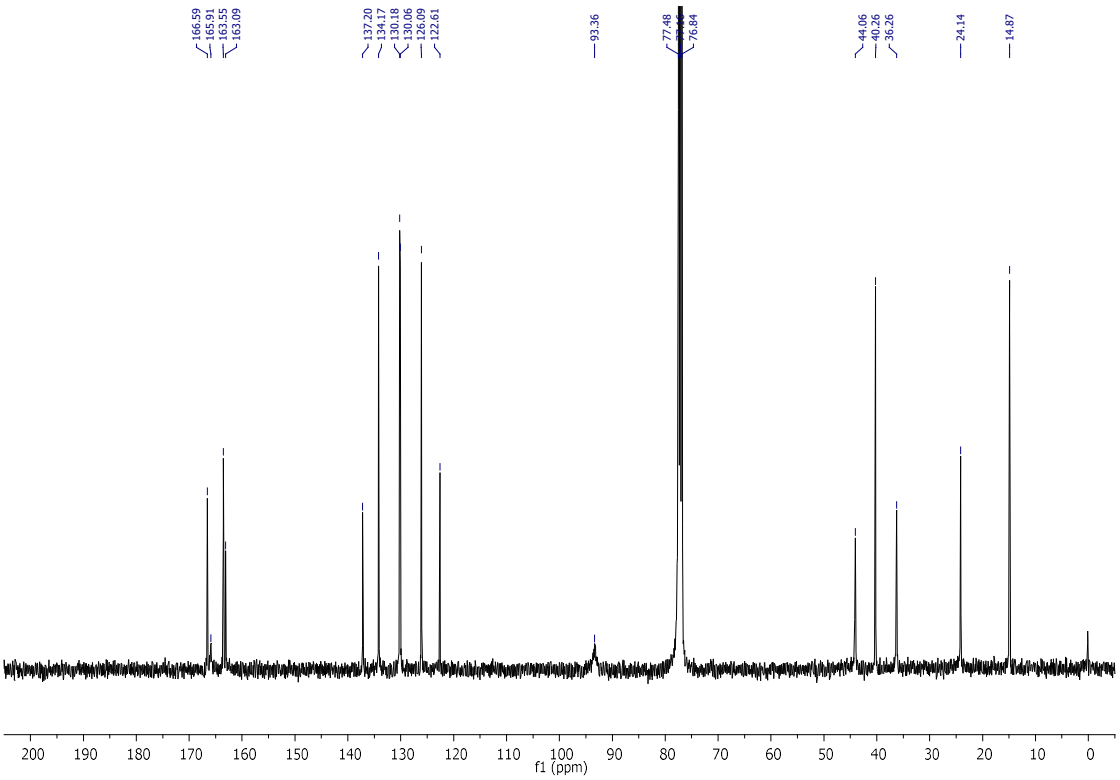

^{13}C NMR spectrum of compound **2.64**

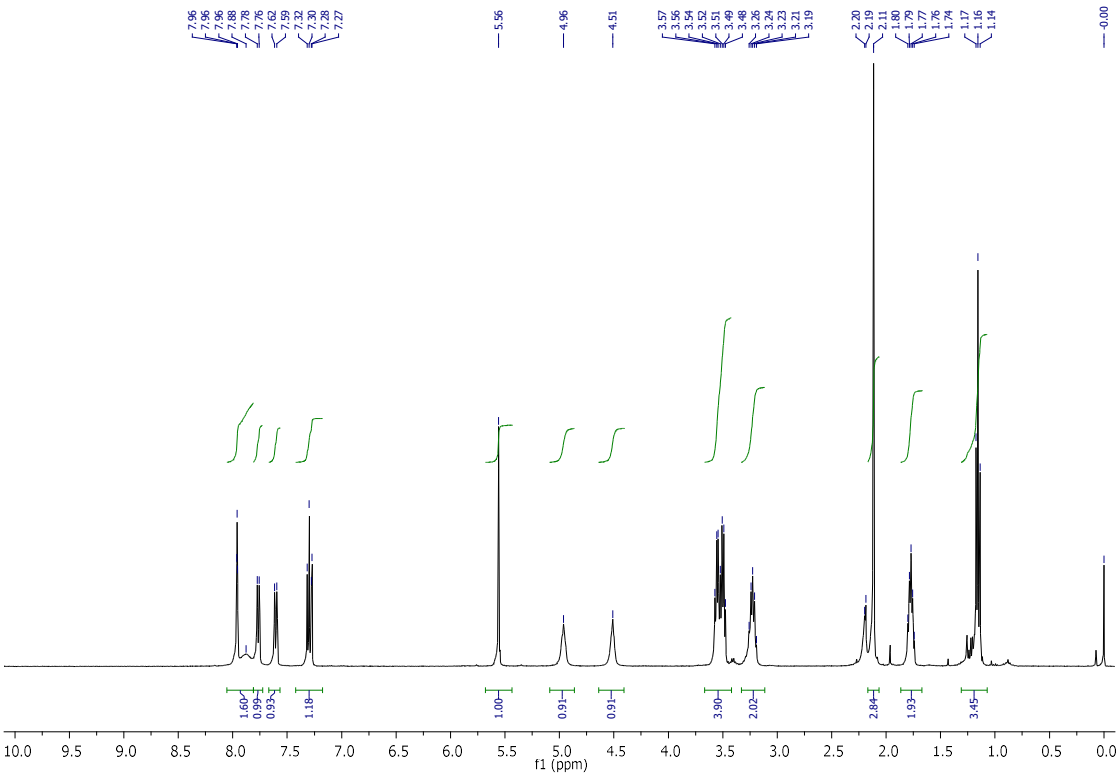

^{1}H NMR spectrum of compound **2.65**

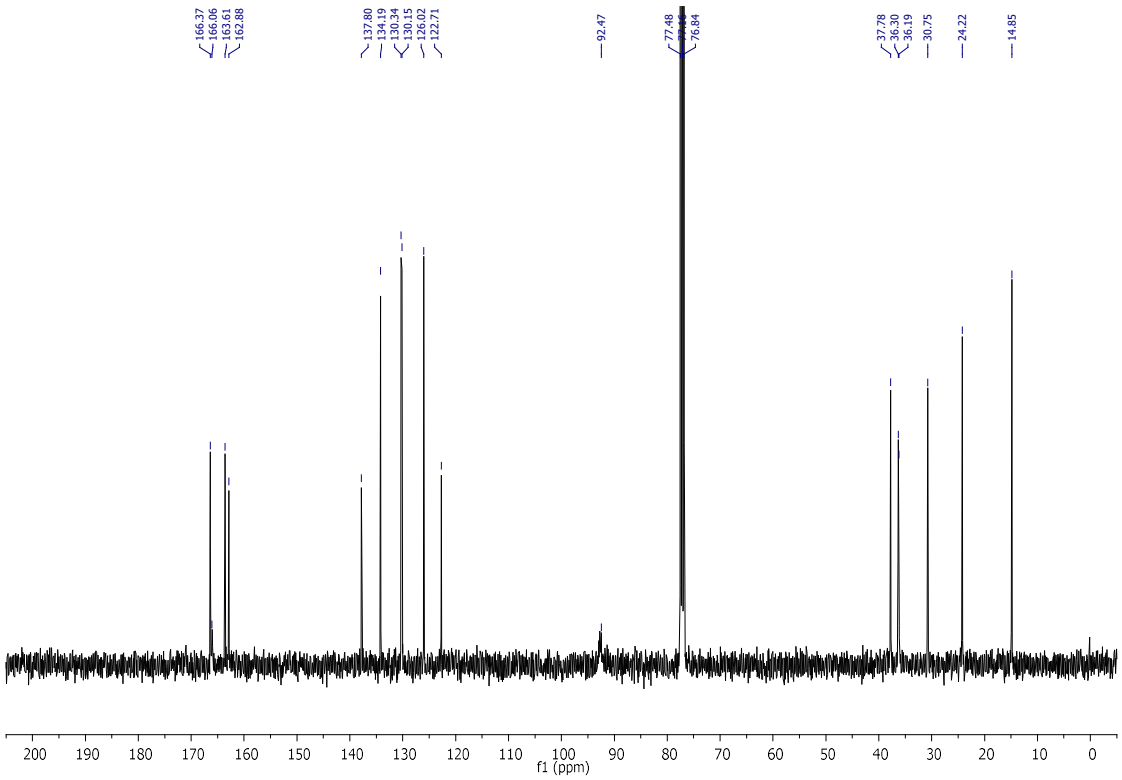

^{13}C NMR spectrum of compound **2.65**

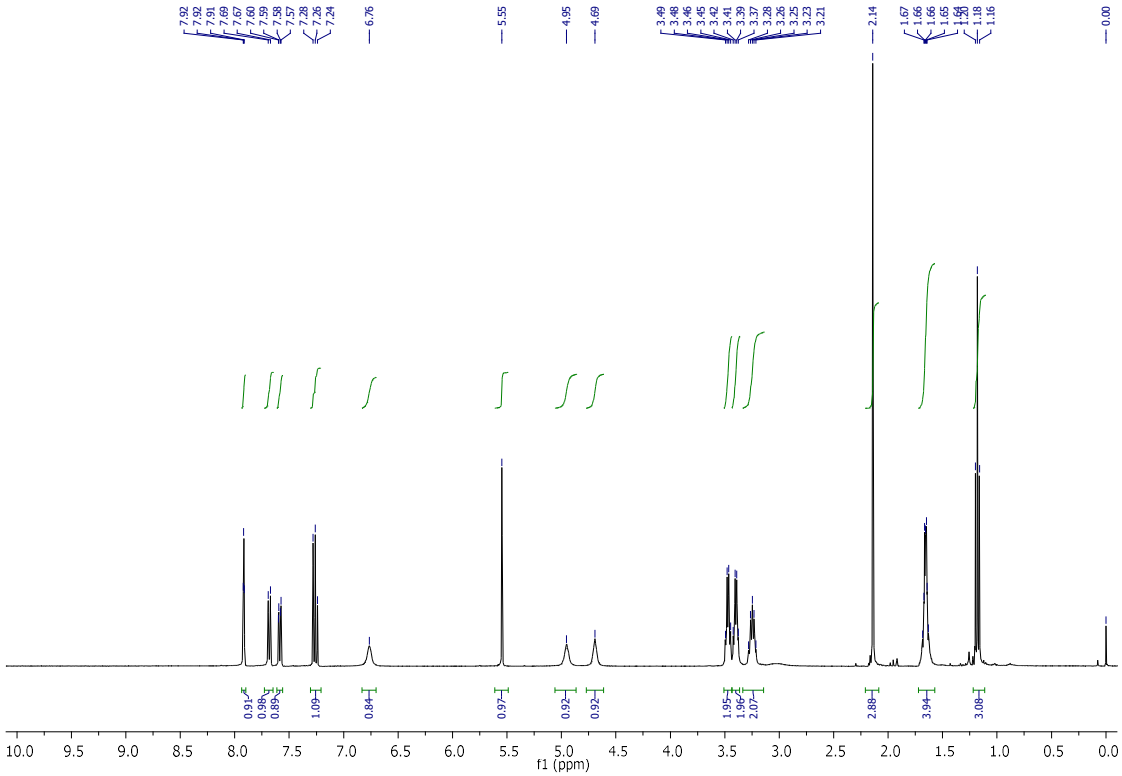

^{1}H NMR spectrum of compound **2.66**

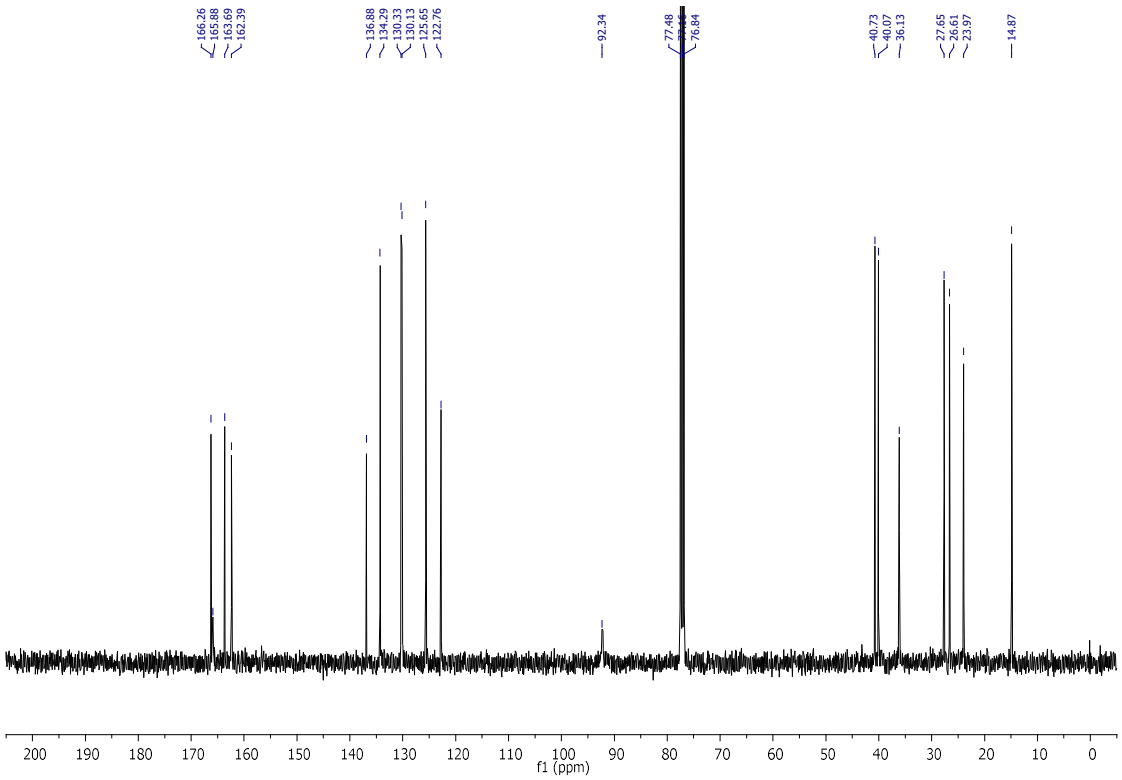

^{13}C NMR spectrum of compound **2.66**

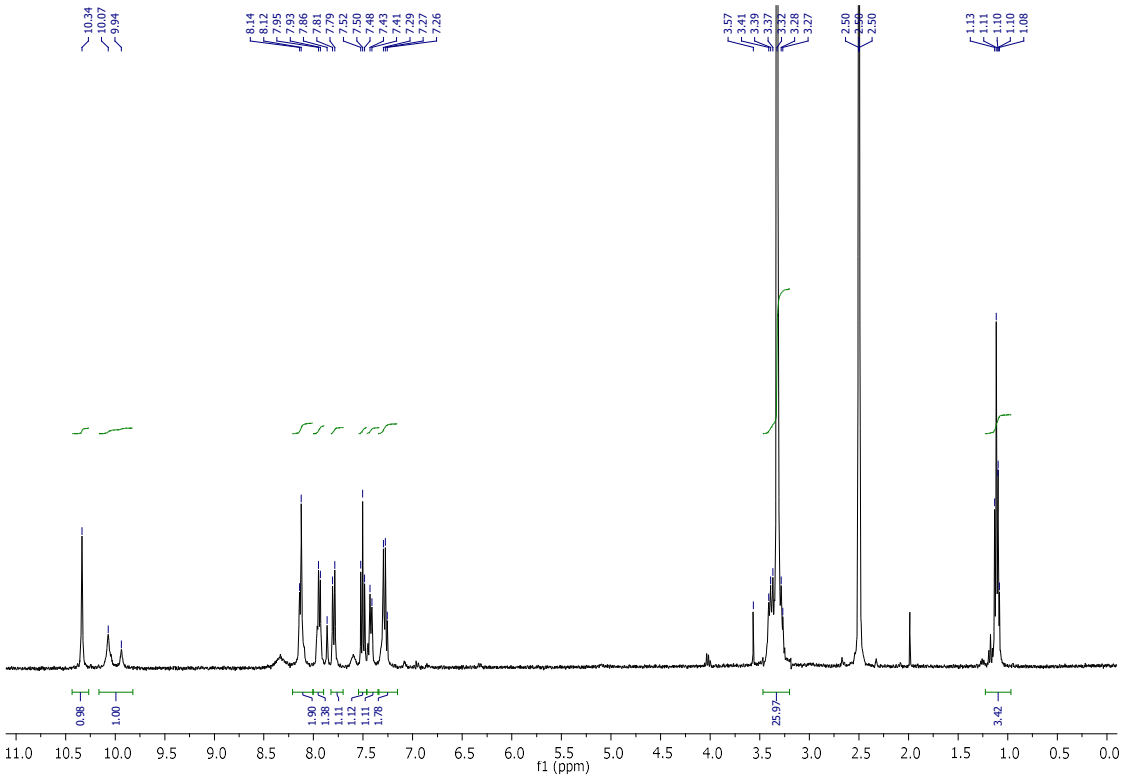

^{1}H NMR spectrum of compound **2.67**

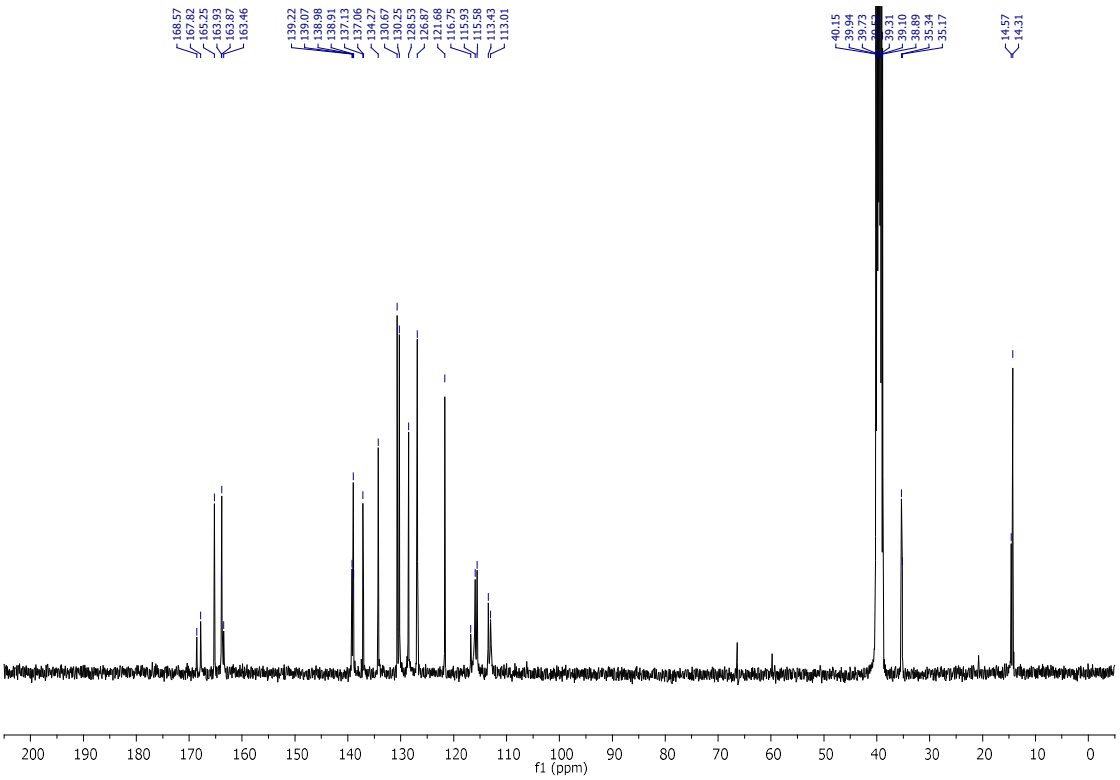

^{13}C NMR spectrum of compound **2.67**

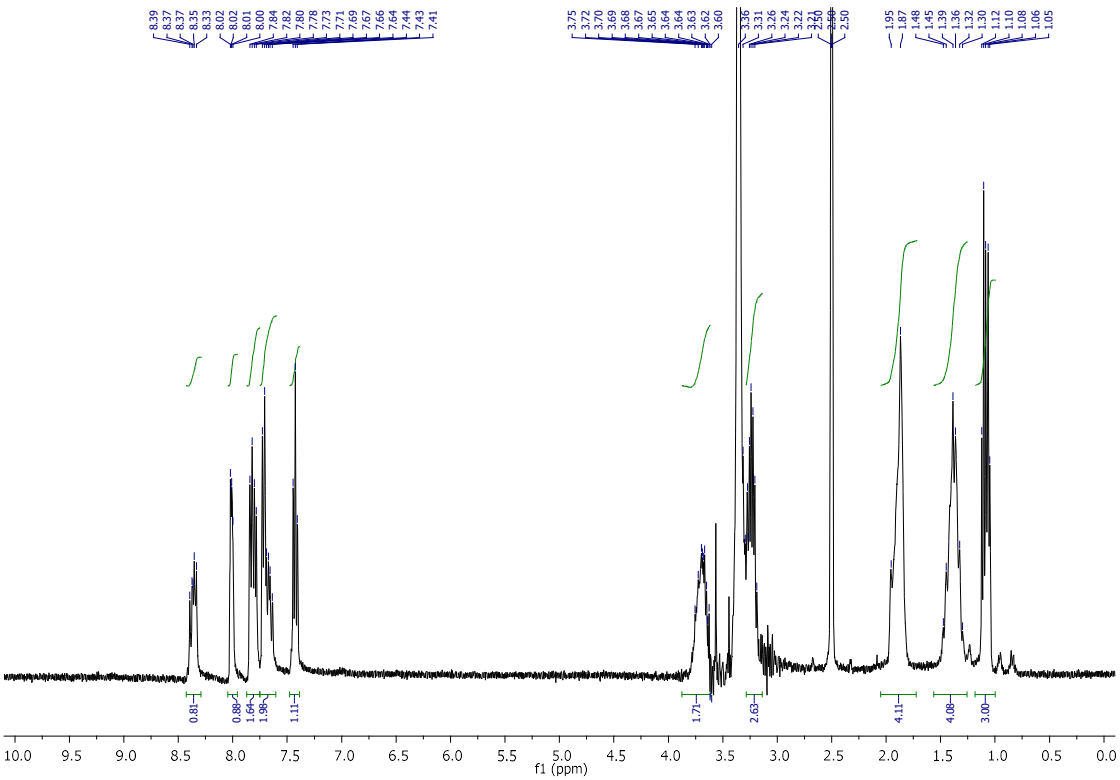

^{1}H NMR spectrum of compound **2.68**

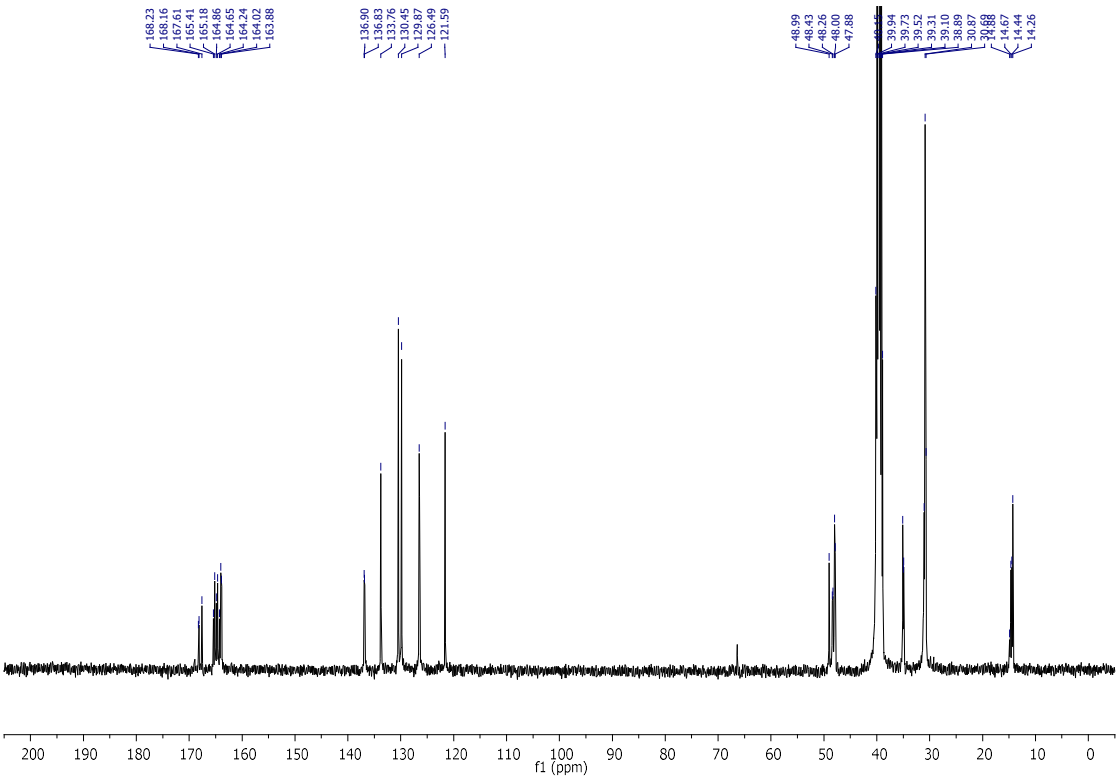

^{13}C NMR spectrum of compound **2.68**

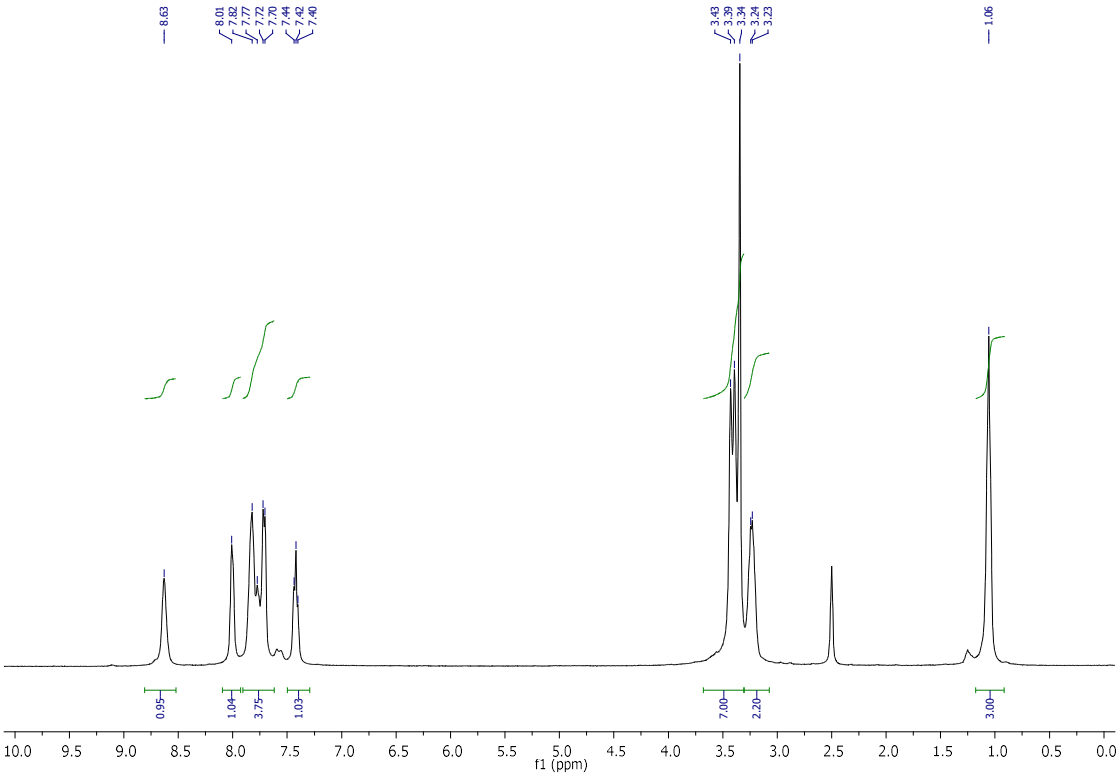

^{1}H NMR spectrum of compound **2.69**

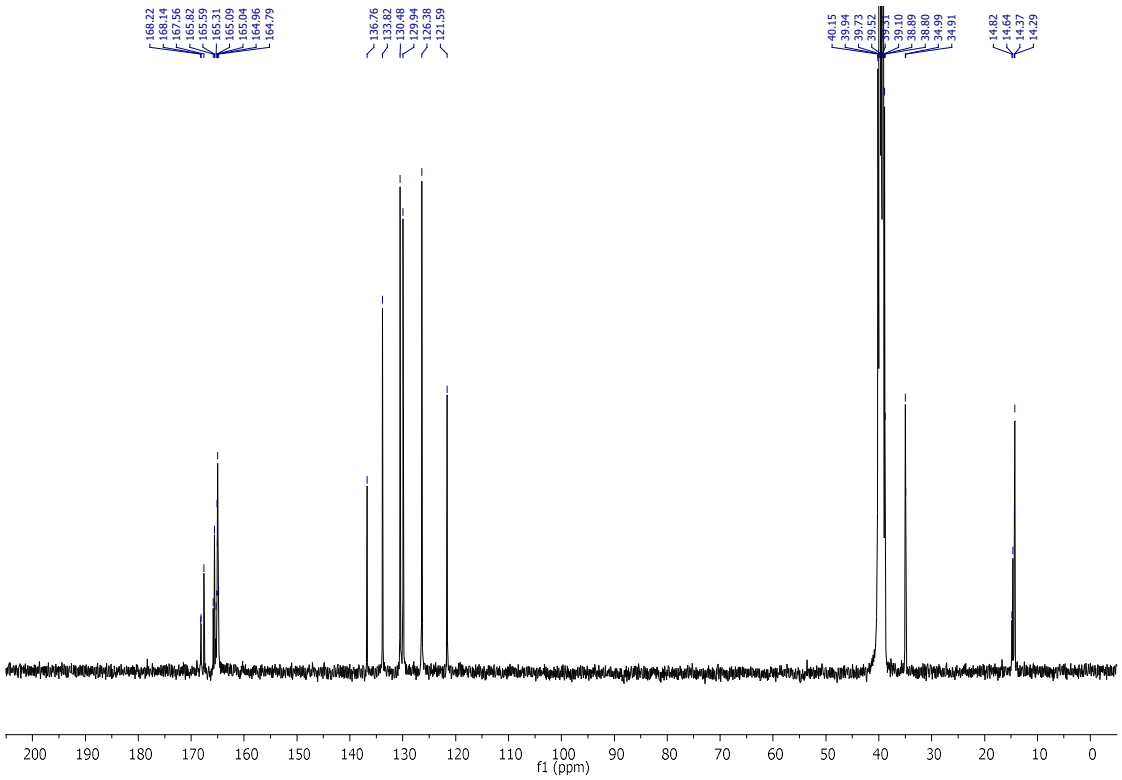

^{13}C NMR spectrum of compound **2.69**

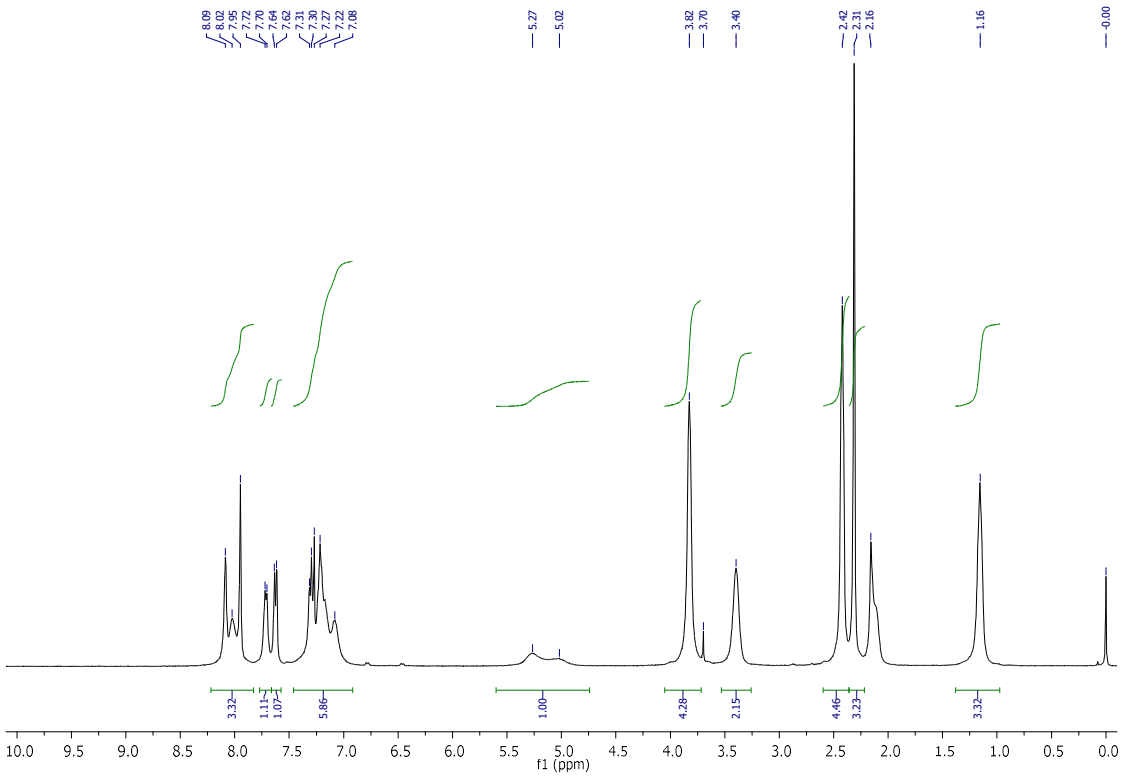

^{1}H NMR spectrum of compound **2.70**

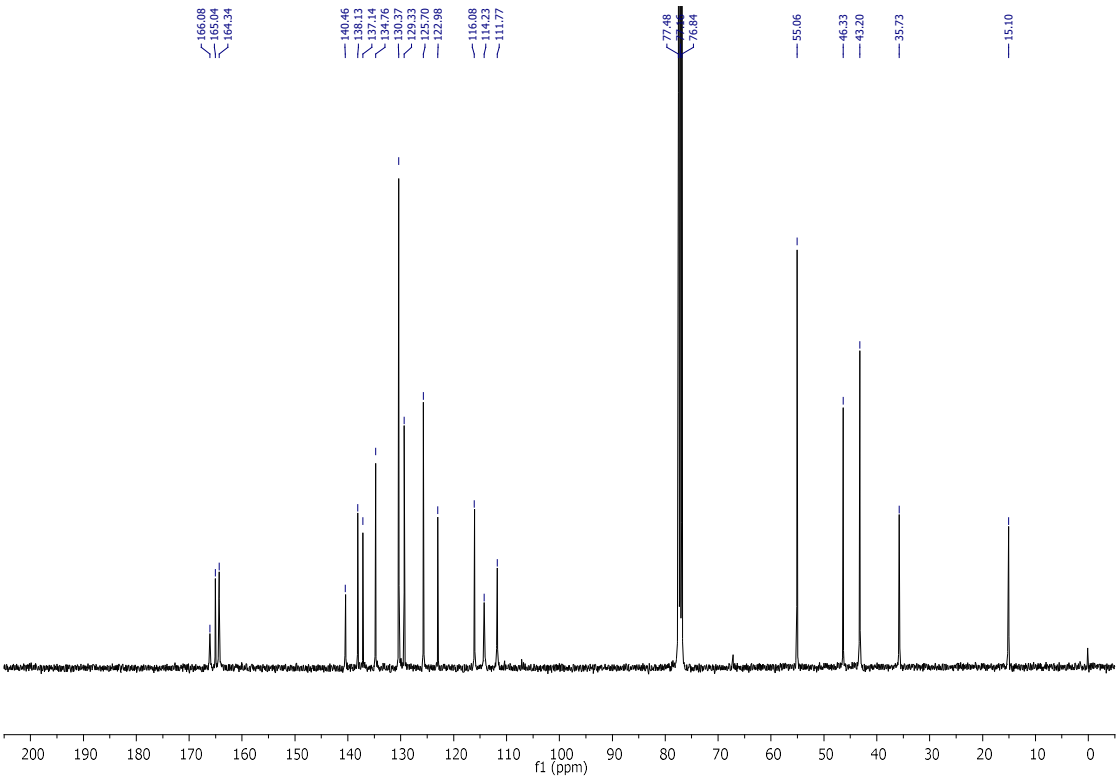

^{13}C NMR spectrum of compound **2.70**

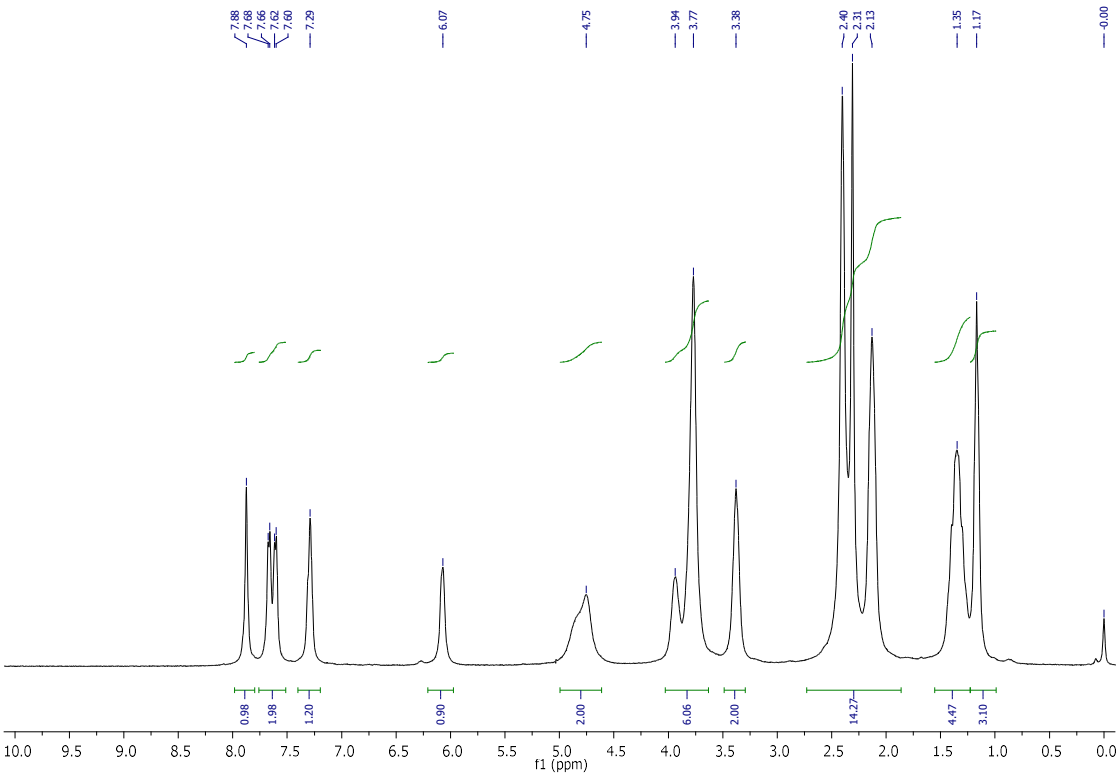

^{1}H NMR spectrum of compound **2.71**

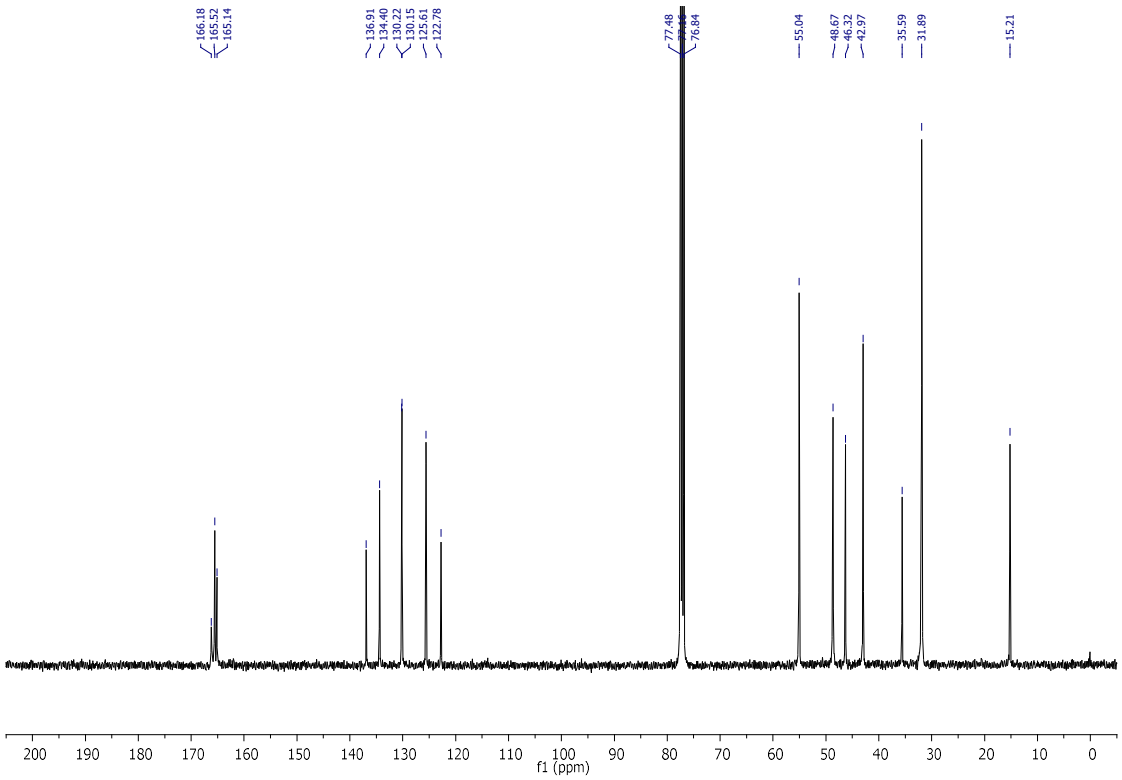

^{13}C NMR spectrum of compound **2.71**

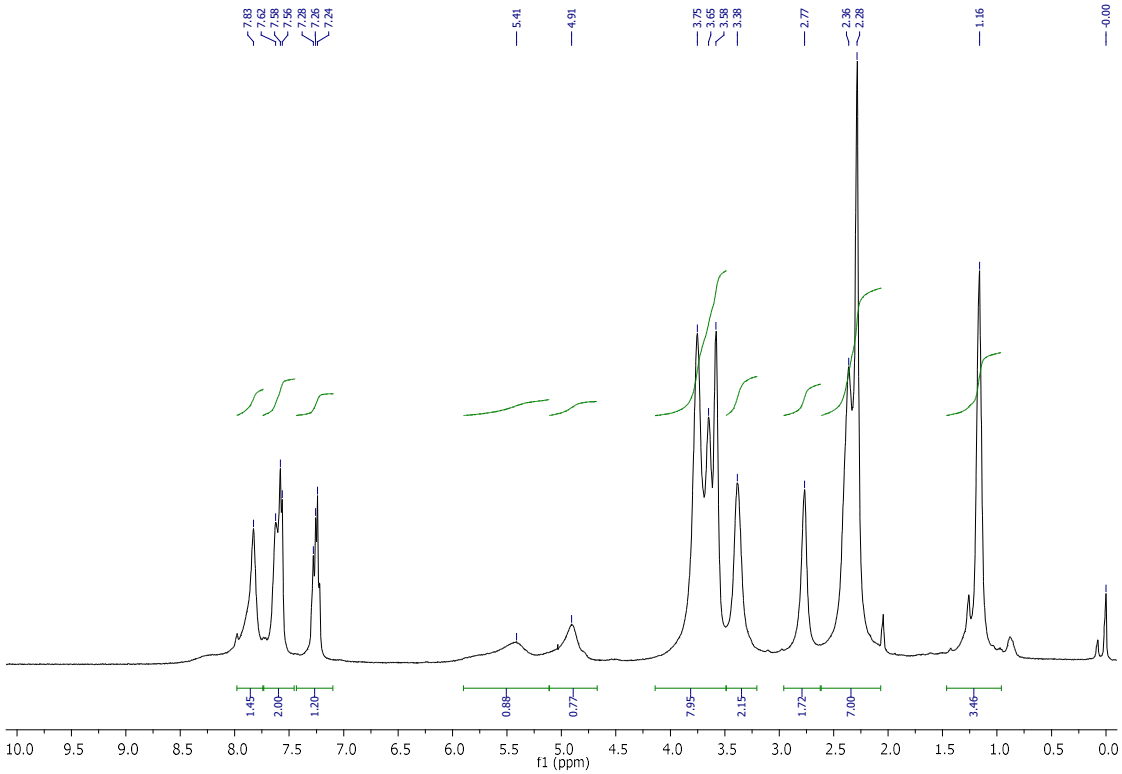

^{1}H NMR spectrum of compound **2.72**

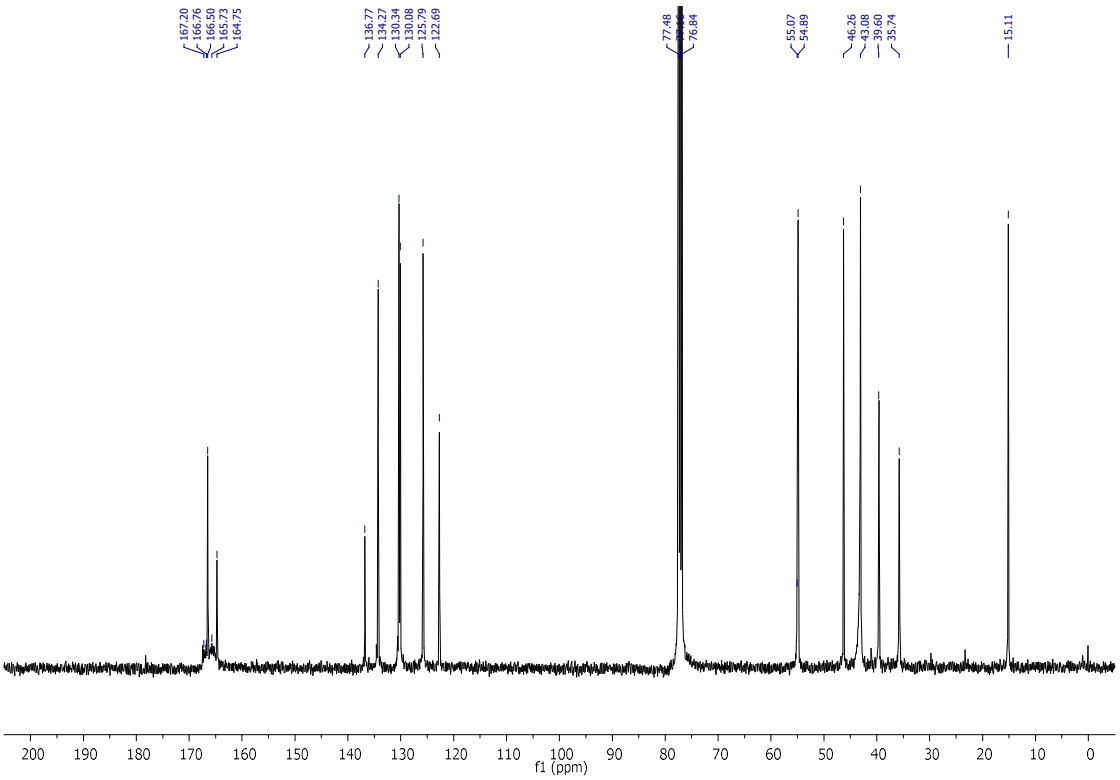

^{13}C NMR spectrum of compound **2.72**

Appendix B

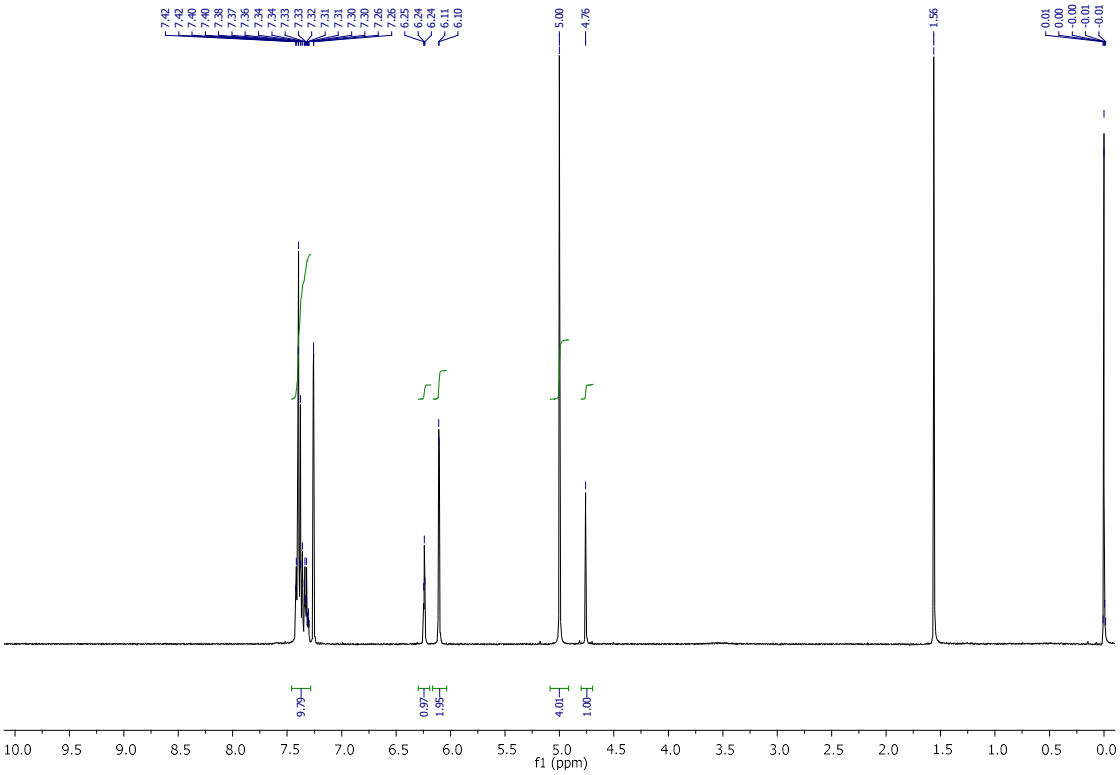

^{1}H NMR spectrum of compound **3.1**

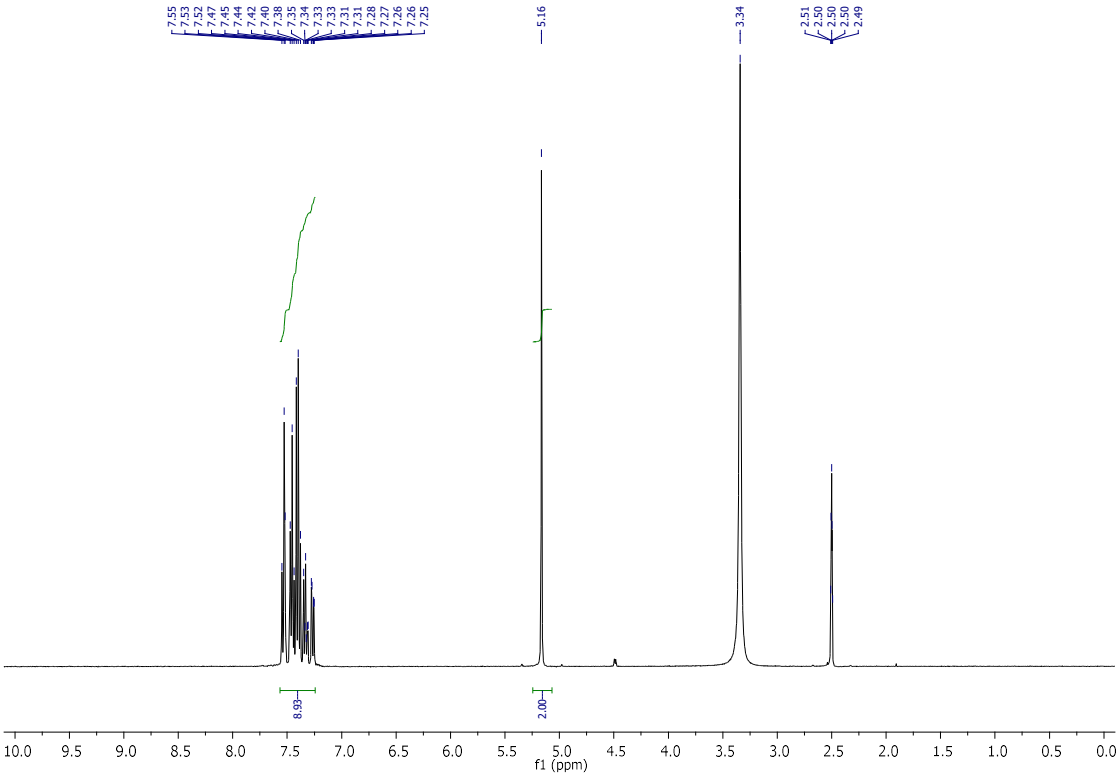

^{1}H NMR spectrum of compound **3.16b**

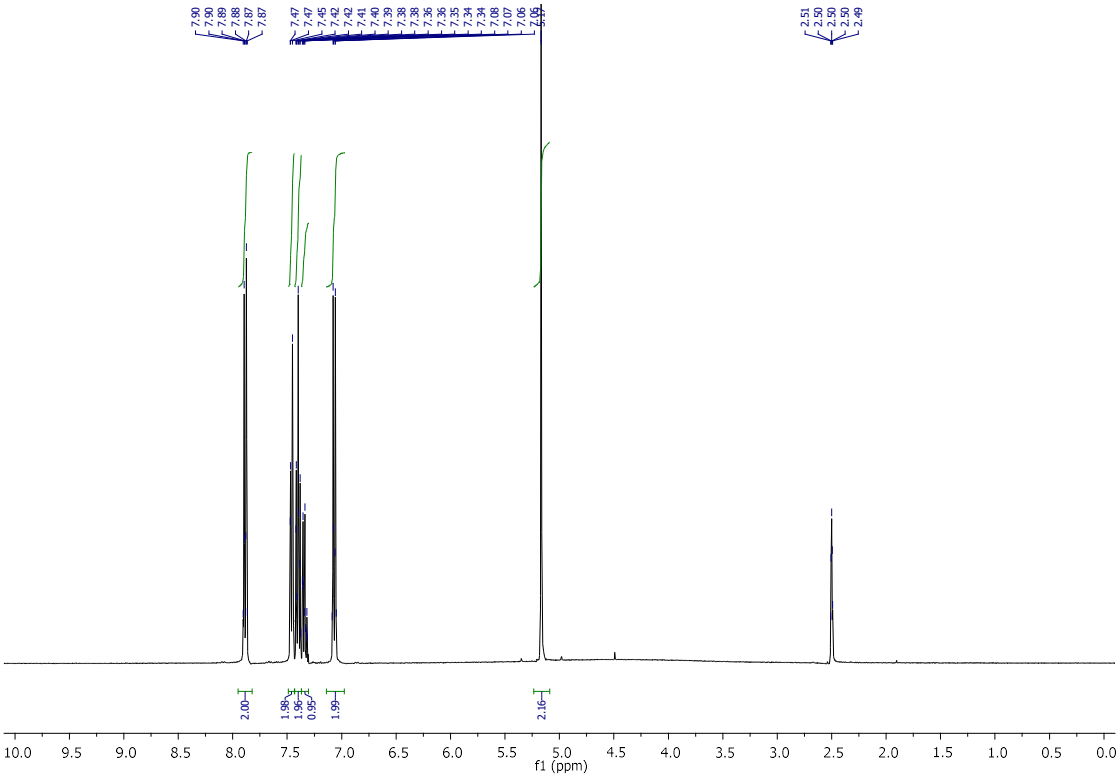

^{1}H NMR spectrum of compound **3.16c**

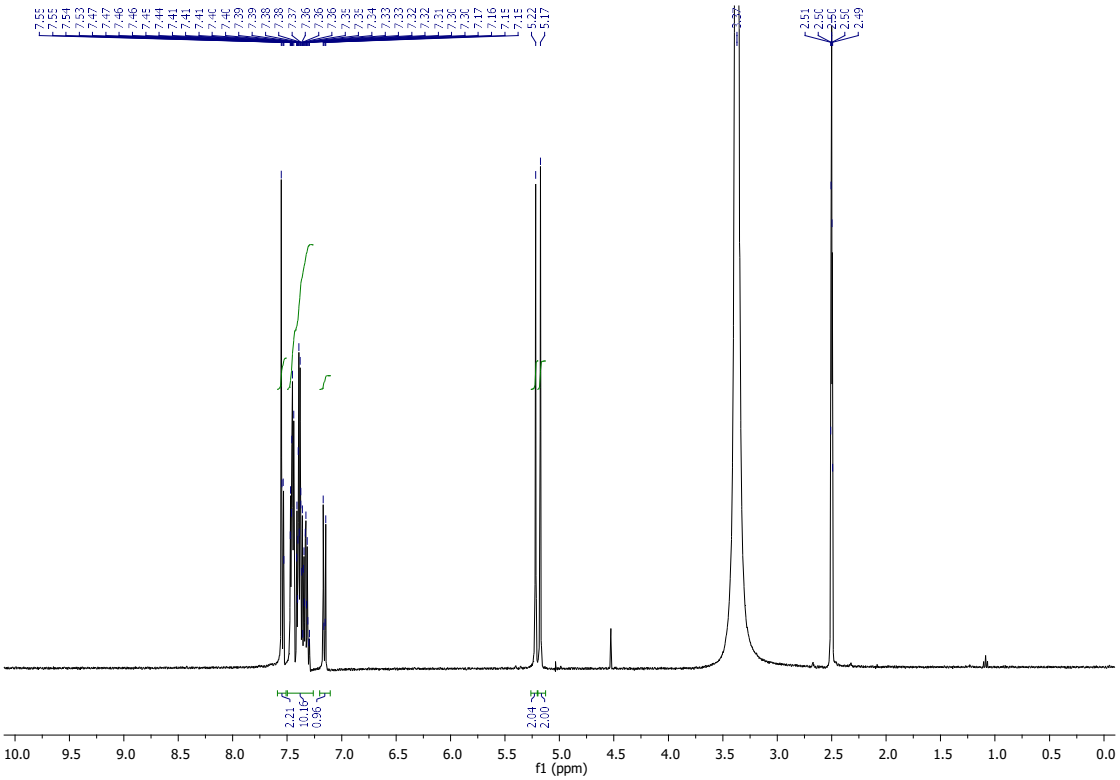

^{1}H NMR spectrum of compound **3.16d**

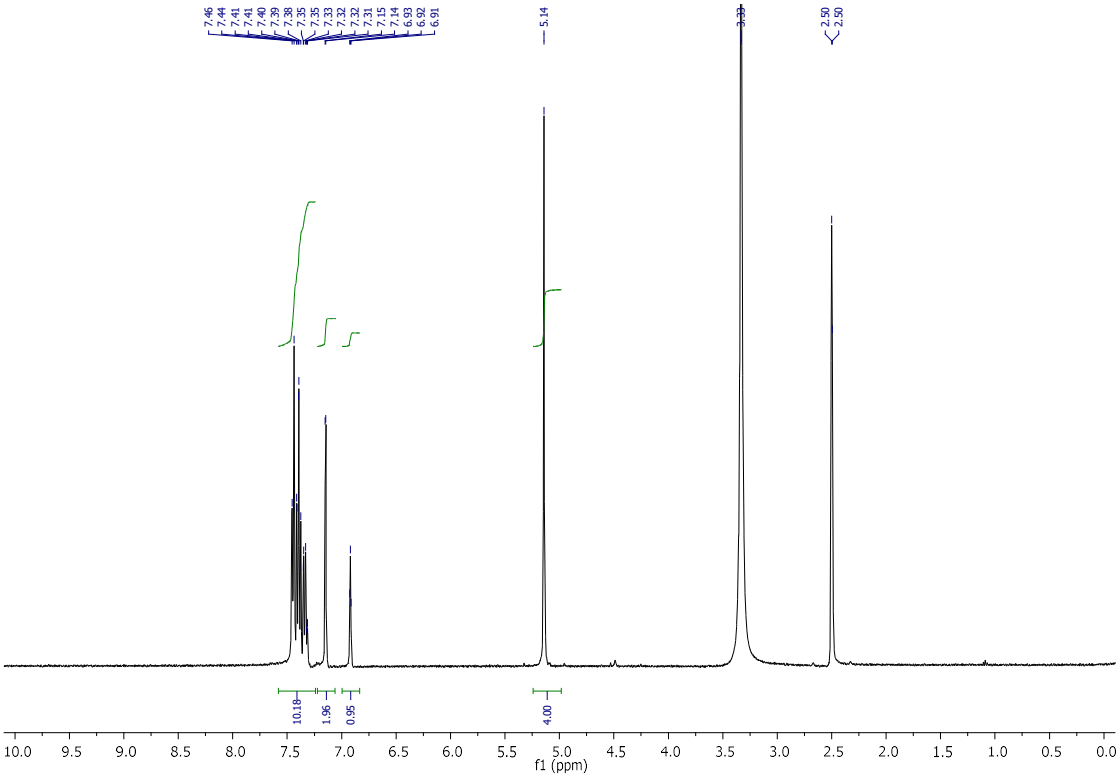

^{1}H NMR spectrum of compound **3.16e**

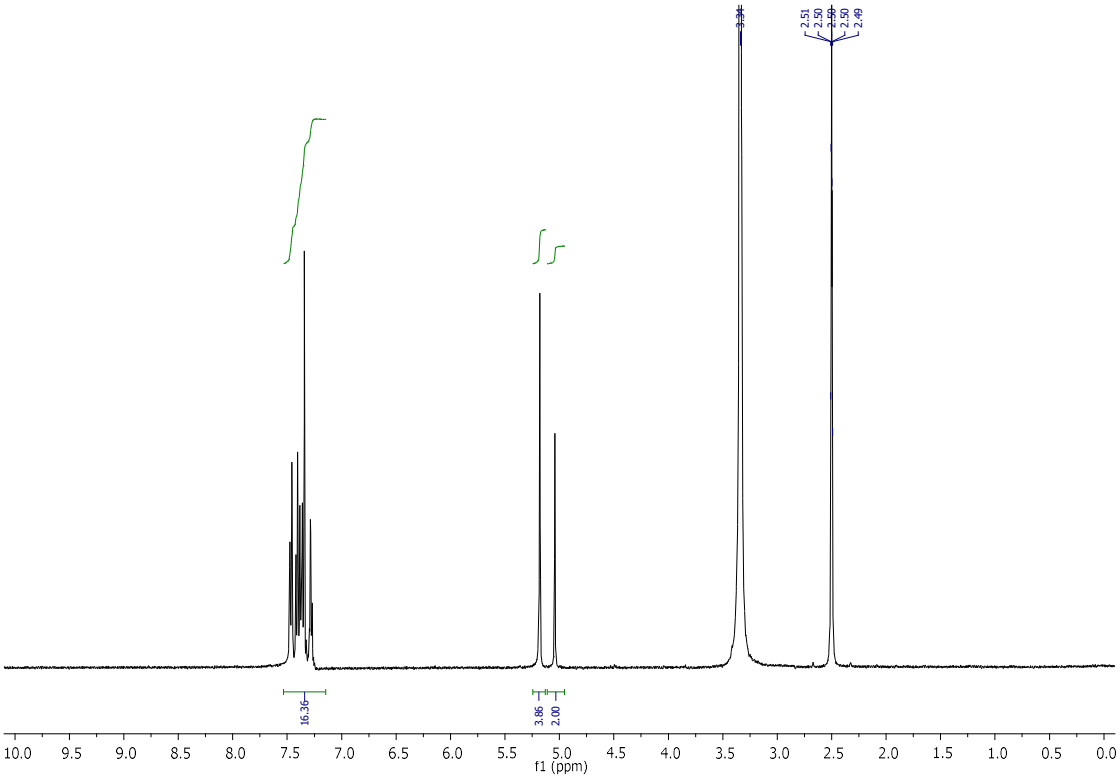

^{1}H NMR spectrum of compound **3.16f**

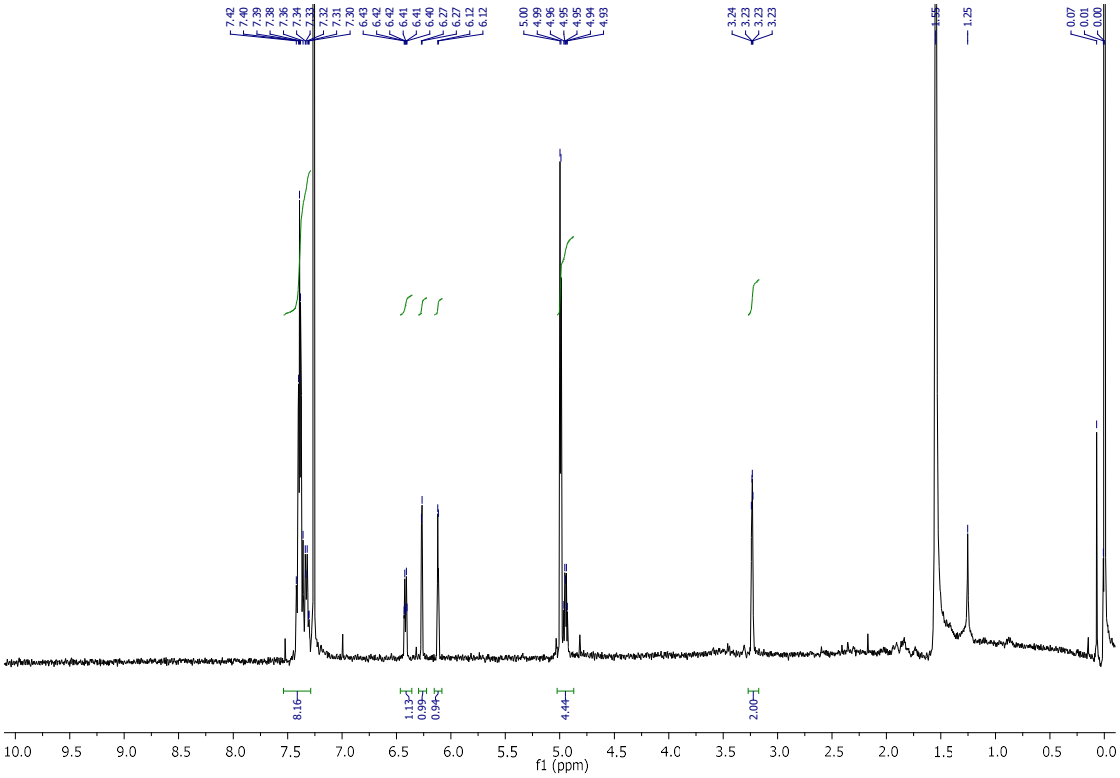

^{1}H NMR spectrum of compound **3.17**

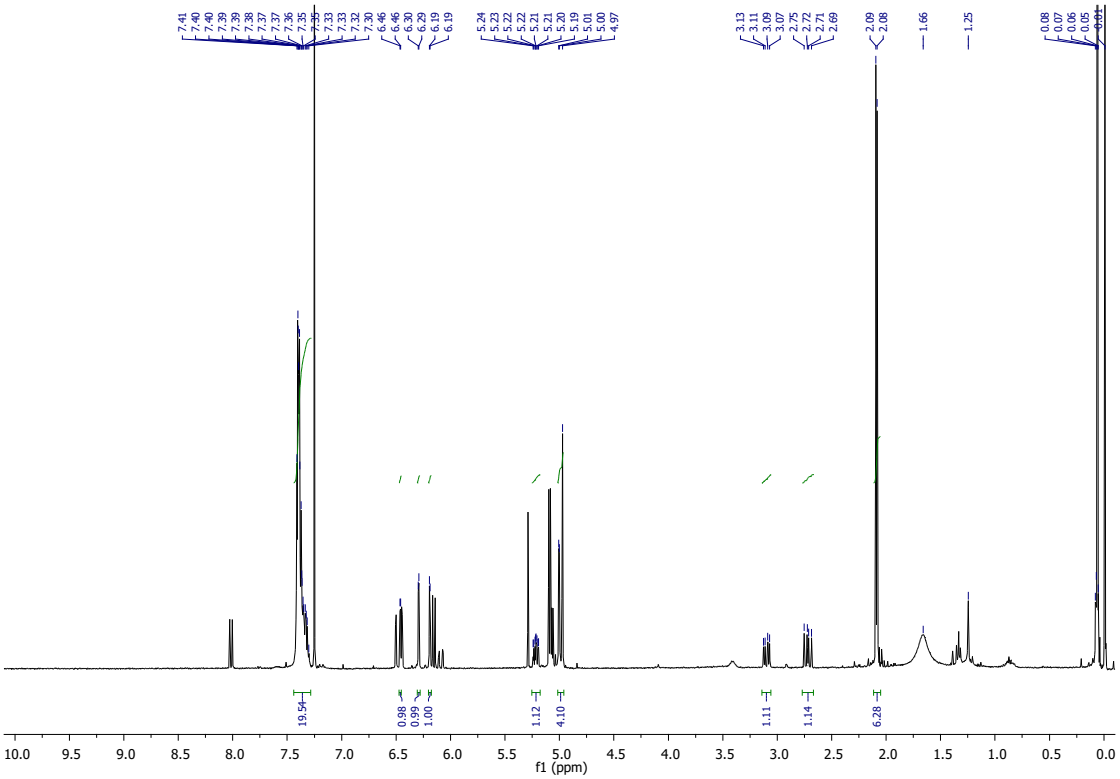

^{1}H NMR spectrum of compound ***rac-cis* 3.19**

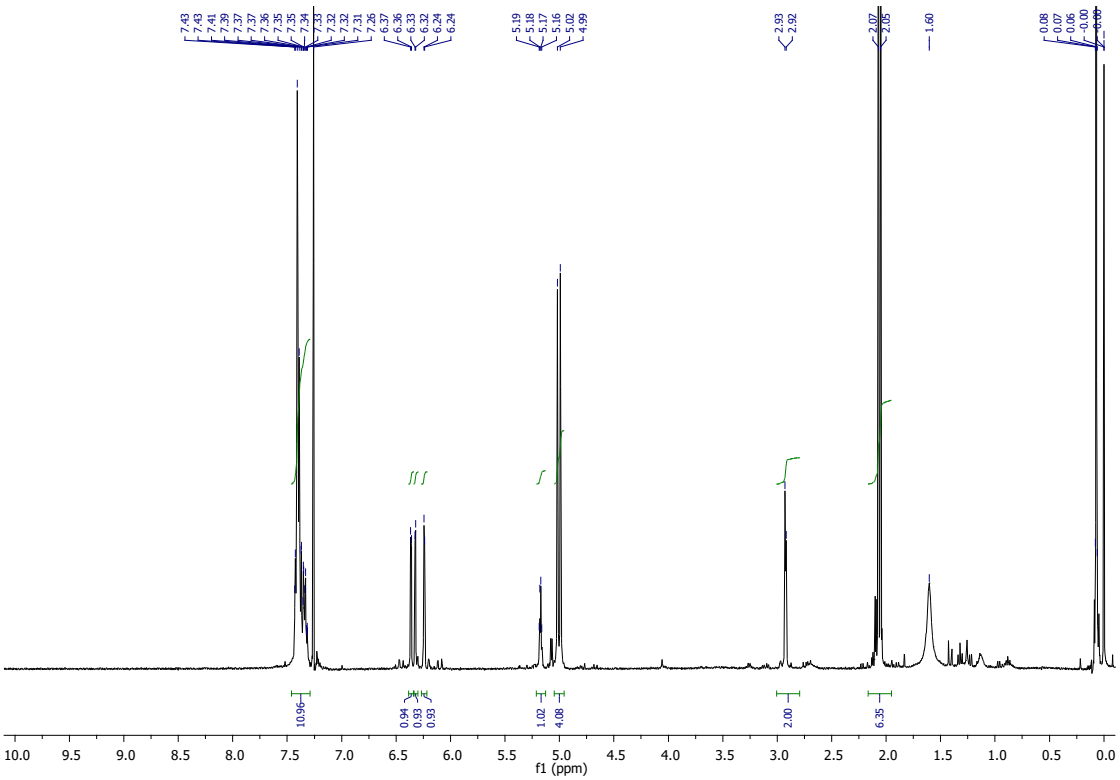

^{1}H NMR spectrum of compound ***rac-trans* 3.19**

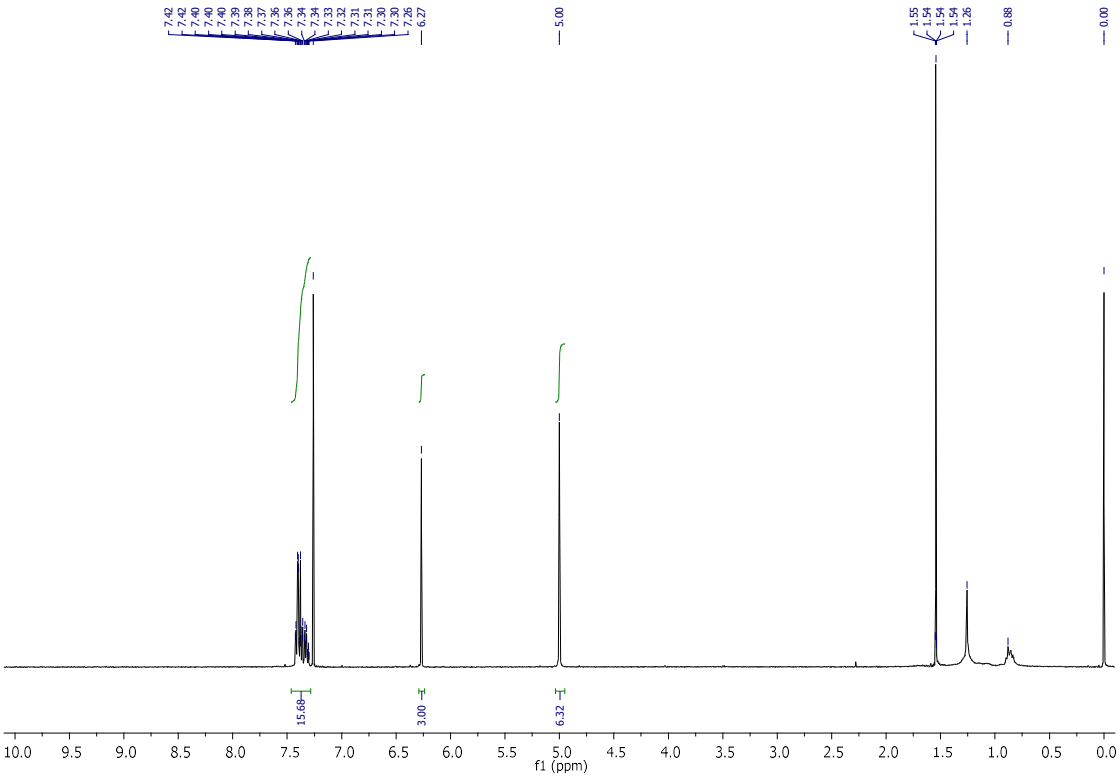

^{1}H NMR spectrum of compound **3.23**

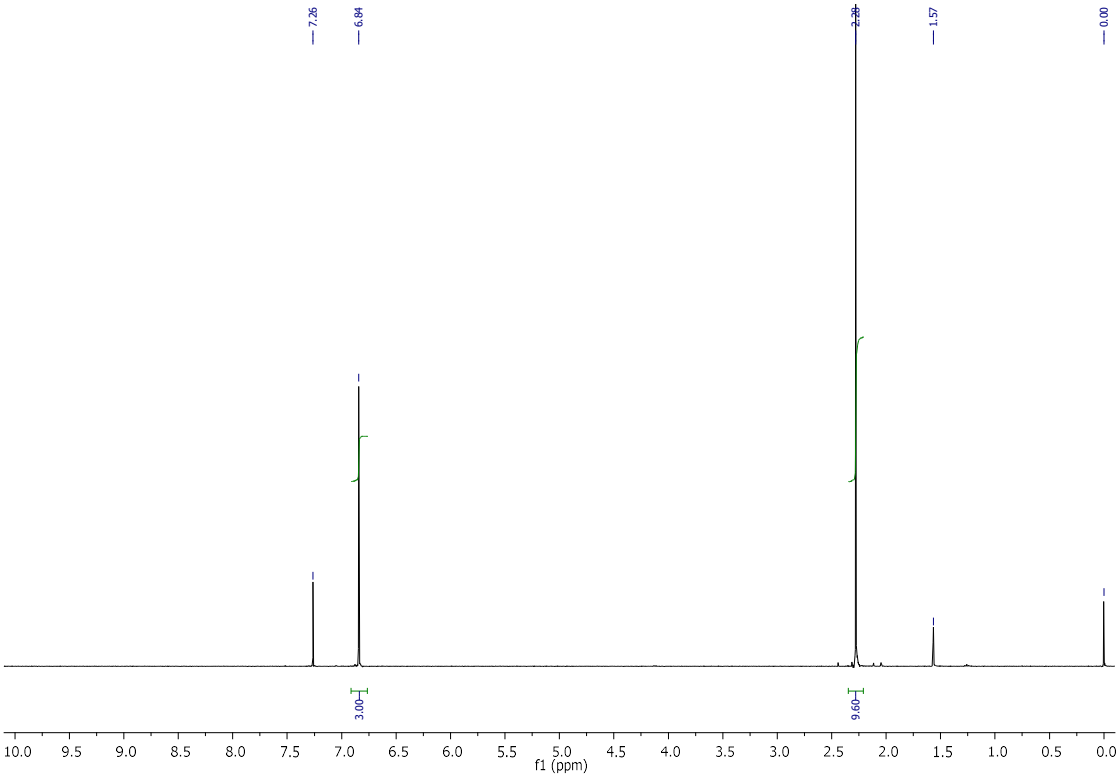

^{1}H NMR spectrum of compound **3.25**

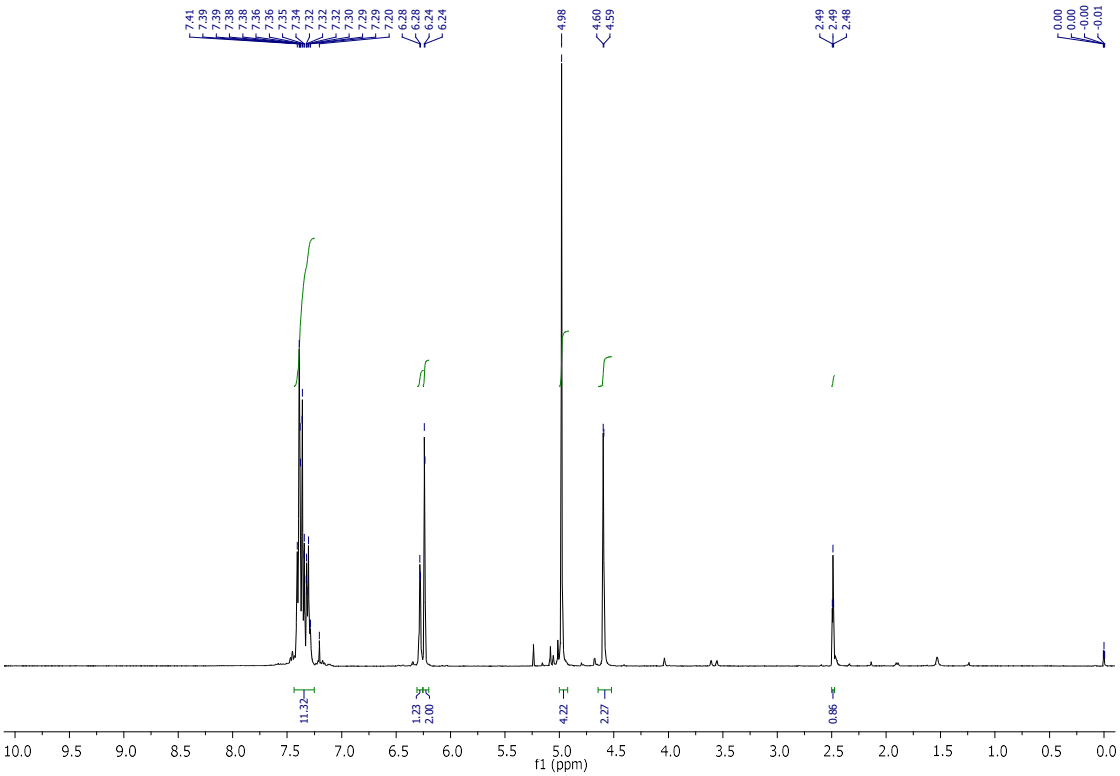

^{1}H NMR spectrum of compound **3.26**

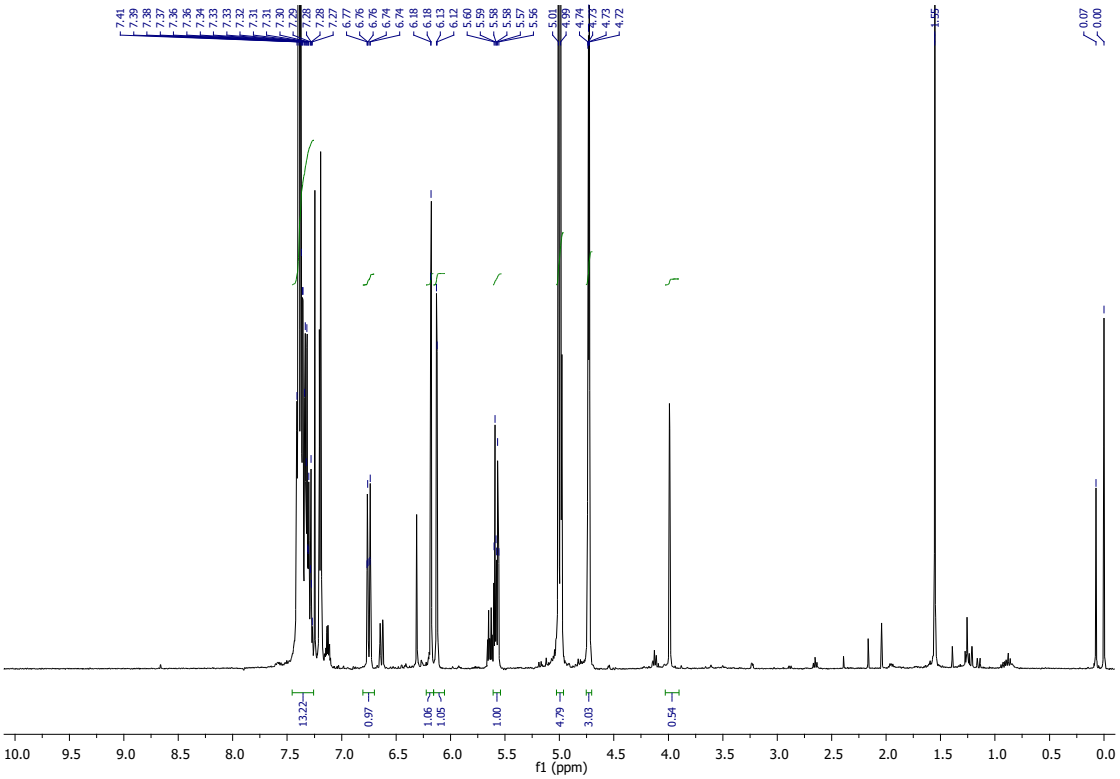

^{1}H NMR spectrum of compound **3.27**

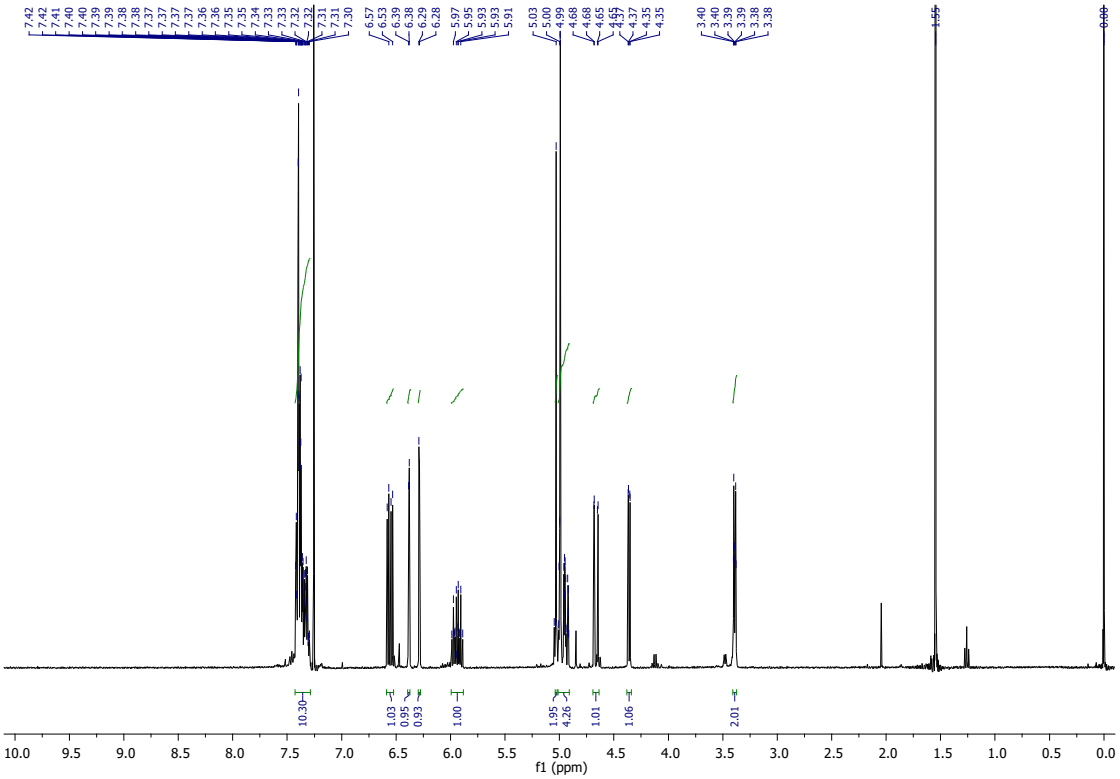

^{1}H NMR spectrum of compound **3.28**

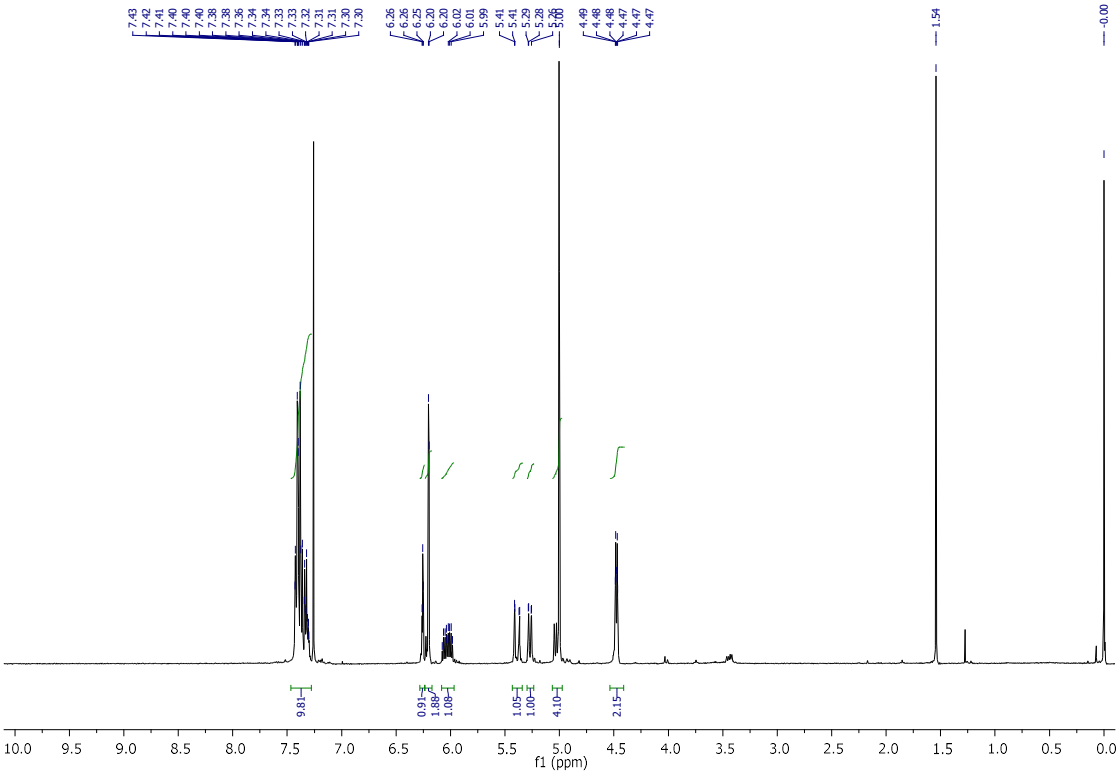

^{1}H NMR spectrum of compound **3.29**

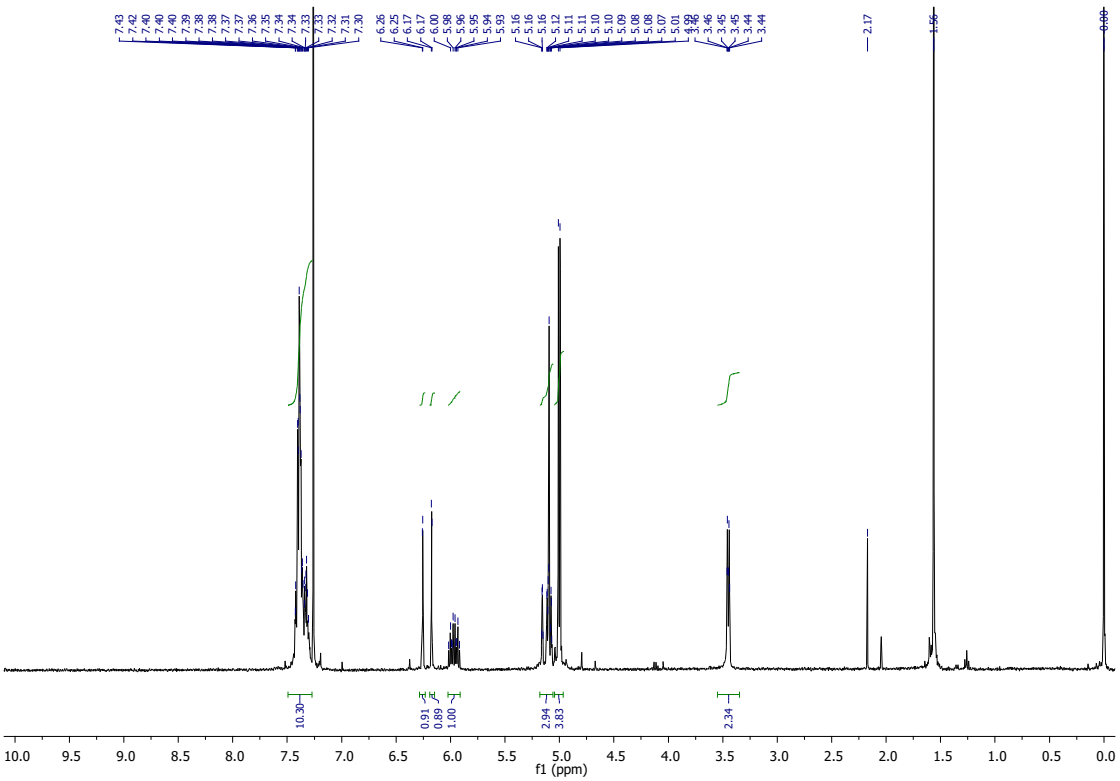

^{1}H NMR spectrum of compound **3.30**

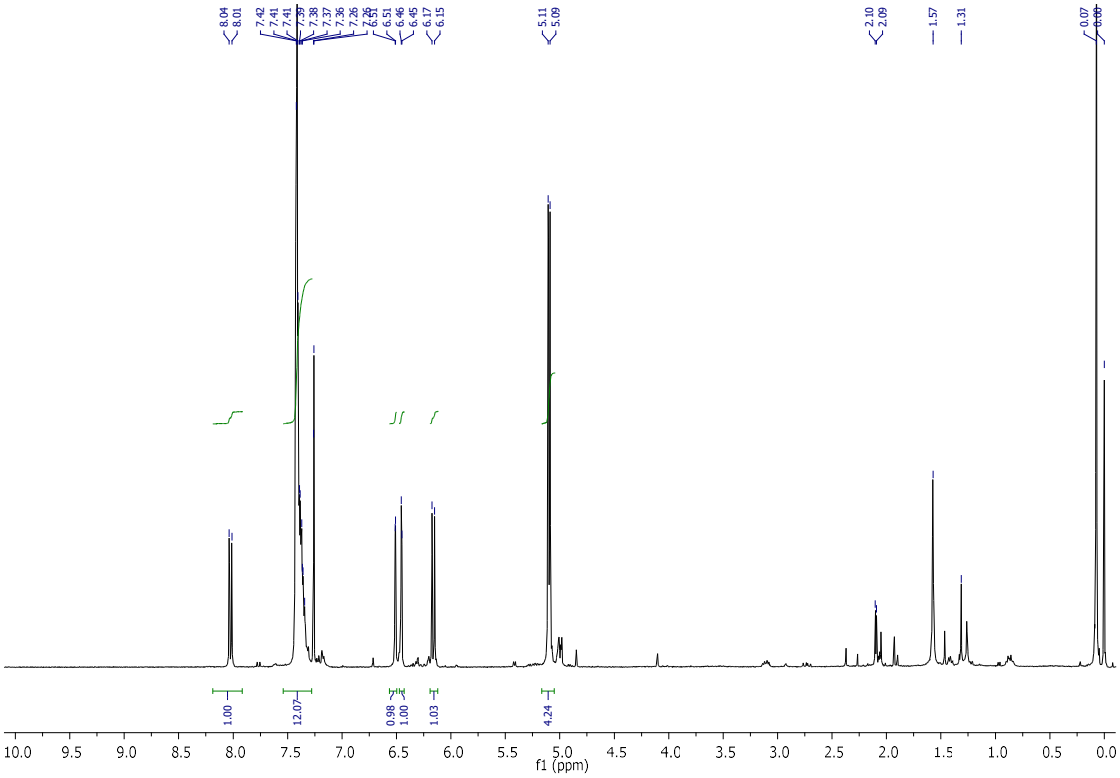

^{1}H NMR spectrum of compound **3.32**

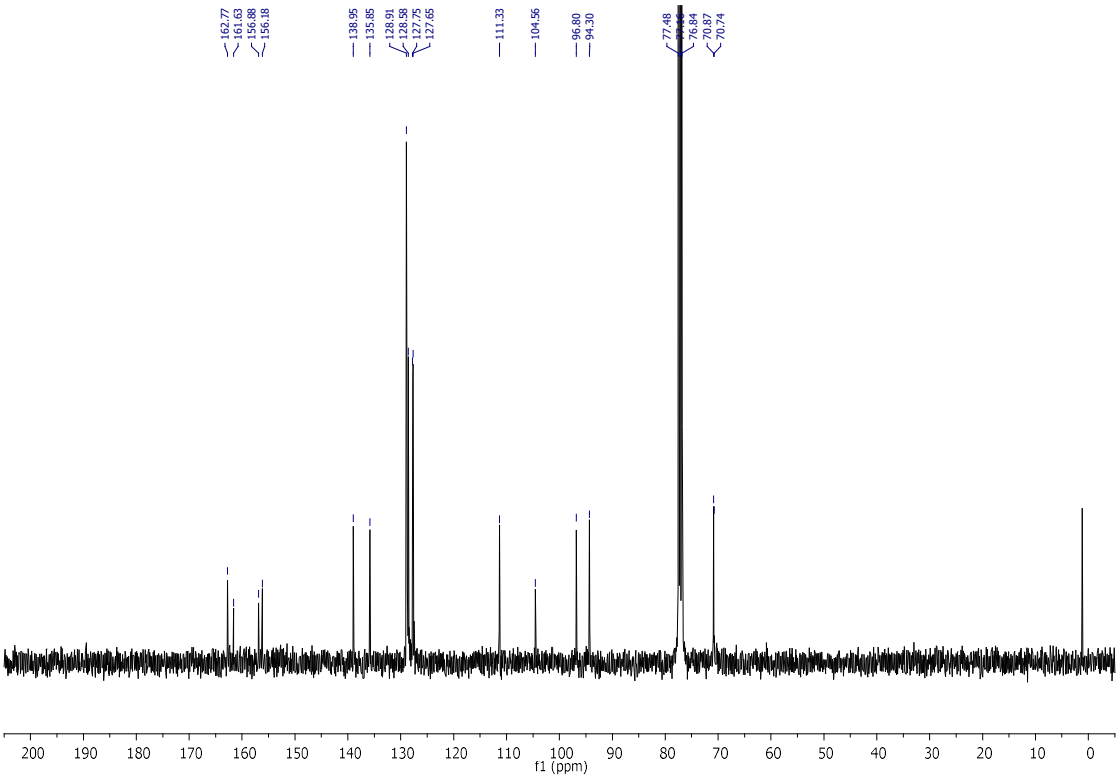

^{13}C NMR spectrum of compound **3.32**

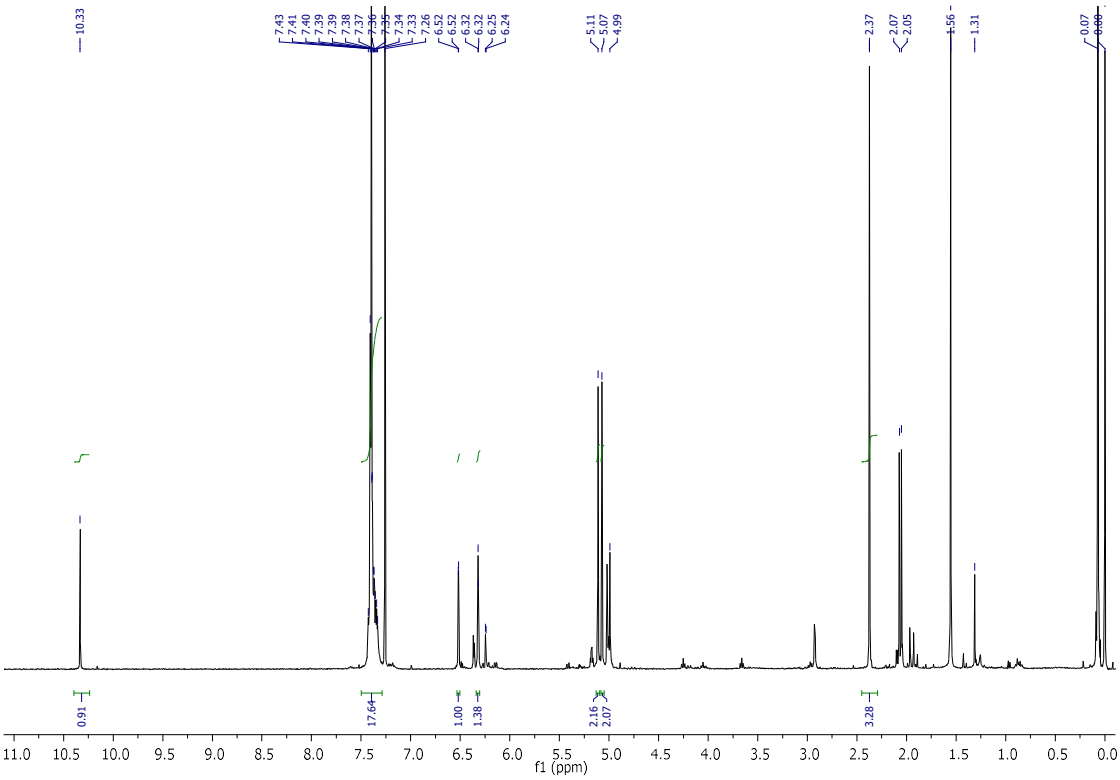

^{1}H NMR spectrum of compound **3.33**

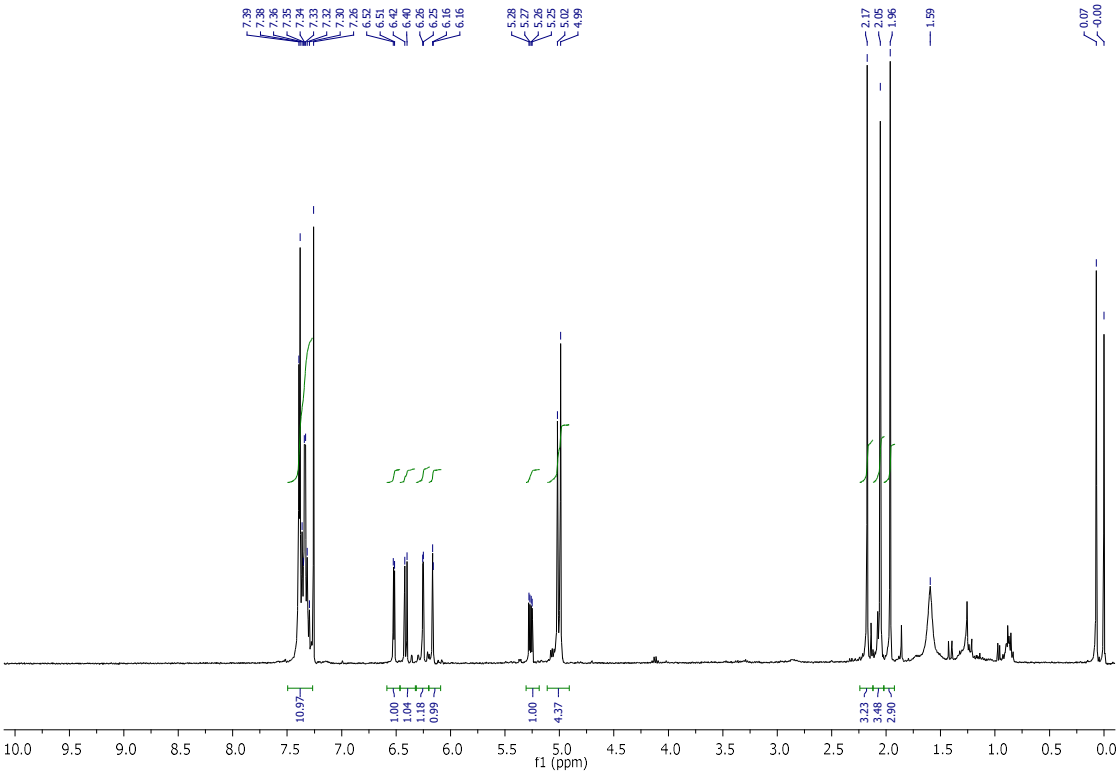

^{1}H NMR spectrum of compound **3.34**

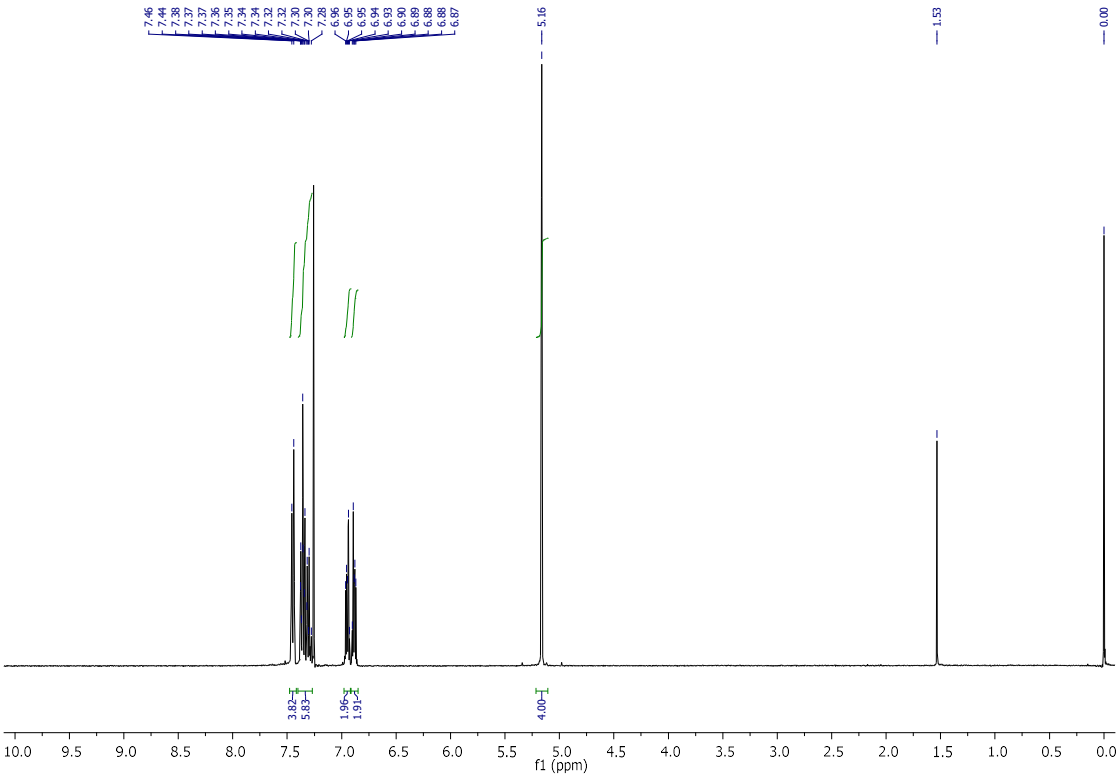

^{1}H NMR spectrum of compound **3.42**

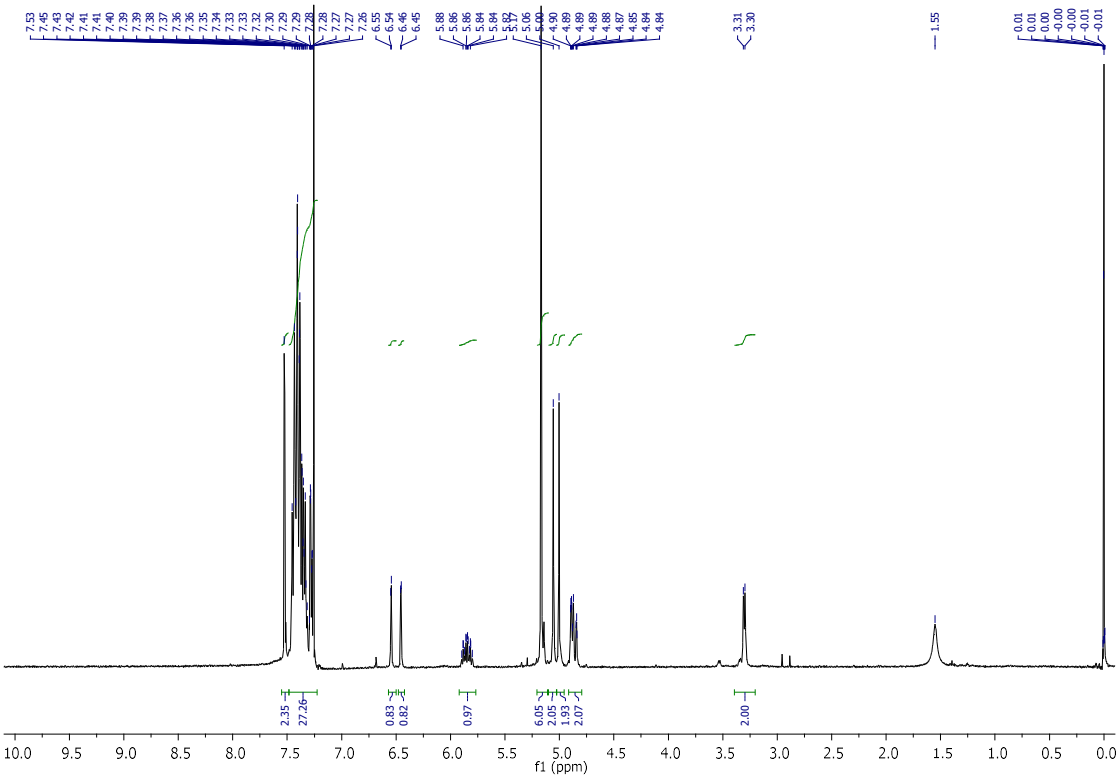

^{1}H NMR spectrum of compound **3.45**

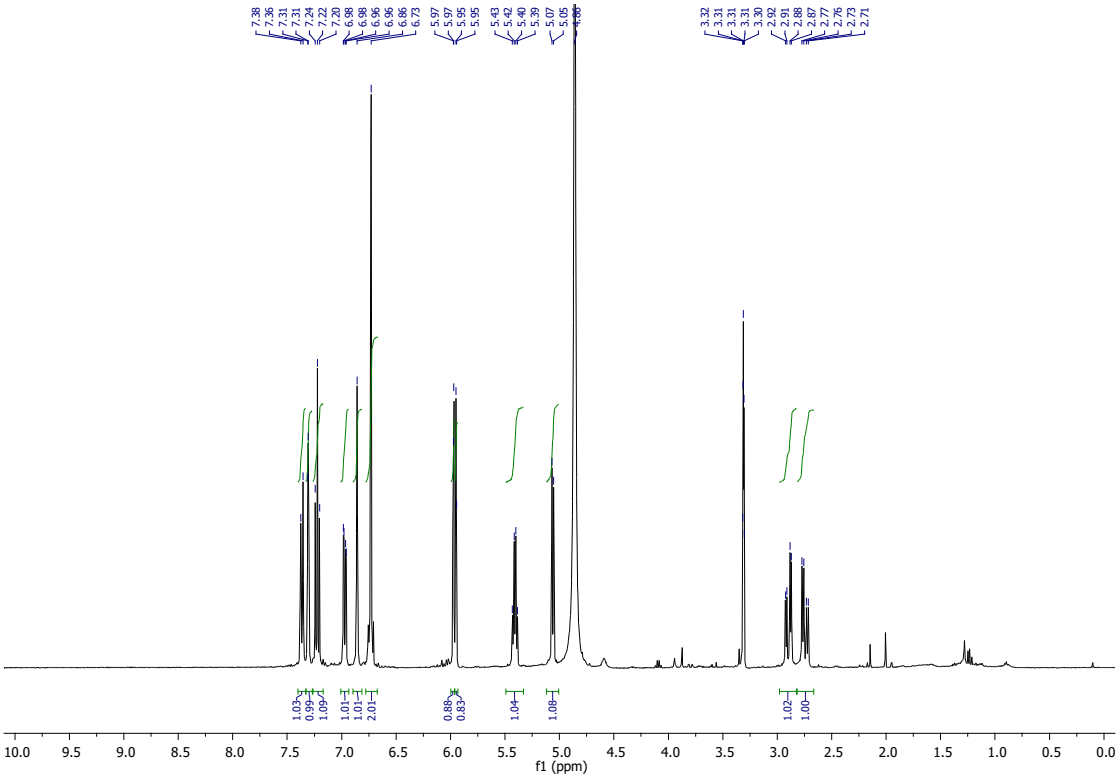

^{1}H NMR spectrum of compound **3.48b**

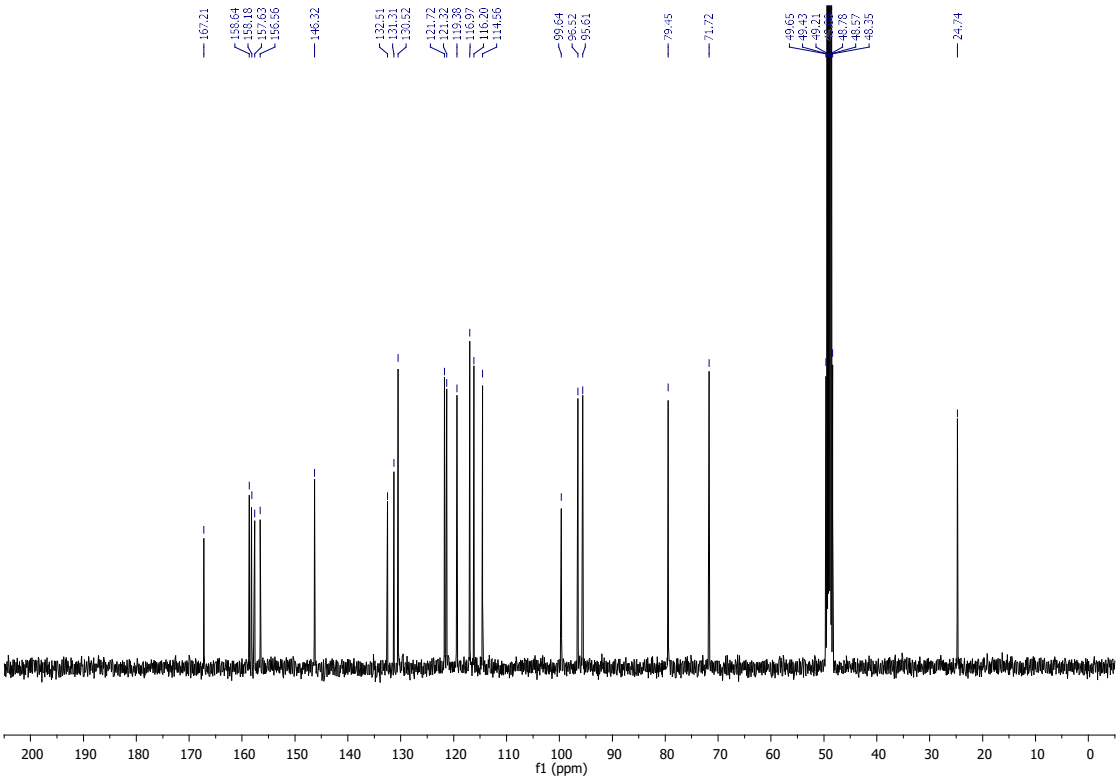

^{13}C NMR spectrum of compound **3.48b**

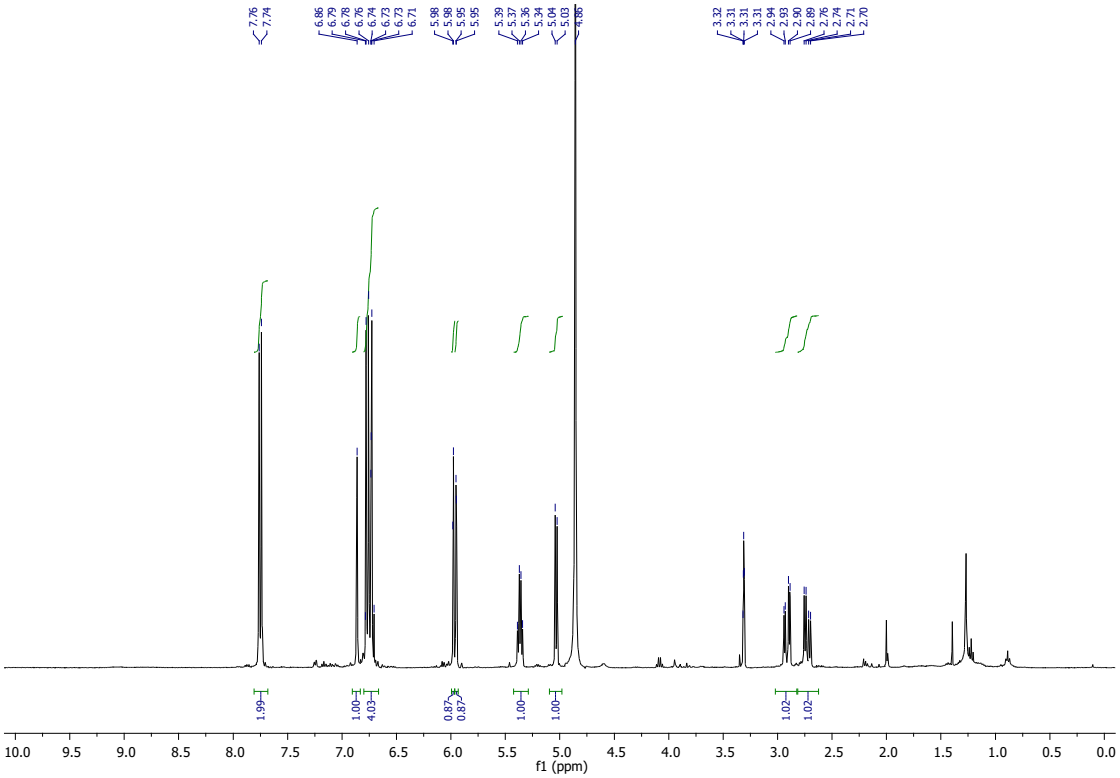

^{1}H NMR spectrum of compound **3.48c**

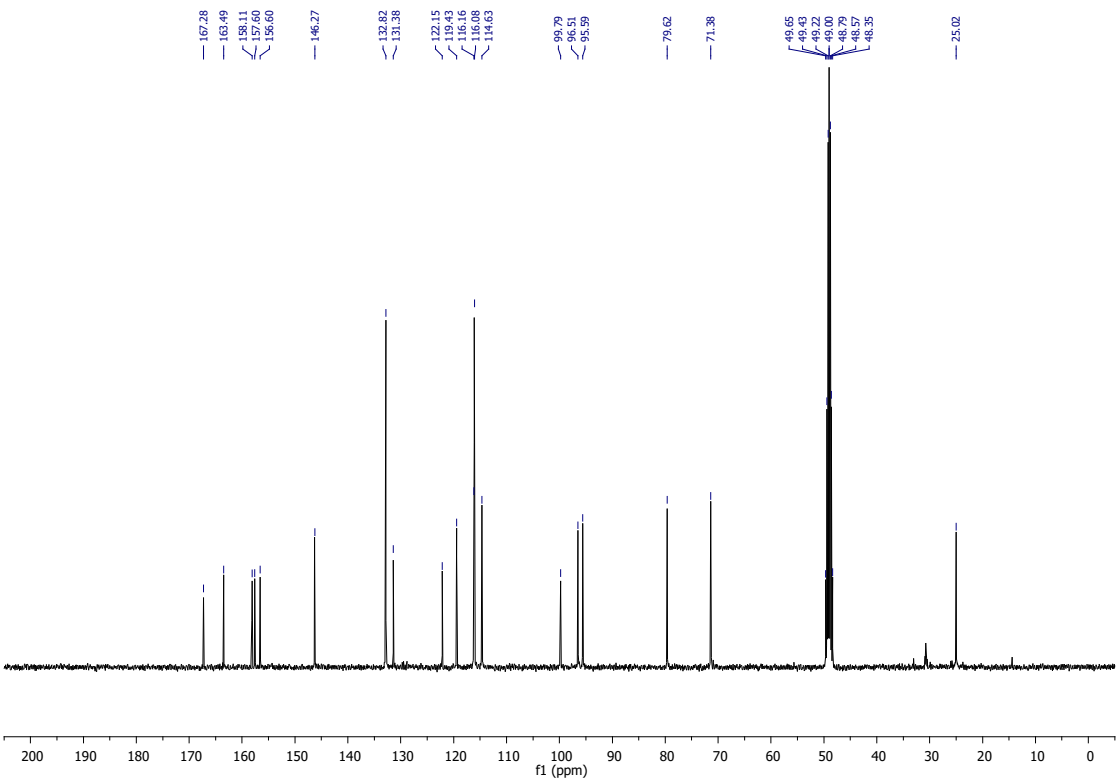

^{13}C NMR spectrum of compound **3.48c**

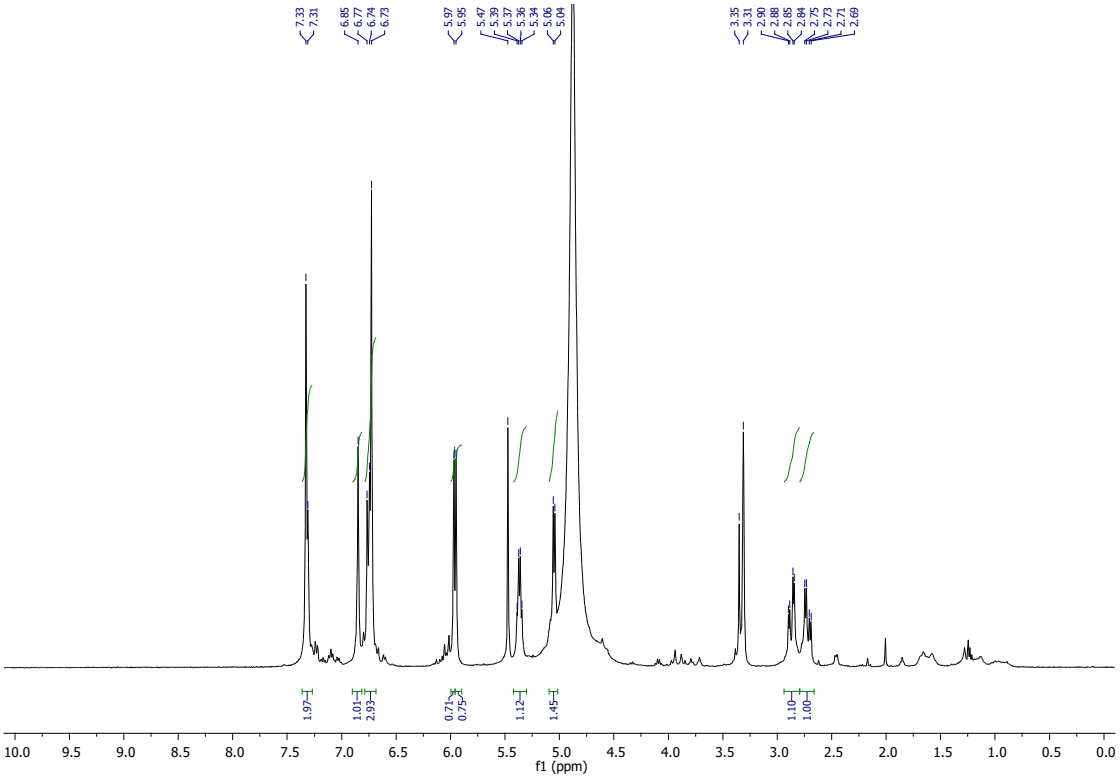

^{1}H NMR spectrum of compound **3.48d**

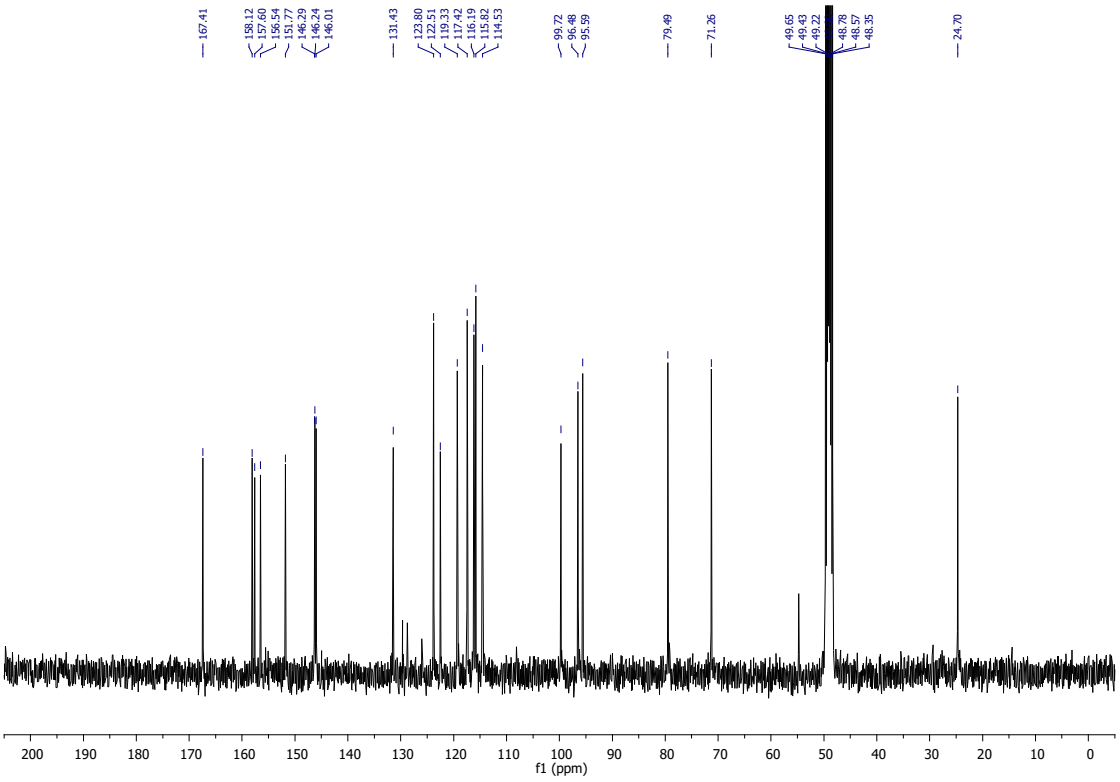

^{13}C NMR spectrum of compound **3.48d**

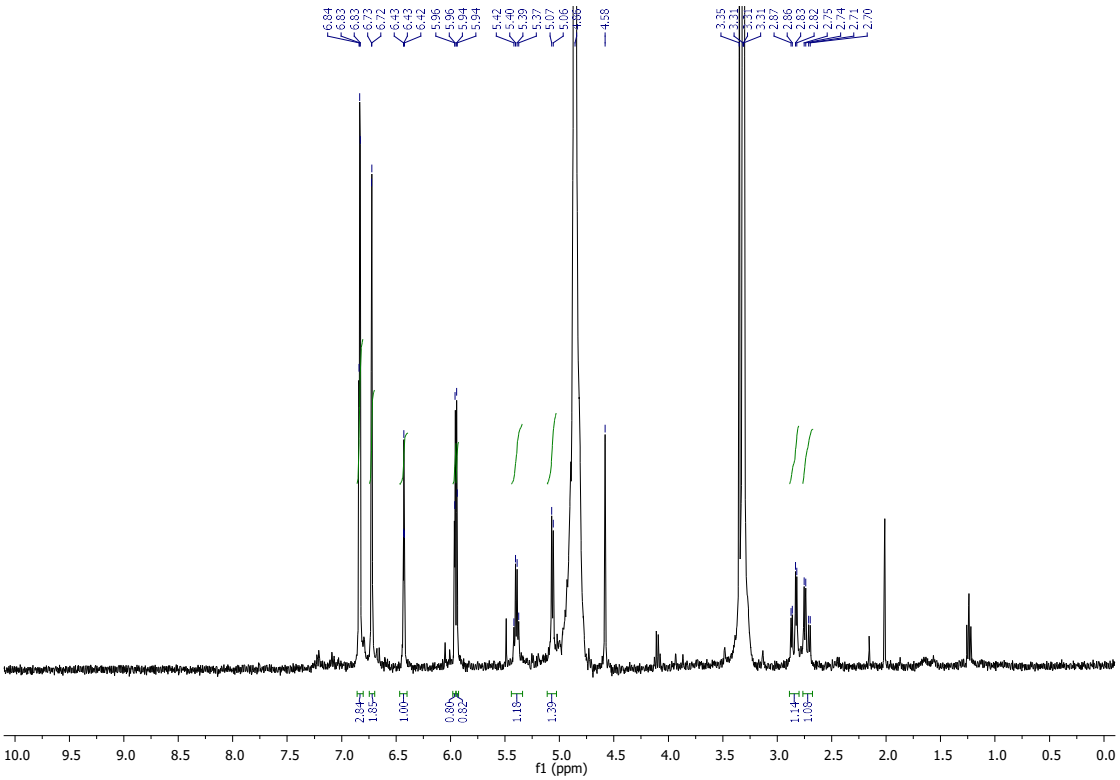

^{1}H NMR spectrum of compound **3.48e**

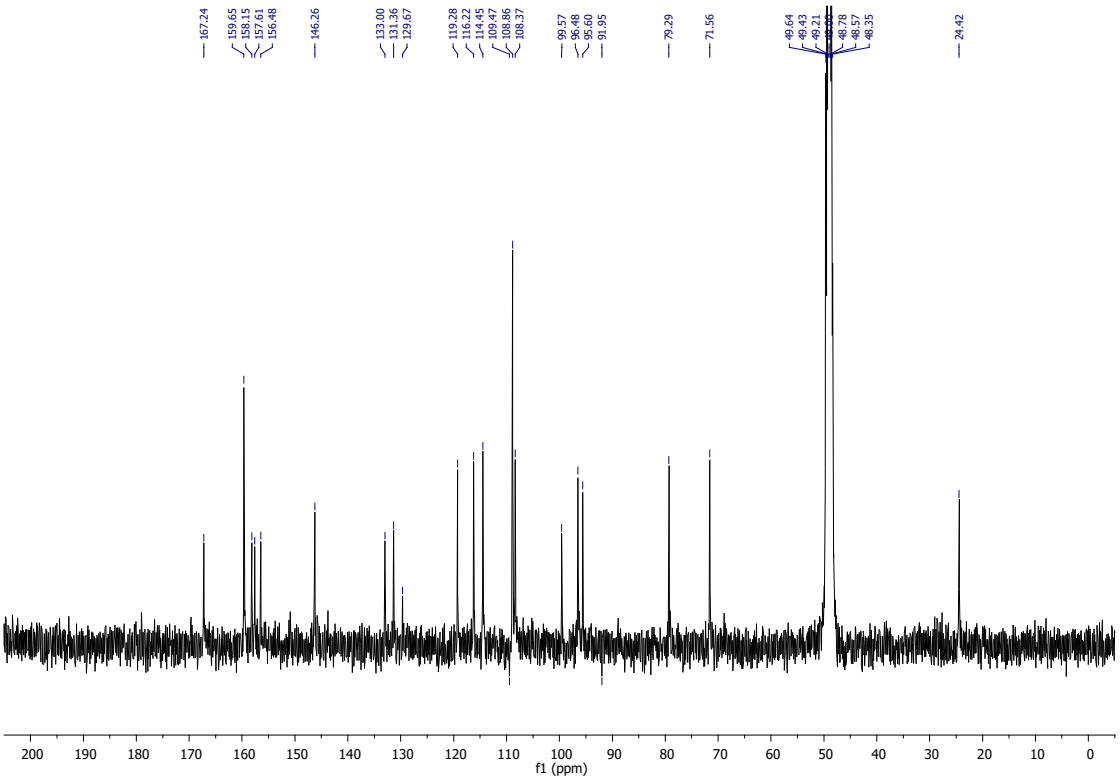

^{13}C NMR spectrum of compound **3.48e**

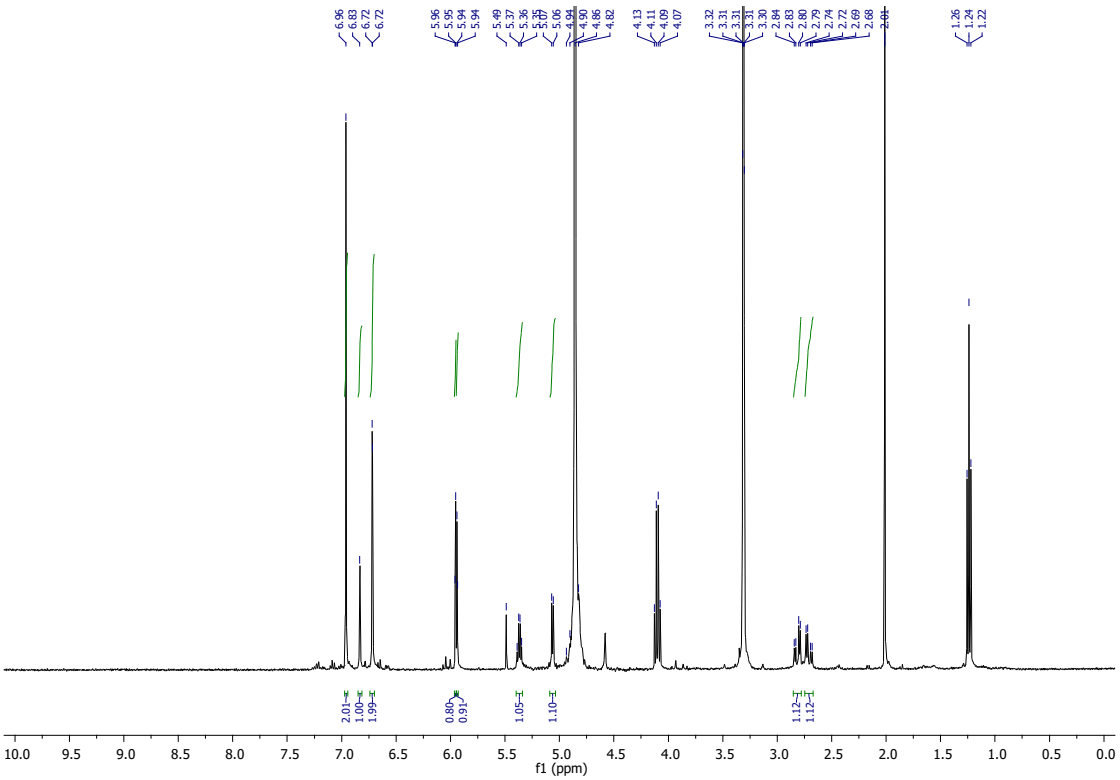

^{1}H NMR spectrum of compound **3.48f**

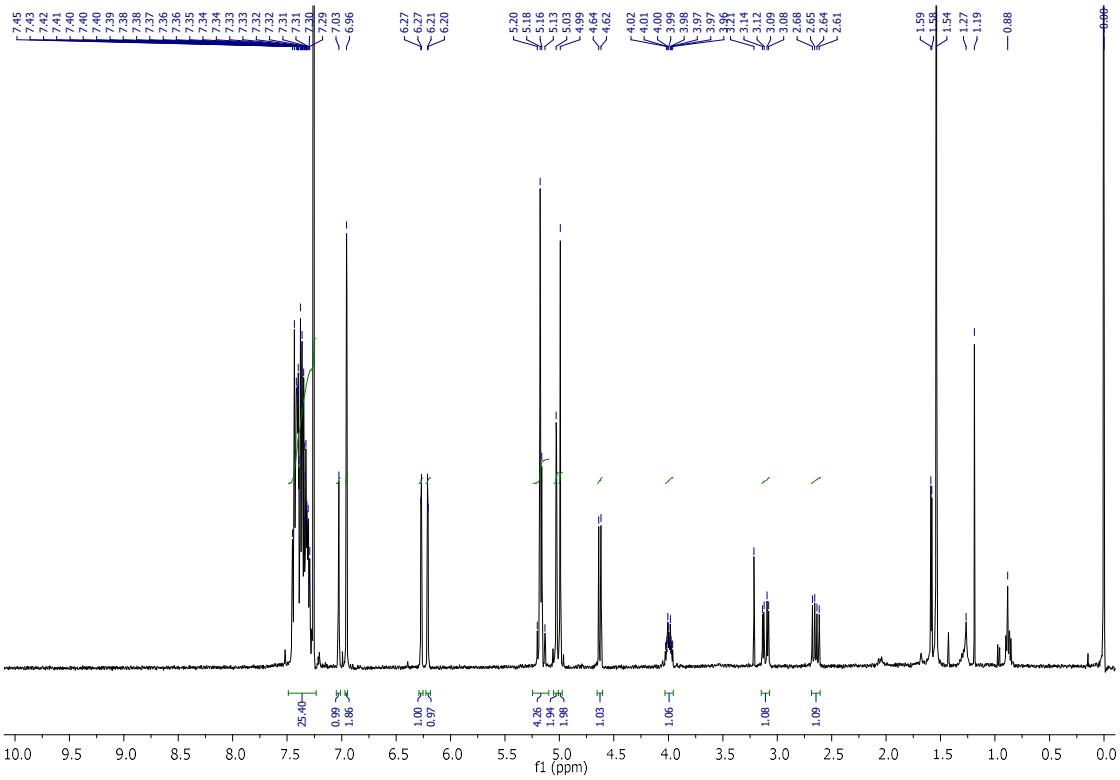

^{1}H NMR spectrum of compound **3.49a**

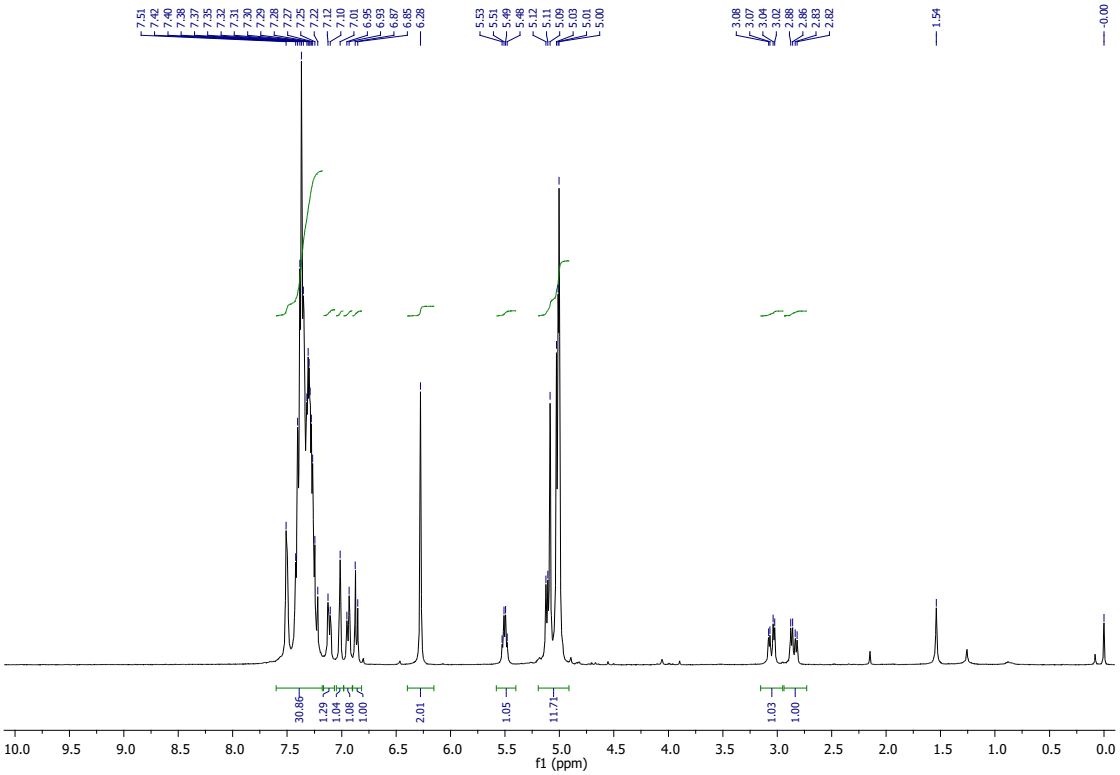

^{1}H NMR spectrum of compound **3.49b**

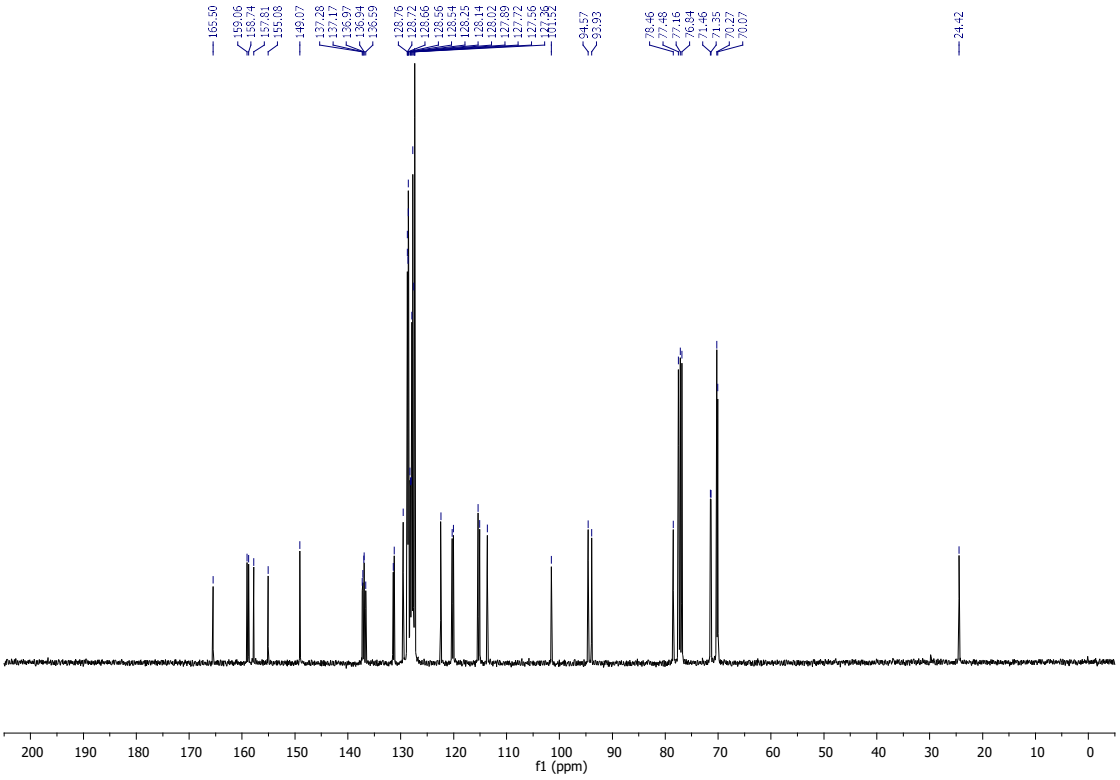

^{13}C NMR spectrum of compound **3.49b**

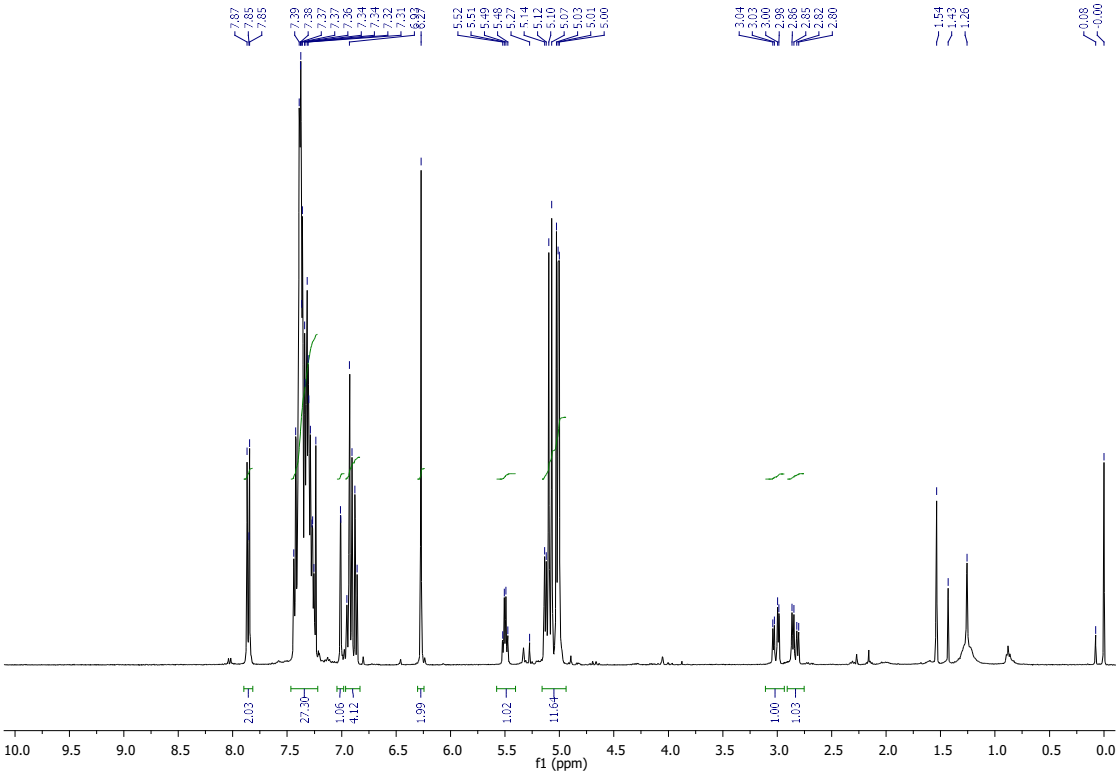

^{1}H NMR spectrum of compound **3.49c**

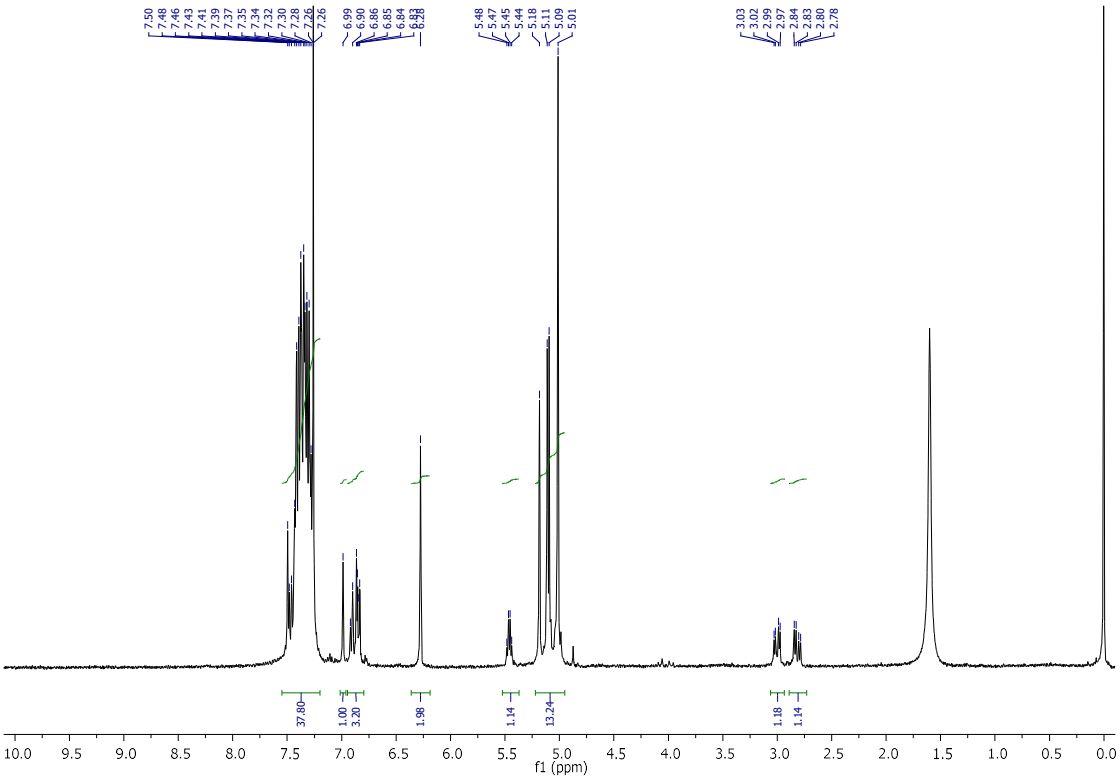

^{1}H NMR spectrum of compound **3.49d**

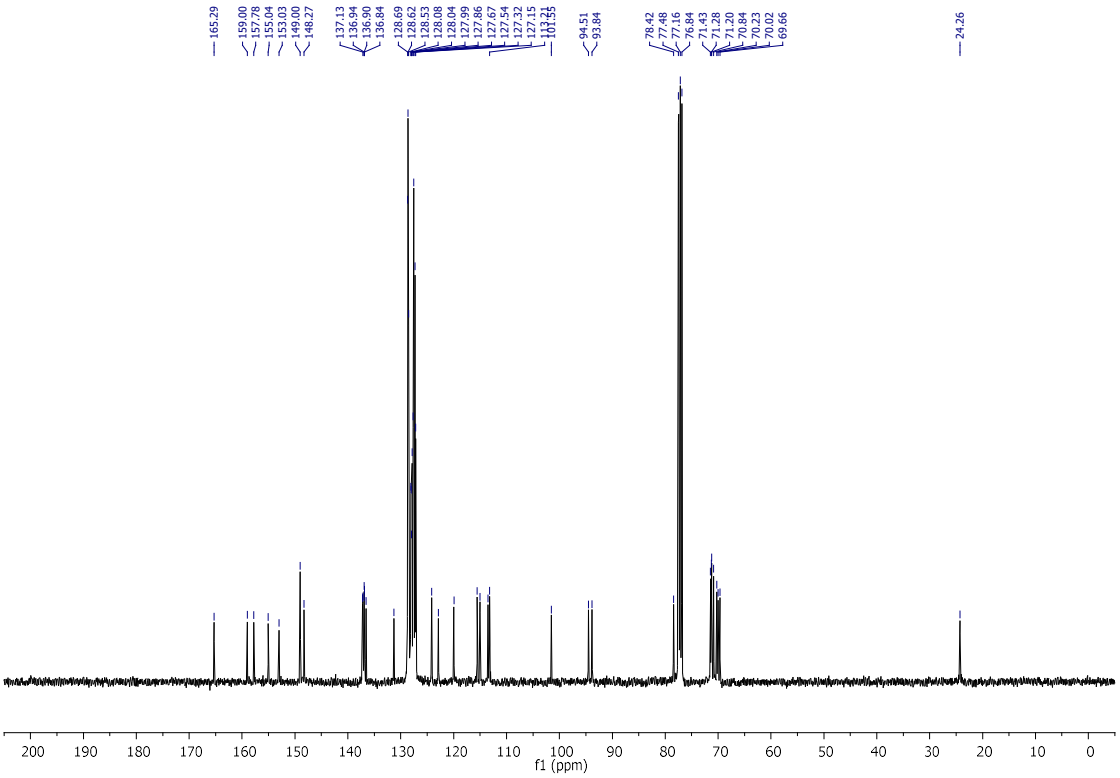

^{13}C NMR spectrum of compound **3.49d**

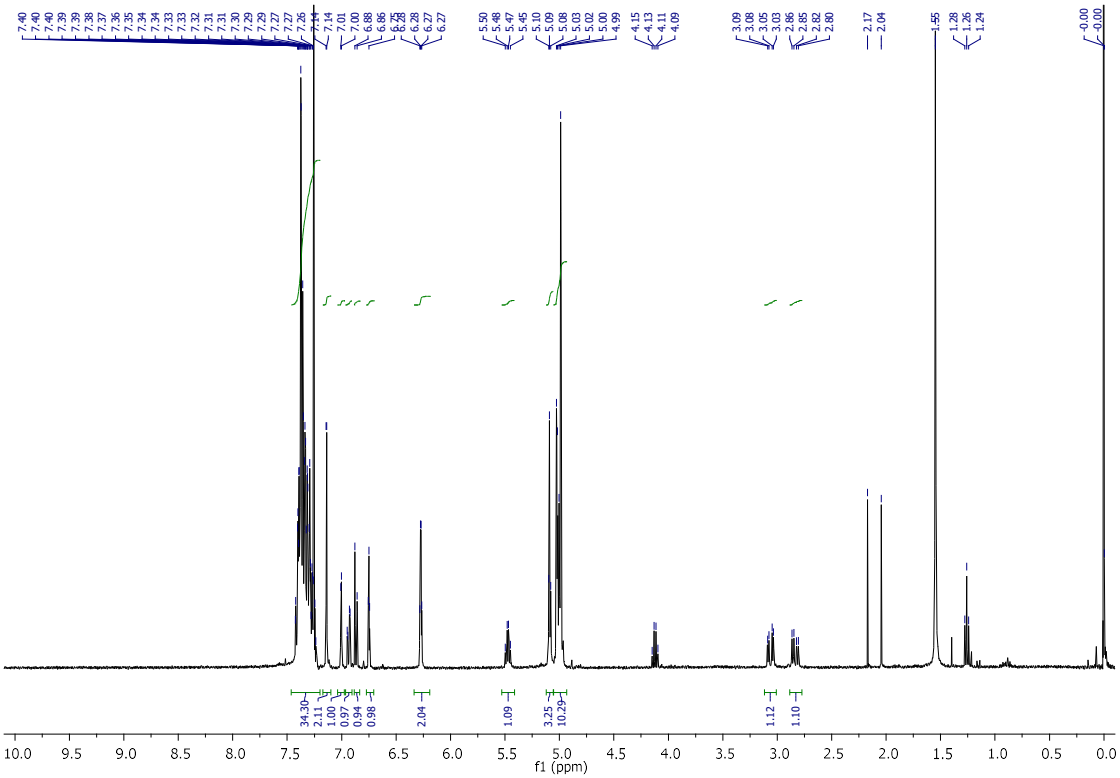

^{1}H NMR spectrum of compound **3.49e**

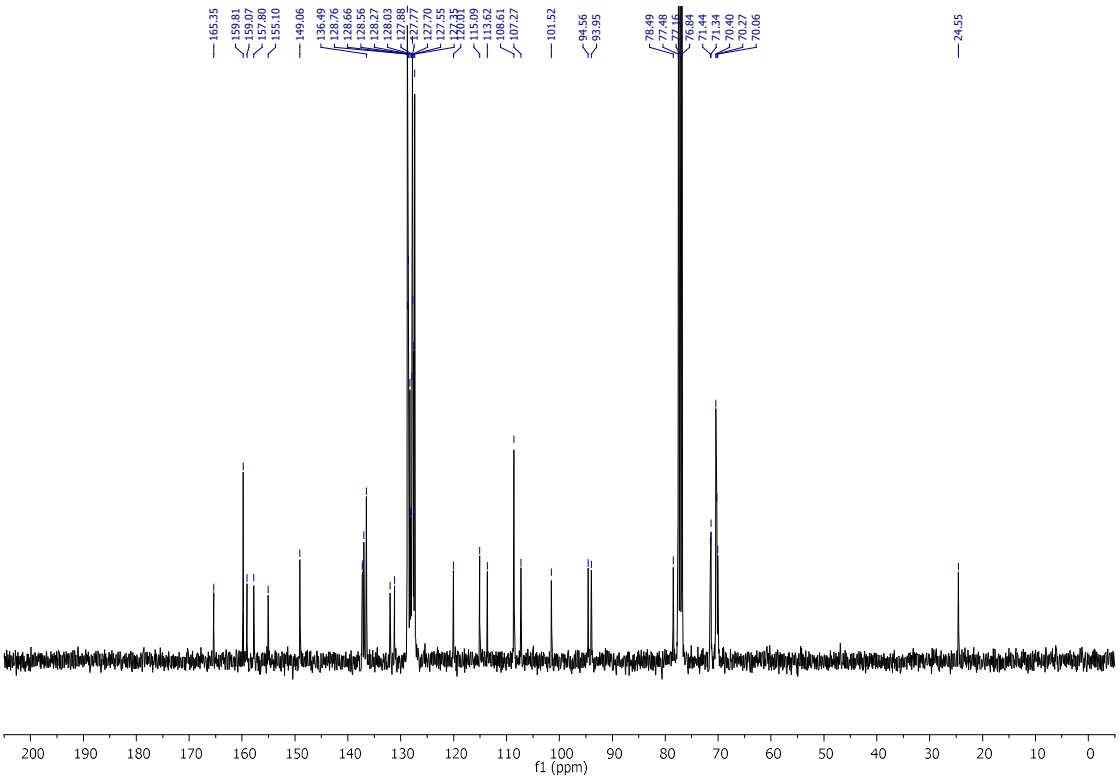

^{13}C NMR spectrum of compound **3.49e**

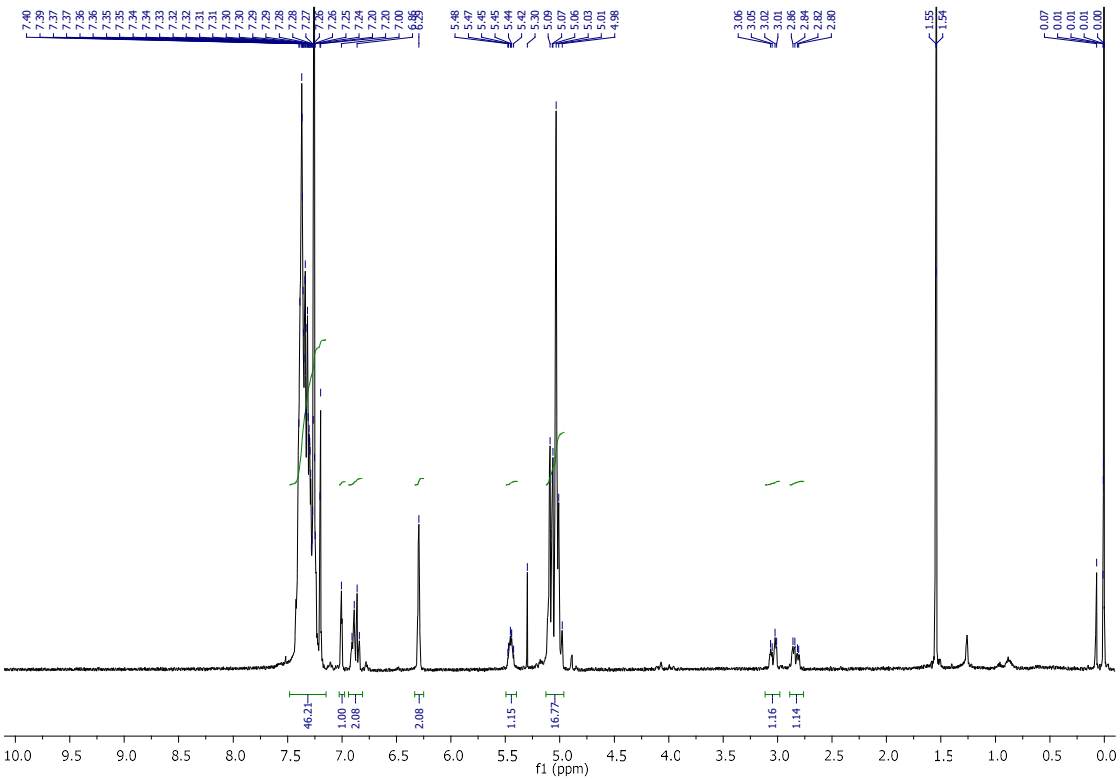

^{1}H NMR spectrum of compound **3.49f**

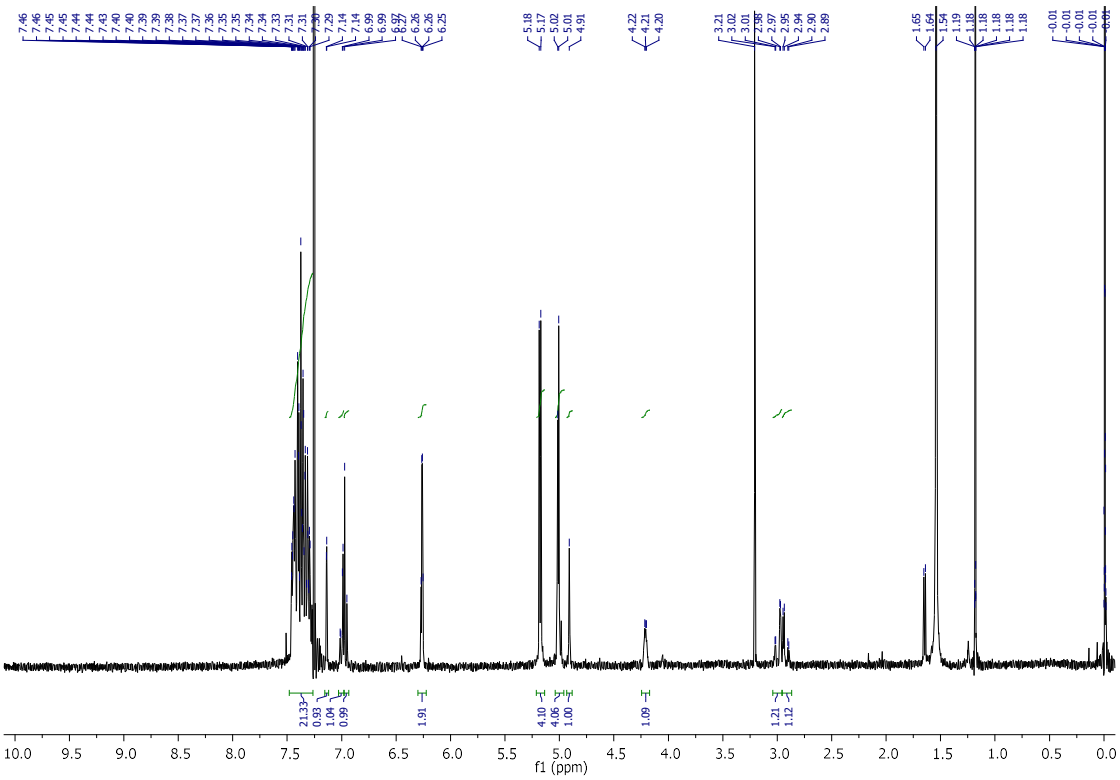

^{1}H NMR spectrum of compound **3.50a**

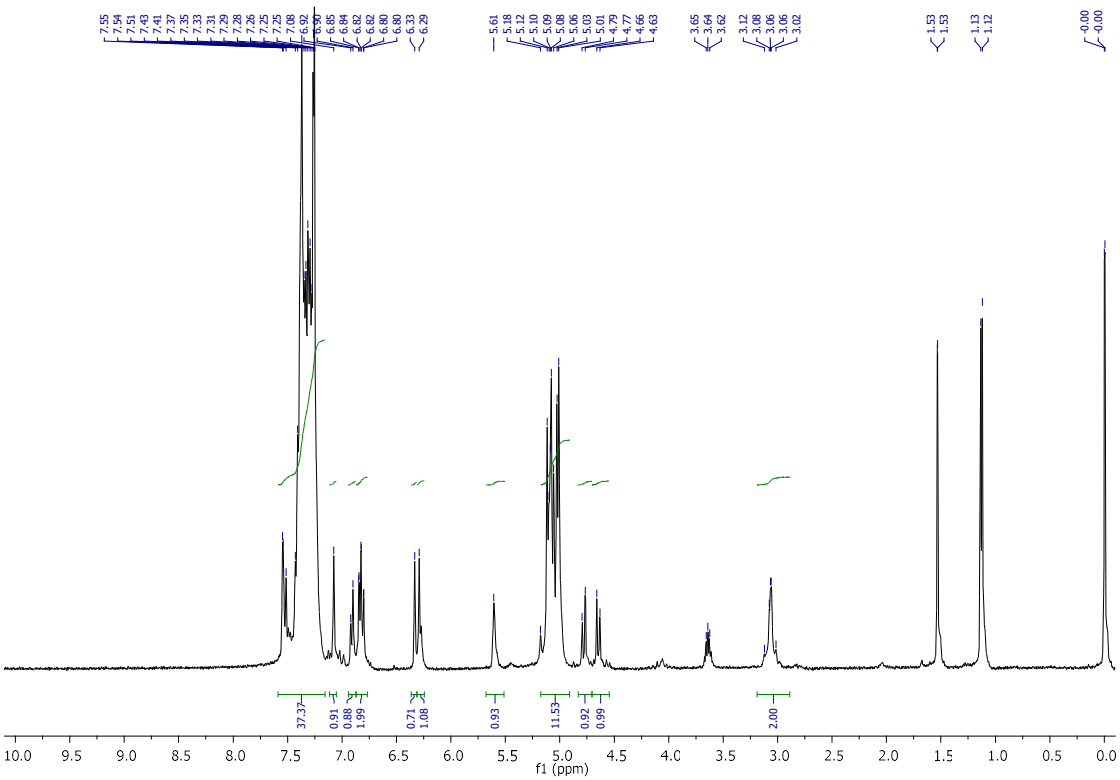

^{1}H NMR spectrum of compound **3.50d**

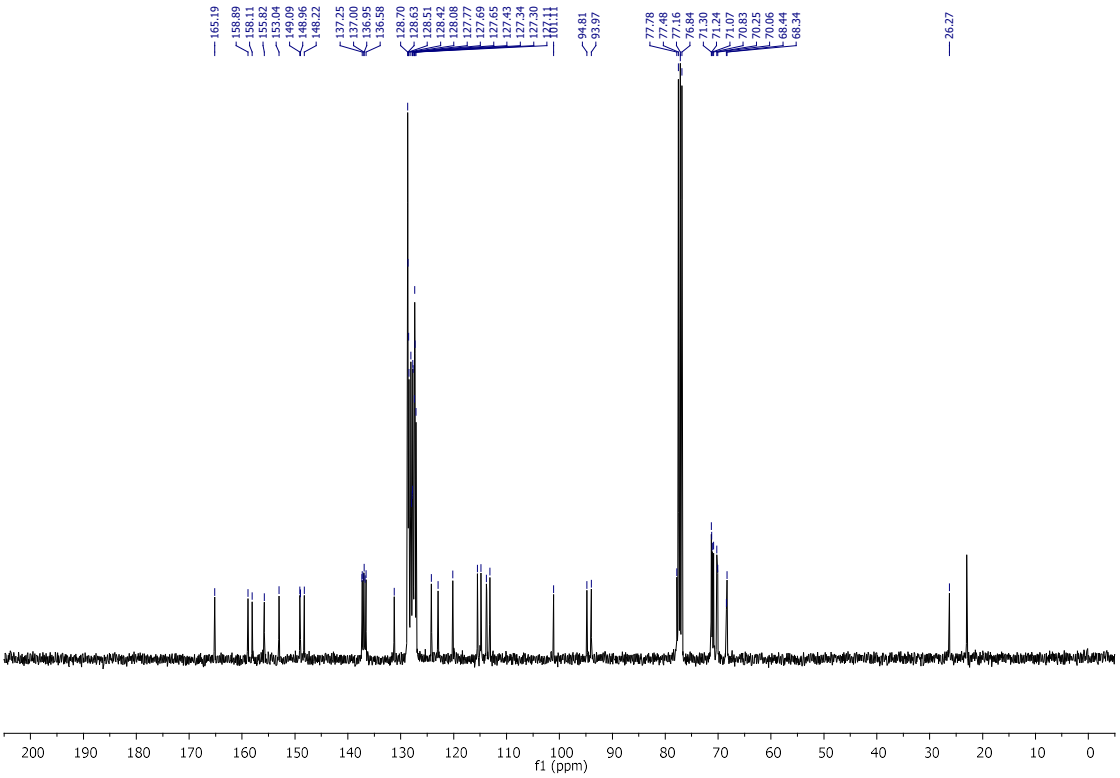

^{13}C NMR spectrum of compound **3.50d**

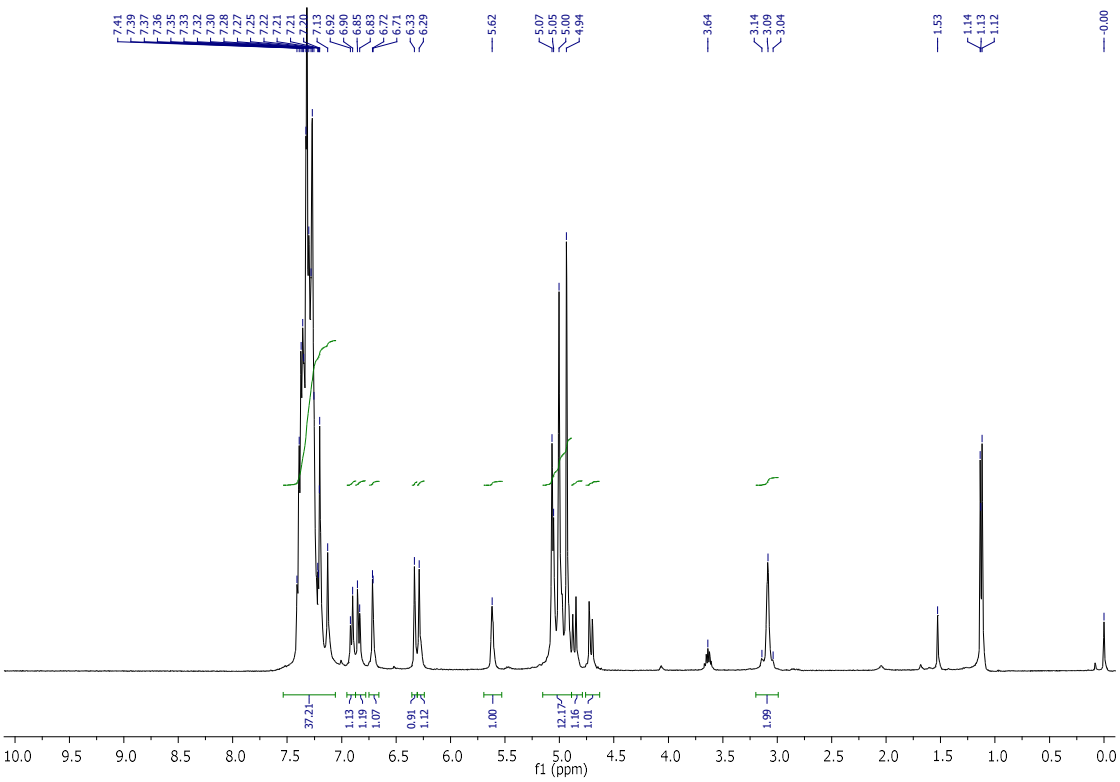

^{1}H NMR spectrum of compound **3.50e**

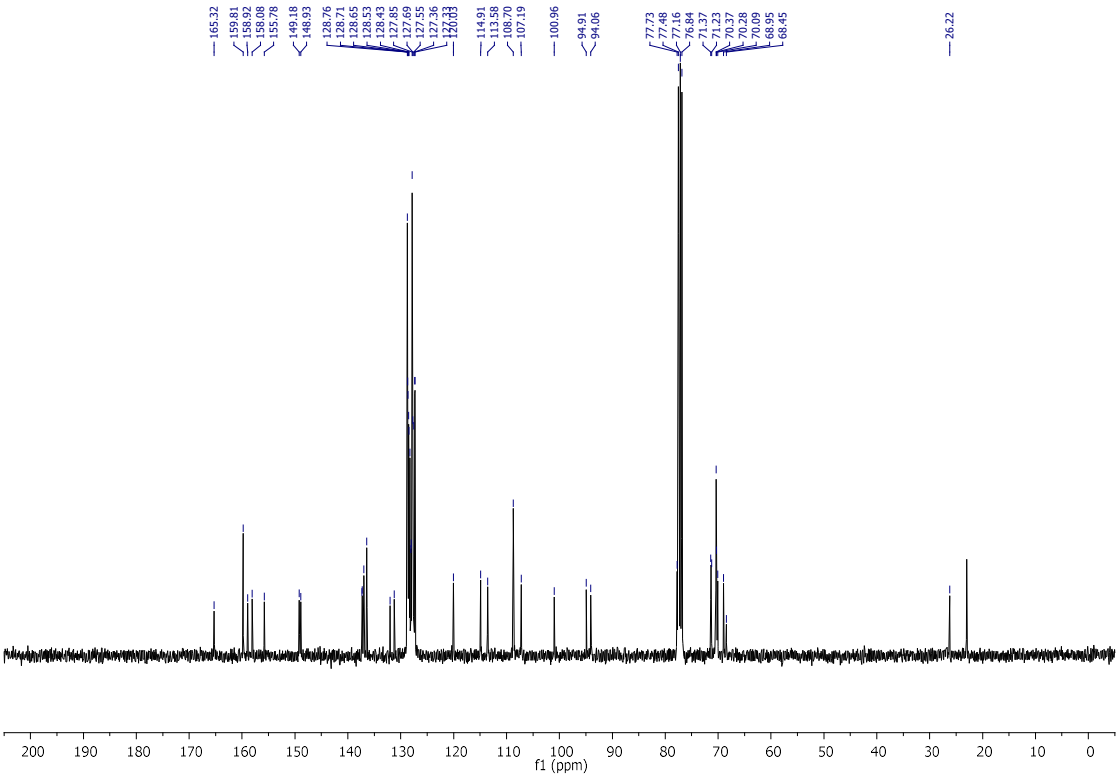

^{13}C NMR spectrum of compound **3.50e**

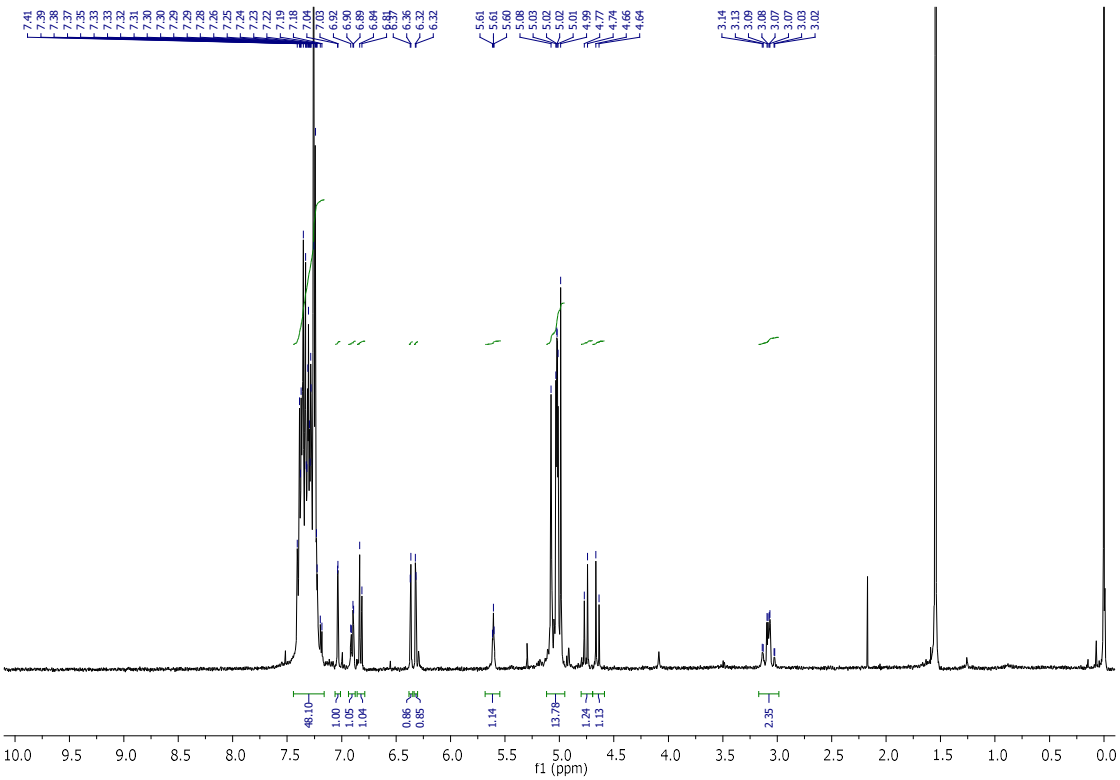

^{1}H NMR spectrum of compound **3.50f**

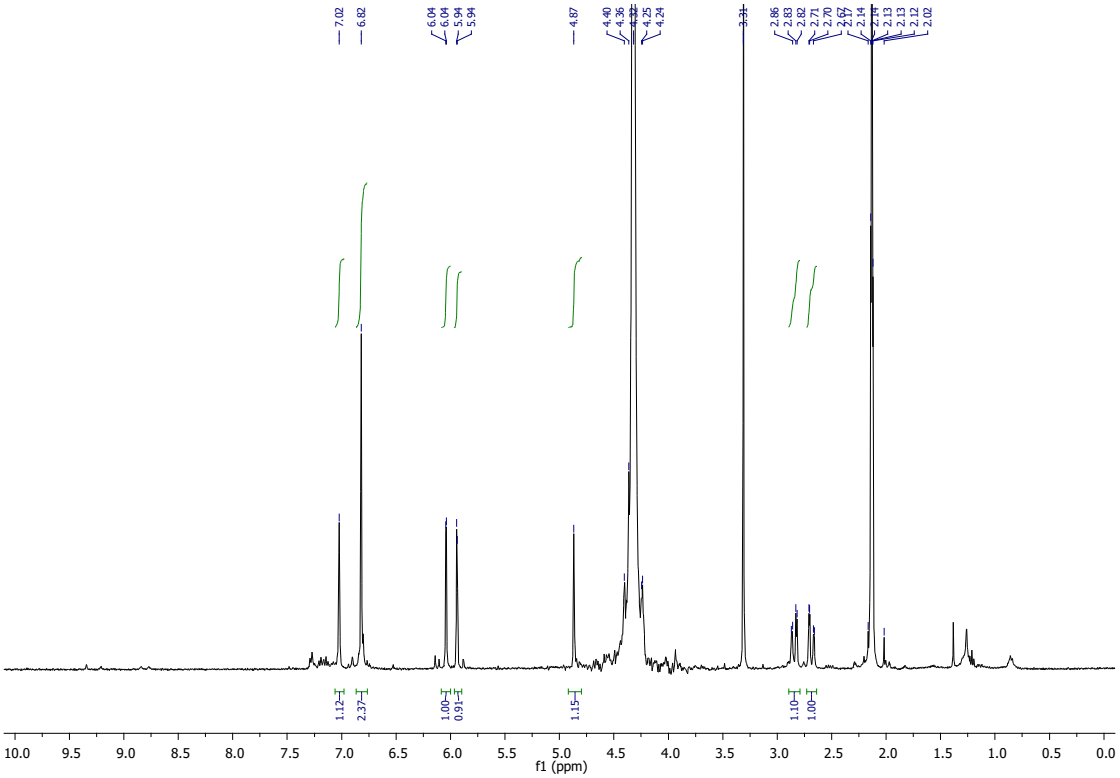

^{1}H NMR spectrum of compound **3.53a**

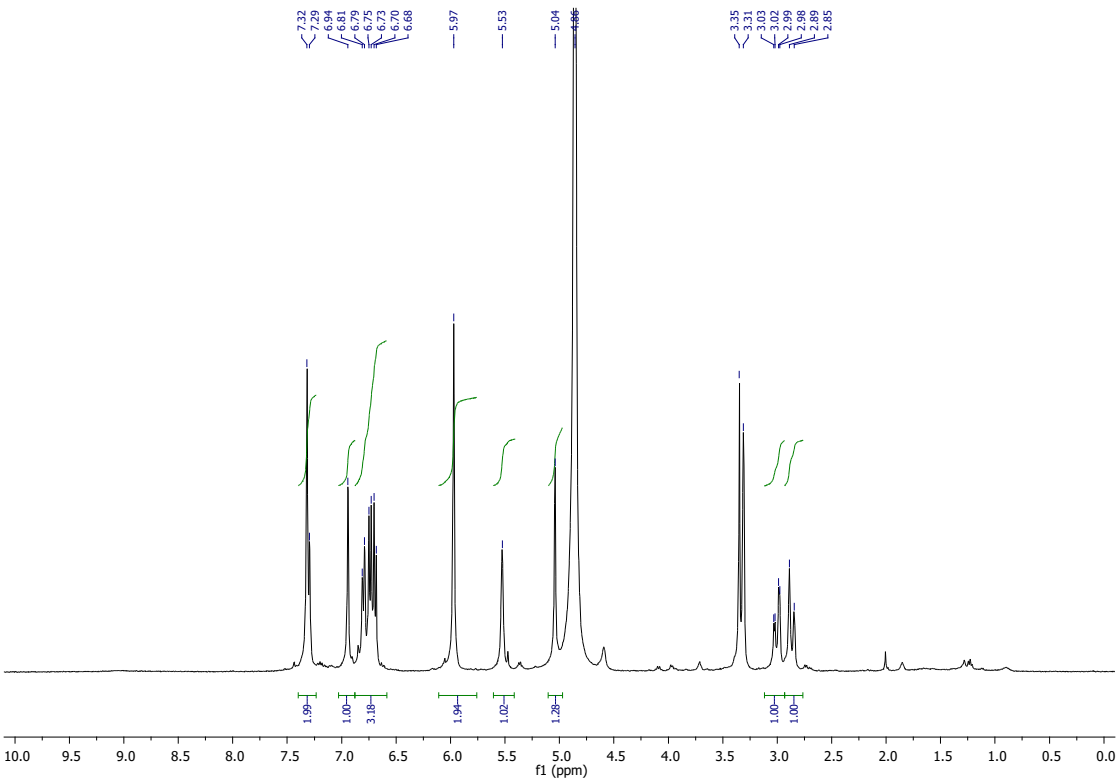

^{1}H NMR spectrum of compound **3.53d**

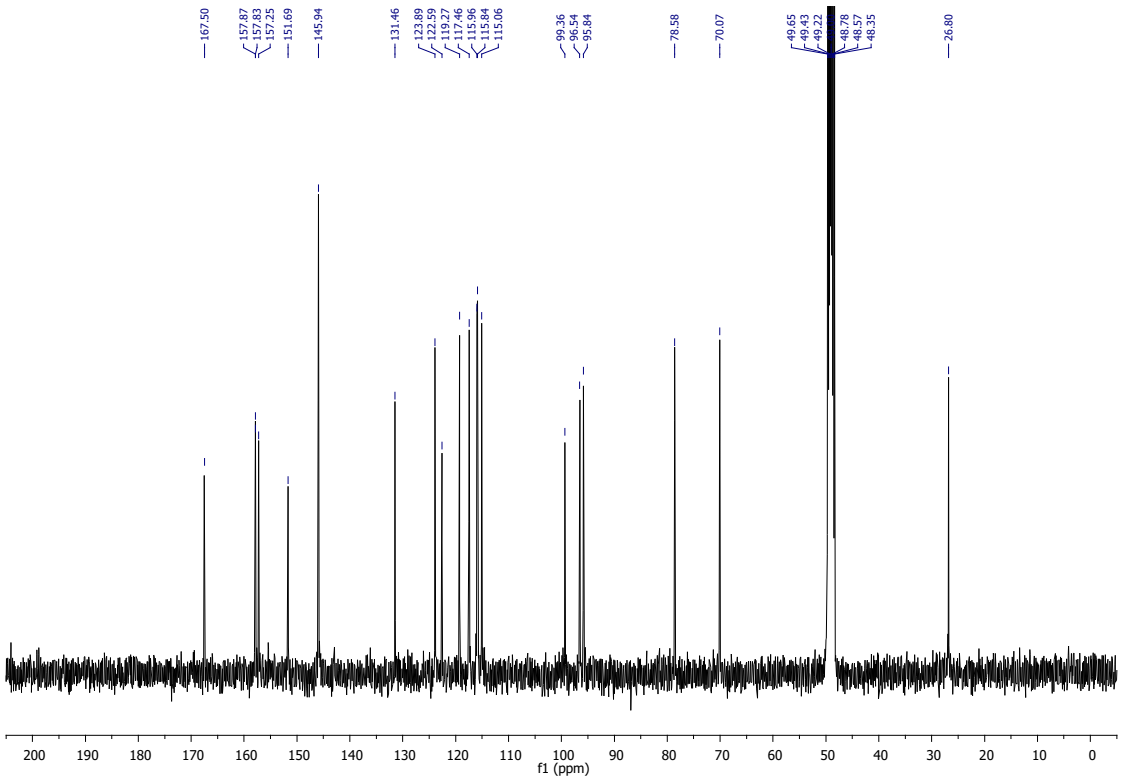

^{13}C NMR spectrum of compound **3.53d**

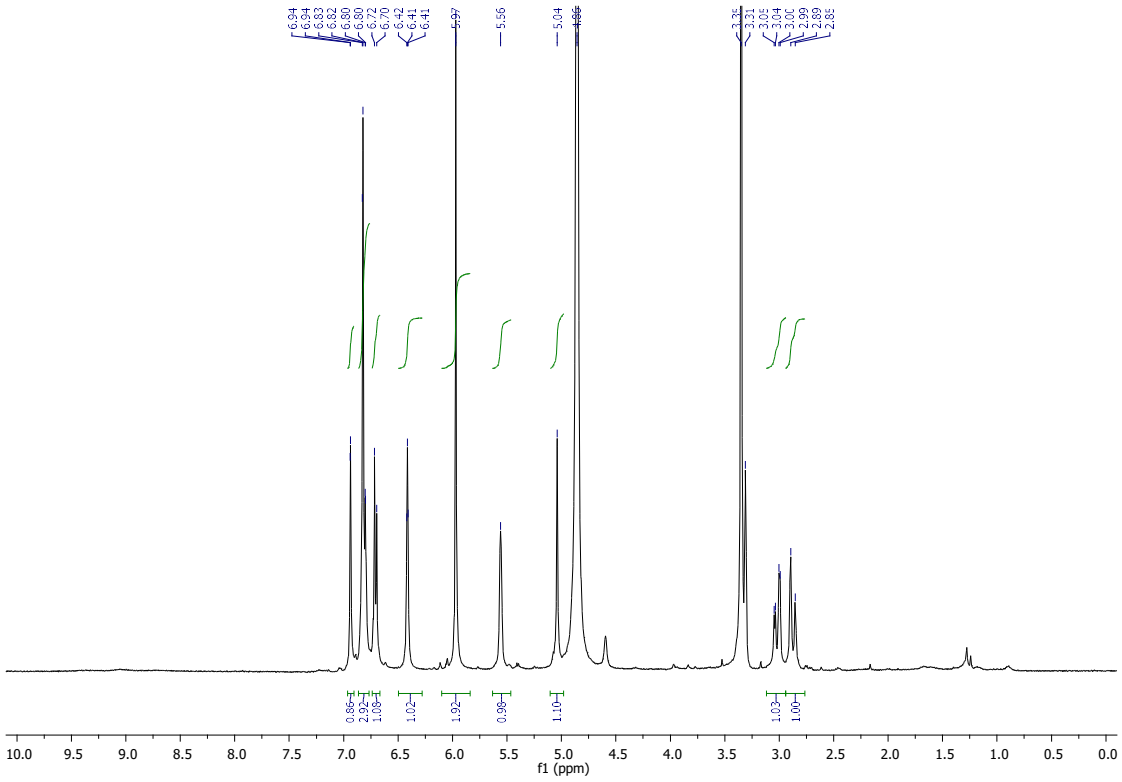

^{1}H NMR spectrum of compound **3.53e**

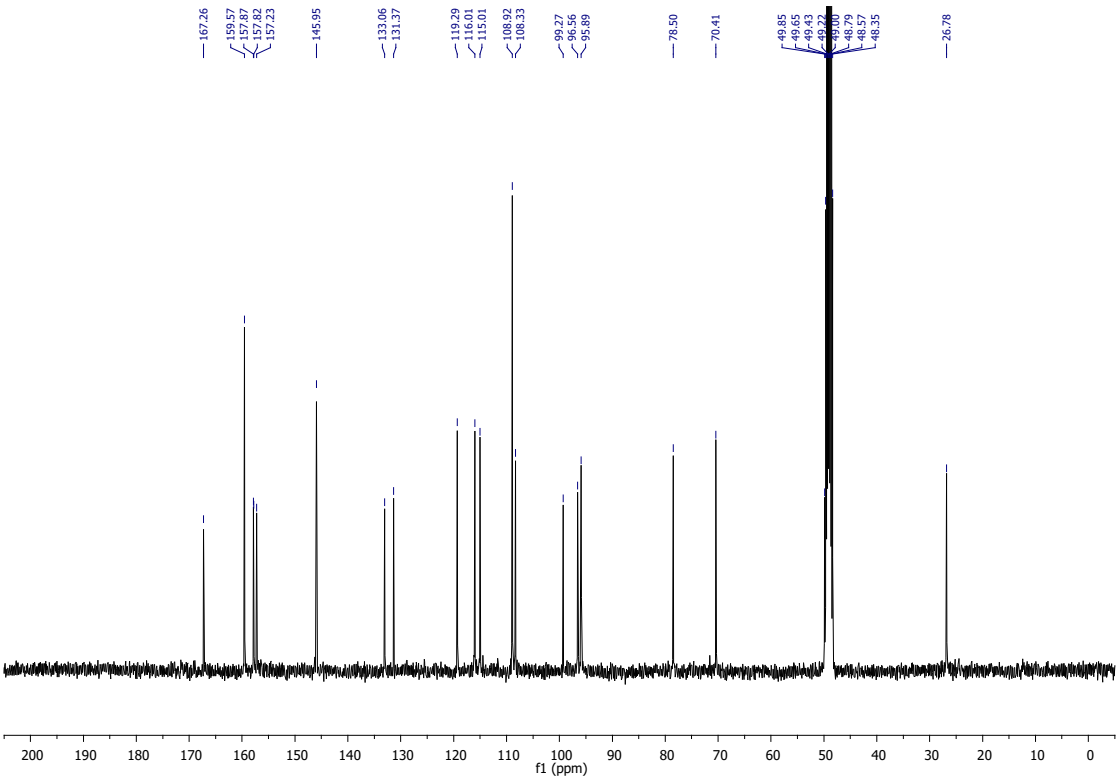

^{13}C NMR spectrum of compound **3.53e**

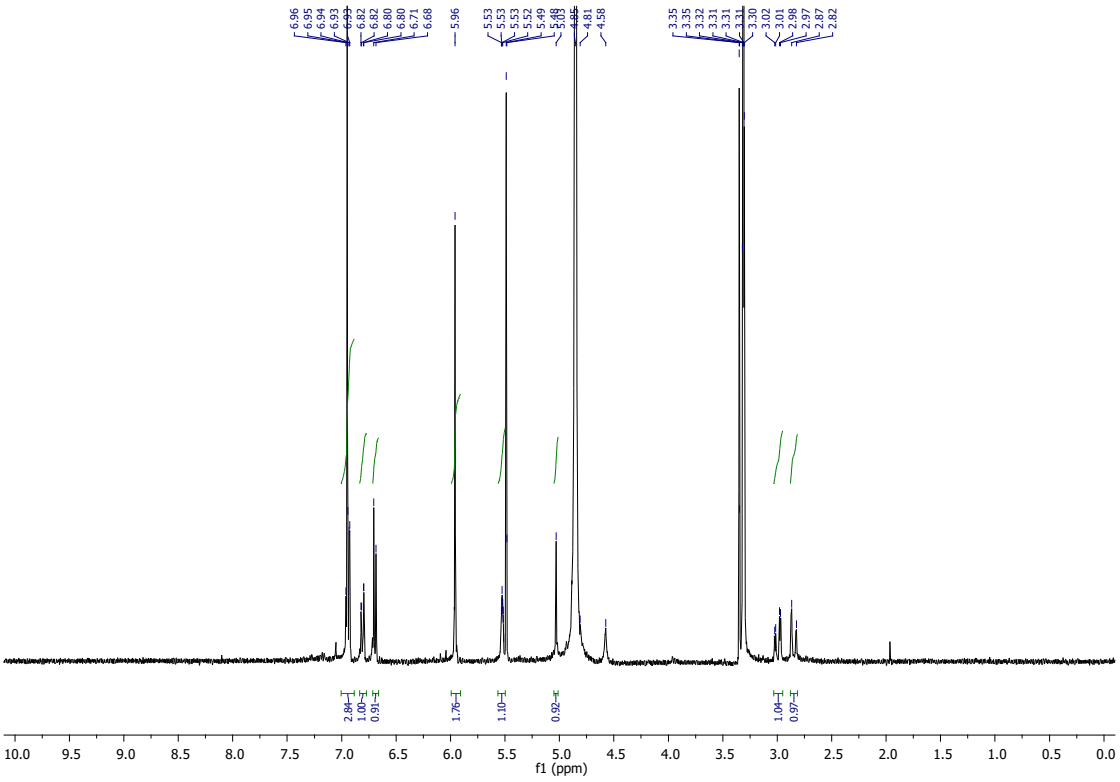

^{1}H NMR spectrum of compound **3.53f**

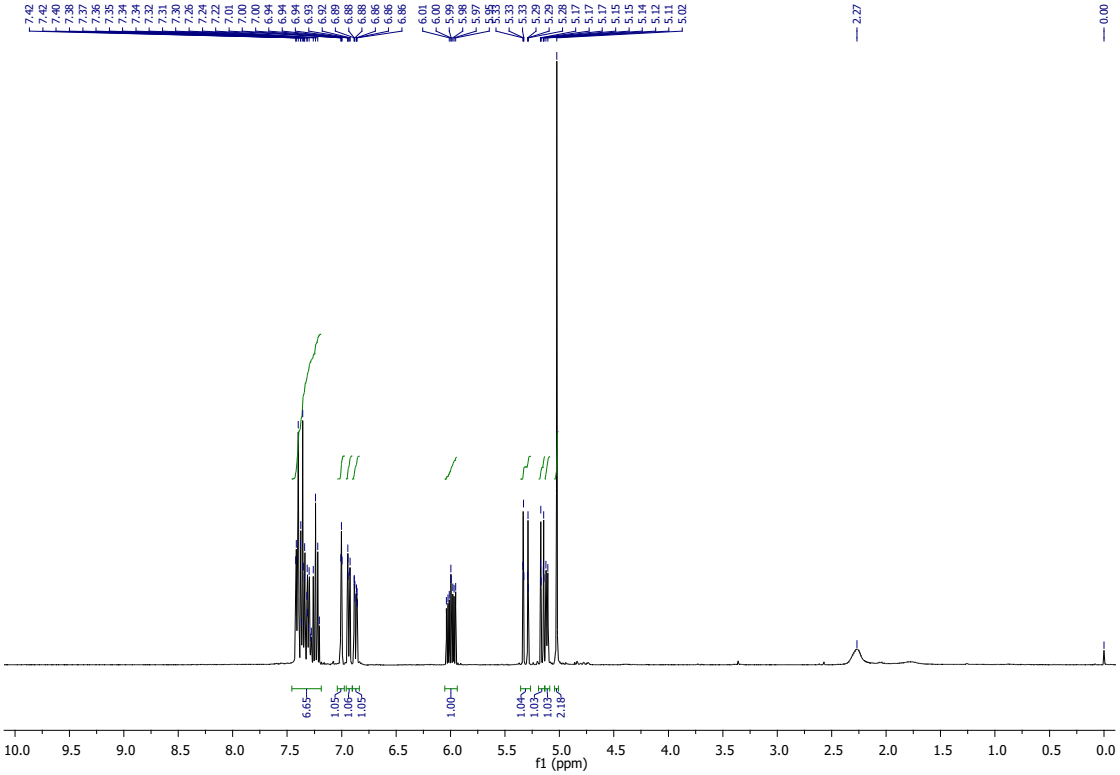

^{1}H NMR spectrum of compound ***rac*-3.55b**

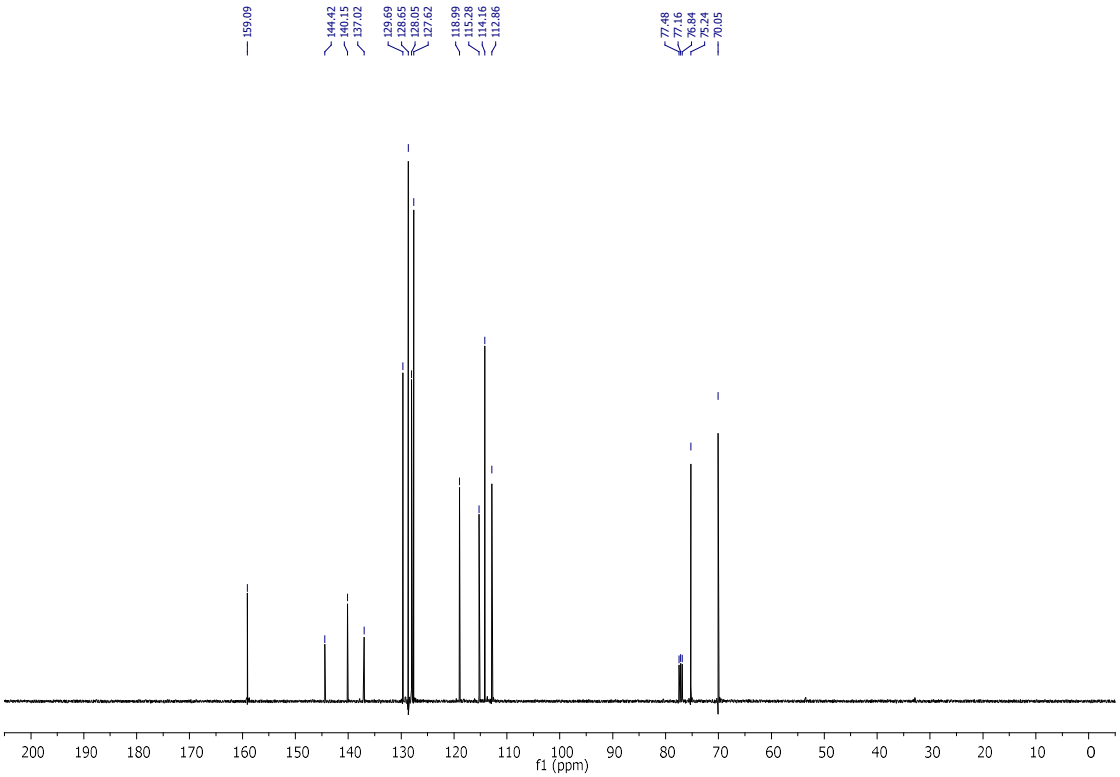

^{13}C NMR spectrum of compound ***rac*-3.55b**

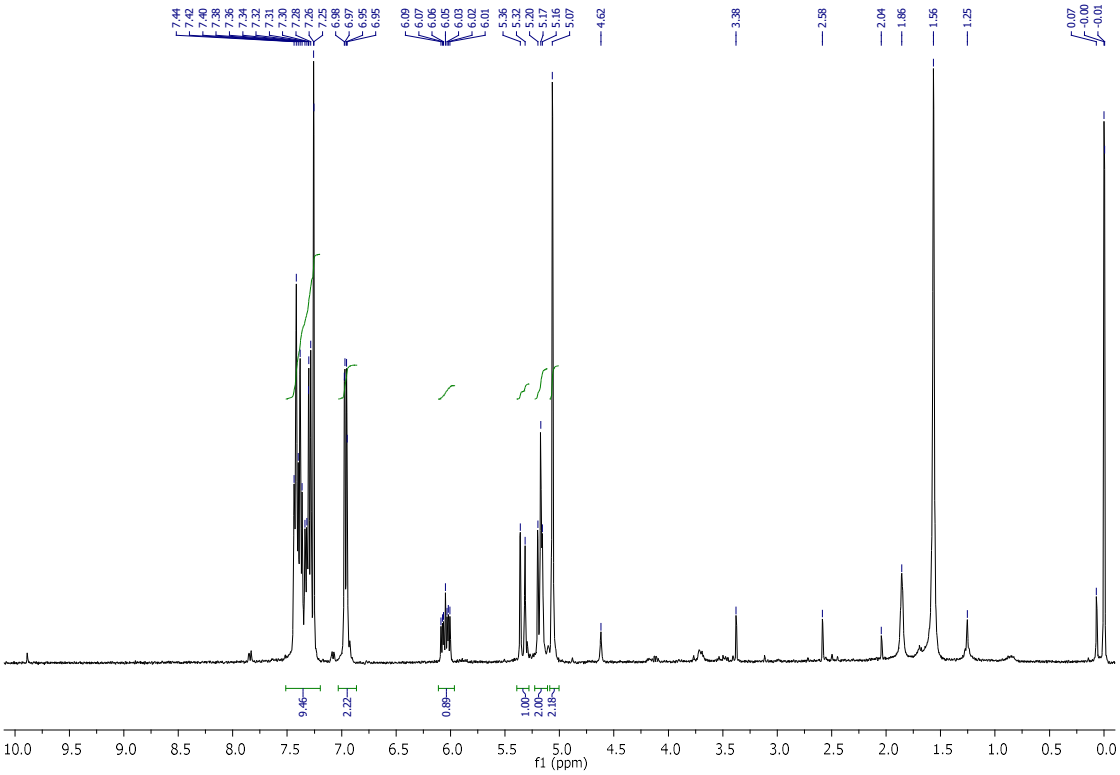

^{1}H NMR spectrum of compound ***rac*-3.55c**

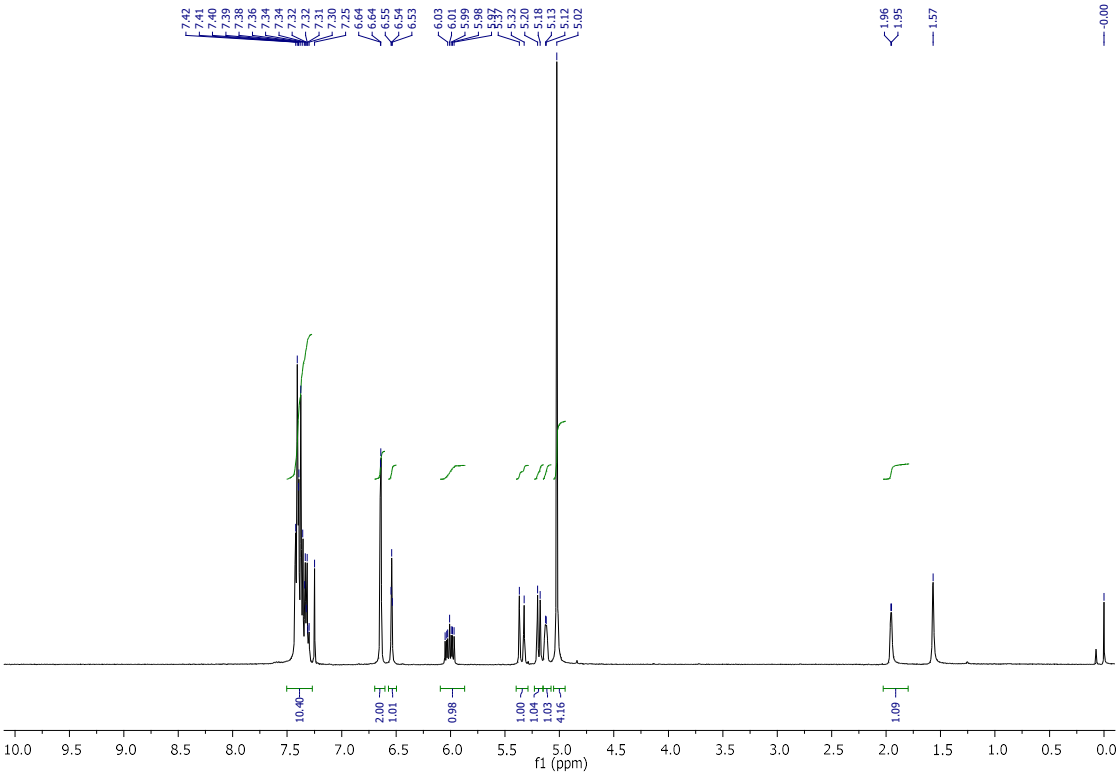

^{1}H NMR spectrum of compound ***rac*-3.55d**

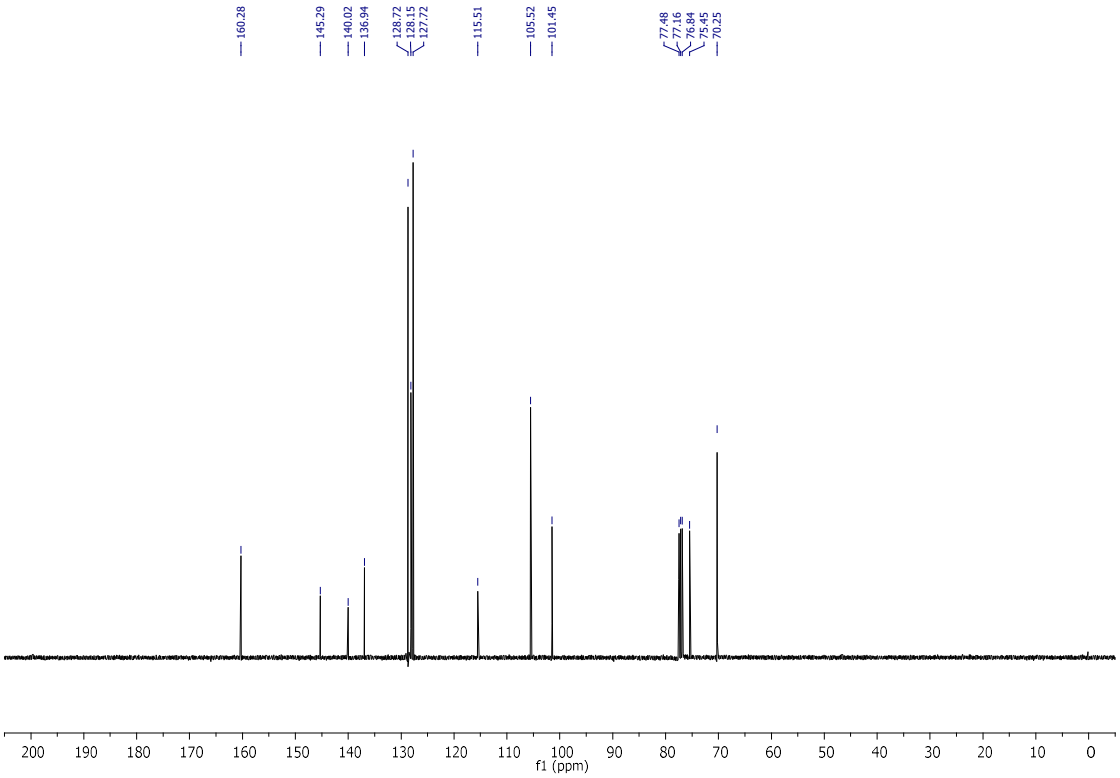

^{13}C NMR spectrum of compound ***rac*-3.55d**

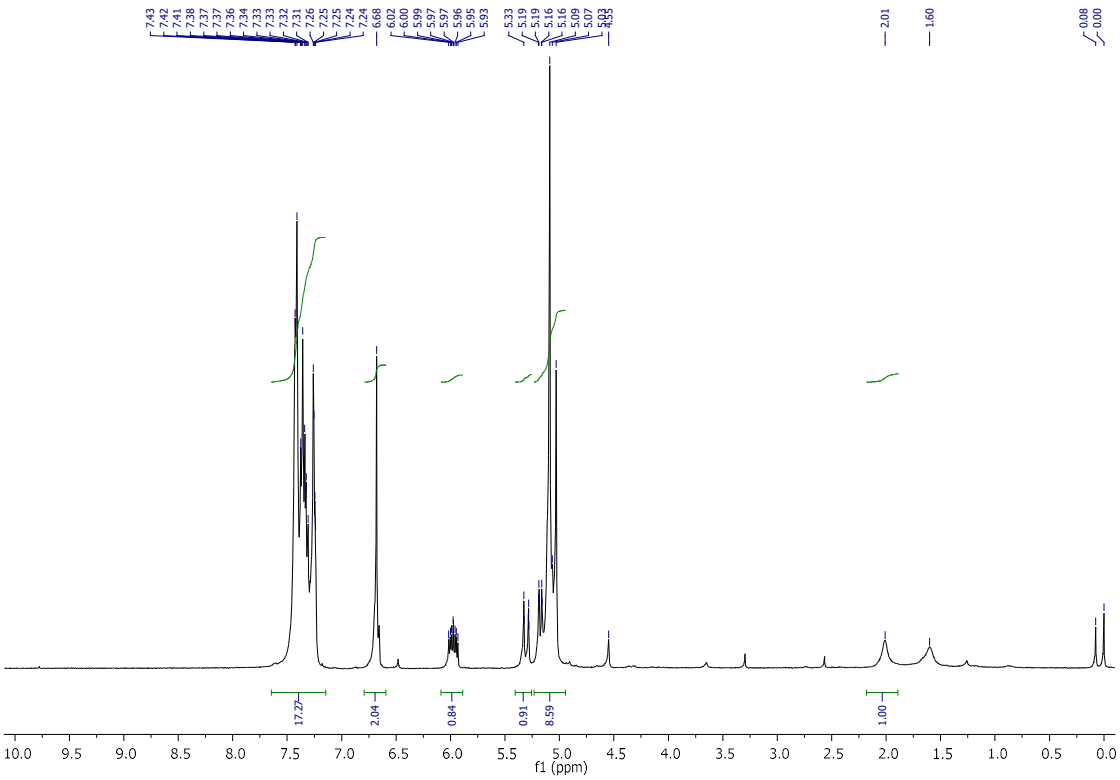

^{1}H NMR spectrum of compound ***rac*-3.55e**

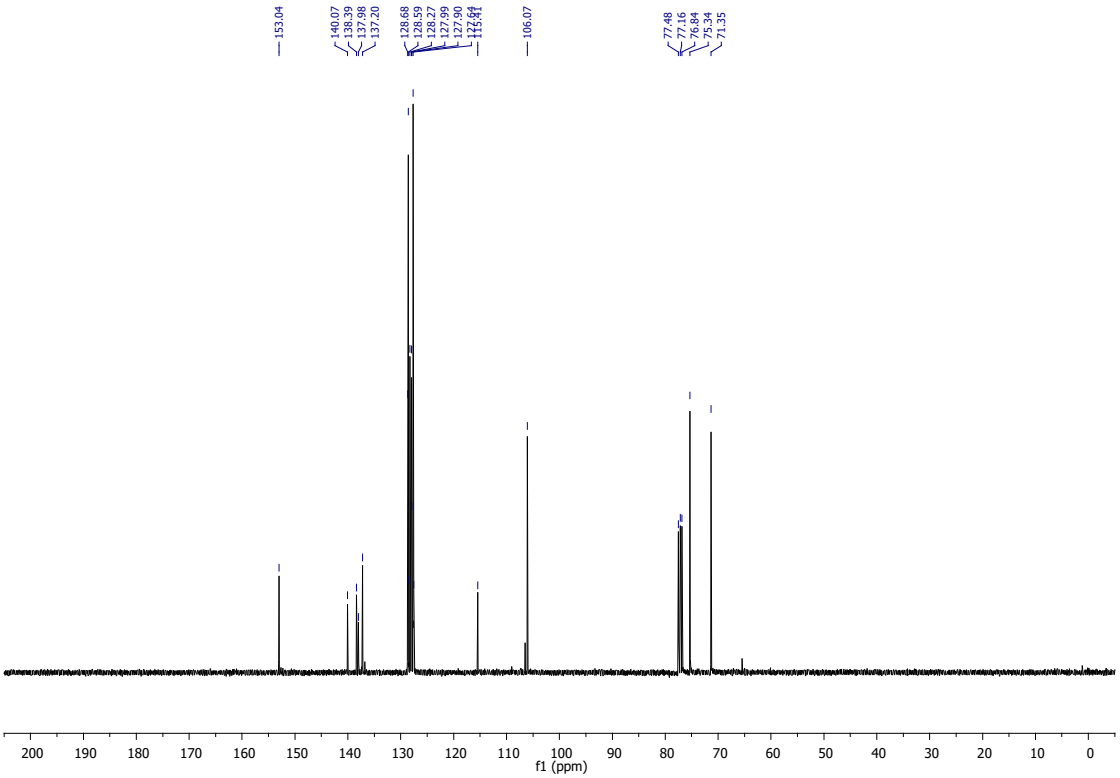

^{13}C NMR spectrum of compound ***rac*-3.55e**

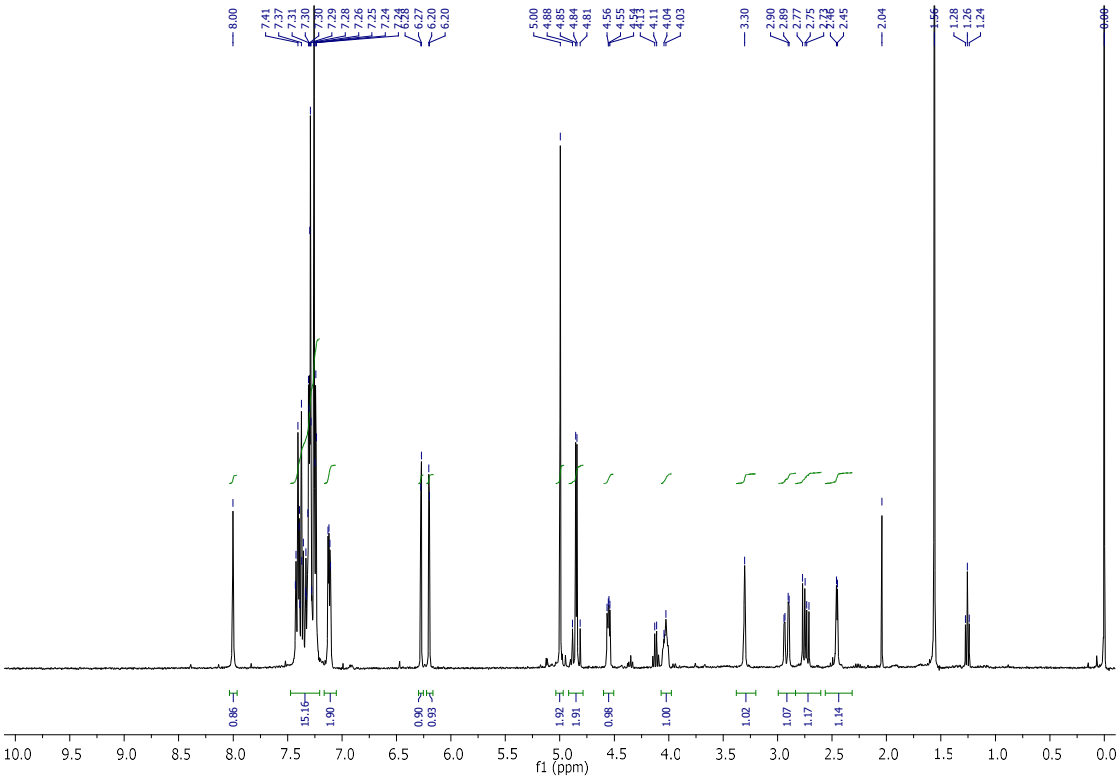

^{1}H NMR spectrum of compound ***rac*-3.56a**

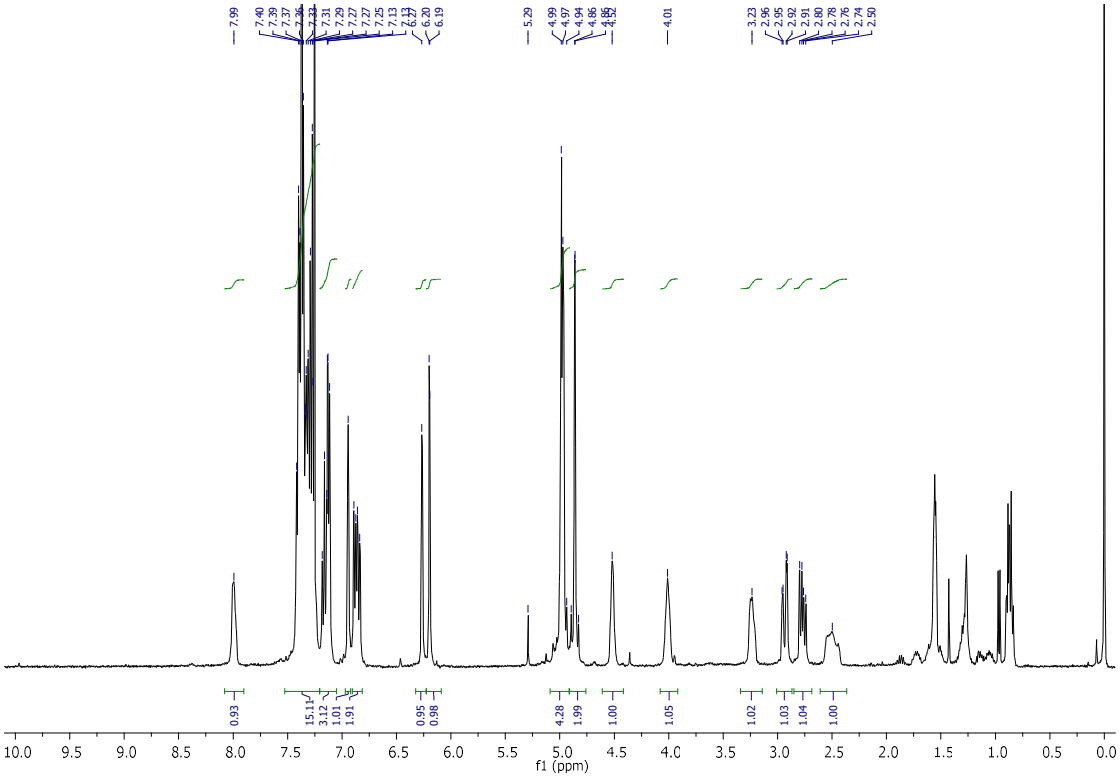

^{1}H NMR spectrum of compound ***rac*-3.56b**

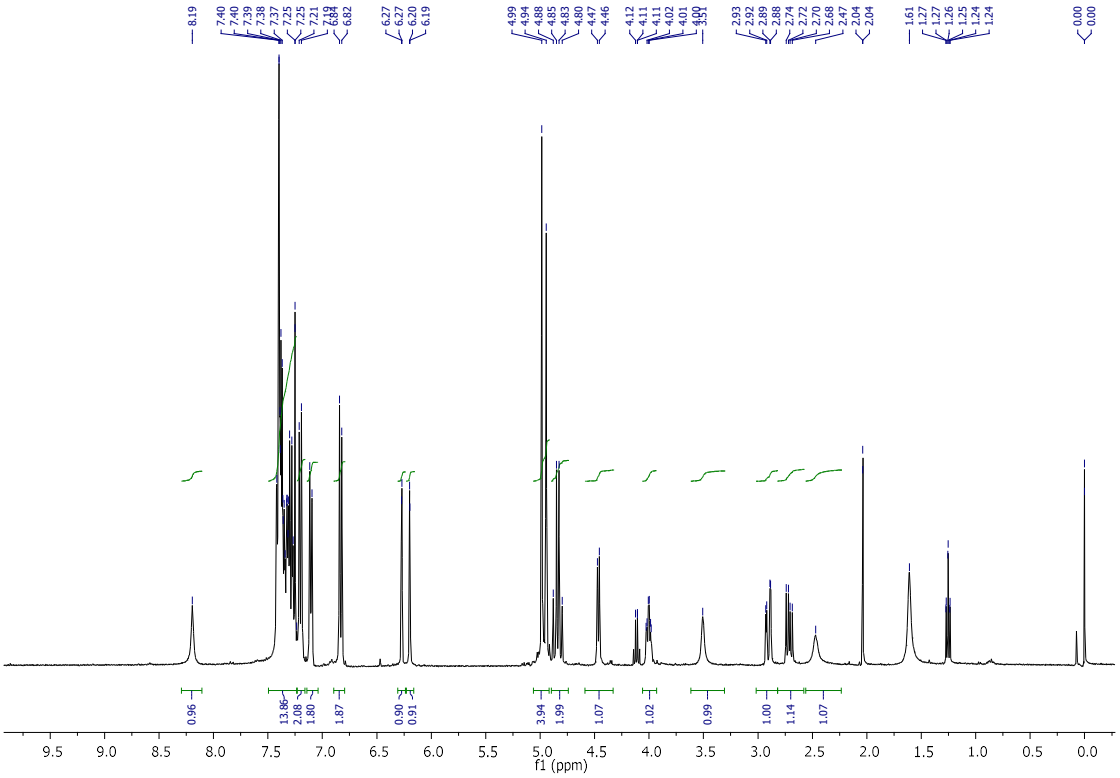

^{1}H NMR spectrum of compound ***rac*-3.56c**

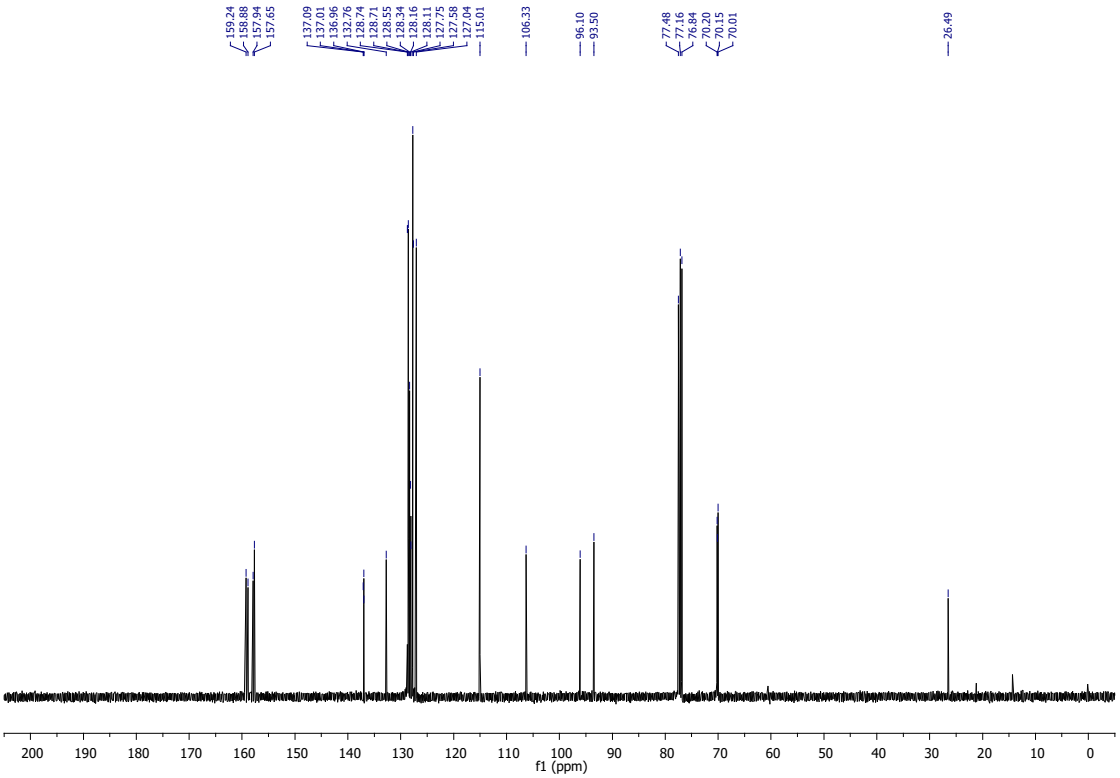

^{13}C NMR spectrum of compound ***rac*-3.56c**

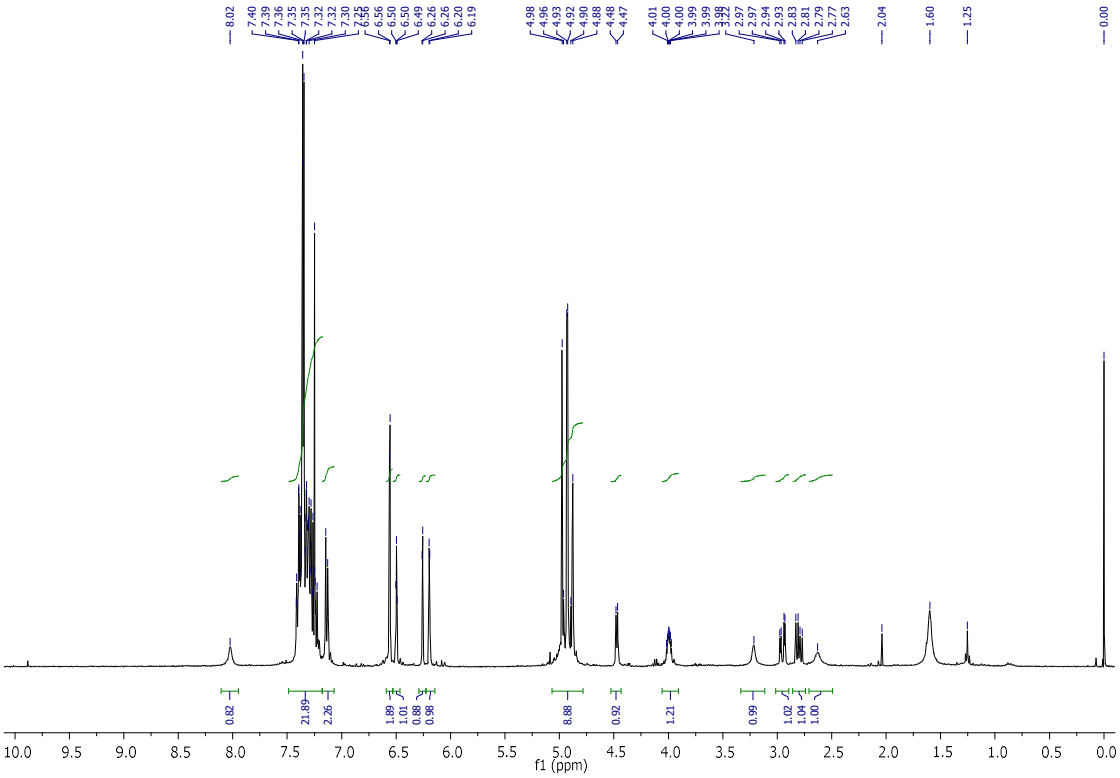

^{1}H NMR spectrum of compound ***rac*-3.56d**

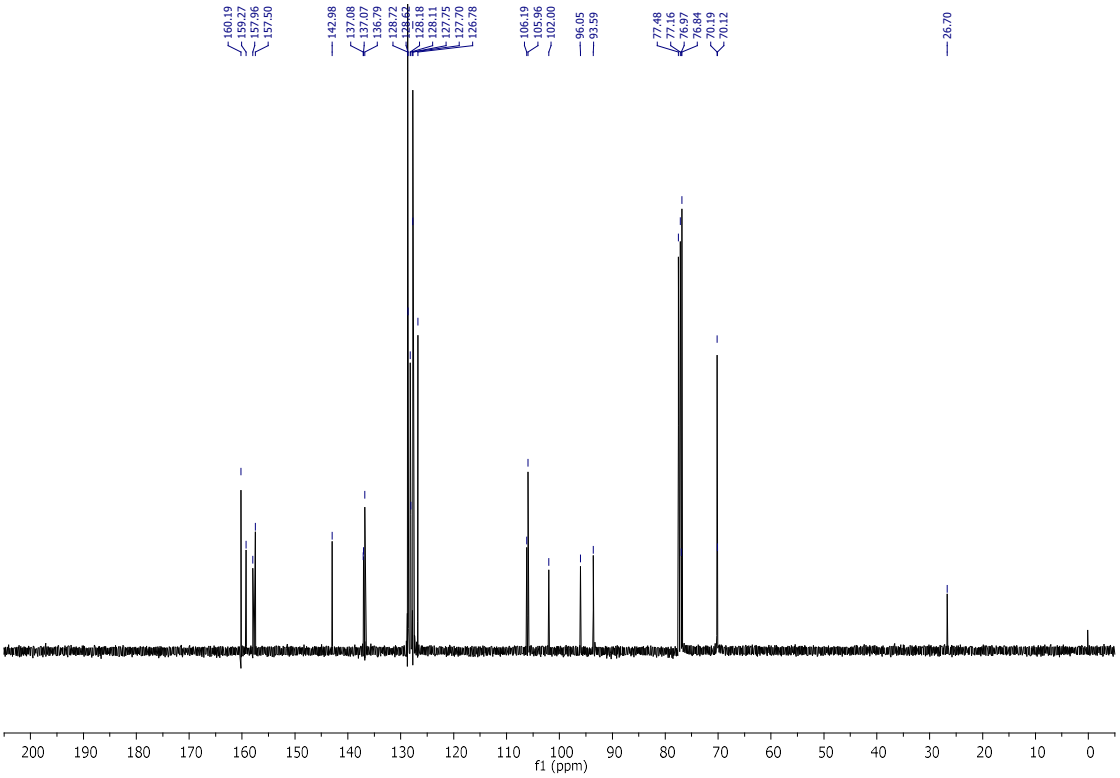

^{13}C NMR spectrum of compound ***rac*-3.56d**

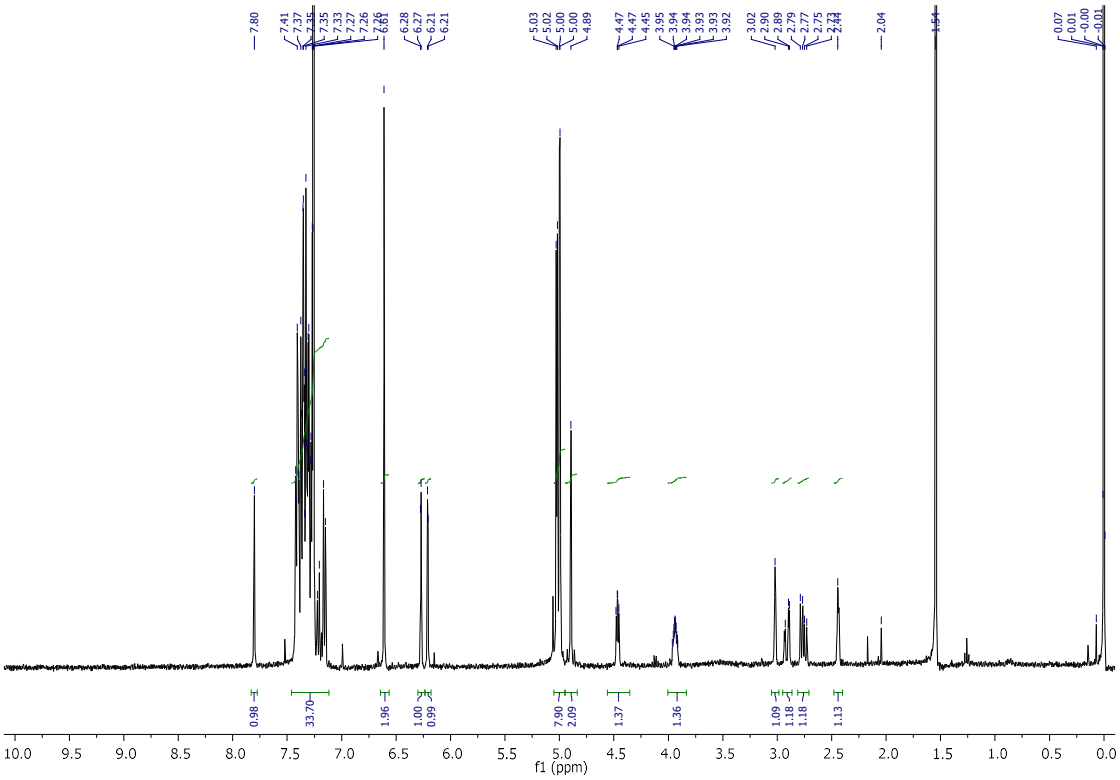

^{1}H NMR spectrum of compound ***rac*-3.56e**

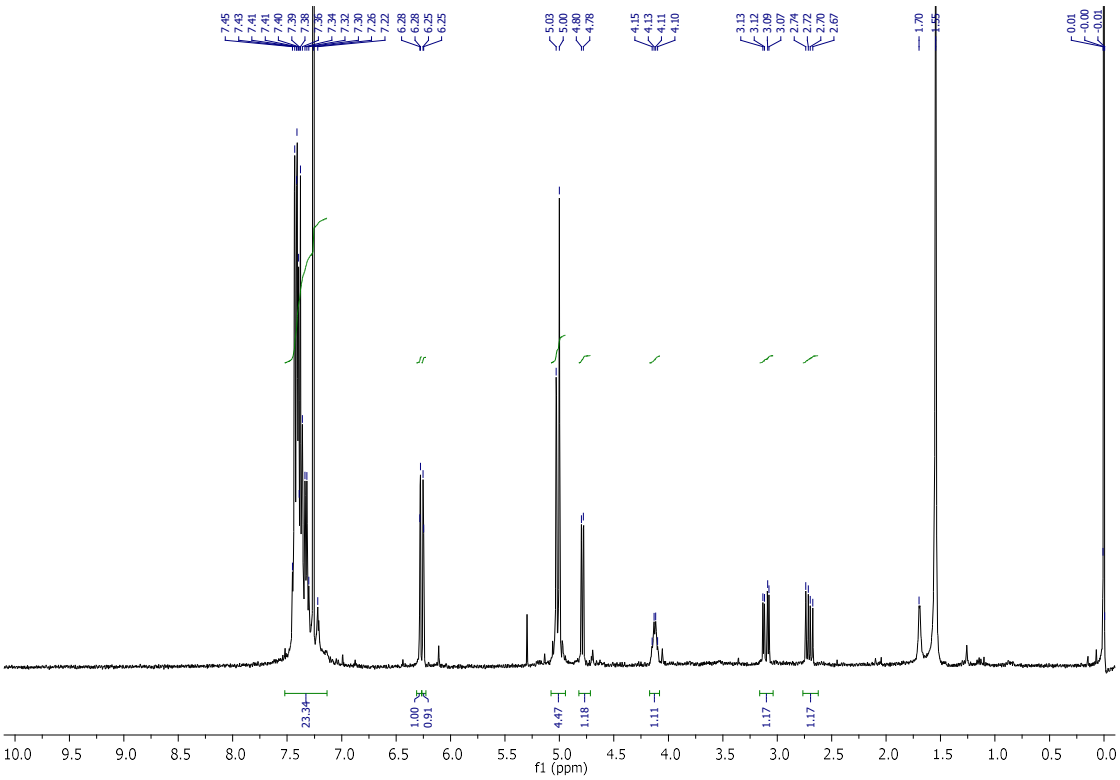

^{1}H NMR spectrum of compound ***rac*-3.57a**

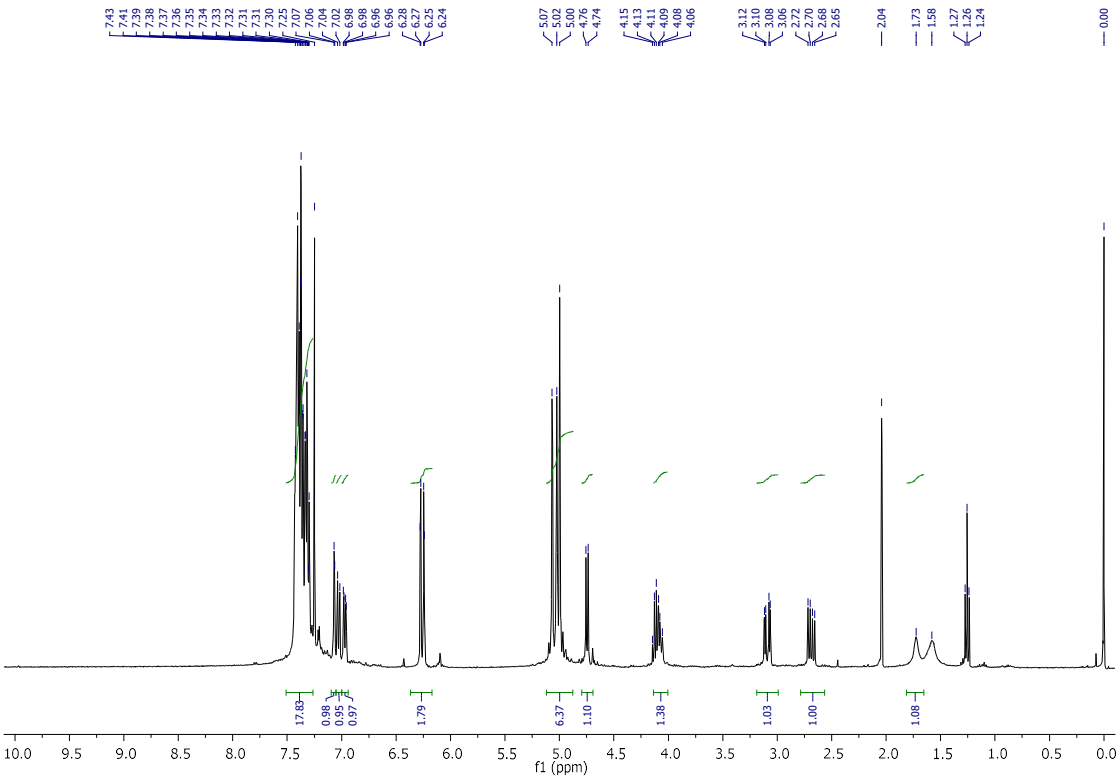

^{1}H NMR spectrum of compound ***rac*-3.57b**

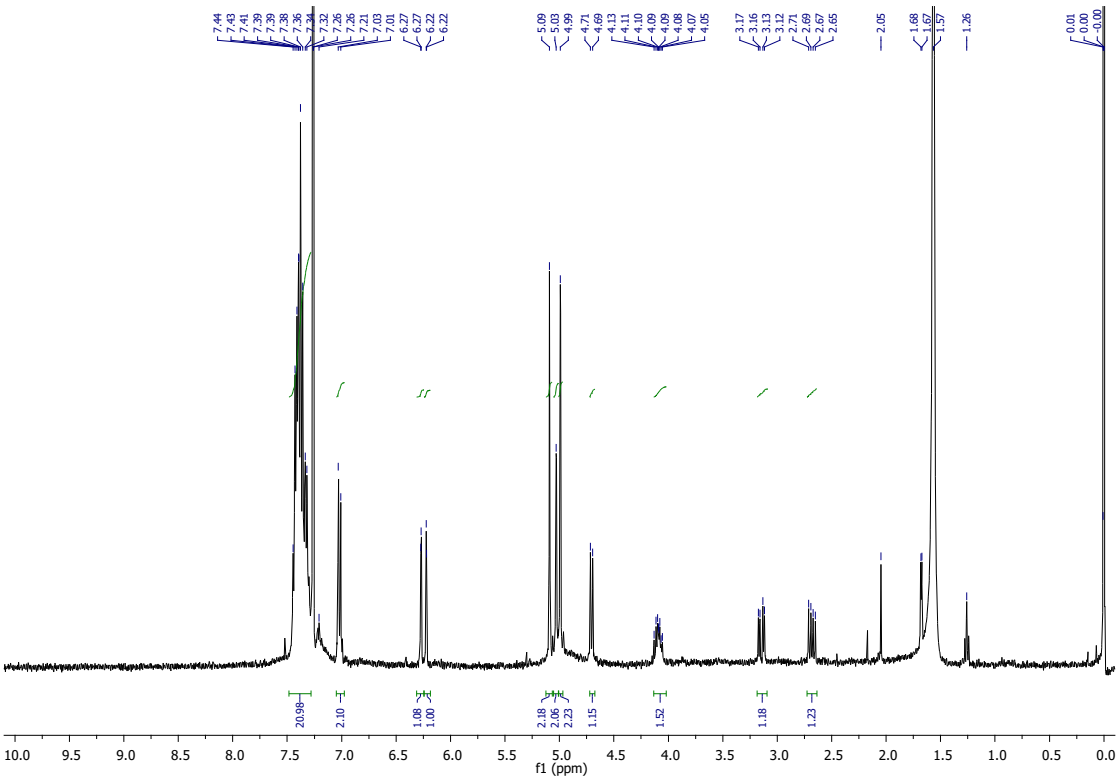

^{1}H NMR spectrum of compound ***rac*-3.57c**

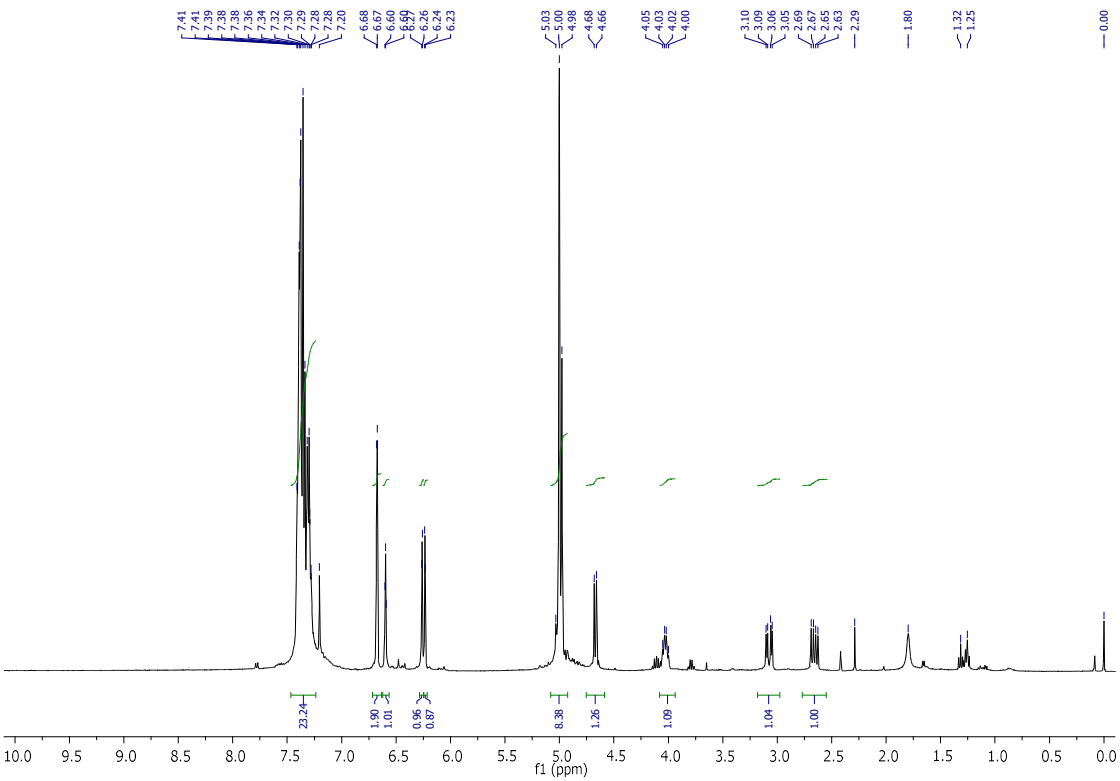

^{1}H NMR spectrum of compound ***rac*-3.57d**

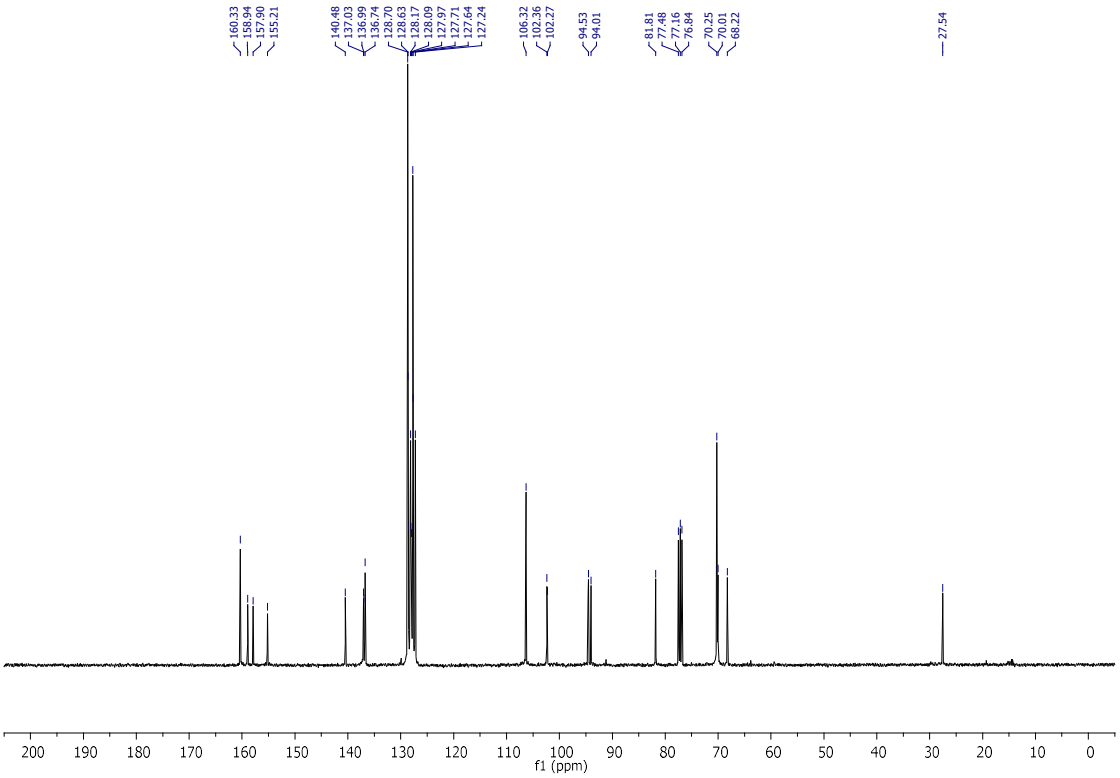

^{13}C NMR spectrum of compound ***rac*-3.57d**

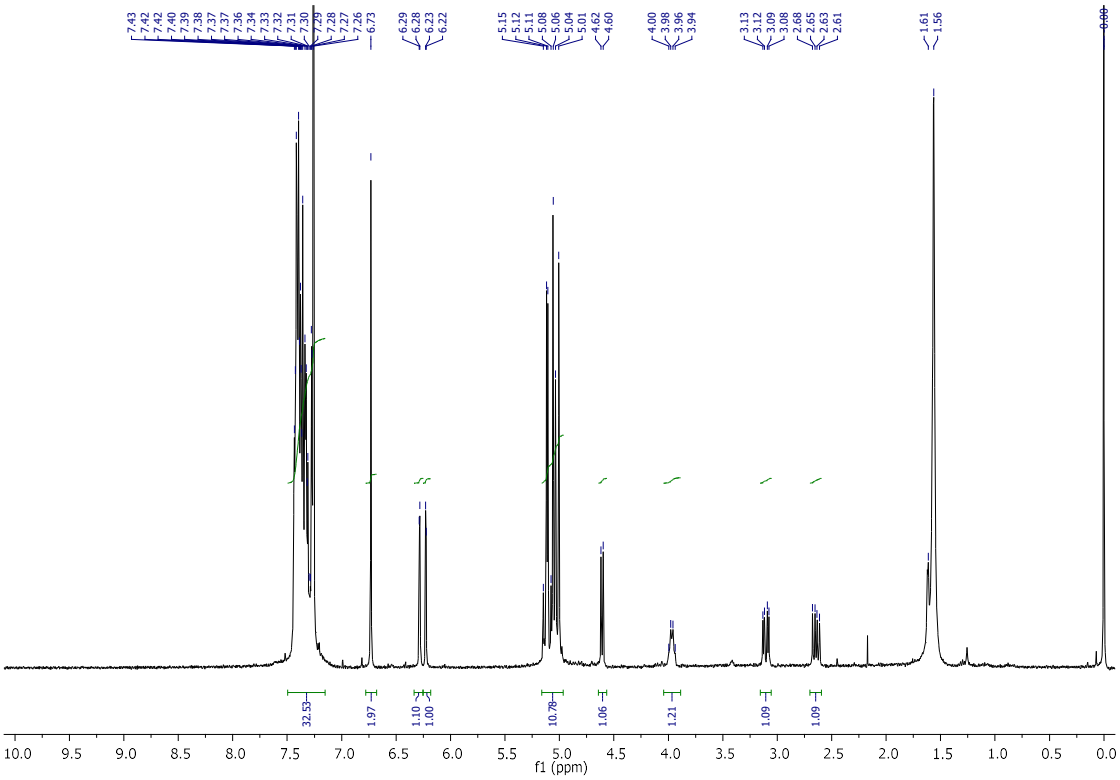

^{1}H NMR spectrum of compound ***rac*-3.57e**

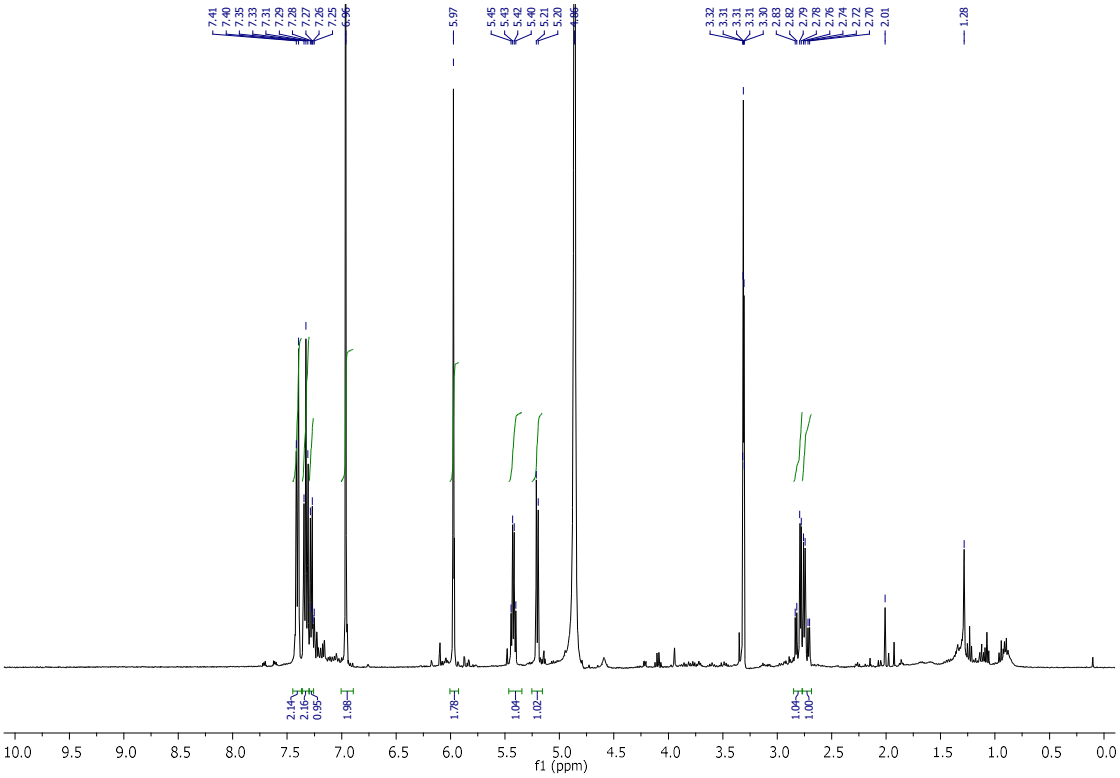

^{1}H NMR spectrum of compound ***rac*-3.58a**

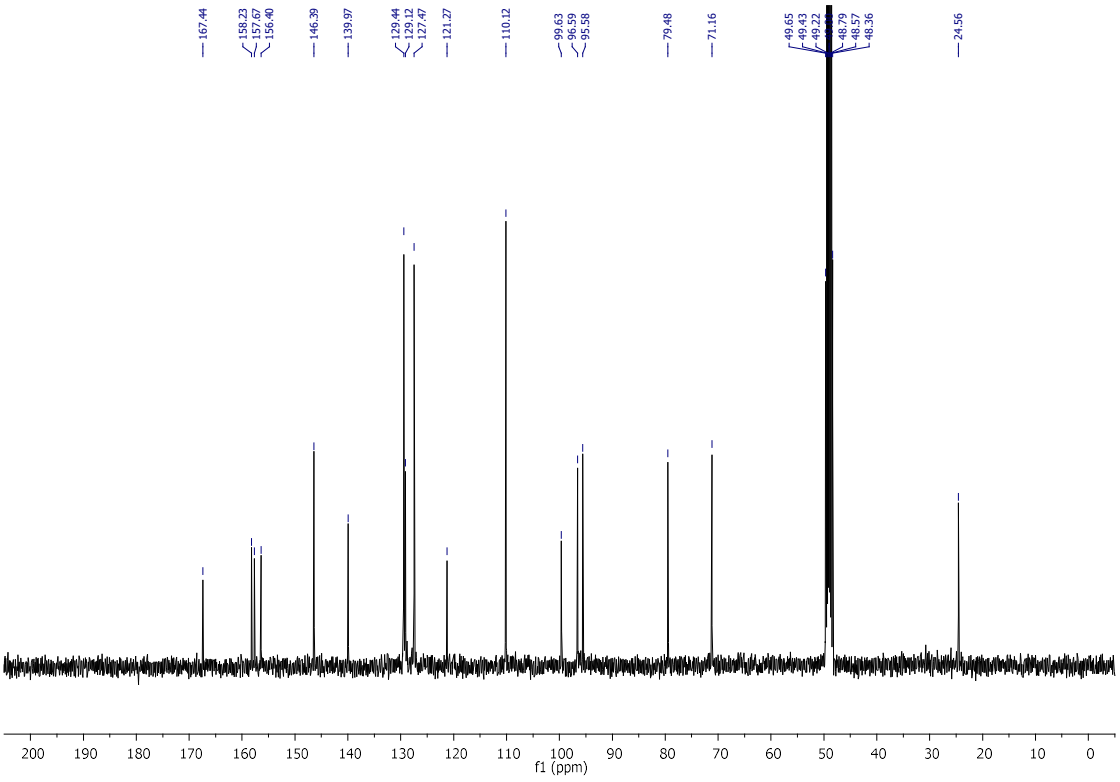

^{13}C NMR spectrum of compound ***rac*-3.58a**

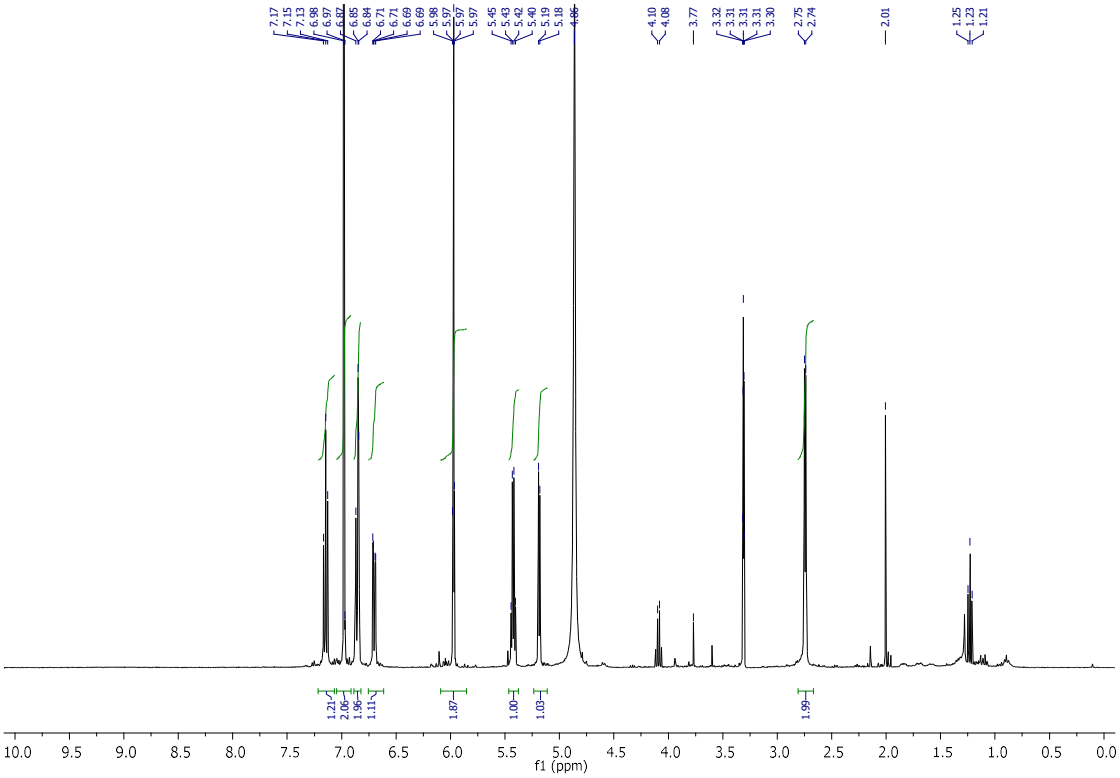

^{1}H NMR spectrum of compound ***rac*-3.58b**

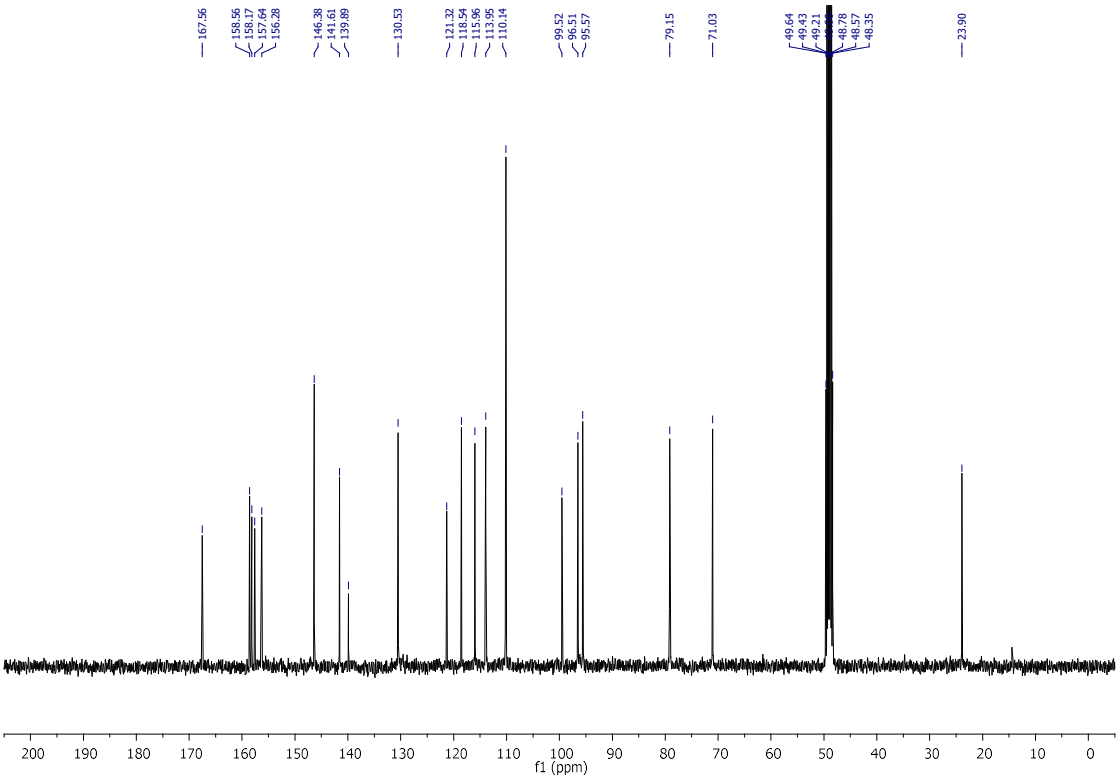

^{13}C NMR spectrum of compound ***rac*-3.58b**

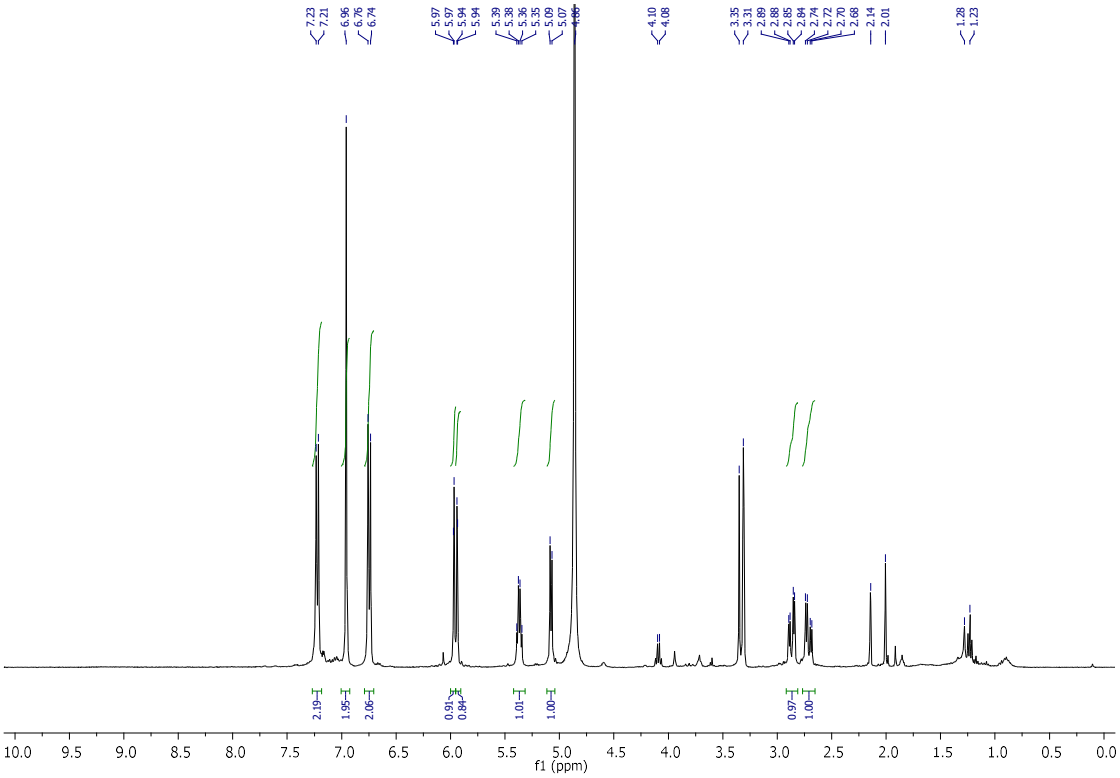

^{1}H NMR spectrum of compound ***rac*-3.58c**

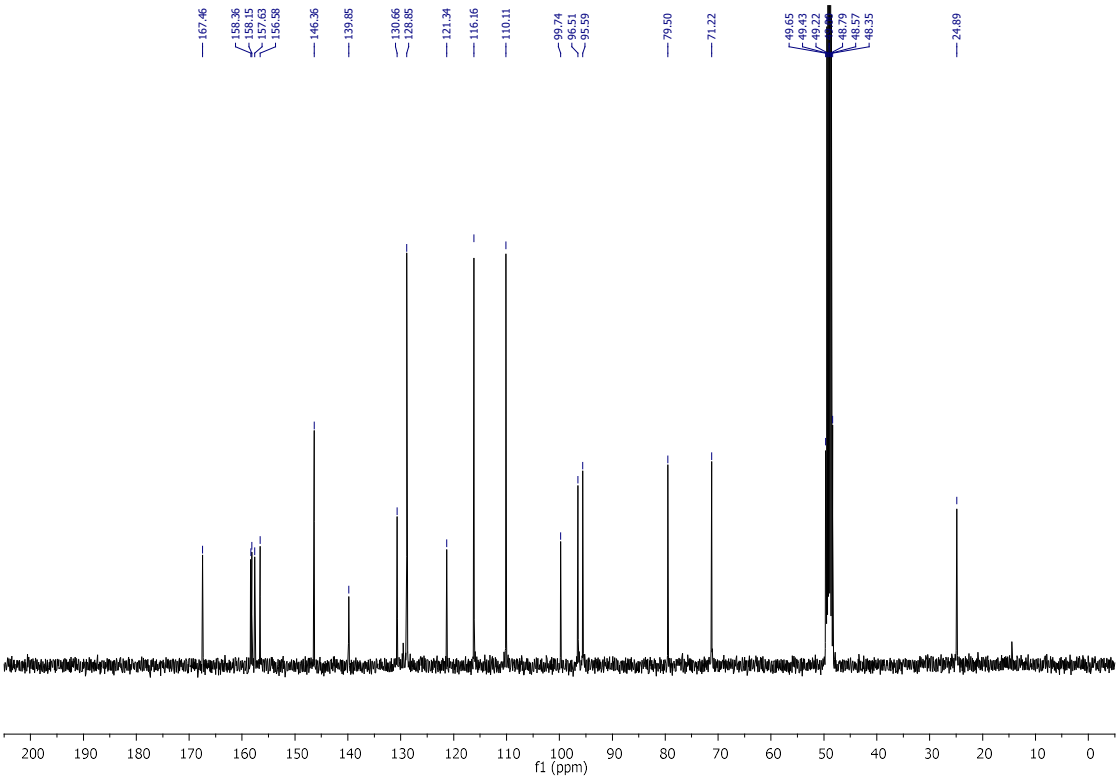

^{13}C NMR spectrum of compound ***rac*-3.58c**

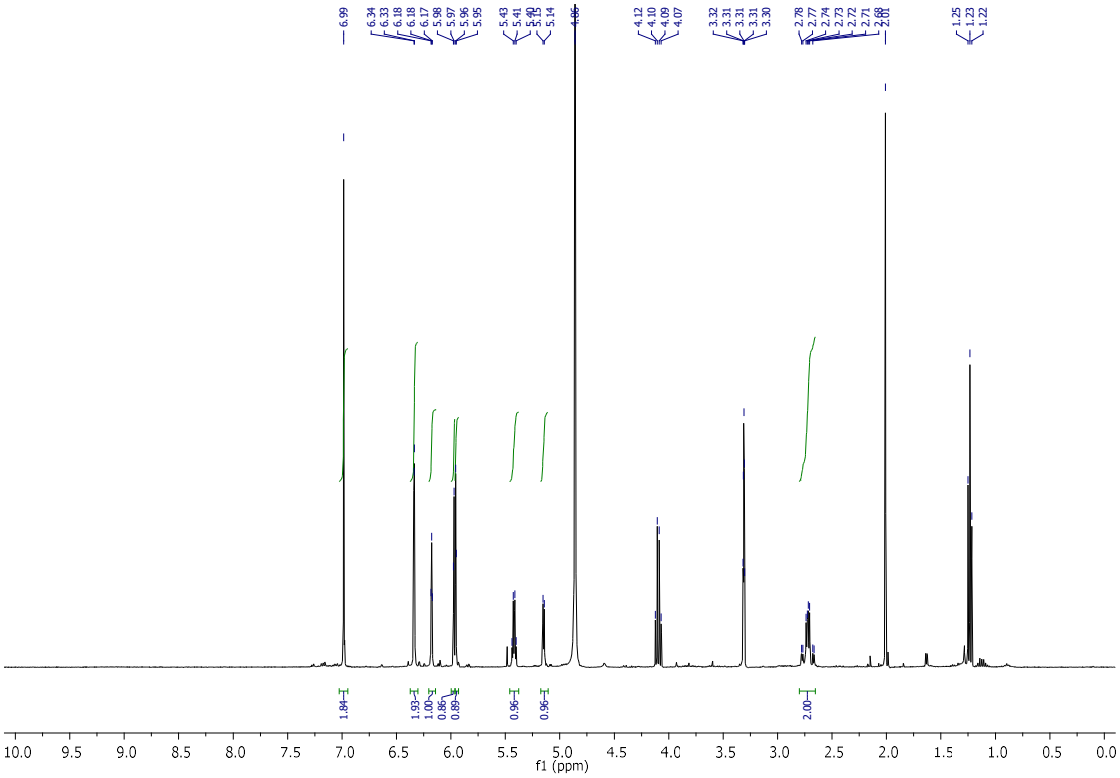

^{1}H NMR spectrum of compound ***rac*-3.58d**

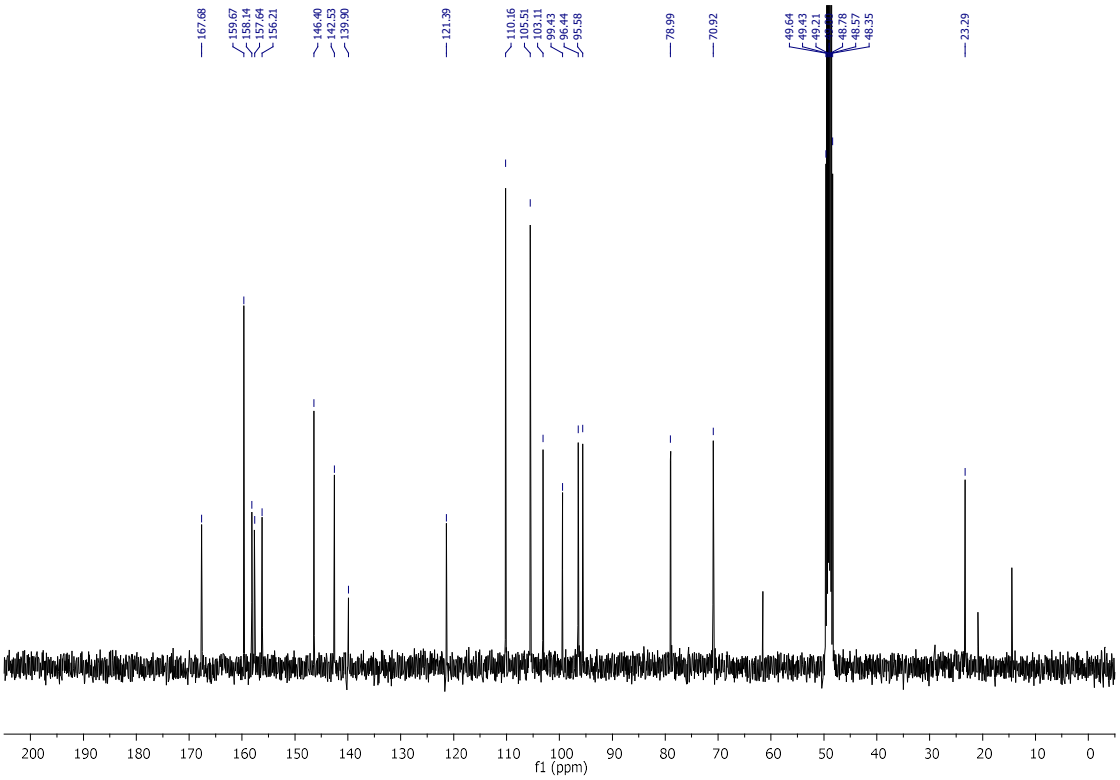

^{13}C NMR spectrum of compound ***rac*-3.58d**

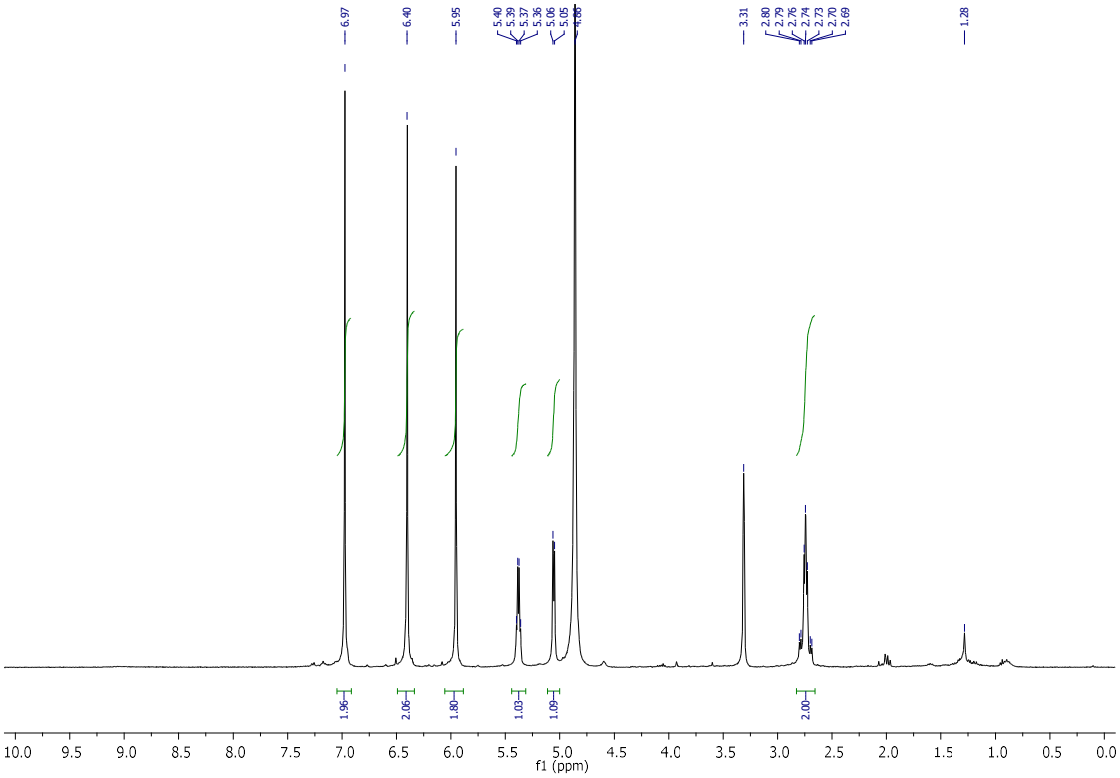

^{1}H NMR spectrum of compound ***rac*-3.58e**

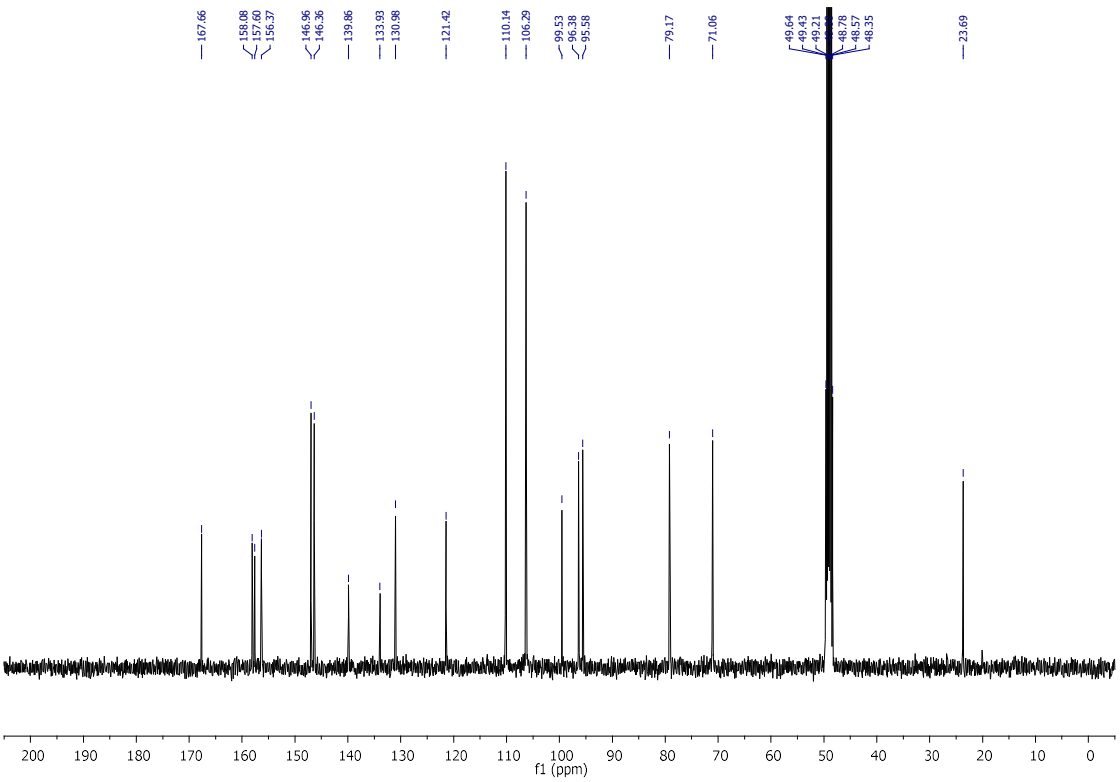

^{13}C NMR spectrum of compound ***rac*-3.58e**

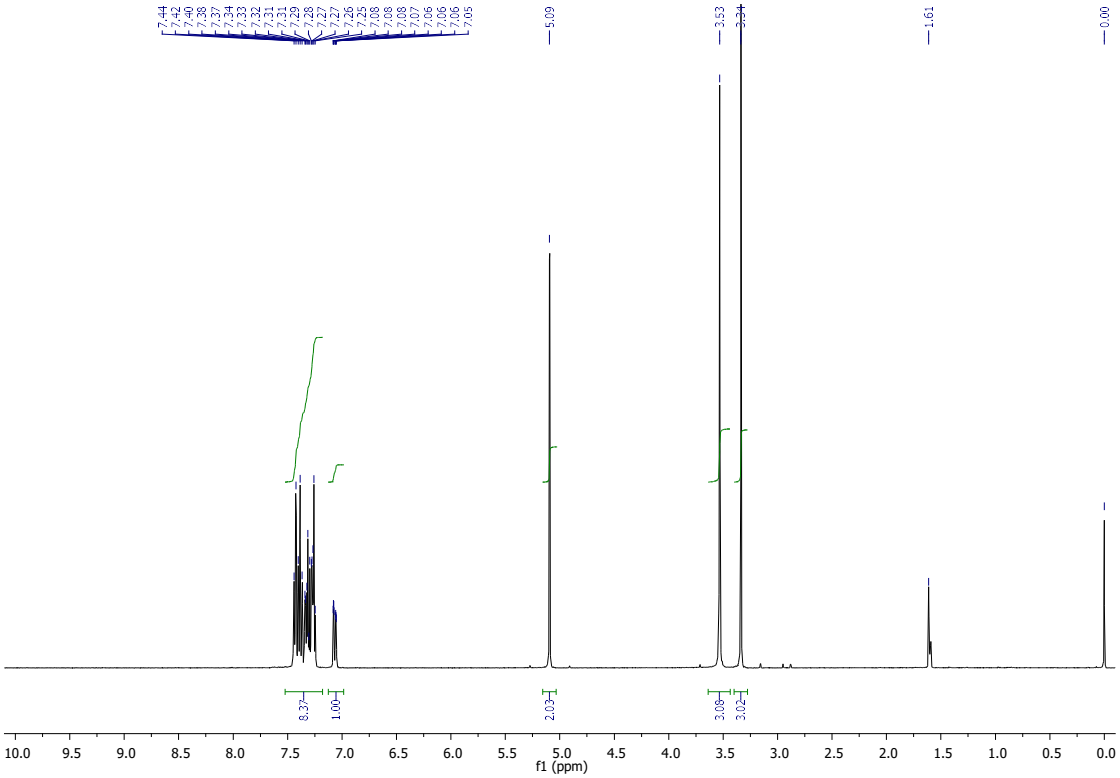

^{1}H NMR spectrum of compound **3.59b**

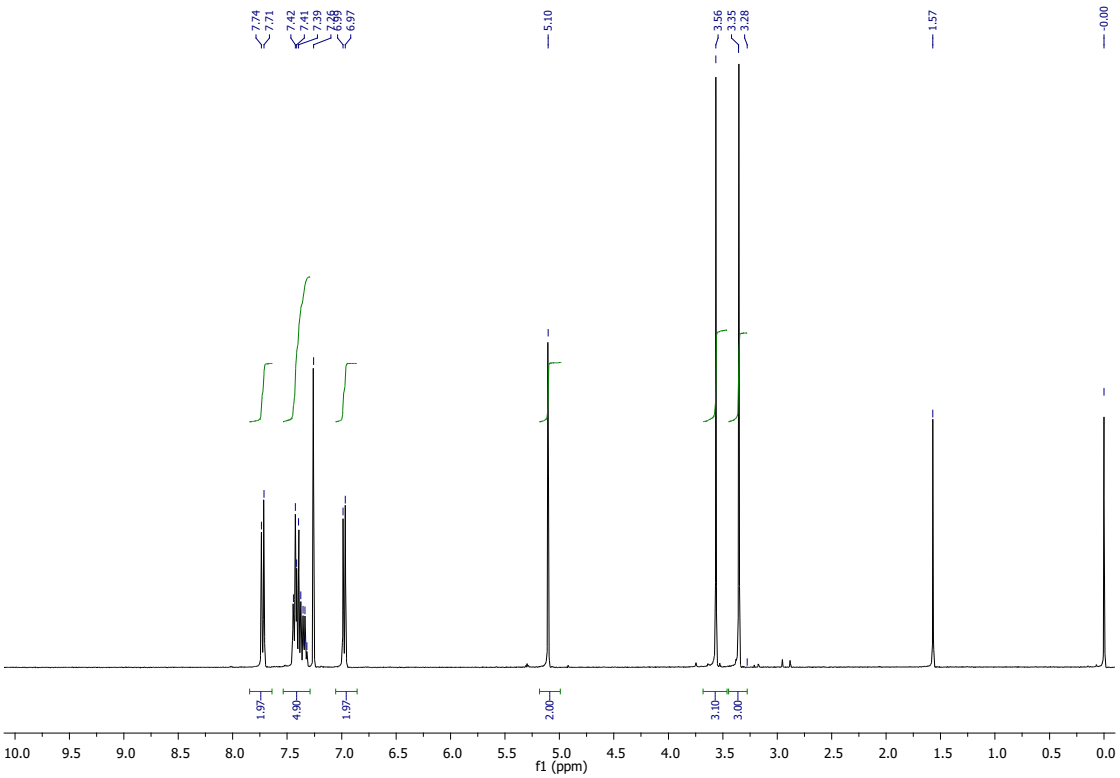

^{1}H NMR spectrum of compound **3.59c**

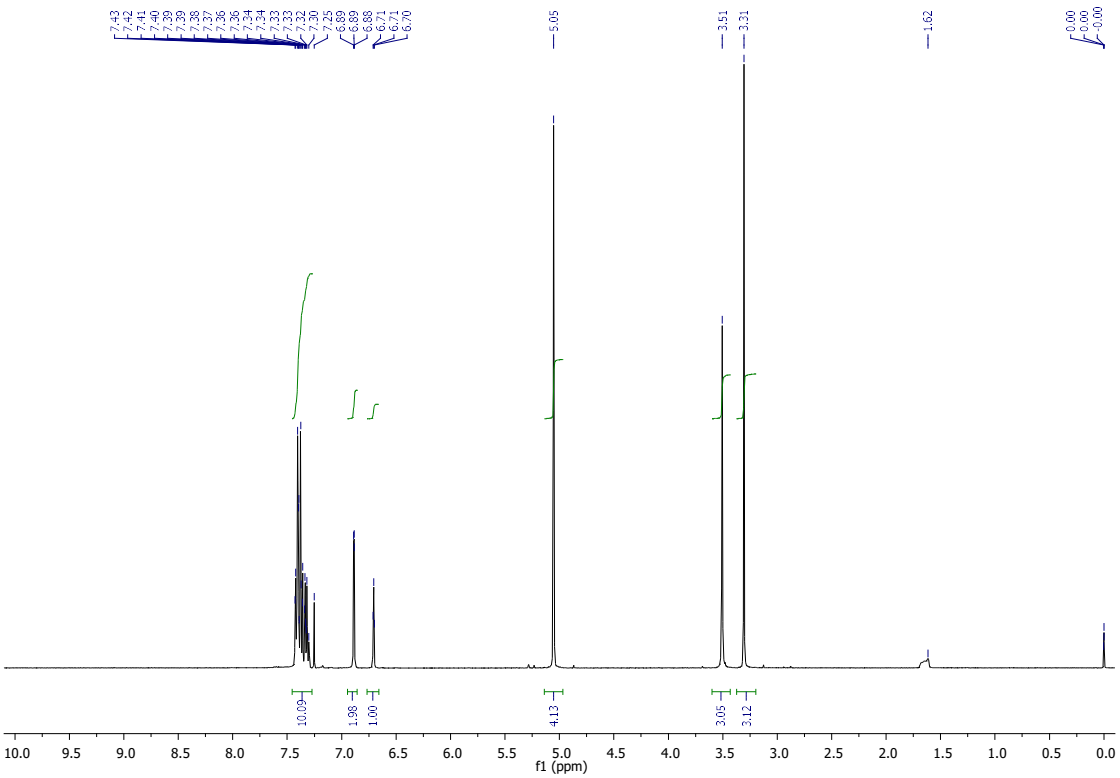

^{1}H NMR spectrum of compound **3.59d**

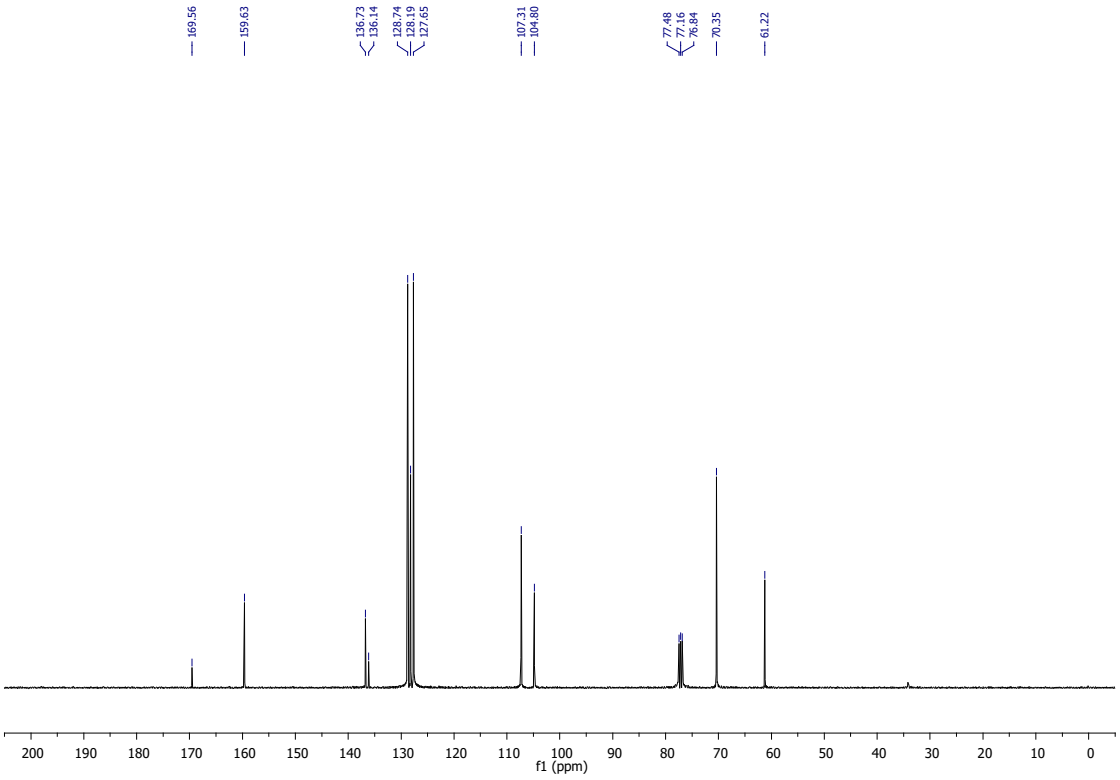

^{13}C NMR spectrum of compound **3.59d**

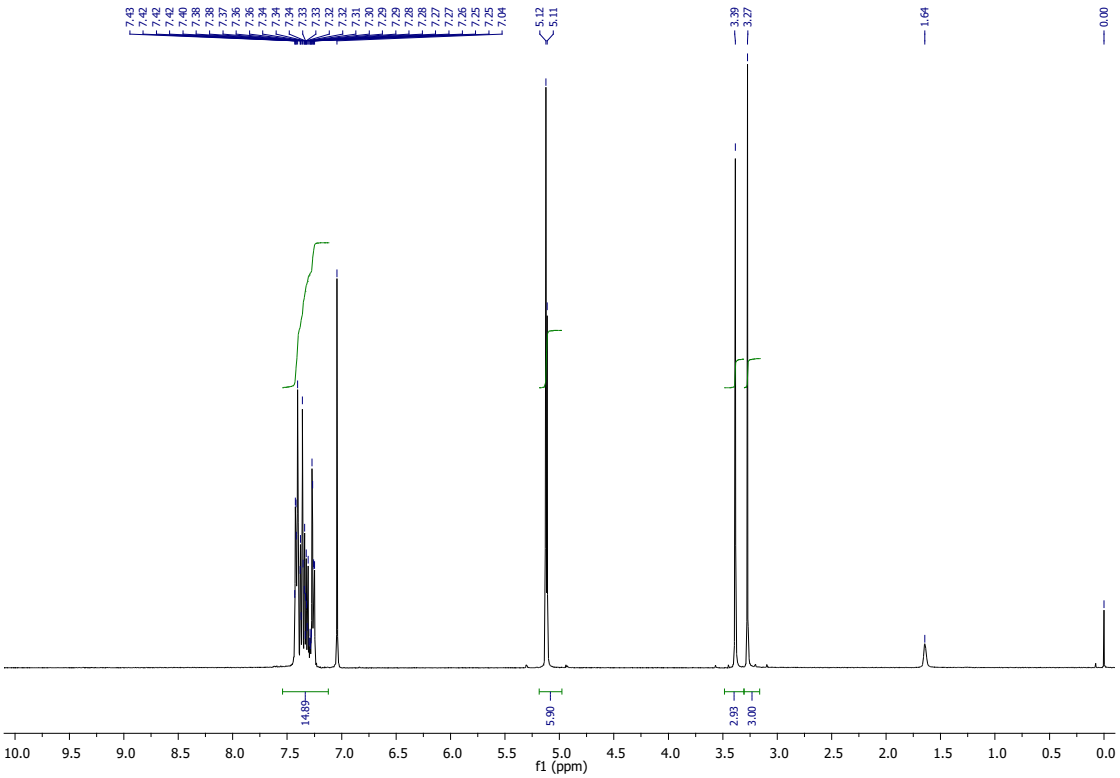

^{1}H NMR spectrum of compound **3.59e**

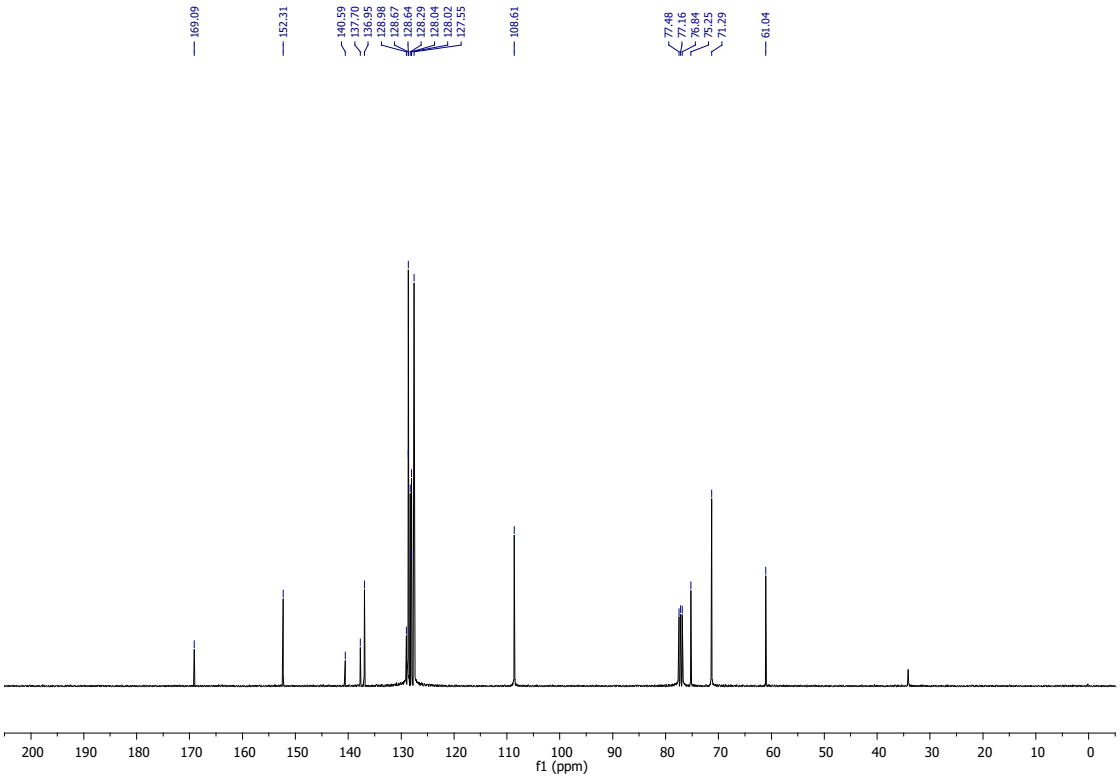

^{13}C NMR spectrum of compound **3.59e**

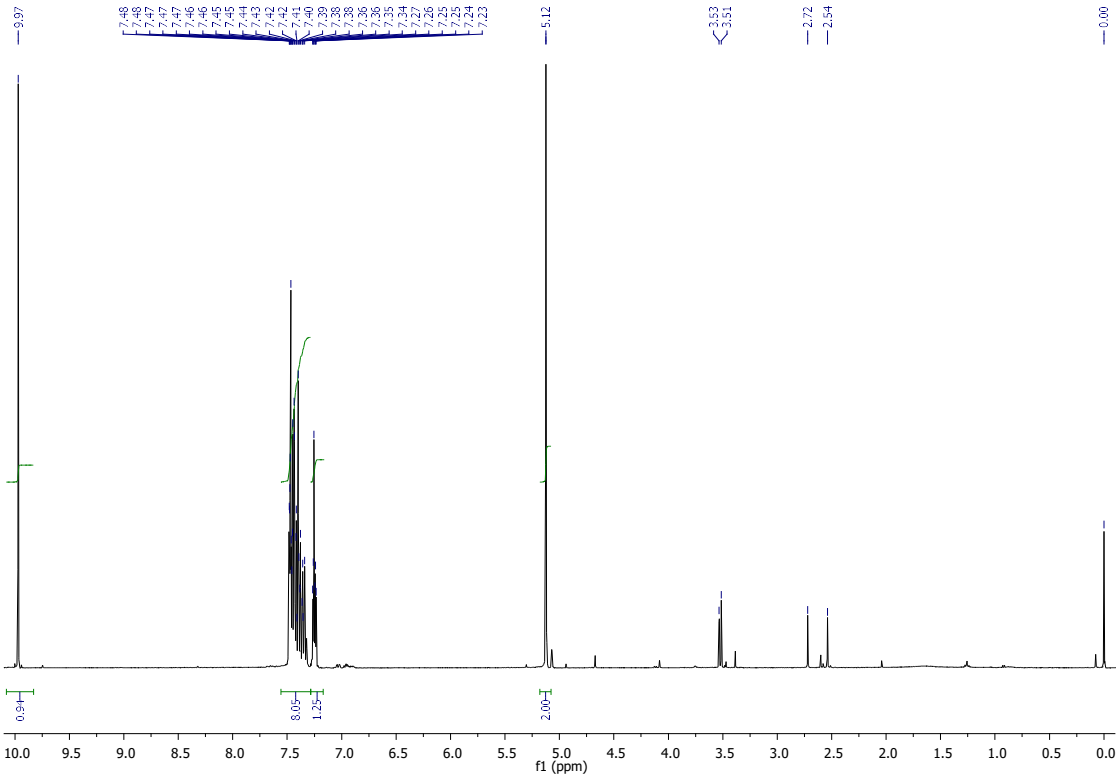

^{1}H NMR spectrum of compound **3.60b**

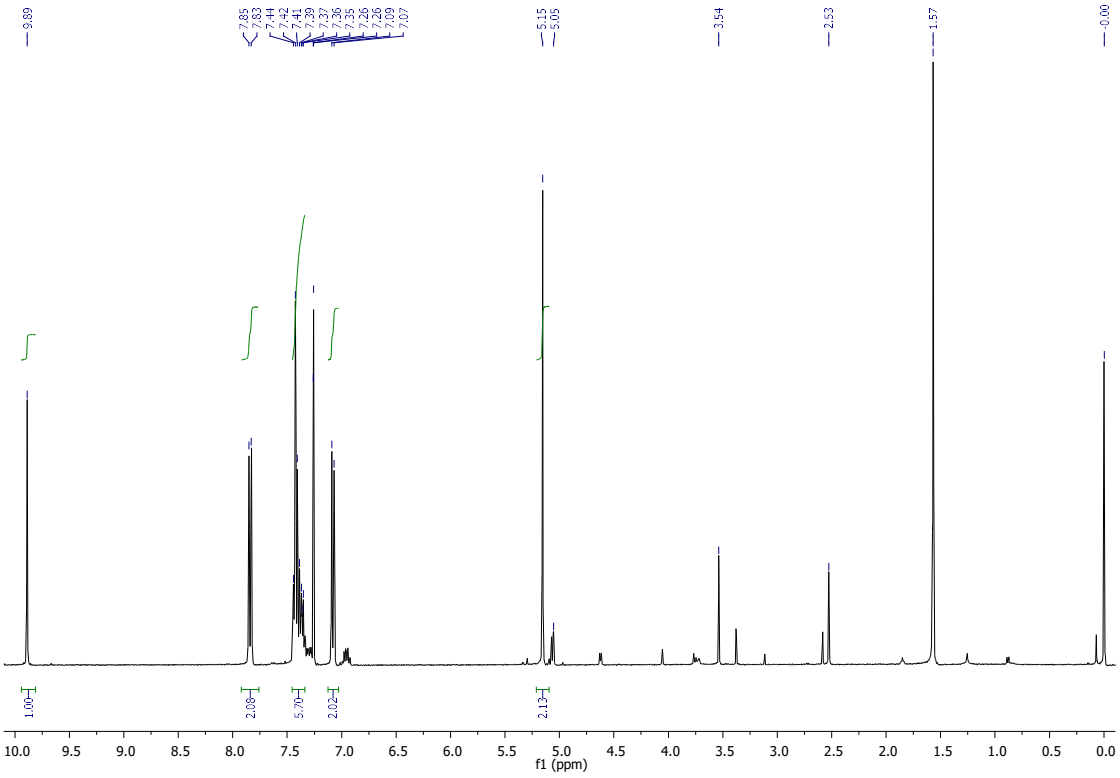

^{1}H NMR spectrum of compound **3.60c**

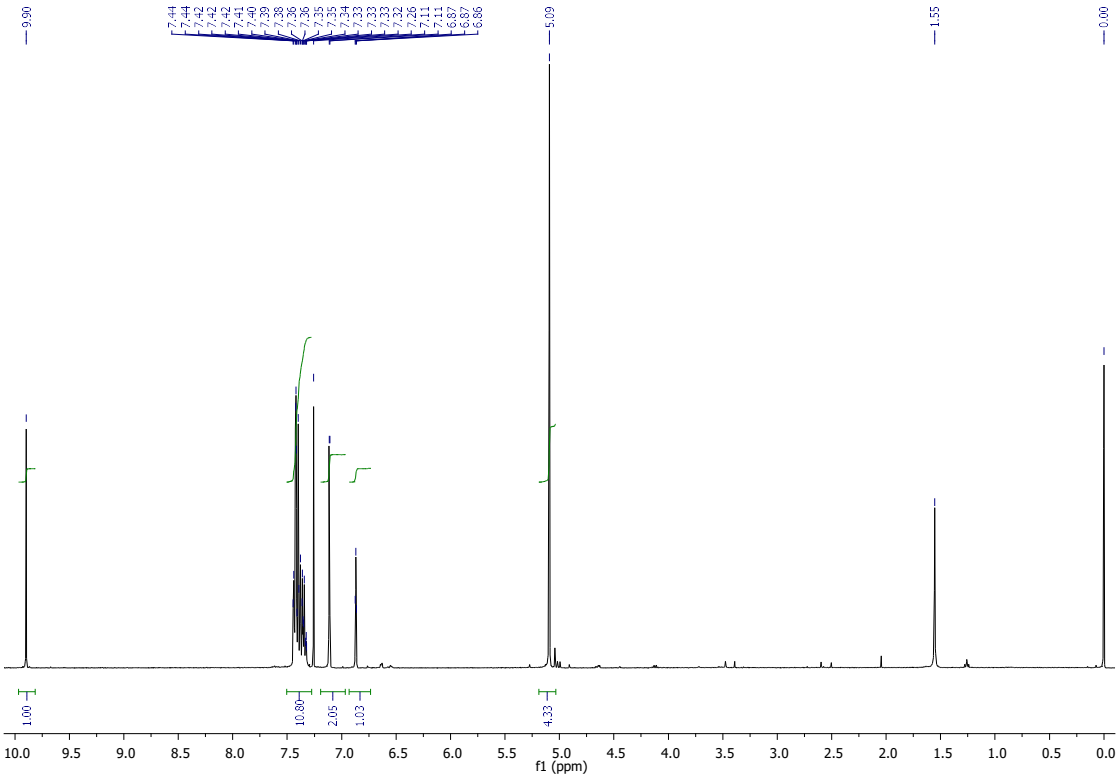

^{1}H NMR spectrum of compound **3.60d**

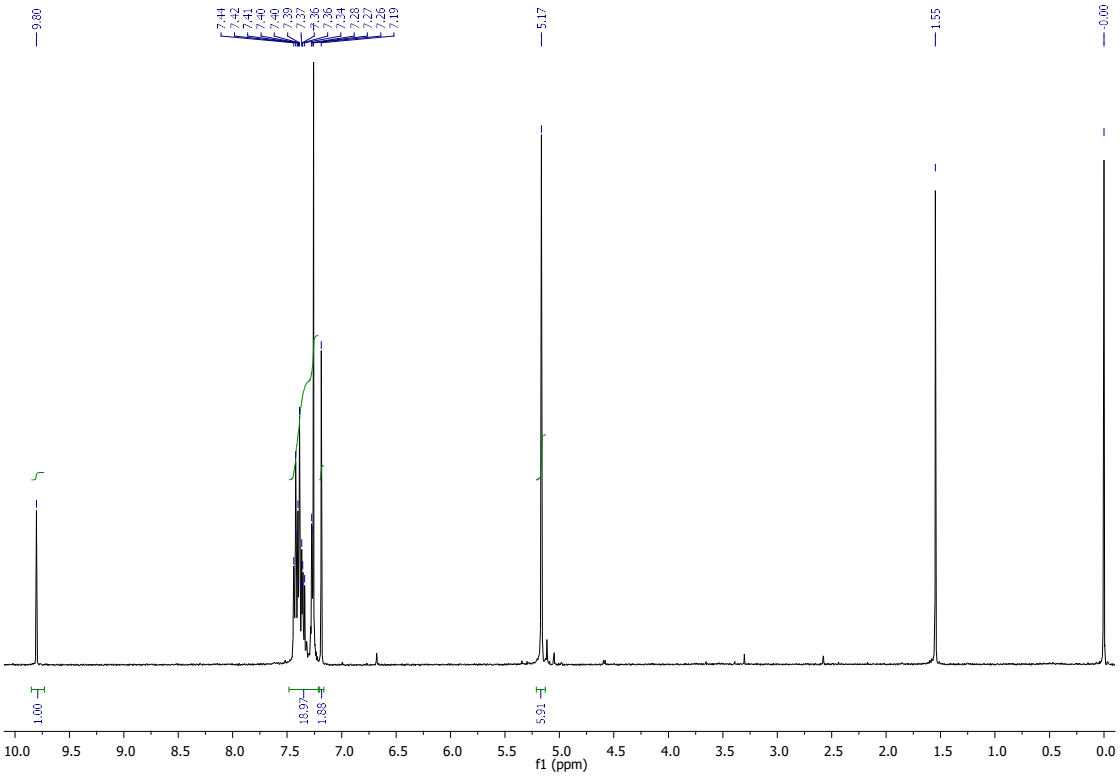

^{1}H NMR spectrum of compound **3.60e**

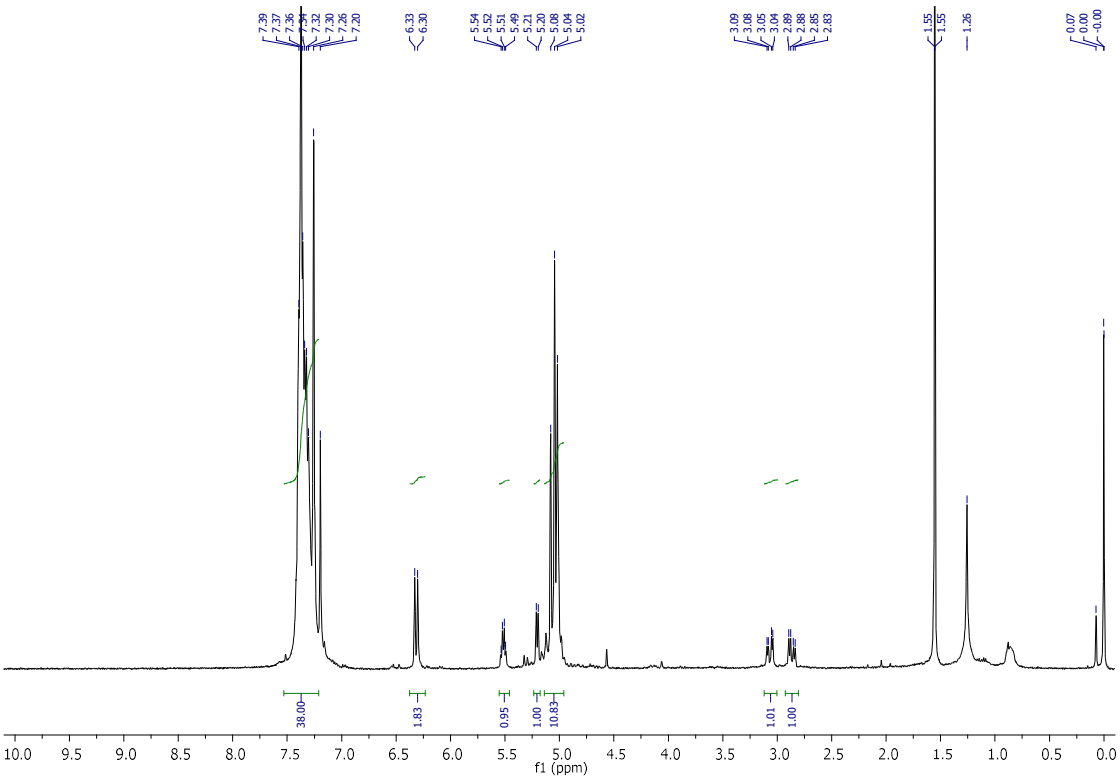

^{1}H NMR spectrum of compound ***rac*-3.61a**

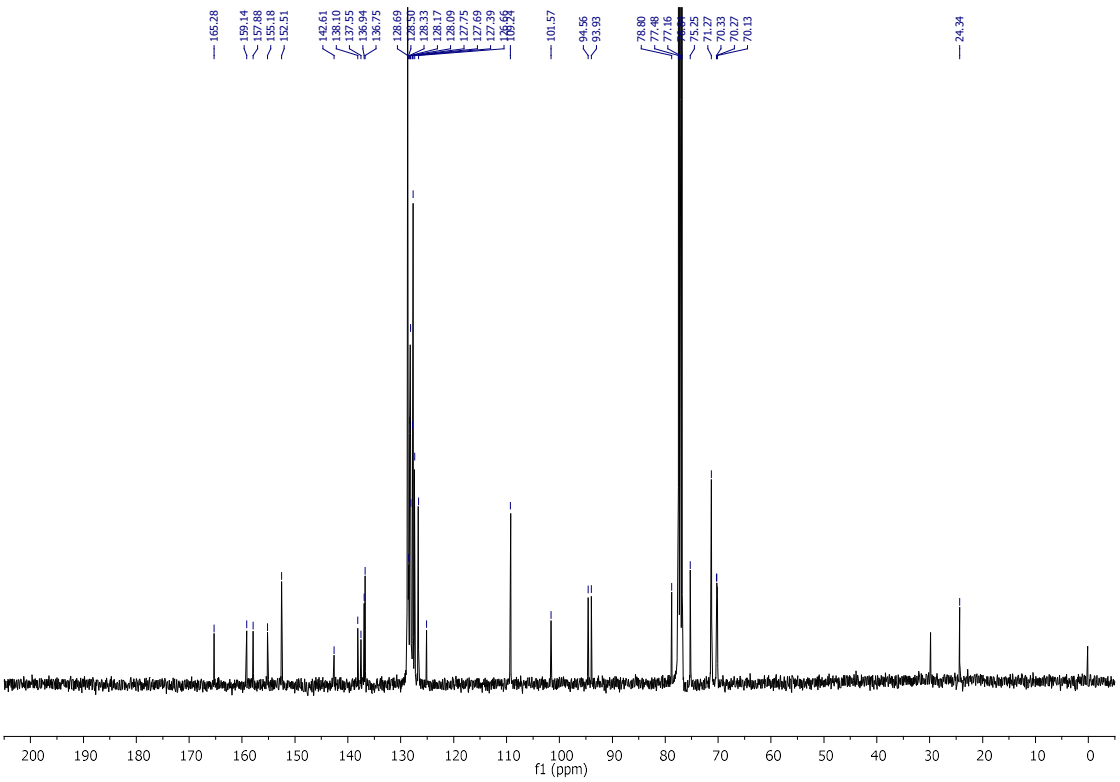

^{13}C NMR spectrum of compound ***rac*-3.61a**

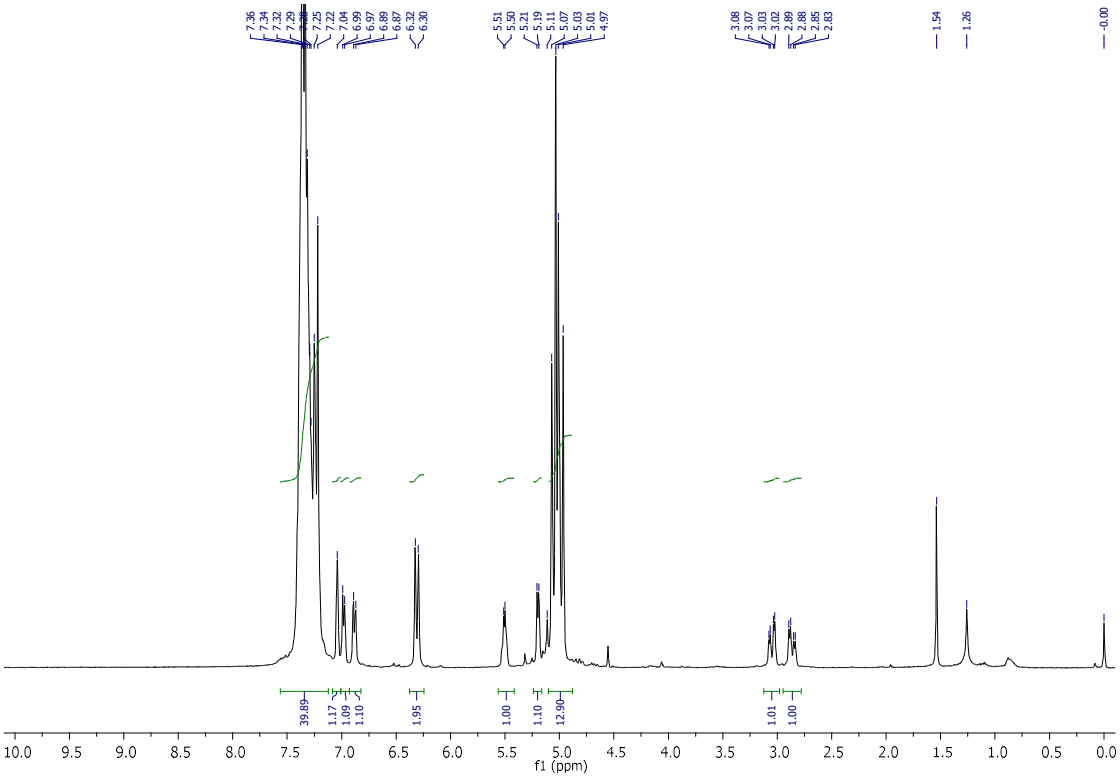

^{1}H NMR spectrum of compound ***rac*-3.61b**

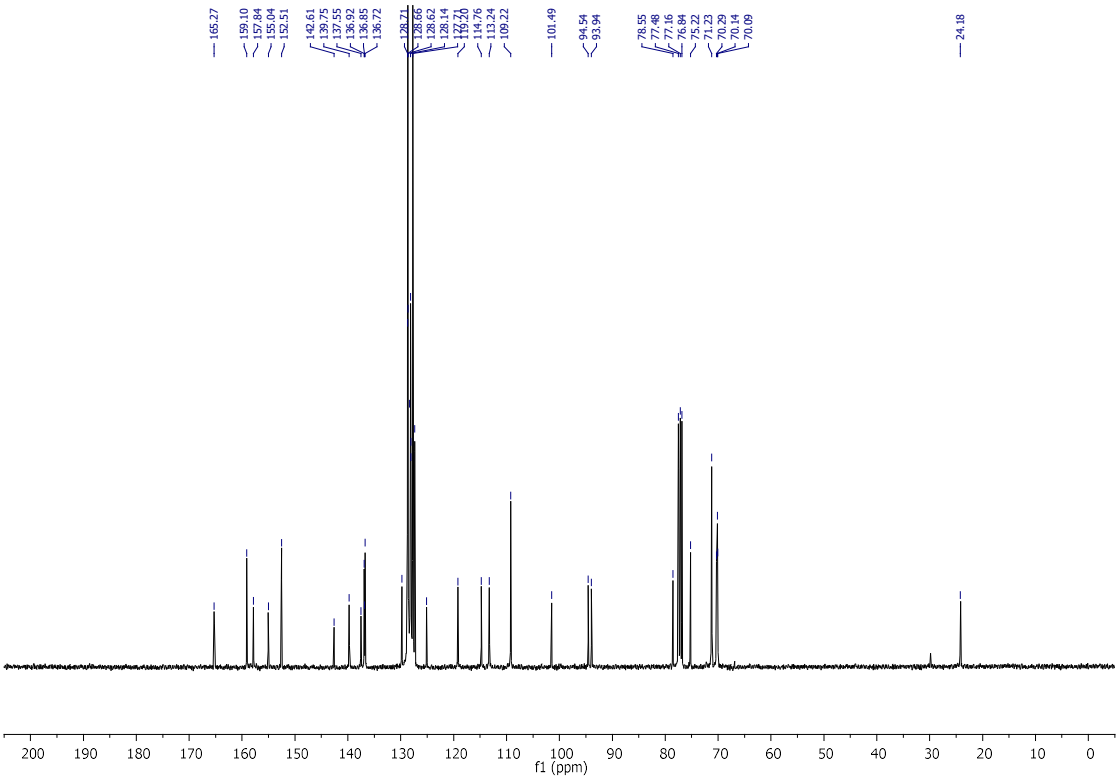

^{13}C NMR spectrum of compound ***rac*-3.61b**

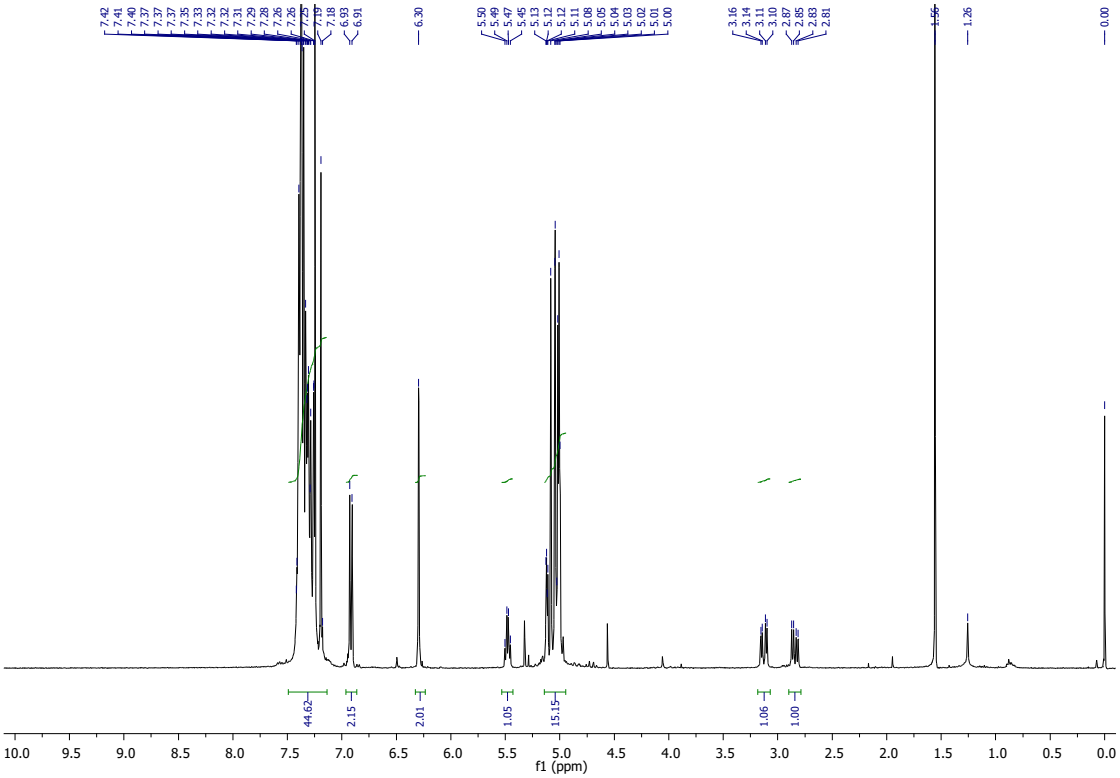

^{1}H NMR spectrum of compound ***rac*-3.61c**

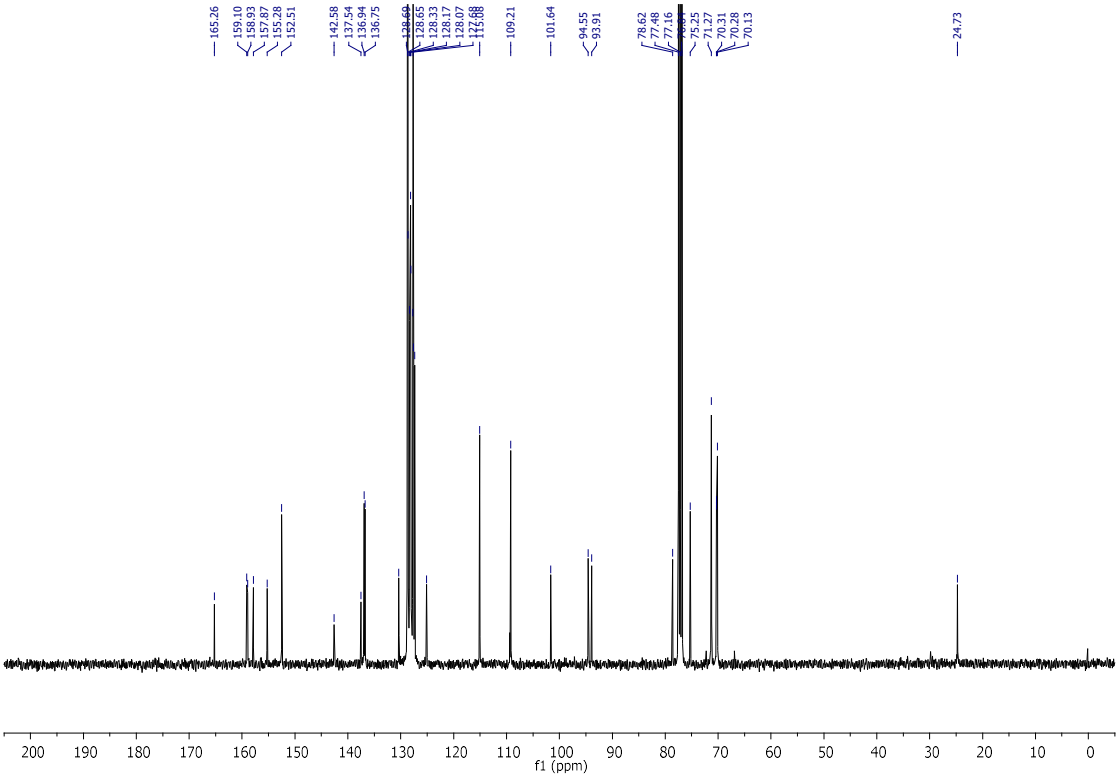

^{13}C NMR spectrum of compound ***rac*-3.61c**

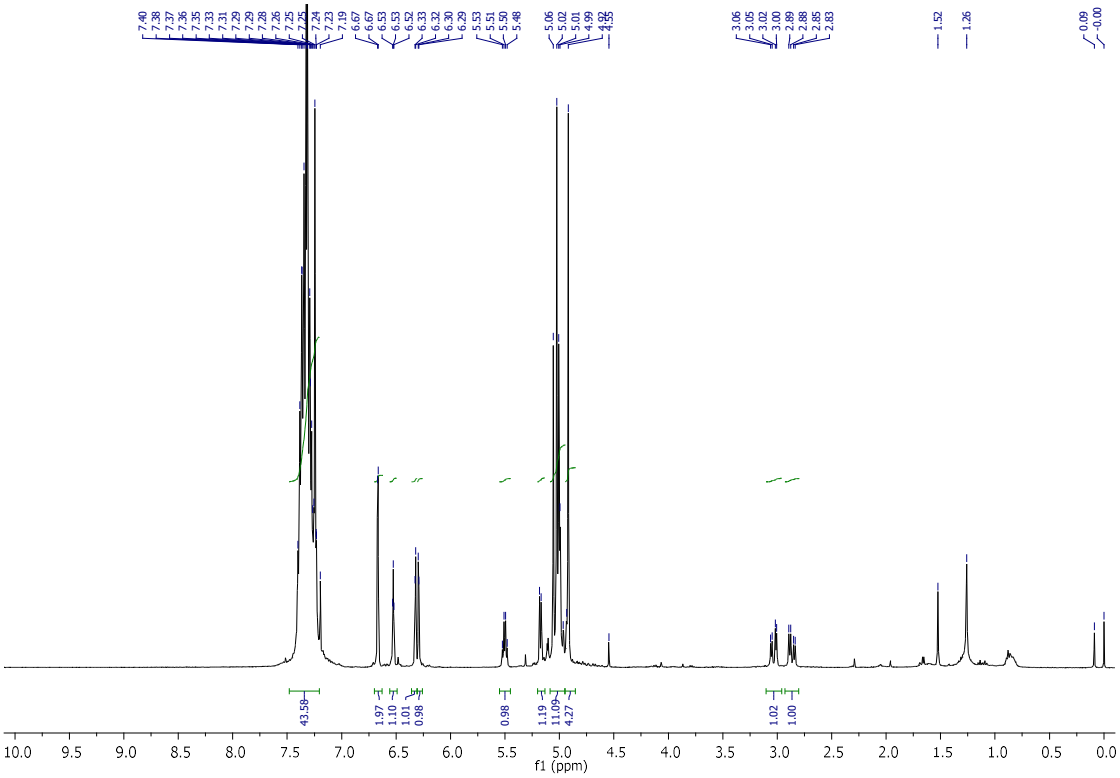

^{1}H NMR spectrum of compound ***rac*-3.61d**

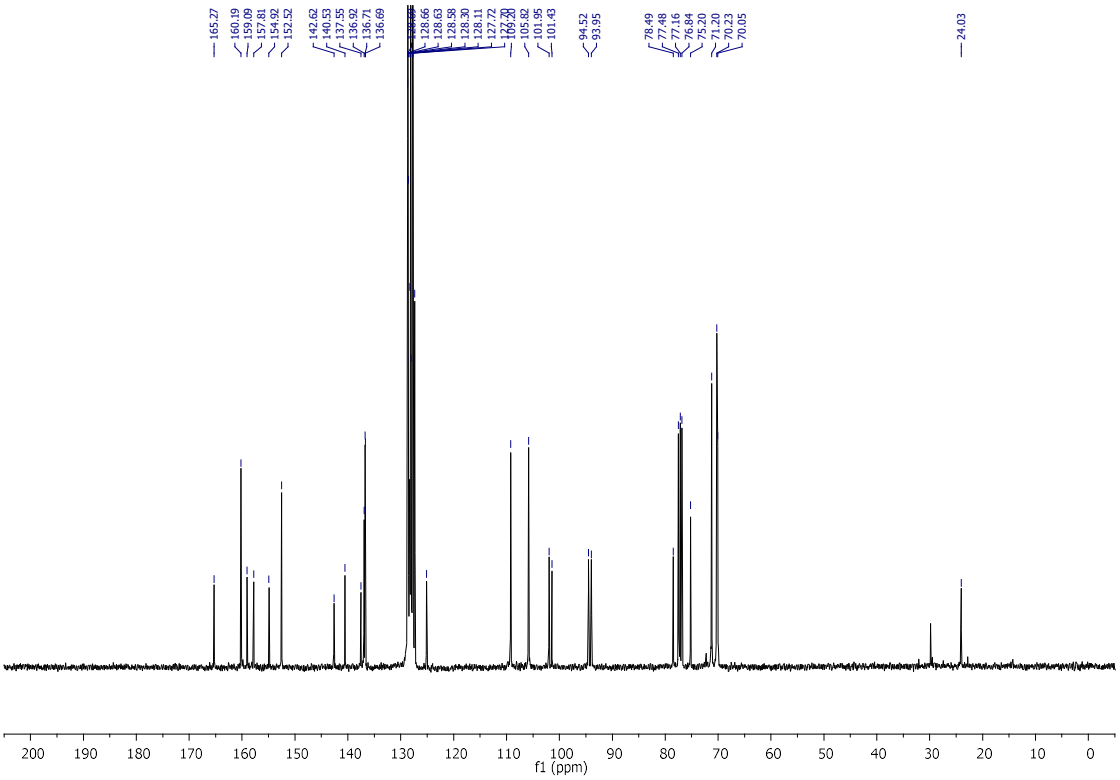

^{13}C NMR spectrum of compound ***rac*-3.61d**

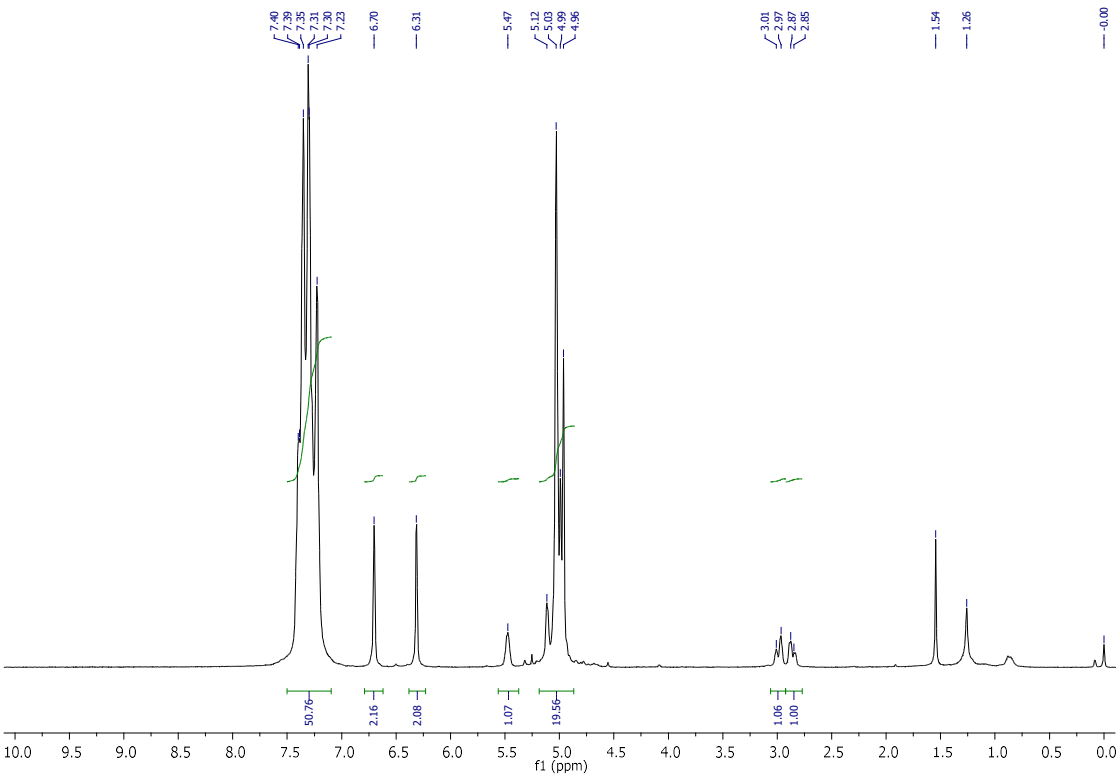

^{1}H NMR spectrum of compound ***rac*-3.61e**

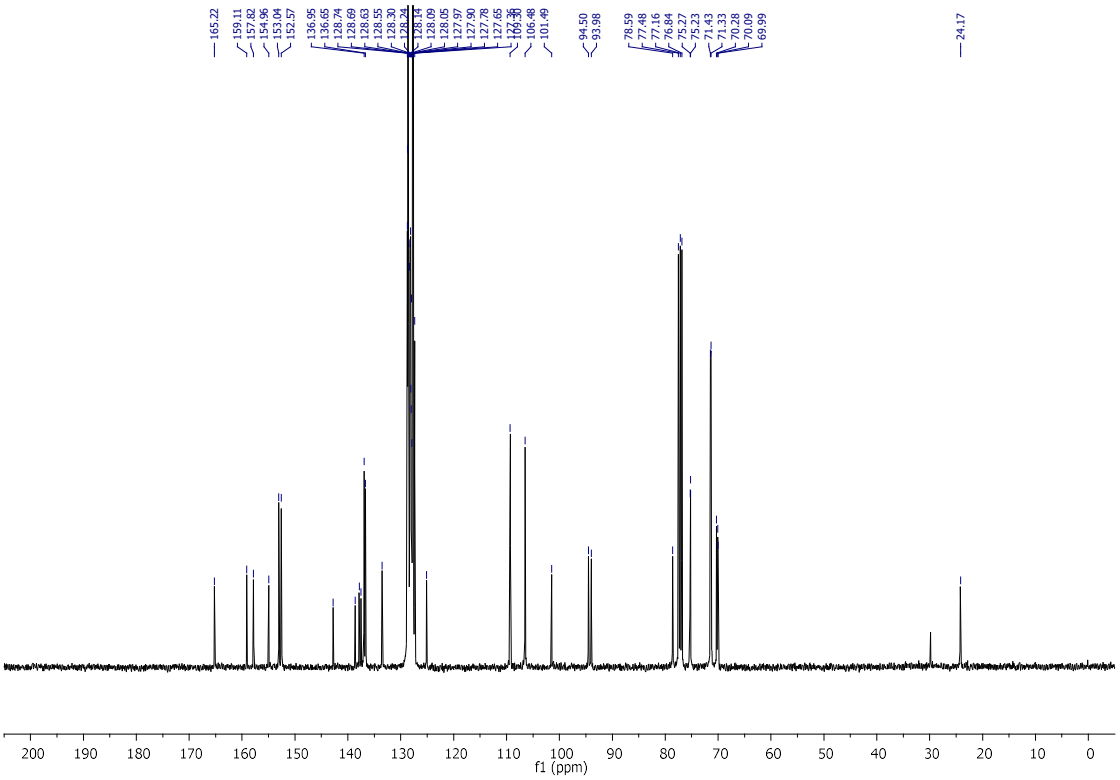

^{13}C NMR spectrum of compound ***rac*-3.61e**

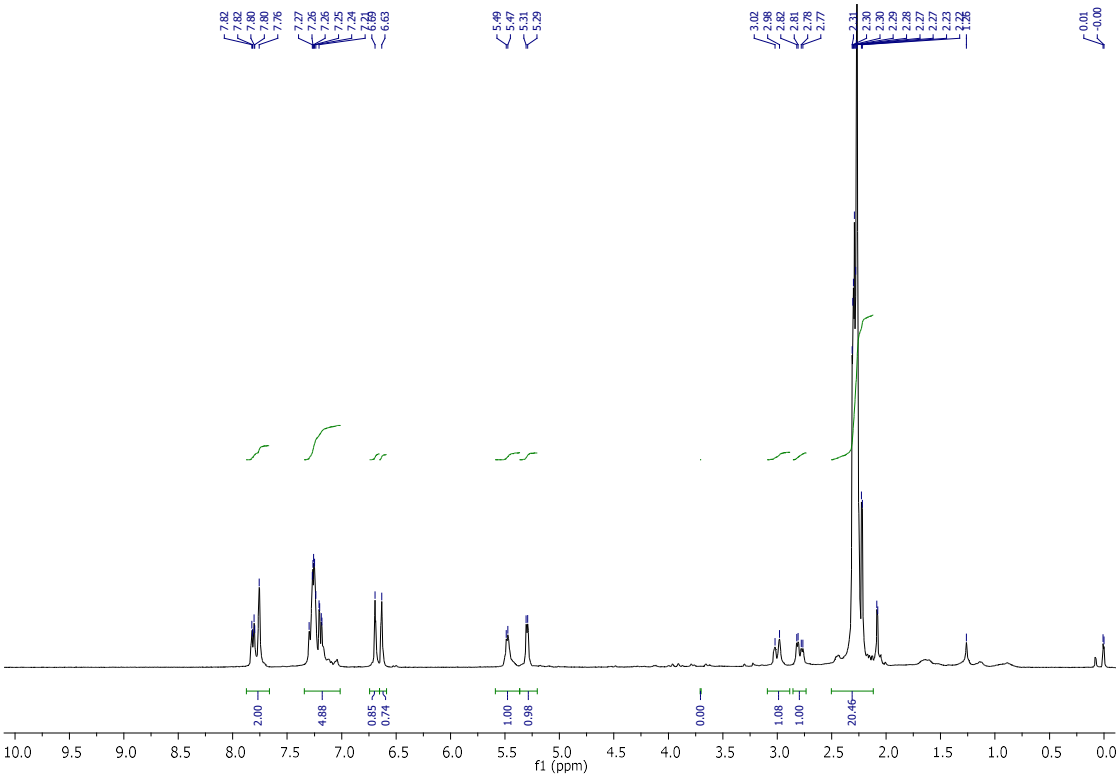

^{1}H NMR spectrum of compound ***rac*-3.63a**

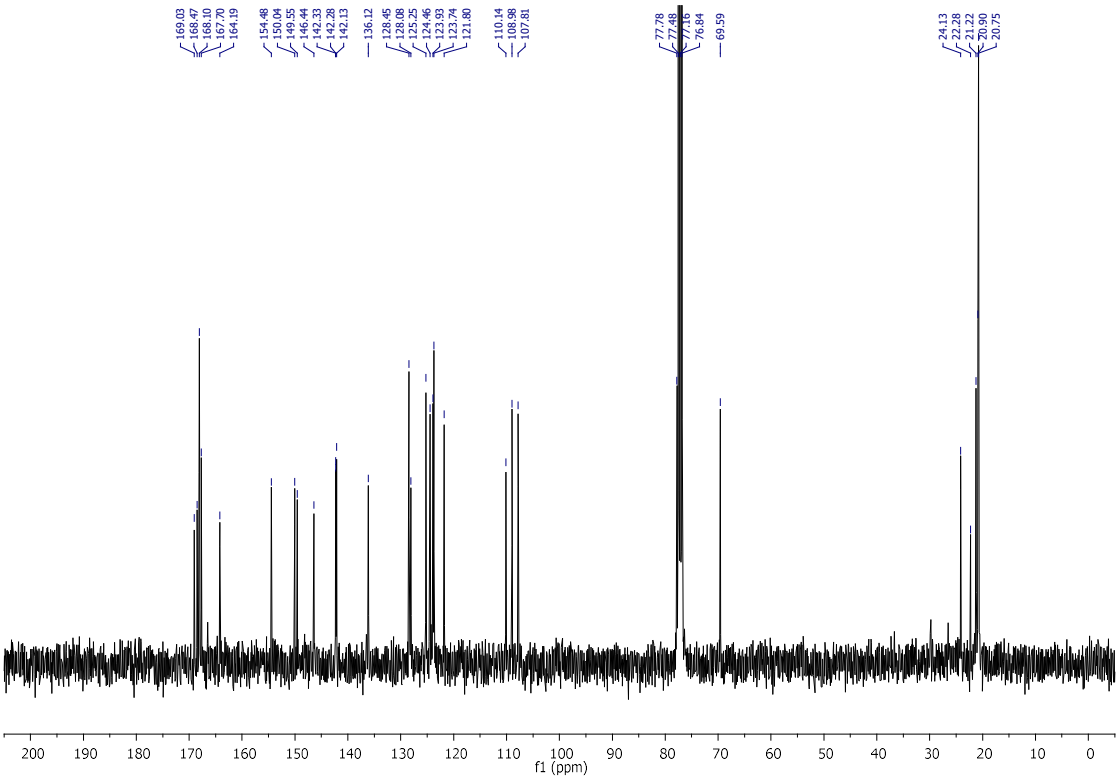

^{13}C NMR spectrum of compound ***rac*-3.63a**

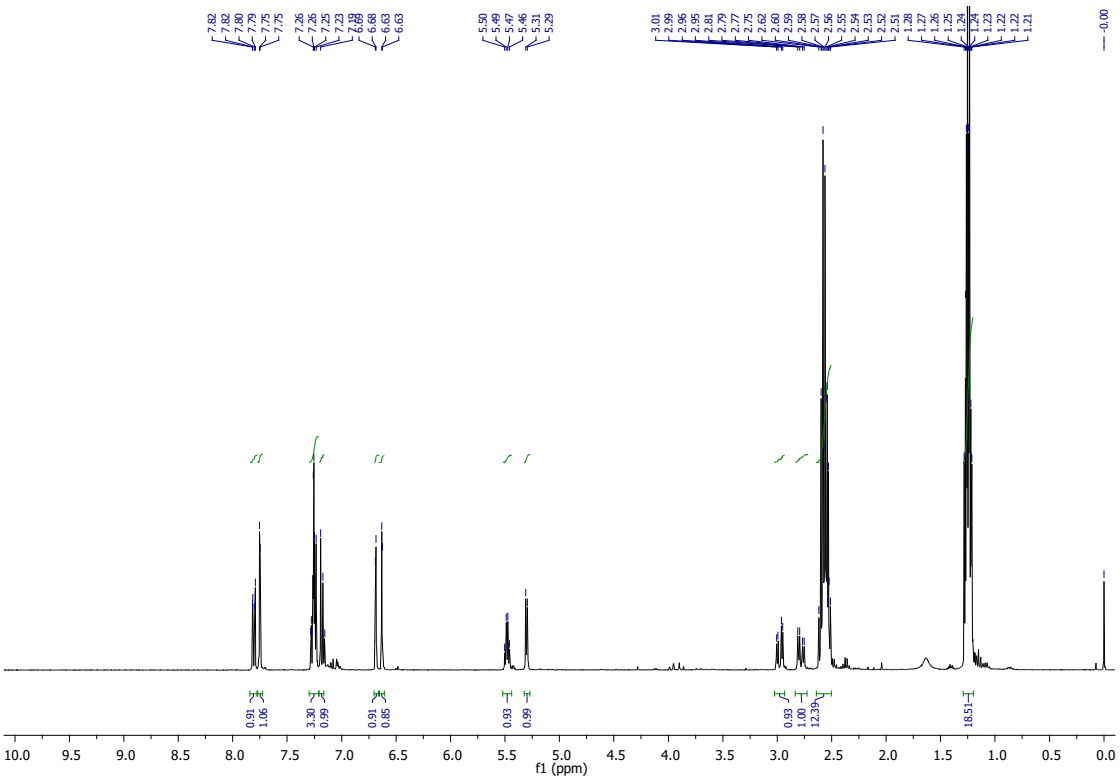

^{1}H NMR spectrum of compound ***rac*-3.63b**

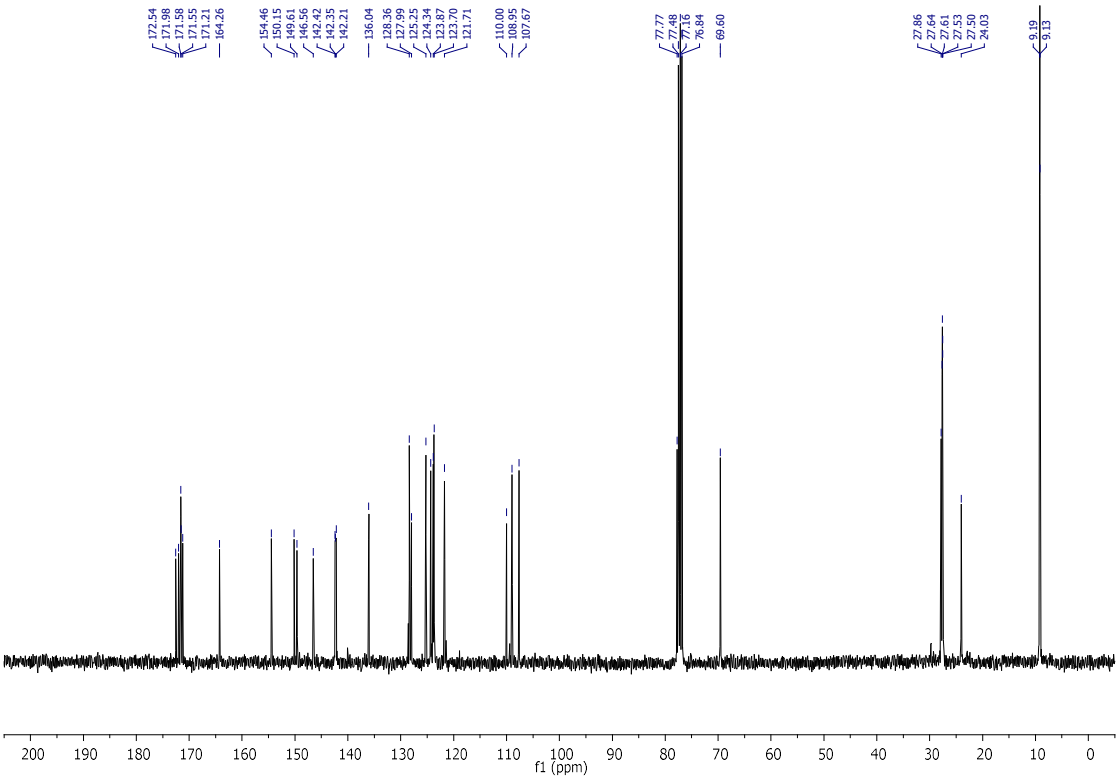

^{13}C NMR spectrum of compound ***rac*-3.63b**

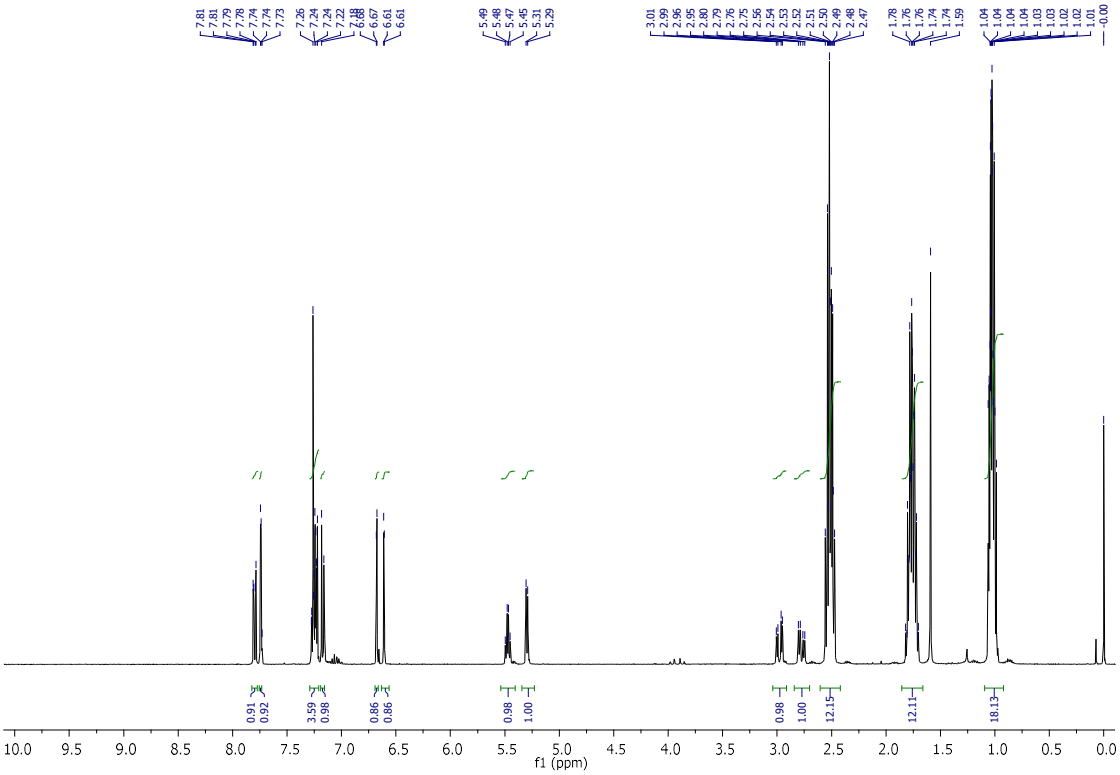

^{1}H NMR spectrum of compound ***rac*-3.63c**

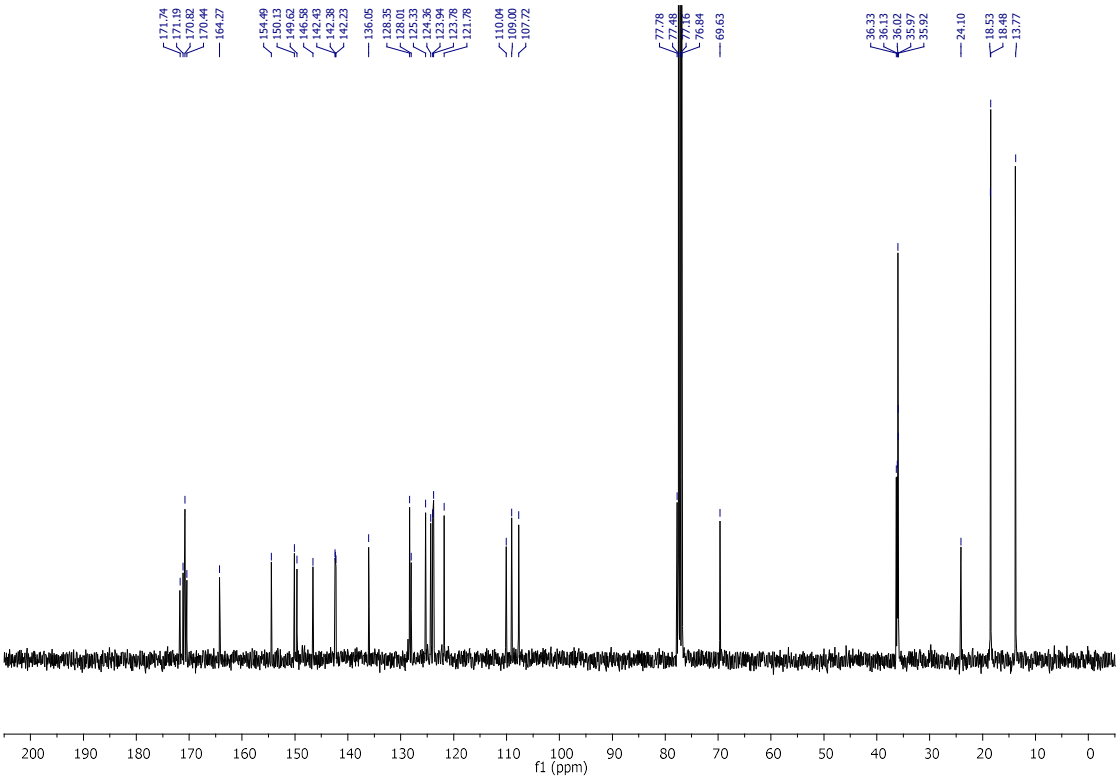

^{13}C NMR spectrum of compound ***rac*-3.63c**

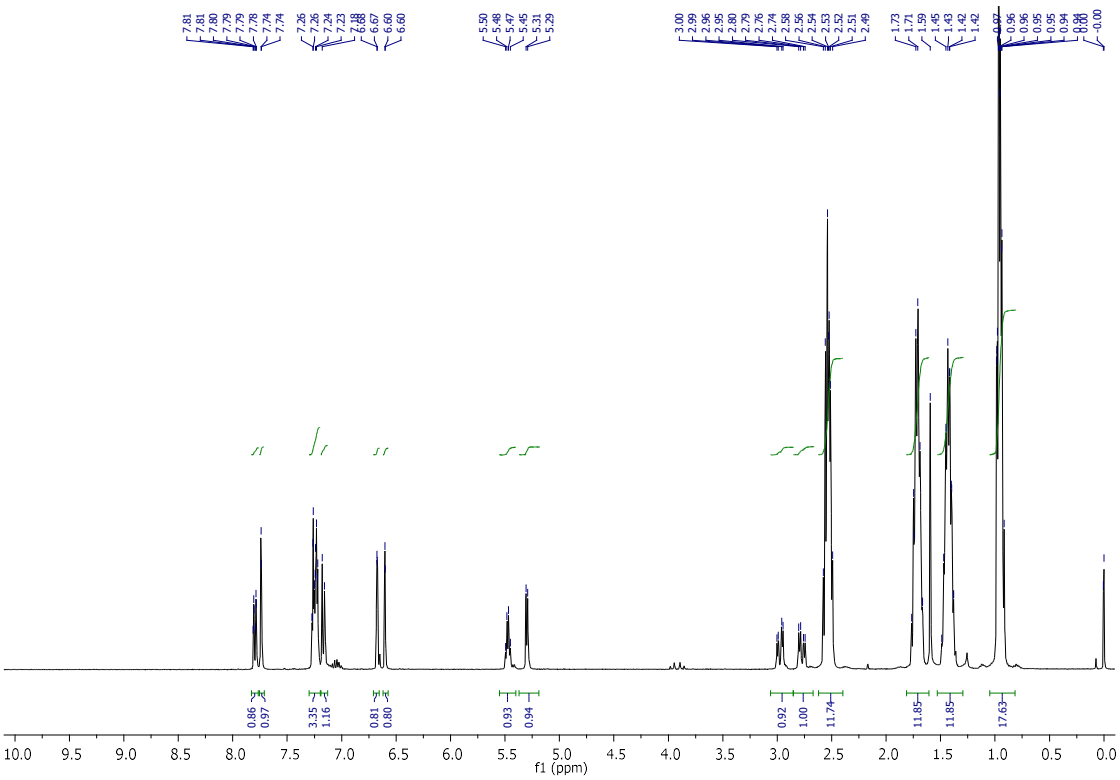

^{1}H NMR spectrum of compound ***rac*-3.63d**

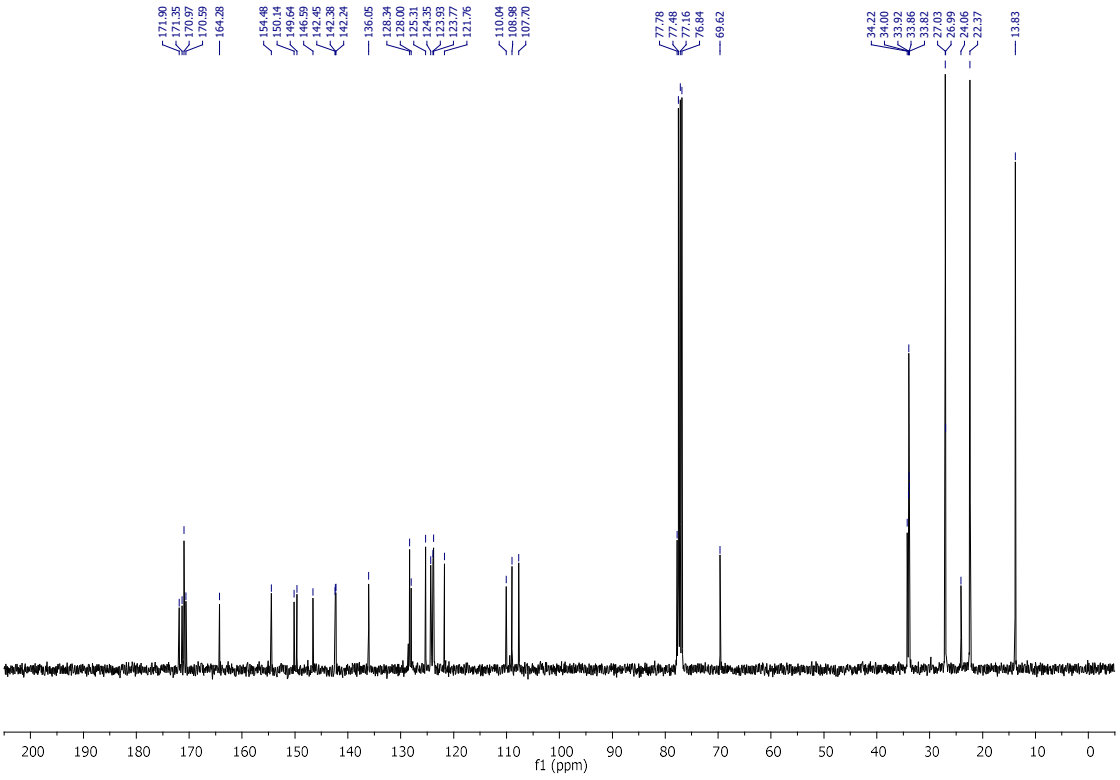

^{13}C NMR spectrum of compound ***rac*-3.63d**

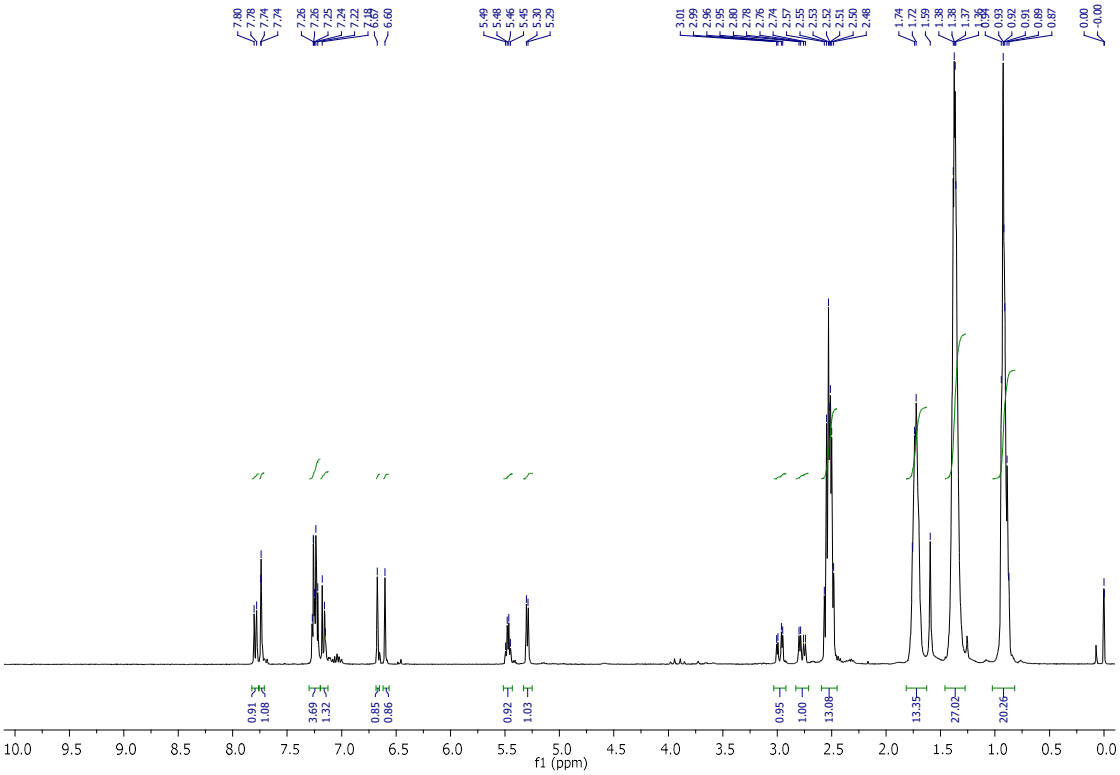

^{1}H NMR spectrum of compound ***rac*-3.63e**

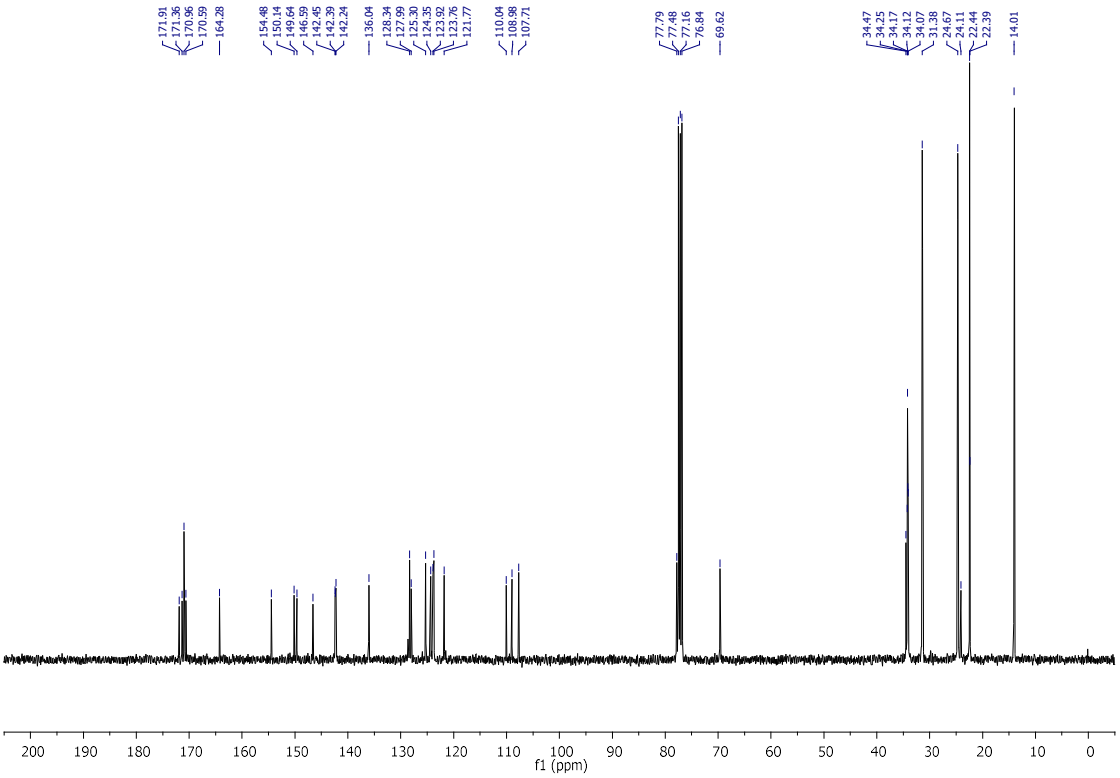

^{13}C NMR spectrum of compound ***rac*-3.63e**